

Universidade de Lisboa
Faculdade de Farmácia



Medicinal Chemistry Approaches
To
Malaria Drug Discovery

Doutoramento em Farmácia
(Especialidade de Química Farmacêutica e Terapêutica)

Sofia Alexandre Santos

Tese orientada pela Prof. Doutora M^a Alexandra Paulo e coorientada pelos Prof. Doutores Rui Moreira e Ralph Mazitschek, especialmente elaborada para a obtenção do grau de doutor.

2016

Universidade de Lisboa
Faculdade de Farmácia



Medicinal Chemistry Approaches To Malaria Drug Discovery

Sofia Alexandre Santos

Orientadores: Prof. Doutora M^a Alexandra Paulo

Prof. Doutor Rui Moreira

Prof. Doutor Ralph Mazitscheck

Tese especialmente elaborada para a obtenção do grau de Doutor em Farmácia e especialidade de Química Farmacêutica e Terapêutica.

Juri:

Presidente:

- Doutor Carlos Alberto Mateus Afonso. Professor Catedrático e Membro do Conselho Científico da Faculdade de Farmácia da Universidade de Lisboa. Presidente do juri por subdelegação de competências:

Vogais:

- Doctor Ralph Mazitschek, Assistant Professor Harvard Medical School, Co-supervisor;
- Doutora Maria Manuel da Cruz Silva, Professora Auxiliar Faculdade de Farmácia da Universidade de Coimbra;
- Doutora Paula Alexandra Carvalho Gomes. Professora Associada com Agregação Faculdade de Ciências da Universidade do Porto;
- Doutora Maria de Fatima Carvalho Nogueira. Investigadora Auxiliar Instituto de Higiene e Medicina Tropical da Universidade Nova de Lisboa;
- Doutora Maria de Lurdes dos Santos Cristiano, Professora Associada com Agregação Faculdade de Ciências e Tecnologia da Universidade do Algarve;
- Doutora Maria Alexandra da Silva Paulo. Professora Auxiliar com Agregação Faculdade de Farmácia da Universidade de Lisboa, Orientadora;
- Doutora Ana Paula Gameiro Francisco. Professora Auxiliar Faculdade de Farmácia da Universidade de Lisboa.

Este trabalho foi financiado pela Fundação para a Ciência e Tecnologia através da bolsa de doutoramento SFRH/BD/80162/2011.

Copyright Statement

The author and the co-promoters give authorization to consult and to copy parts of this thesis for **personal use only** and made **only** in accordance with instructions given by the author. This page must form part of any such copies made. Any other use is limited by the Laws of Copyright, specially the obligation to refer the source whenever results from this thesis are cited.

© 2016 - *Sofia Alexandre Santos*

All rights reserved

Statement

O presente trabalho foi desenvolvido sob orientação da Prof. Doutora M^a Alexandra Paulo e coorientação dos Prof. Doutores Rui Moreira e Ralph Mazitschek. O trabalho foi elaborado em Portugal, no iMed.Ulisboa (Instituto de Investigação do Medicamento) da Faculdade de Farmácia da Universidade de Lisboa e nos Estados Unidos da America, no Center for Systems Biology no Massachusetts General Hospital (Harvard Medical School affiliate hospital). Este trabalho foi financiado pela Fundação para a Ciência e Tecnologia através da bolsa de doutoramento SFRH/BD/80162/2011.

This work was developed under scientific supervision of Dr. M^a Alexandra Paulo and co-supervision of Professor Rui Moreira and Dr. Ralph Mazitschek. This work was done in Portugal, at the iMed.Ulisboa (Research Institute for Medicines) in the Faculty of Pharmacy, University of Lisbon, and in the United States of America, at the Center for Systems Biology in the Massachusetts General Hospital (Harvard Medical School affiliate hospital). The work was financially supported by Fundação para a Ciência e Tecnologia, through the doctoral grant SFRH/BD/80162/2011.

Acknowledgments

This thesis represents roughly four years of focused efforts, during which I have benefited from the guidance and support of mentors, colleagues, friends, and family, without whom none of this would have been possible.

I would like to express my gratitude to my supervisor and co-supervisors. Prof. Alexandra Paulo for her patience, encouragement and constant support. Prof. Ralph Mazitschek for his guidance and help, as well as continuously pushing me to do better. Prof. Rui Moreira for the helpful inputs. I could not have imagined having better advisors for my PhD student life. I would further like to express my gratitude for the insightful comments and proof reading of this thesis.

I offer my sincere appreciation to Prof. Dyann Wirth, and all the lab members for providing precious support, helpful advice and spending their valuable time assisting me in performing *Plasmodium falciparum* biological assays. A particular thanks goes to Dr. Amanda Lukens for all her support in the Wirth lab.

Furthermore, I would like to thank all the collaborators with whom I had the pleasure of working with during this journey.

A special thanks to all my past and present fellow lab members, especially Yelena Wainman and Antoinette Nibbs, for their invaluable assistance and emotional support and Lola Fagbami for insightful discussions. I would like to thank all my colleagues at Center for Systems Biology at MGH for their continuous help and encouragement. I would also like to extend my gratitude to my fellow lab members at iMed, Portugal.

I would like to express my indebtedness gratitude to Fundação para a Ciência e Tecnologia for their financial support (SFRH/BD/80162/2011), to the Faculdade de Farmácia, Universidade de Lisboa, Portugal and to the Center for Systems Biology, Massachusetts General Hospital for the availability of facilities, material and equipment necessary for the development of this study.

I would also like to express my love and gratitude to my beloved family, especially my mother and sister for their unconditional love and encouragement throughout my life. Finally, I would like to thank my husband, who is my rock, for his strength, understanding and continuous support on this roller-coaster ride.

Autobiography

Ph.D, 2012-2016

Faculdade de Farmácia, Universidade de Lisboa, Portugal

Center for Systems Biology, Massachusetts General Hospital, USA

Thesis Title: Medicinal Chemistry Approaches to Malaria Drug Discovery

Supervisors: Prof. Doutor Maria Alexandra da Silva Paulo

Co-Supervisors: Prof. Doutor Ralph Mzitschek and Prof. Doutor Rui Ferreira Alves Moreira

Mestrado Integrado em Ciências Farmacêuticas, 2006 – 2011

Faculdade de Farmácia, Universidade de Lisboa, Portugal

Thesis Title: Multidrug resistance regulation in cancer cells

Supervisors: Prof. Doutor Maria Alexandra da Silva Paulo;

Publications and Communications

Part of the original work presented in this thesis has been already published or communicated.

Papers in international scientific periodicals with referees

1. **Sofia A. Santos**, Amanda K. Lukens, Margarida Ruivo, Dyann F. Wirth, Maria Mota, Rui Moreira, Alexandra Paulo, Ralph Mazitschek, Plasmodium t-RNA Synthetases as Next Generation Druggable Targets for Malaria Elimination (In preparation)
2. **Sofia A. Santos**, Amanda K. Lukens, Lis Coelho, Fátima Nogueira, Dyann F. Wirth, Ralph Mazitschek, Rui Moreira, Alexandra Paulo. Exploring the 3-piperidin-4-yl-1H-indole scaffold as a novel antimalarial chemotype. *Eur J Med Chem.* 2015, 102:320-333
3. Jonathan D. Herman, Lauren R. Pepper, Joseph F. Cortese, Guillermina Estiu, Kevin Galinsky, Vanessa Zuzarte-Luis, Emily R. Derbyshire, Ulf Ribacke, Amanda K. Lukens, **Sofia A. Santos**, Vishal Patel, Clary B. Clish, William J. Sullivan Jr., Huihao Zhou, Selina E. Bopp, Paul Schimmel, Susan Lindquist, Jon Clardy, Maria M. Mota, Tracy L. Keller, Malcolm Whitman, Olaf Wiest, Dyann F. Wirth, Ralph Mazitschek. The cytoplasmic prolyl-tRNA synthetase of the malaria parasite is a dual-stage target of febrifugine and its analogs. *Sci Transl Med.* 2015, 7(288): 288ra77
4. Marta Figueiras, Lis Coelho, Kathryn J. Wicht, **Sofia A. Santos**, João Lavrado, Jiri Gut, Philip J. Rosenthal, Fátima Nogueira, Timothy J. Egan, Rui Moreira, Alexandra Paulo. N10,N11-di-alkylamine indolo[3,2-b]quinolines as hemozoin inhibitors: design, synthesis and antiplasmodial activity. *Bioorg Med Chem.* 2015, 23(7): 1530-9
5. Alexandra M. Courtis, **Sofia A. Santos**, Yinghua Guan, J. Adam Hendricks, Balaram Ghosh, D. Miklos Szantai-Kis, Surya A. Reis, Jagesh V. Shah, and Ralph Mazitschek. Monoalkoxy BODIPYs-A Fluorophore Class for Bioimaging. *Bioconjug Chem.* 2014, 25(6): 1043-1051
6. Alexandra Paulo, Marta Figueiras, Marta Machado, Catarina Charneira, João Lavrado, **Sofia A. Santos**, Dinora Lopes, Jiri Gut, Philip J. Rosenthal, Fátima Nogueira, and Rui Moreira. Bis-alkylamine Indolo[3,2-b]quinolines as hemozoin ligands: implications for antimalarial cytostatic and cytotoxic activities. *J Med Chem.* 2014, 57(8): 3295-313

Oral communications in conferences

1. **Sofia A. Santos**, *et al.*, Plasmodium t-RNA Synthetases as Next Generation Druggable Targets for Malaria Elimination; Gordon Research Seminar on High Throughput Chemistry & Chemical Biology; USA 2015
2. **Sofia A. Santos**, Amanda K. Lukens, Dyann F. Wirth, Ralph Mazitschek, Rui Moreira, Alexandra Paulo; Broad SAR Exploration of 3-Piperidin-4-yl-1H-Indole Scaffold: Towards a New Antimalarial Chemotype; 1st Young Medicinal Chemist Symposium; September 2014

Posters in conferences

1. **Sofia A. Santos**, *et al.*, Plasmodium t-RNA Synthetases as Next Generation Druggable Targets for Malaria Elimination; ACS National Meeting - Merck Women in Chemistry Symposium. USA 2015; P48. (Best Poster Award)
2. **Sofia A. Santos**, *et al.*, Plasmodium t-RNA Synthetases as Next Generation Druggable Targets for Malaria Elimination; Gordon Research Conference on High Throughput Chemistry & Chemical Biology; USA 2015; P38
3. **Sofia A. Santos**, Amanda K. Lukens, Dyann F. Wirth, Ralph Mazitschek, Rui Moreira, Alexandra Paulo; Towards a new antimalarial chemotype: Development of Piperidinyl-Indole based inhibitors of Blood Stage Malaria; 10th Annual Broad Scientific Retreat; Boston, USA; November 2014; P112
4. **Sofia A. Santos**, Amanda K. Lukens, Dyann F. Wirth, Ralph Mazitschek, Rui Moreira, Alexandra Paulo; Broad SAR Exploration of 3-Piperidin-4-yl-1H-Indole Scaffold: Towards a New Antimalarial Chemotype; XXIII International Symposium on Medicinal Chemistry; September 2014; P-L004
5. **Sofia A. Santos**, Ralph Mazitschek, Rui Moreira, Alexandra Paulo; Synthesis of an Indole-based Antimalarial Library; 10th National Meeting of Organic Chemistry; Lisbon, Portugal; September 2013; P76
6. **Sofia A. Santos**, Ralph Mazitschek, Rui Moreira, Alexandra Paulo; Development of Novel Indole-based Antimalarials; Gordon Research Conference-High Throughput Chemistry & Chemical Biology; New Hampshire, USA; June 2013

7. **Sofia A. Santos**, Rui Moreira, Alexandra Paulo; Synthesis Optimization of Indole-based Antimalarial Compounds; IV Post-Graduate iMed.UL Students Meeting; Lisbon, Portugal; December 2012

8. **Sofia A. Santos**, Rui Moreira, Alexandra Paulo; Studies towards the synthesis of indole-based antimalarial compounds; 3rd National Meeting of Medicinal Chemistry; Aveiro, Portugal; November 2012; P117

Abstract

Malaria remains a major burden to global public health, causing nearly 600,000 deaths annually. Efforts to control malaria are hampered by parasite drug resistance, insecticide resistance in mosquitoes, and the lack of an effective vaccine. However antimalarial drugs are a mainstay in efforts to control and eventually eradicate this disease, thus the discovery of new antimalarials is critical. Antimalarial drug discovery is especially challenging due to the unique biology of malaria parasites, the scarcity of tools for identifying new drug targets, and the poorly understood mechanisms of action of existing antimalarials. Therefore, this work describes the use of different medicinal chemistry approaches to address unmet needs in antimalarial drug discovery. Part of this process includes ensuring that sufficient drug leads are available to prime the drug discovery pipeline, particularly those with novel modes of action in order to limit issues of cross-resistance with existing drugs.

The first approach described in this thesis consists on the phenotypic-based hit to lead optimization designed to explore the antimalarial potential of the 3-piperidin-4-yl-1*H*-indole. The hit compound was identified in a phenotypic screen of ~2 million compounds against asexual blood stage *P. falciparum*. Three series of analogs were synthesized following a reagent-based diversity approach, in a total of 38 compounds, and screened for their blood stage antimalarial activity. The SAR shows that 3-piperidin-4-yl-1*H*-indole is intolerant to most *N*-piperidinyl modifications. Out of the analogs synthesized, three were active (**2.19**, **2.20** and **2.29**). Furthermore, the (4-(1*H*-indol-3-yl)piperidin-1-yl)(pyridin-3-yl)methanone (**2.29**) showed *in vitro* antimalarial activity (EC₅₀ values ~3 μM), no cross-resistance with chloroquine, selectivity for the parasite, and lead-like properties (cLogP < 3; MW ~ 300). This represents a promising new antimalarial chemotype with a potential novel mechanism of action. Further medicinal chemistry efforts are needed to improve the potency of compound **2.29** and disclose its antimalarial mechanism of action.

In the second part of this work we focus on exploring the potential of aminoacyl tRNA synthetases (aaRS) as a novel class of antimalarial targets. We hypothesize that the inhibition of some but not all, *P. falciparum* aaRSs will result in activation of amino acid response pathways and that inhibition of this subgroup represents an attractive approach for chemotherapeutic

intervention in malaria. First, a library of 21 aminoacyl-sulfamoyl adenosine (aaSA) analogs was synthesized and used as tool compounds to profile 19 of the *Pf*aaRSs as drug targets. Among the analogs tested, L-PheSA, L-HisSA, L-AlaSA and L-ProSA were the compounds that exhibited higher antimalarial activity (EC_{50} against the Dd2 strain < 120 nM) and selectivity index (> 20). These results allow the prioritization of the phenylalanyl tRNA synthetase (FRS), histidyl tRNA synthetase (HRS), alanyl tRNA synthetase (ARS), and prolyl tRNA synthetase (PRS) as the top four enzymes for further exploration as drug targets in blood stage malaria. aaSA compound treatment of *P. falciparum* increased eIF2 α phosphorylation at 100X concentration, inducing the amino acid starvation pathway through direct inhibition of the corresponding *Pf*aaRS, with few exceptions. Moreover, analogs were also active *in vitro* against liver stage *P. berghei*, with $> 99\%$ parasite growth inhibition at the higher concentration of 10 μ M. Thus, underscoring the potential of the aaRS family as an attractive novel class of antimalarial drug targets.

To further explore cytoplasmic prolyl tRNA synthetase (cPRS) as an antimalarial target, which we have previously identified as the long sought biochemical target of the antimalarial halofuginone (HFG), novel HFG based inhibitors were designed to exploit additional ligand-protein interactions in the active site of cPRS, and may serve as lead compounds in the preclinical development of a mechanistically unique class of malaria drugs with activity against both liver and blood stage life cycle stages. Furthermore, we aimed to characterize the biology of cPRS inhibition and resulting amino acid starvation response. Understanding the enzyme-inhibitor complex formed by the different types of inhibitors (HFG and L-ProSA) would further elucidate on the differential effect observed on the amino acid starvation response in mammalian cells, despite targeting the same enzyme. Thus, a two-step proteomic approach to isolate the protein complex using immunoprecipitation followed by identification of its components using mass spectrometry is proposed. Despite not being able to completely establish the protocol, the results in MCF-7 cells are consistent with the model proposed, thus further work needs to be done towards increasing the amount of the enzyme-inhibitor complex isolated to meet the detection requirements of the techniques used.

Finally, to address the problem of limited target identification and validation tools for novel antimalarial compounds, the third aim of this thesis investigates the use of fluorescently labeled small molecules as a novel target discovery approach in malaria drug discovery efforts. A new methodology, which originated from our efforts to synthesize MayaFluors in a one-pot,

two-step approach via BODIPY-OTf intermediate, was developed to label drugs with the BODIPY fluorophore. The method allows for substitution of either one or both of the canonical fluorides on the BODIPY dye with alkoxy ligands, under mild conditions. We successfully labeled a group of small molecules. Of these, two known drugs ((+) JQ1 and hydroxychloroquine) were evaluated for their activity and cellular localization. In both cases the labeled drug presented comparable activity to the parent drug. Furthermore, the fluorescently labeled antimalarial displayed a subcellular staining pattern in mammalian cells that is consistent with accumulation in acidic vesicles in the cytoplasm. Moreover, the probe was also tested in *Plasmodium falciparum* cultures, where results show subcellular staining pattern that seems consistent with accumulation in the food vacuole. Despite the identified limitation concerning the solvent compatibility of the method, this approach allows direct labeling of hydroxyl-functionalized drugs, which we believe may have broad applications for rapid and specific imaging of elusive biological targets in living cells.

Taken together, in this thesis multiple medicinal chemistry approaches are explored in an effort to identify novel antimalarial chemotypes that act on underexploited targets. Furthermore, these results present new opportunities for malaria drug discovery to aid efforts in malaria control and eventual eradication.

Keywords: malaria, drug discovery, target identification, phenotypic screen, aminoacyl tRNA synthetases, fluorescent probes.

A malária continua a ser uma das doenças infecciosas com maior impacto, causando mais de 600.000 mortes por ano em todo o mundo, e afetando principalmente mulheres e crianças. Esta doença constitui um grave problema de saúde, com enormes consequências sociais e económicas que afetam principalmente os países onde a malária ainda é endémica. Este problema tem vindo a crescer devido ao agravamento do aparecimento de parasitas resistentes aos fármacos antimaláricos em uso clínico. Parasitas do género *Plasmodium*, responsáveis por esta doença, adaptam-se rapidamente, como é demonstrado pelos relatos de resistência a quase todos os fármacos antimaláricos. A Organização Mundial de Saúde recomenda atualmente o uso de terapias combinadas baseadas em artemisininas (“Artemisinin-based Combination Therapies” – ACTs) como primeira linha no combate à malária. Apesar da importância geral desta doença, o desenvolvimento de novos fármacos foi negligenciado pela indústria farmacêutica nos países desenvolvidos durante algum tempo. Porém, nos últimos anos o esforço para desenvolver novos fármacos tem vindo a aumentar, sendo que várias parcerias entre a indústria e a academia têm sido formadas num esforço global de erradicar a malária. Os esforços para controlar a malária têm sido dificultados pela resistência do parasita aos fármacos, a resistência dos mosquitos aos inseticidas e a falta de uma vacina eficaz. No entanto, os fármacos antimaláricos são um pilar nos esforços para controlar e, eventualmente, erradicar esta doença. Assim, a descoberta de novos antimaláricos é crítica. A descoberta de novos fármacos antimaláricos é especialmente difícil devido à escassez de ferramentas para a identificação de novos alvos terapêuticos e à pouca compreensão dos mecanismos de ação dos atuais antimaláricos.

Portanto, este trabalho descreve o uso de diferentes abordagens em química medicinal ao desenvolvimento de novos fármacos para o tratamento da malária. Uma parte importante do processo de desenvolvimento de novos fármacos inclui a garantia de que existe quantidade suficiente de novas moléculas a entrar no processo de desenvolvimento, particularmente potenciais fármacos com novos alvos terapêuticos, de forma a limitar os problemas de resistência cruzada com os fármacos em uso clínico.

A primeira abordagem descrita nesta tese consiste na otimização de um composto identificado num ensaio de rastreio, através de uma estratégia que visa explorar o potencial antimalárico do esqueleto 3-piperidin-4-il-1*H*-indol. O composto inicial foi identificado num

ensaio fenotípico, usando a fase assexuada intra-eritrocítica do *P. falciparum*, que incluiu um conjunto de cerca de 2 milhões de compostos. Foram sintetizadas três séries de análogos seguindo uma estratégia de diversificação estrutural baseada nos reagentes de síntese. Obtiveram-se 38 compostos que foram avaliados *in vitro* quanto à sua atividade contra a forma intra-eritrocítica do parasita. O estudo da relação estrutura-atividade mostra que o esqueleto 3-piperidin-4-il-1*H*-indol é intolerante à maior parte das modificações no grupo *N*-piperidinil. Dos 38 derivados sintetizados, três apresentaram atividade antimalárica contra a fase sanguínea do parasita (**2.19**, **2.20** e **2.29**). Para além disso, o composto (4- (1*H*-indol-3-il) piperidin-1-il) (piridin-3-il) metanona (**2.29**) demonstrou: atividade antimalária *in vitro* ($EC_{50} \sim 3 \mu\text{M}$); não apresentar resistência cruzada com a cloroquina; seletividade para o parasita; e propriedades adequadas a uma molécula protótipo ($c\text{LogP} < 3$; peso molecular ~ 300). Esta molécula representa um potencial novo farmacóforo antimalárico, com possivelmente um novo mecanismo de ação. No entanto, são necessários esforços adicionais visando melhorar a atividade do composto e identificar o seu alvo terapêutico.

Na segunda parte deste trabalho concentramo-nos em explorar o potencial das aminoacil-tRNA sintetases (aaRS) como uma nova classe de alvos terapêuticos para a malária. Esta classe de enzimas é responsável por catalisar a reação de esterificação entre o RNA transferência e o respetivo aminoácido, de forma a formar o complexo aminoacil-tRNA no processo de síntese proteica. Nós propomos que a inibição de algumas destas enzimas no *P. falciparum* resultará na ativação de vias de resposta aos níveis deficitários de aminoácidos (“aminoacid starvation response”) e que a inibição deste subgrupo representa uma abordagem atrativa para a intervenção quimioterapêutica na malária.

Em primeiro lugar, uma biblioteca de 21 aminoacil-sulfamoil adenosina (aaSA), análogos do intermediário de reação, foram sintetizados e usados como ferramentas para a caracterização do perfil de 19 das *Pf*aaRSs como alvos terapêuticos. Entre os análogos testados, o L-PheSA, o L-HisSA, o L-AlaSA e o L-ProSA foram os análogos que exibiram melhor atividade antimalárica (EC_{50} contra a estirpe resistente Dd2 $< 120 \text{ nM}$) e maior índice de seletividade (> 20). Estes resultados permitem a priorização da fenilalanil tRNA sintetase (FRS), histidil tRNA sintetase (HRS), alanil tRNA sintetase (ARS), e prolil tRNA sintetase (PRS) como as quatro enzimas com maior potencial para o desenvolvimento adicional como alvos terapêuticos na malária. O tratamento dos parasitas com os compostos aaSAs em concentrações 100x o EC_{50} ,

resultaram geralmente no aumento da fosforilação da eIF2 α , um marcador da indução da via de resposta aos níveis deficitários de aminoácidos, através da inibição direta das enzimas PfaaRSs correspondentes. Os compostos sintetizados foram também testados contra a fase hepática do parasita, num ensaio *in vitro* usando o modelo do *P. berghei*. Os compostos mostraram capacidade de inibição de crescimento do parasita (> 99%) na concentração mais elevada (10 μ M). Estes resultados demonstram o potencial da família de aaRSs como uma atraente nova classe de alvos terapêuticos para o desenvolvimento de novos antimaláricos. De forma a explorar em mais detalhe a enzima prolil tRNA sintetase citoplasmática (cPRS) como alvo antimalárico, anteriormente identificada pelo nosso grupo como o alvo bioquímico do composto antimalárico halofuginona (HFG), foram desenhados inibidores híbridos de HFG para explorar novas interações entre o ligando e a proteína, no centro ativo da enzima prolil tRNA sintetase citoplasmática, e podem servir como ponto de partida para o desenvolvimento pré-clínico de uma classe mecanisticamente única de fármacos para a malária, ou seja, fármacos com dupla atividade, atingindo não só a fase intra-eritrocítica mas também a fase hepática do parasita. Este estudo, teve também como objetivo caracterizar a biologia da inibição cPRS e consequente indução da via de resposta aos níveis deficitários de aminoácidos. O estabelecimento da composição do complexo enzima-inibidor formado pelos diferentes tipos de inibidores (HFG e L-ProSA), permite elucidar o mecanismo subjacente ao efeito da indução de fosforilação da proteína eIF2 α , observado em resposta à inibição da cPRS em células de mamíferos. Desta forma, é proposto uma abordagem proteómica que consiste em dois passos. Primeiro, o isolamento do complexo formado pela enzima, utilizando a técnica de imunoprecipitação, e segundo, a identificação dos componentes deste complexo utilizando a espectrometria de massa. Apesar de não ter sido possível estabelecer completamente o protocolo, os resultados preliminares em células MCF-7 estão de acordo com o modelo proposto. No entanto, é necessário otimizar a quantidade do complexo enzima-inibidor isolado para satisfazer os limites de deteção das técnicas aplicadas.

No capítulo quatro, abordamos o problema da limitação de ferramentas disponíveis para a identificação e validação dos alvos terapêuticos dos antimaláricos em desenvolvimento. Desta forma, numa terceira abordagem, é explorado o uso de fármacos marcados com fluoróforos. Partindo da síntese dos compostos fluorescentes designados de MayaFluors, foi desenvolvida uma nova metodologia. A síntese inicial consiste em duas reações sequenciais, num só passo,

através do intermediário BODIPY-OTf. O novo método sintético foi desenvolvido para ligar o fármaco ao fluoróforo BODIPY, permitindo a observação da localização celular do fármaco. O método permite a substituição de um ou de ambos os átomos de fluor na estrutura do BODIPY, por ligandos com um grupo alcóxido, sob condições suaves. Este método foi utilizado com sucesso para ligar o BODIPY a um pequeno grupo de fármacos. Destes, dois são fármacos conhecidos ((+) JQ1 e hidroxicloroquina) e foram avaliados quanto à sua atividade e localização celular. Em ambos os casos, o fármaco marcado com o fluoróforo apresentou atividade comparável à do fármaco original. Além disso, o antimalárico marcado apresentou um padrão de localização subcelular, em células de mamífero, que é consistente com a acumulação em vesículas ácidas no citoplasma e em culturas de *Plasmodium falciparum*, os resultados mostram um padrão de localização subcelular consistente com uma acumulação da sonda no vacúolo digestivo do parasita, conforme esperado. Apesar da limitação identificada quanto à compatibilidade de solventes, este método representa uma abordagem inovadora que permite a ligação direta de moléculas funcionalizadas com grupos hidroxilo, e que acreditamos poder ter amplas aplicações na obtenção de imagens rápidas e específicas de alvos terapêuticos em células.

Em conclusão, esta tese explora múltiplas abordagens de química medicinal para identificação de novos compostos antimaláricos que atuem potencialmente em alvos terapêuticos subexplorados, contribuindo assim para os esforços globais de combate à malária. Analisando o conjunto de resultados obtidos no decorrer desta tese, pode-se considerar que são apresentadas oportunidades inovadoras para o desenvolvimento de novos fármacos com atividade antimalárica.

Palavras Chave: Malaria, descoberta de Fármacos, Identificação de Alvos Terapêuticos, Ensaios Fenotípicos, aminoacil-tRNA sintetase, sondas fluorescentes.

Table of Contents

Copyright Statement	i
Statement.....	iii
Acknowledgments.....	v
Autobiography	vii
Publications and Communications.....	ix
Abstract	xiii
Resumo	xvii
Table of Contents.....	xxi
Table of Figures	xxv
List of Tables	xxix
Table of Schemes.....	xxxii
List of Abbreviations	xxxiii
Amino acid Nomenclature.....	xxxix
Scope of this Thesis	xli
1. INTRODUCTION.....	3
1.1 MALARIA	3
1.2 MALARIA CHEMOTHERAPEUTICS	7
1.2.1 Quinoline-containing Drugs.....	8
1.2.2 Artemisinins	14
1.2.3 Cytochrome <i>bc</i> ₁ Inhibitors	16
1.3 DRUG DISCOVERY STRATEGIES.....	18
1.3.1 Virtual Screening	19
1.3.2 Chemical Screening.....	19
1.3.2.1 Sources of Chemical Libraries	20
1.3.2.1.1 Clinical Approved Drugs.....	20
1.3.2.1.2 Diversity Oriented Synthesis (DOS)	20
1.3.2.1.3 Natural Products.....	20
1.3.2.2 Drug Discovery Screen.....	21
1.3.2.2.1 Target-based Screen.....	22
1.3.2.2.2 Phenotypic Screen.....	22
1.3.3 Rational Chemistry-based Approaches.....	23
1.3.3.1 Hit to Lead Optimization.....	23
1.3.3.2 Hybrid Molecules	24
1.3.3.3 Modification of Existing Antimalarials.....	25
1.4 NEW DRUG CANDIDATES	26

1.4.1	<i>Quinolones</i>	28
1.4.2	<i>Pyrimethamines</i>	29
1.4.3	<i>Ozonides</i>	29
1.4.4	<i>Spiroindolones</i>	31
1.4.5	<i>Imidazolopiperazines</i>	32
1.4.6	<i>Others Drug Candidates</i>	33
1.5	TARGET IDENTIFICATION AND VALIDATION	35
1.5.1	<i>Target Identification</i>	35
1.5.1.1	<i>In silico</i> Assignment of Mechanism of Action	35
1.5.1.2	Stage of Action	36
1.5.1.3	<i>In vitro</i> Evolution of Drug-resistant <i>P. falciparum</i> Strains	36
1.5.2	<i>Target Validation</i>	38
1.5.2.1	Bioassays.....	38
1.5.2.2	'-omics' Techniques.....	39
1.5.2.3	Fluorescent Probes.....	40
2.	INDOLE-BASED ANTIMALARIALS	45
2.1	INTRODUCTION	45
2.2	PURPOSE OF THIS STUDY	46
2.3	SYNTHETIC METHODOLOGY	47
2.3.1	<i>Chemical Synthesis Strategy</i>	47
2.3.2	<i>Synthesis of Hit Compound</i>	49
2.3.3	<i>Synthesis of Amine Library</i>	51
2.3.4	<i>Synthesis of Amide Library</i>	52
2.3.5	<i>Synthesis of Bis-amide Library</i>	55
2.4	ANTIMALARIAL AND CYTOTOXICITY ACTIVITIES.....	56
2.5	DISCUSSION OF STRUCTURE ACTIVITY RELATIONSHIPS AND CONCLUSION	59
3.	AMINOACYL-TRNA SYNTHETASE INHIBITORS AS ANTIMALARIALS	65
3.1	INTRODUCTION	65
3.1.1	<i>Aminoacyl-tRNA Synthetases as Drug Targets</i>	65
3.1.2	<i>Classes of Aminoacyl-tRNA Synthetases</i>	67
3.1.3	<i>Quality Control of Aminoacyl-tRNA Synthetases</i>	68
3.1.4	<i>Noncanonical Functions of Aminoacyl-tRNA Synthetases</i>	69
3.1.5	<i>Aminoacyl-tRNA Synthetases in Plasmodium</i>	72
3.1.6	<i>Aminoacyl-tRNA Synthetase Inhibitors</i>	73
3.2	PURPOSE OF THIS STUDY	83
3.3	EXPLORE TRNA SYNTHETASES AS NOVEL TARGETS IN <i>P. FALCIPARUM</i>	86
3.3.1	<i>Synthetic Methodology</i>	87
3.3.1.1	Chemical Synthesis Strategy	87
3.3.1.2	Synthesis of aa-AMP Analogs	87
3.3.2	<i>Antimalarial and Cytotoxic Activities</i>	92
3.3.3	<i>Amino Acid Starvation Pathway Activation</i>	99
3.4	DEVELOP HYBRID-HALOFUGINONE DERIVATIVES WITH HIGH PARASITE SPECIFICITY.....	102
3.4.1	<i>Chemical Synthesis Strategy</i>	104

3.4.2	<i>Synthesis of Halofuginone Hybrid Analogs</i>	105
3.5	CHARACTERIZE THE BIOLOGY OF CPRS INHIBITION AND AMINO ACID STARVATION RESPONSE.....	110
3.5.1	<i>Methodological Approach</i>	112
3.5.2	<i>Studies in Yeast Cultures</i>	113
3.5.3	<i>Studies in Mammalian Cells</i>	119
3.5.4	<i>Discussion and Conclusion</i>	125
4.	FLUORESCENT PROBES FOR TARGET DISCOVERY	131
4.1	INTRODUCTION	131
4.1.1	<i>Fluorescent Probes</i>	131
4.1.2	<i>Indolo[3,2-b]quinoline Antimalarial Scaffold</i>	138
4.2	PURPOSE OF THIS STUDY.....	141
4.3	SYNTHETIC METHODOLOGY	142
4.3.1	<i>Chemical Synthesis Strategy</i>	142
4.3.2	<i>Synthesis of Alkoxy BODIPYs</i>	143
4.3.3	<i>Synthesis of Small Molecule Probes</i>	156
4.3.4	<i>Synthesis of Indolo[3,2-b]quinoline Probe</i>	157
4.4	IN VITRO PROFILING OF LABELED SMALL MOLECULES	159
4.4.1	<i>In Mammalian Cell Cultures</i>	159
4.4.2	<i>In Plasmodium falciparum Intraerythrocytic Cultures</i>	161
4.5	CONCLUSION.....	163
5.	GENERAL CONCLUSIONS AND FUTURE PERSPECTIVES	169
6.	MATERIALS AND METHODS	177
6.1	CHEMISTRY.....	177
6.1.1	<i>General</i>	177
6.1.2	<i>Synthesis of 3-piperidin-4-yl-1H-indole Derivatives</i>	178
6.1.3	<i>Synthesis of Sulfamoyl Aminoacyl AMP Analogs</i>	204
6.1.4	<i>Synthesis of HFG-hybrid Analogs</i>	221
6.1.5	<i>Synthesis of Fluorescent Probes</i>	232
6.1.5.1	<i>Synthesis of CMA-BODIPYs</i>	232
6.1.5.2	<i>Synthesis of HaloTag functionalized CMA-BODIPY</i>	233
6.1.5.3	<i>Synthesis of Monoalkoxy BODIPYs</i>	236
6.1.5.4	<i>Synthesis of Dialkoxy BODIPYs</i>	239
6.1.5.5	<i>Synthesis of Small Molecule Probes</i>	242
6.2	PHYSICO-CHEMICAL CHARACTERIZATION OF BODIPYS	247
6.2.1	<i>Solubility Test</i>	247
6.2.2	<i>LogD Determination</i>	247
6.3	BIOLOGICAL METHODS.....	248
6.3.1	<i>Plasmodium falciparum Blood Stage in vitro Drug Sensitivity Assay</i>	248
6.3.2	<i>Plasmodium berghei Liver Stage in vitro Drug Sensitivity Assay</i>	248
6.3.3	<i>Plasmodium falciparum Whole Cell Lysate Western Blot</i>	248
6.3.4	<i>Yeast Growth Assays</i>	249
6.3.5	<i>Yeast Western Blots</i>	249

6.3.6	<i>MCF-7 Cell Culture</i>	250
6.3.7	<i>Cytotoxicity Assay</i>	250
6.3.7.1	MCF-7	250
6.3.7.2	HepG2.....	250
6.3.8	<i>MCF-7 Western Blots</i>	251
6.3.9	<i>BRD4 in vitro EC₅₀ Determination</i>	251
6.3.10	<i>Pull-down Assays</i>	252
6.3.10.1	Dynabeads® His-Tag.....	252
6.3.10.2	His-Tag (27E8) Mouse mAb Magnetic Bead Conjugate	252
6.3.10.3	Dynabeads® Protein A	252
6.3.11	<i>Cell Imaging</i>	253
REFERENCES		257
APPENDICES		289
	CHEMICAL STRUCTURES	289

Table of Figures

Figure 1.1 – Estimated incidence of malaria per 1000 population, map from 2014 WHO Malaria Report. ¹	3
Figure 1.2 – The <i>Plasmodium</i> life cycle. ²¹	5
Figure 1.3 – Quinoline alkaloid and the first synthetic antimalarial drug	7
Figure 1.4 – Antimalarial drugs (antifolates, artemisinins, quinoline-containing drugs).....	8
Figure 1.5 – Schematic representation of the hemoglobin degradation mechanism in the food vacuole of <i>Plasmodium</i>	9
Figure 1.6 – Pharmacophore of the antimalarial 4-aminoquinoline chloroquine. Adapted from Egan <i>et al.</i> ⁷¹	11
Figure 1.7 – Artemisinin and its proposed active species.....	15
Figure 1.8 – Chemical structures of atovaquone (1.12) and proguanil (1.13), the active molecules in Malarone®.....	17
Figure 1.9 – Binding mode of atovaquone into bc1 complex Qo site.	17
Figure 1.10 – Structure of some experimental antimalarial molecules.....	26
Figure 1.11 – Progression of the clinical development of new antimalarial candidates over the past 5 years. Adapted from Wells <i>et al.</i> ⁷⁹	27
Figure 1.12 – Design of ELQ-300 (1.21) based on the structure of endochin (1.24) and GW844520 (1.25)..	28
Figure 1.13 – P218 : Pyrimethamine to Drug Candidate	29
Figure 1.14 – OZ439: Hit to Drug Candidate.....	30
Figure 1.15 – NITD609: Hit to Drug Candidate.....	31
Figure 1.16 – NITD609: Hit to Drug Candidate.....	32
Figure 1.17 – MMV390048: Hit to Drug Candidate.....	33
Figure 1.18 – DSM265: Hit to Drug Candidate.....	34
Figure 2.1 – Structure of the hit compound TCMDC-134281.....	46
Figure 2.2 – Structures of the explored indole-based scaffold.....	47
Figure 2.3 – Retrosynthetic analysis of compounds from the amine, amide and bis-amide series.....	48
Figure 2.4 – Assignment of ¹ H and ¹³ C NMR of key intermediate 2.3	50
Figure 2.5 – Assignment of ¹ H NMR of hit compound 2.1	51
Figure 2.6 – Assignment of ¹ H and ¹³ C NMR of amine compound 2.11	52
Figure 2.7 – Assignment of ¹ H and ¹³ C NMR of amine compound 2.29	54
Figure 2.8 – Assignment of ¹ H and ¹³ C NMR of amine compound 2.43	56
Figure 3.1 – Protein translation.....	65
Figure 3.2 – Classes of aminoacyl tRNA synthetases. ²⁵³	67
Figure 3.3 – Pre-transfer and post-transfer editing of non-cognate amino acids by aaRS.....	69
Figure 3.4 – Canonical and non-canonical functions of aaRSs.....	70
Figure 3.5 – Phosphorylation of eIF2 α by inhibition of aminoacyl-tRNA synthetases (aaRS).	72

Figure 3.6 – Aminoacyl-tRNA synthetase inhibitors.	75
Figure 3.7 – Proposed epimerization mechanism for halofuginone.	78
Figure 3.8 – Sulfamoyl aminoacyl-AMP analogs.....	84
Figure 3.9 – Molecular dynamics simulations of the ternary complex of <i>Pf</i> PRS with ATP and halofuginone. Image adapted from Herman <i>et al.</i> ⁷	85
Figure 3.10 – a) aaRSs sites: active site, editing site and anticodon binding site; b) PRS transition state and enzyme-complex formed with two different inhibitors (ProSA and HFG).	86
Figure 3.11 – General retrosynthetic scheme of aminoacyl-sulfamoyl-AMP analogs.	87
Figure 3.12 – Assignment of ¹ H and ¹³ C NMR of compounds 3.17 and 3.54	92
Figure 3.13 – Molecular docking of the complex of PRS with ProSA.	96
Figure 3.14 – <i>In vitro</i> <i>P. berghei</i> growth (%) and HepG2 A16 human hepatic cell line viability (%) at 10 μM and 1 μM of drug treatments.....	98
Figure 3.15 – Immunohistochemical detection of eIF2α phosphorylation.	101
Figure 3.16 – (A) Hybrid-analog design; (B) Overlay of ATP-halofuginone complex (green) with hybrid structure (gray) using an acetamide linker.....	103
Figure 3.17 – Hybrid-halofuginone derivatives designed.....	104
Figure 3.18 – General retrosynthetic scheme of hybrid-halofuginone derivatives.	105
Figure 3.19 – Aminoacylation of PRS.....	111
Figure 3.20 – Affinity purification with Dynabeads®.	113
Figure 3.21 – A heterologous yeast model.....	114
Figure 3.22 – Western blot analysis of <i>Pfc</i> PRS after treatment with 10 μM halofuginone, 10 μM ProSA or with corresponding volume of DMSO.	117
Figure 3.23 – Western blot analysis of <i>Pfc</i> PRS following pull-down experiments using three different bead elution buffers.....	118
Figure 3.24 – Western blot analysis of EPRS following native lysis of MCF7 cell line.....	120
Figure 3.25 – Differential induction of eIF2α phosphorylation in MCF-7 cells.	120
Figure 3.26 – Yeast tRNA calibration curve on SDS-PAGE using SYBR® Gold stain as detection method.....	121
Figure 3.27 – Western blot analysis of EPRS following co-immunoprecipitation.	122
Figure 3.28 – MCF-7 cells treatment with 10 μM ProSA or a corresponding volume of DMSO.....	124
Figure 4.1 – Jablonski Diagram ³⁸⁵	132
Figure 4.2 – Plot of fluorophore brightness for the major classes of fluorophores.	134
Figure 4.3 – Structures of BODIPY dyes.....	136
Figure 4.4 – Indoloquinolines from <i>Cryptolepis sanguinolenta</i>	139
Figure 4.5 – Structure of target bioisosteres <i>N</i> 10, <i>N</i> 11-di-alkylamine indolo[3,2- <i>b</i>]quinoline derivatives.	140
Figure 4.6 – Structures of alkoxy-drug and alkoxy-ligand BODIPY dyes accessed by the new synthetic methodology.	142
Figure 4.7 – Retrosynthetic analysis of the alkoxy BODIPY labeled drug.....	143

Figure 4.8 – Structure of 3,7-dichloro- <i>N</i> 10-ethylpyrrolidine parent compound and designed fluorescent probe.....	157
Figure 4.9 – Cellular uptake and intracellular distribution of compound 4.39 (a) and compound 4.37 (b) in MCF-7 cells.....	160
Figure 4.10 – Half-maximal inhibitory concentration (EC ₅₀) of (+) JQ1 and (+) JQ1-CMA-BODIPY 4.39 determined against purified BRD4 protein.....	161
Figure 4.11 – Cellular uptake and intracellular distribution of compound 4.37 in Plasmodium falciparum Dd2 strain.....	162
Figure 5.1 – Outline of the diverse medicinal chemistry approaches used in this work.....	170

List of Tables

Table 2.1 – Optimization of coupling conditions between intermediate 2.3 and carboxylic acids. -----	53
Table 2.2 – Final step yield of synthesized compounds, their drug-like properties (MW, cLogP and compliance with “Lipinski’s Rule of 5”) and results from antimalarial activity screening. -----	57
Table 2.3 – <i>In vitro</i> antimalarial activity (EC ₅₀) and cytotoxicity (EC ₅₀) of selected compounds. -----	59
Table 3.1 – Optimization of the sulfamoylation of 2', 3'-O-isopropylideneadenosine. -----	89
Table 3.2 – Yield of synthesized compounds. -----	90
Table 3.3 – <i>In vitro</i> antimalarial activity (EC ₅₀) and cytotoxicity (EC ₅₀) of aaSA compounds. -----	94
Table 3.4 – Optimization of SmI ₂ -mediated reductive cross-coupling reaction. -----	107
Table 3.5 – Optimization of yeast lysis. -----	115
Table 4.1 – Physico-chemical Characterization of BODIPYs ⁴ -----	146
Table 4.2 – Optimization of CMA-BODIPY synthesis. -----	148
Table 4.3 – Optimization of benzyl-alkoxy BODIPY synthesis. Compound structure for 4.25 and 4.30 in scheme 4.3. -----	150
Table 4.4 – Optimization of catalyst amount for new methodology. Reaction conditions: toluene, 60 °C. -----	151
Table 4.5 – Optimized solvents for the new methodology. Reaction conditions: 50 mg of molecular sieves/ mg of fluorophore (catalyst), 60 °C. -----	153
Table 6.1 – Final step and global yield of synthesized compounds. -----	202

Table of Schemes

Scheme 2.1 – Reagents and conditions: a) KOH, isopropanol, reflux, 6 h, 98%; b) 10% Pd/C, 10% glacial acetic acid in ethyl acetate, H ₂ , 48 h, r.t., 96%; c) DCC, HOBT, CH ₃ CN, 2 h, r.t., 60%; d) DIBAL, THF, 1 h, -78 °C, 35%; e) 2 M HCl/MeOH, 20 min, r.t., 99%; f) DIPEA, isopropanol, 56 h, reflux, 15%. -----	49
Scheme 2.2 – R fragments and yields are given in Table 2.2; Reagents and conditions: a) NaBH(OAc) ₃ , DCE, 1 h, r.t., 58%-70%; b) NaBH(OAc) ₃ , DCE, 4 h, r.t. or NaBH ₃ CN, MeOH, Microwave at 100 °C, 20 min; c) DIPEA, isopropanol, 56 h, reflux, 25%; d) DCM, aq. NaHCO ₃ , 10 min, r.t. or DIPEA, DCM, 30 min, r.t. or PyBOP, DIPEA, DCM, 0.5-1 h, r.t. -----	53
Scheme 2.3 – R fragments and yields are listed in Table 1 ; Reagents and conditions: a) 2 M HCl/MeOH, 40 min, r.t., quantitative yield; b) DCM, aq. NaHCO ₃ , 10 min, r.t. -----	55
Scheme 3.1 – Mechanism of aminoacylation by aminoacyl-tRNA synthetases. ²⁴⁷ -----	66
Scheme 3.2 – Synthesis of sulfamoylated aa-AMP analogs. Reagents and conditions: a) NaH, DME, 0 °C → r.t., 4 h, 65%; b) DBU, DMF, r.t., 4 h; c) TFA/H ₂ O (5:1), r.t., 30 min; d) 10% Pd/C, 0%-1% glacial acetic acid, DMF, H ₂ , 2-8 h, r.t. -----	88
Scheme 3.3 – Synthesis of the β-amido alcohol. Reagents and conditions: a) DMSO, (COCl) ₂ , Et ₃ N, DCM, -60 °C, 3 h, 67%; b) (<i>S</i>)- <i>tert</i> -Butanesulfinamide, anhydrous CuSO ₄ , DCM, r.t., 12 h, 59%; c) TBDPSCl, imidazole, DMAP, DCM, r.t., 12 h, 50%; d) SmI ₂ , <i>t</i> -BuOH, THF, -78 °C, 58%. -----	106
Scheme 3.4 – Synthesis of the <i>N</i> -sulfonyl piperidine. Reagents and conditions: a) RBr, NaHMDS, THF, -20 °C, 16 h; b) MCPBA, DCM, r.t., 3 h; c) HF/Pyridine, THF, r.t., 16 h; d) MsCl, DIPEA, DCM, -78 °C, 3 h; e) NaHMDS, THF, -20 °C, 16 h. -----	108
Scheme 3.5 – Synthesis of the piperidine epoxide. Reagents and conditions: a) PPTS, MeOH, 60 °C, 16 h; b) TsCl, Bu ₂ SnO, Et ₃ N DCM, r.t., 3 h; c) DBU, DMC, r.t., 16 h; -----	108
Scheme 3.6 – Synthesis of the piperidine epoxide. Reagents and conditions: a) KH, 4-quinazolone, DMF, 80 °C, 72 h; b) 6 M HCl/MeOH, r.t., 3 h; c) Boc ₂ O, DIPEA, r.t., 5 h; d) 1 M LiOH, 60 °C, 5 h. -----	109
Scheme 4.1 – Synthesis of CMA-BODIPYs. a) One-pot synthesis of CMA-BODIPY analogs 4.15-4.16 . Reagents: a) TCM, TMSOTf, 0 °C, 150 s; b) TCM, R'OH, 0 °C, 150 s; b) Synthesis of CMA-BODIPY 4.19 . -----	144
Scheme 4.2 – Synthesis of HaloTag functionalized CMA-BODIPY. Reagents and conditions: a) Boc ₂ O, EtOH, r.t., 4 h, 98%; b) NaH, THF:DMF (2:1), r.t., 3 h, 38%; c) 2 M HCl, MeOH, r.t., 2 h, 78%; d) DIPEA, DCM, r.t., 30 min, 37%; e) Ethylene glycol, TMSOTf, DIPEA, TCM, r.t., 2:30 min, 60%. -----	145
Scheme 4.3 – Synthesis of mono- and dialkoxy BODIPY analogs. Reagents and conditions: a) Molecular sieves, Toluene or THF, 60 °C, 24 h; b) Molecular sieves, Toluene, 60 °C, 3 h. Isolated yield after purification is given in parentheses. -----	154
Scheme 4.4 – Synthesis of mono- and dioxetanol BODIPY analogs. Reagents and conditions: a) Molecular sieves, Toluene, 60 °C, 1 h (4.35 : 8% yield) or 8 h (4.36 : 55% yield). -----	155

- Scheme 4.5** – Synthesis of CMA-BODIPY labeled small molecules. Reagents and conditions: **a)** molecular sieves, THF, 60 °C, 8 h; **b)** molecular sieves, Toluene, 60 °C, 8 h.-----156
- Scheme 4.6** – Synthesis of CMA-BODIPY labeled indolo[3,2-*b*]quinoline. Reagents and conditions: **a)** 130 °C, 16 h, 62%; **b)** NaBH(OAc)₃, DCE, r.t., 4 h, 51%; **c)** HF/Pyridine/THF (1/2/7), r.t., 16 h, 58%; **d)** molecular sieves, 60 °C, 8 h.-----158

List of Abbreviations

aa	Amino Acid
aa-AMP	Aminoacyl-adenylate
aaRS	Aminoacyl tRNA Synthetase
aaSA	Aminoacyl-sulfamoyl adenosine
AAR	Amino Acid Starvation Response
ACT	Artemisinin Combination Therapy
ARS	Alanyl-tRNA synthetase
ART	Artemisinin
ATP	Adenosine Triphosphate
br	Broad
Boc	tert-Butyloxycarbonyl Group
cNRS	Cytoplasmic asparaginyl-tRNA synthetase
cLogP	Calculated Partition Coefficient
cPRS	Cytoplasmic prolyl-tRNA Synthetase
CNV	Copy Number Variants
CQ	Chloroquine
CRS	Cysteinyl-tRNA synthetase
CRT	Chloroquine resistance transporter
d	Doublet
DBU	1,8-Diazabicycloundec-7-ene
DCC	N,N'-Dicyclohexylcarbodiimide
DCE	Dichloroethane
dd	Doublet of Doublets
ddd	Doublet of Doublet of Doublets
DHFR	Dihydrofolate Reductase
DHODH	Dihydroorotate Dehydrogenase
DHPS	Dihydropteroate Synthetase
DIBAL	Diisobutylaluminium hydride

DIPEA	N,N-Diisopropylethylamine
DMA	Dimethylacetamide
DME	1,2 Dimethoxyethane
DMAP	4-Dimethylaminopyridine
DMF	N,N-Dimethylformamide
DMSO	Dimethylsulfoxide
DNA	Deoxyribonucleic Acid
DOS	Diversity Oriented Synthesis
DRS	Aspartyl-tRNA synthetase
EC50	Concentration of a drug that gives 50% of maximal response
EDC	1-Ethyl-3-(3-dimethylaminopropyl)carbodiimide
eIF2 α	Alpha subunit of Eukaryotic Initiation Factor 2
EtOAc	Ethyl Acetate
EtOH	Ethanol
EPRS	Glutamylprolyl-tRNA Synthetase
ER	Endoplasmatic Reticulum
FDA	Food and Drug Administration
FP IX	Ferriprotoporphyrin IX
FRS	Phenylalanyl-tRNA synthetase
FV	Food Vacuole
GNC2	General control nonderepressible 2
GSK	GlaxoSmithKline
G6PD	Glucose-6-phosphate dehydrogenase
HCTU	O-(6-Chlorobenzotriazol-1-yl)-N,N,N',N'-tetramethyluronium hexafluorophosphate
HFG	Halofuginone
HFol	Halofuginol
HOBt	Hydroxybenzotriazole
HPPK	Hyoxymethylpterin Pyrophosphokinase
HRS	Histidinyl-tRNA synthetase
HTS	High-Throughput Screening

Hz	Hemozoin
EC ₅₀	Concentration of a drug that is required for 50% inhibition in vitro
IPP	Isopentenyl Pyrophosphate
ISP	Iron-sulfur Protein
IRS	Isoleucyl-tRNA synthetase
ISR	Integrated Stress Response
<i>J</i>	Coupling Constant
KRS	lysyl-tRNA synthetase
LAR	Lipid Accumulation Ratio
LG	Leaving Group
m	Multiplet
mCPBA	meta-Chloroperoxybenzoic Acid
MeOH	Methanol
mETC	Mitochondrial Electron Transport Chain
MDR	Multidrug Resistance
MEF	Mefloquine
MRS	Methionyl-tRNA synthetase
MMV	Medicines for Malaria Venture
MoA	Mechanism of Action
mp	Melting Point
MsCl	Methanesulfonyl Chloride
mTORC 1	Mammalian target of rapamycin complex 1
MW	Molecular Weight
NaHMDS	Sodium Bis(trimethylsilyl)amide
NMR	Nuclear Magnetic Resonance
OSu	N-hydroxysuccinimide
PBS	Phosphate-Buffered Saline
PDB	Protein Data Bank
Pf	Plasmodium falciparum
<i>pfcr</i>	<i>P. falciparum</i> chloroquine resistance transporter gene
<i>pfmdr1</i>	<i>Plasmodium falciparum</i> multidrug resistance gene 1

<i>Pf</i> PI4K	Phosphatidylinositol 4-kinase
PPI	Protein-Protein Interaction
PRS	prolyl-transfer RNA Synthetase
PoC	Proof-of-concept
PyBOP	Benzotriazol-1-yl-oxytripyrrolidinophosphonium hexafluorophosphate
RI	Resistance Index
Ro5	Lipinski rule of 5
RNA	Ribonucleic Acid
r.t.	Room Temperature
ROS	Reactive Oxygen Species
s	Singlet
SAR	Structure-activity relationships
Sc	<i>Saccharomyces cerevisiae</i>
SERCaP	Single-Exposure Radical Cure and Prophylaxis
SI	Selectivity Index
SILAC	Stable isotope labelling amino acid
SNP	Single Nucleotide Polymorphism
t	Triplet
TBAF	Tetra-n-butylammonium Fluoride
TBDPS	tert-Butyldiphenylsilyl Ether
TCP	Target Candidate Profiles
TCAMS	Tres Cantos Antimalarial Set
TEA	Triethylamine
TFA	Trifluoroacetic Acid
THF	Tetrahydrofuran
TMSOtf	Trifluoromethanesulfonic Acid Trimethylsilylester
TPP	Target Product Profile
tRNA	Transfer Ribonucleic Acid
TRS	Threonyl-tRNA synthetase
VAR	Vacuolar Accumulation Ratio
WHO	World Health Organization

WRS

Tryptophanyl-tRNA synthetase

Amino acid Nomenclature

Amino Acid	One Letter	Three Letter
Alanine	A	Ala
Cysteine	C	Cys
Aspartic acid	D	Asp
Glutamic acid	E	Glu
Phenylalanine	F	Phe
Glycine	G	Gly
Histidine	H	His
Isoleucine	I	Ile
Lysine	K	Lys
Leucine	L	Leu
Methionine	M	Met
Asparagine	N	Asn
Proline	P	Pro
Glutamine	Q	Gln
Arginine	R	Arg
Serine	S	Ser
Threonine	T	Thr
Valine	V	Val
Tryptophan	W	Trp
Tyrosine	Y	Tyr
D-Methionine	m	Met
D-Proline	P	Pro

Scope of this Thesis

Malaria, the most devastating of the parasitic diseases, afflicts 300-500 million people and causes an estimated 600,000 deaths annually. Despite great efforts, the decreasing efficacy of existing therapies, due to constantly evolving resistance to the currently used antimalarial chemotherapeutics, has aggravated the malaria threat.¹ To counter these statistics, which are likely to increase, new drugs exploiting novel targets in different stages of the parasite's lifecycle are urgently needed. Furthermore, new technologies and high throughput approaches have been applied to identify a burgeoning number of lead drug candidates and novel drug classes with antimalarial activity.²⁻³

Within our efforts to help address the unmet medical need we have explored different drug discovery strategies to develop novel antimalarial drugs. Prompted by results previously obtained by both our groups and the literature,⁴⁻⁸ the overall objective of this research project is to build on these important findings and apply mainly three different medicinal chemistry approaches to identify and biologically characterize selective small molecules that are suitable as lead candidates for preclinical broad-spectrum malaria drug development.

This PhD thesis includes six chapters:

Chapter 1 gives a short overview of the global malaria spread, the *Plasmodium* life cycle and drugs developed or employed in the malaria therapy, as well as drug discovery strategies used to identify novel antimalarial drugs. Also the target identification and validation methods currently available to aid malaria drug discovery are reviewed.

Chapter 2 will discuss the design and synthetic strategy used to obtain the three libraries of derivatives to explore the antimalarial potential of the 3-piperidin-4-yl-1*H*-indole scaffold.

Chapter 3 establishes that inhibition of aminoacyl-tRNA synthetases in *Plasmodium* by small molecules and simultaneous activation of the integrated stress response is both feasible and attractive, and provides a rational mechanistic basis for future drug discovery and development focused on these novel targets and pathway. Furthermore, novel cytoplasmic prolyl-tRNA

synthetase inhibitors are explored.

Chapter 4 will present the development of a new synthetic methodology, which allows direct fluorescent labeling of drugs. Fluorescent probes are explored as a novel target discovery approach.

Chapter 5 will provide a global overview on the major conclusions and achievements of this work, with focus on the antimalarial profiling and structure-activity relationships of the synthesized libraries and the implications for future drug development. In addition, the major outcomes from the new fluorescent probes reported in this thesis will also be addressed.

Chapter 6 presents all the experimental procedures used in the development of the present study. Synthetic methodologies, physical-chemical properties and biological methods will be described.

Chapter One

1. Introduction

1.1 Malaria

Malaria is one of the most life-threatening diseases with almost one-third of the world's population at risk. It represents a major public health problem due to its morbidity and mortality.^{1,9} An estimated 198 million cases led to nearly 584,000 deaths in 2013, 90% of which were reported in sub-Saharan Africa.¹ Malaria has a broad impact throughout tropical and subtropical areas of the globe, affecting indigenous populations as well as an increasing number of travelers (Figure 1.1).¹⁰⁻¹²

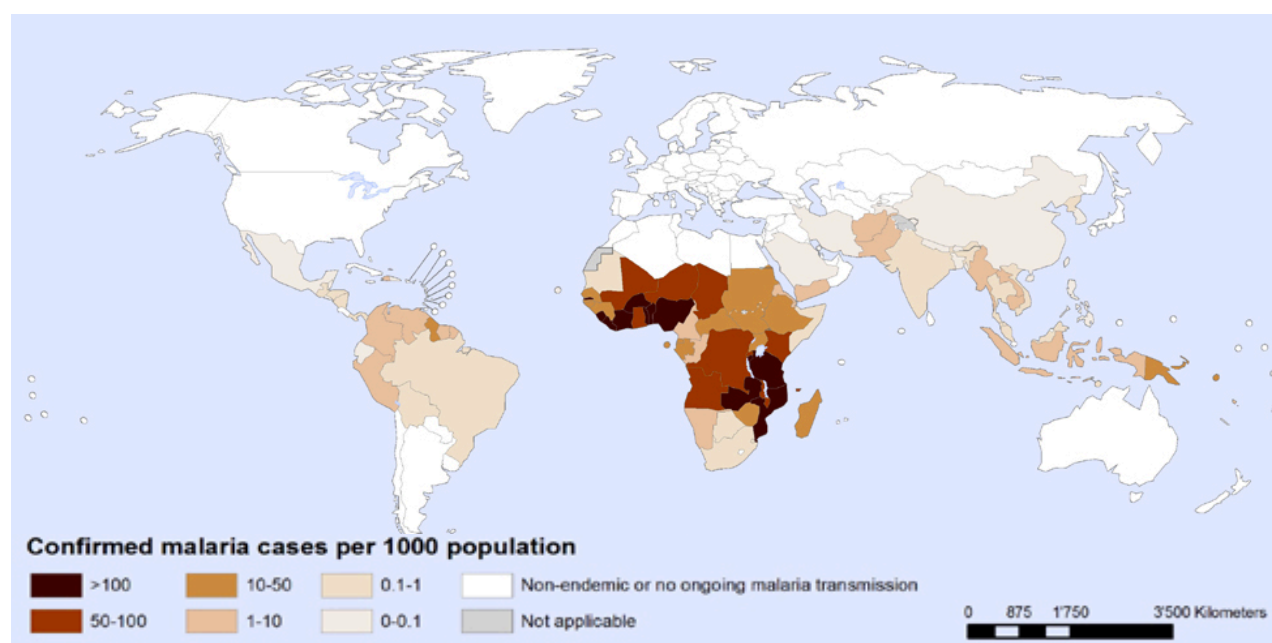


Figure 1.1 – Estimated incidence of malaria per 1000 population, map from 2014 WHO Malaria Report.¹

According to the 2014 World Health Organization (WHO) Malaria Report, about 78% of deaths attributed to malaria occur in African children under age of 5.¹ In addition to the human cost of malaria, the economic burden of the disease is significant with a huge impact upon individual households due to lost wages and healthcare costs, as well as detrimental effect on the national scale with about 40% of African health budgets spent on malaria every year.¹³

Five of the *Plasmodium* species are known to infect humans: *P. vivax*, *P. ovale*, *P. malariae*, *P. knowlesi* and *P. falciparum*.¹⁴ Of these species, *P. falciparum* is the human malaria parasite inflicting the highest burden in Africa, spread in nearly all malaria endemic countries

Chapter 1 – Introduction

and is responsible for the majority of malaria mortality. *P. vivax* is also increasingly recognized as an important contributor to the malaria toll, despite causing benign malaria, since it is considered the most widespread of the five species.¹⁵⁻¹⁶

The parasite has a complex life cycle, which involves alternate developmental stages within the human host and the female *Anopheles* mosquito.^{9,17} The parasites' life cycle (Figure 1.2) begins when sporozoites, present in the infected *Anopheles* mosquito's salivary gland, are injected into the human host during a blood meal.¹⁸⁻¹⁹ The sporozoites inoculated into the skin enter the blood vessels and are carried to the liver where they pass through Kupffer cells and invade hepatocytes.^{14,20} For all *Plasmodium spp.*, parasites incubate and multiply forming liver schizonts, which eventually burst, releasing thousands of merozoites into the blood stream 2-16 days after initial infection.²¹ In the bloodstream, merozoites rapidly collide with erythrocytes, bind to their plasma membrane and actively invade the cells through a cascade of protein-protein interactions.²² Alternatively, *P. vivax* and *P. ovale* can remain in a dormant form within the liver cells as hypnozoites until they activate and cause relapses, months or years later.²⁰ Once inside the red blood cell, the merozoite is hidden from the immune system, and through DNA replication and schizogony, produces 8–32 new merozoites per red blood cell. With the exception of *P. malariae*, the parasite's 48-hour growth cycle is followed by red blood cell rupture and merozoite re-invasion, which further increases the infection and causes the symptoms of the disease. This cycle of asexual reproduction can persist indefinitely in the absence of treatment.^{19,21}

During the asexual cycle, some of the parasite cells develop into male and female sexual stages, gametocytes. These asymptomatic, non-replicating forms can persist for weeks and are responsible for malaria transmission. After the ingestion of gametocytes by a mosquito during a blood meal, they differentiate into male and female gametes that fuse to form a zygote in the midgut of the mosquito. Meiosis occurs in the zygote, which then develops into a motile ookinete that migrates through the gut wall and eventually forms an oocyst. After multiple rounds of DNA replication thousands of sporozoites are produced. These sporozoites migrate to the salivary glands and are transmitted to the next human host during a blood meal.^{14, 18-19, 21} The erythrocytic stage of the infection accounts for the diseases' clinical symptoms which is characterized by fever, chills, headache and nausea in early stages as well as life-threatening anemia. In addition to fever and anemia, *P. falciparum* infections often lead to further

complications due to the sequestration of infected red blood cells in the host microvasculature. Blood-stage *P. falciparum* parasites extensively remodel the surface of their red blood cell hosts, expressing proteins that adhere the infected red blood cell to endothelial cells.²³ Presumably, this enables infected red blood cells to avoid clearance by the host spleen, but can lead to coagulation, breakdown in blood vessel structure, and inflammation in the host,²⁴⁻²⁶ with further complications in individual organs.²⁷ Cerebral malaria has a high mortality rate in children and can lead to permanent neurological impairment.²⁸ Sequestration can also occur in the placenta during pregnancy, leading to anemia in the mother and reducing fetal birth weight, thereby increasing the risk of infant mortality.²⁹⁻³⁰ Malaria caused by *P. falciparum* can progress within a few days from an uncomplicated to a severe scenario with a fatal outcome in 10-40% of all cases.^{17,31}

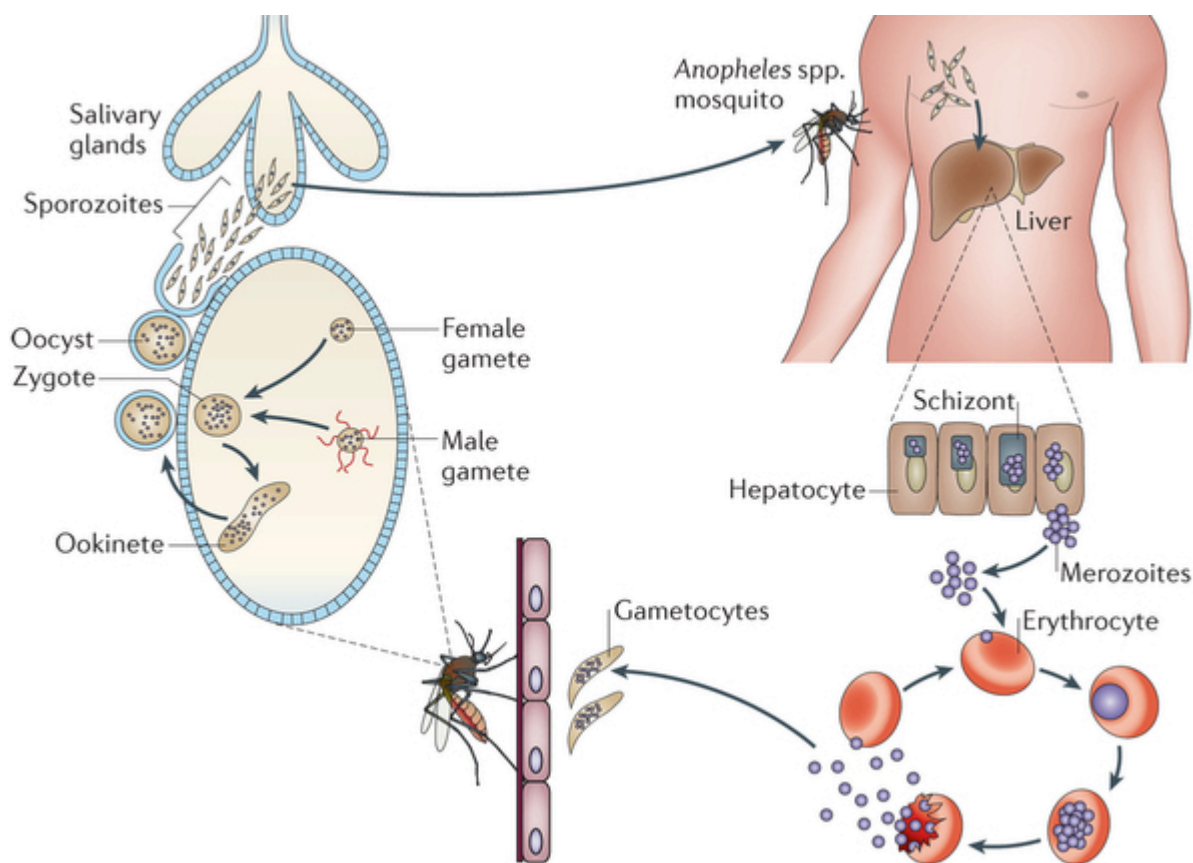


Figure 1.2 – The *Plasmodium* life cycle.²¹

Chapter 1 – Introduction

Each of the developmental stages discussed above provides numerous potential points for intervention, at which the life cycle can be interrupted. Hence new antimalarial drugs and anti-vector measures can be developed to prevent infection, disease and transmission.³²⁻³³

Virtually all stages of the complex life cycle of malaria parasites have been enlightened in several studies by the use of luciferase reporters. These engineered parasites provided key answers to fundamental biological questions and now represent important tools for drug screening.³⁴

Chemoprophylaxis and chemotherapy still plays, and will continue to play, a central role in combating malaria infections. However this role has been compromised throughout the years by the quite modest number of antimalarial drugs currently licensed and the inexorable emergence and spread of parasite strains that are drug-resistant.³⁵

The extensive and inappropriate sequential use of these drugs during a long period of time resulted in a tremendous selection pressure on malaria parasites to develop mechanisms of resistance, which has increased mortality and morbidity in many malaria-endemic regions.³⁶ Drug resistance arises from several factors such as overuse of antimalarial drugs for prophylaxis, inadequate or incomplete treatments of active infections, drugs administered in sub-therapeutic levels and even high degree of parasite adaptability.^{20, 37}

The 2014 WHO guidelines establish that the adequate approach towards malaria containment consists on the appropriate treatment, with the use of combination therapy, as well as control of the *Anopheles* mosquito vector, via use of insecticide-impregnated bed nets.¹

Combining antimalarial drugs has the purpose of both increasing the efficacy of treatment in addition to delaying the emergence of drug resistance. When choosing a drug combination it's important that the constituent drugs have a different, but yet synergetic mode of action and display well-matched pharmacokinetic and pharmacodynamic profiles. Mismatched combinations may jeopardize the efficacy of drugs against which resistance hasn't been extensively recorded. Some of the combinations used are, for example, artesunate-amodiaquine, artesunate-mefloquine.^{36, 38-39} Furthermore, public health challenges in endemic areas place additional constraints on drug development. Future drugs must be, not only well tolerated when given in combination with other drugs to minimize the need for follow-up care which is often limited, but also orally bioavailable and rapidly curing the underlying disease to enable practical mass administration and maximize patient compliance. Finally, drugs must be especially

inexpensive to be broadly accessible to populations in endemic areas.⁴⁰⁻⁴¹ Take together malaria elimination will ultimately require an integrated strategy that includes chemotherapeutics, vaccines⁴²⁻⁴⁵, vector control and public health measures. Although the task seems daunting, efforts are being made to achieve this common goal.

1.2 Malaria Chemotherapeutics

The bark of the *Chinchona* tree, native to South America, provides a rich source of medicinal alkaloids. The first use of the bark in treating malaria is often attributed to the 17th century in Peru, though the indigenous population used hot infusions of the bark much earlier.⁴⁶ Thus, the powdered bark from the *Chinchona* tree, containing the plasmocidal quinoline alkaloid quinine **1.1** (Figure 1.3) was the first medicine used against malaria. William Perkins first attempted quinine synthesis in 1856, but it was only in 1944 that its total synthesis was accomplished. Meanwhile, the microbiologist Paul Ehrlich used methylene blue **1.2** (Figure 1.3) to enhance visibility of microorganisms under the microscope and realized that it was particularly effective in staining malaria parasites, thus speculating that this dye might also be selectively toxic towards the parasite. In 1891 Ehrlich and Guttman cured two malaria patients with methylene blue, becoming the first synthetic drug used in therapy. It became the starting point of a synthetic development and the predecessor to many antimalarial drug classes.⁴⁷

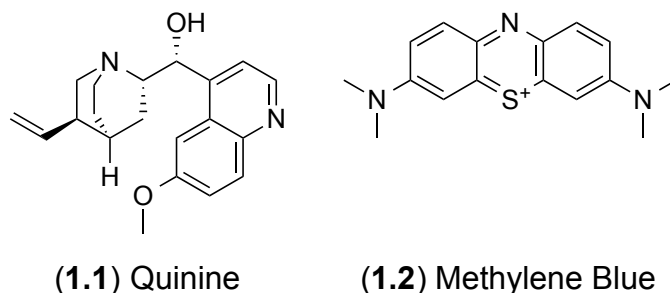


Figure 1.3 – Quinoline alkaloid and the first synthetic antimalarial drug.

Antimalarial drugs are classified according to the stage of the malaria life cycle that they target. In the case of *P. falciparum* malaria where there is no reinfection or relapse from the liver, a single blood schizonticide is sufficient as treatment. Tissue schizonticides (ex. Pyrimethamine **(1.4)**, a folate inhibitor) (Figure 1.4) kill hepatic schizonts preventing the invasion of erythrocytes, thus acting in a casually prophylactic manner, and hypnozoiticides (ex. 8-

Mode of Action

Malaria parasites in the bloodstream reside within host erythrocytes, where they mature and digest a large proportion of the host cell's hemoglobin as a source of amino acids for protein synthesis. Despite the access to abundant host heme during intraerythrocytic infection, parasites retain a complete heme biosynthesis pathway. Although apparently dispensable and inactive it can be activated by exogenous stimuli.⁵¹

Two aspartic proteases and one cysteine protease are responsible for hemoglobin's hydrolysis (Figure 1.5), and there are four distinct hemoglobin uptake pathways proposed.⁵² During the degradation pathway of hemoglobin, heme Fe(II) is released and this free heme is toxic because of its ability to cause lipid peroxidation and to destabilize membranes through a colloid osmotic mechanism in addition to producing reactive oxygen species.⁵³⁻⁵⁶ Instead of excreting, the parasite detoxifies free heme by autoxidizing it to FPIX (Fe(III)) and then converting it into non-toxic, insoluble crystals of hemozoin that accumulate in the food vacuole.⁵³

Hemozoin or malaria pigment represents a striking feature of the trophozoite stage of malaria, seen as a dark brown-black substance in a lysosome-like compartment when examined under a microscope.⁵⁷

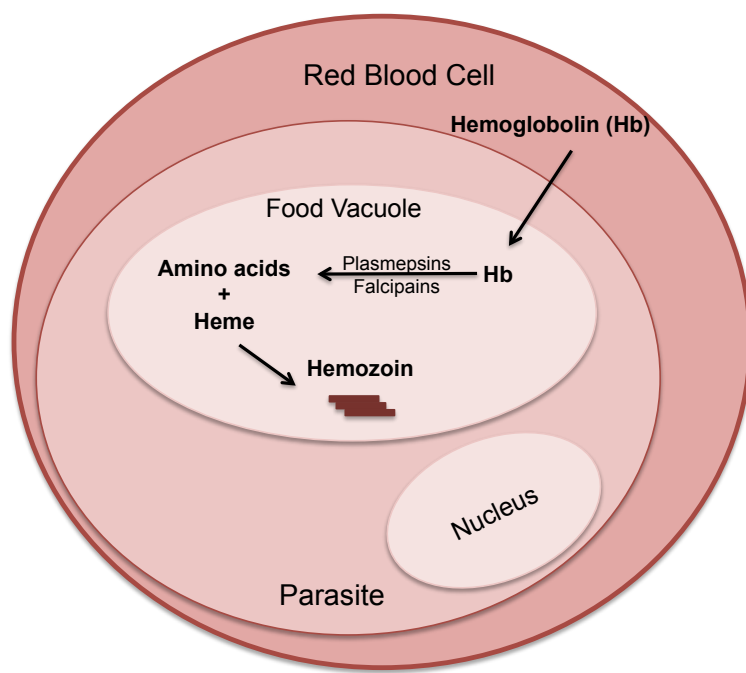


Figure 1.5 – Schematic representation of the hemoglobin degradation mechanism in the food vacuole of *Plasmodium*. Ingested hemoglobin is transported into the FV where it is degraded to heme and globin. The globin fragments are cleaved by several proteases until amino acids used in the peptide synthesis by *Plasmodium*. Heme fragment, which is toxic to the parasite is oxidized and crystallized to hemozoin.⁵⁸

The antimalarial activity of quinoline-containing compounds acting as schizonticides, seems to be correlated with the inhibition of hemozoin formation.^{49, 54, 58} However, the mechanism of hemozoin biocrystallization inhibition by these antimalarials is still a matter of debate. As recently reviewed,⁵⁹ several studies indicate that they may inhibit Hz crystallization by binding to the hemozoin monomer,⁶⁰⁻⁶¹ or the μ -oxodimer,⁶²⁻⁶³ or the “head-to-tail” dimer that is adsorbed on the crystal surface, or even by acting as capping molecules on Hz crystal faces.⁶⁴⁻⁶⁶ The weak base property of these compounds explains its selective accumulation in the food vacuole (FV), as seen with chloroquine ($pK_{a1}=8.1$; $pK_{a2}=10.2$). Its uncharged form diffuses freely into acidic compartments, like *P. falciparum* food vacuole, where it protonates and becomes trapped.⁴⁹⁻⁵⁰

The mechanism of inhibition involves π - π stacking interactions of the quinoline ring with the porphyrin ring system with the potential for a second weak electrostatic interaction of the charged ammonium group with the carboxyl groups of FP IX. It is believed that the build up of toxic concentrations of free FP IX inside the FV leads to the parasite's death.^{49, 54} Even though the main mode of action of these compounds seems to be inhibition of the hemozoin crystals formation, other possible targets have also been described, which may include increased accumulation of hemoglobin in endocytic vesicles (4-aminoquinoline drugs) and induction of morphologic changes (4-aminoquinoline and quinoline-4-methanol drugs).⁶⁷

The mechanism of action of quinoline-containing compounds acting as hypnozoiticides, such as 8-aminoquinoline primaquine **1.9** (Figure 1.4), is not yet fully understood. It is thought that the metabolism at the parasite's mitochondria is impaired, eventually by interference with the ubiquinone function, as an electron carrier in the respiratory chain. Another potential mechanism consists on the production of highly reactive metabolites that generate intracellular oxidative potentials. Previous biotransformation seems to be necessary for their toxicity as well as efficacy. The selective generation of oxidative stress in the parasitized cells is the most plausible mechanism of both toxicity and efficacy.⁶⁸⁻⁶⁹

4-Aminoquinolines

Since the quinoline nucleus was believed to be an important feature in antimalarial activity, in 1934, diethylaminoisopentylamino side chain was introduced into position 4 of 7-chloroquinoline yielding chloroquine (CQ), the most distinct member of the 4-aminoquinoline

class.⁴⁷ CQ **1.10** (Figure 1.6) has been the most successful single drug for the treatment of malaria, being a safe and affordable compound that has saved countless lives.³⁵ This 4-aminoquinoline contains a 7-chloro substituted quinoline ring system with a flexible pentodiamino side chain and since its discovery attempts have been made to obtain a superior antimalarial drug.⁵⁴ Structure-activity relationship studies show that a strong lipophilic and electron withdrawing functional group in the 7-position of the quinoline ring is required for inhibition of hemozoin formation, being the chloride atom optimal for antimalarial activity both *in vivo* and *in vitro*. Also the tertiary amino nitrogen in the alkyl side chain, as well as the quinoline ring nitrogen are essential for accumulation in the acidic food vacuole and the quinoline ring itself to act as a heme binding template. The length of the side chain can determine possible activity against resistant strains. This information allows the description of its pharmacophore (Figure 1.6).^{54, 70}

As a lipophilicity enhancement strategy, an aromatic structure was incorporated into the side chain of chloroquine, thus resulting in amodiaquine **1.7** (Figure 1.4).⁴⁷ This compound is effective against low-level but not high-level chloroquine resistant *P.falciparum* strains. Its therapeutic value is significantly reduced by biotransformation into a quinonimine which is responsible for severe hepatotoxicity and life-threatening agranulocytosis.⁴⁹

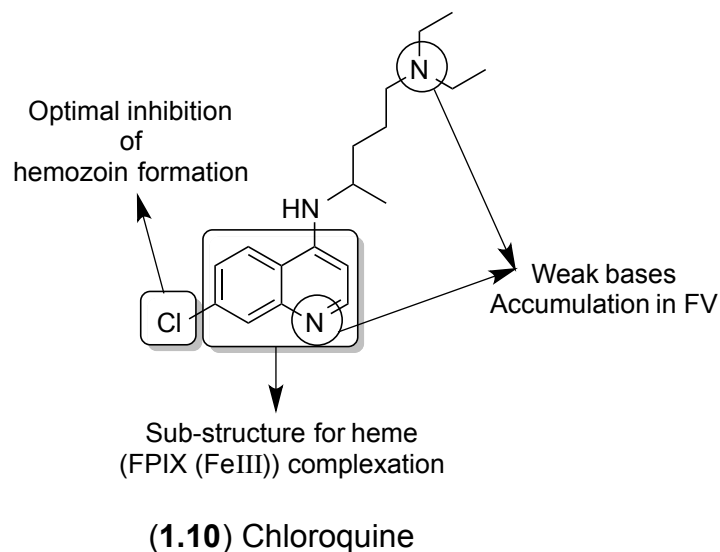


Figure 1.6 – Pharmacophore of the antimalarial 4-aminoquinoline chloroquine. Adapted from Egan *et al.*⁷¹

Chapter 1 – Introduction

Despite the widespread resistance to chloroquine there is a continued interest in compounds of this class and much of the current effort is directed to the development of novel 4-aminoquinoline drugs, since their mode of action and resistance appear to occur via independent mechanisms.⁷²⁻⁷³

The extensive employment of chloroquine as an antimalarial drug, through an extensive period of time, provided a tremendous selection pressure on malaria parasites to evolve mechanisms of resistance. Resistant *P. falciparum* strains have developed independently in four different regions, and have successively spread over almost the entire malaria endemic area, with profound consequences.^{35, 74-76} It is generally accepted that resistance results from a mutation in the gene *pfcr* responsible for the expression of the chloroquine resistance transporter (CRT) located in the membrane of the FV, the so called ‘charged drug leak’ hypothesis.³⁵ The genotyping of resistant strains showed a mutation in *pfcr*, where, a lysine residue (polar and positively charged) is replaced by a threonine residue (neutral and hydrophobic). This positive-to-neutral charged modification caused by this amino-acid substitution may impede the retention of CQ inside the FV. Since the transporter’s positive charge limits the efflux of CQ, a weak diprotic base of which almost 100% will carry two positive charges in acidic conditions, when the mutation occurs the CQ^{2+} can exit down its concentration gradient via the CRT. However, possible reversing strategies have been described, such as, mutations elsewhere in the protein that can restore a positive charge to the pore, thus reversing the resistance phenotype, as well as the use of lipophilic and positively charged compounds (ex. Verapamil), which compete with CQ for binding to CRT.^{35, 77-78}

Nevertheless, other 4-aminoquinolines are currently in clinical use as Food and Drug Administration (FDA) approved artemisinin-based combination therapy, such as dihydroartemisinin-piperazine and pyronaridine-artesunate.⁷⁹

8-Aminoquinolines

The 8-aminoquinoline primaquine (Figure 1.4), has been approved for treatment of malaria since 1952 by the FDA, and is the most representative member of this class since it is the only one in general use.⁶⁸⁻⁶⁹ Primaquine is the only transmission-blocking antimalarial clinically available, since it displays unique gametocytocidal properties against all species of human malaria. This compound is also a tissue schizontocide that kills early liver stages of *P.*

falciparum and *P. vivax*, thereby providing causal and terminal prophylaxis against both infections.⁸⁰⁻⁸¹ Though primaquine is effective, unique and so far irreplaceable, it is also associated with serious hazards and side effects, such as gastrointestinal reactions, methemoglobinemia and severe intravascular haemolysis in glucose-6-phosphate dehydrogenase (G6PD) deficient individuals, which prohibits its use in key groups, like pregnant women.⁸¹ Extensive derivatization approaches to develop 8-aminoquinoline analogs with better pharmacological and reduced toxicological profiles have led to compounds that are still under development such as, tafenoquine, a slowly eliminated 8-aminoquinoline currently in phase III clinical trials, among others.^{79-80, 82} Resistance to primaquine is a difficult entity to quantify due to the fact that it is used in combination with a blood schizontocidal agent, and the lack of efficacy between the two is difficult to quantify separately.⁶⁹

Arylamino Alcohols

Another class of quinoline-containing compounds is the arylamino alcohols, which include mefloquine **1.8** (Figure 1.4), a widely used antimalarial medication for travelers that go to areas where chloroquine-resistant *P. falciparum* is predominant. The drug is an effective schizontocide, active against the blood stages of all the malaria species that infect humans.⁸³ Mefloquine has proven safe as chemoprophylaxis in long-term travellers, pregnant women, breastfeeding women, and children, as well as in treating paediatric malaria.⁸³⁻⁸⁴ Furthermore, a non quinoline-containing arylamino alcohol is currently in clinical use as a FDA approved artemisinin-based combination therapy for both adults and children (artemether-lumefantrine).⁷⁹

Resistance to mefloquine has been reported as a consequence of elevated *pfmdr1* gene copy number, resulting in decreased parasite sensitivity to this compound. This increase is a direct result of the maturation delay at the ring stage and has not proven to affect antimalarial activity of a currently used drug, artemisinin.⁸⁵

Antifolates

Antifolates were demonstrated to be effective against malaria in the 1930s, when they emerge as a part of the antimalarial drugs that have specific enzyme targets in the parasite.

The principal antifolate drugs used against malaria are pyrimethamine and the sulfa drugs, for example sulfadoxine **1.3** (Figure 1.4), among others.²⁰ Pyrimethamine (**1.4**, Figure 1.4)

targets the dihydrofolate reductase (DHFR) activity of the parasite's bifunctional DHFR-thymidylate synthetase (TS) protein, whereas the sulfa drugs affect the dihydropteroate synthetase (DHPS) activity of the bifunctional hydroxymethylpterin pyrophosphokinase (HPPK)-DHPS protein. All of these drugs act as competitive inhibitors of the enzymes' natural substrates. Since DHFR is present in both, host and parasite, the safety and efficacy of the drugs that target this enzyme depends on a several hundred-fold differential binding ability. Resistance appeared rapidly when these drugs were initially deployed as mono-therapy, but synergistic combinations with sulfa drugs have proved to be of long-term utility, especially as a cheap alternative to combat the CQ-resistant parasites, although its use has diminished with the use of artemisinin-based combination therapy.³⁵ The pyrimethamine derivative P218 (**1.23**, Figure 1.10) is a next generation inhibitor of DHFR that has largely finished preclinical development. This clinical candidate has a good pharmacokinetic profile, is selective and highly efficacious, as well as demonstrates a good safety margin.⁸⁶

1.2.2 Artemisinins

The plant sweet wormwood, *Artemisia annua*, used for more than 2000 years as a Chinese herbal medicine against intermittent fever, rendered the antimalarial drug artemisinin (ART) (**1.11**, Figure 1.7) in the 1980's.⁸⁷⁻⁸⁸ Since its discovery, ART has been the most studied antimalarial compound due to its low nanomolar range activity and its general tolerability.^{87, 89-91}

Artemisinins, such as artesunate (**1.5**) and artemether (**1.6**) (Figure 1.4), constitute the only known drug class that effectively functions against multidrug-resistant parasites, although reports of prolonged parasite clearance times in artemisinin-treated patients have raised concerns that the advances of the past few years might be lost.^{21, 92-94} The first signs of artemisinin resistance came from a study that was conducted in 2008, in which parasite clearance times after initial artesunate monotherapy were slower in patients from the Eastern Thailand–Cambodian border.⁹⁵

The expanded use of artemisinin-based combination therapy (ACT) has played a major part in reduction of malaria illness and deaths and is the WHO-recommended treatment for *P. falciparum* malaria worldwide.¹ Artemisin and its derivatives are used as ACTs and are the recommended first-line treatments for malaria because they are effective against all four human-

infecting malaria parasites, produce rapid parasite/fever clearance, and show fewer adverse effects.⁹⁶

The mechanism of action of these compounds (Figure 1.7) is still uncertain, even though it is most likely attributed to the endoperoxide bridge (1,2,4-trioxane).⁹⁶⁻⁹⁷ One of the proposed modes of action consists on the activation of the endoperoxide bridge by free iron (II), present in high amounts inside the parasite, since it is a side-product of the hemoglobin digestion. As a result of the activation, the endoperoxide bridge originates oxygen radicals (ROS), that further rearrange into carbon centered radicals considered very toxic to the parasite.⁹⁷⁻⁹⁸ Due to the generation of ROS, earlier studies suggest that artemisinins modulate parasite oxidative stress and reduce the levels of antioxidants and glutathione in the parasite.⁹⁹ Moreover, P-type ATPases¹⁰⁰ and the respiratory chain of the mitochondria¹⁰¹ have also been proposed as specific targets of artemisinins.¹⁰²

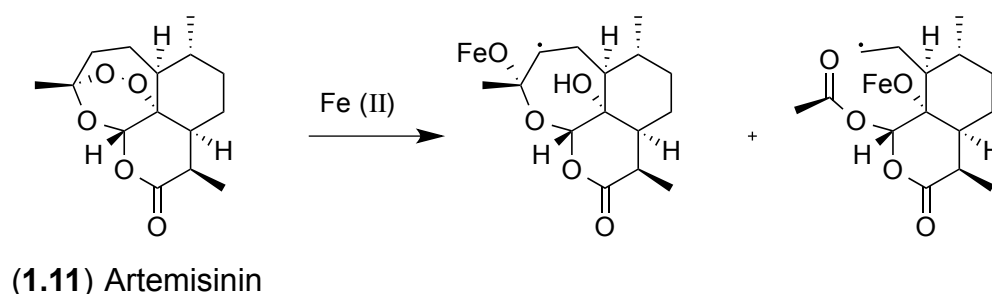


Figure 1.7 – Artemisinin and its proposed active species.

Since ART lacks a good pharmacokinetic profile, low water and oil solubilities as well as low half-life in the bloodstream, further semi-synthetic derivatives were synthesized, such as artesunate and artemether (Figure 1.4). The derivatives' half-life in the blood was not significantly improved, allowing some parasites to survive and eventually develop resistance, which led to drug regimen with multiple administrations.¹⁰³⁻¹⁰⁵ When developing an ACT, the partner drugs should ideally be structurally unrelated, more slowly eliminated *in vivo*, and should target those parasites that have not yet developed resistance. Antimalarial combination therapy with ART derivatives is recommended, since the simultaneous use with other blood schizonticidal drugs with an independent mode of action and different pharmacokinetic properties is more effective, and delays the emergence of parasite resistance against each drug,

for example artesunate-amodiaquine.^{96, 106} Moreover, the current clinical approved antimalarial drugs have been screened for their activity in other stages of the parasite's life cycle, where both artesunate and artemether were active against the liver stage parasites ($IC_{50} < 1\mu M$).¹⁰⁷

1.2.3 Cytochrome *bc*₁ Inhibitors

The cytochrome *bc*₁ complex is a key enzyme of the respiratory electron transfer chain, which is an attractive and validated drug target in the fight against malaria. The mitochondrial electron transport-chain is fundamental in *Plasmodium* sp., since the parasites do not possess the requested enzymatic machinery to salvage pyrimidines from their metabolism and, therefore, have to perform *de novo* pyrimidine biosynthesis to enable their survival, leading to its death when this pathway is inhibited.¹⁰⁸

Cytochrome *bc*₁ contains three polypeptides, which display catalytic functions: cytochrome *b*, cytochrome *c*₁ and the Rieske protein, or iron-sulfur protein (ISP). It catalyzes the transfer of electrons from ubiquinol to cytochrome *c* and couples this electron transfer to the vectorial translocation of protons across the inner mitochondrial membrane. This catalytic mechanism, called the Q-cycle, requires two distinct quinone-binding sites, the quinol oxidation site (Q_0) and the quinone reduction site (Q_i), which are located on opposite sides of the membrane and linked by a transmembrane electron-transfer pathway.¹⁰⁹⁻¹¹¹

Currently, the 1,4-Naphthoquinone atovaquone **1.12** (Figure 1.8) is the only drug targeting the *bc*₁ complex in clinical use.¹¹¹⁻¹¹² This antimalarial drug was developed in the 1990's and acts as a competitive inhibitor of cytochrome *bc*₁ that targets specifically the Q_0 site and locks the conformation of the Rieske (iron-sulfur) complex, which immobilizes the cluster and reduces electron transfer. Atovaquone induces collapse of the mitochondrial membrane potential at very low concentrations and, as a result, the mammalian system is not affected substantially. Initially, this drug was found to be a very effective antimalarial compound, but soon was considered inappropriate for use as a single agent due to the relatively quick emergence of resistance. In an attempt to improve its efficiency and overcome the emergence of resistance, atovaquone is now used in combination with the synergistic agent proguanil **1.13** (Figure 1.8).¹¹³

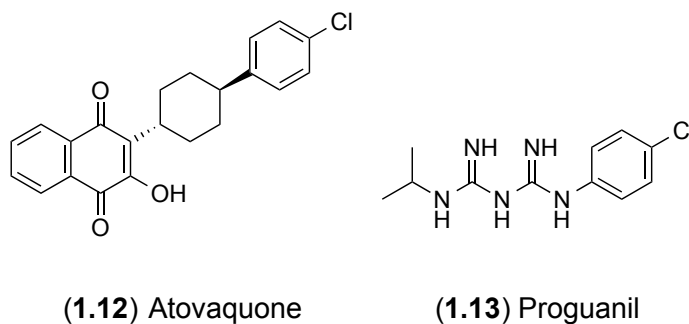


Figure 1.8 – Chemical structures of atovaquone (1.12) and proguanil (1.13), the active molecules in Malarone®.

Structurally the hydroxyl group of the hydroxynaphthoquinone binds, via a hydrogen bond, to a imidazole nitrogen of ISP, and on the opposite side of the ring system, the carbonyl group at position 4 interacts via a water molecule with cytochrome b (Figure 1.9).¹¹¹

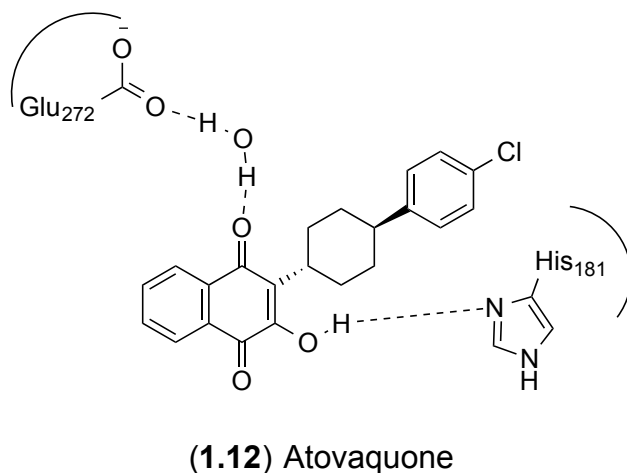


Figure 1.9 – Binding mode of atovaquone into bc1 complex Qo site.

Since resistance to atovaquone has been reported as a result of mutations responsible for the changes in the volume of the inhibitor-binding pocket, interfering with drug binding.¹¹² Therefore efforts have been made to develop other inhibitors, emerging drug classes such as the acridones, quinolones and tetracyclic benzothiazepines, but few compounds display all the desired properties.^{111, 114-115}

1.3 Drug Discovery Strategies

The emergence of drug resistance has already rendered once-effective malaria treatments, such as chloroquine and sulfadoxine-pyrimethamine, less reliable. Today, ACTs are the weapon of choice against malaria, and the possibility of losing them with the first signs of resistance, rendered the urgent need for novel antimalarial chemotypes.^{76, 87} Such facts highlight the parasite's ability to evolve and adapt to every drug introduced thus far, which mandates the research to identify novel chemotypes as well as new targets for antimalarial therapy.²⁻³

Nonetheless, in an attempt to streamline the number of available malaria therapeutics, the reformulation of existing drugs to increase their therapeutic efficacy has also been used. Thus improving the drug's bioavailability, decreasing pharmacokinetic variability, and lowering the total daily intake have extended the life of some antimalarial drugs.¹¹⁶ An example of such an approach is the reformulation of bitter crushed artemether/lumefantrine tablets to palatable and rapidly dispersible (<1 min) formulations, which has improved their efficacy in children. This sweet tasting paediatric formulation has been approved in 24 African countries.¹¹⁷ Treatments with greater efficiency have also been discovered, by combining different antimalarial drugs.^{21, 118-119} Pyronaridine-artesunate¹²⁰ and azithromycin-chloroquine¹²¹ are two such new drug combinations currently in clinical trials for malaria treatment.

Furthermore, new technologies and high throughput approaches are being applied to identify a burgeoning number of lead drug candidates and novel drug classes with antimalarial activity.²⁻³ Although efforts have been made to improve existing molecules, most new classes of potential antimalarials have come from high-throughput screens. Thus, drug discovery strategies include extensive compound screening, of which, natural sources, chemical libraries and virtual screening stand out.^{21, 122-123}

The global concerns that the efficacy of all currently used anti-malarial drugs will erode, creates a pressing need to develop inexpensive yet effective agents that can both treat and eradicate malaria. With such goals in mind the antimalarial target product profiles (TPP) have recently been reevaluated and defined. Future antimalarial combination treatments will need to cure the disease efficiently, by rapid clearance of parasitemia in patients, thereby reducing the risk of resistance and preventing recrudescence. In addition, these new medicines will be expected to block transmission and eliminate all liver forms of the parasite including dormant hypnozoites. This profile corresponds to the main treatment TPP at the Medicines for Malaria

Venture (MMV) in which the ideal criterion constitutes a medicine administered as a single dose, the SERCaP (single-exposure radical cure and prophylaxis).¹²⁴ Furthermore four different target candidate profiles (TCPs) were also defined regarding pharmacodynamics, pharmacokinetics, and safety parameters that a drug candidate should exhibit to fulfill the radical cure or prophylaxis criteria.¹²⁴⁻¹²⁵

Broadly, drug discovery efforts to develop novel antimalarial drugs include virtual and chemical screening, as well as rational chemistry-based approaches.

1.3.1 Virtual Screening

Virtual screening emerged in the 1990s as a way of predicting bioactive compounds using computational methods. These methods are usually defined as either structure-based or ligand-based, where structure-based approaches use knowledge of the 3D structure of the biological target, whereas ligand-based approaches rely on the knowledge of the structure of compounds exhibiting the desired activity.¹²⁶ Using computational approaches to expedite the identification of hit molecules that are predicted to possess the desired properties is an efficient approach to discover the best set of compounds with predicted activity. Following virtual screen, hit confirmation is necessary through *in vitro* testing.¹²⁶⁻¹²⁷ A high-throughput screening (HTS) has been established, for example, to identify novel inhibitors of the parasite's mitochondrial enzyme NADH:quinine oxidoreductase adopting the ligand-based approach.¹²⁶

1.3.2 Chemical Screening

Current successful approaches to discover drugs with new targets and chemotypes have come largely from high-throughput screening of chemical libraries of structurally diverse small molecules. In an effort to diversify the current stock of antimalarial chemotherapeutic agents, HTS campaigns have been developed for novel, drug-like compounds with whole-cell antimalarial activity, limited susceptibility to established mechanisms of drug resistance and minimal toxicity to mammalian cells, as a pathway to medicinal chemistry optimization and preclinical development of lead compounds.^{115, 128-129}

1.3.2.1 Sources of Chemical Libraries

1.3.2.1.1 Clinical Approved Drugs

Recent drug discovery approaches utilize compounds or compound classes that have already been evaluated or approved for clinical use against other diseases as a starting point for the discovery of new antimalarial agents.¹³⁰⁻¹³² Advantages of this approach include availability of safety and tolerability data, as well as, knowledge of possible mechanisms of action and resistance, which is time and cost efficient.¹³⁰ The value of this approach for malaria and other parasitic diseases is being recognised with recent interest in “clinical” drug libraries. Screens for antimalarial activity with some of the libraries have been carried out against asexual blood stage¹³³⁻¹³⁵, liver stage¹³⁶ and gametocyte stage *P. falciparum* parasites¹³⁷. Currently, the drug trimethoprim **1.14** (Figure 1.10), a clinically approved antibiotic, is being evaluated as an antimalarial drug in a Phase III clinical trial.⁷⁹

1.3.2.1.2 Diversity Oriented Synthesis (DOS)

Structural diversity plays an important role in discovering quality molecules that can generate favorable biological response for complex targets, thus DOS is an efficient tool, which has been utilized to generate structurally diverse libraries with novel biological properties. Traditional combinatorial chemistry is typically dependent on diversifying a common template, while libraries of compounds from DOS are usually architecturally more varied, allowing the interrogation of a more diverse chemical space.¹³⁸ In 2012, Schreiber *et al.* discovered an antimalarial macrocyclic lactam ML238 **1.15** (Figure 1.10) using a phenotypic screening of a DOS library, against *P. falciparum* asexual blood-stage parasites. This small molecule displayed picomolar activity and belongs to a novel structural class of antimalarials.¹³⁹⁻¹⁴⁰

1.3.2.1.3 Natural Products

Nature has been a major source of pharmacological drugs throughout history and the most efficient antimalarial drugs such as quinine and artemisinin were isolated from natural products. Thus, the interest in using libraries of natural-product extracts for high-throughput screening against *P. falciparum*.¹⁴¹⁻¹⁴³ As malaria is a disease that has historically been treated by herbal medicinal products, selecting extracts with demonstrable clinical activity could clearly lead to new drugs.¹⁴⁴ Thus, surveys of selected molecules from natural sources have been carried

out and antimalarial activity was evaluated through *in vitro* testing.^{122, 141} However, strategies based on medicinal plants render compounds with complex structures, which slow down the identification process, and present problems regarding supply.^{122, 142} Furthermore, additional challenges include seasonal or environmental variations in the composition of living organisms and loss of source through extinction or legislation, complexity of the mixtures after fractionation, the isolation of very small quantities of bioactive substance and challenging physicochemical properties such as solubility and stability.¹⁴⁵

Nevertheless, exploring natural products as a source of antimalarial drugs continues to be a powerful drug discovery approach, which has yield many active compounds. Alkaloids from traditional herbal medicines have contributed greatly over the centuries not only to the discovery of new antimalarial and therapeutic agents but also to the elucidation of biochemical pathways allowing the development of modern pharmaceutical industry.¹⁴⁶⁻¹⁴⁸ Two examples of great interest to our group, which will be further addressed in this thesis, include the febrifugine derivatives and the indoloquinoline derivatives. The febrifugine derivatives are a family of small molecules derived from the active component of *Dichroa febrifuga*. Used as an antipyretic in traditional Chinese medical practice, extracts of *D. febrifuga* were shown to have antimalarial properties in 1945. In the 1960s, the Walter Reed Army Institute of Research (WRAIR) developed halofuginone and other febrifugine analogs as part of a large antimalarial drug development program.¹⁴⁹ The indoloquinolines are unique natural alkaloids, characterized by an indole and a quinoline fused rings, found almost exclusively in the West African climbing shrub *Cryptolepis sanguinolenta* (Lindl.) Schltr. The roots' aqueous extracts of this plant have been used for centuries by African traditional healers mainly for the treatment of fevers including malaria, hepatitis and bacterial infections, among others.¹⁵⁰

1.3.2.2 Drug Discovery Screen

The drug discovery screens of chemical libraries has historically benefited from the phenotypic (whole-cell) screening approach to identify lead molecules in the search for new drugs. However over the past two decades there has been a shift in the pharmaceutical industry to move away from whole-cell screening to target-based approaches, fuelled by the genomic revolution.¹⁵¹⁻¹⁵²

1.3.2.2.1 Target-based Screen

Target-based screens start with the identification of an essential enzyme or pathway, ideally specific to the parasite, followed by the development of an *in vitro* biochemical assay, and an HTS can then be executed to identify hit compounds.¹⁵² This approach is often operationally simpler as it can use pure proteins in the biochemical assay and renders candidate molecules with known mechanism of action enabling structure-based lead optimization. The process can be further enhanced if crystal structures of the protein are available to guide the design of potential inhibitors and to increase selectivity and specificity against the parasite protein, relative to the host protein.¹⁵³ Several target-based screens, for suitable therapeutic agents have been developed in the past 10 years, such as the dihydrofolate reductase, among others. An undesirable common outcome is an *in vitro/in vivo* disconnect where excellent potency on the target does not translate to similar cellular activity or *in vivo* efficacy.¹⁵¹⁻¹⁵²

Among drug candidates identified using target-based approaches is the compound DSM-265 (**1.16**, Figure 1.10), an inhibitor of *P. falciparum* dihydroorotate, which will be further discussed below.¹⁵⁴

Although target-based approaches in the search for new antimalarials remains an active area of research, new chemical entities from HTS phenotypic campaigns of large chemical libraries are beginning to bolster the antimalarial pipeline at a more efficient pace than target-based screening.¹⁵⁵⁻¹⁵⁶

1.3.2.2.2 Phenotypic Screen

Phenotypic screens involve whole cells or even whole organisms and identify libraries or classes of compounds with potential biological activity against the parasite. This approach renders molecules that are permeable and active on the *Plasmodium* sp., but its disadvantage is that the activity can result from multiple pathways, leading to very poor or narrow structure-relationship activities during lead optimization.^{151-152, 155}

Malaria drug discovery has, until recently, focused on finding replacements for compounds that are active against blood-stage *P. falciparum*, such as artemisinin. With the recent progress that has been made in the development of high-throughput screens for both asexual and sexual stages, as well as for the liver stage of the parasite life cycle, efforts are made towards identifying compounds that are active against multiple stages.^{136-137, 151, 157-162}

As a consequence of the extensively debated drug resistance, there is an urgent need for novel drugs, preferably new chemotypes acting on underexploited parasite targets. This has triggered a great number of drug discovery and development programs from public institutions, private institutions, and public-private partnerships, using phenotypic screening with *P. falciparum* sensitive and resistant strains.¹⁶³ Among them were large libraries from Novartis, St. Jude Children's Research Hospital and GlaxoSmithKline (GSK)^{6, 155}.

On the basis of these public screen results, a library of 400 unique compounds with blood-stage antimalarial activity was created. These compounds have been resynthesized and this 'malaria box' of potential chemical starting points can be obtained from the Medicines for Malaria Venture (MMV). The malaria box concept enables biologists, who cannot resynthesize compounds, to participate in the drug discovery process and to help to identify how the compounds function. The MMV requests that the results of tests that use the malaria box are made public and encourages collaboration between groups. A total of ~6 million compounds have been screened to date and, excitingly, more than 25,000 of these have shown half-maximal (IC₅₀) activity at approximately 1 μ M or lower against *P. falciparum*.^{155, 164}

Among the new classes of antimalarial drugs identified using phenotypic-based approaches are the spiroindolones and the imidazolopiperazines, which will be further discussed below^{79, 165}.

1.3.3 Rational Chemistry-based Approaches

1.3.3.1 Hit to Lead Optimization

As described above several large libraries have been screened and thousands of cell-active compounds have been identified and made publicly available. Furthermore, different drug design strategies can be used for hit to lead optimization of these compounds. Moreover, rational drug design can be applied in the development of small molecule hits with known or unknown targets. Nonetheless, the challenge of the phenotypic-based approach develops when compound optimization stalls, and identification of the hit compounds' molecular targets for biochemical or structural analysis is necessary for further development from hit to lead.¹⁶⁶⁻¹⁶⁷

The process of hit to lead optimization is interactive and often proceeds through multiple cycles before an optimized lead goes into phase I clinical trials. Thus, specific criteria have been proposed for defining hits and leads in the development of antimalarial drugs.¹⁶⁸

Many of the improvements needed as the lead is converted to a drug candidate, such as reducing off-target interactions or improving metabolic stability, may be most easily achieved through the addition of functional groups that increase MW and often lipophilicity. Based on these studies, a set of thresholds for lead-likeness can be specified, for example, MW < 400 and log P < 3.5, to rank hits for their suitability for further exploration and optimization.¹⁶⁹

Among drug hits identified using phenotypic-based approaches, which were optimized to lead compounds using medicinal chemistry approaches, are the spiroindolone NITD609¹⁷⁰ (**1.17**, Figure 1.10) and the imidazolopiperazine KAF156¹⁷¹ (**1.18**, Figure 1.9), further discussed below.

1.3.3.2 Hybrid Molecules

Another rational chemistry-based approach is the design of hybrid molecules that combine several chemical groups to provide stability, solubility and potency.¹⁷²⁻¹⁷⁴ A new generation of hybrid antimalarial drugs, instead of combined drugs, is being developed due to lower risk of drug-drug adverse interactions and greater treatment adherence. Thus, the design of antimalarials based on the covalent linking of drugs into a single hybrid molecule is a relatively new approach and the resulting molecule tends to be more effective than the isolated components. A series of hybrids containing drugs with different biological functions, distinct pharmacophores, reduced toxicity and improved activity (as compared to the isolated compounds) are being developed.^{122, 175} In addition, hybrid compounds have the potential to act against different life-cycle stages of malaria parasites, a required feature to facilitate the ultimate goal of eradicating malaria.¹⁷⁶

Since quinolines are considered to be privileged antimalarial building blocks, the synthesis of quinoline-containing antimalarial hybrids has been elaborated extensively in recent years. Four types of hybrid strategies using quinolines have been pursued, including coupling with well-known antimalarial drug, artemisinin or one of its derivatives, a synthetic peroxide, a synthetic reversal agent (chemosensitizers) or a new biologically active motif.^{172, 177-178}

The most successful story emerges from the extensive optimization of endoperoxide–aminoquinoline hybrids carried out by Meunier's group in partnership with Sanofi-Aventis, where trioxaquine—PA1103/SAR116242 (**1.19**, Figure 1.10) emerged from this optimization as the first antimalarial hybrid to reach clinical trials. This compound effectively displayed a

dual mechanism of action, being an important asset to face the highly adapting malaria parasites.¹⁷⁹

1.3.3.3 Modification of Existing Antimalarials

Another rational chemistry-based approach is to chemically modify existing antimalarials in order to overcome its drawbacks.¹²²⁻¹²³ Such an example is the class of the 4-aminoquinolines, where the alkylamine side chains allow for structural modifications, resulting in compounds that have different lipophilicity and drug-resistance profiles.^{70, 180} Among the CQ analogs that have been synthesized by linking 4,7-dichloroquinoline with monoalkynes and dialkynes, 12 compounds have demonstrated activity against *P. berghei* in mice, especially those with methylene groups in the side chain.¹⁸¹ Furthermore, ferroquine (**1.20**, Figure 1.10), a metallocenic CQ analog, that is considered to be the most advanced organometallic drug candidate, is in Phase II clinical trials for the treatment of uncomplicated malaria.¹⁸²

Other drug candidates currently in clinical trials, that were obtained by applying this rational chemistry-based approach include: ELQ-300¹⁸³ (**1.21**, Figure 1.10), which resulted from *in vivo* optimization of the avian antimalarial endochin; OZ439¹⁸⁴ (**1.22**, Figure 1.10), which resulted from *in vivo* optimization of 1,2,4-trioxolane arterolane; and P218⁸⁶ (**1.23**, Figure 1.10), which resulted from structure optimization of pyrimethamine.

Chapter 1 – Introduction

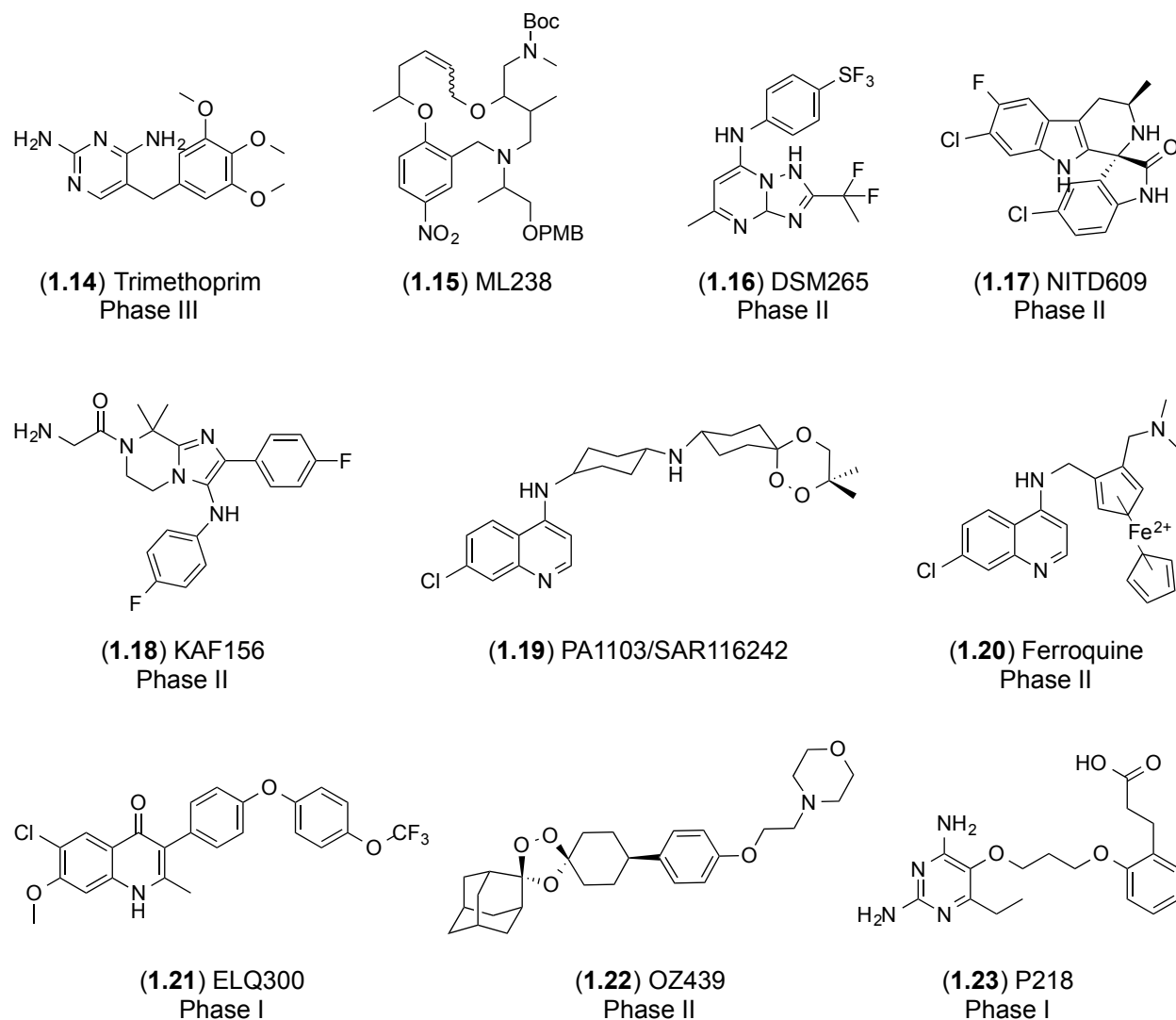


Figure 1.10 – Structure of some experimental antimalarial molecules.

1.4 New Drug Candidates

The past decade has seen a transformation of the portfolio of malaria medicines, with a dozen or so new chemical entities entering clinical development and breakthroughs in translational research. The phenotypic screens have proven to be very productive as many of the compounds identified have been successfully optimized and progressed to preclinical and clinical development. Nonetheless, target- and chemistry-based approaches have also yielded novel candidates currently under development.

Through a collaborative effort, among MMV, their partners and others, new molecules with novel modes of action are entering preclinical development and beyond (Figure 1.11).⁷⁹ The Global Malaria Portfolio can also be found at <http://www.mmv.org/interactive-rd-portfolio> and is updated on a quarterly basis.

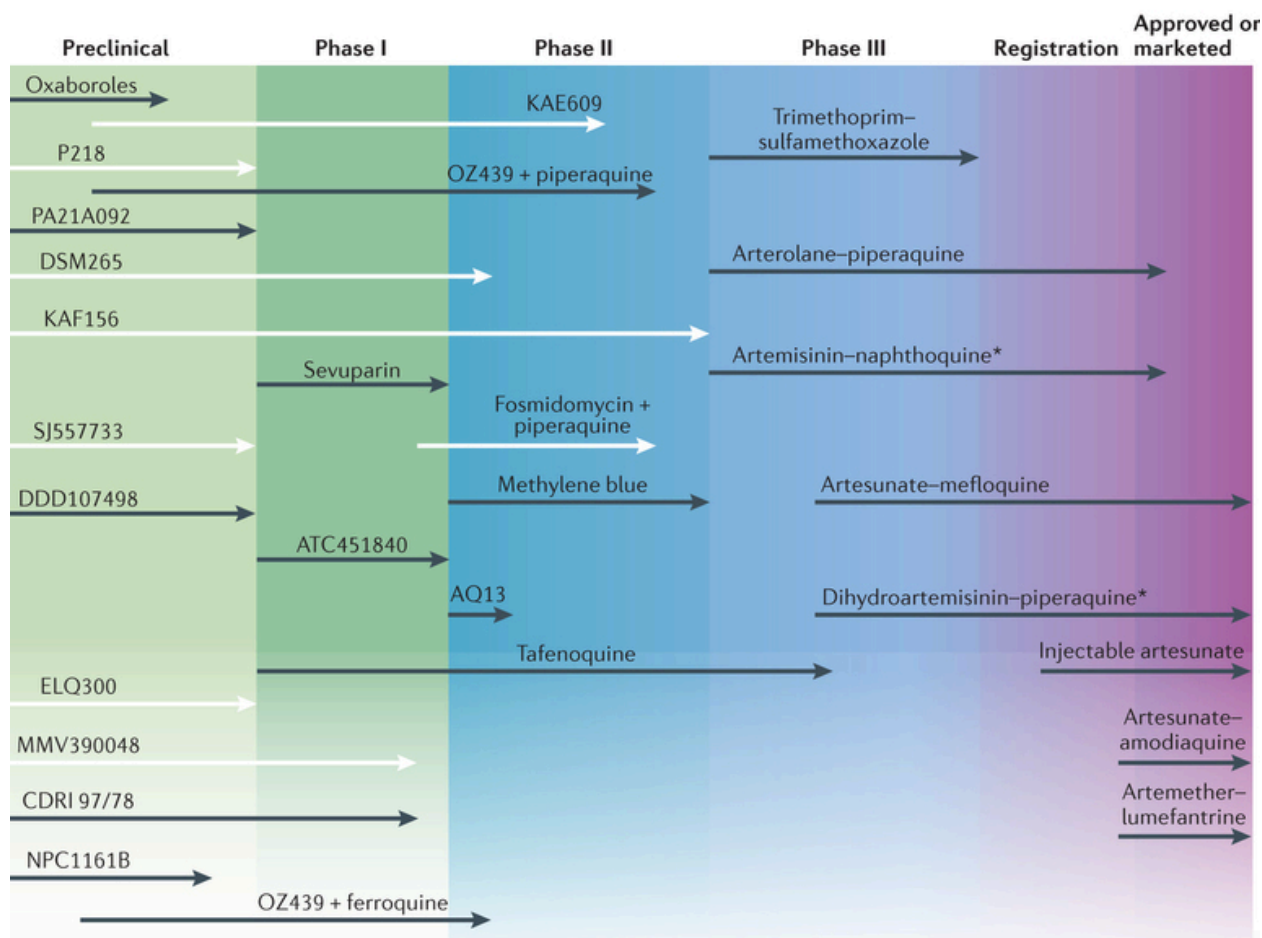


Figure 1.11 – Progression of the clinical development of new antimalarial candidates over the past 5 years. Adapted from Wells *et al.*⁷⁹ Drug candidates with white arrows have molecularly defined targets. Some molecules have been approved by disease-endemic countries and not by stringent regulatory authorities or prequalified by the WHO (World Health Organization), and these are indicated by asterisks. Phase II includes both Phase IIa (tests of compounds in patients as monotherapies) and Phase IIb (tests of compounds in patients as combination therapies).

Despite the relative abundance of projects at certain stages, taking into account the attrition between each phase and the need for combination medicines, it is clear that a sustained

delivery of high quality antimalarial preclinical candidates is still of the utmost importance.

Within the MMV portfolio, a selection of the new compounds, at different stages of development, is described below.

1.4.1 Quinolones

Antimalarial activity of 4(1H)-quinolones was first recognized in the 1940's when endochin (**1.24**, Figure 1.12) was identified as a causal prophylactic, killing growing liver stage parasites, and potent erythrocytic stage agent in avian malaria models. However, this inhibitor was not efficacious against malaria parasites of mammals.¹⁸⁵ Recently, several efforts have been made to develop new quinolones targeting the *P. falciparum* bc₁ complex, resulting in several compounds which display exceptional antimalarial activity.^{136, 183, 186-187} From these efforts, ELQ-300 (**1.21**), which contains a diarylether moiety and acts selectively against *Plasmodium falciparum* bc₁ complex, was identified.¹⁸³ This compound was designed based on the chemical structure of endochin (**1.24**) through replacement of its metabolic unstable alkyl chain by the side chain from the, well-known, bc₁ complex inhibitor GW844520 (**1.25**, Figure 1.12). This compound demonstrated improved metabolic stability when compared with endochin and increased selectivity ratio for *P. falciparum* bc₁ over the human homolog. Moreover, due its superior properties, this compound was selected for preclinical studies and is currently in Phase I clinical trials.^{79, 183, 188}

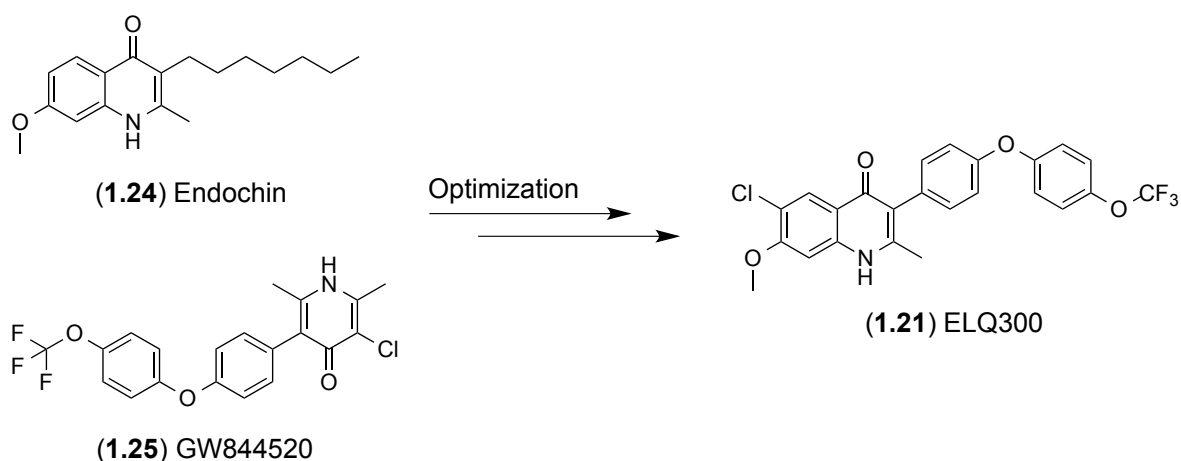


Figure 1.12 – Design of ELQ-300 (**1.21**) based on the structure of endochin (**1.24**) and GW844520 (**1.25**).

1.4.2 Pyrimethamines

Dihydrofolate reductase (DHFR) inhibitors such as pyrimethamine (**1.4**) have been widely used for the treatment of malaria, although widespread resistance has compromised clinical efficacy. P218 (**1.23**) is a next generation inhibitor of DHFR, it has largely finished preclinical development and is currently in Phase I clinical trials.^{79, 165} This compound was designed using structure-based methods to have a high affinity to both the parent and mutated enzymes and to also kill both wild type and clinically-relevant resistant strains. The challenge of sustaining activity across even quadruple-mutated enzymes was overcome by starting with the pyrimethamine scaffold and then using a flexible side-chain that could adopt a variety of conformations to achieve potency, which led to compound P65 (**1.26**). Further optimization found that a carboxylic acid was optimal for selective binding to a key protein arginine in the parasite but not in the human homolog, which led to compound P218 (Figure 1.13). This clinical candidate has a good pharmacokinetic profile, is selective and highly efficacious, as well as demonstrates a good safety margin.^{86, 189-190}

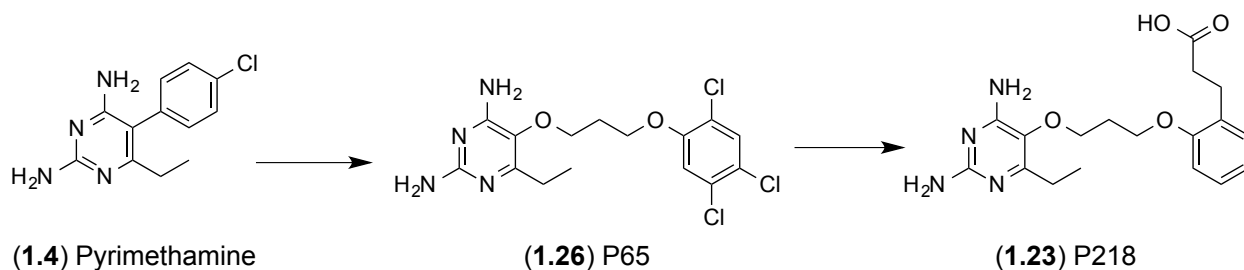


Figure 1.13 –P218: Pyrimethamine to Drug Candidate.

1.4.3 Ozonides

One of the best examples of the chemistry-based approach is the development of the synthetic ozonides. Given that artemisinin endoperoxides and their derivatives, such as artesunate, are the mainstay of current malaria chemotherapy, these endoperoxides have been attractive starting points for drug discovery efforts. Ozonides (which are synthetic peroxides) retain the endoperoxide bridge that gives artemisinin its potent blood-stage activity, but they also contain a bulky amantadine ring, which increases their stability in the plasma.^{21, 79} It has been proposed that their activity results from the peroxide bond being reduced by ferrous iron or

Chapter 1 – Introduction

heme, which are liberated through the digestion of hemoglobin by the parasite. This reduction produces carbon-centred radicals that alkylate heme and parasite proteins, which ultimately leads to parasite death.¹⁹¹

Vennerstrom and co-workers demonstrated that a stabilized ozonide, OZ03 (**1.27**), with a simple structure was sufficient to give excellent *in vitro* potency. To address the high lipophilicity and low solubility, polar and ionizable groups were introduced in the region of the molecule that was synthetically tractable, resulting in compound OZ277 (**1.28**) (arterolane), which was the first clinical candidate of this class (Figure 1.14).¹⁹¹⁻¹⁹² This first-generation ozonide is as potent as artesunate *in vitro* and has increased activity in the *P. berghei* mouse models, curing mice with three 10mg/kg oral doses.¹⁹¹ Nonetheless, OZ277 had lower exposure in patients than expected, therefore further optimization was required. To increase stability the amide was replaced by a phenyl ring with an ether-linked base, resulting in the newer generation synthetic ozonide OZ439 (**1.22**) (Figure 1.14).

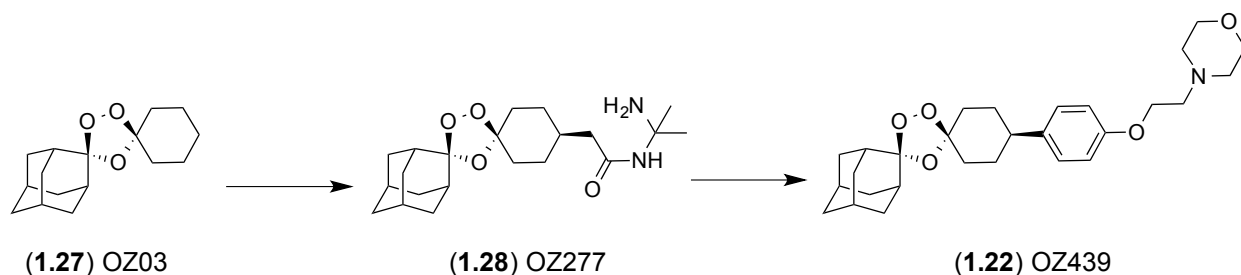


Figure 1.14 – OZ439: Hit to Drug Candidate.

OZ439 (also known as artefenomel) is potent and fast-acting, as well as being pharmacologically active for longer time and having improved bioavailability. The drug candidate is able to cure and to prevent *P. berghei* blood-stage mouse infections with a single 30 mg/kg dose and blocks transmission in the *in vitro* membrane feeding assay,^{184, 193} and has now progressed to Phase IIb combination studies, whereby it is being tested in combination with piperazine.⁷⁹

Despite the successful clinical development thus far, the ozonides, as with artemisinins, are mainly active against blood stages and, because their activity relies on the endoperoxide bridge present in artemisinins, they might be less effective against artemisinin-resistant parasites.

1.4.4 Spiroindolones

One of the first novel drug classes to be identified using modern phenotypic screening methods was the spiroindolones. The lead for this class, a racemic spiroazepineindole (**1.29**), was identified from a screen of natural products and “natural product like” compounds that were analysed for their activity against blood-stage *P. falciparum*. A medicinal chemistry approach was applied to contract the seven-membered ring, to define the stereochemical structure-activity relationship and to replace the lipophilic bromine atom (Compound **1.30**). Furthermore, to increase metabolic stability halogens were positioned on the tetrahydro-beta-carboline ring, resulting in the drug candidate KAE609, also known as NITD609 (**1.17**) (Figure 1.15). Compound **1.17** is being further developed by Novartis as part of the company’s efforts to contribute to global malaria elimination.^{3, 194}

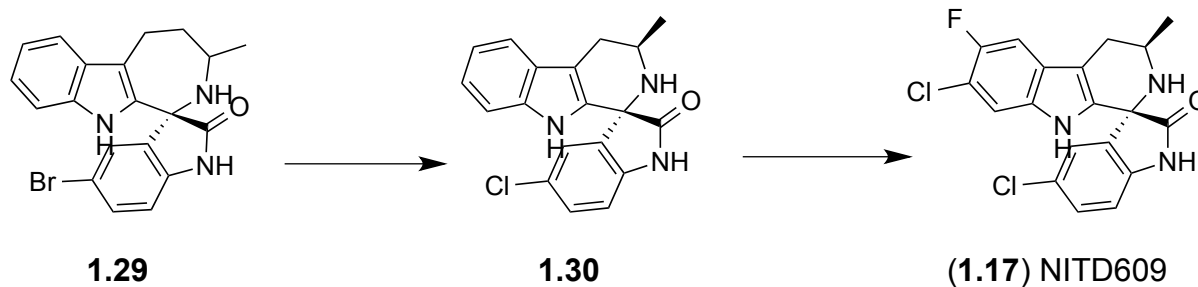


Figure 1.15 – NITD609: Hit to Drug Candidate.

In preclinical studies it displayed pharmacokinetic profiles consistent with once-daily oral dosing in humans. In the *P. berghei* malaria mouse model, the compound had a fast onset of action and potently reduced parasitaemia. No significant risks have been identified in safety pharmacological assays and the overall risk of resistance is viewed as moderate.¹⁹⁵ **1.17** underwent an open-label proof-of-concept (PoC) Phase II trial involving 21 patients with *P. falciparum* or *P. vivax* mono-infection. After treatment with 30 mg daily for three days, parasites were cleared in a median of 12 h, an effect that is more rapid than that observed with artemisinin-based combination therapies. In addition, in the five patients for whom gametocytaemia was detected at baseline (all with *P. vivax* malaria), it was cleared by 8 h post-dose, confirming the potent transmission-blocking potential of this novel class of compounds.¹⁹⁴ ¹⁹⁵ The spiroindolone class has a novel mechanism of action, which was identified using *in vitro* evolution and whole-genome scanning. This drug is believed to target the outer membrane

transporter, P-type ATPase 4 (*PfAtp4*), which is reported to be important for maintaining sodium homeostasis in the parasite.¹⁷⁰ Several preclinical and clinical studies are underway or planned to evaluate potential drug partners to enable combination therapy in the clinic.¹⁹⁵

1.4.5 Imidazolopiperazines

The imidazolopiperazine class of compounds was also discovered using modern phenotypic screen methods. The library was initially screened for asexual blood-stage activity, followed by liver stage activity. One hit that was identified in the screen was compound **1.31** (Figure 1.16). The mechanism of action is currently unknown, but drug resistance is mediated by the emergence of mutations in the cyclic amine resistance locus (*PfCarl*), which encodes a protein of unknown function and contains several transmembrane domains.^{3, 21, 194-195} In lead optimization, metabolically labile aromatic substituents were replaced and likely positions susceptible of metabolism were blocked with halogens, resulting in compound **1.32**. Further optimization, through metabolite identification and excellent medicinal chemistry then led to the isomer, whereby the metabolically susceptible position on the piperazine was blocked with two methyl groups, resulting in the drug candidate KAF156, also known as GNF156 (**1.18**) (Figure 1.16).

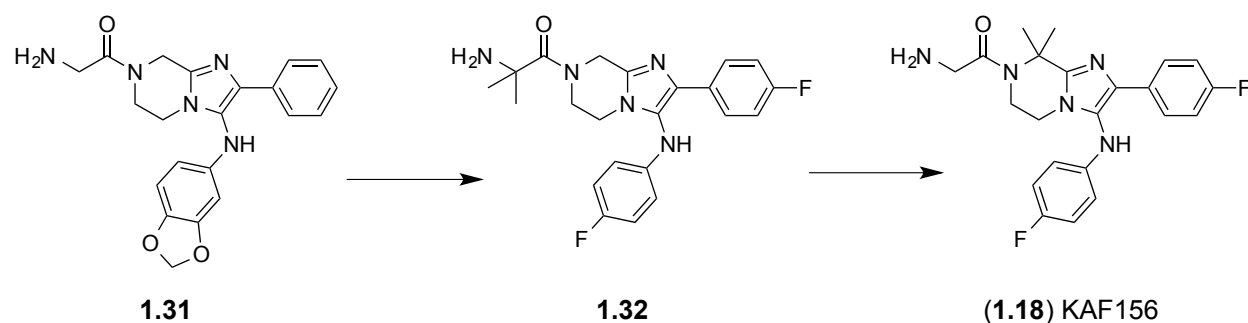


Figure 1.16 – NITD609: Hit to Drug Candidate.

KAF156 displayed potent parasitaemia reduction in blood-stage models (IC₅₀ of 6 to 17.4 nM against *P. falciparum* drug-sensitive and drug-resistant strains), as well as potent therapeutic activity in *P. berghei* mouse models of malaria with 99% effective doses of 1.4 mg/kg. This compound is slightly less potent than **1.17** but it provides prophylactic protection in animal

models and has activity against gametocytes, thus having the potential to prevent infection, treat acute disease, and reduce transmission.^{171, 194}

Following a strategy similar to **1.17**, a Phase I study in healthy adults has been completed for **1.18** and a Phase II PoC study in patients with uncomplicated *P. vivax* or *P. falciparum* infection is underway.¹⁹⁵⁻¹⁹⁶

1.4.6 Others Drug Candidates

MMV390048

Since the first high-throughput screens that used blood-stage parasites, several other screens have been implemented that focus on specialized compound libraries or parasite lines. A novel class of orally active antimalarial 3,5- diaryl-2-aminopyridines has been identified from a phenotypic whole cell high-throughput screening of a commercially available SoftFocus kinase library, led by the University of Cape Town, South Africa. Initial screening identified a aminopyridine hit (**1.33**), which was optimized by replacement of both the hydroxyl and methoxy groups on the phenyl ring, to produce an early lead compound (**1.34**). Upon refinement, it resulted in the drug candidate MMV390048 (**1.35**) (Figure 1.17).^{79, 197}

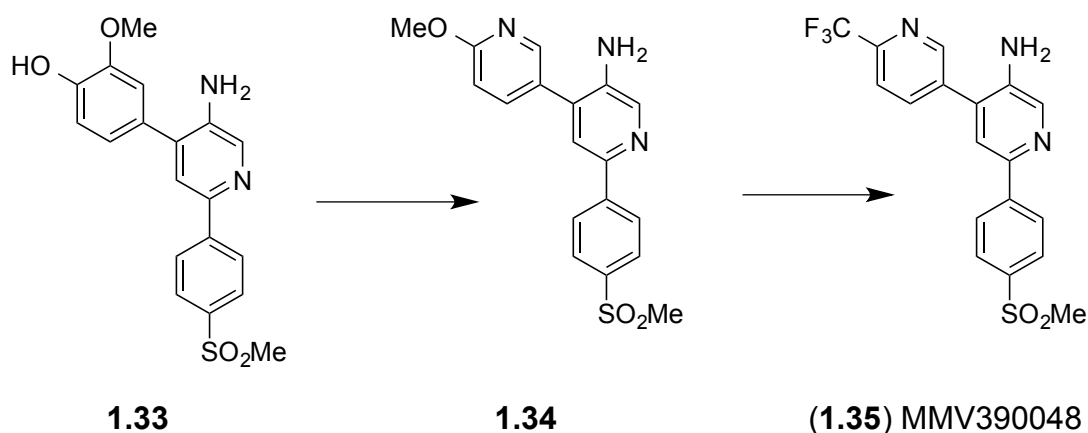


Figure 1.17 – MMV390048: Hit to Drug Candidate.

This drug candidate is equipotent against CQ-resistant and CQ-sensitive strains ($IC_{50} \approx 25$ nM), curing 100% of *P. berghei*-infected mice after a single 30 mg/kg dose. Pharmacokinetic studies indicated that this compound has good oral bioavailability (51% at 20 mg/kg) and a

reasonable half-life ($t_{1/2} \approx 7-8$ h).¹⁹⁷ While successfully completing the preclinical programme, the cellular target was identified to be the lipid phosphatidylinositol 4-kinase (*Pf*PI4K), and in 2014 MMV390048 began Phase I clinical trials.⁷⁹

DSM265

The target-based screening as a drug discovery approach towards lead compound identification has also resulted in new drug candidates. A good example of this process for malaria is the high-throughput enzyme screen against *Plasmodium* dihydroorotate dehydrogenase (DHODH). This mitochondrial enzyme has long been recognized as a potential antimalarial target because it catalyses the fourth step in the essential *de novo* pyrimidine biosynthesis pathway.¹⁹⁸

The triazolopyrimidines, a chemical class from the original screen, was shown to have potent activity in whole-cell assays (IC_{50} of 79 nM in *P. falciparum*) and >5000-fold specificity for parasite DHODH over human DHODH. However the hit compound DSM1 (**1.36**, Figure 1.18) was inactive in the *P. berghei in vivo* model and presented unfavorable pharmacokinetics.^{3,}

21

First, progress was made to improve pharmacokinetics by substituting electron-withdrawing groups in the aniline ring, since the binding site was hydrophobic in nature, resulting in compound **1.37**. After further chemical modifications and analysis of drug–enzyme co-crystal structures to optimize binding, the inhibitor DSM265 (**1.16**, Figure 18) emerged as a drug candidate. This compound has similar potency to chloroquine in the humanized SCID (severe combined immunodeficient) mouse *P. falciparum* model, and rodent pharmacokinetic studies demonstrated it has excellent oral bioavailability, a long half-life and low clearance.

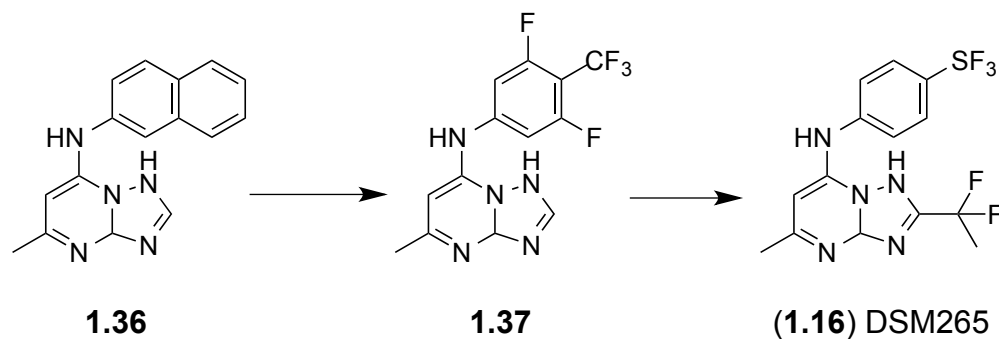


Figure 1.18 – DSM265: Hit to Drug Candidate.

DSM265 was tested in a challenge cohort only 7 months after the first-in-human (Phase I) study, which provided an early readout as to the efficacy and pharmacodynamics in patients. The drug candidate began Phase IIa monotherapy studies in 2015.⁷⁹

1.5 Target Identification and Validation

New antimalarials with a novel mode of action (MoA) are critical to combat the continued emergence and dissemination of drug-resistant parasites that threaten the efficacy of current malaria treatments. Thus, global efforts with increased number of high-throughput screening campaigns have been initiated, as discussed above. These have led to the unprecedented identification of thousands of new antimalarial compounds, which, inherently, have poorly defined modes of action.¹⁹⁹

Although drugs can be approved without a clear known target or MoA, the full characterization of the protein binding profile of a small molecule is an important prerequisite for a complete picture of the biology behind it. While some of the compounds may have recognizable targets, the majority of phenotypic-based hits are comprised of unique chemical scaffolds usually lacking cross-resistance with known drugs. These novel antimalarial scaffolds will most likely reveal new targets.¹⁹⁹⁻²⁰⁰

Target identification and validation for small molecules is often the rate limiting step in drug discovery, and knowledge of the MoA and the molecular target(s) could help guide the development of backup compounds, as well as help researchers monitor patients for the emergence of drug-resistant parasites.²⁰⁰

A variety of methods and technologies for identifying target proteins of bioactive compounds have been reported. Target candidates can emerge by profiling the biological data of the compounds, using connectivity maps. On the other hand by using techniques such as affinity chromatography, biochemical fractionation and radioactive ligand binding assays, one can directly identify the interaction partners of the compound.²⁰⁰⁻²⁰¹ Efforts to identify the MoA for antimalarials have traditionally been met with ambiguous results.

1.5.1 Target Identification

1.5.1.1 *In silico* Assignment of Mechanism of Action

One way to establish a compound's MoA is by comparing its chemical scaffold to the

scaffolds of compounds with a known drug target. If a scaffold is more than 95% identical to a known drug it is likely to bind to the same target. A disadvantage of this method is that two very dissimilar scaffolds, which only share a small pharmacophore critical to drug target specificity, may not be recognized due to the scoring function.¹⁹⁹ Using this approach GlaxoSmithKline analyzed data from pre-existing biochemical assays for each chemotype resulting in 31% of the cell-active hit collection being assigned to human or microbial targets with orthologs in *Plasmodium*.⁶ Using chemical similarity between structures, a probable MoA can only be assigned to a minority of the compounds.

1.5.1.2 Stage of Action

Due to the stage specificity of some antimalarial compounds, analysing the morphology of drug-treated parasites can provide preliminary clues to the MoA. Giemsa-stained thin blood smears of synchronized intraerythrocytic stage parasites subjected to drug concentrations at or above the 90% inhibitory concentration are sufficient to determine the stage of action.¹⁹⁹ For example, Wilson *et al.*, aimed to more precisely define the timing of action of antimalarial agents, particularly those with a history of clinical use, by determining the inhibitory effects of these drugs on merozoite invasion, schizont rupture, and intraerythrocytic development.²⁰²

1.5.1.3 *In vitro* Evolution of Drug-resistant *P. falciparum* Strains

The whole genome sequences for the different *Plasmodium* species have been resolved and provide blueprints for exploitation, revealing multiple potential target candidates. Thus, classical genetic approaches have been scaled to a genomic level and together these approaches can close major gaps in knowledge, providing insights into drug transport and metabolism, facilitating drug target prioritization, as well as target validation and deconvolution.²⁰³

A powerful approach that has been employed with great success involves the *in vitro* selection of resistant mutants using small molecule inhibitors. Once resistance has been acquired, the resultant parasite clones are analyzed to identify novel genetic changes relative to the parental genome sequence that could be associated with drug-resistance. Mutations conferring resistance are revealed using genome scanning with either high-density tiling DNA microarray or with whole genome sequencing, and will often directly reveal the drug target.^{199, 203} The technique of evolving drug-resistant *P. falciparum* parasites *in vitro* has been well established

and has been successfully used to determine drug targets since the advent of high-density microarrays, to reveal newly emerged single nucleotide polymorphisms and copy number variations.²⁰⁴ A software analysis platform to compare the DNA microarray hybridization differences between a parental drug-sensitive and a drug-resistant clone has been developed, making genomic analysis user friendly, resulting in the identification of novel drug targets.¹⁹⁹

Plasmodium often acquires mutations in the drug target as a means of combating drug toxicity, so this method can be very powerful for target identification, as seen with the spiroindolones¹⁷⁰, cladosporin²⁰⁵ and febrifugine derivatives.^{7, 206}

There are several examples of where this systematic strategy has yielded the discovery of novel antimalarial targets, including the spiroindolone, NITD609 (**1.17**), the derivative of a natural product-like molecule, discovered in a phenotypic-based screen, as mentioned in the above section.¹⁷⁰ After 4 months of *in vitro* selection, the IC₅₀ values of NITD609 increased ~10X. Genomic analysis with the *P. falciparum* tiling array identified several hybridization differences, most of which were found in a single gene (*PfATP4*) and the rest being mostly in randomly assorted sub-telomeric or intergenic regions. Further inspection of the hybridization patterns also showed that one strain carried copy number variants (CNV) that surrounded the gene encoding for a cation-transporting P-type ATPase (*PfATP4*).²⁰⁷⁻²⁰⁹ Transgenic parasites were created that showed that only mutations in *PfATP4* conferred resistance.¹⁷⁰ Recent functional data also indicates that *PfATP4* is a sodium pump and is the likely target of the spiroindolones.²¹⁰ The likely target of cladosporin, a natural compound that was subsequently found to inhibit lysyl-tRNA synthetase was also identified using this approach. In the case of cladosporin, all three resistant lines harbored CNVs surrounding the *P. falciparum* lysyl-tRNA synthetase gene.²⁰⁵

Our group has identified the long sought biochemical target of febrifugine, the active ingredient of a traditional Chinese herbal remedy for malaria, by using this target identification approach. Moreover, we used an integrated chemogenomics approach that combined drug resistance selection and whole-genome sequencing, and demonstrated that the cytoplasmic prolyl-tRNA (transfer RNA) synthetase (*PfcPRS*) of the malaria parasite *P. falciparum* is a biochemical and functional target of febrifugine and its synthetic derivative halofuginone. The only gene with nonsynonymous single-nucleotide polymorphisms (SNPs) identified in both resistant lines was annotated as a putative cytoplasmic proline aminoacyl-tRNA synthetase that

resembled the *P. falciparum* PRS.⁷

Using this technique the detected changes in the genome of the drug-resistant parasites should directly reveal the mechanism of resistance. However, mutations unrelated to resistance might also emerge spontaneously, thus independent cultures are evolved in triplicate to determine which changes are significant.¹⁹⁹ A practical concern is that nearly 50% of the *Plasmodium* genome remains unannotated, thus using orthologs is an alternative to study and characterize the gene product in follow-up biochemical or biological assay systems. For example, *Plasmodium* proteins with a yeast ortholog can be introduced on a complementation vector into a yeast background engineered to abolish ortholog expression under nonpermissive conditions.^{7, 211} An additional factor that makes identifying molecular targets in *Plasmodium* complicated is that RNAi does not work since the enzyme necessary to degrade the dsRNA is lacking.¹⁹⁹

Other approaches have also been used to match the genetic change to a certain phenotype, such as genome-wide association studies and perturbation of gene expression.²⁰³ Due to the limitation factors referenced above, additional techniques to validate the mechanism of action have been employed.

1.5.2 Target Validation

Target identification is always followed by validation to eliminate false-positive target candidates. Diverse validation assays establish the biological relevance of the small molecule and its target protein.²¹²

1.5.2.1 Bioassays

The most straightforward experiment is to directly assay the gene product responsible for its inhibitory activity, however this is contingent on successful heterologous expression of that gene and development of an assay to detect inhibition, which in some cases is challenging. An alternative approach is to use transgenic models to do the bioassay. Some examples include using yeast complementation, orthologs in related organisms and transgenic *P. falciparum* strains.¹⁹⁹ This approach has been used to further validate the cytoplasmic prolyl-tRNA synthetase (*Pfc*PRS) of the malaria parasite *P. falciparum* as the functional target of febrifugine and its synthetic derivative halofuginone. Our group used an orthogonal yeast transgenic system,

which showed that treatment with febrifugine derivatives activated the amino acid starvation response in both *P. falciparum* and a transgenic yeast strain expressing *PfcPRS*. Thus, results validated that *PfcPRS* is the functional target of febrifugine and halofuginone.⁷ Another example of successful target validation using this method is the cladosporin. The interaction between lysyl-tRNA synthetase and cladosporin was also validated using this approach, by using a model organism, the yeast *Saccharomyces cerevisiae*. Here, precise removal of one copy of the yeast lysyl-tRNA synthetase in a diploid strain resulted in an increase in sensitivity to the compound.²⁰⁵

1.5.2.2 '-omics' Techniques

Advances in the '-omics' techniques that have emerged and have been developed over the years have promoted new drug discovery strategies based on assays with increased content and better appreciation of the molecular context in which protein targets operate. These methodologies are providing complementary approaches to drug target identification and validation.²¹²⁻²¹⁴

Metabolomics

Metabolomics-based studies are proving of great utility in the analysis of modes of action and resistance mechanisms of drugs in parasitic protozoa. Metabolic labeling has traditionally consisted in the incorporation of radiolabeled cysteine and/or methionine to monitor protein synthesis, while nucleic acid synthesis can be investigated using radiolabeled hypoxanthine. An increased repertoire of labeled metabolites, as well as advances in mass spectrometry have improved the analysis of endogenous metabolites, which allows the identification of original pathways and networks of regulatory interactions within the parasite. Metabolic assays can be extended to comparative studies to evaluate incorporation differences between untreated and drug-treated parasites. Furthermore, the utilization of targeted metabolomics techniques has enabled validation of existing hypotheses regarding antiprotozoal drug mechanisms.²¹⁵⁻²¹⁸

Thus, the continued advances in metabolic labeling methodologies are best exemplified by studies elucidating mechanistic details in *P. falciparum*. Bulusu *et al.* utilized the purine salvage pathway for both radiolabel uptake studies and ¹³C-nuclear magnetic resonance spectroscopy to follow the conversion of fumarate, a product of tricarboxylic acid metabolism, to

aspartate, which led to the identification of functional roles for fumarate hydratase, malate quinone oxidoreductase and aspartate aminotransferase, in fumarate conversion. Furthermore, in this study they also utilized atovaquone as a chemical tool to demonstrate that the electron transport chain was linked to fumarate conversion.²¹⁹ A second study using metabolomics aimed to validate glutamate dehydrogenase as a drug target by an untargeted LC-MS approach. Thus, heavy atom–labeled glutamine tracking was used to show that there is no difference in the labeling of the tricarboxylic acid cycle intermediates after knock out of this gene, nor is there an increased sensitivity to oxidative stresses, which lead to the conclusion that, contrary to previous suggestions, glutamate dehydrogenase is not suitable as a drug target.²²⁰

Proteomics

Proteomics enables the study of native proteins in cell extracts or cell fractions, under conditions carefully optimized to preserve protein integrity, folding, post-translational modifications, and interactions with regulatory proteins. The global proteomic strategies involve drug treatment of cells or animals followed by whole-cell or organ-wide proteome analysis and are attractive because of the unbiased nature of the analysis.^{214, 221} There are a handful of proteomic studies to determine MoA for antimalarials in *P. falciparum*.¹⁹⁹ Prieto *et al.* investigated the differential expression of proteins treated with ART or CQ using mass spectrometry and, found 41 and 38 uniquely upregulated proteins, respectively.²²²⁻²²³ In another effort to employ this technique, a 2D electrophoresis and tandem mass spectrometry identification study was performed by Radfar *et al.* that established that CQ treatment of parasites results in the oxidation of proteins involved in protein folding, proteolysis, energy metabolism, signal transduction and pathogenesis.²²⁴ In both cases, the results obtained suggest that specific drugs may produce a ‘fingerprint’ of uniquely deregulated protein expression.

1.5.2.3 Fluorescent Probes

The challenges of discovering a compound’s MoA and subsequent validation of the macromolecular target have driven innovative approaches, such as the use of a nonperturbing chemical handle within the incorporated biomolecule, which allows for selective attachment of a fluorophore or affinity tag. For example, small molecules with fluorescence can be used as probes for localization and detection markers, thus treatment of cells with fluorophore-linked

drug can be used to assess co-localization with organelle markers using fluorescent imaging.^{212, 225} Furthermore, without methods to confirm that chemical probes reach and selectively engage their protein targets, in living systems, it is difficult to attribute pharmacological effects to perturbation of the protein(s) of interest versus other mechanisms. Additionally, most drugs will bind to more than one target (polypharmacology), and therefore, measuring cellular pharmacology requires the use and development of new technologies, ideally those that can be applied *in vivo*.^{221, 226} To follow the drug's distribution at the cellular level, fluorescently labeled drugs have been developed, which will maintain comparable specificity and affinity for the unlabeled drug target. When used in combination with confocal or two-photon fluorescence microscopy, fluorescent analogs provide high spatial and temporal resolution maps of the drug.²²⁶⁻²²⁷ In the literature, fluorescent derivatives of small molecules and drugs have been employed as probes to identify their subcellular localizations and further elucidate on MoA. There have been only a handful of fluorescently labeled antimalarials reported in the literature. Most of which are fluorescent artemisinin compounds used in the antimalarial mechanistic studies.^{100, 228-230} Liu *et al.*, synthesized a cytotoxic artemisinin compound conjugated with a fluorescent dansyl moiety and accessed its subcellular localization in Hep3B cells. Colocalization by organelle specific dyes revealed that endoplasmic reticulum (ER) was the main site of its accumulation.²²⁹ Furthermore, very recently an additional fluorescently labeled antimalarial was reported in the literature. The fluorescent chloroquine-BODIPY used as a proxy for chloroquine accumulation. This compound localized to the food vacuole of the parasite, as observed under confocal microscopy, and inhibited growth of chloroquine-sensitive strain 3D7 more extensively than in the resistant strains, and it is being used as a marker for chloroquine resistance and uptake in a 96-well plate assay.²³¹

One of the biggest challenges in pharmaceutical research and development is to reduce phase II attrition rates. The identification of target protein candidates provides the first clue to the signaling mechanism modulated by the small molecule. Furthermore, a network analysis of target protein candidates provides additional insight into the small molecule's bioactivity, connecting related signal pathways and the endpoint phenotype. The last step in the discovery process is validation of target proteins to eliminate false-positive candidates. As noted above, validation assays may take a variety of forms, but must establish the biological relevance of the small molecule and its target proteins to aid in the development of an effective therapeutic drug.

Chapter Two

2. Indole-based Antimalarials

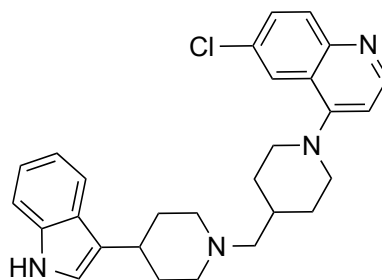
2.1 Introduction

The *Plasmodium* parasite has demonstrated an ability to evolve and adapt to every drug introduced thus far, and with this in mind, it is crucial that efforts are made to develop new analogs active against resistant strains, to identify new drugs, or even identify new therapeutic targets in the parasite²⁻³. The strategies currently used for the development of novel antimalarial drugs, as well as the current efforts to address this issue have been reviewed above.

GlaxoSmithKline (GSK) published the Tres Cantos Antimalarial Set, which resulted from the screening of the in-house chemical library of almost 2 million compounds against asexual blood stage *P. falciparum*. Setting the threshold for growth inhibition to greater than 80%, at a concentration cut-off of 2 micromolar, the authors identified more than 13,500 active compounds, 8,000 of these being equally active against multi-drug-resistant *P. falciparum* parasites. This fast-track filtering process identified many high-quality starting points for lead optimization efforts.⁶ Analyses using historic assay data suggested novel mechanisms of antimalarial action for these compounds, such as inhibition of protein kinases and host–pathogen interaction related targets.⁶ Furthermore, an agglomerative structural clustering technique followed by computational filters such as antimalarial activity, physicochemical properties, and dissimilarity to known antimalarial structures, was used and identified 47 clusters for lead optimization, among which was an indole-based series.¹⁶³

The main characteristics that the selected starting points should ideally possess are (a) the scaffold (chemotype) should be structurally different to known antimalarial scaffolds as various parasite strains are resistance to many of these drugs; (b) high tractability to facilitate rapid lead optimizations programs; (c) physicochemical profiles that are compatible with good oral absorption and reasonable aqueous solubility; (d) no known toxicity issues; (e) drug-like functionality; (f) no known intellectual property issues; and (g) moderate to good antimalarial activity.^{163, 232} Further studies identified compounds from the GSK collection that are capable of escaping drug resistance, have polypharmacology profiles that cover multiple essential targets and perturb different points of the parasite's metabolic network.²³³

Joining the international efforts, we analyzed the disclosed Tres Cantos Antimalarial Set (TCAMS) to identify novel indole-based antimalarials as starting points for the development of a possible next-generation antimalarial drugs. Indoles are an emerging antimalarial fragment present in several lead drug candidates with new mechanisms of action, such as the spiroindolone^{170, 234-237} and aminoindole classes.^{236, 238} We were intrigued by TCMDC-134281 (**2.1**, Figure 2.1), which emerged as a very potent antimalarial compound, with a reported EC₅₀ of 34 nM against the chloroquine-sensitive *P. falciparum* 3D7 strain.



(**2.1**) TCMDC-134281

Figure 2.1 – Structure of the hit compound TCMDC-134281.

Additionally, the compound did not demonstrate significant cytotoxicity, as its EC₅₀ against the human HepG2 hepatoma cell line was greater than 10 μ M. Moreover, this analog did not have a predicted target in the *P. falciparum*, in spite of being annotated as a possible adrenergic receptor antagonist in mammalian cells.⁶ Nonetheless, this compound showed poor drug-like properties and cross-resistance with chloroquine, possibly due to the presence of the 4-aminoquinolinyl fragment, which is the essential pharmacophore of CQ.

2.2 Purpose of This Study

This project is designed to explore the antimalarial potential of the 3-piperidin-4-yl-1H-indole scaffold (Figure 2.2). To address the liabilities aforementioned, we decided to remove one of the piperidin-4-yl fragments and to replace the 4-aminoquinoline fragment. This resulted in an overall reduction of the compound's LogP and MW and chemically differentiates the molecule from the 4-aminoquinoline antimalarials, which we hypothesized would overcome the observed cross-resistance with CQ.

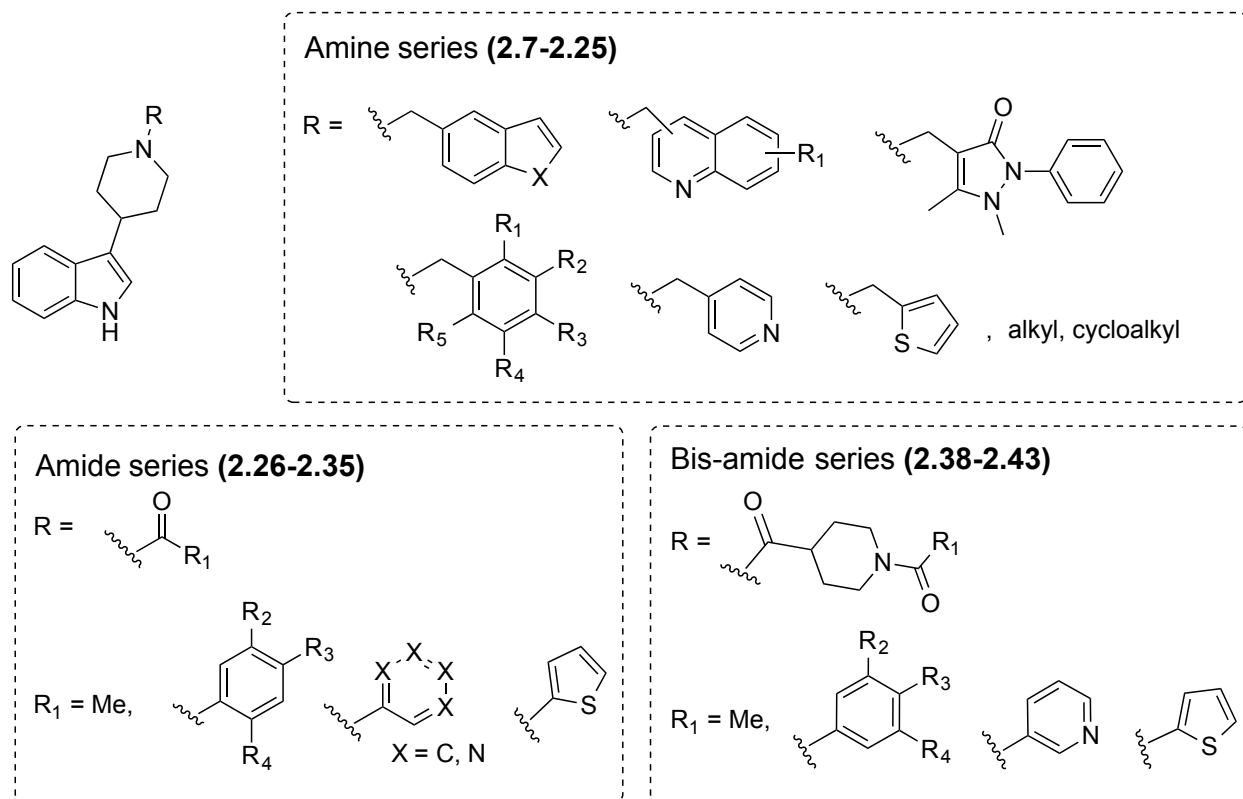


Figure 2.2 – Structures of the explored indole-based scaffold.

We synthesized three series of derivatives following a reagent-based diversity approach, in a total of 38 compounds, and assayed them against the multidrug resistant *P. falciparum* Dd2 strain at a fixed 5 μ M concentration. The most potent derivatives were further profiled in dose-response against both *P. falciparum* drug-resistant (Dd2) and sensitive (3D7) strains to determine activity and parasite selectivity. (Work done at the Harvard School of Public Health together with the help of Dr. Amanda Lukens)

2.3 Synthetic Methodology

2.3.1 Chemical Synthesis Strategy

The retrosynthetic analysis of the three series of derivatives shows a key intermediate A that can be prepared by condensation of the indole with 4-piperidone in the presence of a base and subsequent reduction under hydrogenation conditions. The 4-piperidone used must be protected in order to increase condensation yields. Both the amine and amide series can be prepared directly from the key intermediate A. The bis-amide series is obtained by conversion of

the key intermediate A into the intermediate B, through coupling with 1-(*tert*-butoxycarbonyl)piperidine-4-carboxylic acid followed by amine deprotection (Figure 2.3)

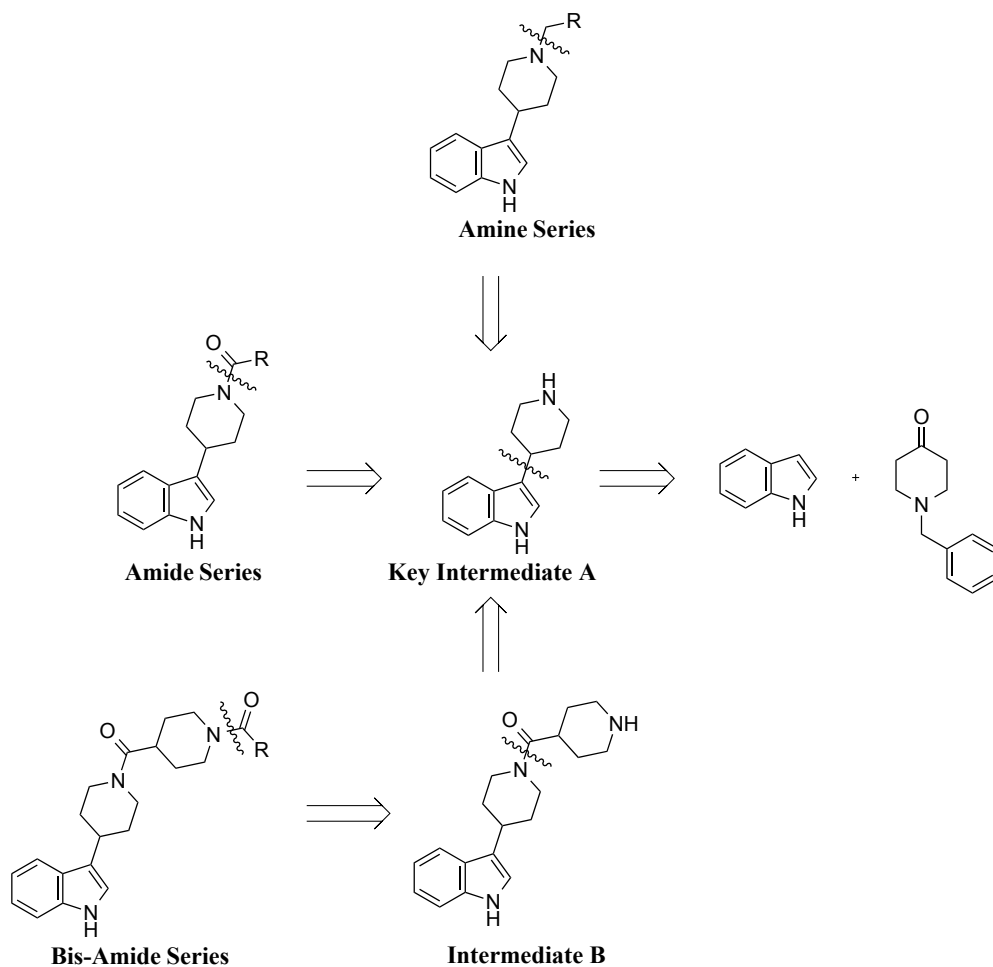
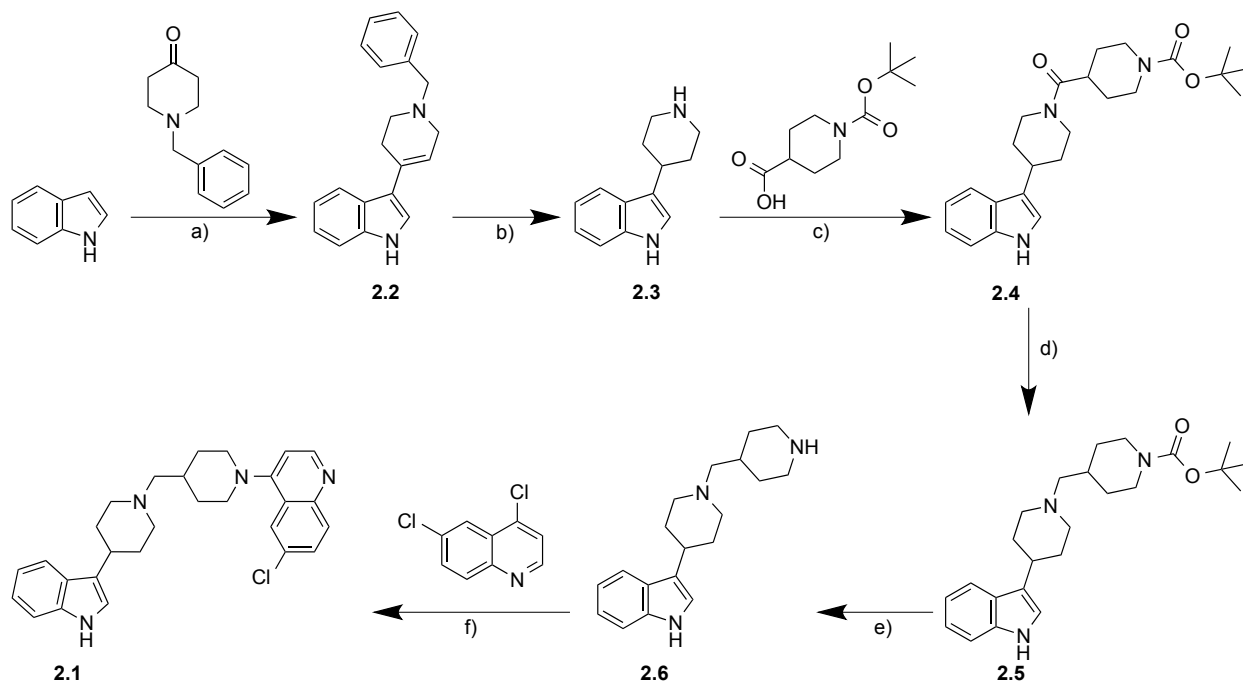


Figure 2.3 – Retrosynthetic analysis of compounds from the amine, amide and bis-amide series.

All synthesized compounds were purified by flash chromatography and the purity was assessed with HPLC-ELSD-MS prior to profiling for antiparasitic activity (purity was >90%). The structures of all compounds were confirmed by NMR spectroscopy using $^1\text{H-NMR}$, $^{13}\text{C-NMR}$ and two-dimensional experiments, including $^1\text{H-}^1\text{H}$ COSY, HMQC and HMBC (see details in Experimental).

2.3.2 Synthesis of Hit Compound

We first resynthesized the original hit compound **2.1**, following a six-step synthesis, as shown in scheme 2.1. Starting with the condensation of the indole with *N*-benzyl-4-piperidone in the presence of a base, compound **2.2** was obtained in high yield (98%). Subsequent debenzylation with concurrent olefin reduction afforded the common intermediate 3-piperidin-4-yl-1*H*-indole (**2.3**) with 96% yield.



Scheme 2.1 – Reagents and conditions: **a)** KOH, isopropanol, reflux, 6 h, 98%; **b)** 10% Pd/C, 10% glacial acetic acid in ethyl acetate, H₂, 48 h, r.t., 96%; **c)** DCC, HOBt, CH₃CN, 2 h, r.t., 60%; **d)** DIBAL, THF, 1 h, -78 °C, 35%; **e)** 2 M HCl/MeOH, 20 min, r.t., 99%; **f)** DIPEA, isopropanol, 56 h, reflux, 15%.

The attribution of the ¹H and ¹³C NMR of key intermediate **2.3** is shown in Figure 2.4. The results are in accordance with the chemical structure of the compound (Chapter 6) and the analysis of the NMR spectra confirms the formation of the desired product through the presence of five aromatic protons from the indole and nine aliphatic protons from the piperidine group. The ¹H NMR coupling pattern of **2.3**, shows two *d*, two *ddd* and one *s* signal between 7.60 ppm and 7.01 ppm, which corresponds to the signals of the indole. Next, the aliphatic region of the spectra shows one *dt*, two *m* and one *d* signals corresponding to the signals of the piperidine H.

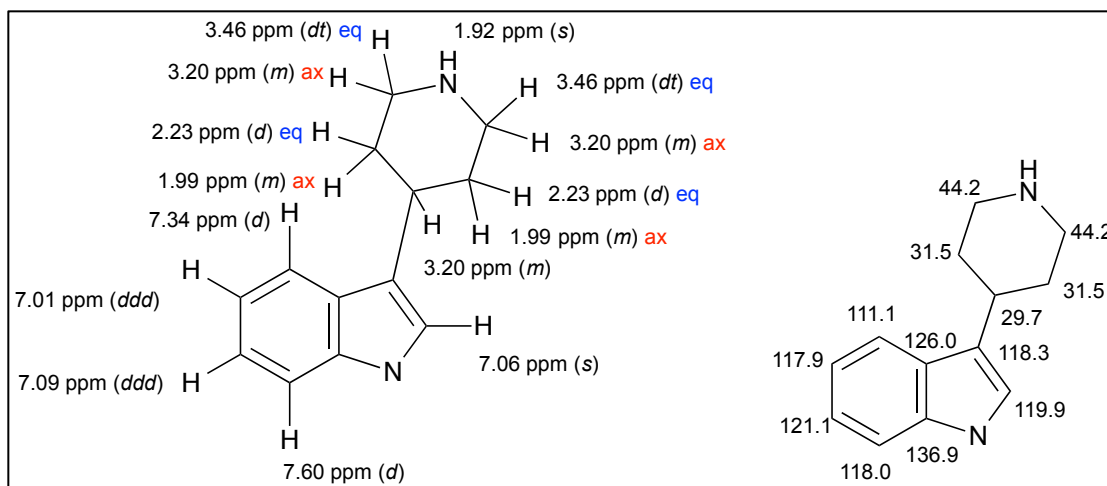


Figure 2.4 – Assignment of ^1H and ^{13}C NMR of key intermediate **2.3**.

Next, compound **2.3** was coupled with 1-(*tert*-butoxycarbonyl)piperidine-4-carboxylic acid to give the amide intermediate **2.4** in moderate yield (60%). Reduction of the carbonyl group afforded compound **2.5**, followed by Boc-deprotection to yield the amine compound **2.6**. Compound **2.1** was obtained by nucleophilic aromatic substitution of 4,6-dichloroquinoline with the amine intermediate **2.6** (Scheme 2.1). The product of the reaction was characterized by NMR spectroscopy and LC/MS. Results are in agreement with the compounds structure (Chapter 6).

The analysis of the NMR spectra, reveals the presence of five additional aromatic signals when compared to intermediate **2.3**, which is consistent with the presence of the quinoline group. Furthermore, in the aliphatic region, additional signals corresponding to nine protons, as well as, one doublet with a chemical shift of 2.11 ppm, integrating to two protons, corroborates the presence of the methylpiperidinyl group (Figure 2.5).

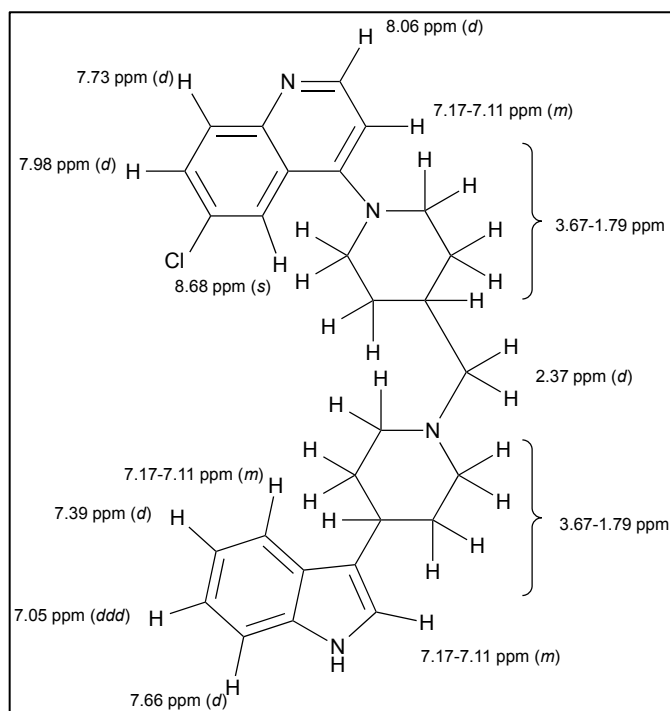


Figure 2.5 – Assignment of ¹H NMR of hit compound **2.1**.

2.3.3 Synthesis of Amine Library

The first series of derivatives was designed to explore the structure-activity relationships (SAR) of *N*-piperidinyl modifications. These compounds were obtained by reductive amination²³⁹ of the corresponding aldehydes with the amine intermediate **2.3** to give the title compounds **2.7-2.25** (Scheme 2.2), with yields ranging from 25%-100% (Table 2.2) and overall yield ranging from 24%-96% (Table 6.1 in the materials and methods chapter). All but two derivatives from this series were obtained using commercially available aldehydes. Aldehydes **A** and **B**, used in the synthesis of compounds **2.21** and **2.20**, were previously obtained by reductive amination of terephthalaldehyde with piperidine or morpholine, respectively (Scheme 2.2).

All the amine derivatives were characterized by NMR techniques and LC/MS (Chapter 6). The results are in good agreement with the chemical structure of the compounds. For instance, the attribution of ¹H and ¹³C NMR chemical shifts for **2.11** is shown in Figure 2.6.

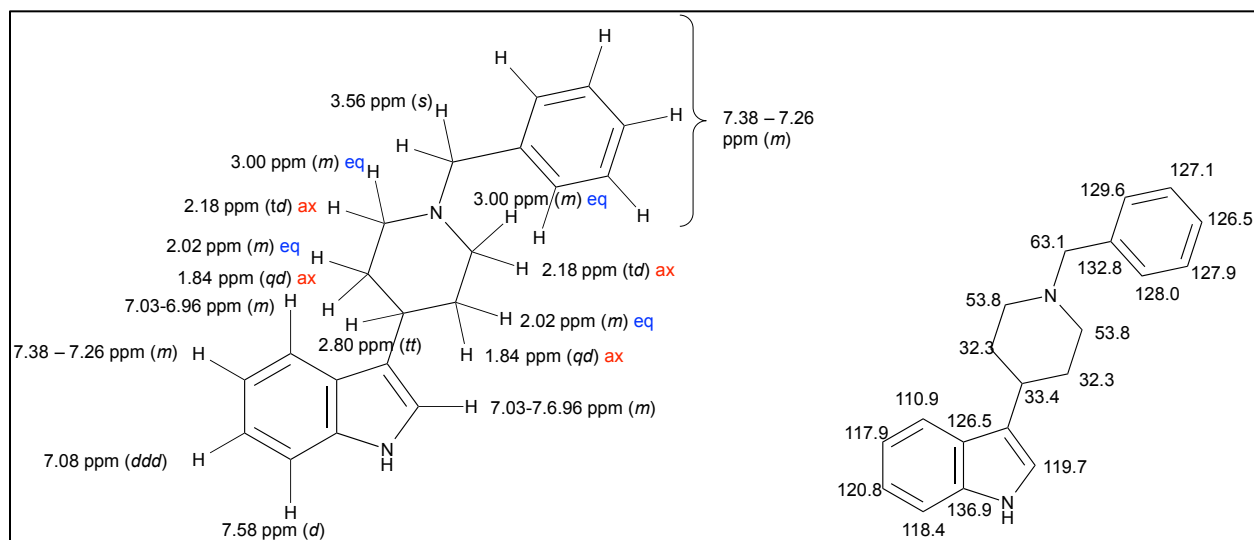
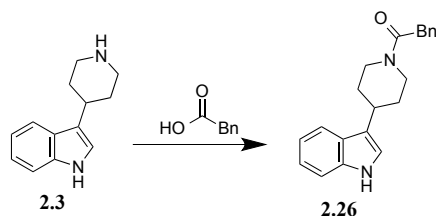


Figure 2.6 – Assignment of ^1H and ^{13}C NMR of amine compound **2.11**.

The product of the reaction between key intermediate **2.3** and benzaldehyde resulted in desired product **2.11**. The assignment of the NMR spectra reveals the presence of five additional aromatic protons, consistent with the presence of the new benzyl group. Furthermore, in the aliphatic region one additional signal integrating to two protons, with a chemical shift of 3.56 ppm, corroborates the presence of the newly formed bond.

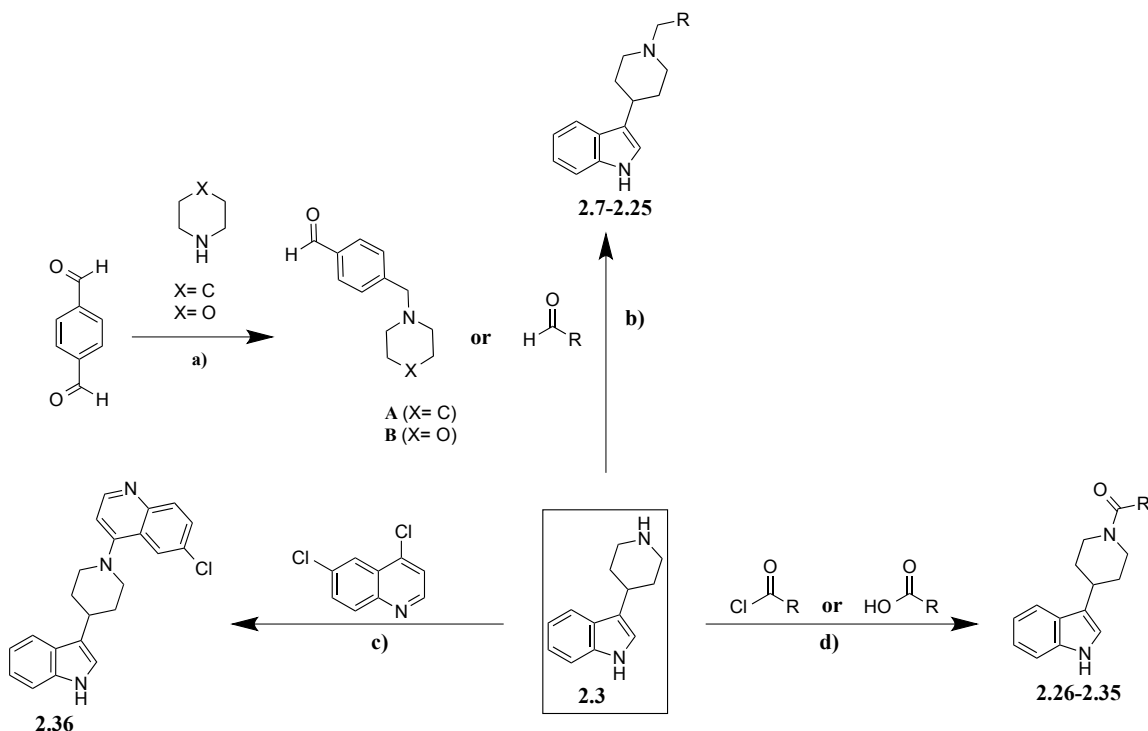
2.3.4 Synthesis of Amide Library

We next synthesized a series of amide derivatives to assess the importance of the basic amine versus an amide linkage and resulting rotational hindrance. These compounds were synthesized by coupling the amine intermediate **2.3** with commercially available acid chlorides under standard Schotten Baumann conditions to afford the desired compounds **2.26-2.35** (Scheme 2.2), in 25% to quantitative (Quant.) yields (Table 2.2) and overall yield ranging from 24%-96% (Table 6.1 in the materials and methods chapter). To access the derivatives **2.32-2.35** (Scheme 2.2) in high yields we screened several coupling reagents and found PyBOP to give the best results (Table 2.1).

Table 2.1 – Optimization of coupling conditions between intermediate **2.3** and carboxylic acids.

Entry	Coupling Reagent	Conversion
1	PyBOP/DIPEA	High
2	HOBt/EDC	Moderate
3	DCC/DMAP	Moderate

Conditions: DCM or DMF, 0.5-1 h, r.t.



Scheme 2.2 – R fragments and yields are given in Table 2.2; Reagents and conditions: **a)** NaBH(OAc)₃, DCE, 1 h, r.t., 58%-70%; **b)** NaBH(OAc)₃, DCE, 4 h, r.t. or NaBH₃CN, MeOH, Microwave at 100 °C, 20 min; **c)** DIPEA, isopropanol, 56 h, reflux, 25%; **d)** DCM, aq. NaHCO₃, 10 min, r.t. or DIPEA, DCM, 30 min, r.t. or PyBOP, DIPEA, DCM, 0.5-1 h, r.t.

Chapter 2 – Indole-based Antimalarials

Compound **2.35**, which consisted of two amide units linked by a benzyl group, was synthesized by reacting excess of the amine intermediate **2.3** with terephthalic acid using PyBOP coupling conditions, with quantitative yield (Scheme 2.2; Table 2.2).

All the amide derivatives were characterized by NMR techniques and LC/MS (Chapter 6). The results are in good agreement with the chemical structure of the compounds. For instance, the attribution of ^1H and ^{13}C NMR chemical shifts for **2.29** is shown in Figure 2.7. Compound **2.29** is the product of the reaction between key intermediate **2.3** and nicotinoyl. The assignment of the NMR spectra reveals the presence of four additional aromatic signals, which is consistent with the presence of the pyridine-3-yl group. Furthermore, in the ^{13}C NMR spectra a signal at 167.8 ppm is consistent with the presence of the carbonyl group.

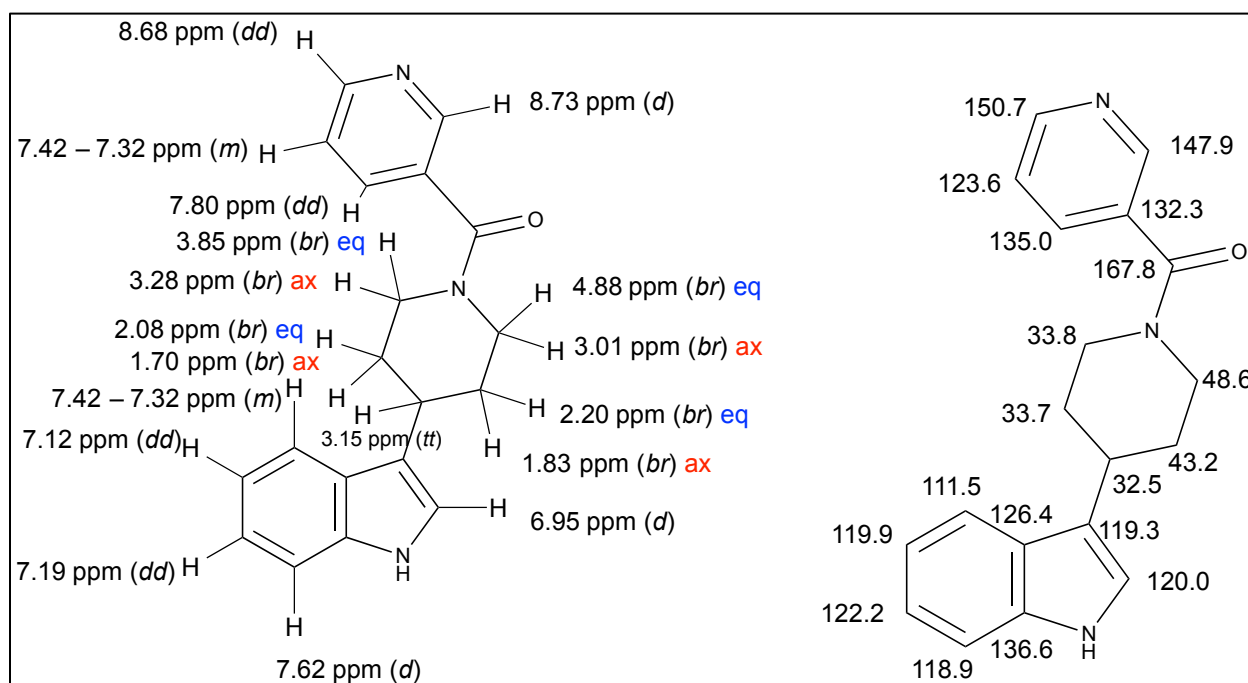
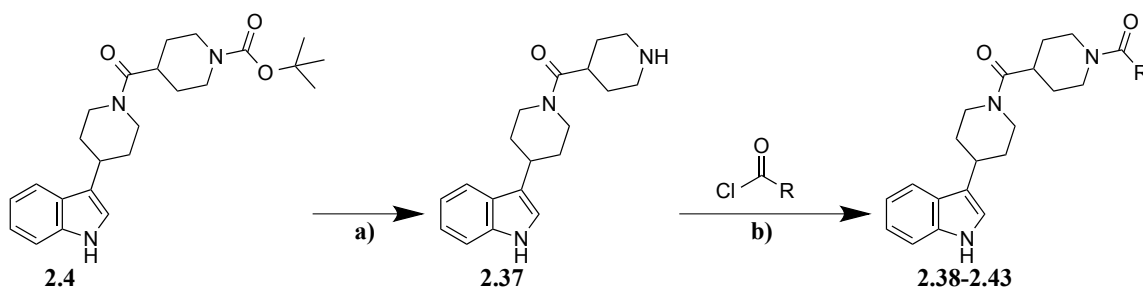


Figure 2.7 – Assignment of ^1H and ^{13}C NMR of amine compound **2.29**.

Next we examined the importance of the 4-aminoquinoline fragment, the essential pharmacophore of chloroquinoline. We synthesized derivative **2.36**, which was obtained through a nucleophilic substitution between 4,6-dichloroquinoline and the amine intermediate **2.3** (Scheme 2.2; Table 2.2).

2.3.5 Synthesis of Bis-amide Library

As a part of our SAR studies an additional series of derivatives was designed in order to maintain both the second piperidinyl group, as well as the amide linkages, while exploring the chemical variation at the terminal piperidinyl fragment. To synthesize this set of analogs the intermediate compound **2.4** was Boc-protected, followed by acylation of the free amine **2.37** with commercially available acid chlorides using standard Schotten Baumann conditions to obtain the desired compounds **2.38-2.43** (Scheme 2.3), in 25% to quantitative yields (Table 2.2)



Scheme 2.3 – R fragments and yields are listed in **Table 1**; Reagents and conditions: **a)** 2 M HCl/MeOH, 40 min, r.t., quantitative yield; **b)** DCM, aq. NaHCO₃, 10 min, r.t.

All the bis-amide derivatives were characterized by NMR techniques and LC/MS (Chapter 6). The results are in good agreement with the chemical structure of the compounds. For instance, the attribution of ¹H and ¹³C NMR chemical shifts for **2.43** is shown in Figure 2.8.

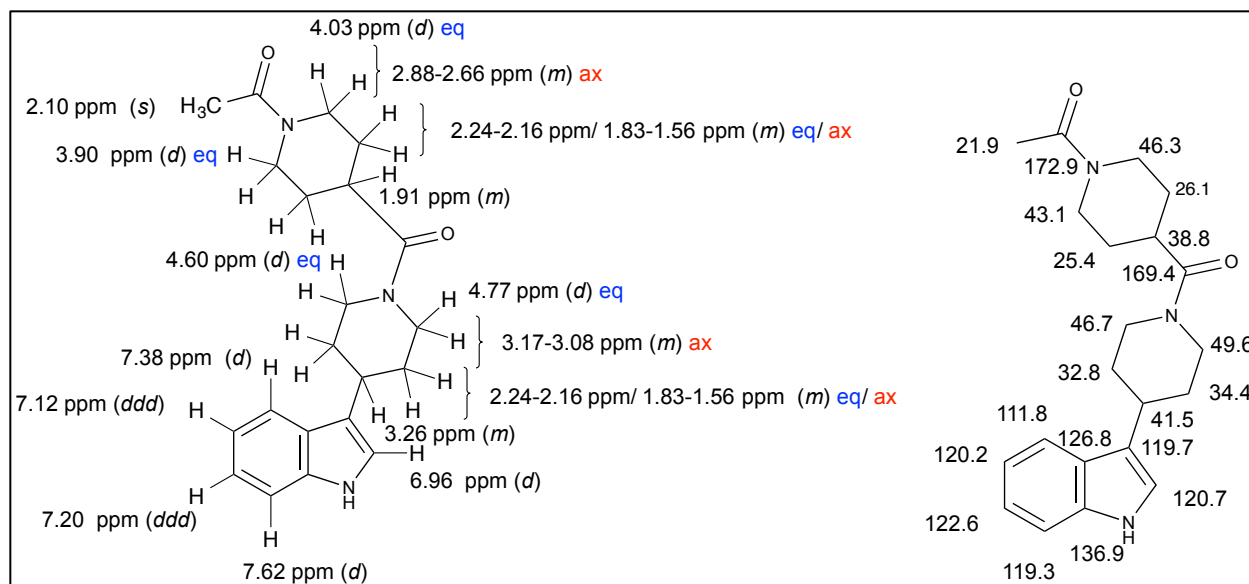


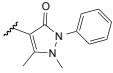
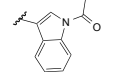
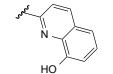
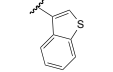
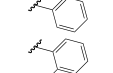
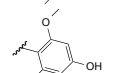
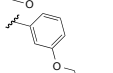
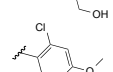
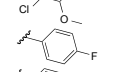
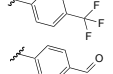
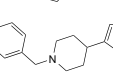
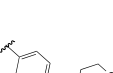
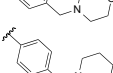
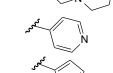
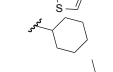
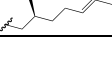



Figure 2.8 – Assignment of ¹H and ¹³C NMR of amine compound **2.43**.

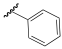
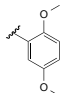
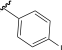
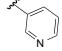
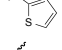
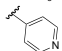
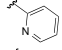
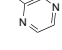
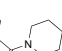
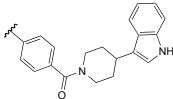
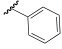
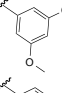
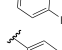
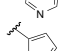
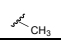

Compound **2.43** is the product of the reaction between key intermediate **2.37** and acetyl chloride. The NMR spectra reveals the absence of additional aromatic signals, and the presence of a singlet peak, which integrates to three protons, at 2.10 ppm. Moreover, in the aliphatic region of the spectra, additional signals integrating to nine protons, corroborate the presence of the second piperidinyl group. Furthermore, in the ¹³C NMR spectra, two signals at 172.1 and 167.8 ppm are consistent with the presence of two carbonyl groups.

2.4 Antimalarial and Cytotoxicity Activities

The synthesized derivatives were first evaluated at 5 μM fixed concentration for their growth inhibitory activity against the erythrocytic stage of the CQ-resistant *P. falciparum* strain Dd2 (Table 2.2). Lipophilicity of the synthesized indole compounds, expressed in terms of their partition coefficient values (cLogP), molecular weight in g/mol and violations of Lipinski's rule of 5 (Ro5) were calculated in Instant JChem (Chemaxon) and considered as a preliminary test of the drug-likeness of the compounds (Table 2.2).

Table 2.2 – Final step yield of synthesized compounds, their drug-like properties (MW, cLogP and compliance with “Lipinski’s Rule of 5”) and results from antimalarial activity screening.

Series	Compound	R	Yield (%)	MW (g/mol)	cLogP	Ro5 (≤ 2 violations)	% Inhibition at 5 μ M <i>P. falciparum</i> Dd2
	2.1	-	15	459.03	5.70	Yes	100
	2.3	-	96	200.28	2.18	Yes	<10
	2.6	-	Quant.	297.44	2.66	Yes	<10
Amine	2.7		79	400.52	3.41	Yes	<10
	2.8		76	371.47	3.70	Yes	70
	2.9		99	357.45	3.98	Yes	<10
	2.10		55	346.49	5.16	Yes	16
	2.11		53	290.40	4.28	Yes	15
	2.12		55	304.43	4.80	Yes	11
	2.13		42	366.45	3.47	Yes	<10
	2.14		99	350.45	3.44	Yes	<10
	2.15		60	419.34	5.18	Yes	<10
	2.16		72	308.39	4.43	Yes	14
	2.17		69	358.40	5.16	Yes	<10
	2.18		25	318.41	4.00	Yes	20
	2.19		30	502.69	6.60	Yes	100
	2.20		38	389.53	4.01	Yes	66
	2.21		54	387.56	5.08	Yes	100
2.22		97	291.39	3.07	Yes	<10	
2.23		65	296.43	4.20	Yes	<10	
2.24		Quant.	296.45	4.67	Yes	<10	
2.25		98	340.55	5.10	Yes	17	

Series	Compound	R	Yield (%)	MW (g/mol)	cLogP	Ro5 (≤ 2 violations)	% Inhibition at 5 μ M <i>P. falciparum</i> Dd2
Amide	2.26		55	304.39	3.64	Yes	<10
	2.27		Quant.	364.44	3.33	Yes	<10
	2.28		95	322.38	3.78	Yes	<10
	2.29		25	305.37	2.42	Yes	100
	2.30		66	310.41	3.55	Yes	<10
	2.31		73	242.32	1.79	Yes	<10
	2.32		60	305.37	2.42	Yes	14
	2.33		95	305.37	2.81	Yes	<10
	2.34		Quant.	306.36	1.59	Yes	<10
	2.35		Quant.	530.66	5.31	Yes	80
	2.36	-	25	361.87	5.21	Yes	32
Bis-amide	2.38		80	415.53	3.35	Yes	<10
	2.39		75	475.58	3.04	Yes	10
	2.40		75	433.52	3.50	Yes	<10
	2.41		10	416.52	2.14	Yes	30
	2.42		73	415.53	3.35	Yes	<10
	2.43		40	475.58	3.04	Yes	10

Compounds inhibiting more than 95% of parasite growth at 5 μ M concentration were further profiled for dose-response to determine half maximal effective concentrations (EC₅₀) against CQ-resistant Dd2 and CQ-sensitive 3D7. The reference antimalarials chloroquine, atovaquone, amodiaquine and artesunate were included as controls and resulted in EC₅₀s in agreement with published results. The original hit molecule **2.1** and its simplified derivative **2.36** were also tested for comparison to the newly synthesized compounds (Table 2.3). Cytotoxicity

(EC₅₀) of selected compounds for human cells (HepG2) and selectivity index for CQ-resistant Dd2 (SI_{res}) and CQ-sensitive 3D7 strains (SI_{sen}) are reported in Table 2.3.

Table 2.3 – *In vitro* antimalarial activity (EC₅₀) and cytotoxicity (EC₅₀) of selected compounds.

Compound	<i>P. falciparum</i>		HepG2 EC ₅₀ (μM) ±SD	Selectivity Index	
	EC ₅₀ (μM) ±SD			SI _{res} ^a	SI _{sen} ^b
	Dd2	3D7			
2.1	0.94±0.51	0.24±0.08	3.86±0.50	4.10	16.08
2.19	0.21±0.05	0.08±0.03	0.46±0.03	2.19	5.75
2.21	2.91±0.35	1.35±0.45	n.d.	n.d.	n.d.
2.29	2.95±0.30	3.80±0.50	12.80±0.28	4.33	3.37
2.36	5.01±1.50	6.30±1.50	4.24±0.21	0.85	0.67
Chloroquine	285±58 ^c	23±1 ^c	n.d.	n.d.	n.d.
Atovaquone	0.19±0.06 ^c	0.35±0.14 ^c	n.d.	n.d.	n.d.
Amodiaquine	12.30±4.21 ^c	5.85±2.20 ^c	n.d.	n.d.	n.d.
Artesunate	1.76±0.43 ^c	1.97±0.29 ^c	n.d.	n.d.	n.d.

^a SI_{res} = EC₅₀ HepG2 / EC₅₀ PfDd2; ^b SI_{sen} = EC₅₀ HepG2 / EC₅₀ Pf3D7; n.d.= not determined; ^c EC₅₀ values in nM; n.d.= not determined.

2.5 Discussion of Structure Activity Relationships and Conclusion

The hit compound **2.1** was resynthesized and tested against the Dd2 and 3D7 strains and exhibited an EC₅₀ of 0.94 μM (Dd2) and 0.24 μM (3D7) which confirmed our previously observed cross-resistance with CQ (resistance index (RI) calculated as EC₅₀ Dd2/EC₅₀ 3D7 = 4). Interestingly, we found significantly decreased activity for this compound in our assay compared to that reported (EC₅₀ 3D7 = 0.03 μM).⁶ This discrepancy in activities could be the consequence of different assays conditions, or possibly the result of inaccurate compound assay concentration, or presence of a biological active contaminant in the original HTS assay plates.

In a first approach to determine the requirement of each fragment of hit **2.1** for its antimalarial activity, we tested intermediates **2.3** and **2.6**, and concluded that the 4-amino-chloroquinoline moiety is essential for activity. Next, we investigated the requirement of the

distal piperidinyl fragment for the antimalarial activity of **2.1**. Removal of this fragment leads to a compound (**2.36**), which had substantially decreased antimalarial activity when compared to compound **2.1** (Tables 2.2 and 2.3).

We then further explored the 3-piperidin-4-yl-1*H*-indole scaffold. The effect of chemically diverse substituents linked to the *N*-piperidinyl group was investigated within the first series of amine derivatives (**2.7-2.25**). Various aromatic fragments, including bicyclic (**2.7-2.10**), monocyclic (**2.11-2.18**) and mono heterocyclic (**2.22-2.23**), as well as alkyl fragments (**2.24-2.25**) were introduced in place of the 4-aminoquinoline. The results indicate that, with the exception of the *N*-acyl indole fragment (**2.8**), none of the smaller fragments tested lead to compounds with anti-parasitic activity. However, the introduction of a second 3-piperidin-4-yl-1*H*-indole group linked through the *p*-position of the benzyl ring afforded a compound (**2.19**) with significant antimalarial activity against both Dd2 and 3D7 strains of *P. falciparum* (EC_{50} s of 0.21 and 0.08 μ M, respectively). Due to the increased lipophilic properties of **2.19**, simplification of the latter benzyl substitution was investigated. The introduction of a basic piperidine group resulted in a compound (**2.21**) with some antimalarial activity against both strains of *P. falciparum* (Dd2 EC_{50} = 2.91 and 3D7 EC_{50} = 1.35 μ M), whereas the introduction of a less basic morpholine group (**2.20**) decreases the activity. Overall, the results indicate that in the amine series the antimalarial activity depends mostly on lipophilicity and the basic characteristics of the compounds, which may be a nonspecific antiproliferative effect as compound **2.19** also showed an equivalent EC_{50} (0.46 μ M) against the HepG2 cell line.

We next investigated the effect of an amide linkage in place of the basic amine, conferring rotational hindrance to the molecules, decreased basicity, as well as providing a hydrogen bond acceptor. A series of *N*-acyl substituted 3-piperidin-4-yl-1*H*-indoles with a wide variety of aromatic groups was synthesized. However, only one of the tested amide derivatives (**2.26-2.35**) was active against Dd2. Compound **2.29**, which was derived from *N*-acyl pyridin-3-yl substitution, demonstrated antimalarial activity (EC_{50} = 2.95 μ M) comparable to analog **2.21**. Notably **2.29** has a significantly improved cLogP compared to **2.21** (2.42 vs 5.08). Moreover, **2.29** did not show cross-resistance with CQ (RI = 1.3) and was modestly selective (4x) for *P. falciparum* over the tested human cell line (EC_{50} = 12.8 μ M). Interestingly, the activity was highly susceptible to the substitution position of the pyridinyl moiety, with the *N*-acyl pyridine-4-yl (**2.32**) and *N*-acyl pyridine-2-yl (**2.33**) derivatives being inactive against the parasite,

suggesting that the relative spatial disposition of the carbonyl group and the nitrogen atom is required for activity.

Comparison of the activity of bis-3-piperidin-4-yl-1*H*-indole compound **2.19** and its bis-amide counterpart **2.35**, suggests that the amide bond significantly reduces the antimalarial activity (**2.35** with EC₅₀ > 5 μM). To broaden our structure-activity relationship study we also examined a small series of analogs containing the 4-(piperidine-1-carbonyl)piperidin-1-yl) scaffold with structurally diverse *N*-acyl substituents (**2.38-2.43**). No significant antimalarial activity was observed for the tested *N*-acyl derivatives, (**2.38-2.43** with EC₅₀ > 5 μM). Moreover, when comparing the *N*-acyl pyridin-3-yl substitution in the 3-piperidin-4-yl-1*H*-indole series (**2.29**) to the same *N*-acyl substitution in the 4-(4-piperidine-1-carbonyl)piperidin-1-yl-1*H*-indole series (**2.41**), the introduction of the second piperidinyl group results in loss of antimalarial activity.

Despite efforts to protect the useful lifespan of frontline therapies, antimalarial drug resistance remains an ever-present threat. This challenge demands new drugs, preferably new chemotypes active against drug resistant parasites, with a good pharmacologic profile and affordable to endemic areas. Here we applied a rational fragment-based approach to design three related series of 3-piperidin-4-yl-1*H*-indoles around TCMDC-134281 (**2.1**), which was previously identified by GSK in a HTS campaign, to develop robust SAR and to validate this chemotype for further preclinical development. Altogether, 38 compounds were synthesized and evaluated for antimalarial activity. Compounds that demonstrate promising activity against the multidrug-resistant *P. falciparum* Dd2 strain were also tested in the 3D7 parasite strain and counter screened in human HepG2 cells.

The SAR study revealed that the 4-aminoquinolinyl moiety present in hit **2.1** can be replaced by some smaller groups without significantly affecting activity. Compounds, which retained activity in spite of the absence of the chloroquine motif, demonstrate the potential of the 3-piperidin-4-yl-1*H*-indole scaffold as a new class of antimalarial drugs independent from the 4-aminoquinolines.

The results suggest that the 3-piperidin-4-yl-1*H*-indole scaffold is very sensitive to most *N*-piperidinyl modifications. Out of the analogs synthesized, only three were active (**2.19**, **2.21** and **2.29**). While **2.21** showed cross-resistance to chloroquine and **2.19** was not selective in HepG2 cytotoxicity assays, the (4-(1*H*-indol-3-yl)piperidin-1-yl)(pyridin-3-yl)methanone (**2.29**)

Chapter 2 – Indole-based Antimalarials

showed *in vitro* antimalarial activity (EC_{50} values $\sim 3 \mu\text{M}$), no cross-resistance with chloroquine, selectivity for the parasite, and lead-like properties ($c\text{LogP} < 3$; $\text{MW} \sim 300$). This represents a promising new antimalarial chemotype with a potential novel mechanism of action. Further medicinal chemistry efforts are needed to improve the potency of compound **2.29** and disclose its antimalarial mechanism of action.

Chapter Three

3. Aminoacyl-tRNA Synthetase Inhibitors as Antimalarials

3.1 Introduction

3.1.1 Aminoacyl-tRNA Synthetases as Drug Targets

The cell is the functional unit of living organisms, and it contains DNA, RNA and proteins. The central dogma of molecular biology consists on the sequential transmission of information from DNA to RNA to protein, and the regulation of gene expression is required to meet the changing environmental and developmental demands of the cell. Proteins comprise nearly 50% of the cellular mass and serve as enzymes, signaling molecules, structural, storage and mechanical components of the cell.²⁴⁰⁻²⁴¹

The process of translation of the genetic message contained in mRNA into proteins is a universal mechanism conserved, with minor modifications, in the all branches of the tree of life, from bacteria to archaea, and eukaryotes.²⁴²

Aminoacyl-tRNA synthetases are central enzymes in protein translation, providing the aminoacid-charged tRNAs needed as building blocks for the construction of peptide chains (Figure 3.1). These enzymes have long been pursued as drug targets in bacteria and fungi, and in the past decade there has been considerable research on aminoacyl-tRNA synthetases in eukaryotic parasites.²⁴³⁻²⁴⁶

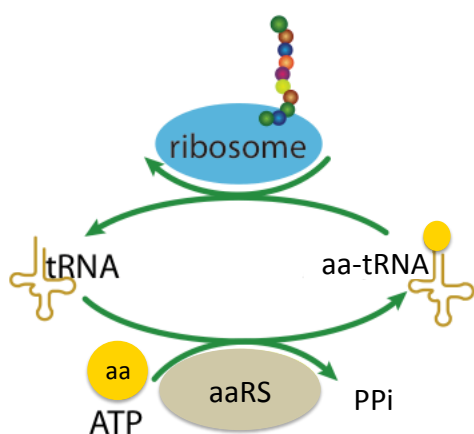


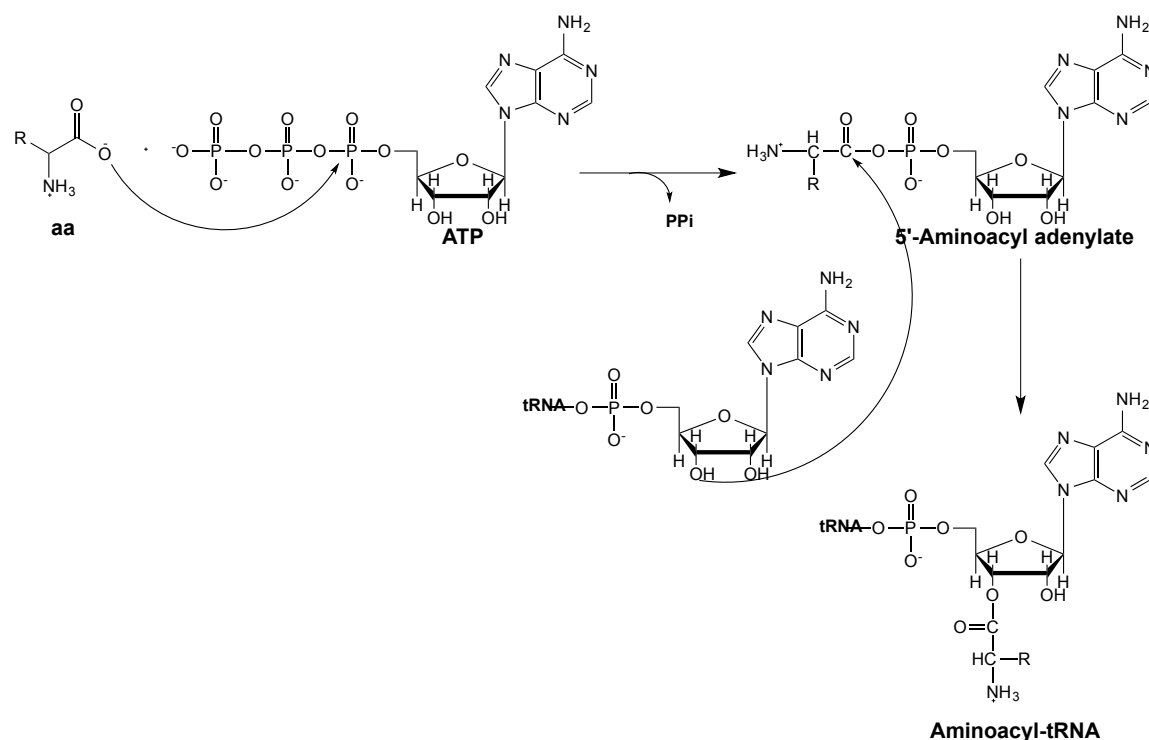
Figure 3.1 – Protein translation. Aminoacyl tRNA synthetases (aaRS) charge unloaded tRNAs with their cognate amino acids (aa), which in turn are used as substrates by the ribosome during protein biosynthesis.

Aminoacylation reaction

Aminoacyl-tRNA synthetases (aaRS) are, together with tRNA, the main players in the first step of the protein translation: the aminoacylation reaction. These enzymes catalyze a two-

Chapter 3 – Aminoacyl-tRNA Synthetase Inhibitors as Antimalarials

step process involving the attachment of a specific amino acid to the cognate tRNA resulting in the formation of aminoacyl-tRNAs. The first step catalyzed by all aaRSs consists of activation of their corresponding amino acid to form an aminoacyl-adenylate intermediate (aa-AMP) by the reaction with ATP. In the second step, the activated amino acid is transferred to the 2'- or 3' hydroxyl of the adenosine of the tRNA through aminoacyl ester bond to be use for protein biosynthesis, this step constitutes the rate-limiting step (Scheme 3.1).



Scheme 3.1 – Mechanism of aminoacylation by aminoacyl-tRNA synthetases.²⁴⁷ The covalent attachment of an amino acid to its cognate tRNA happens in two steps. First an amino acid carboxylate attacks the alpha phosphate of an ATP, producing an aminoacyl adenylate intermediate. In the second step, the 2'- or 3'-hydroxyl of the tRNA A76 subsequently displaces the AMP, resulting in a “charged” tRNA attached to its amino acid.

This aminoacylation reaction occurs and the charged tRNAs are transported to the site of protein biosynthesis, the ribosome, where the amino acid is transferred to a growing polypeptide chain.²⁴⁷⁻²⁴⁹ In summary, the accurate synthesis of proteins, dictated by the corresponding nucleotide sequence encoded in mRNA, is a two-part process. First, amino acids are covalently

linked to their cognate tRNAs by aaRSs, then the aminoacyl-tRNAs (aa-tRNAs) are delivered to the ribosome by elongation factors (EF-Tu in bacteria and EF-1A in archaea and eukaryotes).²⁵⁰⁻²⁵¹ Moreover, in addition to their fundamental role in translation, aaRSs are also involved in unrelated non-canonical functions, which are further discussed below.

3.1.2 Classes of Aminoacyl-tRNA Synthetases

Plasmodium has genes for 37 aaRSs, which recognize the 20 amino acids, and these are apparently sufficient to translate the nuclear, apicoplasmic, and mitochondrial genomes. These aaRS are universally distributed across the tree of life.^{247, 252} Although the basic chemical reaction is the same in each case, the aaRSs fall into two classes based on their chemical properties, architecture of their catalytic domains, as well as the presence of certain consensus sequences (Figure 3.2).^{248, 253}

	Class I	Class II	
Ia	MetRS	SerRS	IIa
	ValRS	ThrRS	
	LeuRS	AlaRS	
	IleuRS	GlyRS	
	CysRS	ProRS	
	ArgRS	HisRS	
Ib	GluRS	AspRS	IIb
	GlnRS	AsnRS	
	LysRS I	LysRS II	
Ic	TyrRS	PheRS	IIc
	TrpRS		

Figure 3.2 – Classes of aminoacyl tRNA synthetases.²⁵³ The two major classes can be organized into subclasses that hold enzymes that are most closely related to each other in their sequences. Significantly, the subclasses also group tRNA synthetases according to their amino acid chemical types.

Class I and class II enzymes appear to have originated from two separate ancestral active site domains or catalytic cores, that contained both amino acid activation and tRNA aminoacylation activity. With the exception of lysyl-tRNA synthetase, each of the 20 types of aaRS can be assigned to only one of these two classes. Each class is then further separated into three subclasses a, b, and c based on their unique mechanistic properties, anticodon-binding

domain characteristics as well as the organization of structural motifs unique to each of the two main classes.²⁵³⁻²⁵⁵

The differences between the two classes extend beyond their active site structure. Class I aaRS transfer initially the aminoacyl group of aa-AMP to the 2'-OH of the terminal ribose in tRNA and is then moved to the 3'-OH by a transesterification, while for class II aaRS, the aminoacyl group is transferred directly to the 3'-OH.²⁴⁷

Interestingly, aaRS of the same subgroup tend to recognize similar types of amino acids. For instance, class Ic aaRS recognize aromatic amino acids such as tyrosine and tryptophan while class Ib recognizes amino acids with charged side chains such as lysine, glutamate and its derivative glutamine.

3.1.3 Quality Control of Aminoacyl-tRNA Synthetases

Faithful translation of genetic information from mRNA to protein is critical for cellular function. In spite of the fact that the active site of aaRSs excludes most non-cognate amino acids, selection of correct amino acid is more challenging for the amino acids that are chemically similar. It has been postulated, that the overall error rate of one in 10,000 is maintained for correct codon-anticodon recognition on the ribosome and pairing of each amino acid to its corresponding tRNA.²⁵⁶⁻²⁵⁹ When error rates exceed this threshold, the incorrect products are hydrolyzed at the secondary amino acid binding sites (editing sites), either by pre-transfer (hydrolysis of aminoacyl-adenylate) or post-transfer (hydrolysis of aminoacyl-tRNA) editing mechanisms. Thus, additional domains appended to or inserted in the body of aaRS have increased efficiency and specificity of the aminoacylation process (Figure 3.3).²⁵⁹⁻²⁶⁰

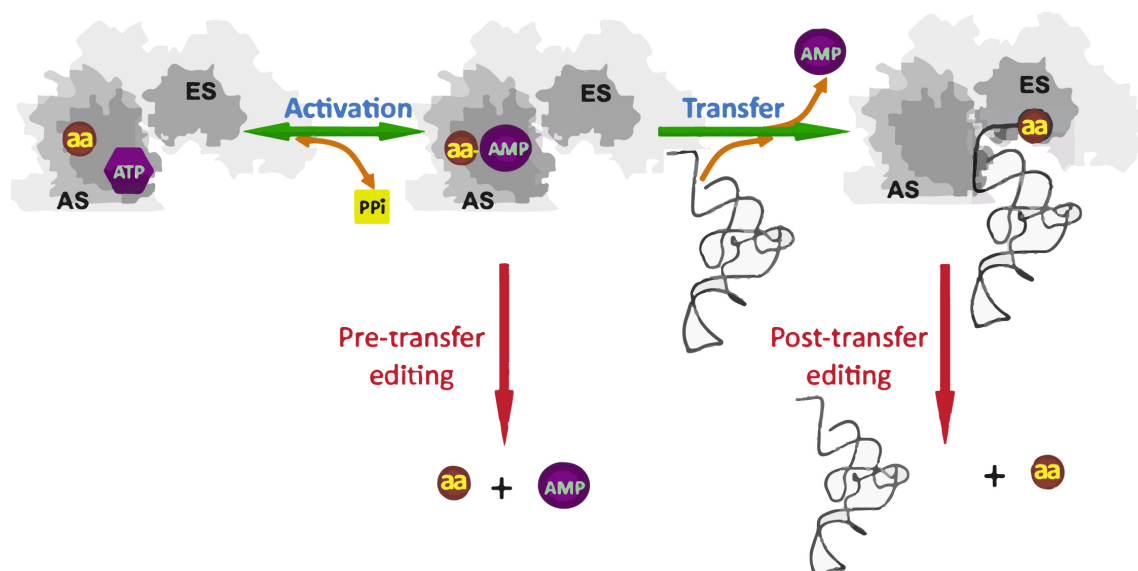


Figure 3.3 – Pre-transfer and post-transfer editing of non-cognate amino acids by aaRS. The amino acid (aa) is activated at the active site (AS) to form aminoacyl-adenylate (aa-AMP). In pre-transfer editing, aa-AMP is hydrolyzed directly, whereas in post-transfer editing, the mischarged tRNA is translocated to the editing site (ES), where the aa is removed. Image adapted from Yadavalli *et al.*²⁶⁰

3.1.4 Noncanonical Functions of Aminoacyl-tRNA Synthetases

In the course of evolution, besides the basic domains (aminoacylation, anticodon binding and editing), aaRS have acquired additional domains and insertions, which have expanded the range of functions performed by these enzymes.²⁶¹ These appended domains, often dispensable for aminoacylation, are considered as markers for the aaRS associated functions beyond translation.²⁶² Thus, in addition to their fundamental role in translation, aaRS are also involved in unrelated noncanonical functions, such as regulation of gene expression, apoptosis, angiogenesis and cellular signaling, among others (Figure 3.4).^{248, 263-264}

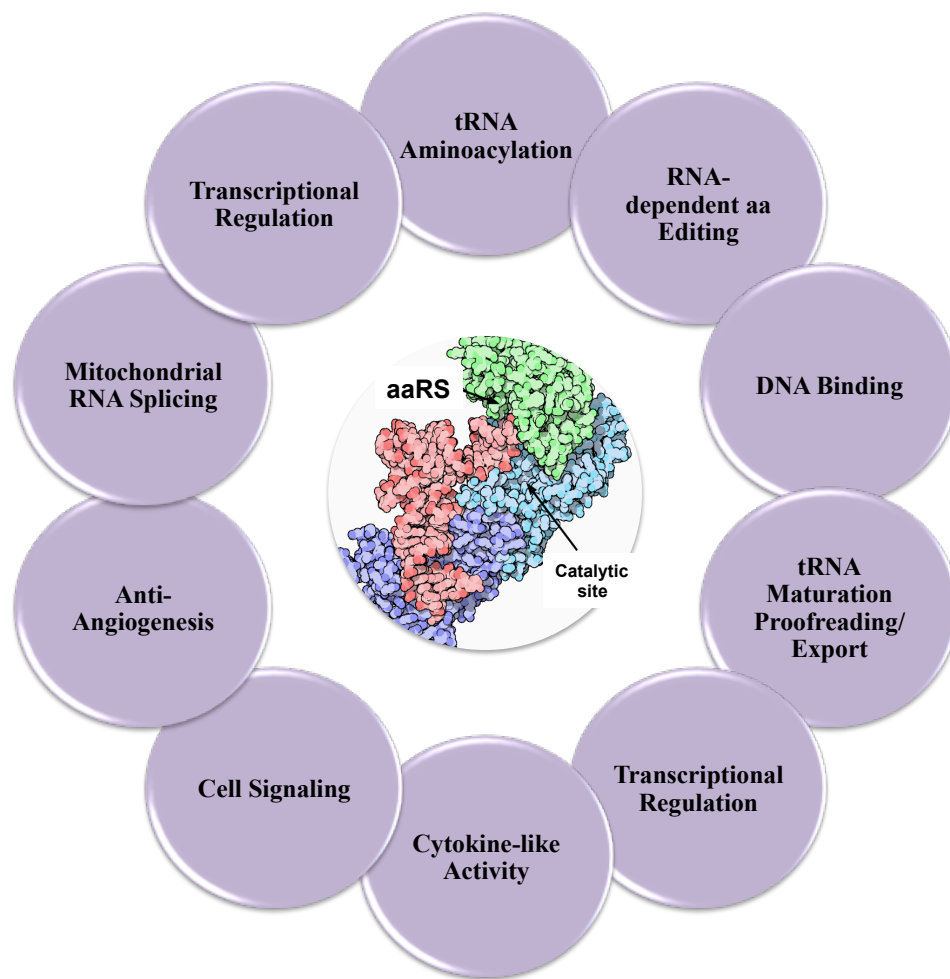


Figure 3.4 – Canonical and non-canonical functions of aaRSs.

The secondary functions mentioned, often involve the association of the aaRS with cellular partners that are distinct from their regular partners in translation and vary among different organisms.^{242, 262} In mammalian cells these multiprotein complexes in which aaRSs are included have also been implicated in several different human diseases²⁶⁵⁻²⁶⁶ such as cancer,²⁶⁷⁻²⁶⁸ neuronal diseases,²⁶⁹ diabetes,²⁷⁰ and autoimmune diseases.²⁷¹ Due to this diversity of functions, aaRS have a tremendous impact on the life of cells and contribute to the regulation and coordination of processes in the cell and the organism as a whole. Additionally, cells also use these enzymes as measurements of overall amino acid homeostasis.

In eukaryotic cells, the Amino Acid Starvation Response (AAR) and Mammalian target of rapamycin complex 1 (mTORC1) pathways both play a role in sensing nutrient status and

activating cellular programs that mitigate restriction in the supply of environmental amino acids. These metabolic stress pathways are differentially activated, however, eliciting distinct sets of transcriptional responses and biological effects.²⁷²⁻²⁷⁴ The multiprotein mTORC1 protein kinase complex is the central component of a pathway that promotes growth in response to insulin, energy levels, and amino acids.²⁷⁵ In contrast to the AAR, the mTORC1 pathway is inhibited by amino acid restriction by possibly sensing amino acid levels directly.²⁷⁶ AAR pathway activation, on the other hand, is triggered by the intracellular accumulation of uncharged tRNAs.²⁷⁷

Cells directly sense the amount of uncharged tRNAs and reprogram their behavior via a signal transduction pathway (AAR). The AAR is a stress response pathway well appreciated in yeast and mammalian biology as part of the larger Integrated Stress Response (ISR). It reprograms cellular behavior in response to deprivation of available amino acids.²⁷⁸⁻²⁷⁹ The aggregate effect of the AAR is to inhibit cell-wide protein synthesis and selective translation of stress-response proteins. Despite redundant amino acid supplies, the *P. falciparum* parasite remains vulnerable to amino acid starvation. In fact, *in vitro* experimentation has demonstrated that growing parasites in media lacking isoleucine activates the AAR.²⁸⁰⁻²⁸¹

Thus, the AAR pathway senses the levels of uncharged tRNAs as a surrogate for free amino acid availability. Uncharged tRNAs bind to and activate GCN2, which in turn phosphorylates the regulatory subunit eIF2 α of the eukaryotic initiation factor complex eIF2 (Figure 3.5). Phosphorylation of eIF2 α results in the direct inhibition of cap-dependent protein translation and the initiation of specific stress response pathways including apoptosis and autophagy.^{246, 282-283}

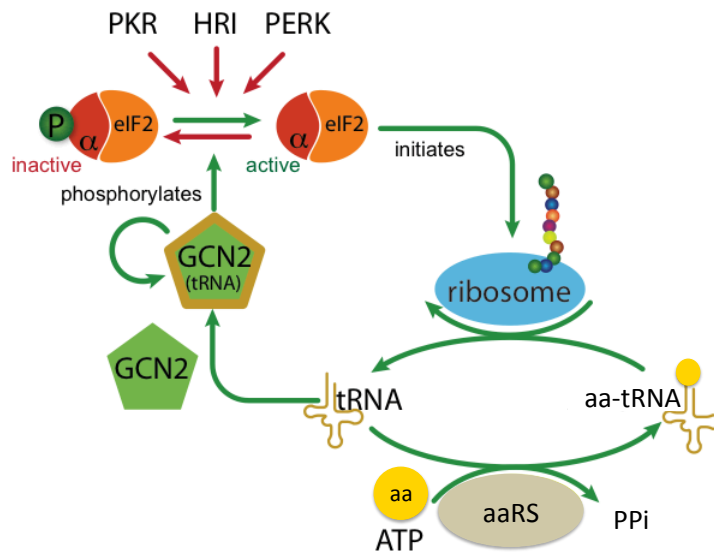


Figure 3.5 – Phosphorylation of eIF2 α by inhibition of aminoacyl-tRNA synthetases (aaRS). The aaRS charge unloaded tRNAs with their cognate amino acids (aa), which in turn are used as substrates by the ribosome during protein biosynthesis. Inhibition of aaRS (or lack of amino acids) results in accumulation of uncharged tRNAs that bind and activate GCN2. Active GCN2 phosphorylates the alpha-subunit of the eukaryotic initiation factor eIF2. Phosphorylated eIF2 α can no longer initiate the ribosome assembly, resulting in inhibition of translation.

3.1.5 Aminoacyl-tRNA Synthetases in *Plasmodium*

In spite of the sequence similarity for homologous synthetases from the three different phyla (bacteria, archaea and eukaryotes), there is a notable variation in the structural organization. An intricate network of protein-protein interactions is required for efficient translation.²⁸⁴

The protein translation machinery in *P. falciparum* remains poorly characterized. *Plasmodium* parasites have three subcellular compartments that house genomes: the nucleus, the mitochondria and the apicoplast (an essential organelle that is present in all Apicomplexans and is thought to be derived from a secondary endosymbiosis of a red algae). Each of these three compartments requires its own compartmentalized transcription and translation apparatus for its survival.²⁵²

P. falciparum encodes for only 37 aaRSs, and these are apparently sufficient to translate genomes from all three compartments. The subcellular distribution of most aaRSs remains unclear, although computational studies suggest that most of these proteins are either targeted to the apicoplast or the cytosol, but not to the mitochondria.²⁸⁵⁻²⁸⁶ Several *P. falciparum* aaRS

(GlyRS, AlaRS, CysRS and ThrRS) are present only once in the genome, and thus should be dually targeted to both, the apicoplast or the cytosol.²⁸⁷ With respect to mitochondrial protein translation, it is probable that in *P. falciparum* mitochondrial tRNAs are aminoacylated in the cytosol and transported into the mitochondria for use in protein synthesis, in a similar fashion to what has been suggested for *Toxoplasma gondii* and *Trypanosoma brucei*.²⁸⁸⁻²⁸⁹

The protein translation machinery of the *P. falciparum* parasite is the target of some antimalarial drugs, and encompasses many promising targets for future drugs.

3.1.6 Aminoacyl-tRNA Synthetase Inhibitors

Despite the fact that all aaRS share the same reaction mechanism, the high level of phylogenetic divergence between bacterial and eukaryote/archaea enzymes can allow aaRS inhibitors to discriminate effectively between pathogen and host aaRS.²⁹⁰⁻²⁹¹

An important example of the clinical application of an aaRS inhibitor is provided by the antibiotic mupirocin (**3.1**, Figure 3.6), marketed as Bactroban, which selectively inhibits bacterial isoleucyl-tRNA synthetase (IleRS). This product is currently the world's most widely used topical antibiotic for the control of methicillin-resistant *Staphylococcus aureus* infections (MRSA).²⁹²⁻²⁹³ Besides mupirocin there is currently only one other aaRS inhibitor that is on the market: benzoxaborole AN2690 (**3.7**, Figure 3.6), used for the topical treatment of onychomycosis.²⁹⁴ These drugs prove that selective and efficacious inhibition of aaRS is a feasible approach for anti-infective development.

Other aaRS inhibitors described to date include natural products, such as febrifugine (**3.4**),⁸ borrelidin (**3.3**),²⁹⁵ granaticin,²⁹⁶ indolmycin,²⁹⁷ furanomycin,²⁹⁸ ochratoxin A,²⁹⁹ cispentacin,³⁰⁰ and several semisynthetic products,³⁰¹ including halofuginone (**3.5**), a febrifugine derivative which our group identified as an inhibitor of *P. falciparum* prolyl tRNA synthetase.⁷ We have established for the first time in *Plasmodium* that inhibition of tRNA synthetases by a small molecule and simultaneous activation of the integrated stress response is both feasible and attractive, and provides a rational mechanistic basis for future drug discovery and development focused on this novel target and pathway.⁷⁻⁸

Moreover, most efforts on the design of new synthetic drugs targeting aaRS have focused on mimicking the aminoacyl adenylate intermediate (aa-AMP).³⁰²⁻³⁰⁴ Most inhibitors bind to the highly conserved synthetic active sites and act as competitive inhibitors of the respective

Chapter 3 – Aminoacyl-tRNA Synthetase Inhibitors as Antimalarials

substrate amino acid. Compounds can be analogs of natural aaRS inhibitors or mimics of the reaction intermediate, aminoacyl-adenylate. However, a number of inhibitors bind to other regions of the aaRS outside the active site, either allosterically affecting the synthetic active site or binding to alternative active sites, such as the editing domain.²⁴⁵

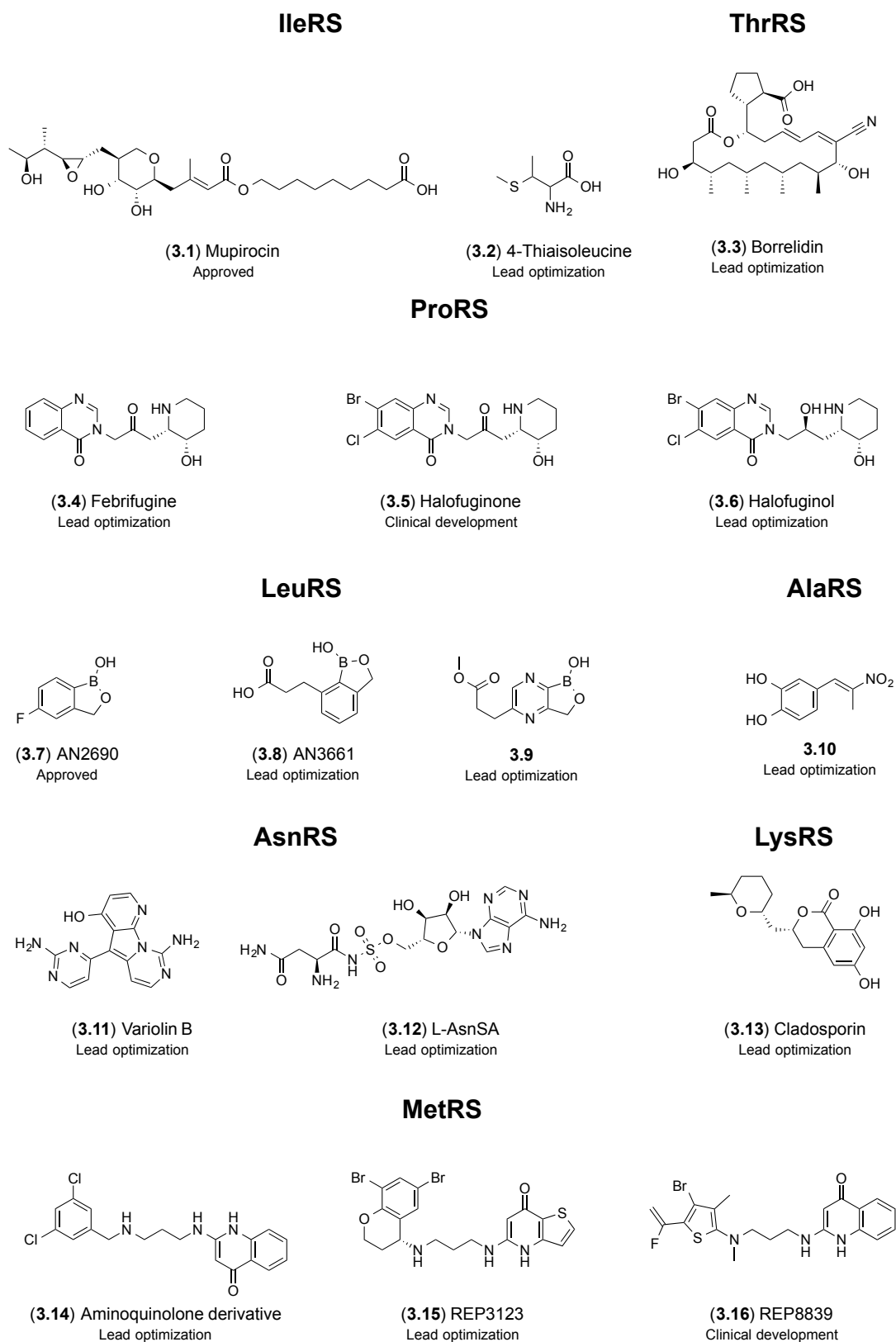


Figure 3.6 – Aminoacyl-tRNA synthetase inhibitors.

Isoleucyl-tRNA synthetase inhibitors

As mentioned above, mupirocin targets IleRS and is the most widely used drug that inhibits an aminoacyl-tRNA synthetase. Crystal structures of mupirocin bound to IleRS indicate that mupirocin inhibits bacterial IleRS by blocking the binding of the Ile-AMP intermediate.³⁰⁵ Furthermore, the *Trypanosoma brucei* isoleucyl-tRNA synthetase (IRS) has been validated as a potential drug target, with *ex vivo* and *in vivo* RNAi knockdowns showing IleRS to be essential for *Trypanosoma brucei* growth, a protist parasite that causes human African trypanosomiasis.³⁰⁶

Plasmodium parasites can obtain its amino acid requirement, with the exception of Ile, by degrading host cell hemoglobin. Mupirocin and thiaisoleucine (**3.1** and **3.2**, Figure 3.6), an isoleucine analog, were screened against *in vitro* cultures of CQ-sensitive strain *P. falciparum* 3D7, killing parasites with EC₅₀ of 11.7 nM and 16.3 μM, respectively. Furthermore, using a genome-wide high-density tiling microarray, the apicoplast IleRS was validated as the target of mupirocin, whereas thiaisoleucine inhibited the *Plasmodium* cytosolic IRS.²⁸¹

Prolyl-tRNA synthetase inhibitors

Our group has identified the cytoplasmic prolyl-tRNA synthetase (*Pfc*PRS, PFL0670c) in *Plasmodium falciparum* as the long-sought biochemical target of halofuginone (**3.5**) (HFG) and the natural product febrifugine (**3.4**) (Figure 3.6).⁷

The quinazoline-type alkaloid febrifugine was isolated from the plant *Dichroa febrifuga*, which was used as an ancient herbal remedy in Traditional Chinese Medicine for over 2000 years for the treatment of fevers and malaria.¹⁴⁹ In the 1960s, the Walter Reed Army Institute of Research (WRAIR) developed halofuginone and other febrifugine analogs as part of a large antimalarial drug development program. In spite of the potent antimalarial activity displayed by febrifugine and its analog halofuginone, the severe emetic and gastrointestinal side effects has precluded their clinical development.³⁰⁷ Subsequent identification of the broad-spectrum antiprotozoal activity of halofuginone led to its approval and common use in veterinary medicine.³⁰⁸ During recent years, halofuginone has attracted much attention because of its wide range of beneficial biological activities, not only as an antimalarial but also in the treatment of cancer, as well as in fibrosis-related and autoimmune diseases.³⁰⁹⁻³¹⁰ In parallel, with the work our group has developed in *P. falciparum* parasites, we have also demonstrated in mammalian cells that halofuginone targets the glutamylprolyl-tRNA synthetase (EPRS), activating the amino

acid starvation response pathway which in turn potently inhibits the differentiation of proinflammatory Th17 cells.^{8, 311} Moreover, our collaborators showed that halofuginone specifically blocks the formation of the Pro-AMP adenylate complex, by interaction with ATP.³¹² Furthermore, Hwang and Yogavel have recently solved the structures of free human EPRS and *PfcPRS*, respectively, demonstrating significant conformational changes in the apoenzyme.³¹³⁻³¹⁵

Halofuginone affects both the asymptomatic liver stage that is the first stage of the *Plasmodium* parasite's life cycle and the sporozoite propagation within liver cells, as well as the blood stage that elicits characteristic malaria symptoms. In the liver stage, halofuginone inhibited the *P. berghei* sporozoite load in HepG2 cells, with an IC₅₀ value of 17 nM, without affecting sporozoite traversal.³¹⁶

To provide an unbiased and comprehensive approach to target identification, our group has carried out independent stepwise resistance selections under intermittent drug pressure using HFG as a selection agent. *P. falciparum* strains with decreased sensitivity to HFG were isolated, cloned, and subjected to increased drug pressure to yield stable clones with high levels of resistance. Two resistant parasite strains were independently selected along with the parental Dd2 strain, which were analyzed using full genome sequencing to identify the genetic loci that contribute to resistance. The only locus with nonsynonymous SNPs identified in both resistant strains was PFL0670c, previously assigned as putative cytoplasmic proline aminoacyl tRNA synthetase (cPRS).⁷ Using the induced resistance parasite lines, a non-genetic drug resistance mechanism was identified, where *P. falciparum* upregulates its proline amino acid homeostasis in response to halofuginone pressure prior to genetic modification of the cPRS.²⁰⁶ Halofuginone binds to the cPRS in a novel mode, forming a ternary complex with ATP and simultaneously mimics proline and the 3' end of bound tRNA. As seen using molecular dynamics simulations, a network of hydrogen bond interactions stabilizes the *N*-protonated hydroxypiperidine moiety. The interactions between halofuginone, ATP, and *PfcPRS* were similar to the binding mode observed for human cPRS consistent with the similarity of the *PfcPRS* core catalytic domains. These results show that halofuginone is a competitive inhibitor of the proline and tRNA binding sites of *PfcPRS*.^{7, 312}

Further investigation showed that both halofuginone and febrifugine treatment significantly increased eIF2 α phosphorylation in *P. falciparum* asynchronous Dd2 cultures, in a dose dependent manner within 90 min, comparable to amino acid starvation.⁷

Dose-limiting toxicity, rather than lack of efficacy, has precluded clinical development of febrifugine and its analogs as antimalarials. Our group has hypothesized that the observed side effects of HFG and febrifugine could be caused by off-target effects originating from the compounds' reported ability to epimerize in solution through formation of a reactive intermediate (Figure 3.7).³¹⁷

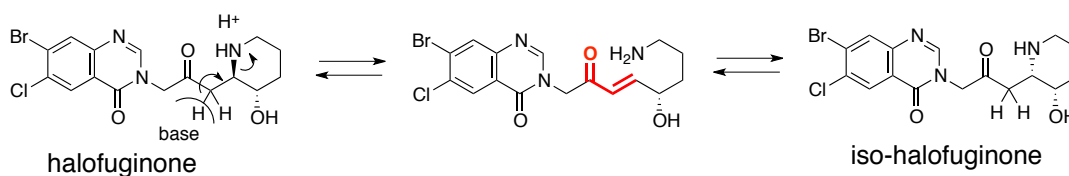


Figure 3.7 – Proposed epimerization mechanism for halofuginone. Halofuginone and febrifugine have been reported to epimerize. The mechanism is reversible and likely proceeds through the formation of a reactive unsaturated ketone (shown in red) as the result of a retro-Michael reaction. The enone can react intramolecularly or with other nucleophiles (e.g. cysteine residues) to form covalent adducts.

Thus, we reasoned that formal reduction of the ketone to yield a secondary alcohol would retain the potential to form critical hydrogen bonds within the target complex while eliminating the ability to form a reactive Michael-acceptor. The resulting compound, Halofuginol (HFol) (**3.6**, Figure 3.6), demonstrated low nanomolar *in vitro* potency against 3D7 (EC_{50} = 5.8 nM) comparable to febrifugine (4.0 nM). Cytotoxicity profiling in primary mouse embryonic fibroblasts (EC_{50} = 373 nM) revealed that HFol was about 65 times more selective for *P. falciparum*. Halofuginol had similar activity (EC_{50} = 14 nM) to halofuginone (EC_{50} = 17 nM) in the *in vitro* *P. berghei* ANKA liver-stage model, and was highly efficacious *in vivo* in both asexual blood- and liver-stage, resulting in >99% reduction of parasites with the regimens used.⁷

Although halofuginol is an attractive starting point for rational development of *Pfc*PRS inhibitors as next-generation dual-stage antimalarials, it is important to understand the consequences of blocking human EPRS, thus *Pfc*PRS inhibitors with improved biochemical selectivity might be more attractive candidates for clinical development.

Leucyl-tRNA synthetase inhibitors

Leucyl-tRNA synthetase (LeuRS) is a proofreading aaRS that is involved in post-transfer editing, which consists on the translocation of mischarged tRNA from the aminoacylation to the editing active site where mischarged tRNA binds for hydrolysis of the noncognate amino acid to enhance fidelity.³¹⁸

One of the two aaRS inhibitors currently on the market in a topical formulation, is the small molecule 5-fluoro-1,3-dihydroxy-2,1-benzoxaborole (**3.7**, AN2690), which targets the editing site of LeuRS and traps the tRNA^{Leu}. AN2690 contains a boron atom that mediates the adduct formation responsible for trapping the enzyme-bound tRNA^{Leu} in the editing site halting catalytic turnover. This antifungal agent also kills a wide range of organisms including yeasts, molds and dermatophytes.³¹⁹⁻³²⁰

Inspired by the success of AN2690, inhibitors based on the benzoxaborole core, which contain a boronic acid and forms an adduct with the tRNA, have been explored as LeuRS inhibitors in other organisms.³²¹⁻³²² The unique ability of benzoxaboroles to inhibit the function of LeuRS from other organisms allowed them to be pursued as a novel class of antibiotics. For example, benzoxaborole-based derivatives GSK2251052 and ZCL039 inhibit *Enterobacteriaceae* LeuRS and *Streptococcus pneumoniae*, respectively.³²³⁻³²⁴

Benzoxaboroles also offer new opportunities for treating neglected diseases, such as malaria and human african trypanosomiasis. Many Benzoxaboroles *T. brucei* LeuRS inhibitors have been reported^{304, 325}, and most recently the *N*-(4-sulfamoylphenyl)thioureas, discovered through the screening and modification of a targeted library of putative aaRS inhibitors, that targets the catalytic site.³²⁶

Several benzoxaboroles with 7-carboxyethyl substituents, such as AN3661 (**3.8**, Figure 3.6) have been reported to have very potent antimalarial properties with IC₅₀ values in the nM range.³²⁷ Most recently a series of 6-aryloxy benzoxaborole compounds was designed and synthesized, where a highly potent 6-(2-(alkoxycarbonyl)pyrazinyl-5-oxy)-1,3-dihydro-1-hydroxy-2,1-benzoxaborole (**3.9**, Figure 3.6) was identified. This compound demonstrated excellent *in vitro* blood stage activity (IC₅₀ = 1.9 nM in *P.f.* 3D7 strain) and *in vivo* efficacy against *P. berghei* in infected mice (ED₉₀ = 7.0 mg/kg).³²⁸

Alanyl-tRNA synthetase inhibitors

Alanyl-tRNA synthetase (AlaRS) has been a focus of extensive research due to its unusual secondary catalytic site, which has an editing activity. Thus, AlaRS enzymes can edit products of misacylation to ensure they do not accumulate to toxic levels.³²⁹⁻³³⁰ The reduced translational fidelity, caused by a hypomorphic mutation in the editing domain of alanyl-tRNA synthetase (ARS), results in accumulation of misfolded proteins, which in turn caused severe pathological phenotypes in mice, such as neurodegeneration and cardioproteinopathy.³³¹⁻³³²

AlaRS has also been characterized in *Plasmodium* parasites, where one version of this enzyme is encoded and post-translationally targeted to both the *P. falciparum* cytosol and the apicoplast.²⁸⁷

4-(2-nitro-1-propenyl)-1,2-benzenediol (**3.10**, Figure 3.6) is a putative inhibitor of PfAlaRS identified in a *in silico* docking screen, which inhibited parasite growth at low micromolar ($EC_{50} \approx 8 \mu\text{M}$) and produced limited mammalian cytotoxicity.^{246, 285}

Asparaginyl-tRNA synthetase inhibitors

The cytoplasmic asparaginyl-tRNA synthetase (cNRS) has been a long-standing drug target in *Brugia malayi*, a nematode that is one of the causative agents of lymphatic filariasis.³³³⁻³³⁵ Two distinct strategies have been employed to find inhibitors of the *B. malayi* enzyme, *in silico* docking and high throughput screening. Using the first approach Sukuru and co-workers successfully identified diverse compounds, including Variolin B (**3.11**, Figure 3.6), which can inhibit the activity of NRS with micromolar affinity.³³⁶ The second approach makes use of an assay that focuses on the enzyme's capacity to recognise and edit misacylation prior to transfer.³³⁷ The assay was then used to experimentally screen for inhibitors of *BmNRS* among tens of thousands of extracts from diverse microbial strains, which resulted in the identification of multiple natural compound inhibitors.³³⁸⁻³³⁹

Furthermore, the reaction intermediate asparaginyl-adenylate (AsnSA (**3.12**), Figure 3.6) was screened against *in vitro* cultures of *P. falciparum* 3D7, with an IC_{50} of 88.3 nM, validating the potential of AsnRS as a drug target in the malaria parasite.³⁴⁰

Lysyl-tRNA synthetase inhibitors

As a result of a phenotypic screen of a natural product library with the goal to identify inhibitors of *Plasmodium falciparum* blood- and liver-stage proliferation, cladosporin (**3.13**, Figure 3.6) was identified. The fungal secondary metabolite inhibits both blood and liver proliferation of *P. falciparum* at a nanomolar range ($EC_{50} \approx 40-90$ nM).³⁴¹ Using reverse genomic approach the *P. falciparum* lysyl-tRNA synthetase was identified as cladosporin's target and demonstrated that *PfKRS* was a druggable drug target for both blood and liver stages of malaria.²⁰⁵ The crystal structure of the ternary complex *PfKRS*-lysine-cladosporin, reveals structural differences among the different homologs that may allow for the design of selective inhibitors that act against the *Plasmodium* but not the human KRS.³⁴² Furthermore, research to understand the high selectivity of cladosporin, in spite of the drug acting by interaction with the ATP binding pocket of KRS, revealed that the binding of lysine to *PfKRS* induces a series of conformational changes in the active site of the enzyme that further favors the binding of cladosporin and stabilizes the complex *PfKRS*-lysine-cladosporin.³⁴³⁻³⁴⁴

To investigate the potential of the apicoplast *PfKRS* isoform as a drug target, inhibitors based on the lysyl-adenylate intermediate were designed and synthesized. Two of the tested compounds had potent delayed death inhibition and inhibited aminoacylation by recombinant apicoplast *PfKRS*.²⁸²

Methionyl-tRNA synthetase inhibitors

Due to the successful inhibition of bacterial MRS by diaryl diamine inhibitors, where high selectivity of bacterial versus mammalian enzyme was observed,³⁴⁵⁻³⁴⁶ efforts have been made to identify novel inhibitors of the *Trypanosoma brucei* MRS.³⁴⁷

Homology models based on several MetRS structures were used to guide synthesis of related *T. brucei* MRS inhibitors, and these were tested for binding to *TbMetRS*. Compounds were also screened using *ex vivo* cultures of *T. brucei* and *T. cruzi*, the most effective compound, an aminoquinolone derivative (**3.14**, Figure 3.6), showed an IC_{50} of 4 nM and low toxicity for mammalian cells.³⁴⁷ Further studies have also characterized the structures of *Leishmania* MRS³⁴⁸ and the *TbMRS*³⁴⁹⁻³⁵⁰ bound to substrates (Met, Met-AMP) and inhibitors, in the case of the *TbMetRS*, and have shown for the latter that the mechanism of resistance consists on an amplification of the target gene.³⁵¹ Two orthogonal highthroughput screening assays have recently

been developed to identify inhibitors of the *TbMRS*.³⁵²

Plasmodium falciparum nuclear genome encodes two copies of methionyl-tRNA synthetase,²⁸⁶ a recent report provides evidence of the localization of each *PfMRS* isoform and screened a small molecule drug-like library identifying two bacterial MRS inhibitors, REP3123 ($EC_{50} = 144$ nM) and REP8839 ($EC_{50} = 155$ nM) (**3.15**, Figure 3.6), as well as three new hit compounds ($EC_{50} < 500$ nM).³⁵³

Threonyl-tRNA synthetase inhibitors

Borrelidin (**3.3**, Figure 3.6), a structurally unique 18-membered macrolide, acts as a selective inhibitor that binds to some bacterial and eukaryotic threonyl-tRNA synthetase (TRS) enzymes.³⁵⁴ This polyketide natural product displays antibacterial, antifungal, antimalarial, anticancer, insecticidal and herbicidal activities through the selective inhibition of TRS. This broad activity seems to be related to the occupation of a significant fraction of the total volume of the TRS enzymatic pocket, physically excluding all three of the physiological substrates of TRS. Although occupying the canonical active site cavity, borrelidin also extends into a fourth ‘orthogonal’ pocket.³⁵⁵

Plasmodium possesses only one *PfTRs*, a dual-targeted enzyme, which is trafficked to the apicoplast and cytosol.²⁸⁷ The immediate inhibition of *P. falciparum* cultures seen with Borrelidin is consistent with the requirement of the cytosolic *PfTRs* for its activity. The effect of M-threonine was also tested, which appears to curtail its antimalarial activity, possibly through effect on threonyl-tRNA synthetase.³⁵⁶

Borrelidin was found to express antimalarial activity against drug-resistant *P. falciparum* parasites, with an IC_{50} value of 0.97 nM. However, it also displays strong cytotoxicity against mammalian cells.³⁵⁷ To circumvent this problem, borrelidin-like series have been generated and tested for their antimalarial activity as well as for their toxicity. Some of the semisynthetic borrelidin analogs were found to effectively lose toxicity against human cells while retaining potent antiparasitic activity both *in vitro* and *in vivo*.³⁴⁰

Other aa-tRNA synthetases inhibitors

Due to their essential role in protein synthesis, all of the parasite's aminoacyl-tRNA synthetases represent a potential drug target in the fight against malaria. Nonetheless not all of these enzymes have been further pursued as drug targets and inhibitors have not been reported thus far in the *Plasmodium falciparum* parasite.

More recently, studies including *PfWRS*,³⁵⁸⁻³⁵⁹ *PfFRS*,²⁸⁹ *PfCRS*³⁶⁰ or *PfDRS*³⁶¹ have aimed at further characterizing each enzyme in *P. falciparum*, in an effort to provide additional background for unraveling the functional properties of each of the parasite's aaRS and creating a platform for the development of specific inhibitors. In a different approach, five reaction intermediate analogs, GluSA, GlnSA, AsnSA, TyrSA and SerSA, were screened for *in vitro* antimalarial activity against *P. falciparum* 3D7 strain. Inhibitors exhibited high to moderate activity ranging from 39.5 nM to 372 nM.³⁴⁰

3.2 Purpose of This Study

Aminoacyl-tRNA synthetases and associated pathways have been proposed as attractive targets for chemotherapeutic intervention in malaria.²⁵² While some tRNA synthetase inhibitors that were identified in other organisms display antimalarial activity, validation of actual on target mechanism has been elusive.^{281, 287, 327} The repertoire of aaRSs in *Plasmodium* diverges from other organisms because of the need to carry out protein synthesis in multiple subcellular compartments.²⁸⁷ Although underexploited for many years, it has been demonstrated that the plasmodial aaRS are not only druggable enzymes but also that selective inhibition of these enzymes versus their human homologs is feasible.²⁴⁶

As mentioned above, our group has established for the first time in *Plasmodium* that inhibition of tRNA synthetases by a small molecule and simultaneous activation of the integrated stress response is both feasible and attractive, and provides a rational mechanistic basis for future drug discovery and development focused on this novel target and pathway. We hypothesized that the inhibition of some but not all, *P. falciparum* aaRSs will result in activation of amino acid response pathways and that inhibition of this subgroup represents an attractive approach for chemotherapeutic intervention in malaria.

The general aim of this research project is to build on these important findings and apply an integrated chemogenomic approach to identify and biologically characterize selective small

molecule inhibitors for the cPRS that are suitable as lead candidates for preclinical broad-spectrum malaria drug development. This work has the potential to have a major impact on both basic malaria biology and applied biomedical research. This project is organized into three different, but complementary, objectives.

1. Explore tRNA synthetases as novel targets in *P. falciparum*

Our goal is to better understand the biological consequences of inhibiting the different aaRSs and identify the critical downstream events responsible for the killing of the malaria parasite. To explore the potential of the aminoacyl-tRNA synthetase family as a source of antimalarial drug targets, we have designed a library of 21 reaction intermediate analogs to profile 19 of the *PfaaRS* as drug targets. The desired aa-AMP analogs (Figure 3.8) will be obtained through robust synthetic methods and will be used as tool compounds to gain insights into the potential of each tRNA synthetase as a target for chemotherapeutic intervention in *P. falciparum*.

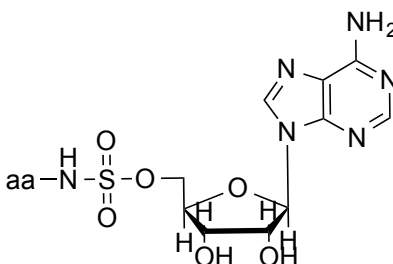


Figure 3.8 – Sulfamoyl aminoacyl-AMP analogs.

2. Develop Hybrid-Halofuginone derivatives with high parasite specificity

This aim is designed to pharmacologically characterize and develop novel HFG analogs. Common to all aaRSs are three potential target sites, including the active site, editing site and anticodon binding site (Figure 3.10a). Most aaRS inhibitors bind to the catalytic site, mimicking ATP and/or the cognate amino acid. HFG binds in a novel mode, forming a ternary complex with ATP and simultaneously mimicking proline and the 3' end of bound tRNA (Figure 3.9).⁷ Based on the complex formed by HFG and ATP in the active site of cPRS, hybrid-halofuginone derivatives were designed and will be synthesized following a strategy that is based on a concise asymmetric synthetic strategy (23% overall yield, 14 steps) by Lin and coworkers.

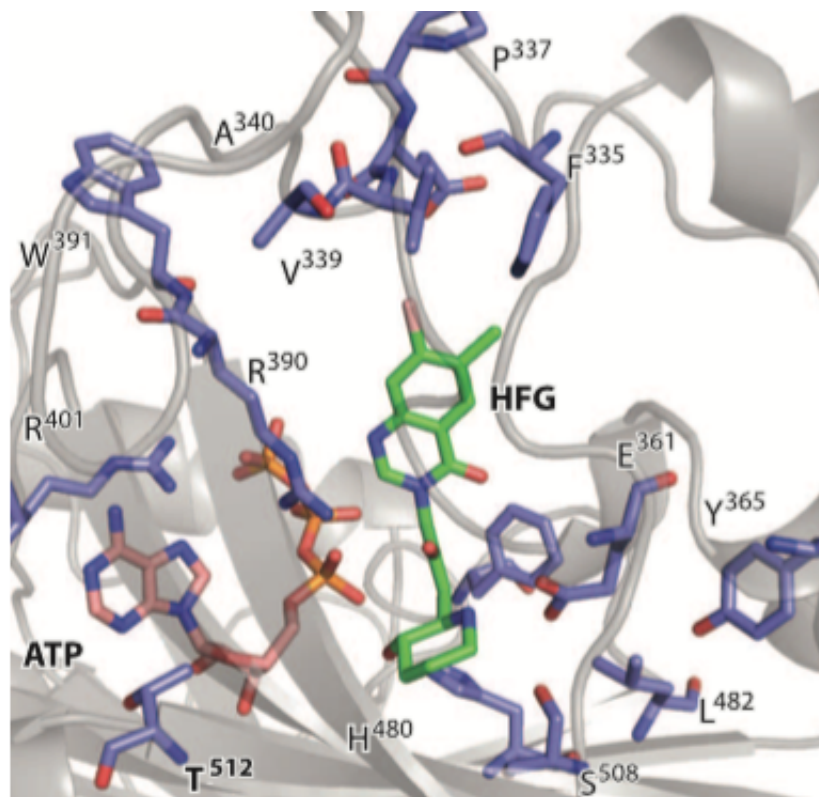


Figure 3.9 – Molecular dynamics simulations of the ternary complex of *Pf*PRS with ATP and halofuginone. Image adapted from Herman *et al.*⁷

3. *Characterize the biology of cPRS inhibition and amino acid starvation response*

The objective of this aim is to provide functional insights in the biology of cPRS inhibition, thus characterizing the enzyme-inhibitor complex underlying the mechanism of action of the inhibitors and potential activation of the amino acid starvation response. Unlike halofuginone and halofuginol, the nonhydrolyzable L-prolyl sulfamoyl adenosine substrate analog (ProSA) does not induce the phosphorylation of eIF2 α in mammalian cell lines (data not published), which is a sensitive indicator of the starvation response.

Understanding the enzyme-inhibitor complex formed by the different types of inhibitors (Figure 3.10b) will further elucidate on the differential effect observed on the amino acid starvation response, despite targeting the same enzyme.

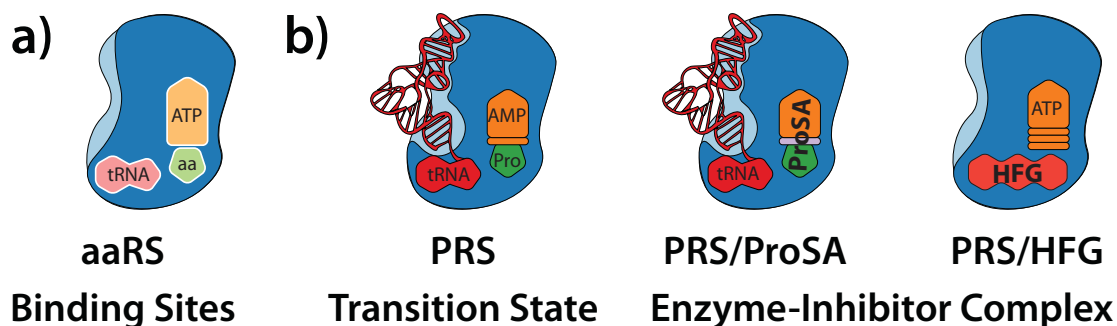


Figure 3.10 – a) aaRSs sites: active site, editing site and anticodon binding site; b) PRS transition state and enzyme-complex formed with two different inhibitors (ProSA and HFG).

3.3 Explore tRNA Synthetases as Novel Targets in *P. falciparum*

As discussed above, reaction intermediate-based inhibitors of aminoacyl-tRNA synthetases have been used as potential anti-infectives. The structures of the reaction intermediates have been the focus for the development of novel synthetic compounds that target aaRS. Aminoacyl-adenylates (aa-AMP) have lower dissociation constants than the amino acids and ATP, and thus, the choice of the intermediate is advantageous in the design of novel synthetic compounds with high affinity.³⁶²⁻³⁶³ The synthesis of aa-AMP analogs bearing non-hydrolyzable phosphate isosteres is of great value as chemical tools in exploring the different tRNA synthetases as potential novel targets in *P. falciparum*. Modifications of the aminoacyl-adenylate have been investigated for the purpose of improving chemical stability, tight binding and pathogen selectivity. Many of the modifications were made in the linker region since the mixed anhydride acyl-phosphate bond of the intermediate is readily susceptible to hydrolysis. Several types of stable analogs of aa-AMP inhibit their cognate aaRSs. Moreover, the aminoacyl-sulfamate bioisoster yields the most potent inhibitors with improved hydrolytic stability and a well-established synthetic strategy, ideal for tool compounds to profile the class of aaRSs. Unfortunately, these analogs have poor *in vivo* efficacy due to lack of efficient cell-penetration.^{290-291, 301, 303, 364}

We designed, synthesized and evaluated the antimalarial activity of a series of sulfamoyl-aminoacyl-adenosines. We envisioned that the developed protocol should be general and applicable to the various different amino acids.

3.3.1 Synthetic Methodology

3.3.1.1 Chemical Synthesis Strategy

The synthesis of sulfamoyl-aminoacyl-AMP derivatives has been established for a subset of the analogs. The retrosynthetically deconstruct according to what has been cited in the literature³⁶⁵ (Figure 3.11) shows a short and robust approach starting with a commercially available protected adenosine. After sulfamylation of 2', 3'-O-isopropylideneadenosine, the desired analogs can be obtained by coupling with the protected *N*-hydroxysuccinimide ester of each amino acid under basic conditions, followed by full deprotection of the obtained intermediates. Deprotection conditions vary depending on the protective group used for each functional group on the intermediates and may require multiple steps.

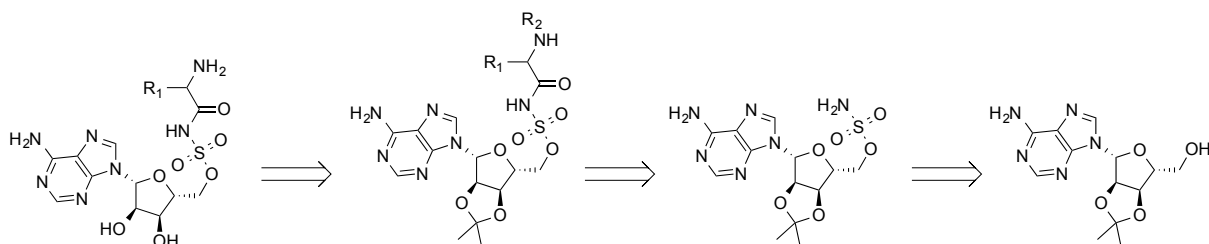
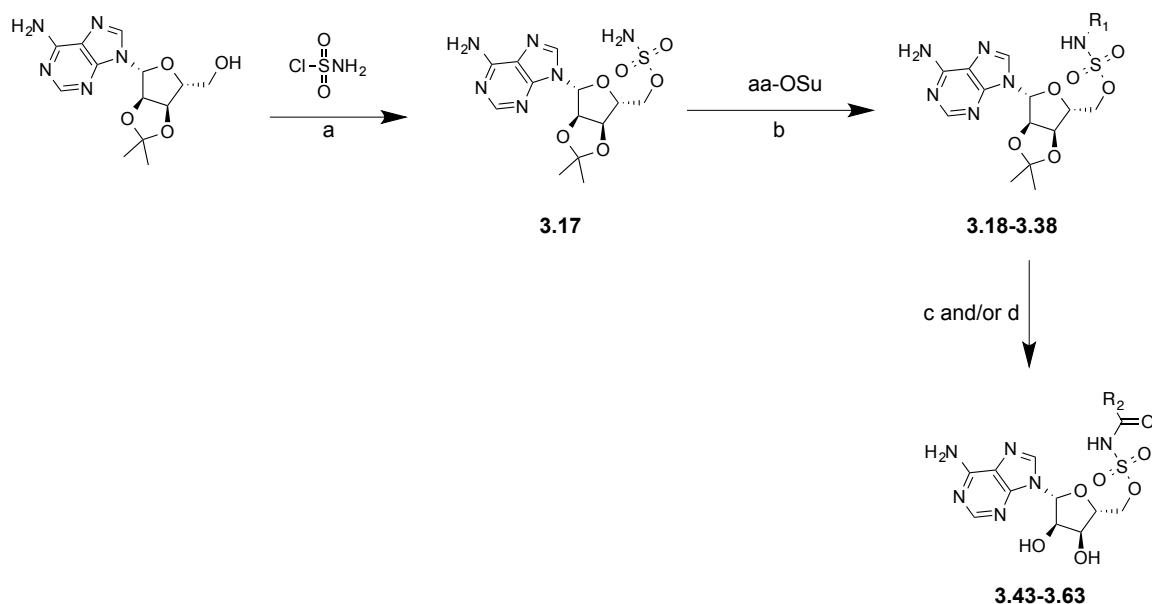


Figure 3.11 – General retrosynthetic scheme of aminoacyl-sulfamoyl-AMP analogs.

3.3.1.2 Synthesis of aa-AMP Analogs

Sulfamoyl based analogs of aa-AMP are useful for structural and biochemical studies of aaRSs and as potential lead compounds for drug development. The overall yields are very dependent on the amino acid and the protecting groups used in the synthesis and consequently some sulfamoylated analogs of aa-AMP are difficult to attain.

Herein, we report a short synthetic strategy enabling the rapid synthesis of a library of sulfamoyl analogs of the aa-AMP intermediate (aaSA). The synthesis of the target compounds is illustrated in Scheme 3.2.



Scheme 3.2 – Synthesis of sulfamoylated aa-AMP analogs. Reagents and conditions: **a)** NaH, DME, 0 °C → r.t., 4 h, 65%; **b)** DBU, DMF, r.t., 4 h; **c)** TFA/H₂O (5:1), r.t., 30 min; **d)** 10% Pd/C, 0%-1% glacial acetic acid, DMF, H₂, 2-8 h, r.t.

We synthesized the library of desired aaSA compounds, in 3-4 steps, as shown in scheme 3.2, starting with the synthesis of the key sulfamoyl intermediate **3.17**.

Several different experimental procedures for the sulfamoylation of the 5'-hydroxyl moiety have been reported in the literature including the use of sulfamoyl chloride as reagent in the presence of different bases.^{303, 363, 366-368} A set of different reaction conditions was evaluated to identify the optimal system for high yielding formation of **3.17** in a large scale (Table 3.1).

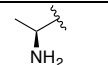
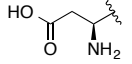
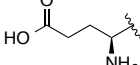
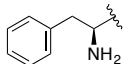
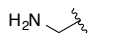
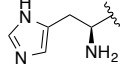
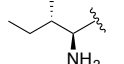
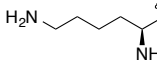
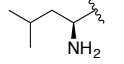
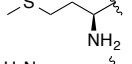
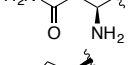
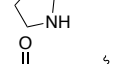
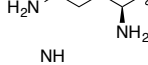
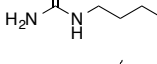
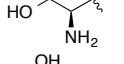
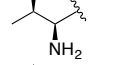
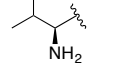
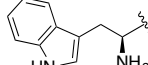
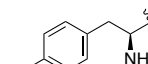
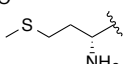
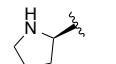
Table 3.1 – Optimization of the sulfamoylation of 2', 3'-O-isopropylideneadenosine.

Entry	Sulfamoyl chloride (equiv.)	Base	Solvent	Reaction conditions (Temp. (°C), time (h))	Scale (g)	Yield (%)
1	2.3	-	DMA	0 → rt, 4	2	67%
2	1.5	NaH	DME	0 → rt, 4	2	93%
3	1.5	NaH	DME	0 → rt, 4	20	65%

Two different conditions were tested with varying strengths. When DMA was used without the addition of any base (Entry 1) compound **3.17** was obtained in 67% yield, while the use of a strong base such as NaH (Entry 2) gave the desired sulfamoyl intermediate in 93% yield, in the same scale. Since using a strong base in DME gave a higher yield, the same conditions were used to scale-up the reaction (Entry 3) to 20 g, where the desired compound was obtained in 65% yield. The protected amino acids were coupled following sulfamoylation. The most frequently reported literature method for the formation of acylsulfamates is the use of *N*-Boc protected *N*-hydroxy succinimide (OSu) amino acid esters in the presence of DBU.^{303, 363, 367, 369} All amino acids were commercially available as OSu esters and had only few, major protecting groups (Boc, Cbz or OtBu) depending on the different functional groups present. The acylsulfamate compounds were obtained by coupling of the sulfamoyl intermediate **3.17** with the corresponding amino acids to give the title compounds **3.18-3.38** (Scheme 3.2), with yields ranging from 12%-69% (Table 3.2).

Protecting groups were removed in the final step to afford compounds **3.43-3.63** (Scheme 3.2), in 0.36%-97% yield (Table 3.2). Deprotection was done with strong acidic conditions, followed by catalytic hydrogenation, in a two-step synthesis originating intermediates **3.39-3.42**, before affording the desired compounds **3.49** and **3.56-3.58**. The lower yields obtained in some aaSA were probably due to either the amino acid side chains having favorable lengths to perform undesired reactions once deprotected or decomposition of the adenosine moiety under deprotection conditions.

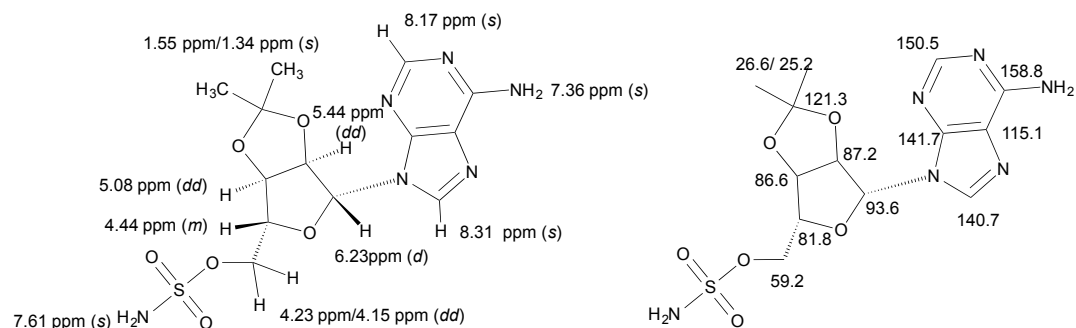
Table 3.2 – Yield of synthesized compounds. *Yield over two steps.

Compound	R ₁	Yield (%)	Compound	R ₂	Yield* (%)	
3.18	Boc-Ala-	42	3.43	AlaSA		35
3.19	Z- Asp(OtBu)-	40	3.44	AspSA		0.9*
3.20	Boc- Glu(OtBu)-	23	3.45	GluSA		39
3.21	Boc-Phe-	39	3.46	PheSA		64
3.22	Boc-Gly-	42	3.47	GlySA		34
3.23	Boc-His(1- Boc)-	29	3.48	HisSA		30
3.24	Boc-Ile-	32	3.49	IleSA		40
3.25	Boc-Lys-	22	3.50	LysSA		35
3.26	Boc-Leu-	31	3.51	LeuSA		19
3.27	Boc-Met-	56	3.52	MetSA		34
3.28	Boc-Asn-	15	3.53	AsnSA		97
3.29	Boc-Pro-	40	3.54	ProSA		36
3.30	Boc-Gln-	30	3.55	GlnSA		44
3.31	Z-Arg(Z) ₂ -	39	3.56	ArgSA		9.5*
3.32	Z-Ser(Bn)-	69	3.57	SerSA		4.1*
3.33	Z-Thr(tBu)-	46	3.58	ThrSA		2.6*
3.34	Boc-Val-	38	3.59	ValSA		43
3.35	Boc-Trp-	12	3.60	TrpSA		34
3.36	Boc-Tyr-	48	3.61	TyrSA		30
3.37	Boc-D-Met	19	3.62	D-MetSA		31
3.38	Boc-D-Pro-	35	3.63	D-ProSA		37

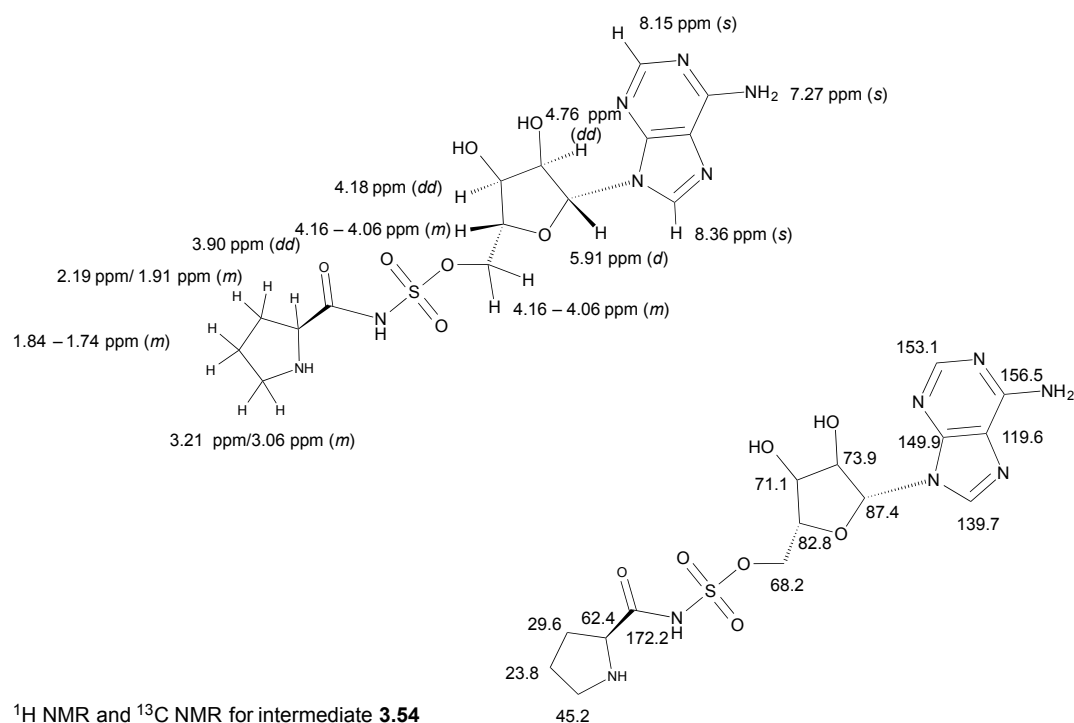
All synthesized compounds were purified by flash chromatography and the purity was assessed with HPLC-ELSD-MS prior to profiling for antiparasitic activity and cytotoxicity (purity was > 90%). The structures of all compounds were confirmed by NMR spectroscopy using ^1H -NMR, ^{13}C -NMR and two-dimensional experiments, including ^1H - ^1H COSY, HMQC and HMBC (see details in Chapter 6).

The attribution of the ^1H and ^{13}C NMR of key intermediate **3.17** and final analog **3.54** is shown in Figure 3.12. The results are in accordance with the chemical structure of the compounds (Chapter 6). When analyzing the NMR spectra of the adenosine intermediate **3.17** we observe four singlet signals in the aromatic region, two of which integrates to two protons (the $-\text{NH}_2$ in the adenosine and the $-\text{NH}_2$ in the sulfamoyl group) and the other two integrate to one proton (8.31 ppm and 8.17 ppm). Furthermore, five signals integrating to six protons (one *d*, four *dd* and one *m* signal) are present in the spectra region from 6.23 – 4.15 ppm, accounting for the rest of the adenosine protons. Moreover, two singlets integrating to three protons each, confirm the presence of the acetal-protecting group. When analyzing data regarding analog **3.54**, the assignment of the NMR spectra reveals the presence of three additional proton signals that integrate to seven protons, when compared to intermediate **3.17**, which is consistent with the presence of the proline group. Furthermore, the ^{13}C NMR displays a signal at 172.2 ppm consistent with the presence of the carbonyl group and a shift in the signals corresponding to the carbons adjacent to the hydroxyl groups (73.9 and 71.1 ppm) due to the acetal deprotection (Figure 3.12).

Chapter 3 – Aminoacyl-tRNA Synthetase Inhibitors as Antimalarials



^1H NMR and ^{13}C NMR for intermediate **3.17**



^1H NMR and ^{13}C NMR for intermediate **3.54**

Figure 3.12 – Assignment of ^1H and ^{13}C NMR of compounds **3.17** and **3.54**.

3.3.2 Antimalarial and Cytotoxic Activities

The synthesized aaSA analogs were profiled for dose-response in intraerythrocytic stage parasites to determine half maximal effective concentrations (EC_{50}) against CQ-sensitive 3D7, CQ-resistant Dd2 and ProRS mutant (cPRS:L482H) strains. The reference antimalarials atovaquone, amodiaquine and artesunate were included as controls and resulted in EC_{50} s in agreement with published results. Halofuginone, a febrifugine derivative, which targets cPRS was also included (Table 3.3). Cytotoxicity (EC_{50}) of selected compounds for human cells

(MCF-7) and selectivity index for CQ-resistant Dd2 (SI_{res}) and CQ-sensitive 3D7 strains (SI_{sen}) are also reported in Table 3.3.

Furthermore, HFG was tested against the three strains and exhibited an EC_{50} of 1.16 nM (3D7), 1.05 nM (Dd2) and 255 nM (cPRS:L482H) (Table 3.3) which confirmed our previously observed cross-resistance with the mutant strain.⁷

Our results show that most of the aaSA analogs were equally active *in vitro* against both blood stage *P. falciparum* strains in the nanomolar range (Table 3.3). Among these compounds, we found that L-PheSA, L-HisSA, L-AlaSA and L-ProSA were the analogs that exhibited higher antimalarial activity, with EC_{50} against the Dd2 strain of 120 nM, 98.4 nM, 119 nM and 96.9 nM, respectively. Among the tool compounds with lower antimalarial activity were L-IleuSA, L-TrpSA, L-LysSA and L-GluSA, with EC_{50} against the Dd2 strain of 2390 nM, 1220 nM, 1130 nM and 1210 nM, respectively.

Aminoacyl-tRNA synthetases in many instances discriminate between the L- and D-amino acids due to their stereospecificity, thus we hypothesized that D-aaSA analogs would not be recognized by the respective enzyme, and would display decreased activity compared to its L-aaSA counterpart. To experimentally verify this possibility we synthesized two D-aaSA analogs, D-ProSA and D-MetSA, and profiled their antimalarial activity.

Table 3.3 – *In vitro* antimalarial activity (EC₅₀) and cytotoxicity (EC₅₀) of aaSA compounds.

Compound	<i>P. falciparum</i>			MCF7	Selectivity Index (SI _{res} ^a)	
	EC ₅₀ ±SD (nM)			EC ₅₀ ±SD		
	3D7	Dd2	PRS: L482H	(µM)		
3.5	HFG	1.2±0.2	1.0±0.2	255±15	0.04±0.03	38.0
3.43	AlaSA	99.5±27	119±25	135±22	>50	>420
3.44	AspSA	414±150	963±340	25.8±6.6	0.5±0.1	0.5
3.45	GluSA	734±290	1210±90	1120±50	2.0±0.2	1.7
3.46	PheSA	84.6 ±7.9	120±37	96.5±5.1	3.3±0.3	27.3
3.47	GlySA	209±82	337±55	380±73	3.2±0.4	9.4
3.48	HisSA	78.3±11	98.4±17	105±15	3.3±0.01	33.9
3.49	IleSA	1560±130	2390±210	2280±140	13.7±0.04	5.7
3.50	LysSA	812±230	1130±170	1260±160	3.5±0.2	3.1
3.51	LeuSA	348±30	645±68	621±49	11.2±0.3	17.3
3.52	MetSA	291±30	610±52	594±51	0.9±0.2	1.4
3.53	AsnSA	134±5.6	517±87	502±160	5.0±0.3	9.7
3.54	ProSA	87.3±16	96.9±7.1	122±31	2.0±0.03	20.7
3.55	GlnSA	112±26	149±6.8	170±14	1.5±0.02	10.0
3.56	ArgSA	519±7.2	336±78	253±42	2.6±0.6	7.7
3.57	SerSA	478±73	628±91	1070±81	11.6±1.2	18.7
3.58	ThrSA	98.3±13	296±110	312±41	2.2±0.5	7.4
3.59	ValSA	122±21	153±26	162±16	1.1±0.1	6.9
3.60	TrpSA	862±60	1220±170	1710±920	>50	>41
3.61	TyrSA	256±62	398±33	474±110	7.9±0.1	19.9
3.62	D-MetSA	1280±300	1760±320	1700±400	1.8±0.8	1.0
3.63	D-ProSA	781±280	1190±120	1190±83	4.4±0.1	3.7
	Atovaquone	0.2±0.05	0.2±0.03	0.17±0.02	nd	n.d.
	Amodiaquine	2.7±0.5	3.3±0.3	1.2±0.2	nd	n.d.
	Artesunate	14.4±4.3	14.4±4.8	nd	nd	n.d.

^a SI_{res} = EC₅₀ MCF7 / EC₅₀ PfDd2; n.d.= not determined;

When comparing the activity of the L- and D-aaSA against Dd2 strain, we can detect a 3-fold decrease in activity for MetSA (L-MetSA EC_{50} 610 nM and D-MetSA EC_{50} 1760 nM), and a 10-fold decrease in activity when comparing L-ProSA (EC_{50} 96.9 nM) to D-ProSA (EC_{50} 1190 nM).

The library of aaSA analogs was also tested against the *P. falciparum* PRS mutant (PRS:L482H) strain in order to verify that none of the analogs targeted PRS non-specifically.

Interestingly, the ProSA analog did not present significant decrease in activity when comparing the EC_{50} between both strains, EC_{50} against the Dd2 strain of 96.9 nM and EC_{50} against the PRS:L482H strain of 122 nM, as it might have been expected since it targets the same enzyme as HFG. Previously, we investigated the L482H *Pfc*PRS mutant to understand the observed decreased sensitivity to halofuginone. Molecular modeling studies show Leu482 is adjacent to the proline-binding pocket, and although it does not directly participate in the hydrogen bond network formed between halofuginone and *Pfc*PRS, it does support the binding geometry of the amino acid residues that directly interacts with halofuginone. The histidine in the L482H mutant provides an alternative hydrogen bond acceptor, thus destabilizing the network, which in turn impacted the halofuginone-ATP interaction, likely to explain the experimental observation.

Analysis of the interactions between ProSA and each of the enzymes (*wtPfc*PRS and *Pf*PRS:L482H) may further explain the absence of cross-resistance observed (Data not Published-Figure 3.13)

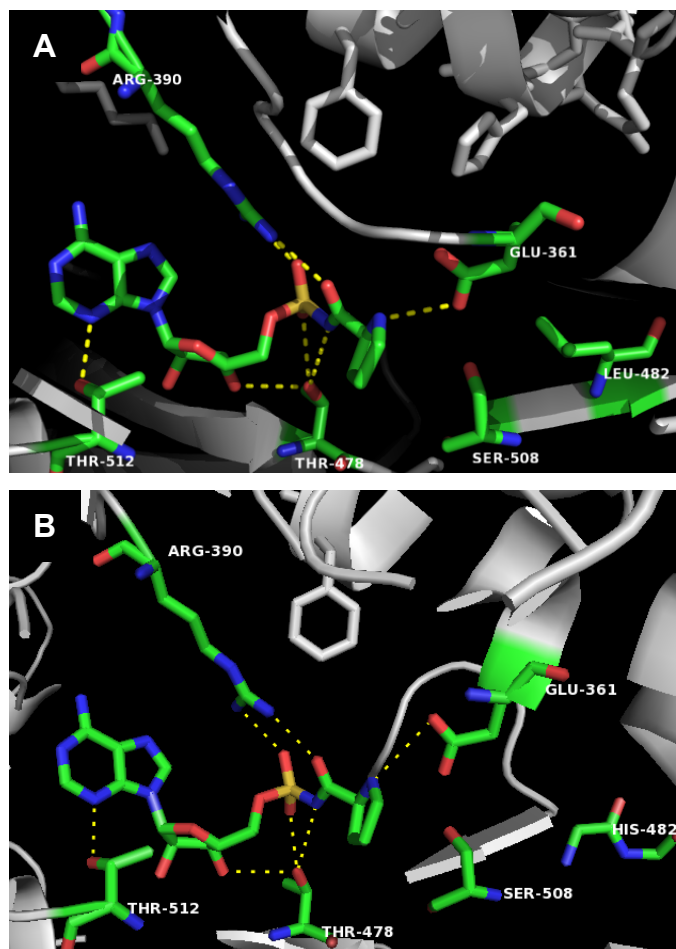


Figure 3.13 – Molecular docking of the complex of PRS with ProSA. (A) Interaction with the wild-type *fc*PRS of *P. falciparum* and (B) the *Pfc*PRS L482H mutant of *P. falciparum*. The lack of cross-resistance can be explained by the fact that the mutation in residue 482 does not interfere with the network of possible hydrogen bonds between the enzyme and the inhibitor. Image generated using PyMOL version 1.7.0.5 for Mac.

Thus, one possible justification is, since ProSA's antimalarial activity does not rely on the interaction with ATP and consequent formation of the ternary complex, as seen for halofuginone, its activity may not be affected by the mutation, when tested against *P. falciparum* PRS:L482H strain. As such, a mutation adjacent to the proline-binding pocket, as the one present in PRS:L482H strain, which does not directly interfere in the hydrogen bond network between the inhibitor and the enzyme, may not significantly affect the antimalarial activity of the ProSA analog.

Cytotoxicity profiling in human MCF-7 cell line shows a wide range of EC_{50} and selectivity index among the aaSA analogs, underscoring the potential to specifically target the parasite aaRS with little to no effect over the human homolog, in some cases (Table 3.3). We found that some analogs have effectively decreased toxicity against human cells, when compared to halofuginone (EC_{50} against MCF-7 cells of 0.04 μ M and SI=38.0). Among the analogs with lower cytotoxicity were L-LeuSA, L-IleuSA, L-TrpSA, L-AlaSA and L-SerSA, with EC_{50}

against MCF-7 cell line of 11.2 μM , 13.7 μM , >50 μM , >50 μM and 11.6 μM , respectively. Interestingly, when comparing the EC_{50} of halofuginone to that of ProSA against MCF-7 cells, we can see a 50-fold decrease in cytotoxicity, although targeting the same enzyme (Table 3.3). Thus, emphasizing the potential to improve specificity towards the parasite's enzyme over the human aaRS by modifying the compound's scaffold or targeting different sites within the enzyme. Furthermore, amongst the analogs with higher antimalarial activity, L-AlaSA stands out by being one of the compounds with lower cytotoxicity, with EC_{50} against the Dd2 strain of 119 nM and EC_{50} against MCF-7 cell line greater than 50 μM , with a selectivity index higher than 420.

The wide range of EC_{50} observed for the different analogs underlines the differential potential among these enzymes to act as antimalarial drug targets. Furthermore it can be argued that any of the aaRS can be potential antimalarial drug targets since the inhibitor with lowest activity still has a low micromolar EC_{50} . Thus, taken together the blood stage *in vitro* *P. falciparum* activity results allow the prioritization of the phenylalanyl tRNA synthetase (FRS), histidyl tRNA synthetase (HRS), alanyl tRNA synthetase (ARS) and prolyl tRNA synthetase (PRS) as the top four enzymes for further exploration as drug targets in blood stage malaria.

Since HFG and its derivatives, which target *P. falciparum* prolyl-tRNA synthetase are equally active against both *in vitro* and *in vivo* *P. berghei* liver stage parasites,^{7, 316} we decided to profile the library of aaSA analogs for its *in vitro* liver stage activity in order to investigate the potential for dual-stage activity when targeting each of these enzymes. The synthesized derivatives were evaluated at 1 μM and 10 μM for their growth inhibitory activity against an *in vitro* *P. berghei* ANKA liver-stage model (Figure 3.14).

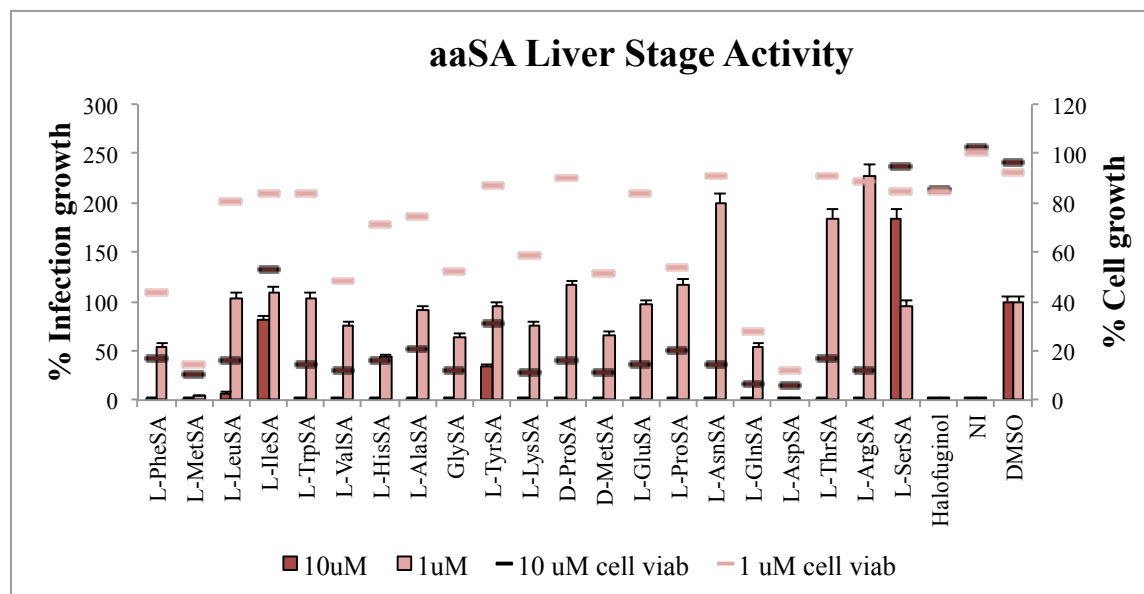


Figure 3.14 – *In vitro* *P. berghei* growth (%) and HepG2 A16 human hepatic cell line viability (%) at 10 μ M and 1 μ M of drug treatments. DMSO and not infected cultures (NI) were used as controls.

Our results show that most of the aaSA analogs were active against liver stage *in vitro* *P. berghei*, with >99% parasite growth inhibition at the higher concentration of 10 μ M. Compounds L-SerSA, L-IleuSA and L-TyrSA, were the exception, with no growth inhibition, 29% and 66% growth inhibition, respectively (Figure 3.14). Furthermore, HepG2 A16 human hepatic cell line viability was also determined and most compounds displayed cytotoxicity at the higher concentration. Among the derivatives tested, we found that only three compounds presented moderate to high parasite growth inhibition at the lower concentration of 1 μ M (L-HisSA, L-MetSA and L-Asp, showed 45%, 95% and 99% parasite growth inhibition, respectively), while the rest of the analogs showed < 50% parasite growth inhibition at 1 μ M.

Furthermore, halofuginol was also tested against the *in vitro* *P. berghei* ANKA liver-stage model and exhibited >99% parasite growth inhibition at both concentrations (Figure 3.14) which confirmed our previous results.

Taken together results allow the prioritization of the phenylalanyl tRNA synthetase (FRS), histidyl tRNA synthetase (HRS), and prolyl tRNA synthetase (PRS) as the top three enzymes for further exploration as potential dual-stage drug targets.

Dual-stage activity is essential for antimalarial drugs that will be used to eliminate malaria. The results obtained, together, are consistent with our hypothesis that aaRS family in

general is attractive as a novel class of antimalarial drug targets, with some of these enzymes having potential for dual-stage activity.

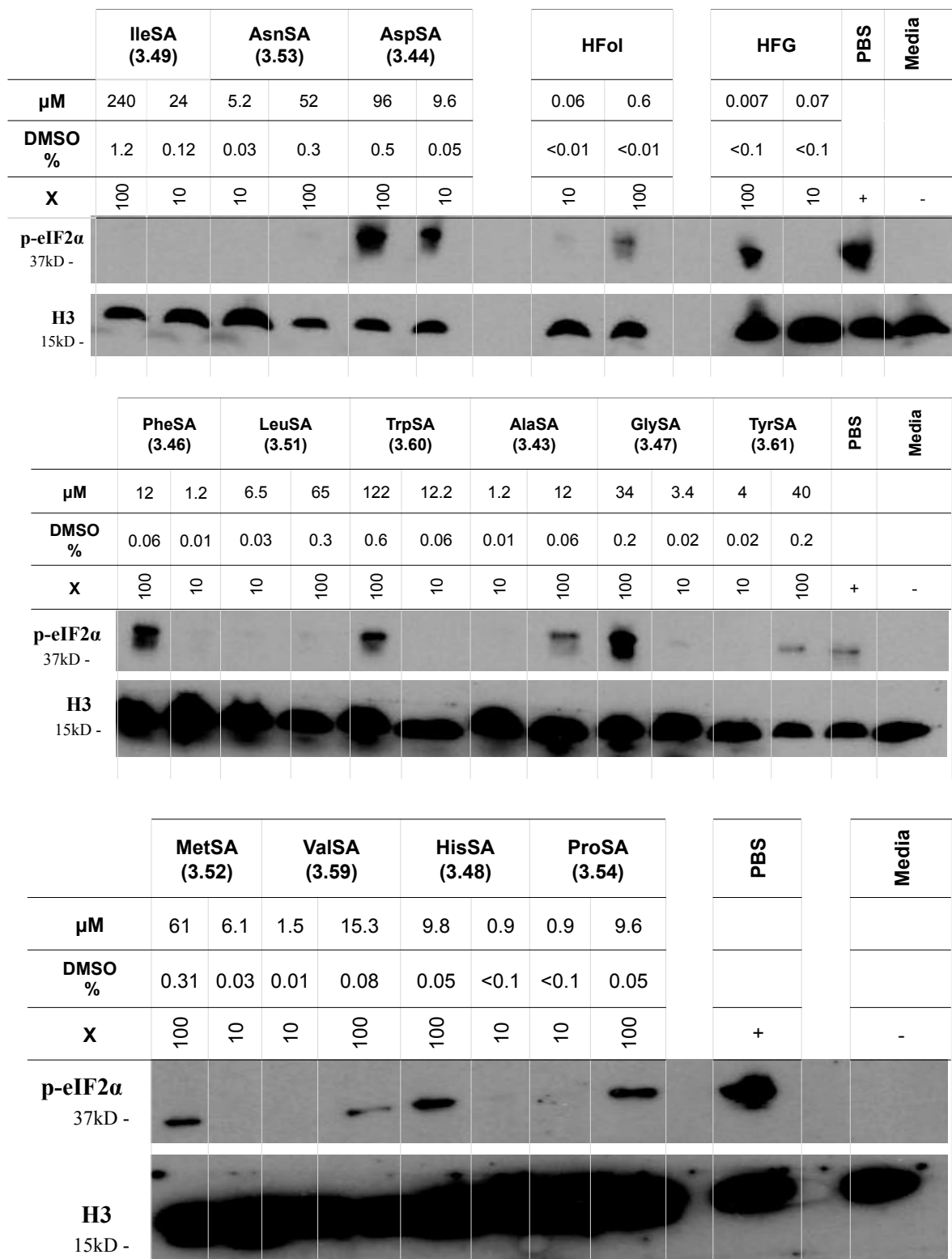
3.3.3 Amino Acid Starvation Pathway Activation

After profiling the synthesized aaSA analogs for *in vitro* activity against the different *P. falciparum* strains, we next investigated how these analogs dysregulate the amino acid sensing mechanism in the parasite.

Recent research has confirmed the existence of a functional AAR in the intraerythrocytic stage of *P. falciparum* and has demonstrated induction of phosphorylated eIF2 α in response to amino acid starvation.²⁸¹ In mammalian cells, inhibition of EPRS by halofuginone or direct amino acid deprivation results in phosphorylation of the eukaryotic initiation factor 2 α (eIF2 α) and consequent activation of the amino acid response (AAR) pathway.⁸ Additionally, we have recently demonstrated the same effect in *P. falciparum* Dd2 strain.⁷

To probe for the activation of the AAR, we treated asynchronous *P. falciparum* Dd2 cultures with two concentrations of each aaSA (10x and 100x of each compounds' EC₅₀), using PBS as a positive control and media as a negative control, and compared the amount of phosphorylated eIF2 α by Western blot analysis (Figure 3.15).

Chapter 3 – Aminoacyl-tRNA Synthetase Inhibitors as Antimalarials



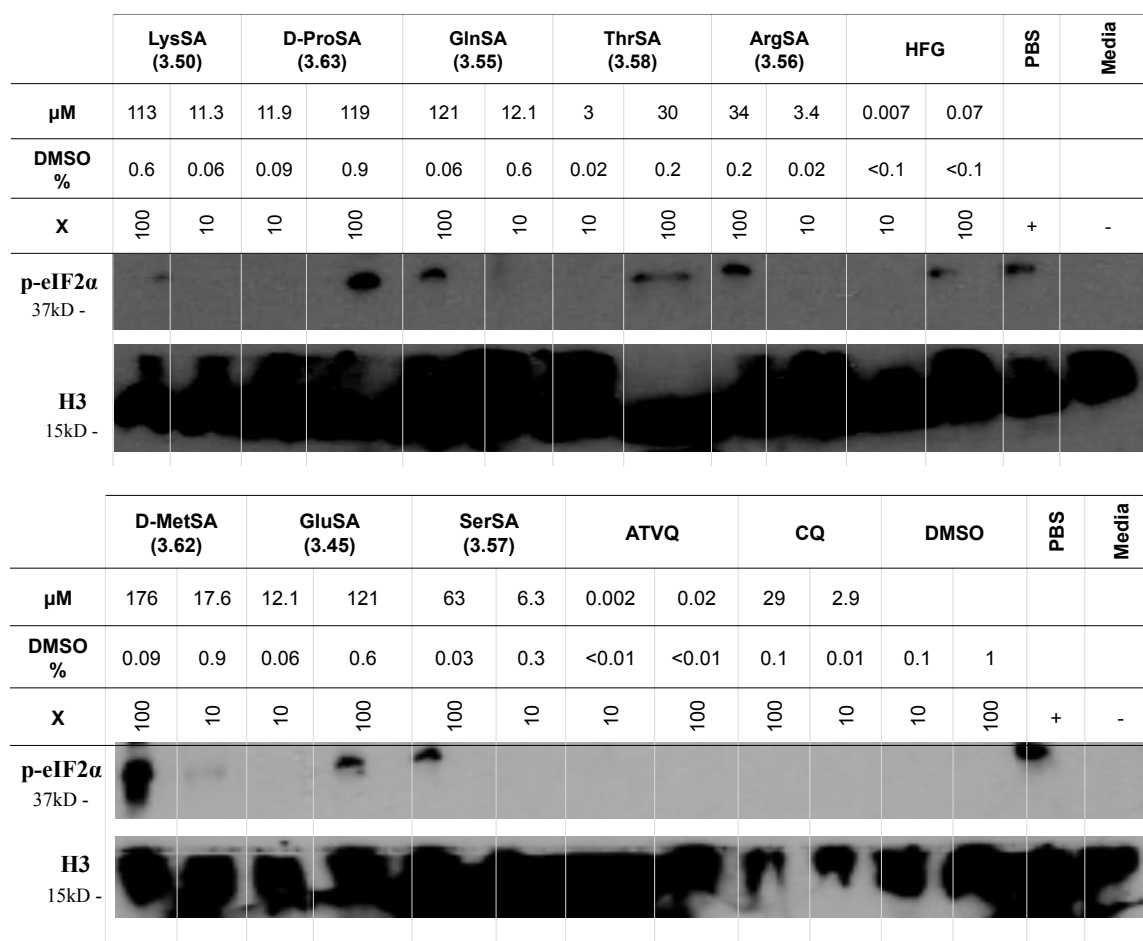


Figure 3.15 – Immunohistochemical detection of eIF2 α phosphorylation. In brief, the asexual Dd2 parasites were exposed to the experimental treatments for 90 minutes and the protein lysates from each sample were prepared from saponin released parasite pellets. All lysis buffers contained 1x Complete protease inhibitor cocktail (Roche) and 1x phosphatase inhibitor cocktail PhosStop (Roche). Western blots were probed with a phospho-specific eIF2 α pAb raised to a *P. falciparum* peptide antigen MSELpSKRRFRS, an eIF2 α pAb raised to *T. gondii* peptide KGYIDLSKRRVS which recognizes total eIF2 α protein and a histone-H3 rabbit pAb (Abcam ab1791). PBS treatment was used as a positive control for eIF2 α phosphorylation and untreated media as negative control.

Halofuginone and halofuginol, treatment increased eIF2 α phosphorylation in a dose-dependent manner that was comparable to eIF2 α phosphorylation during amino acid starvation (PBS treatment), in accordance to our previously observed results .

Atovaquone and chloroquine, two known antimalarials that act by different mechanisms of action, were also tested. Neither of the compounds increased eIF2 α phosphorylation, even at 100x of EC₅₀, consistent with what was expected since the amino acid sensing mechanism is linked to aaRS inhibition, which is not targeted by these compounds . Dimethyl sulfoxide (DMSO) and media control treatments also failed to increase eIF2 α phosphorylation.

Treatment with aaSA compounds increased eIF2 α phosphorylation at 100X concentration, with the exception of L-LeuSA, L-IleuSA and L-AsnSA. At the lower concentration (10x of EC₅₀), only treatment with L-Asp resulted in increased eIF2 α phosphorylation. These results, together, demonstrate that aaSA treatment induced the amino acid starvation pathway through direct inhibition of the corresponding *PfaaRS*, with few exceptions.

Taken together, the results allow the prioritization of the ARS, HRS, TRS, FRS and PRS as the top five enzymes for further exploration as drug targets in blood stage malaria. Furthermore, the HRS, FRS and PRS are identified as the top three enzymes for further exploration as potential dual-stage drug targets.

3.4 Develop Hybrid-Halofuginone Derivatives with High Parasite Specificity

Within the scope of our efforts to help address the unmet medical need for novel antimalarials, we have designed a new chemical cPRS inhibitor series that potentially satisfies the development criteria of a lead candidate based on potency, selectivity, *in vivo* pharmacology and efficacy in blood and liver stage *P. berghei* mouse model.

It is highly desirable to identify additional cPRS inhibitor chemotypes with alternate binding modes, as they provide additional opportunity to develop inhibitors with selectivity over the host cPRS homolog. Furthermore, such compounds may retain activity should resistance emerge to halofuginol-derived drugs or potentially show a lower propensity to generate resistance.

We aim to develop cPRS inhibitor classes that follow a “traditional” tRNA inhibitor design, including targeting the adenosyl-binding pocket. We expect that this strategy will allow

us to exploit structural differences between the parasite and host proteins that are not utilized by HFOI and therefore offers potential to gain high selectivity over the host PRS homolog.

Taking into account the recently published crystal structure of *Pf*PRS with HFG, we propose a structure-based rational design that aims to exploit the three potential target sites in aaRS, which may offer a way to explore the structural differences between the human and *Plasmodium* proteins.⁷ Furthermore, this approach is inspired by the unique complex formed by HFG/HFOI and ATP in the active site of EPRS. Halofuginone and halofuginol establish a strong hydrogen bond between the hydroxyl-group of the piperidine substituent and the α -phosphate of ATP. Our preliminary modeling studies show a very good overlap between the proposed hybrid compounds and the parent complex (Figure 3.16).

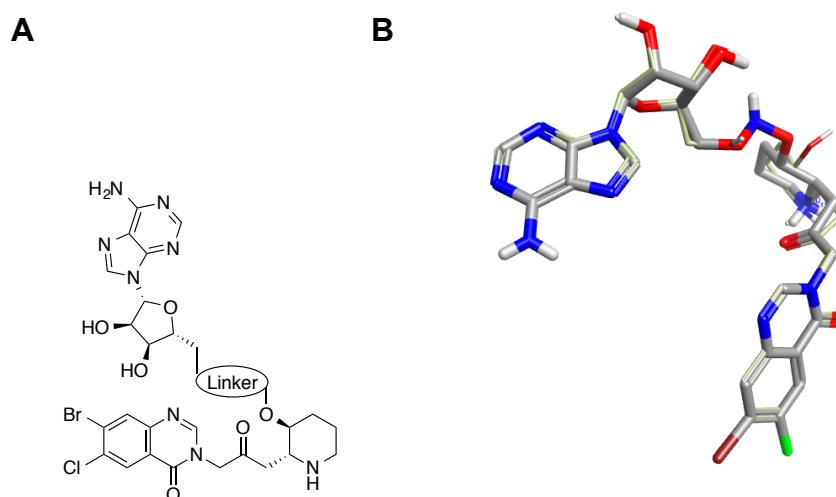


Figure 3.16 – (A) Hybrid-analog design; (B) Overlay of ATP-halofuginone complex (green) with hybrid structure (gray) using an acetamide linker.

Thus, we propose to synthesize both halofuginone- and halofuginol-adenosyl hybrid molecules by replacing the triphosphate of ATP with an appropriate linker to join both ligands (Figure 3.17). The hybrid molecules that have been designed enable direct comparison between the halofuginone and halofuginol based hybrids, as well as the different points of attachment with the adenosyl-substituent.

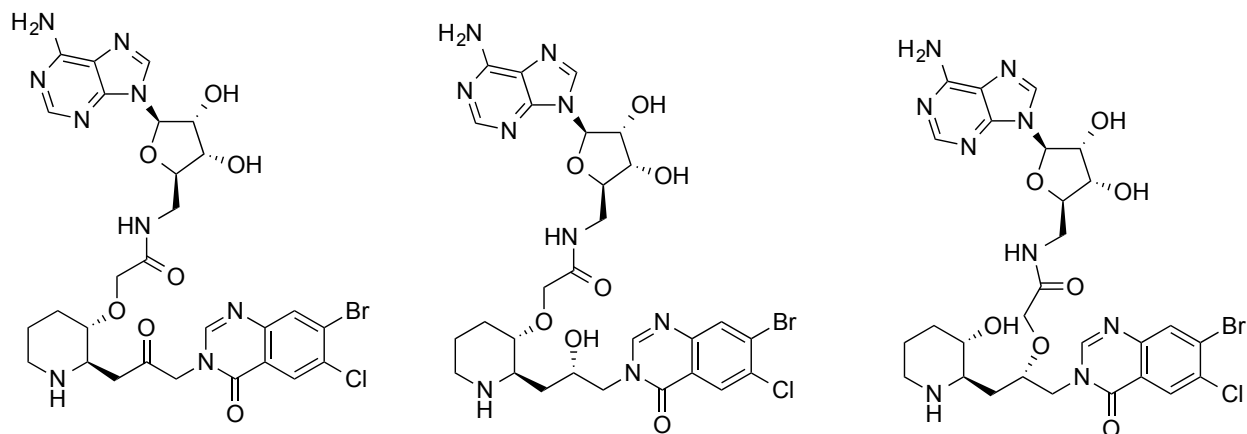


Figure 3.17 – Hybrid-halofuginone derivatives designed.

3.4.1 Chemical Synthesis Strategy

As depicted in Figure 3.18, the retrosynthetically deconstruct shows that the desired hybrid compounds can be obtained by coupling with adenosine after reaction of the 4-quinazolone and the piperidine epoxide, according to what has been cited in the literature.³⁷⁰ Containing all the necessary functional groups with desired stereochemistry, the β -amido alcohol represents a suitable precursor for the key intermediate, piperidine epoxide. The amido alcohol can be derived from N-tert-butanesulfinyl imine and TBDPS-protected hydroxyaldehyde by employing SmI_2 -mediated reductive cross-coupling.

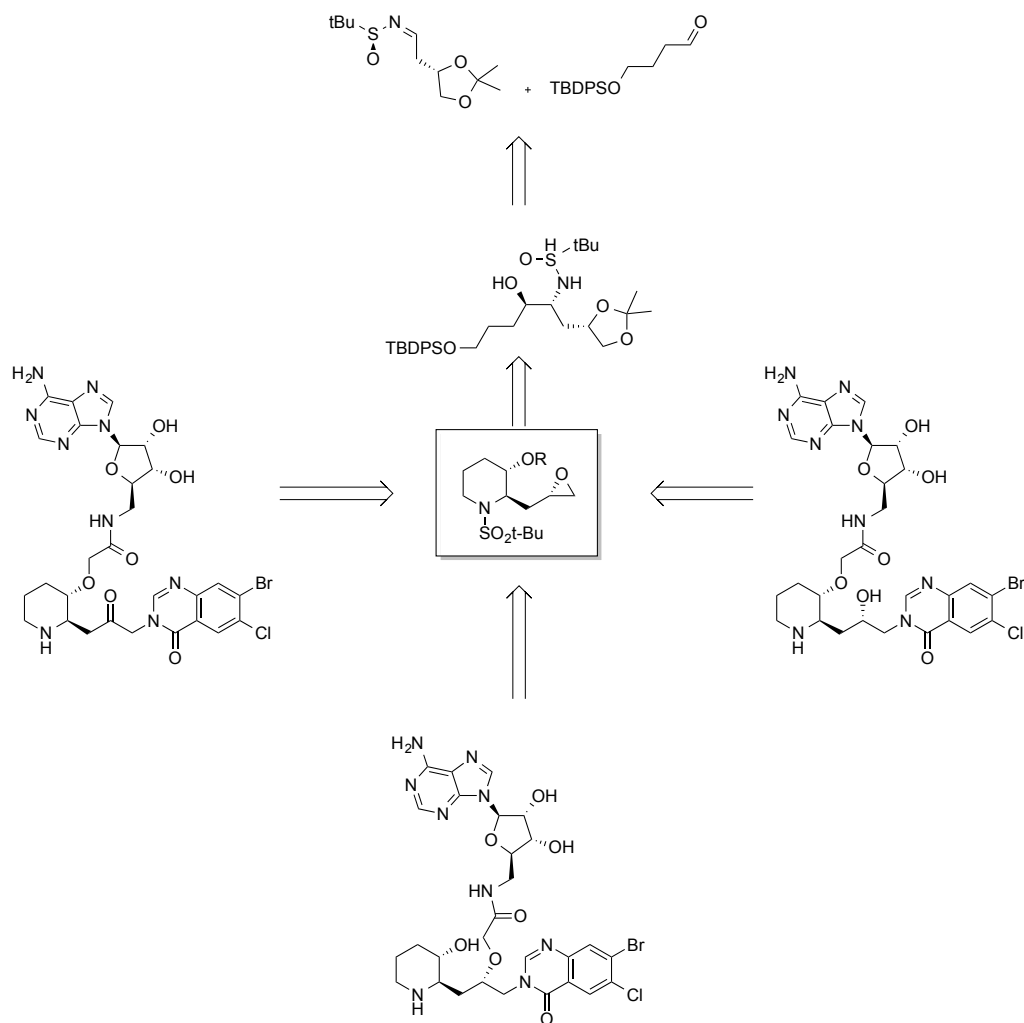
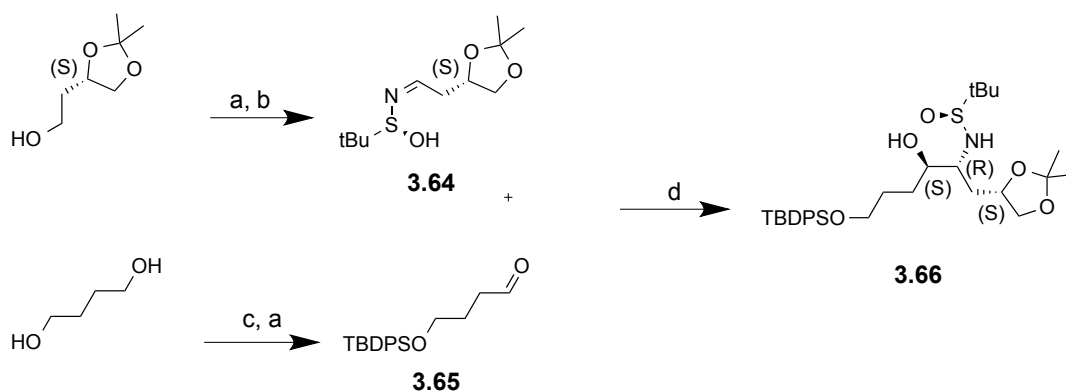


Figure 3.18 – General retrosynthetic scheme of hybrid-halofuginone derivatives.

3.4.2 Synthesis of Halofuginone Hybrid Analogs

The synthesis of the hybrid analogs started with the preparation of the β -amido alcohol through a convergent approach using commercially available materials (Scheme 3.3), following published procedure by Lin and co-workers.³⁷⁰ Many approaches have been described in the literature to synthesize febrifugine and its derivatives, nonetheless this is enantioselective and compatible with the introduction of the adenosine moiety. In one of the branches we started with the mono-protection of 4-butanediol using TBDPSCl followed by Swern oxidation to afford aldehyde **3.65** in 93% yield. On the other branch of the convergent synthesis, the commercially available primary alcohol (*S*)-2-(2,2-dimethyl-1,3-dioxolan-4-yl)ethanol, was subjected to oxidation under Swern's conditions to afford crude aldehyde which, without further purification,

was treated with Ellman's reagent to afford imine **3.64** in 40% overall yield.



Scheme 3.3 – Synthesis of the β -amido alcohol. Reagents and conditions: **a)** DMSO, $(\text{COCl})_2$, Et_3N , DCM, $-60\text{ }^\circ\text{C}$, 3 h, 67%; **b)** (*S*)-*tert*-Butanesulfinamide, anhydrous CuSO_4 , DCM, r.t., 12 h, 59%; **c)** TBDPSCl, imidazole, DMAP, DCM, r.t., 12 h, 50%; **d)** SmI_2 , *t*-BuOH, THF, $-78\text{ }^\circ\text{C}$, 58%.

With both, the imine **3.64** and aldehyde **3.65** in hand, we moved on to the crucial SmI_2 -mediated reductive cross-coupling reaction (Scheme 3.3). Initial attempts did not afford the coupling product, due to degradation of the SmI_2 reagent. Using the Hilmersson method to synthesize SmI_2 we found that the formation of the coupling reagent is remarkably resilient to the presence of water and oxygen, however upon contact with metal needles it would degrade within a couple of minutes. Furthermore, examination of the literature suggests that commercial solutions of SmI_2 in THF vary significantly in concentration from the advertised value, where the average concentration was found to be 0.04M, instead of 0.1M.³⁷¹ Thus, the initial attempt to synthesize the amido alcohol **3.66** failed likely due to the unexpected lower concentration of SmI_2 (Entry 1, Table 3.4). Next, we increased the amount of equivalents of SmI_2 in an attempt to form the desired product, which resulted in a low yielding reaction (Entry 2). The packaging of the reagent being used had a sure/seal™, which led to the use of needles to add the reagent to the reaction mixture, resulting in increased degradation of the SmI_2 . Moreover, the literature examined suggested that a specific commercial source of SmI_2 (Strem Chemicals) had an increased concentration relative to the other sources. Thus, we acquired the SmI_2 solution from the new source, increased the amount of SmI_2 added to the reaction mixture, as well as, avoided the use of needles to handle the reagent, which resulted in increased yield (Entry 3). Since we were successful in increasing the reaction yield, next we investigated the possibility of

decreasing the amount of SmI₂ (Entry 4) and increasing the reaction scale (Entry 5), which resulted in comparable yields (Table 3.4).

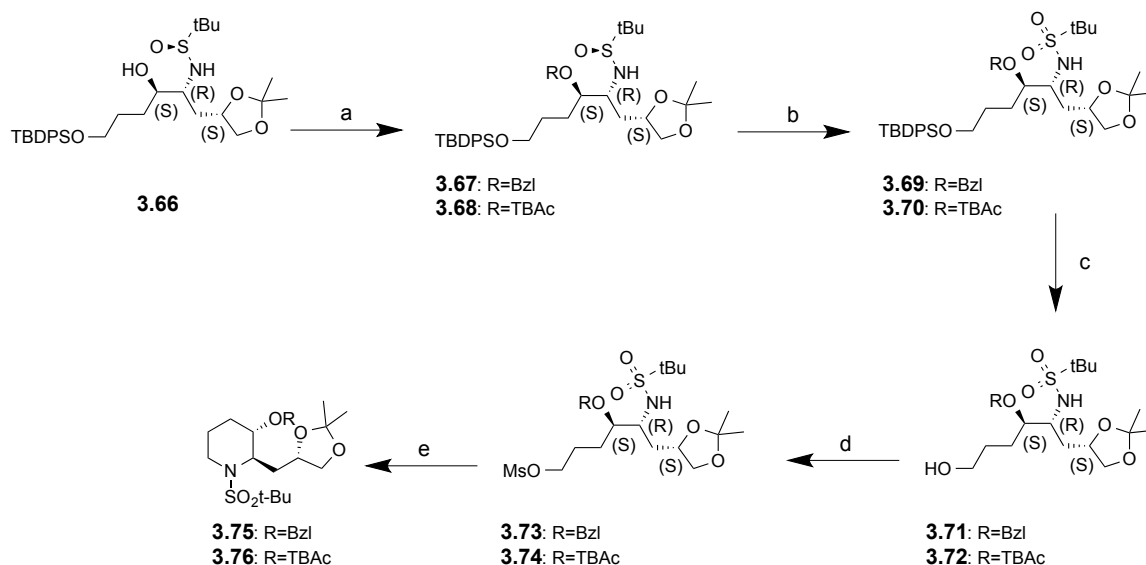
Table 3.4 – Optimization of SmI₂-mediated reductive cross-coupling reaction.

Entry	SmI ₂ (0.1M)		Solvent	Sure/Seal™ Package	Addition via Needle	Scale (mg)	Yield (%)
	Source	Equiv.					
1	Sigma aldrich	2.1	THF	✓	✓	100	-
2	Sigma aldrich	4.2	THF	✓	✓	100	20%
3	Strem	6.5	THF	×	×	380	50%
4	Strem	3.2	THF	×	×	380	52%
5	Strem	2.3	THF	×	×	1000	58%

After synthesis of the β-amido alcohol **3.66**, the key intermediate piperidine epoxide can be obtained following 8 steps, first the β-amido alcohol is converted to the *N*-sulfonyl piperidine (Scheme 3.4), which is then converted to the piperidine epoxide as shown in Scheme 3.5.

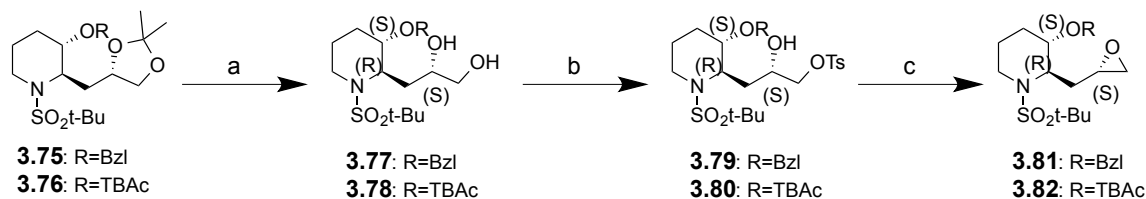
The newly formed hydroxyl group in the β-amido alcohol was first converted into benzyl ether **3.67** or *tert*-butyl acetate **3.68**, in 52% and 44% yield, respectively, by treatment with sodium hexamethyldisilazide (NaHMDS) in THF. Subsequent exposure of each of the sulfonamides to meta-chloroperoxybenzoic acid (mCPBA) afforded compounds **3.69** and **3.70** in 99% and 98% yield, respectively. The silyl group was successfully removed with HF/pyridine/THF (1:2:7), resulting in the free hydroxyl intermediates **3.71** and **3.72**, in 77% and 78% yield, respectively. Next, the free hydroxyl group was activated with methanesulfonyl chloride (MsCl) under basic conditions followed by cyclization with NaHMDS in THF, providing the *N*-sulfonyl piperidines **3.75** and **3.76** in 60% and 51% yield, respectively, over 2 steps (Scheme 3.4).

Chapter 3 – Aminoacyl-tRNA Synthetase Inhibitors as Antimalarials



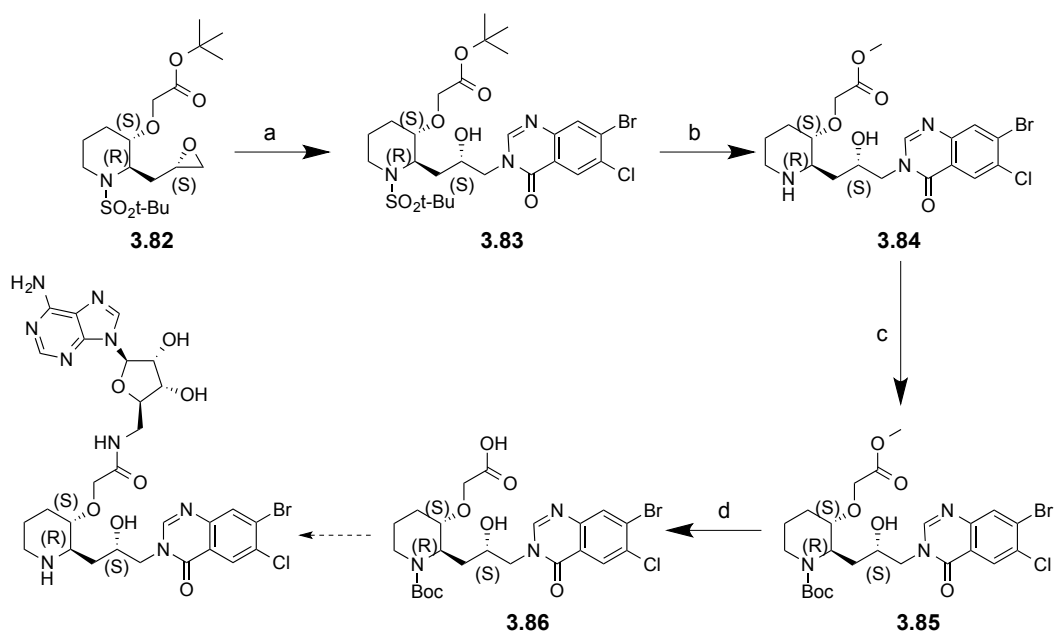
Scheme 3.4 – Synthesis of the *N*-sulfonyl piperidine. Reagents and conditions: **a)** RBr, NaHMDS, THF, -20 °C, 16 h; **b)** MCPBA, DCM, r.t., 3 h; **c)** HF/Pyridine, THF, r.t., 16 h; **d)** MsCl, DIPEA, DCM, -78 °C, 3 h; **e)** NaHMDS, THF, -20 °C, 16 h.

To convert the *N*-sulfonyl piperidine into the key intermediate piperidine epoxide, three additional steps are required (Scheme 3.5). First, we optimized the deprotection conditions by evaluating three acidic catalysts, camphorsulfonic acid (CSA), *p*-toluenesulfonic acid (TsOH) and pyridinium *p*-toluenesulfonate (PPTS). The latter, a mild acidic catalyst, afforded the desired diol in higher yield compared to the others. Thus, compounds **3.75** and **3.76** were exposed to PPTS in methanol to give diols **3.77** and **3.78**, which were converted to epoxides **3.81** and **3.82** in 98% and 91% yield, by sequential monotosylation and then base-induced cyclization.



Scheme 3.5 – Synthesis of the piperidine epoxide. Reagents and conditions: **a)** PPTS, MeOH, 60 °C, 16 h; **b)** TsCl, Bu₂SnO, Et₃N DCM, r.t., 3 h; **c)** DBU, DMC, r.t., 16 h;

To prioritize our efforts, we chose to progress with the synthetic scheme using the *tert*-butyl acetate derivative since it would enable access to two of the desired final hybrid compounds. Once the key intermediate piperidine epoxide is obtained the desired halofuginol-hybrid analog can be synthesized in five steps following Scheme 3.6. Compound **3.82** was reacted with the halogenated 4-quinazolone in the presence of potassium hydride to give alcohol **3.83** in 84% yield, which in turn was treated with 6 M HCl/MeOH, resulting in transesterification and amine deprotection, followed by Boc re-protection furnishing **3.85** in 28% yield, over two steps. The resulting Boc protected ester was saponified with LiOH in methanol, yielding the desired carboxylic acid intermediate **3.86**, by LC/MS analysis.



Scheme 3.6 – Synthesis of the piperidine epoxide. Reagents and conditions: **a**) KH, 4-quinazolone, DMF, 80 °C, 72 h; **b**) 6 M HCl/MeOH, r.t., 3 h; **c**) Boc₂O, DIPEA, r.t., 5 h; **d**) 1 M LiOH, 60 °C, 5 h.

Next, to obtain the desired hybrid compounds two additional steps are necessary, amide bond formation by coupling with the adenosine followed by full deprotection under acidic conditions. Initial optimization of the coupling of compound **3.86** with the adenosine was done in small scale using well-known coupling reagents, such as PyBOP, however we were unable to isolate sufficient amount of the desired compound to continue the synthesis of the hybrid analogs. Thus, further optimization is necessary to scale-up the latter reaction.

3.5 Characterize the Biology of cPRS Inhibition and Amino Acid Starvation Response

Understanding the mode of action, systemic responses and mechanisms of resistance to novel antimalarials is critical for future therapeutic development efforts, as it will allow to better evaluate the potential of new drug targets, address possible issues early in the drug development process, help to guide the preclinical drug development process and inform the design of treatment strategies.

Our preliminary data has demonstrated that *Pfc*PRS is the target of HFG and further identifies the AAR pathway as a potential downstream consequence of treatment. Like direct amino acid deprivation, inhibition of aaRSs results in the accumulation of uncharged tRNA, which in turn binds and activates the eIF2 α kinase GCN2 as the central control element of the conserved Amino Acid Starvation Response pathway, as mentioned (Chapter 3, Section 3.3.3).^{283, 372} Recent work by our group in *P. falciparum* has also demonstrated that amino acid starvation results in a broad transcriptional perturbation.^{7-8, 206} Research has confirmed the existence of a functional AAR in *P. falciparum*'s intraerythrocytic stage and demonstrated the phosphorylation of eIF2 α in response to isoleucine starvation (the sole amino acid that can be fully depleted as it is the only amino acid that is absent from hemoglobin).²⁸⁰⁻²⁸¹ However, treatment with isoleucine tRNA synthetase inhibitors unexpectedly did not induce eIF2 α phosphorylation.²⁸¹

We have demonstrated in the first section of this chapter that induction of eIF2 α phosphorylation is not common to all tRNA synthetase inhibitors in *P. falciparum* Dd2 strain. Moreover, in *P. falciparum* cultures, HFG and ProSA induced eIF2 α phosphorylation in a similar manner. Nonetheless, in mammalian cells, halofuginone induced phosphorylation to a higher extent than ProSA, when compared to the amino acid starvation controls (data not published). To fully understand the latter outcome we must further comprehend the mode of action of the two different PRS inhibitors, thus we propose to characterize the enzyme-inhibitor complex formed by each of these two inhibitors, to gain insights that could justify the observed difference.

Under physiological conditions aminoacylation proceeds in two main steps, in the first step the amino acid is adenylated by reaction with ATP to yield aminoacyl adenylate and pyrophosphate. The aminoacyl adenylate remains tightly bound to the aaRS until the aa-AMP-

aaRS complex encounters a tRNA molecule, which fits in the tRNA binding pocket and accepts the activated amino acid. The charged tRNA is released to continue protein translation (Figure 3.19a). We hypothesize that in the presence of ProSA, a transition state analog, the enzyme will remain in a high-affinity state, where the compound occupies both ATP and amino acid binding pockets. This complex will scavenge the tRNA molecules to form a stable tRNA-enzyme-inhibitor complex (Figure 3.19b). In contrast, HFG occupies the tRNA and proline binding pockets and forms a ternary complex with ATP bound to the prolyl tRNA synthetase. In this case the uncharged tRNA is unable to interact with the enzyme and will accumulate in the cell resulting in activation of the amino acid starvation response (Figure 3.19c).

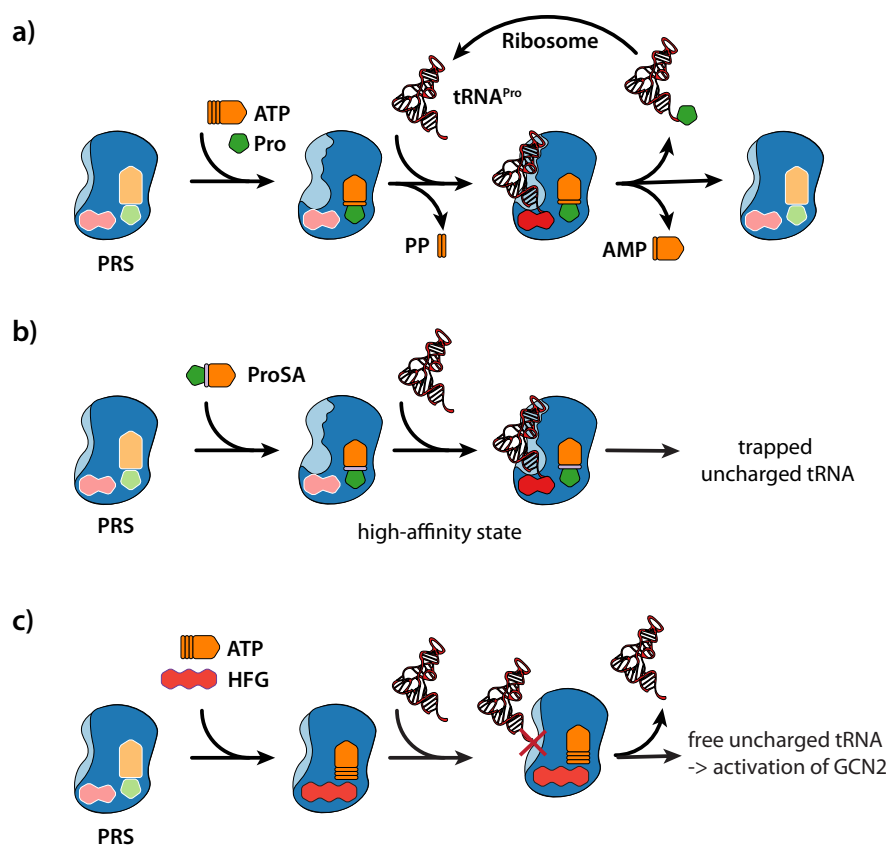


Figure 3.19 – Aminoacylation of PRS. **a)** Aminoacylation of PRS under physiological conditions; **b)** Treatment with ProSA results in trapped uncharged tRNA; **c)** Treatment with HFG results in free uncharged tRNA which in turn activates the amino acid starvation response.

To test our hypothesis we will apply a two-step proteomic approach to isolate the protein complex using immunoprecipitation followed by identification of its components using mass spectrometry.

We expect to obtain detailed mechanistic insights in the biology underlying cPRS inhibition through the two different types of inhibitors. We anticipate that our findings will not only provide a better understanding of the amino acid starvation response in *Plasmodium*, but will also validate both cPRS specifically and the amino acid starvation response generally as pharmaceutically tractable and attractive targets for malaria drug discovery.

3.5.1 Methodological Approach

In the post-genomic era, the importance of protein–protein interactions is becoming even more apparent. We are coming to recognize that most, if not all, catalytic and regulatory pathways operate as networks, with frequent and extensive input from signaling pathways, feedback, and cross-talk. Owing to the central importance of protein–protein interactions (PPIs) in biology, methods have been developed to study multiple aspects of PPIs.³⁷³ The identification of the components of protein complexes can be obtained by shotgun proteomics using affinity purification coupled to mass spectrometry. Affinity purification combined with mass spectrometry (AP-MS) has emerged as a particularly attractive method for PPI mapping. A major advantage is that this method allows unbiased detection of PPIs under physiological conditions. Importantly, AP-MS can assess PPIs in relevant biological contexts such as mammalian cell lines or even tissues. Moreover, AP-MS experiments have the advantage that they can provide quantitative information.³⁷⁴

The most commonly used technique for isolating protein complexes using affinity purification is Co-Immunoprecipitation (Co-IP), which usually employs ectopically expressed tagged bait proteins. In this methodology, the protein of interest and any complex it forms in the cell are recovered by the use of high affinity reagents (e.g. antibodies or peptides coupled to beads) to the tag. This reliable and flexible approach has been applied in a range of biological contexts to study both small protein complexes as well as global protein–protein interaction networks.³⁷⁵

Here, we report the attempted optimization of the co-immunoprecipitation of the PRS complex with and without inhibitor treatment.

First, we tested the general method of affinity purification by Co-IP using His-tag coupled metal magnetic beads. These Dynabeads® are coated in a cobalt-based Immobilized

Metal Affinity Chromatography (IMAC) chemistry, which binds histidine-tagged proteins with higher selectivity.

We chose two orthogonal systems to test the pull-down conditions, the protein ladder (Novex® Sharp Pre-Stained Protein Standard) which has His-tagged proteins (Figure 3.20A), and pure His-tagged HDAC8 (Figure 3.20B). In both cases, the Dynabeads® His-Tag protocol was followed and the His-tagged proteins were successfully isolated. Samples obtained by affinity purification were loaded on SDS-PAGE and differential bands between samples were identified by Coomassie blue staining and western blot analysis.

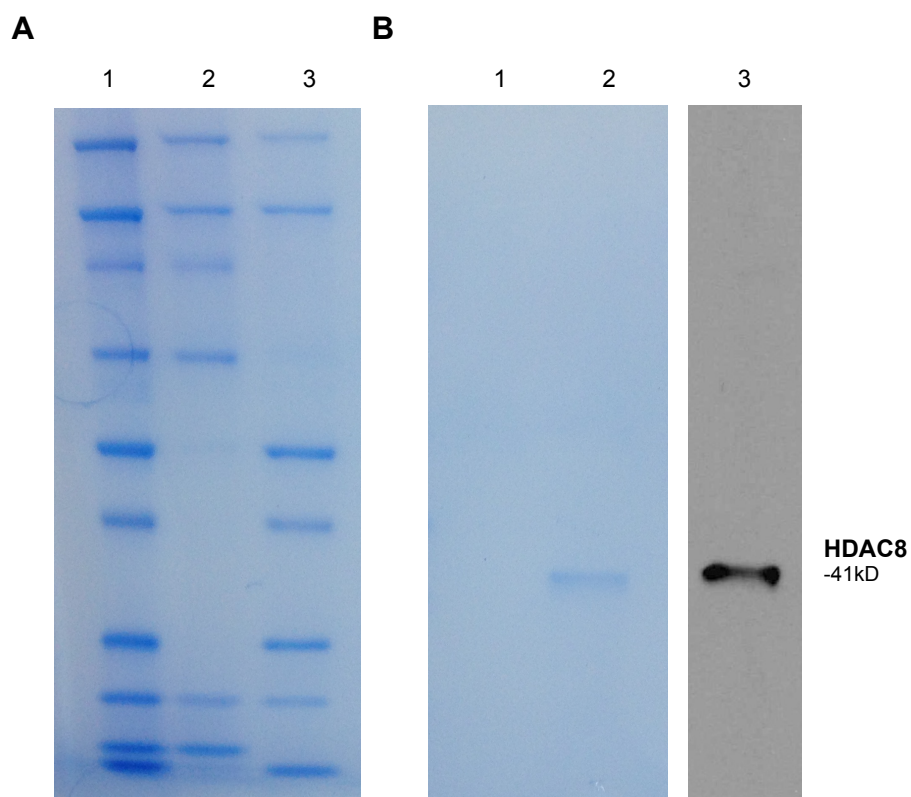


Figure 3.20 – Affinity purification with Dynabeads®. Reducing SDS-PAGE (NuPAGE® Novex® 4-12% Bis-Tris Gels) stained in coomassie brilliant blue of two representative experiments performed with the protein ladder (**A**) or His-tagged HDAC8 (**B**). **A**) Lane 1: Novex® Sharp Pre-Stained Protein Standard; Lane 2: Supernatant; Lane 3: pull-down; **B**) Lane 1: Supernatant; Lane 2: pull-down in coomassie brilliant blue; Lane 3: pull-down in western blot.

3.5.2 Studies in Yeast Cultures

Saccharomyces cerevisiae PRS (ScPRS, YHR020w) is very similar to the *P. falciparum* cPRS and *H. sapiens* EPRS. Within the core Class II catalytic domains, the yeast PRS shares

77% and 70% similarity with human and plasmodium enzymes, respectively. Despite the high similarity, we discovered that *S. cerevisiae* was not sensitive to halofuginone. This allowed us to use a yeast model for both target confirmation of halofuginone and validation of the resistance phenotype of the mutant alleles identified in our drug resistance selections, in our previous work.⁷

Our group has performed a complementation test of *PfcPRS* in *S. cerevisiae*. We deleted the chromosomal copy of *ScPRS*, an essential gene and the only locus that codes for a prolyl tRNA synthetase in *S. cerevisiae*. We found that episomal expression of *PfcPRS* could complement the *ScPRS* knock-out strain. Next, we generated transgenic yeast strains that would express only *ScPRS*, wild-type and mutant *PfcPRS*, respectively (Figure 3.21A). The constructs included a His-tag fused protein on the *N*-terminus of *PfcPRS*, which allowed the use of His as bait in the pull-down experiments. While all strains exhibit comparable growth characteristics, only the wild type *PfcPRS*-expressing strain displayed a dose-dependent sensitivity to halofuginone treatment (Figure 3.21B).⁷

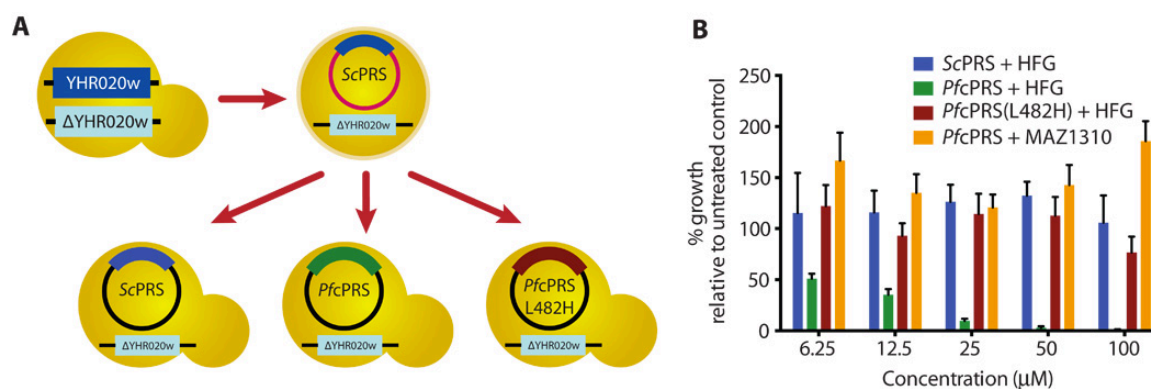


Figure 3.21 – A heterologous yeast model. **(A)** The +/- YHR020w (*ScPRS*) heterozygous strain of *S. cerevisiae* was transformed with a YHR020w-containing plasmid, and haploid spores were selected for genomic deletion of YHR020w. The intermediate strain was transformed with a second plasmid with an orthogonal selection marker and YHR020w, wild-type *PfcPRS* (codon-optimized) or mutant *PfcPRS* (codon-optimized), and was subsequently selected for loss of the first plasmid. **(B)** Only transgenic *S. cerevisiae* expressing wild-type *PfcPRS* (green) displayed dose-dependent sensitivity to halofuginone, whereas strains expressing *ScPRS* (blue) or the L482H *PfcPRS* mutant (red) were insensitive to halofuginone treatment up to 100 mM (all strains were *pdr1,3*-deleted). The control compound MAZ1310 did not affect growth of *PfcPRS* expressing yeast (orange). (Work done by another member of our group)⁷

Next, using these constructs with a His-tag fused protein on the *N*-terminus of *Pfc*PRS, we optimized the pull-down experiments, the first step in our proteomic approach. Thus, aiming to isolate the protein complex, to identify its components thereafter using mass spectrometry.

Co-immunoprecipitation Optimization

Preliminary studies were performed to identify the best conditions for cell lysis following standard protocol the pump-deleted yeast strains were grown overnight in assay media at 23 °C, after which either 10 µM halofuginone, 10 µM ProSA or a corresponding volume of DMSO was added to cultures, which were then grown at 30 °C for six hours. Yeast pellets were made from different amounts of yeast ranging from 10-50 mL (Table 3.5). After pellets were formed, they were washed with water and resuspended in 1 mL of lysis buffer, followed by addition of corresponding volume of beads. Pellets were bead beaten using one of three techniques for increasing periods of time, at 4 °C (Table 3.5).

The initial attempts to lyse the yeast strains relied on the use of the vortex for the bead beating step (Entry 1-4). Increasing amount of yeast, as well as longer duration of lysis was tested using acid washed beads, however after SDS-PAGE separation *Pf*PRS band was absent in both western blot analysis and commassie blue staining. Next, the mini Bead Beater96 was used for lysis with acid washed beads (Entry 5-11). Increasing the amount of yeast from 10 to 50 mL using the same lysis duration did not result in identification of *Pf*PRS band. Furthermore decreasing durations of lysis were tested (Entry 7-10) in an attempt to decrease the other bands present, which might indicate degradation of the desired protein. *Pf*PRS was not identified in any of the entries and the amount of undesired proteins present plateaued after 2 min of lysis (Entry 9).

Table 3.5 – Optimization of yeast lysis.

Entry	Yeast (mL)	Bead Beating		Time (Min.)	Western Blot		Coomassie Blue	
		Bead Beater	Beads		<i>Pfc</i> PRS	Other	<i>Pfc</i> PRS	Other
1	10	Vortex	Acid washed	5	×	✓	×	✓
2	50	Vortex	Acid washed	5	×	✓	×	✓
3	50	Vortex	Acid washed	30	×	✓	×	✓
4	50	Vortex	Acid washed	60	×	✓	×	✓
5	10	Bead Beater96	Acid washed	5	×	✓	×	✓
6	50	Bead Beater96	Acid washed	5	×	✓	×	✓
7	50	Bead Beater96	Acid washed	4	×	✓	×	✓
8	50	Bead Beater96	Acid washed	3	×	✓	×	✓
9	50	Bead Beater96	Acid washed	2	×	✓	×	✓
10	50	Bead Beater96	Acid washed	1	×	✓	×	✓
11	50	Bead Beater96	Acid washed	2 ^a	×	✓	×	✓
12	50	FastPrep-24™	Acid washed	40 s	×	✓	×	✓
13	50	FastPrep-24™	Matrix A	40 s	✓	✓	×	✓
14	20	FastPrep-24™	Matrix A	3X40 s	×	✓	×	×
15	30 ^b	FastPrep-24™	Matrix A	40 s	×	✓	×	×
16	30 ^b	FastPrep-24™	Matrix A	3X40 s	×	✓	×	×

^aEthanol Lysis buffer; ^bOD600 0.01

Additionally a different lysis buffer was unsuccessfully used under the same conditions (Entry 11). To continue our efforts to establish lysis conditions, which would render enough *Pfc*PRS to move forward with the pull-down experiments, we tested a third instrument for the bead beating step. The FastPrep-24™ instrument is a high-speed reciprocating homogenizer with lysing matrix beads specific for protein isolation from yeast samples. In entries 12 and 13 the FastPrep-24™ was used under the same conditions with exception of the type of beads used.

When using the matrix A beads with one lysis cycle of 40 s (Entry 13), *Pf*PRS band was present after western blot analysis (Figure 3.22) but absent in the commassie blue staining, indicating that the amount of protein present was below the stain's sensitivity.

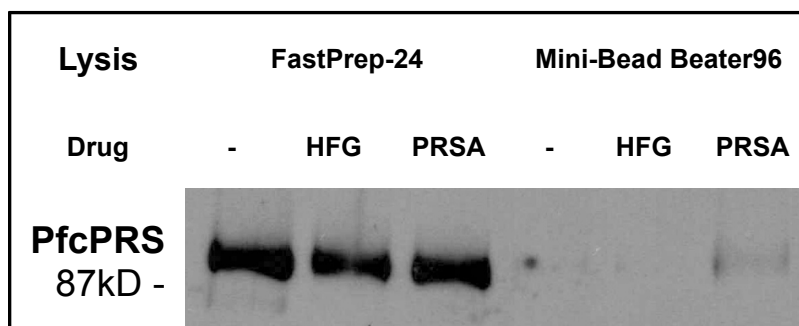


Figure 3.22 – Western blot analysis of *Pfc*PRS after treatment with 10 μ M halofuginone, 10 μ M ProSA or with corresponding volume of DMSO. Yeast pellets were lysed using one of two instruments; FastPrep-24™ or Mini BeadBeater96. Each blot is representative of two independent replicates.

In an attempt to further increase the amount of *Pf*PRS isolated, the number of lysis cycles was increased (Entry 14 and 16) and the yeast were treated at log phase of growth (Entry 15 and 16). Neither strategy yielded the desired result. The presence of other bands in all entries indicates that the lysis was potentially efficient despite the desired protein not being present or present in small amounts. Taken together we concluded that only a small amount of *Pf*PRS was produced in these strains, and it was stable in very specific conditions, which would point to revising the plasmid used for complementation of *Pfc*PRS in *S. cerevisiae*.

Having investigated the best conditions for lysis, next we studied the conditions for co-immunoprecipitation of the *Pf*PRS complex. First, we tested the general method of affinity purification using the His-tag coupled metal magnetic beads used before. The Dynabeads® were incompatible with components of the lysis buffer which required dialysis prior to the pull down experiment. Three different sized Amicon ultra-0.5 centrifugal filters were used (30 KDa, 50 KDa and 100 KDa) for buffer exchange. Samples were loaded on SDS-PAGE and *Pf*PRS band was not identified by commassie blue staining or western blot analysis. To avoid the buffer exchange step in this protocol we repeated the general method of affinity purification using the His-Tag (27E8) mouse mAb magnetic bead conjugate.

Preliminary experiments using 10 μ M halofuginone, 10 μ M ProSA or a corresponding volume of DMSO were done to test the conditions optimized thus far. The standard protocol for the pump-deleted yeast strain growth and drug treatment was followed. Samples were lysed according to conditions in Table 3.5 -Entry 13. Next, to 200 μ L of cell lysate was added 10 μ L of the His-Tag antibody magnetic bead conjugate, which incubated overnight at 4 $^{\circ}$ C. After washing the beads 3-4 times, proteins were eluted from the beads using denaturing conditions (SDS). Samples were analyzed by western blot, which revealed the *Pf*PRS band.

To characterize the enzyme-inhibitor complex formed by the different types of inhibitors with *Pf*PRS, and identify its components, both the lysis and co-immunoprecipitation should be done under non-denaturing conditions to enable the pull-down of the intact complex. Thus, non-denaturing conditions were tested to elute the complex from the His-Tag antibody magnetic beads. One of three common methods was used to elute the complex from the beads. The SDS buffer is the harshest, which will also elute non-covalently bound antibodies and antibody fragments along with the protein of interest, and may result in separation of the complex components. The Glycine buffer gently elutes the protein with reduced amount of eluted antibody, while the His elution buffer consists on less stringent conditions thus yielding more functional isolated proteins. As seen above, elution of the protein under denaturing conditions resulted in identification of a band at about 90 kD by western blot analysis, while the other two elution methods failed to do so (Figure 3.23). The corresponding band was absent when using the commassie blue stain.

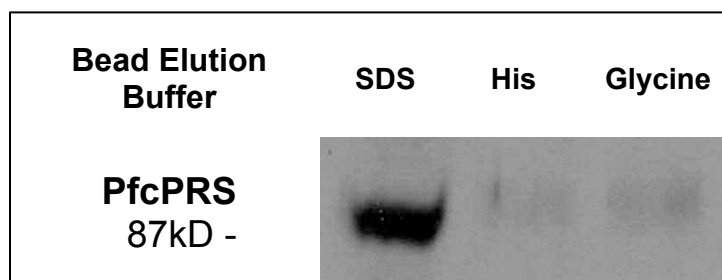


Figure 3.23 – Western blot analysis of *Pfc*PRS following pull-down experiments using three different bead elution buffers.

Nonetheless, based on western blot analysis, bands were excised from the commassie blue stained gel and sent for mass spectrometry analysis. When analyzing the peptides identified

from the samples it was evident that the *Pf*PRS protein was not being isolated, underscoring the potential problem associated with the efficient transcription of the plasmid used in the complementation of *Pfc*PRS in *S. cerevisiae*.

Within the scope of our efforts to help establish optimal conditions for co-immunoprecipitation of the PRS complex we decided to apply the same principles and techniques using a mammalian cell line.

3.5.3 Studies in Mammalian Cells

In previous work, we have also shown that febrifugine and its derivatives activate the AAR in mammalian cells by directly inhibiting the prolyl-tRNA synthetase activity of glutamyl-prolyl-tRNA synthetase (EPRS). The derivatives compete with proline for the prolyl-tRNA synthetase active site, causing the accumulation of uncharged tRNA^{Pro} and mimicking reduced cellular proline availability. Our group has demonstrated that, in the absence of true nutritional deficit, febrifugine-derived compounds block EPRS activity to send intracellular signals indicative of proline limitation, activating the AAR pathway and thereby reproducing a key component of the beneficial effects of caloric restriction.⁸

Based on the validation of EPRS as the molecular target of febrifugine and analogs, we turned our interest to understanding the biology underlying EPRS inhibition through the two different types of inhibitors in a mammalian model. To test our hypothesis we will apply the same two-step proteomic approach to isolate the protein complex using immunoprecipitation followed by identification of its components using mass spectrometry.

Co-immunoprecipitation Optimization

Preliminary studies were performed to identify the best conditions for cell lysis. First we used RIPA buffer, a harsher more reliable buffer, next we used a native lysis buffer, which allows the protein to be isolated in its active form, thus remaining in complex with all its components. The results by western blot analysis were comparable in both cases. Furthermore the amount of EPRS present in the MCF-7 cell line using the native lysis buffer was assessed (Figure 3.24).

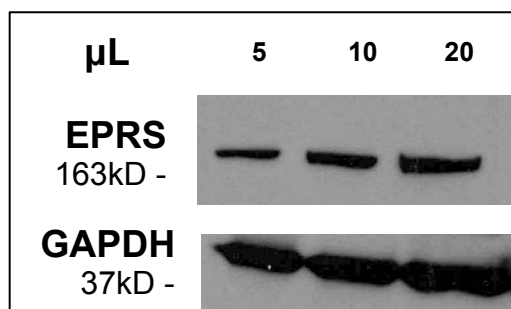


Figure 3.24 – Western blot analysis of EPRS following native lysis of MCF7 cell line. Increasing amounts of lysate loaded on the SDS-PAGE gel. GAPDH was used as loading control.

To probe for the induction of the AAR, we have treated MCF7 cells with halofuginone, halofuginol, ProSA, or equivalent amount of DMSO and quantified the amount of eIF2 α and p-eIF2 α by Western blot analysis relative to untreated cells (Figure 3.25).

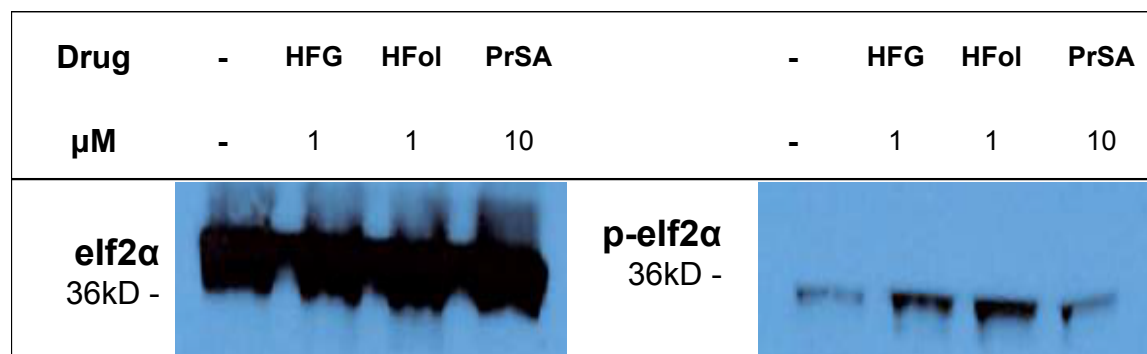


Figure 3.25 – Differential induction of eIF2 α phosphorylation in MCF-7 cells. Western blot analysis of p-eIF2 α and total eIF2 α protein in drug-treated cultures relative to DMSO treated cultures. Each blot is representative of two independent replicates. Both DMSO and drug-treated cultures had similar amount of eIF2 α . Halofuginone and halofuginol induce phosphorylation of eIF2 α after 90 minutes treatment, while ProSA is comparable to DMSO treated cultures.

Halofuginone and halofuginol treatment significantly increased eIF2 α phosphorylation compared to untreated cultures. ProSA, like DMSO control treatment failed to increase levels of eIF2 α phosphorylation. The differential activation of AAR observed by the two types of inhibitors is consistent with our hypothesis that in the presence of ProSA, the enzyme-inhibitor complex will scavenge the tRNA molecules to form a stable tRNA-enzyme-inhibitor complex

whereas, HFG occupies the tRNA and proline binding pockets forming a ternary complex with ATP, which leads to accumulation of uncharged tRNA in the cell resulting in activation of the amino acid starvation response.

Following standard protocol for SYBR® Gold nucleic acid gel stain we established a calibration curve for tRNA detection, which identified how much tRNA would be detectable when analyzing the samples obtained from the co-immunoprecipitation experiments (Figure 3.26). Despite the fact that the amount of tRNA isolated in the protein complex via co-immunoprecipitation is potentially below the detection limit of the SYBR® Gold stain method, we decided to move forward with the affinity purification experiments because the samples isolated would be analyzed by mass spectrometry, which is a more sensitive technique.

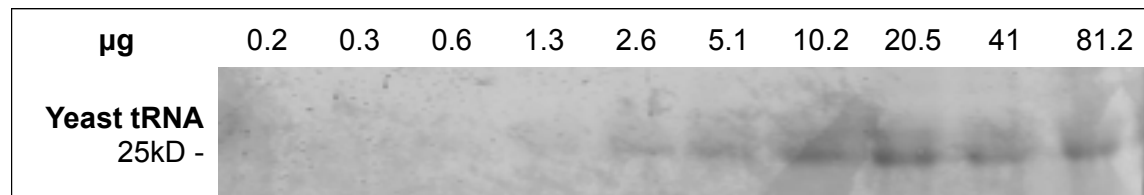


Figure 3.26 – Yeast tRNA calibration curve on SDS-PAGE using SYBR® Gold stain as detection method.

Having established the best conditions for native lysis, next we optimized the conditions for co-immunoprecipitation of the EPRS complex. Immunoprecipitation can be performed by two different methods using antibodies. We tested both methods using the Protein A coupled magnetic beads. In the first approach the anti-glutamyl prolyl tRNA synthetase antibody (ab31531) is added to the lysate and allowed to interact with the protein overnight, followed by addition of the Protein A Dynabeads®. In the second approach the antibody is allowed to bind to the Protein A coupled magnetic beads first, followed by addition to the cell lysate. In both methods samples were loaded on SDS-PAGE and western blot analysis revealed the presence of EPRS. Nonetheless, the latter approach resulted in less isolated protein when compared to the other approach, thus the following experiments were done according to the first method. As mentioned in the above section to characterize the enzyme-inhibitor complex formed with EPRS when treated with the different inhibitors, and to identify its components, both the lysis and co-immunoprecipitation should be done under non-denaturing conditions to enable the pull-down of

the intact complex. Thus, non-denaturing conditions were tested to elute the complex from the magnetic beads. The SDS buffer is the harshest and will also elute non-covalently bound antibodies and antibody fragments along with the complex components, which mostly likely disaggregates under these conditions. Both the glycine buffer and the Protein A Dynabeads® elution gently elutes the protein with reduced amount of eluted antibody. Elution of the protein using the glycine buffer as well as under denaturing conditions resulted in identification of a band at about 163 kD by western blot analysis, while the other elution method failed to do so. Moreover, we analyzed how associating the different methods of lysis, immunoprecipitation and elution would ultimately affect the amount of isolated protein. When using RIPA buffer or native lysis buffer, the first immunoprecipitation approach yielded higher amounts of isolated protein in both cases. In each of the latter cases the three different elution buffers were also tested and the results were consistent among the experiments. Nonetheless, only one set of conditions resulted in identification of the EPRS band in both western blot analysis and Coomassie blue stain.

Preliminary experiments using 1 μM halofuginone, 10 μM ProSA or a corresponding volume of DMSO were done to test the conditions optimized thus far. The standard protocol for the MCF-7 culture growth and drug treatment was followed. Samples were lysed using the native lysis buffer. Next, to 250 μL of cell lysate was added 2.5 μL of the anti-glutamyl prolyl tRNA synthetase antibody, which incubated overnight at 4 $^{\circ}\text{C}$. Followed by incubation with 35 μL of Protein A Dynabeads® for 4 h at 4 $^{\circ}\text{C}$. After washing the beads 3-4 times, proteins were eluted from the beads using denaturing conditions (SDS). Samples were analyzed by western blot, which revealed the EPRS band (Figure 3.27).

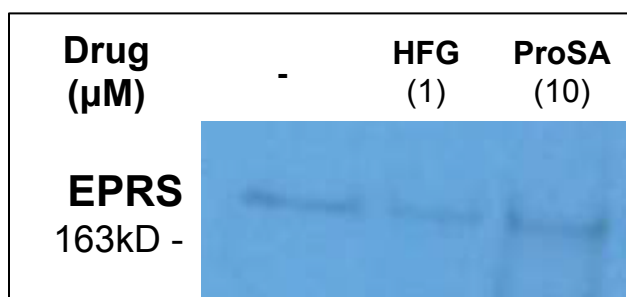


Figure 3.27 – Western blot analysis of EPRS following co-immunoprecipitation. MCF-7 cells were treated with 1 μM halofuginone, 10 μM ProSA or a corresponding volume of DMSO. Each blot is representative of two independent replicates.

To increase the amount of EPRS isolated, in the ratio of cell lysate to antibody was increased as well as the quantity of magnetic beads used.

Next, cultures were treated with 10 μ M ProSA or a corresponding volume of DMSO for 2 h at 37 °C. Samples were lysed using non-denaturing conditions. To 450 μ L of cell lysate was added 2.5 μ L of the anti-glutamyl prolyl tRNA synthetase antibody, which incubated overnight at 4 °C. Followed by incubation with 50 μ L of Protein A Dynabeads® for 4 h at 4 °C. After the beads were washed, proteins were eluted under denaturing conditions (SDS). Samples were loaded on 4–20% SDS-PAGE gel and analyzed by western blot, commassie blue stain and SYBR® Gold stain (Figure 3.28). Both lysate and supernatant from the pull-down experiment was analyzed. Western blot analysis revealed increased amount of EPRS in the lanes where pull-down sample was loaded versus lysate. In the commassie stained gel it is apparent that the lysis is efficient, since the lanes where lysate was loaded a smear of proteins is observed. The lanes where the supernatant was loaded reveal a small band consistent with EPRS, nonetheless the amount of protein isolated does not seem sufficient for mass spectrometry analysis (Figure 3.28a).

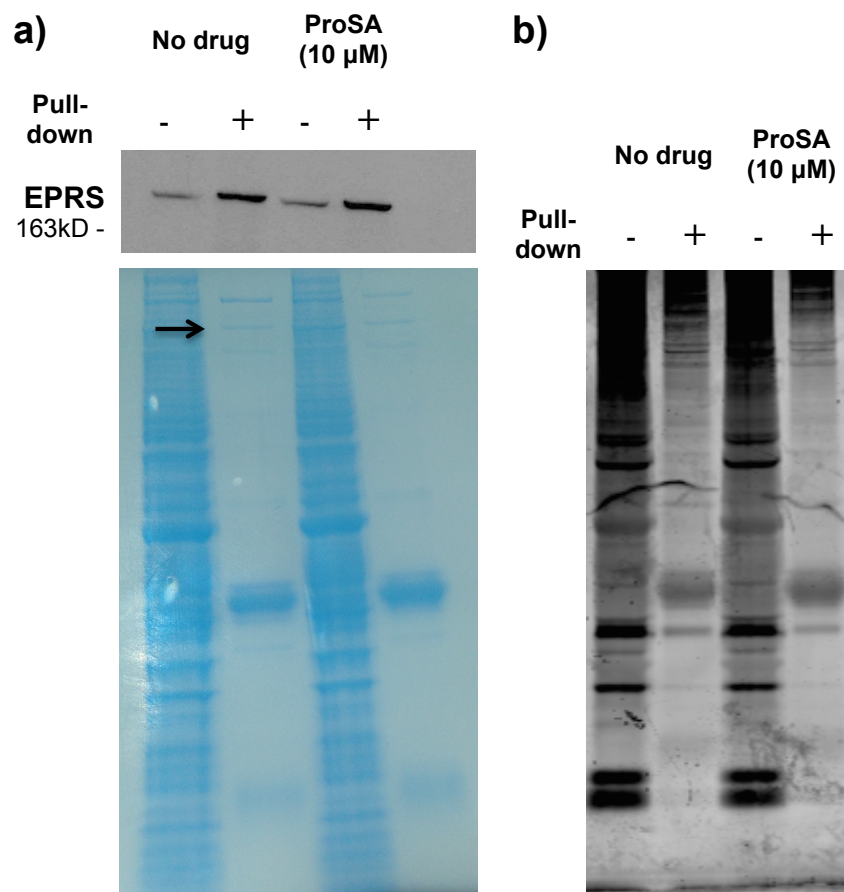


Figure 3.28 – MCF-7 cells treatment with 10 μM ProSA or a corresponding volume of DMSO. **a)** Western blot analysis of EPRS and commassie blue stained gel with potential EPRS band indicated with an arrow. **b)** SYBR® Gold stain of the same gel shows non-specific nucleic acid bands present in pull-down lanes (Lane 2 and 3) and absence of bands consistent with tRNA. Each blot is representative of two independent replicates.

Furthermore, the SYBR® Gold stain of this gel (Figure 3.28b), shows that even after the pull-down experiment there is still a significant amount of non specific nucleic acid bands in the sample as well as absence of a band consistent with tRNA migration, which may indicate that the amount of tRNA isolated is under the detection limit and underscores the need to further optimize the efficiency of the co-immunoprecipitation, as well as potentially use alternative methods for tRNA detection.

The preliminary results obtained thus far are consistent with our hypothesized model, nonetheless additional optimization is required to establish this technique. Therefore further work needs to be done towards increasing the amount of the enzyme-inhibitor complex isolated

to meet the detection requirements of the techniques used, and explore alternative approaches that might be more sensitive.

3.5.4 Discussion and Conclusion

The need for new targets for anti-malarial drug development is universally recognized, and many have been proposed. However, well-defined, pharmacologically practical paths forward to new classes of drugs remain scarce. Many traditional druggable targets, such as kinases, proved challenging to yield promising candidate targets.³⁷⁶

In addition, widespread resistance to mainstay drugs such as chloroquine, atovaquone, pyrimethamine, and sulfadoxine has aggravated the malaria threat.³⁷⁷ Most recently, the appearance of parasite strains resistant to artemisinin, last line of defense, has once more demonstrated the parasite's ability to quickly adapt to new treatment regimens.^{94, 378}

Within the scope of our efforts to help address this unmet medical need, we used an integrated chemogenomics approach that combined drug resistance selection, whole-genome sequencing, and an orthogonal yeast model, to demonstrate that the cytoplasmic prolyl-tRNA (transfer RNA) synthetase (*PfcPRS*) of the malaria parasite *Plasmodium falciparum* is a biochemical and functional target of febrifugine and its synthetic derivative halofuginone.⁷ *PfcPRS* is highly conserved across *Plasmodium* species and related protozoan parasites, representing an ideal target for broad-spectrum drug development. This concept is supported by our recent findings that *P. berghei* liver stage parasites are equally susceptible to HFG.³¹⁶ Thus, it is expected that inhibitors of cPRS will be comparably active against *P. vivax*, possibly also targeting the hypnozoite stage, which would be of critical importance for malaria elimination and eradication.

Aminoacyl-tRNA synthetases and associated pathways have been proposed as attractive targets for chemotherapeutic intervention in malaria.²⁵² The repertoire of aaRSs in *Plasmodium* diverges from other organisms because of the need to carry out protein synthesis in multiple subcellular compartments.²⁸⁷ Our group has established for the first time in *Plasmodium* that inhibition of tRNA synthetases by a small molecule and simultaneous activation of the integrated stress response is both feasible and attractive, and provides a rational mechanistic basis for future drug discovery and development focused on this novel target and pathway. We hypothesized that the inhibition of some but not all, *P. falciparum* aaRSs will result in activation of amino acid

response pathways and that inhibition of this subgroup represents an attractive approach for chemotherapeutic intervention in malaria. In this chapter we aimed to build on these important findings and in the one hand identify and biologically characterize selective small molecule inhibitors for the cPRS, and on the other identify novel targets within the aaRS class. This work has the potential to have a major impact on both basic malaria biology and applied biomedical research. This project was organized into three different, but complementary, objectives.

First, to explore tRNA synthetases as novel targets in *P. falciparum* we designed and synthesized a library of 21 reaction intermediate analogs, which allowed us to profile 19 of the *PfaaRSs* as drug targets. The desired aa-AMP analogs were successfully synthesized and tested against three different *P. falciparum* strains. Our results show that most of the aaSA analogs were active against blood stage *in vitro* *P. falciparum* strains in the nanomolar range with no chloroquine cross-resistance. Among the derivatives tested, L-PheSA, L-HisSA, L-AlaSA and L-ProSA were the analogs that exhibited higher antimalarial activity, with EC_{50} against the Dd2 strain of 120 nM, 98.4 nM, 119 nM and 96.9 nM, respectively. Cytotoxicity profiling in human MCF-7 cell line revealed a wide range of EC_{50} and selectivity index among the aminoacyl-tRNA synthetase inhibitors tested, underscoring the potential to specifically target the parasite aaRS with little to no effect over the human homolog, in certain cases. Furthermore, most of the aaSA analogs were active against liver stage *in vitro* *P. berghei*, with >99% parasite growth inhibition at the higher concentration of 10 μ M. aaSA compound treatment increased eIF2 α phosphorylation at 100X concentration, inducing the amino acid starvation pathway through direct inhibition of the corresponding *PfaaRS*, with few exceptions. Taken together, the results allow the prioritization of the ARS, HRS, FRS and PRS as the top four enzymes for further exploration as drug targets in blood stage malaria. Furthermore, the HRS, FRS and PRS are identified as the top three enzymes for further exploration as potential dual-stage drug targets. Thus, underscoring the potential of the aaRS family as an attractive novel class of antimalarial drug targets, with some of these enzymes having potential for dual-stage activity.

Second, to develop novel HFG based inhibitors that will serve as lead compounds in the preclinical development of a mechanistically unique class of malaria drugs with activity against both liver and blood stage life cycle stages, we designed hybrid-halofuginone derivatives based on the complex formed by HFG and ATP in the active site of cPRS. We followed a general synthetic approach developed by Lin and coworkers, with optimization of certain steps that were

modified to accommodate our target compounds. Despite being a concise asymmetric synthetic strategy, there were some challenges that had to be overcome. Nonetheless, further optimization efforts regarding the last two steps in the synthesis are necessary to obtain the desired hybrid compounds.

The third and last objective of this chapter consisted in characterizing the biology of cPRS inhibition and resulting amino acid starvation response. Understanding the enzyme-inhibitor complex formed by the different types of inhibitors would further elucidate on the differential effect observed on the amino acid starvation response, despite targeting the same enzyme. Thus, we applied a two-step proteomic approach to isolate the protein complex using immunoprecipitation followed by identification of its components using mass spectrometry. In this methodology, the protein of interest and any complex it forms in the cell is recovered by the use of high affinity reagents (e.g. antibodies or peptides coupled to beads) to the tag. When optimizing the co-immunoprecipitation of the PRS complex optimal conditions had to be established for lysis, immunoprecipitation and protein elution from the beads. Initially, experiments were optimized using the *S. cerevisiae* strains, which had been previously transformed using a complementation test of *PfcPRS*, by our group. The constructs included a His-tag fused protein on the *N*-terminus of *PfcPRS*, which allowed the use of His as bait in the pull-down experiments. Despite extensive optimization of lysis and co-immunoprecipitation conditions using this system, we concluded that only a small amount of *PfcPRS* was produced in these strains, and that it was stable only in very specific conditions, which would point to revising the plasmid used in the complementation experiment of *PfcPRS* in *S. cerevisiae*. Furthermore, based on our previous work validating EPRS as the molecular target of febrifugine and analogs, we turned our interest to understanding the biology underlying EPRS inhibition through the two different types of inhibitors in a mammalian model. Using the MCF-7 cell line, optimal conditions had to be established once again for lysis, immunoprecipitation and protein elution from the beads, to successfully isolate the EPRS complex. Complementary techniques were used to assist identification of the different components directly on the gel. Even though western blot analysis revealed EPRS isolation, the amount of protein present was not enough to successfully identify the complex components using mass spectrometry. Despite not being able to establish the protocol and prove beyond doubt that in the presence of ProSA the complex will scavenge the tRNA molecules to form a stable tRNA-enzyme-inhibitor complex (AAR not

activated), while in the presence of HFG the uncharged tRNA is unable to interact with the enzyme and will accumulate in the cell resulting in activation of the amino acid starvation response. The results obtained in MCF-7 cells are still consistent with the model proposed, thus more work needs to be done towards increasing the amount of the enzyme-inhibitor complex isolated to meet the detection requirements of the techniques used, and explore alternative approaches that might be more sensitive. Furthermore, the different induction levels of eIF2 α phosphorylation by ProSA, when comparing MCF-7 cells to *Plasmodium falciparum* cultures, may be related to differences in the amounts of tRNA present in each organism.

In our work we designed and synthesized valuable chemical tools that establish the amino acyl tRNA synthetases as attractive targets for the development of new classes of antimalarials active against both the red blood cell and liver stages of malaria. In this project we have also designed novel HFG analogs, the hybrid-halofuginone derivatives that target cPRS in an innovative form to exploit the differences between the *PfcPRS* and human EPRS, thus increasing parasite specificity. Furthermore we propose an explanation to our previous observation that not all aaRS inhibitors are capable of inducing the phosphorylation of eIF2 α , which is a sensitive indicator of the starvation response and a hallmark of isoleucine withdrawal, and proposed a viable methodology to prove our hypothesis. Despite the need for further improvement the preliminary results are encouraging.

We believe that the encouraging results obtained, combined with our published work on the identification of cPRS and EPRS, in *P. falciparum* and humans, respectively, as the biochemical targets of halofuginone, provides useful insights for future structure-based drug design efforts to identify novel inhibitors that target other aaRSs, as well as *PfcPRS* inhibitors with increased selectivity and potency.

Chapter Four

4. *Fluorescent Probes for Target Discovery*

4.1 Introduction

Small molecule therapeutic drugs typically exert their effects through binding to one or a few protein targets. This critical interaction - a prerequisite of therapeutic drug efficacy - is often poorly understood and can generally not be visualized in live cells or entire organisms due to the lack of methods to directly measure drug target engagement in a biological setting. As a result, most of our knowledge is incomplete, as it relies on target extraction assay systems or indirect measurements where critical spatiotemporal information is lost, which further complicates drug development.²²⁷

The challenges of discovering a compound's MoA and subsequent validation of the macromolecular target have driven innovative approaches, such as the use of a nonperturbing chemical handle within the incorporated biomolecule, which allows for selective attachment of a fluorophore or affinity tag.^{212, 225} Thus, approaches can be used in combination with chemical probes, including tagged inhibitors, designed to label proteins targets within cells or cell extracts.³⁷⁹⁻³⁸⁰ Nonetheless, incorporation of bulky tags may eventually limit the probe uptake and circulation in living cells.³⁸⁰ As a result two-step labeling may also be introduced via a Cu-catalyzed azide-alkyne 1,3-dipolar cycloaddition (CuAAC reaction) with a ligation handle, which clicks with a chemical tag after the enzyme capturing.³⁸¹

Recent advances in chemical techniques have allowed the creation of fluorescently labeled drugs, prodrugs and activity based probes to interrogate target engagement.^{4, 226, 382}

The use of fluorescently labeled small molecules has not yet been extensively exploited effectively for malaria drug discovery,^{228, 231, 383} but has potential for application to target validation.

4.1.1 Fluorescent Probes

Fluorescence is a three-stage process that occurs in certain types of molecules (fluorophores), which typically possess heterocyclic or polyaromatic structures.³⁸⁴ The fluorescent process is illustrated by Jablonski's simple electronic state diagram (Figure 4.1) and can be summarized in the following sequence of transformations: 1) Excitation-photon absorption by a fluorophore; 2) Life time-existence of an excited state; 3) relaxation of the

excited state by the emission of a photon.³⁸⁵ It is important to note that not all excited molecules decay through a photon emission (i. e., fluorescence) but some of the energy dissipates through other mechanisms. Examples of these processes are: collisional quenching, bond rotation or vibration, intersystem crossing, and fluorescence resonance energy transfer (FRET) to a suitable acceptor molecule.³⁸⁶

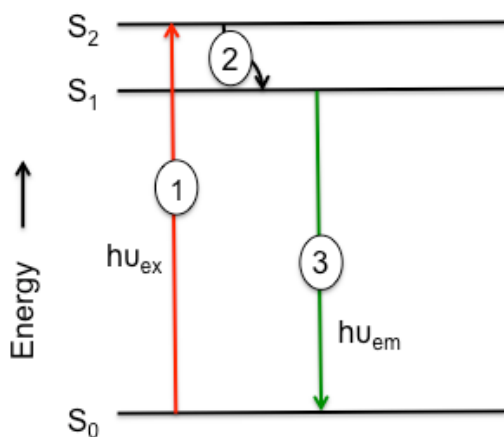


Figure 4.1 – Jablonski Diagram³⁸⁵: (1) absorption of a photon to an excited state; (2) internal conversion to excited state S_1 ; (3) fluorescence.

In fluorescence, the difference between the absorption maxima and the emission maxima is known as the Stokes shift and it is a distinct property for each fluorophore. The Stokes shift is essential for the sensitivity of various fluorescent techniques and often fluorophores with a small Stokes shift are susceptible to self-quenching. Another critical property, which determines the fluorescence output of a given fluorophore, is the efficiency with which it absorbs and emits photons, termed as the fluorescent brightness (Product of quantum yield (Φ) and molar extinction coefficient (ϵ)). The absorption efficacy is usually quantified in terms of molar extinction coefficient and it ranges from 5000 to 200,000 $\text{cm}^{-1}\text{M}^{-1}$.³⁸⁶⁻³⁸⁷

Fluorescence microscopy and fluorescence molecular tomography (FMT) are arguably amongst the most important and most powerful imaging techniques currently utilized to study biological systems with resolutions spanning from single molecules to whole animals.^{226, 388-390} Nonetheless, the *in vivo* penetration capacity may pose as a limitation. Next to fluorescent proteins and quantum dots, small molecule fluorescent dyes have been critical components for the development of these approaches.³⁸⁵ For the observation of specific phenotypes, fluorescent dyes are orthogonal and often superior to alternative probe strategies due to their small size,

increased stability and ease of synthetic access. Furthermore, fluorescent dyes can be designed as probes to interrogate reactive biological species in their native environment.³⁹¹ Tagging biologically active compounds of interest with a fluorescent tracer can enable visualization of the temporal and spatial perturbation of biological systems in their endogenous state, thus allowing to map the distribution of bound and unbound drug.²²⁷ From these agents, real-time information can be gathered on the cellular localization of a small molecule probe as well as other indicators, such as the quantitative expression levels of an intended target.³⁹²

In chemical biology, the application of such small molecule tool compounds has been fruitful, allowing for the exploration of critical physiological events. Similarly, in drug development such fluorescent probes can serve an equally pivotal role in the mechanistic investigation of promising clinical candidates and already established chemotherapeutics, to study their function in various disease states of importance to human biology.³⁹³⁻³⁹⁴

Fluorophores are used in many ways and include molecules with endogenous, fluorescence such as quinine, and many polycyclic aromatics, such as naphthalene derivatives (Figure 4.2). Organic fluorophores can be divided according to the absorption and emission wavelength values of their conjugates, thus broadly grouped into either near-ultraviolet to 500 nm or 500 nm to near-infrared. The second group includes the most important type of fluorophores, such as the fluoresceins, rhodamines, BODIPY dyes, squaraines, and cyanines, among others (Figure 4.2).^{385, 395-396}

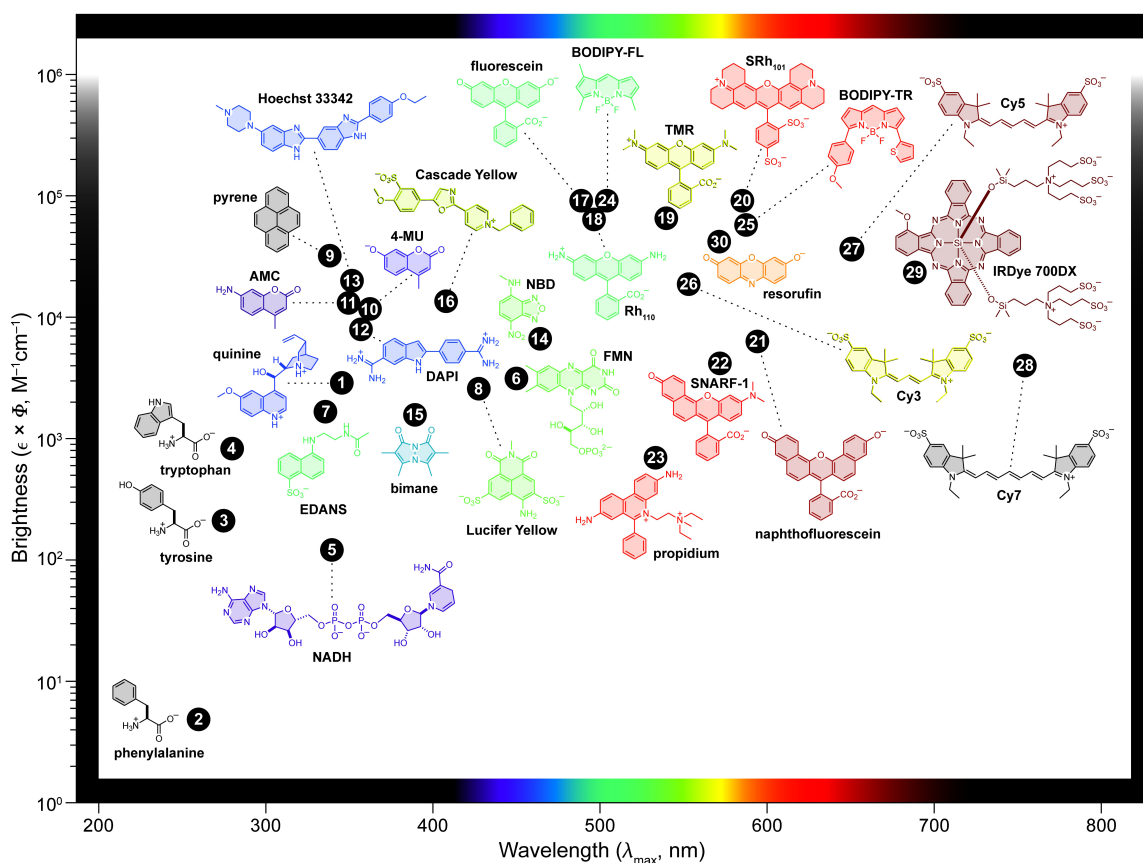


Figure 4.2 – Plot of fluorophore brightness for the major classes of fluorophores. The color of the structure indicates its wavelength of maximum emission (λ_{em}). For clarity, only the fluorophoric moiety of some molecules is shown. (Figure adapted from Luke *et al.*)³⁸⁵

The identification of an organic fluorophore that is suitable for tagging a compound of interest without perturbing its biomolecular activity is a critical, yet frequently problematic, aspect of probe development. While a wide variety of fluorescent dye classes have been reported in the literature, many of which are commercially available, only a few are viable for biological applications.³⁸⁵ Moreover, members of this select pool frequently suffer from at least one key drawback.

For bioimaging approaches, the fluorescent tags must have an appropriate balance of favorable physical properties. Most importantly they should possess high brightness (the product of extinction coefficient to quantum yield), which ideally is independent from the molecular environment (e.g. polarity and pH), and exhibit good aqueous solubility while retaining a

favorable lipophilicity. The latter two factors are particularly critical for live cell and *in vivo* imaging as they ensure that the dye can easily diffuse through membranes and organelles with minimal non-specific staining of lipid membranes.³⁹⁷ Tied with these attributes is a necessity that the dye moiety remains a neutral, uncharged species in aqueous environments. Finally, the fluorophore should be small and provide a modular functional group for bioconjugate chemistry. The endpoint of these stipulations would be a chemically stable fluorophore that readily traffics through pertinent cellular compartments, maintains ideal optical properties in the cell, and possesses minimal drug-like attributes that would interfere with untangling the mechanism of the molecule of interest.²²⁶⁻²²⁷

Recent efforts to develop fluorescent dyes that satisfy the rigorous conditions required for routine live cell imaging have involved in the development of non-planar cyanine fluorophores, which exhibit low-levels of non-specific staining in preliminary cell studies.³⁹⁸ Novel near-IR and cell-permeable fluorophores have also been robustly tested for routine live-cell imaging studies and point towards the importance of fluorophore development with explicit consideration of the eventual challenges to be faced in the imaging environment of interest.³⁹⁹⁻⁴⁰⁰ The importance of multiplexing fluorescent signals has also spurred innovation in small organic probe development such as the recently optimized second-generation multicolor oligodeoxyfluoroside class.⁴⁰¹

Yet, in our estimation, for chemogenomic applications, the difluoro-boron-dipyrromethene dyes (BODIPYs) (4.1) (Figure 4.3) comprise the compound class that fulfills most of the parameters outlined for routine imaging and conjugation to small-molecule and protein targets of interest. BODIPYs are fluorescent on account of a highly compact boron dipyrromethene core and boast excellent brightness.⁴⁰² Importantly, their absorption and emission profiles can be tuned via accessible chemistry on the dipyrromethene ligand. Finally, a series of substitutions on the BODIPY core scaffold have shown the relevancy of this probe class for two-photon imaging applications.⁴⁰³⁻⁴⁰⁴ Unfortunately, the core fluorophore of the BODIPY dyes and their derivatives is inherently lipophilic and thus poorly water-soluble. These physical attributes, while allowing for passive cellular uptake, prepossess the fluorophore (or tagged small molecule) into lipophilic compartments, resulting in non-specific staining of membranes and intracellular organelles. The typical background staining, which we attribute to the endoplasmic reticulum (ER) and Golgi membranes, is commonly observed with cell permeable BODIPY dyes

and other lipophilic dye classes.^{401, 403-406} This characteristic is troublesome as it significantly biases cellular distribution of labeled small molecules to membranes, albeit non-specifically, and requires stringent washing steps to minimize background signal that is only compatible with very tight small molecule-target interactions.

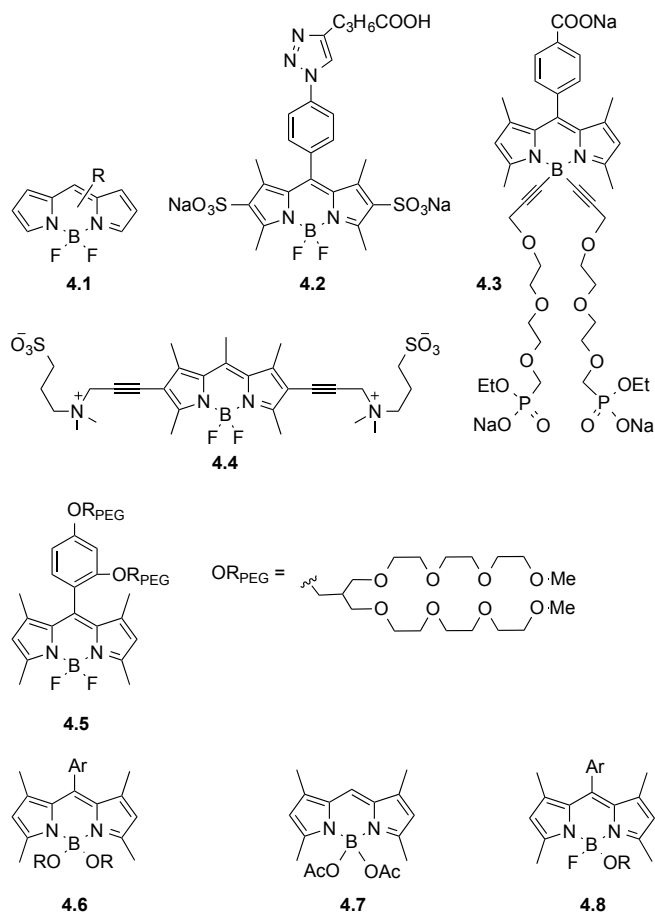


Figure 4.3 – Structures of BODIPY dyes.

To counteract the main drawback of poor aqueous solubility that plague BODIPYs, extensive efforts have focused via the addition of charged functional groups such as sulfonate groups (4.2)⁴⁰⁷ and phosphonates (4.3), including the symmetric functionalization of the boron-core.⁴⁰⁸⁻⁴⁰⁹ Ligands with a net formal charge of zero have also been explored such as zwitterionic sulfobetaines (4.4).⁴¹⁰ While such approaches yield BODIPY dyes with improved water solubility, the applicability for live cell and *in vivo* imaging is limited due to the ionic character of the solubilizing groups, which impair membrane permeability and often result in a significantly increased molecular weight of the fluorescent tag. Similarly, modification with

multiple PEG-groups (4.5) can improve aqueous solubility, again at the cost of increased size (in some examples the solubilizing groups account for >80% of the molecular weight).⁴¹¹ Also of interest in this context are dialkoxy (4.6) and diacetoxy (4.7) BODIPY dyes that have been reported to exhibit improved aqueous solubility compared to the difluoro analogs.⁴¹²⁻⁴¹⁴ It is important to note that recent departures from the canonical BODIPY structure have shown promise for chemical biology imaging applications although these derivatives have yet to demonstrate applicability in live cell imaging with respect to stability and specificity. Notable efforts have also involved stabilization of the core BODIPY scaffold and bioconjugation via the Boranil dye class, characterized with an N-B-O versus N-B-N heteroatom center.⁴¹⁵ Increased cell permeability has been accessed with a rigid triazaborolopyridinium core structure that appears to address the membrane permeability challenge, however, non-specific intracellular staining patterns comparable to our findings with the BODIPY dyes remain.⁴⁰⁵

Our previous synthetic aim was to develop a method to improve the biological imaging compatibility of the BODIPY fluorophore while retaining opportunities in multimodal imaging and ease of bioconjugation. These methods originated from our group's work on BODIPY dyes for hybrid optical/Positron Emission Tomography imaging.⁴¹⁶ However instead of ¹⁹F/¹⁸F exchange, we then explored selective access to singly alkoxy-substituted (core mono-alkoxy) BODIPY (CMA-BODIPY) dyes (4.8) and evaluated their applicability for biological imaging in comparison to BODIPY and dialkoxy-BODIPY dyes (4.6). In this work we found that retaining one the fluorine atoms on the dye scaffold allows for exquisite tuning of the physicochemical properties of the fluorophore while providing an attachment site for bioconjugate and multimodal imaging chemistries. Most importantly, CMA-BODIPYs are characterized by excellent membrane permeability, homogenous distribution and low non-specific background in living cells.⁴ Importantly, prior to our work, following published procedures, CMA-BODIPYs (4.8) were only obtained as byproducts in mixtures with the corresponding dialkoxy derivatives (4.6) that are difficult to separate.⁴¹²⁻⁴¹³

Furthermore, accessing CMA-BODIPYs using a synthetic methodology that is compatible with a broad array of functional groups will allow for direct modification of the well-established BODIPY dyes, thus providing easy access to diversely functionalized reporters, as well as small molecule fluorescent labeling.

4.1.2 Indolo[3,2-*b*]quinoline Antimalarial Scaffold

The scarcity of validated malaria drug targets and the stringent requirements for successful drug candidates suggest that understanding the mechanisms of action of existing antimalarial drugs is critical. Antimalarials with demonstrated clinical efficacy like the aminoquinolines have represented promising basis for rational drug development.^{54, 417}

Blood-stage malaria parasites ingest roughly 75% of the hemoglobin from the host red blood cell into the lysosome-like food vacuole. Here, the polypeptide chains of hemoglobin are cleaved into short peptides and individual amino acids by the concerted action of multiple classes of proteases.⁵⁵ High concentrations of cytotoxic free heme are released. To prevent vacuolar damage from free heme accumulation, due to its affinity for lipids in cellular membranes and its ability to generate reactive oxygen species the parasite sequesters liberated heme into inert crystals of heme dimers termed hemozoin (Hz).^{53, 418}

Hemoglobin degradation and Hz formation are essential for parasite survival, making these processes important targets for antimalarial drug development. Heme detoxification into Hz, believed to be the primary target of quinoline antimalarials such as chloroquine (CQ),^{64, 71} remains one of the most attractive drug development targets, in part due to the immutable nature of heme. Resistance to CQ is associated with mutations in the gene encoding the food vacuole (FV) membrane protein *P. falciparum* chloroquine resistance transporter (*PfCRT*),⁷⁸ which appears to result in reduced drug concentration at the target without altering the target itself.

Within the scope of our efforts, we have explored the indoloquinoline scaffold as a starting point to develop new antimalarials.^{5, 419-422} Alkaloids from traditional herbal medicines have contributed greatly over the centuries towards the discovery of new therapeutic agents.^{145, 423-424} Indoloquinolines are unique natural alkaloids, characterized by an indole ring fused to a quinoline ring, which are found almost exclusively in the West African climbing shrub *Cryptolepis sanguinolenta* and have been used for centuries by African traditional healers mainly for the treatment of fevers from malaria, hepatitis and bacterial infections.¹⁵⁰ Most of the compounds isolated from *C. sanguinolenta* displayed the indolo[3,2-*b*]quinoline nucleus and of these Cryptolepine (Figure 4.4) is by far the most studied. It has two nitrogens but only one (N10) has an acidic proton with a pKa of 11.1-11.8.⁴²⁵⁻⁴²⁶

The pharmacological activities of extracts from *C. sanguinolenta* and its major indoloquinoline alkaloid cryptolepine as well as its isomers, neocryptolepine, isocryptolepine

and the synthetic isoneocryptolepine (Figure 4.4) have been extensively studied.

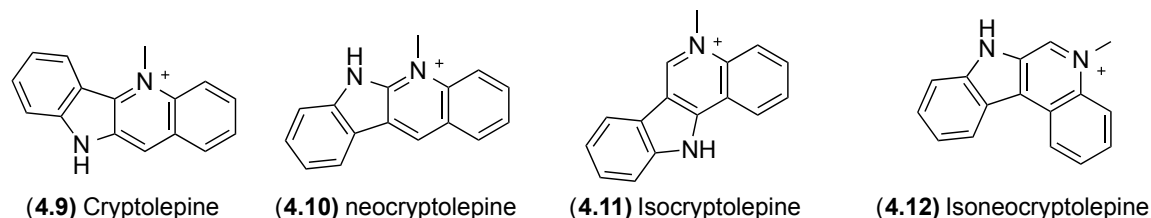


Figure 4.4 – Indoloquinolines from *Cryptolepis sanguinolenta*.

Since 1937, several groups have demonstrated that indoloquinolines have a variety of biological activities including antibacterial, antifungal, antiprotozoal, antitumoral, antihyperglycemic, anti-inflammatory, hypotensive, antithrombotic and vasodilation. Due to its synthetic achievable structure and scope of derivatization, the indolo[3,2-*b*]quinolines have been intensively investigated for finding of new derivatives with improved biological properties.^{150,}

427-428

Taking into consideration the diverse biological activities demonstrated by these compounds, our group has further explored the indolo[3,2-*b*]quinoline scaffold as a starting point in the development of both antimalarial and anticancer drugs.

Anticancer activity

Since indoloquinolines are tetracyclic aromatic alkaloids and can potentially intercalate into DNA these compounds have a high potential to be developed into anticancer drugs. Additionally, derivatives of natural indolo[3,2-*b*]quinolines and cryptolepine have been shown to be good G-quadruplex (G4) DNA structure ligands, telomerase inhibitors, oncogene (c-Myc) transcription inhibitors, and are able to induce cell-growth arrest. Furthermore, our group has identified indolo[3,2-*b*]quinolines with a 7-carboxylate group and three alkylamine side chains, as well as 5-methyl-indolo[3,2-*c*]quinoline derivatives as effective G4 stabilizers and promising selective anticancer leads.⁴²⁹⁻⁴³¹ The compounds target, more specifically G4 motifs present in oncogene KRAS promoter, down-regulate the expression of the mutant KRAS gene through inhibition of transcription and translation, and induce cell death by apoptosis in colon cancer cell

lines. Thus, targeting KRAS at the genomic level with G4 ligands may be a new anticancer therapy strategy for colon cancer.^{429, 431}

Antimalarial activity

Our group has designed, synthesized and profiled for malaria therapy new compounds based on this natural indoloquinoline alkaloid. The C-11 cryptolepine derivatives showed improved *in vitro* cytostatic activity and parasite selectivity.^{419, 421} However, the most promising compound (C11-alkylamine derivative) was only as active as the parent compound cryptolepine in a rodent malaria model, showing modest antimalarial efficacy when administered orally and high toxicity when administered ip at 50 mg/kg.⁴³²

Previous studies suggest that cryptolepine may act like chloroquine (CQ), due to its ability to bind to hemozoin monomer and inhibit Hz formation. Nonetheless, this compound displayed a low capacity to reach its target due to its low accumulation in acidic food vacuole. We have previously reported that a basic amino side chain is needed for CQ accumulation in the acidic vacuole of the parasite.⁴¹⁹ Furthermore, to get insight into the relevance of targeting hemozoin (Hz) crystals, we have evaluated two isomeric bis-alkylamine indolo[3,2-*b*]quinolines for their *in vitro* activity against chloroquine (CQ)-resistant and sensitive strains of *Plasmodium falciparum*. Both series bounded to hemozoin monomer, inhibited β -hemozoin formation *in vitro*, delayed intraerythrocytic parasite development with apparent inhibition of Hz biocrystallization, and showed higher cytotoxic activity against schizonts.⁴²² Moreover, to improve access and binding to the target we then designed novel *N*10,*N*11-di-alkylamine bioisosteres (Figure 4.5).

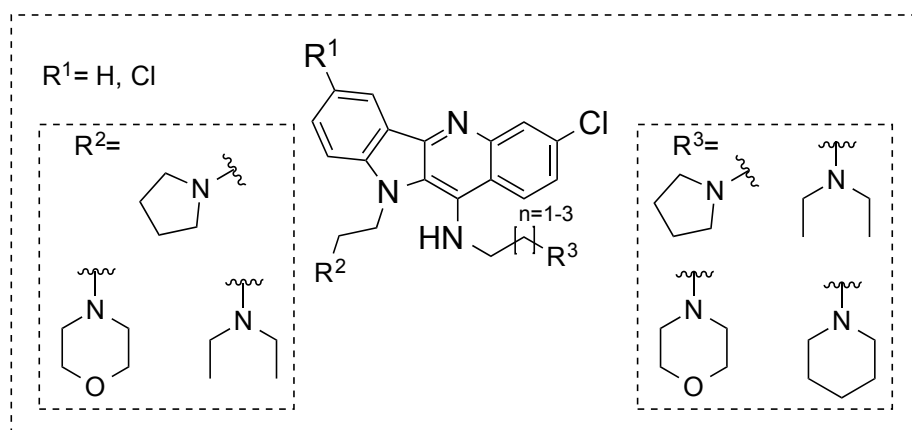


Figure 4.5 – Structure of target bioisosteres *N*10,*N*11-di-alkylamine indolo[3,2-*b*]quinoline derivatives.

All new indolo[3,2-*b*]quinoline derivatives showed selectivity for malaria parasites compared to human hepatic cells (SI > 30) and potent antimalarial activity, with EC₅₀ values in the nM range. Bioisosteric replacement of –O– by –NH– at C11 led to slightly more hydrophilic compounds, with increased vacuolar accumulation ratios (VAR) but lower lipid accumulation ratios (LAR).

In particular, 3-chloro derivatives showed high activity against *Plasmodium falciparum* chloroquine (CQ)-resistant strain W2 with EC₅₀s between 20 and 158 nM. Nonetheless, antimalarial activity of the 3-chloro-*N*10-ethylpyrrolidine series did not correlate with VAR but correlated with β-hematin inhibition. Interestingly, all compounds of this series showed similar potential to accumulate in lipid phases and in the vacuolar aqueous phase (LAR/VAR~1). On the other hand, antimalarial activity of 3,7-dichloro-*N*10-ethylpyrrolidine derivatives increased with VAR values and they were better inhibitors of β-hematin formation. Thus, for both series, the results suggest inhibition of Hz growth as one possible mechanism of action for these indolo[3,2-*b*]quinoline compounds.⁵ To further elucidate the mechanism of action of the 3-chloro-*N*10-ethylpyrrolidine derivatives we aimed to develop fluorescent probes that will allow subcellular fluorescence co-localization of the compound in *Plasmodium falciparum* cultures, which has not been done to the best of our knowledge.

4.2 Purpose of This Study

This project is designed to explore our synthetic methodology and further develop it to enable the use of CMA-BODIPY dyes to label small molecule drugs using an innovative point of attachment between drug and dye, which simultaneously labels the drug and increases solubility and cell permeability.

In this work we report the development of a methodology to selectively substitute either one or both of the canonical fluorides common to most BODIPY dyes with alkoxy ligands, and show that the alkoxy substituent provides an additional, unique attachment site, which can be readily exchanged by either an alkoxy-drug or another an alkoxy-ligand without perturbing the fluorophore scaffold (Figure 4.6).

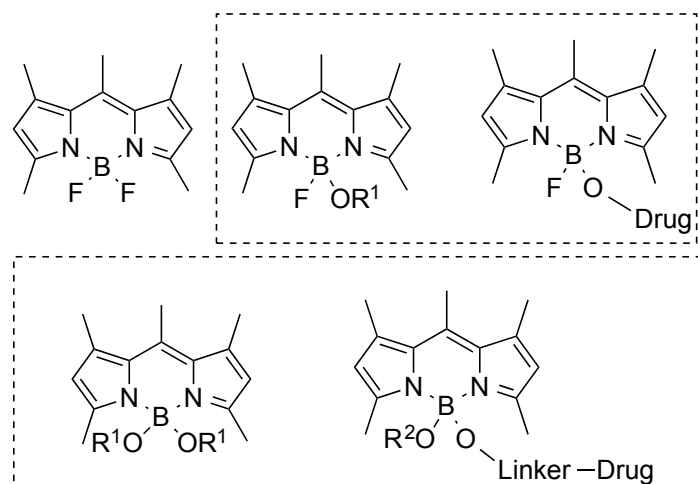


Figure 4.6 – Structures of alkoxy-drug and alkoxy-ligand BODIPY dyes accessed by the new synthetic methodology.

The mild and efficient methodology developed allows access to mono or dialkoxy substituted BODIPYs and we further evaluated its applicability for imaging small molecules in live cells. Nonetheless, despite having great applicability, this method has limitations regarding the acidic conditions required, which are incompatible with some functional groups. Moreover, the broad impact of our approach is demonstrated by directly functionalized small molecules of interest that feature an appropriate hydroxyl group, using the newly developed methodology. This novel synthetic method will be used to label several drugs including a known antimalarial drug, thus enabling the subcellular localization in both mammalian and *Plasmodium falciparum* cultures, which may constitute an additional target validation approach. Moreover, to further validate the drug target of the 3-chloro-*N*(10-ethylpyrrolidine) indoloquinoline derivatives developed by our group, we designed a fluorescent probe that will allow subcellular localization of the compound in *Plasmodium falciparum* cultures.

4.3 Synthetic Methodology

4.3.1 Chemical Synthesis Strategy

The retrosynthetic analysis of the alkoxy BODIPY labeled small molecules (Figure 4.7) shows a short and robust synthetic approach starting with 1,3,5,7,8-Pentamethyl BODIPY. After fluorine/alkoxy exchange to obtain the mono or dialkoxy substituted BODIPYs, a second

exchanged occurs between an alkoxy group from the dye and a hydroxyl functionalized molecule. To obtain a monoalkoxy fluorescently labeled drug, the alkoxy group in the monoalkoxy BODIPY is directly exchanged by the hydroxyl functionalized small molecule, in a boronic acid transesterification. Moreover, the monoalkoxy fluorescently labeled drug can also be obtained by direct displacement of the fluorine atom. Alternatively, to obtain a dialkoxy fluorescently labeled drug, one of the alkoxy groups in the dialkoxy BODIPY is exchanged by a hydroxyl-linker followed by coupling with the drug (Figure 4.7).

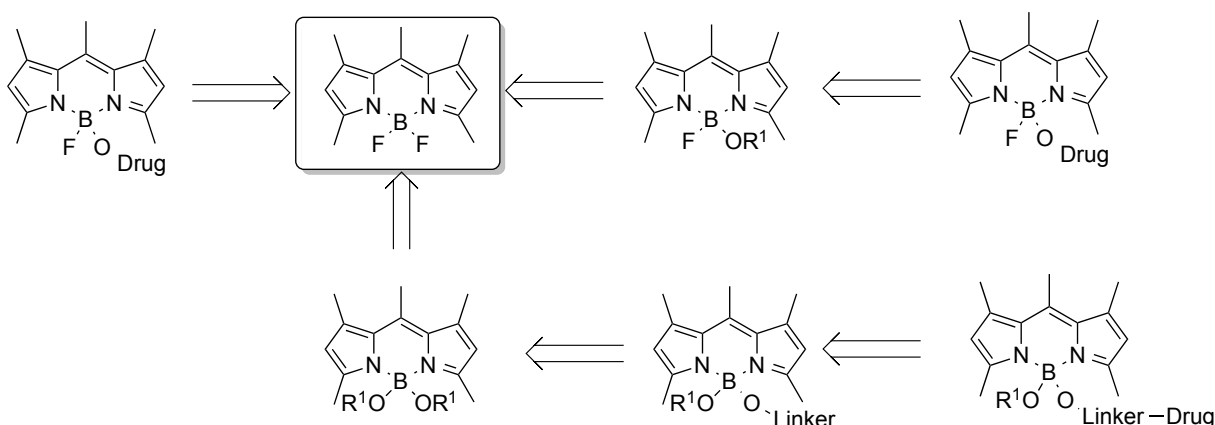
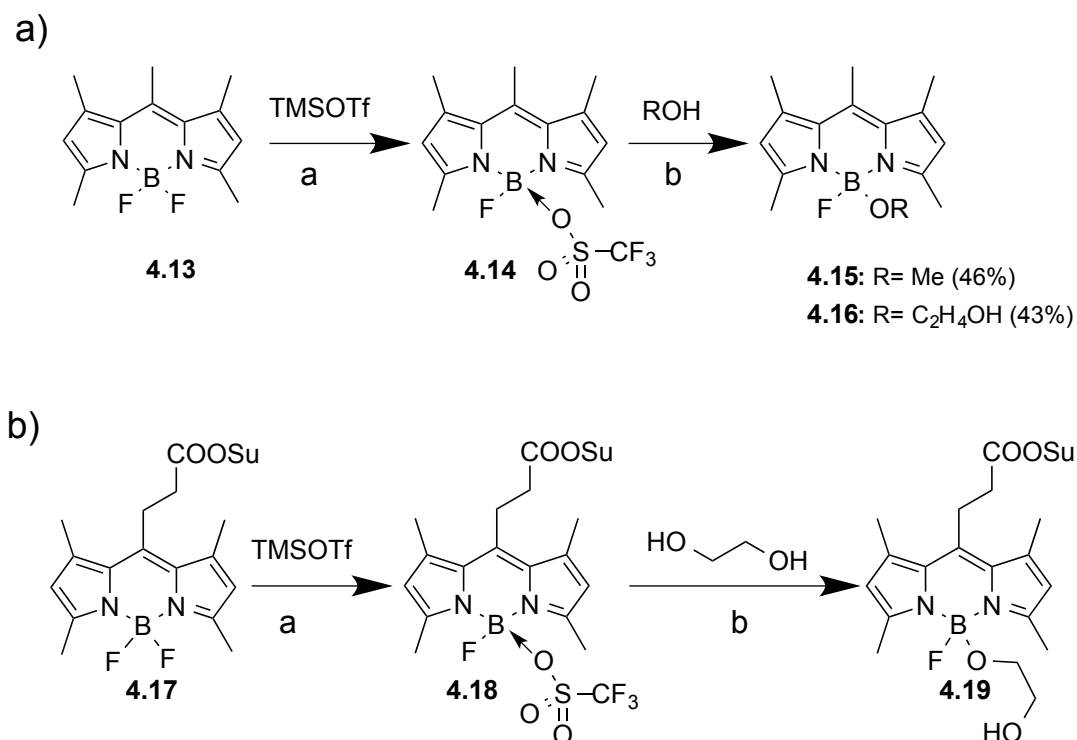


Figure 4.7 – Retrosynthetic analysis of the alkoxy BODIPY labeled drug.

4.3.2 Synthesis of Alkoxy BODIPYs

We have selected BODIPY (**4.13**) as a model substrate since it is well established and provides direct access to dimethoxy BODIPY.^{412, 433} To selectively substitute only one the fluorines we applied a two-step one-pot strategy, guided by previous work in our group on $^{19}\text{F}/^{18}\text{F}$ exchange on BODIPYs for hybrid optical/Positron Emission Tomography imaging.⁴¹⁶ The approach relies on abstraction of a single fluoride from the BF_2 -core to generate a reactive boronium intermediate (**4.14**),⁴³⁴⁻⁴³⁵ which we found readily reacted with suitable alcohols to yield the desired monoalkoxy-BODIPY (CMA-BODIPYs) (**4.15-4.16**) in high-yields without the formation of dialkoxy BODIPY (Scheme 4.1a).⁴



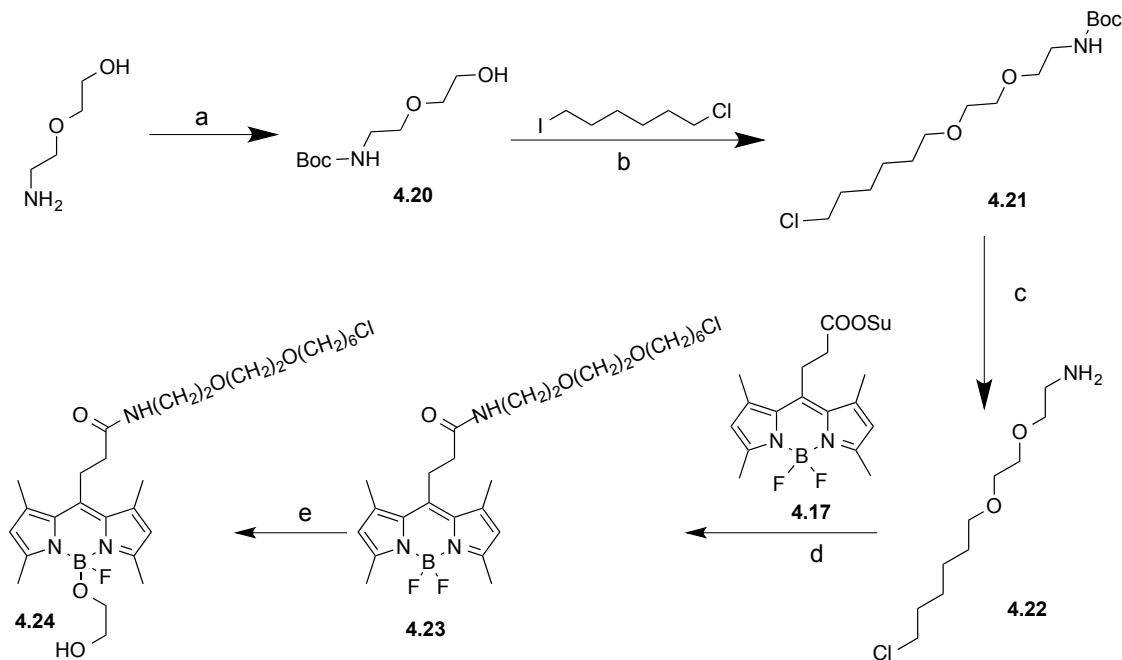
Scheme 4.1 – Synthesis of CMA-BODIPYs. **a)** One-pot synthesis of CMA-BODIPY analogs **4.15-4.16**. Reagents: a) TCM, TMSOTf, 0 °C, 150 s; b) TCM, R'OH, 0 °C, 150 s; **b)** Synthesis of CMA-BODIPY **4.19**.

Specifically, CMA-BODIPYs were obtained by activation of difluoro-BODIPY with excess trimethylsilyl trifluoromethanesulfonate (TMSOTf) to access the reactive BODIPY-OTf (**4.14**) intermediate,⁴³⁵ which is directly quenched by addition of a suitable alcohol to afford the desired monoalkoxy-BODIPY in high yields (**4.15-4.16**). The activated BODIPY-OTf is not stable for a prolonged time under the reaction conditions and slowly degrades, forming the free pyrrole ligand. Therefore, the addition of the desired alcohol ligand has to be timed carefully. Simultaneous addition of DIPEA as a mild, non-nucleophilic base to buffer the acidity of the crude reaction solution, as well as maintaining the whole system at 0 °C, was found to be beneficial.

This synthesis is highly modular and allows for easy access to an array of different alkoxy BODIPY derivatives. Notably, the presented methodology tolerates a wide number of

functional groups. For example, as illustrated in Figure 4.1b, the *N*-hydroxysuccinimide (OSu) functionalized BODIPY **4.17** was efficiently converted into the glycol-analog **4.19**. We expect that these functionalities would be synthetically incompatible with the existing strategies (referenced above) to access these analogs as mono and dialkoxy mixtures of compounds such as **4.16**.

To demonstrate that the favorable properties of CMA-BODIPYs are retained upon conjugation to small molecules, we synthesized a HaloTag functionalized BODIPY **4.23** and CMA-BODIPY **4.24** from the common NHS-ester precursor **4.17** (Scheme 4.2). The latter was coupled with the amine HaloTag, which was obtained in a three-step synthesis starting with the Boc protection of the aminoethoxyethanol, followed by S_N2 coupling with 1-chloro-6-iodohexane and Boc deprotection (Scheme 4.2).



Scheme 4.2 – Synthesis of HaloTag functionalized CMA-BODIPY. Reagents and conditions: **a**) Boc₂O, EtOH, r.t., 4 h, 98%; **b**) NaH, THF:DMF (2:1), r.t., 3 h, 38%; **c**) 2 M HCl, MeOH, r.t., 2 h, 78%; **d**) DIPEA, DCM, r.t., 30 min, 37%; **e**) Ethylene glycol, TMSOTf, DIPEA, TCM, r.t., 2:30 min, 60%.

HaloTag ligands bind selectively and covalently to HaloTag, a small protein that can be expressed as a fusion protein with a target protein of interest, to allow for selective labeling of intracellular targets.⁴³⁶⁻⁴³⁷ We selected the HaloTag system over other tags like SNAP-tag and

CLIP-tag, as the chloroalkane HaloTag ligand is very hydrophobic, thus representing a demanding test system.^{353, 437-438}

To assess the suitability of CMA-BODIPY dyes for biological applications, we investigated their physical properties in direct comparison to the relevant reference compound difluoroBODIPY **4.13** in aqueous buffer at physiological pH.

We first investigated the solubility characteristics in aqueous buffer at physiological pH. Dry powders of the respective compounds in excess were used to prepare saturated solutions in PBS (pH=7.4). The alkoxy derivatives have excellent water solubility while the difluoro-BODIPY **4.13** appears to be virtually insoluble in PBS. Quantitative measurements showed that the alkoxy derivatives are generally soluble at medium to high micromolar concentrations in PBS without the requirement of co-solvents or detergents (Table 4.1). Next, we determined the $\log D_{7.4}$, which is an important characteristic to gauge membrane permeability and the propensity of a small molecule to distribute between aqueous and hydrophobic cellular compartments. Compounds with a $\log D_{7.4}$ of 1-3 strike this balance best and demonstrate the greatest membrane permeability.³⁹⁷ The increased aqueous solubility of CMA-BODIPYs correlates with a lower $\log D_{7.4}$ compared to difluoro BODIPY **4.13** (Table 4.1). Notably, the methoxy (**4.15**) and glycol analogs (**4.16**) exhibit ideal $\log D$ s of 1.4 and 2.2, respectively. In contrast, the difluoro-BODIPY **9** had an unfavorable $\log D$ of >5. Furthermore, the solubility of compound **4.24** in PBS was 231 μM , almost two orders of magnitude greater than the BODIPY **4.23** (Table 4.1). Similarly, this increased aqueous solubility also translated into an improved $\log D$.

Table 4.1 – Physico-chemical Characterization of BODIPYs⁴

Compound	LogD ^a	Solubility (μM) ^b
4.13	> 5	3
4.15	1.4	24
4.16	2.2	122
4.23	> 5	2.4
4.24	3.85	230

^a LogD was determined via the shake-flask method by partitioning a saturated solution of the probes in 1X PBS (pH=7.4) with 1-octanol; ^b Solubility was determined in 1X PBS (pH=7.4) from the concentration of a saturated solution of each probe.

Since we had established that the new class of BODIPY fluorophores, which we term MayaFluors, display significantly improved physicochemical properties that are ideally suited for biological applications, we then turned our focus into exploring the possibility of selectively substituting one of the fluorines with a hydroxyl functionalized small molecule, using the same two-step one-pot strategy.

The first drawback encountered, was regarding the amount of hydroxyl-reagent (100 equiv.) used when synthesizing the CMA-BODIPYs, which is inefficient in some cases. Furthermore, the synthetic conditions used also resulted in some degradation products, as mentioned above, which still had room for improvement. The first approach to address these problems was to optimize the current conditions to enable the use of reduced amounts of the hydroxyl functionalized small molecule as well as increase overall stability, thus decreasing the amount of degradation products (Table 4.2).

To optimize the CMA-BODIPY synthesis we chose to start by using the mono-methoxy BODIPY as a reference system, thus aiming to substantially decrease the number of equivalents of MeOH required in this reaction. First, in an attempt to decrease the amount of degradation products observed using the original synthetic methodology (Entry 1), the solvent was changed to DCM and the temperature decreased to $-78\text{ }^{\circ}\text{C}$ (Entry 2), which did not result in the desired product. Next, a Lewis acid catalyst was added after the trifluoromethanesulfonic acid trimethylsilylester (TMSOTf), resulting in elimination of degradation products by LC/MS analysis of the crude reaction (Entries 3-4). This may occur due to a stabilizing effect of the SnCl_4 on the reactive BODIPY-OTf intermediate. The results obtained when using low (2 equiv.) and high (30 equiv.) amounts of SnCl_4 were comparable. Once conditions were optimized to eliminate the degradation products observed, the amount of hydroxyl-reagent was gradually reduced (Entries 5-10), which also required reduction of the catalysts used, to avoid degradation products. Nonetheless, an alternative solvent and a different Lewis acid catalyst (Entries 8-9) were both tested with no improved results.

Therefore, the mono-methoxy BODIPY was accessed by activation of difluoro-BODIPY with a slight excess of TMSOTf (1.5 equiv.) to access the reactive BODIPY-OTf intermediate, which was stabilized by a small amount of SnCl_4 (0.5 equiv.), followed by addition of one equivalent of methanol to afford the desired monoalkoxy-BODIPY in high yield (Entry 10).

Table 4.2 – Optimization of CMA-BODIPY synthesis.

Entry	ROH		Catalyst (Equiv.)	Solvent	Time (min.)	Temp. (°C)	Degradation Products	Product
	R	Equiv.						
1	Me	100	TMSOTf (5)	TCM	2	0	30%	4.15
2	Me	100	TMSOTf (5)	DCM	2	-78	-	4.15
3	Me	100	TMSOTf (5)/ SnCl ₄ (30)	TCM	2	0	< 5%	4.15
4	Me	100	TMSOTf (5)/ SnCl ₄ (2)	TCM	2	0	< 5%	4.15
5	Me	10	TMSOTf (5)/ SnCl ₄ (2)	TCM	2	0	15%	4.15
6	Me	10	TMSOTf (1.5)/ SnCl ₄ (2)	TCM	2	0	< 5%	4.15
7	Me	5	TMSOTf (1.5)/ SnCl ₄ (0.5)	TCM	2	0	< 5%	4.15
8	Me	5	TMSOTf (1.5)/ SnCl ₄ (0.5)	MeCN	2	0	15%	4.15
9	Me	5	TMSOTf (1.5)/ ZnCl ₂ (2)	MeCN	2	0	20%	4.15
10	Me	1	TMSOTf (1.5)/ SnCl ₄ (0.5)	TCM	5	0	< 5%	4.15
11	CH ₂ CH ₂ OH	5	TMSOTf (5)/ SnCl ₄ (2)	TCM	2	0	20%	4.16
12	CH ₂ CH ₂ OH	10	TMSOTf (5)/ SnCl ₄ (30)	TCM	2	0	20%	4.16
13	Bn	5	TMSOTf (5)/ SnCl ₄ (2)	TCM	2	0	-	-
14	Bn	10	TMSOTf (5)/ SnCl ₄ (30)	TCM	2	0	-	-

Next, to test the applicability of the improved synthetic methodology to other monoalkoxy-BODIPYs, we used ethylene glycol (Entries 11-12) or benzyl alcohol (Entries 13-14) as the hydroxyl-reagent. In the first case, using the Lewis acid catalyst to stabilize the reactive BODIPY-OTf intermediate, allowed a substantial reduction of the ethylene glycol used

(5 equiv.), despite the presence of some degradation products. Unfortunately, when using this methodology with benzyl alcohol, as the hydroxyl-reagent, the desired product was not formed, which indicated that further optimization would be required. Thereafter, the optimization of the latter reaction involved assessment of the ideal catalyst to promote reactivity and adjustment of the solvent used to allow increase in the temperature, thus we chose toluene as the reaction solvent since it is a common solvent with a high boiling point (111 °C) (Table 4.3). Since the reactive BODIPY-OTf intermediate is not stable under temperatures above 0 °C, the TMSOTf was not used in these reactions.

First, difluoro-BODIPY was dissolved in toluene followed by addition of SnCl₄ and benzyl alcohol. The reaction was heated to 60 °C, and stirred for 30 min. The starting material decomposed and the desired product was not formed (Entry 1). Next, the reaction was set up without the Lewis acid catalyst and heated to reflux for 3 h (Entry 2), resulting in formation of desired product as well as decomposition products. Additionally, three other catalysts with a wide array of characteristics were tested, including camphorsulfonic acid, which is a relatively strong acid (Entry 3), DIPEA, which is a mild base (Entry 4) and 5Å molecular sieves, which is a porous material able to trap smaller molecules (Entry 5). Furthermore, the 5Å molecular sieves are an aluminum silicate, which will scavenge the displaced group. The presence of the first two catalysts resulted in a mixture of desired and degradation products, while the last catalyst yielded a clean conversion to a mix of the mono- and dialkoxy BODIPY. Next, using the 5Å molecular sieves, the amount of benzyl alcohol used was decreased by 10 fold, also resulting in a mix of the mono- and dialkoxy BODIPY products (Entry 6).

Table 4.3 – Optimization of benzyl-alkoxy BODIPY synthesis. Compound structure for **4.25** and **4.30** in scheme 4.3.

Entry	ROH		Catalyst (Equiv.)	Solvent	Time (min.)	Temp. (°C)	Degradation Products	Product
	R	Equiv.						
1	Bn	10	SnCl ₄ (30)	Toluene	30	60	–	–
2	Bn	10	-	Toluene	180	reflux	25%	4.25 (25%)
3	Bn	10	CSA (30)	Toluene	30	60	35%	4.25 (20%)
4	Bn	10	DIPEA (30)	Toluene	30	60	35%	4.25 (15%)
5	Bn	10	5Å molecular sieves	Toluene	30	60	–	4.25/4.30 (2:1.5)
6	Bn	1	5Å molecular sieves	Toluene	30	60	–	4.25/4.30 (2:1)
7	Bn	1	5Å molecular sieves	Toluene	180	r.t.	–	4.25/4.30 (2:2)
8	Bn	1	4Å molecular sieves	Toluene	30	60	–	4.25/4.30 (2:1)
9	Bn	1	Silica	Toluene	30	60	–	–
10	Bn	1	Basic Alumina Oxide	Toluene	30	60	–	–
11	Bn	1	Neutral Alumina Oxide	Toluene	30	60	–	–

Furthermore, in an attempt to slow down the kinetics of the reaction, thus increasing the proportion of mono- to dialkoxy BODIPY products, the temperature was decreased, with no success (Entry 7). Moreover, a different size of molecular sieves, as well as other catalyst supports, such as silica, basic alumina oxide and neutral alumina oxide were tested to evaluate the potential to singly form the monoalkoxy product (Entries 8-11). Despite not establishing

conditions, which would only yield the monoalkoxy BODIPY product, we identified a catalyst that allows the synthesis of both species in a step-wise manner.

Once we identified the 5Å molecular sieves as the best catalyst support for this new methodology, we turned our focus to studying the kinetics of the conversion, as well as determining the ideal amount of the catalyst necessary (Table 4.4).

Table 4.4 – Optimization of catalyst amount for new methodology. Reaction conditions: toluene, 60 °C.

Entry	Catalyst (ms/mg fluorophore)	ROH (2.5 Equiv.)	Product (Ratio)			
			0.1	1	2	24
1	1	Bn	4.13	4.13/4.25 (4:1)	4.13/4.25 (3:1)	4.13/4.25/4.30 (1:2:1)
2	2	Bn	4.13	4.13/4.25 (3:1)	4.13/4.25 (2:1)	4.13/4.25/4.30 (1:2:2)
3	4	Bn	4.13	4.25/4.30 (2:1)	4.13/4.25/4.30 (1:2:1)	4.25/4.30 (1:4)
4	6	Bn	4.13/4.25 (2:1)	4.13/4.25/4.30 (2:2:1)	4.25/4.30 (1:1)	4.30

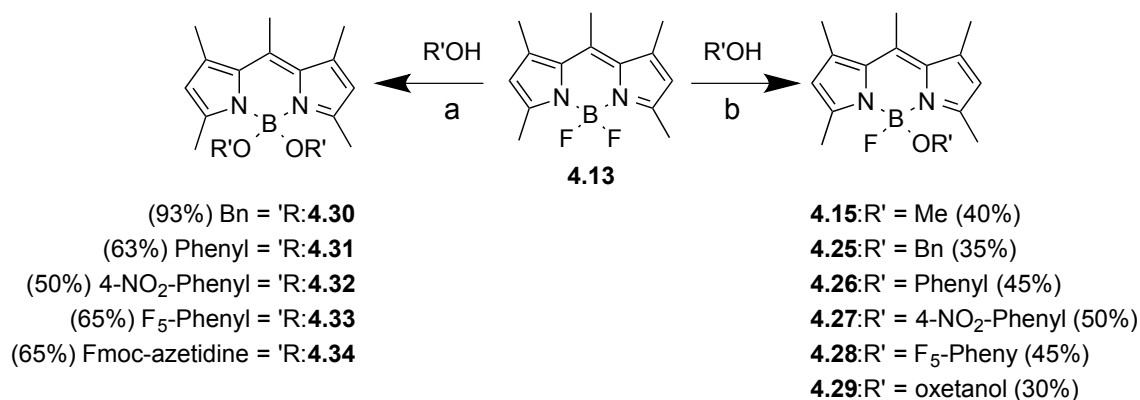
The difluoro-BODIPY starting material was dissolved in toluene followed by addition of 2.5 equiv. of benzyl alcohol. The reaction was heated to 60 °C and the 5Å molecular sieves were added. Four different amounts of catalyst were tested (1, 2, 4 and 6 molecular sieves (ms) per mg of difluoro-BODIPY) and LC/MS analysis of the crude reaction was done at four time points to assess the amount of starting material, mono- and dialkoxy BODIPY. The kinetics of the reaction becomes faster with the increase of molecular sieves used. At 6 ms/mg (50 mg of molecular sieves/ mg of fluorophore), we achieve ideal proportion of monoalkoxy to dialkoxy BODIPY at 2 h and after 24 h we observed a clean conversion to the dialkoxy BODIPY (Entry 4). To further evaluate the potential of the new synthetic method we used the optimized conditions with four different hydroxyl-reagents and tested eight additional solvents, which included pyridine, DMSO, DMF, NMP, THF, 2-Methyl THF, lutidine and 1,4-dioxane, of these only three were compatible with the new methodology. Each of the four alcohols was tested in all nine solvents

following the procedure described above and LC/MS analysis of the crude reaction was done at three time points to assess the amount of starting material, mono- and dialkoxy BODIPY products (Table 4.5). The results show that all four alcohols tested display a stepwise reaction with similar kinetics (Table 4.5). Furthermore, from the nine solvents tested only three (Toluene, THF and 1,4-dioxane) were compatible with our synthetic method, resulting initially in the formation of mono- and dialkoxy BODIPYs followed by full conversion to the dialkoxy product after 24 h (Table 4.5). The fact that this synthesis works with more than one solvent expands the solubility compatibility of this approach, when compared to the initial method, which required chloroform under acidic conditions.

Table 4.5 – Optimized solvents for the new methodology. Reaction conditions: 50 mg of molecular sieves/ mg of fluorophore (catalyst), 60 °C.

Solvent	ROH (2.5 Equiv.)	Product (Ratio)		
		Time (h)		
		1	8	24
Toluene	Bn	4.13/4.25/4.30 (2:2:1)	4.25/4.30 (1:5)	4.30
	Phenyl	4.13/4.26/4.31 (1:1:1)	4.26/4.31 (1:5)	4.31
	4-NO ₂ - Phenyl	4.13/4.27/4.32 (1:1:1)	4.27/4.32 (1:5)	4.32
	F ₅ -Phenyl	4.13/4.28/4.33 (1:1:1)	4.28/4.33 (1:2)	4.33
THF	Bn	4.13/4.25 (10:1)	4.13/4.25/4.30 (4:1:1)	4.13/4.25/4.30 (2:3:2)
	Phenyl	4.13/4.26 (10:1)	4.13/4.26 (5:1)	4.13/4.26 (5:1)
	4-NO ₂ - Phenyl	4.13/4.27 (10:1)	4.13/4.27 (5:1)	4.13/4.27 (5:1)
	F ₅ -Phenyl	4.13/4.28/4.33 (10:1)	4.28/4.33 (5:1)	4.33 (5:1)
1,4-dioxane	Bn	4.13/4.25 (10:1)	4.13/4.25/4.30 (4:1:1)	4.13/4.25/4.30 (1:2:1)
	Phenyl	4.13/4.26 (10:1)	4.13/4.26/4.31 (2:2:1)	4.13/4.26/4.31 (1:2:1)
	4-NO ₂ - Phenyl	4.13/4.27 (10:1)	4.13/4.27/4.32 (2:2:1)	4.13/4.27/4.32 (1:2:1)
	F ₅ -Phenyl	4.13/4.28 (10:1)	4.13/4.28 (3:2)	4.28

Once the new synthetic methodology had been established, a variety of mono- and dialkoxy BODIPY dyes was synthesized (Scheme 4.3).



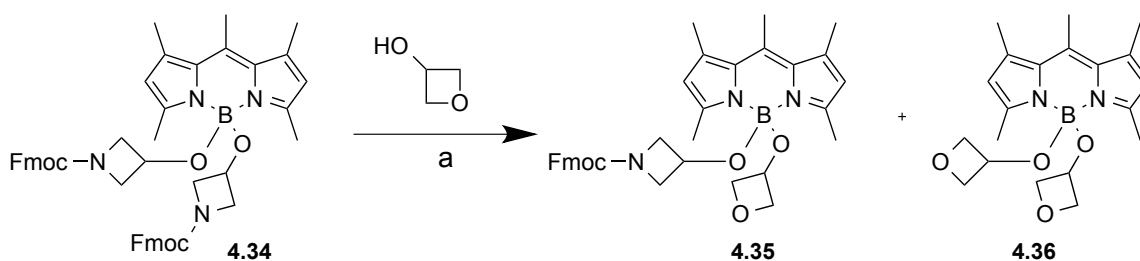
Scheme 4.3 – Synthesis of mono- and dialkoxy BODIPY analogs. Reagents and conditions: **a)** Molecular sieves, Toluene or THF, 60 °C, 24 h; **b)** Molecular sieves, Toluene, 60 °C, 3 h. Isolated yield after purification is given in parentheses.

We found that using this methodology the difluoro-BODIPY readily reacts with a slight excess (1.5 - 2.5 equiv.) of the suitable alcohols to yield the desired monoalkoxy-BODIPYs in moderate yields (**4.15**, **4.25-4.29**) and the dialkoxy BODIPYs in moderate to high yields (**4.30-4.34**), without any degradation products. Alcohols, such as 3-oxetanol and 1-Fmoc-3-hydroxyazetidide are of particular interest due to its particular properties, suitable for bioimaging. On the one hand, 3-oxetanol is an alcohol with increased solubility and has the smallest footprint⁴³⁹, on the other 1-Fmoc-3-hydroxyazetidide provides an additional site for further functionalization. Moreover, secondary alcohols display higher stability towards hydrolysis (data not published).

Specifically, monoalkoxy-BODIPYs were accessed by dissolving difluoro-BODIPY in toluene, followed by addition of a suitable alcohol (2.5 equiv.) and 5 Å molecular sieves (50 mg of molecular sieves/ mg of fluorophore), at 60 °C for 3 h to afford the desired monoalkoxy-BODIPY in moderate yields (**4.15**, **4.25-4.29**). The yields observed result from the balance between monoalkoxy and dialkoxy formation at the time the reaction is stopped. Furthermore, following the same procedure the reaction mixture is heated at 60 °C for 24 h to afford the desired dialkoxy-BODIPYs in moderate to high-yields (**4.30-4.34**). All three BODIPY species (difluoro-, mono- and dialkoxy BODIPYs) are stable for a prolonged time (96 h) under the reaction conditions and no degradation is observed by LC/MS analysis. We therefore predict this strategy will tolerate a wider number of functionalities and allow for easy access to an array of different alkoxy BODIPY derivatives, including BODIPY labeled hydroxyl functionalized small

molecules.

To further test the applicability of the newly developed method we attempted to displace the alkoxy group on the synthesized BODIPYs (**4.15**, **4.25-4.34**) with other alcohols, as well as with tetra-*n*-butylammonium fluoride (TBAF). Regarding the displacement of one alkoxy group by another, using our reaction conditions, we observed that the mono-methoxy BODIPY had a fast kinetic reaction when compared to the parent difluoro-BODIPY, which we could use to our advantage when applying this method to labeling small molecules. Moreover, most alkoxy BODIPYs were stable but unreacted. Furthermore, regarding the reactivity of the synthesized dialkoxy BODIPYs, only the Fmoc-azetidine BODIPY reacted under these conditions with other alcohols, namely with 3-oxetanol (Scheme 4.4).



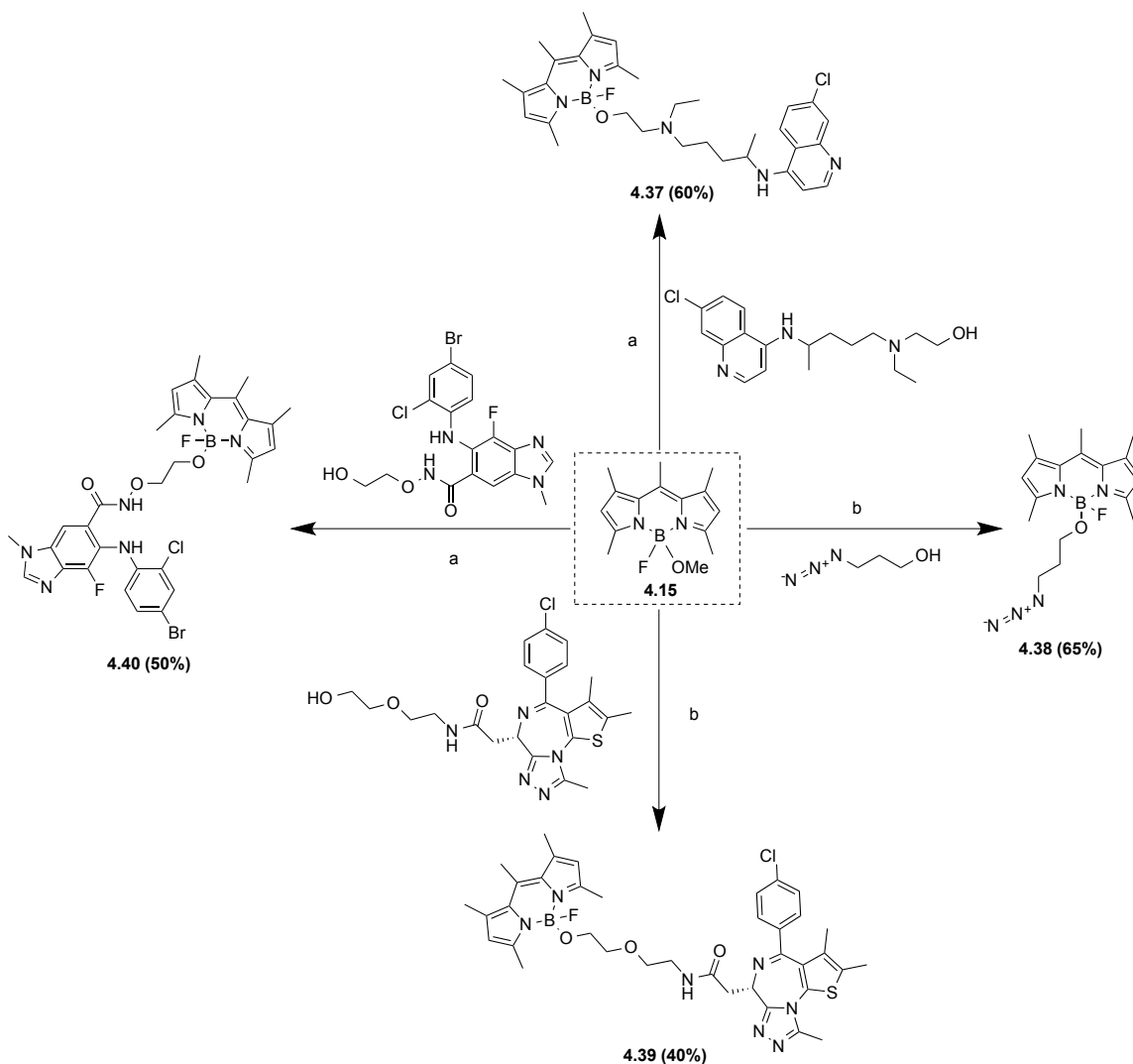
Scheme 4.4 – Synthesis of mono- and dioxetanol BODIPY analogs. Reagents and conditions: **a)** Molecular sieves, Toluene, 60 °C, 1 h (**4.35**: 8% yield) or 8 h (**4.36**: 55% yield).

When attempting to synthesize an asymmetrical dialkoxy BODIPY, starting with the bis-Fmoc-azetidine BODIPY, thus displacing one of the Fmoc-azetidine groups with a 3-oxetanol, we observed that the kinetics of this reaction was very fast and at any point in time the mixture of products favored the dialkoxy BODIPY product. The isolated yield of the monoalkoxy displacement (**4.35**) product after a 1 h reaction was low (8%) compared to the other monoalkoxy BODIPY dyes synthesized. When the reaction is heated at 60 °C for 8 h, a complete conversion to the bis-3-oxetanol BODIPY (**4.36**) is observed and the desired product is isolated in moderate yield (55%). The asymmetrical dialkoxy BODIPY derivatives would represent interesting materials, but with the low yield obtained for compound **4.35**, it requires further optimization to use these dyes for small molecule labeling. Nonetheless, it further demonstrates the potential of the new synthetic methodology to enable the synthesis of a new class of CMA-BODIPY dyes.

4.3.3 Synthesis of Small Molecule Probes

We first synthesized the monomethoxy BODIPY **4.15**, following a two-step one-pot strategy via the reactive BODIPY-OTf (**4.14**) intermediate, as shown in Scheme 4.1a.

Next, a series of BODIPY labeled small molecules was designed to explore small molecules of interest that feature an appropriate hydroxyl group, which may be directly functionalized by reaction with the monomethoxy BODIPY (Scheme 4.5).



Scheme 4.5 – Synthesis of CMA-BODIPY labeled small molecules. Reagents and conditions: **a)** molecular sieves, THF, 60 °C, 8 h; **b)** molecular sieves, Toluene, 60 °C, 8 h.

These compounds were obtained by displacement of the methoxy group, in the presence of 5Å molecular sieves at 60 °C, to give the title compounds **4.37-4.40** (Scheme 4.5), with yields ranging from 40%-65%.

Two of the derivatives from this series were obtained using commercially available hydroxyl functionalized small molecules (**4.37** and **4.40**). The 3-azidopropanol, used in the synthesis of compound **4.38**, was obtained from our collaborator Vamsi Mootha (at MGH) and used without further modification. Whereas, the alcohol used in the synthesis of compound **4.39**, was previously obtained by HCTU coupling of 2-(2-aminoethoxy)ethanol with (+) JQ1 carboxylic acid, which was a gift from our collaborator James Bradner at Dana–Farber Cancer Institute.

This new methodology allowed us to synthesize three BODIPY labeled small molecules and an azide alkoxy BODIPY, which may be further used in click chemistry reactions suitable for the chemical labeling of biomolecules for live fluorescence imaging.⁴⁴⁰

4.3.4 Synthesis of Indolo[3,2-*b*]quinoline Probe

Our group has previously reported that bis-alkylamine indolo[3,2-*b*]quinoline derivatives target hemozoin crystals. The results suggest inhibition of Hz growth as one possible mechanism of action for these antimalarials.^{5, 422} To further elucidate the mechanism of action of these derivatives we aim to develop a fluorescent probe that will allow subcellular fluorescence co-localization of the compound in *Plasmodium falciparum*. We sought to develop an imaging agent for 3,7-dichloro-*N*10-ethylpyrrolidine inhibitors by making minor modifications to the parent inhibitor scaffold (Figure 4.8).

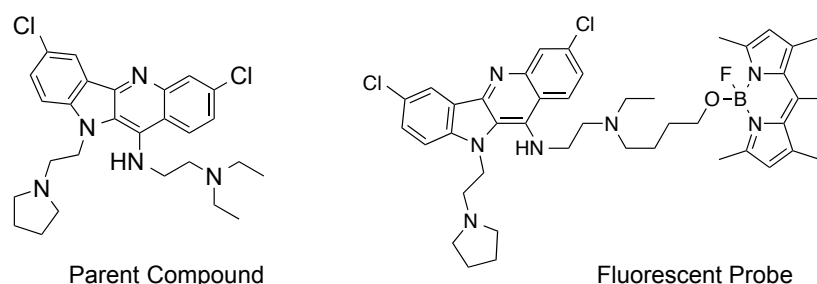
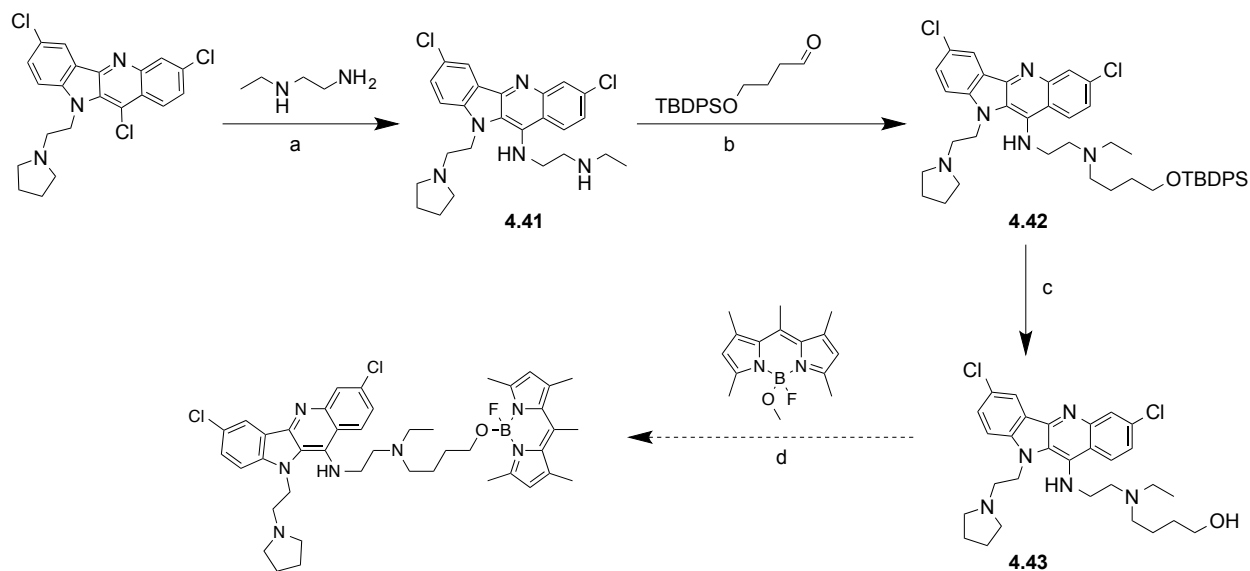


Figure 4.8 – Structure of 3,7-dichloro-*N*10-ethylpyrrolidine parent compound and designed fluorescent probe.

A CMA-BODIPY modified 3,7-dichloro-*N*10-ethylpyrrolidine was designed to be access in four steps, starting with synthesis of the hydroxyl functionalized di-alkylamine indolo[3,2-*b*]quinoline (Scheme 4.6).



Scheme 4.6 – Synthesis of CMA-BODIPY labeled indolo[3,2-*b*]quinoline. Reagents and conditions: **a**) 130 °C, 16 h, 62%; **b**) NaBH(OAc)₃, DCE, r.t., 4 h, 51%; **c**) HF/Pyridine/THF (1/2/7), r.t., 16 h, 58%; **d**) molecular sieves, 60 °C, 8 h.

Briefly, nucleophilic substitution of 3,7,11-trichloro-10-[2-(pyrrolidin-1-yl)ethyl]-10*H*-indolo[3,2-*b*]quinoline by ethylethane-1,2-diamine, followed by reductive amination²³⁹ of the amine intermediate **4.41** with the TBDPS protected hydroxyl-butanal yielded compound **4.42**. Next, deprotection using HF/pyridine afforded the desired hydroxyl functionalized di-alkylamine indolo[3,2-*b*]quinoline in 18% overall yield. Thereafter, we attempted to displace the methoxy group of the monoalkoxy BODIPY dye, in the presence of 5 Å molecular sieves, unfortunately compound **4.43** was not soluble in any of the three solvents compatible with our newly developed methodology, thus preventing the coupling. The novel di-alkylamine indolo[3,2-*b*]quinolines obtained in this synthetic scheme were tested against CQ-resistant Dd2 strain for their antimalarial activity. EC₅₀ of compounds **4.41**, **4.42**, and **4.43**, was 0.47 μM, 2.6 μM and 0.23 μM, respectively. The hydroxyl functionalized di-alkylamine indolo[3,2-*b*]quinoline shows

comparable activity to the parent compound (EC_{50} of $0.22 \mu\text{M}$)⁵, which validates the chemical modification proposed. An alternative synthetic approach to overcome the solubility problem observed in the latter coupling, which involved synthesis of the of mono-butanoxy BODIPY prior to reaction with the di-alkylamine indolo[3,2-*b*]quinoline **4.41**, was tested with little to no success.

Despite the solubility problem observed with the synthesis of di-alkylamine indolo[3,2-*b*]quinoline probe, we are confident on the broad applicability of the methodology developed.

4.4 In vitro Profiling of Labeled Small Molecules

To evaluate the applicability of this unique attachment site for CMA-BODIPY labeling of small molecules for live cell imaging, we interrogated representative derivatives for their ability to penetrate mammalian cell membranes and their propensity for non-specific background staining. Furthermore, the hydroxychloroquine probe was also profiled for its ability to penetrate *Plasmodium falciparum* and determine its subcellular localization.

4.4.1 In Mammalian Cell Cultures

MCF-7 cells were incubated with $10 \mu\text{M}$ of **4.39** and **4.37**. Following a 30 minutes incubation at $37 \text{ }^\circ\text{C}$, the culture medium was replaced twice over 10 minutes to remove excess dye. Live cells were imaged by multi-channel fluorescence microscopy to assess penetration efficiency and subcellular staining patterns. Both of the tested compounds exhibited efficient cell uptake (Figure 4.9).

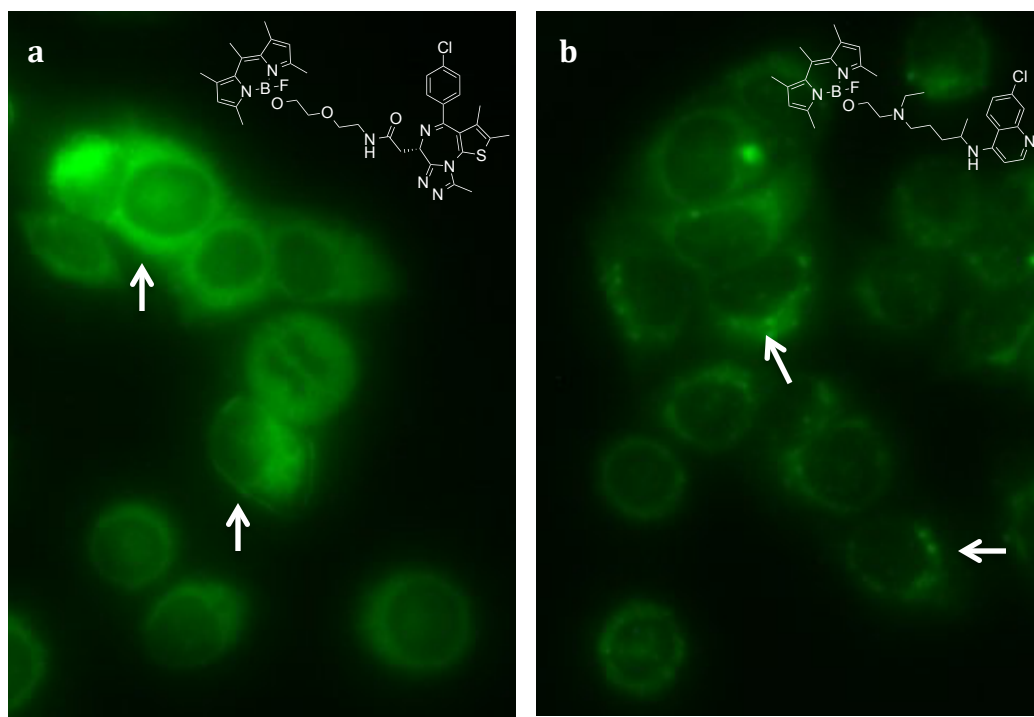


Figure 4.9 – Cellular uptake and intracellular distribution of compound **4.39** (a) and compound **4.37** (b) in MCF-7 cells. Accumulation is indicated by white arrows.

Importantly, (+) JQ1 labeled compound (**4.39**, Figure 4.9a) showed a relatively homogenous intracellular distribution, while probe **4.37** displayed a subcellular staining pattern that is consistent with accumulation in acidic vesicles in the cytoplasm (Figure 4.9b). Since hydroxychloroquine, like chloroquine, is a known lysosomotropic agent⁴⁴¹, the latter was expected.

To confirm the effect of CMA-BODIPY modification on the inhibition efficacy of the drug, half-maximal inhibitory concentration (EC_{50}) of (+) JQ1 and (+) JQ1-CMA-BODIPY were determined against purified BRD4 protein. The labeled compound had an EC_{50} of 26 nM, which is comparable to the parent compound (EC_{50} of 17 nM) (Data obtained with my colleague Dr. Yelena Wainman).

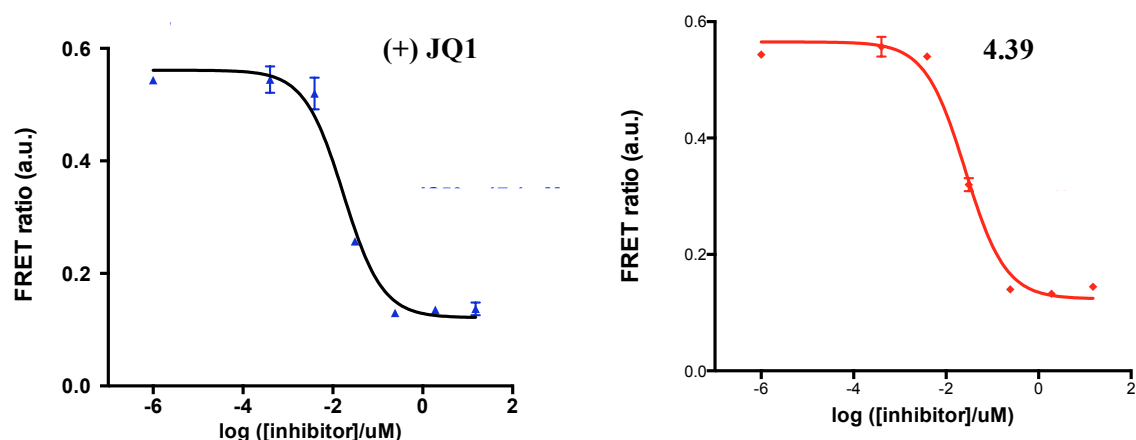


Figure 4.10 – Half-maximal inhibitory concentration (EC_{50}) of (+) JQ1 and (+) JQ1-CMA-BODIPY **4.39** determined against purified BRD4 protein.

Furthermore, JQ1 is a cell-permeable small molecule that binds competitively as a potent inhibitor of the BET family of bromodomain proteins, thus acting on the nucleus of the cell. Nonetheless, bromodomain proteins may also be present in the cytoplasm. Moreover, BRD4 exists in tight complexes that may not tolerate binding of labeled drugs.⁴⁴² In spite of exhibiting cellular uptake, compound **4.39** does not seem to preferably accumulate in the nucleus as expected.

We found favorable membrane permeability in both examples shown above, despite the low specificity of the (+) JQ1 probe towards the nucleus as it was expected due to its known target. Nonetheless, the latter compound had comparable activity to the parent compound in an *in vitro* assay with BRD4 protein, thus demonstrating that our synthetic approach does not affect the compound's activity. Moreover, the hydroxychloroquine probe was distributed throughout the cytoplasm with increased accumulation in acidic vesicles, consistent with what would be expected due to its chemical structure.

4.4.2 In *Plasmodium falciparum* Intraerythrocytic Cultures

Plasmodium falciparum chloroquine resistant and sensitive strains, Dd2 and 3D7, respectively, were incubated with 10 μ M, 1 μ M, 100 nM, 10 nM or 1 nM of the hydroxychloroquine CMA-BODIPY labeled compound (**4.37**). Following a 30 minute incubation at 37 $^{\circ}$ C, the culture medium was replaced twice to remove excess dye. Live parasites

Chapter 4 – Fluorescent Probes for Target Discovery

were imaged by multi-channel fluorescence microscopy to assess penetration efficiency and subcellular staining patterns. Images were comparable amongst both strains. At the two lowest concentrations no signal was observed. Furthermore, at 10 μM and 1 μM concentration there was only faint staining of the membrane but the majority of the probe is in the parasites as expected, while at a 100 nM there is only staining in the parasites.

The probe exhibited efficient parasite uptake at a 100 nM, with subcellular staining pattern that is consistent with accumulation in the food vacuole (Figure 4.11).

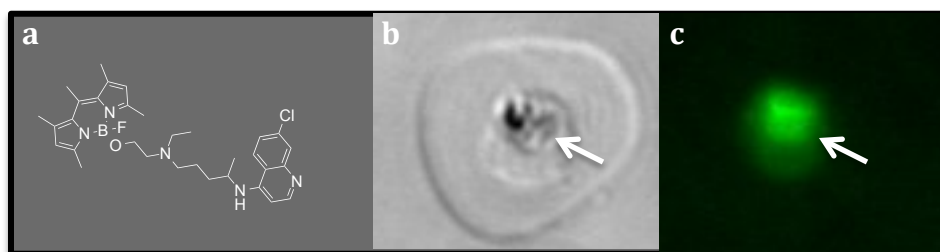


Figure 4.11 – Cellular uptake and intracellular distribution of compound **4.37** in *Plasmodium falciparum* Dd2 strain. **a)** Structure of the hydroxychloroquine CMA-BODIPY labeled compound; Brightfield (**b**) and Fluorescent (**c**) images of an infected erythrocyte with ring stage parasite using 100X immersion oil objective. Accumulation is indicated by white arrows.

Hydroxychloroquine, like chloroquine, is a 4-aminoquinoline antimalarial drug that acts, at least in part, by inhibition of hemozoin formation. Thus, as expected the free base of our probe can diffuse freely and rapidly across the membranes of cells and organelles, but once inside the acidic food vacuole, it protonates and becomes trapped. Microscopy experiments revealed that the hydroxychloroquine CMA-BODIPY labeled probe accumulated in the food vacuole at a higher concentration, compared to the rest of the parasite, as reported in the literature.²³¹

Next, to confirm the effect of CMA-BODIPY modification on the inhibition efficacy of the drug, half-maximal inhibitory concentration (EC_{50}) of chloroquine, hydroxychloroquine and hydroxychloroquine-CMA-BODIPY, were determined against CQ-resistant Dd2 and CQ-sensitive 3D7 strains. The labeled compound had an EC_{50} of 25 nM against the sensitive strain, which is comparable to both the parent compound (EC_{50} of 19 nM) and CQ (EC_{50} of 14 nM), thus the modification does not affect the compound's activity (Data obtained by my colleague Lola Fagbami).

These results thus validate the unique attachment site on the BODIPY dye, which is

accessed by our new synthetic methodology.

4.5 Conclusion

The challenges of discovering a compound's MoA and subsequent validation of the macromolecular target have driven innovative approaches, such as the use of a non-perturbing chemical handles within the small molecule, which allows for selective attachment of a tag. Thus, target identification and validation approaches have included the use of chemical probes, such as fluorescently tagged inhibitors, which allows co-localization within cells or cell extracts and further elucidate on drug target.

The BODIPY dyes are an exciting fluorophore class for diverse imaging applications. They are particularly promising for tagging bioactive compounds for intracellular live cell imaging. However, poor aqueous solubility and high lipophilicity significantly limit the scope of BODIPYs for bioimaging. Although extensive efforts have focused on developing derivatives that have improved water solubility by either installing charged substituents or large PEG chains, these modifications also severely impair or inhibit cell permeability.

In an effort to develop broadly applicable dyes that are suitable for tagging bioactive compounds for intracellular live cell imaging, we developed a new class of BODIPY dyes based on an alkoxy-fluoro-boron-dipyrrromethene core. These novel fluorescent dyes, which we term MayaFluors, are characterized by good aqueous solubility and favorable *in vitro* pharmacological properties.

MayaFluors are readily accessible in good to excellent yields in a one-pot, two-step approach starting from well-established BODIPY dyes and allow facile modification with a broad array of functional groups commonly used in bioconjugate chemistry and bioorthogonal labeling.⁴ This new class of BODIPY fluorophores has significantly improved physicochemical properties that are ideally suited for biological applications. MayaFluors retain the optical attributes of the parent BODIPY dye class while enjoying significant improvements in their lipophilicity. We have validated the applicability of these dyes as fluorescent reporters for live cell imaging and demonstrated that MayaFluors have excellent membrane permeability and show little to no nonspecific staining.⁴ We hypothesize that the low propensity of MayaFluors to insert into biological membranes is the result of aqueous solubility imparted by the increased out of plane dipole moment these analogs experience as opposed to difluoro BODIPYs. Furthermore,

addition of the alkoxy substituent disrupts the planarity of the BODIPY core, which is expected to reduce their ability to self-aggregate and insert into lipid leaflets via the formation of π - π stacks.⁴⁴³

In this work we report the development of a new methodology, which originated from our efforts to synthesize MayaFluors in a one-pot, two-step approach via BODIPY-OTf intermediate. The latter method presented one main drawback with regards to the amount of hydroxyl-reagent (100 equiv.) required when synthesizing the CMA-BODIPYs. Therefore we successfully developed a new synthetic methodology, which overcomes aforementioned problem. Thus, allowing substitution of either one or both of the canonical fluorides on the BODIPY dye with alkoxy ligands. Moreover, we show that the alkoxy substituent provides an additional, unique attachment site, which can be readily exchanged by either an alkoxy-drug or another alkoxy-ligand, using the new synthetic conditions.

We synthesized a small library of novel mono- and dialkoxy BODIPY dyes in moderate to high yields, as well as a series of three BODIPY labeled small molecules and an azide alkoxy BODIPY, which may be further used in click chemistry reactions. Thus, our synthetic method allows for direct modification of the well-established BODIPY dyes and provides easy access to diversely functionalized small molecule probes.

Importantly, (+) JQ1 labeled compound showed a relatively homogenous intracellular distribution in MCF-7 cells, while BODIPY labeled hydroxychloroquine displayed a subcellular staining pattern that is consistent with accumulation in acidic vesicles in the cytoplasm. Furthermore, the latter probe was also tested in *Plasmodium falciparum* cultures, where results show a subcellular staining pattern that seems consistent with accumulation in the food vacuole. The half-maximal inhibitory concentration (EC_{50}) of both probes was determined to confirm the effect of CMA-BODIPY modification on the inhibition efficacy of the drug.

In the first example, (+) JQ1-CMA-BODIPY had an EC_{50} of 26 nM against purified BRD4 protein, which is comparable to the parent compound (EC_{50} of 17 nM), demonstrating that the structural modification does not affect the activity of the probe but other factors, such as for example, size of the molecule, may lead to low accumulation in the nucleus.

In the second example, EC_{50} of chloroquine, hydroxychloroquine and hydroxychloroquine-CMA-BODIPY, were determined against CQ-sensitive 3D7 strain. The

labeled compound had an EC₅₀ of 26 nM, which is comparable to the parent compound (EC₅₀ of 19 nM) and CQ (EC₅₀ of 14 nM), thus the modification does not affect the compound's activity.

The results obtained with both of these probes thus validate the unique attachment site on the BODIPY dye, which is accessed by our new synthetic methodology. Nonetheless, our method has a limitation regarding its solvent compatibility that in some cases prevents the reaction from occurring.

We aimed to further elucidate the mechanism of action of the di-alkylamine indolo[3,2-*b*]quinoline derivatives previously developed by our group, thus designing a fluorescent probe that would allow subcellular fluorescence co-localization of the compound in *Plasmodium falciparum* cultures. A CMA-BODIPY modified 3,7-dichloro-N10-ethylpyrrolidine was designed to be accessed in four steps, starting with synthesis of the hydroxyl functionalized di-alkylamine indolo[3,2-*b*]quinoline. We successfully synthesized the hydroxyl intermediate and attempted the labeling with the dye, using our newly developed synthesis. However, the intermediate was not soluble in Toluene, THF or 1,4-dioxane, the three solvents compatible with the synthesis, thus preventing access to the desired probe. Nevertheless, the hydroxyl intermediate retained antimalarial activity comparable to the parent compound, which underscores the potential of the new methodology.

To conclude, here we have developed a promising novel synthetic methodology utilizing molecular sieves as a catalyst, which, for the first time, allows direct labeling of small molecules through a unique attachment site on the BODIPY dye. Despite the identified limitation, this method allows direct labeling of hydroxyl-functionalized drugs, which we believe may have broad applications for rapid and specific imaging of elusive biological targets in living cells.

Chapter Five

5. *General Conclusions and Future Perspectives*

Malaria is one of the most life-threatening diseases. With almost one-third of the world's population at risk it represents a major public health problem due to its morbidity and mortality.¹
⁹ An estimated 198 million cases led to nearly 584,000 deaths in 2013, 90% of which were reported in sub-Saharan Africa.¹ Malaria has a broad impact throughout tropical and subtropical areas of the globe, affecting indigenous populations as well as an increasing number of travelers.¹⁰⁻¹²

According to the 2014 World Health Organization (WHO) Malaria Report, about 78% of deaths attributed to malaria occur in African children under age of 5.¹ In addition to the human cost of malaria, the economic burden of the disease is significant, with a huge impact upon individual households due to lost wages and healthcare costs as well as detrimental effects on the national scale with about 40% of African health budgets spent on malaria every year.¹³

The emergence of drug resistance has already rendered once-effective malaria treatments such as, chloroquine and sulfadoxine-pyrimethamine, less reliable. Today, ACTs are the weapon of choice against malaria, and the possibility of losing them with the first signs of resistance, rendered the urgent need for novel antimalarial chemotypes.^{76, 87} Furthermore, new technologies and high throughput approaches are being applied to identify a burgeoning number of lead drug candidates and novel drug classes with antimalarial activity.²⁻³ Although efforts have been made to improve existing molecules, most new classes of potential antimalarials have come from high-throughput screens. Thus, drug discovery strategies include extensive compound screening, of which, natural sources, chemical libraries and virtual screening stand out.^{21, 122-123}

In this thesis we have explored three different medicinal chemistry approaches to address the unmet needs in malaria drug discovery.

Here we have employed two different drug discovery strategies to develop novel antimalarials, as well as, a novel target identification and validation tool:

- I. Hit to lead optimization
- II. aaRS as a new class of antimalarial drug target
- III. Fluorescent labeling of drugs for bioimaging

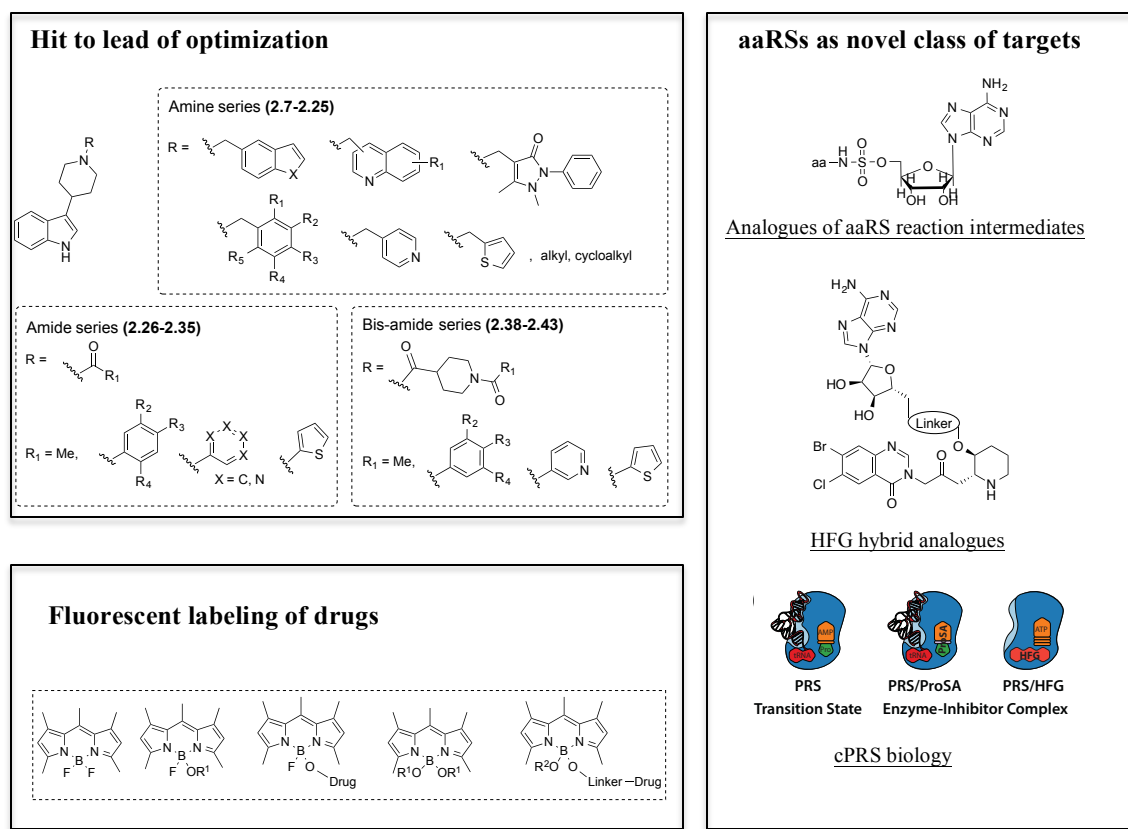


Figure 5.1 – Outline of the diverse medicinal chemistry approaches used in this work.

The first approach focused on a hit to lead optimization strategy designed to explore the antimalarial potential of the 3-piperidin-4-yl-1*H*-indole scaffold.

A library of 2 million compounds from GlaxoSmithKline's chemical library was screened against *P. falciparum* cultures, from which 13,500 inhibited parasite growth and more than 8,000 also showed potent activity against a multidrug resistant strain.⁶ The public availability of these results provides reasonable starting points for further drug development. Furthermore, we were intrigued by TCMDC-134281 (**2.1**, Figure 2.1), which emerged as a very potent antimalarial compound, with a reported EC₅₀ of 34 nM against the chloroquine-sensitive *P. falciparum* 3D7 strain. Moreover, indoles are an emerging antimalarial fragment present in several lead drug candidates with new mechanisms of action, such as the spiroindolone^{170, 234-237} and aminoindoles classes.^{236, 238}

Three series of derivatives were synthesized following a reagent-based diversity

approach, in a total of 38 compounds, and profiled for their antimalarial activity. SAR analysis suggests that the 3-piperidin-4-yl-1*H*-indole scaffold is very sensitive to most *N*-piperidinyl modifications. Furthermore, the (4-(1*H*-indol-3-yl)piperidin-1-yl)(pyridin-3-yl)methanone (**2.29**) showed *in vitro* antimalarial activity (EC_{50} values $\sim 3 \mu\text{M}$), no cross-resistance with chloroquine, selectivity for the parasite, and lead-like properties ($c\text{LogP} < 3$; $\text{MW} \sim 300$), which represents a promising new antimalarial chemotype with a potential novel mechanism of action. Further medicinal chemistry efforts are needed to improve the potency of compound **2.29** and disclose its antimalarial mechanism of action

Although high-throughput screens are powerful tools for identifying novel antimalarial scaffolds, the inverse approach in drug discovery, starting from the target, is still extremely useful. Thus, in a second approach we explored the aaRSs as a potential new class of antimalarial drug target.

Aminoacyl-tRNA synthetases are already the target of commercialized drugs (Bactroban, GlaxoSmithKline), and have been used as drug targets in the search of novel antibacterials. However, until recently, they have remained unexplored as potential antimalarial drug targets.²⁴⁶ Our group has established in *Plasmodium* that inhibition of tRNA synthetases by a small molecule and simultaneous activation of the integrated stress response is both feasible and attractive, and provides a rational mechanistic basis for future drug discovery and development focused on this novel target and pathway.⁷ Furthermore, we aimed to build on these important findings and in the one hand identify and biologically characterize selective small molecule inhibitors for the cPRS, and on the other identify novel targets within the aaRS class. This part of the project was organized into three different, but complementary, objectives.

First, to explore tRNA synthetases as novel targets in *P. falciparum* we designed and synthesized a library of 21 reaction intermediate analogs, which allowed us to profile 19 of the *Pf*aaRSs as drug targets. Analogues were profiled for their antimalarial activity, against blood and liver stage *in vitro* *P. falciparum* strains, cytotoxicity and eIF2 α phosphorylation induction. Among the derivatives tested, L-PheSA, L-HisSA, L-AlaSA and L-ProSA were the analogs that exhibited higher antimalarial activity, (EC_{50} against the Dd2 strain $< 120 \text{ nM}$) and lower cytotoxicity ($\text{SI} > 20$). Most of the aaSA analogs were active against liver stage *in vitro* *P. berghei*, with $>99\%$ parasite growth inhibition at the higher concentration of $10 \mu\text{M}$, and increased eIF2 α phosphorylation at 100X concentration. Taken together, the results allow the

prioritization of the ARS, HRS, FRS and PRS as the top four enzymes for further exploration as drug targets in blood stage malaria. Furthermore, the HRS, FRS and PRS are identified as the top three enzymes for further exploration as potential dual-stage drug targets.

Second, to further explore *Pfc*PRS, which our group has identified as the target of antimalarial halofuginone, we designed hybrid-halofuginone derivatives based on the complex formed by HFG and ATP in the active site of cPRS. We followed a general synthetic approach developed by Lin and coworkers,³⁷⁰ with optimization of certain steps. Despite being a concise asymmetric synthetic strategy, there were some challenges that had to be overcome. Nonetheless, further optimization efforts regarding the last two steps in the synthesis are necessary to obtain the desired hybrid compounds.

Third, we aimed to characterize the biology of cPRS inhibition and resulting amino acid starvation response. Understanding the enzyme-inhibitor complex formed by the different types of inhibitors (HFG and ProSA) would further elucidate on the differential effect observed on the amino acid starvation response observed in mammalian cells, despite targeting the same enzyme. Moreover, the induction of eIF2 α phosphorylation differs when comparing MCF-7 cell culture to *P. falciparum*, which may be potentially explained by differences in the amounts of tRNA available in each organism. We applied a two-step proteomic approach to isolate the protein complex using immunoprecipitation followed by identification of its components using mass spectrometry. Despite not being able to completely establish the protocol, the results in MCF-7 cells are consistent with the model proposed, thus further work needs to be done towards increasing the amount of the enzyme-inhibitor complex isolated to meet the detection requirements of the techniques used. In conclusion, in the second part of this thesis we aimed to characterize the set of aaRS in *P. falciparum*, then select the best potential drug targets amongst the set of plasmodial aaRS, and finally design hybrid-HFG analogs, which would selectively inhibit plasmodial aaRS. From this work we find that plasmodial aminoacyl-tRNA synthetases are indeed druggable enzymes that can be used as antimalarial drug targets.

The third approach used in this project focused on developing a method to fluorescently label drugs, towards a target identification/validation approach. The challenges of discovering a compound's MoA and subsequent validation of the macromolecular target have driven innovative approaches, such as the use of a non-perturbing chemical handles within the small

molecule, which allows for selective attachment of a tag. Thus, target identification and validation approaches have included the use of chemical probes, such as fluorescently tagged inhibitors, which allows co-localization within cells or cell extracts and further elucidate on drug target. First, we developed a new class of BODIPY fluorophores with significantly improved physicochemical properties that are ideally suited for biological applications, which were termed MayaFluors.⁴ We successfully developed a new synthetic methodology, which uses molecular sieves as a catalyst under mild conditions. The latter originated from our efforts to synthesize MayaFluors in a one-pot, two-step approach via BODIPY-OTf intermediate. We synthesized a small library of novel mono- and dialkoxy BODIPY dyes in moderate to high yields, as well as a series of three BODIPY labeled small molecules and an azide alkoxy BODIPY, which may be further used in click chemistry reactions. Thus, our synthetic method allows for direct modification of the well-established BODIPY dyes and provides easy access to diversely functionalized small molecule probes. Of these, two known drugs ((+) JQ1 and hydroxychloroquine) were evaluated for their activity and cellular localization. In both cases the labeled drug presented comparable activity to the parent drug and were cell permeable. Furthermore, the fluorescently labeled antimalarial displayed a subcellular staining pattern in mammalian cells that is consistent with accumulation in acidic vesicles in the cytoplasm. Moreover, the probe was also tested in *Plasmodium falciparum* cultures, where results show subcellular staining pattern that seems consistent with accumulation in the food vacuole. Despite the identified limitation concerning the solvent compatibility of the method, this approach allows for direct labeling of hydroxyl-functionalized drugs, which we believe may have broad applications for rapid and specific imaging of elusive biological targets in living cells.

In conclusion, the work developed during this project demonstrated how different medicinal chemistry approaches might contribute to the malaria drug discovery global efforts. The results obtained are of the utmost importance towards the malaria agenda and will certainly contribute to its further scientific development, since we have: *i*) identified a promising new antimalarial chemotype with a potential novel mechanism of action, *ii*) we have profiled the set of aaRS in *P. falciparum* as a novel class of antimalarial targets, selecting the most promising drug targets amongst the set of plasmodial aaRS, as well as further explored the inhibition of PfcPRS, and *iii*) developed a new synthetic methodology which enables cellular localization of fluorescently labeled drugs for target identification and validation.

Chapter 5 – General Conclusions and Future Perspectives

Finally, in this work we present a wide range of promising results for future development. The results obtained when profiling the aaRS class as novel targets for malaria drug discovery provides a rationale to prioritize the enzymes for further development. Although our studies identify the most promising targets, the tool aaSA compounds synthesized also constitute an attractive starting point for rational development of aaRS inhibitors as next-generation antimalarials. Future efforts to further explore cPRS as an antimalarial target, include the synthesis of the designed hybrid derivatives, which we expect will yield lead candidate compounds with increased parasite selectivity, suitable for preclinical development. Moreover, novel small molecule inhibitors of *PfcPRS* will be developed through a rational structural design approach that follows a traditional aaRS targeting strategy based on the aminoacyl-AMP analogs and will allow us to exploit distinct structural features that will enable higher selectivity.

Chapter Six

6. Materials and Methods

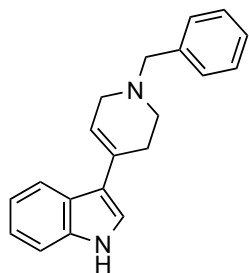
6.1 Chemistry

6.1.1 General

All chemicals were purchased from Chem-Impex International, Fluka, and Sigma-Aldrich Co. and used without further purification unless otherwise noted. All solvents for syntheses were anhydrous. Thin layer chromatography was performed with precoated aluminum-backed TLC plates obtained from VWR: Aluminum Oxide 60, Neutral F254 & Silica Gel 60, Neutral F254. Visualization of TLC plates was performed with ninhydrin, iodine, or an UVGL-25 Compact UV Lamp 254/365 UV (UVP 115V~60Hz/0.16 Amps). Purifications were performed on a Biotage Isolera 4 Purification System equipped with a 200-400 nm diode array detector. For flash purifications, Biotage SNAP Flash Chromatography Cartridges were used. Purity of compounds was determined by analytical LC-ELSD-MS performed on a Waters 2545 HPLC equipped with a 2998 diode array detector, a Waters 3100 ESI-MS module, using a XTerraMS C18 5 μm , 4.6 x 50 mm column at a flow rate of 5 mL/min with a linear gradient (95% A: 5% B to 100% B with 90 seconds and 30 seconds hold at 100% B, solvent A = water + 0.1% formic acid, solvent B = acetonitrile + 0.1% formic acid). Proton and carbon nuclear magnetic resonance (^1H and ^{13}C NMR spectra) were recorded on a Bruker AscendTM instrument at 400 and 101 MHz, respectively. Chemical shifts for protons are reported in parts per million (ppm) and are referenced to residual solvent peaks for DMSO (2.5 ppm), CHCl_3 (7.26 ppm), H_2O (4.79 ppm) and CH_3OH (3.31 ppm). Data is reported as follows: chemical shift, multiplicity (s = singlet, d = doublet, t = triplet, q = quadruplet, m = multiplet, br = broad), coupling constants (Hz) and integration. Instant JChem was used for structure database management, search and prediction, Instant JChem 5.9.3, 2012, ChemAxon (<http://www.chemaxon.com>).

6.1.2 Synthesis of 3-piperidin-4-yl-1H-indole Derivatives

3-(1-benzyl-1,2,3,6-tetrahydropyridin-4-yl)-1H-indole (2.2)

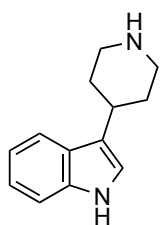


5 g (42.7 mmol) of indole were dissolved in isopropanol (50 mL). To this solution, potassium hydroxide (7.18 g, 128 mmol) in isopropanol (50 mL) was added, followed by the addition of 1-benzypiperidine-4-one (20 mL, 108 mmol) in isopropanol (50 mL). The reaction refluxed for 6 h, after which it was cooled to room temperature. The solvent was removed under reduced pressure. The crude product was purified by flash chromatography using a gradient elution of Hexane/Ethyl Acetate. The desired product was obtained as a yellow solid (12.0 g, 98%).

ESI-MS: $C_{20}H_{20}N_2$, m/z calculated for $[M+H]^+$: 289.2, Found: 289.2.

1H NMR δ (MeOD) 7.84 (d, $J = 8.1$ Hz, 1H), 7.47 – 7.31 (m, 6H), 7.28 (s, 1H), 7.14 (ddd, $J = 8.2, 7.0, 1.2$ Hz, 1H), 7.07 (ddd, $J = 8.1, 7.0, 1.2$ Hz, 1H), 6.20 (tt, $J = 3.5, 1.5$ Hz, 1H), 3.70 (s, 2H), 3.26 (m, 2H), 2.80 (t, $J = 5.8$ Hz, 2H), 2.67 (m, 2H); **^{13}C NMR** δ (MeOD) 138.8, 138.3, 131.7, 130.9, 129.4, 128.5, 126.4, 123.1, 122.5, 121.2, 120.4, 118.3, 117.7, 112.5, 63.8, 54.1, 51.1, 29.6.

3-(piperidin-4-yl)-1H-indole (2.3)



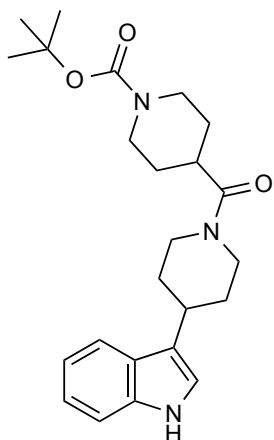
4 g (13.8 mmol) of compound **2.2** were dissolved in 10% acetic acid in ethyl acetate (160 mL). To this solution, 1.2 g of 10% Pd/C were added. The reaction was placed under 1 atm of H_2 (balloon) and stirred at r.t. for 50 h. The reaction mixture was filtered over Celite™ and washed with ethyl acetate followed by acetonitrile:water:methanol (1:1:1). The solvent was removed under reduced pressure and the crude product purified with flash chromatography using a gradient elution of ethyl acetate/acetonitrile:water:methanol (1:1:1) with 1% ammonium hydroxide to afford compound **2.3** as a yellow solid (2.66 g, 96%).

ESI-MS: $C_{13}H_{16}N_2$, m/z calculated for $[M+H]^+$: 201.1, Found: 201.4.

1H NMR δ (MeOD) 7.60 (d, $J = 8.0$ Hz, 1H), 7.34 (d, $J = 8.1$ Hz, 1H), 7.09 (ddd, $J = 8.1, 7.1, 1.2$ Hz, 1H), 7.06 (s, 1H), 7.01 (ddd, $J = 8.1, 7.1, 1.2$ Hz, 1H), 3.46 (dt, $J = 12.8, 3.1$ Hz, 2H),

3.22 – 3.06 (m, 3H), 2.23 (d, $J = 12.3$ Hz, 2H), 1.99 (m, 2H), 1.92 (s, NH); ^{13}C NMR δ (MeOD) 136.9, 126.0, 121.1, 119.9, 118.3, 118.0, 117.9, 111.1, 44.2, 31.5, 29.7.

tert-butyl 4-(4-(1H-indol-3-yl)piperidine-1-carbonyl)piperidine-1-carboxylate (2.4)

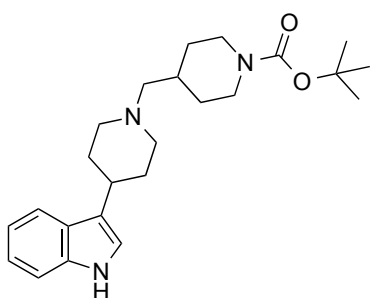


To 1-(*tert*-butoxycarbonyl)piperidine-4-carboxylic acid (1.00 g, 4.36 mmol) in acetonitrile (25 mL) was added compound **2.3** (873.2 mg, 4.36 mmol) in acetonitrile (25 mL), followed by *N,N*-dicyclohexylcarbodiimide (900 mg, 4.36 mmol) and 1-hydroxybenzotriazole (590 mg, 4.36 mmol). The reaction stirred at room temperature for 2 h. The suspension was filtered and the solvent removed under reduced pressure. The crude product was purified by reverse phase flash chromatography using a gradient elution of water/acetonitrile to afford compound **2.4** as a white solid (1.08 g, 60%).

ESI-MS: $\text{C}_{24}\text{H}_{33}\text{N}_3\text{O}_3$, m/z calculated for $[\text{M}^+ \text{H}]^+$: 412.3, Found: 412.4.

^1H NMR δ (MeOD) 7.61 (d, $J = 7.9$ Hz, 1H), 7.37 (d, $J = 8.1$ Hz, 1H), 7.12 (ddd, $J = 8.1, 7.9, 1.2$ Hz, 1H), 7.08 – 6.99 (m, 2H), 4.69 (d, $J = 13.2$ Hz, 1H), 4.21 (d, $J = 13.2$ Hz, 1H), 4.15 (d, $J = 13.4$ Hz, 2H), 3.32 (m, 1H), 3.21-3.13 (tt, $J = 12.8, 3.5$ Hz, 1H), 2.97 (m, 2H), 2.85 (m, 2H), 2.21 (d, $J = 12.9$ Hz, 1H), 2.12 (d, $J = 13.0$ Hz, 1H), 1.79 – 1.60 (m, 6H), 1.50 (s, 9H); ^{13}C NMR δ (MeOD) 173.7, 155.0, 136.9, 126.3, 120.9, 119.9, 119.8, 119.0, 118.1, 110.9, 79.7, 45.9, 42.5, 37.9, 33.7, 32.5, 28.2, 27.3.

tert-butyl 4-((4-(1H-indol-3-yl)piperidin-1-yl)methyl)piperidine-1-carboxylate (2.5)



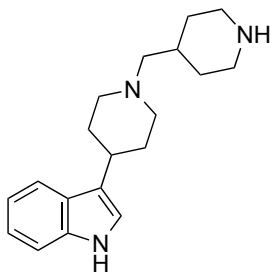
To a solution of **2.4** (100 mg, 0.24 mmol) in THF (3 mL) at -78 °C was added DIBAL in THF (730 μL of 1M solution, 0.73 mmol). The reaction stirred at -78 °C for 1 h and then quenched with MeOH followed by addition of 1 M aq. sodium potassium tartrate. The reaction mixture stirred until clear and was extracted with ethyl acetate. The organic phase was washed with brine and dried over anhydrous Na_2SO_4 . Solvent was removed under reduced pressure and the crude product purified with flash chromatography using a gradient elution of ethyl

acetate/acetonitrile:water:methanol (1:1:1) to afford compound **2.5** as an off-white solid (33.4 mg, 35%).

ESI-MS: C₂₄H₃₅N₃O₂, *m/z* calculated for [M⁺ H]⁺: 398.3, Found: 398.5.

¹H NMR δ (CDCl₃) 8.05 (s, NH), 7.64 (d, *J* = 8.1 Hz, 1H), 7.35 (d, *J* = 7.9 Hz, 1H), 7.17 (ddd, *J* = 7.9, 7.1, 1.2 Hz, 1H), 7.09 (ddd, *J* = 8.1, 7.1, 1.1 Hz, 1H), 6.96 (d, *J* = 2.1 Hz, 1H), 4.10 (d, *J* = 11.5 Hz, 2H), 2.99 (d, *J* = 11.5 Hz, 2H), 2.82 (m, 1H), 2.71 (t, *J* = 12.3 Hz, 2H), 2.23 (d, *J* = 6.9 Hz, 2H), 2.11 (td, *J* = 11.9, 1.9 Hz, 2H), 2.03 (d, *J* = 12.3 Hz, 2H), 1.87 – 1.64 (m, 5H), 1.46 (s, 9H), 1.11 (qd, *J* = 12.1, 3.4 Hz, 2H); **¹³C NMR** δ (CDCl₃) 154.8, 136.2, 126.5, 121.7, 121.4, 119.5, 118.9, 118.8, 111.0, 79.0, 64.9, 54.8, 33.7, 33.4, 32.8, 30.8, 28.3, 28.2.

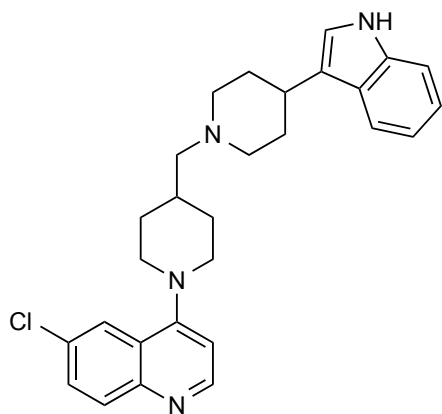
3-(1-(piperidin-4-ylmethyl)piperidin-4-yl)-1H-indole (2.6)



Compound **2.5** (30 mg, 0.08 mmol) was dissolved in a solution of 2 M HCl in MeOH (3 mL) and stirred at room temperature for 20 min. The solvent was removed under reduced pressure and the crude product was purified by reverse phase flash chromatography using a gradient elution of water/acetonitrile to afford the desired product as a yellow solid (22.4 mg, quantitative yield).

ESI-MS: C₁₉H₂₇N₃, *m/z* calculated for [M⁺ H]⁺: 298.2, Found: 298.5.

¹H NMR δ (D₂O) 7.75 (d, *J* = 8.0 Hz, 1H), 7.55 (d, *J* = 8.1 Hz, 1H), 7.29 (dd, *J* = 8.2, 8.1 Hz, 1H), 7.25 (s, 1H), 7.20 (dd, *J* = 8.2, 8.0 Hz, 1H), 3.71 (d, *J* = 12.5 Hz, 2H), 3.53 (d, *J* = 13.2 Hz, 2H), 3.24 – 3.05 (m, 7H), 2.32 (d, *J* = 12.5 Hz, 2H), 2.16 – 1.97 (m, 4H), 1.85 (m, 1H), 1.60 (q, *J* = 11.9 Hz, 2H); **¹³C NMR** δ (D₂O) 136.3, 125.4, 122.1, 121.3, 119.3, 118.7, 117.5, 112.1, 61.3, 53.7, 43.2, 30.5, 29.6, 28.7, 26.2.

4-(4-((4-(1H-indol-3-yl)piperidin-1-yl)methyl)piperidin-1-yl)-6-chloroquinoline (2.1)

To a solution of compound **2.6** (20 mg, 0.07 mmol) and DIPEA (35.2 μ L, 0.20 mmol) in isopropanol (2 mL) was added 4,6-dichloroquinoline (19.8 mg, 0.10 mmol). The reaction mixture stirred under reflux for 56 h. The solvent was removed under reduced pressure and the crude product was purified by flash chromatography using a gradient elution of ethyl acetate/acetonitrile:water:methanol (1:1:1) to afford compound **2.1** as an off-white oil (4.6 mg, 15%).

ESI-MS: $C_{28}H_{31}ClN_4$, m/z calculated for $[M^+ H]^+$: 459.22, Found: 459.37.

1H NMR δ (MeOD) 8.68 (d, $J = 5.1$ Hz, 1H), 8.46 (br, 1H), 8.06 (d, $J = 2.3$ Hz, 1H), 7.98 (d, $J = 9.0$ Hz, 1H), 7.73 (dd, $J = 9.0, 2.3$ Hz, 1H), 7.66 (d, $J = 7.8$ Hz, 1H), 7.39 (d, $J = 8.1$ Hz, 1H), 7.17 – 7.11 (m, 3H), 7.05 (dd, $J = 8.0, 7.9$ Hz, 1H), 3.67-3.81 (m, 4H), 3.24-3.29 (m, 5H), 3.04 (t, $J = 12.1$ Hz, 2H), 2.37 (d, $J = 13.4$ Hz, 2H), 2.28-2.16 (m, 3H), 2.11 (d, $J = 13.3$ Hz, 2H), 1.79 (qd, $J = 12.5, 3.7$ Hz, 2H).

General Procedure A:

Aldehyde (1.5 equiv.) and amine (1 equiv.) were mixed in 1,2-dichloroethane, followed by addition of sodium triacetoxyborohydride (1.4 equiv.). The reaction was stirred at room temperature under inert atmosphere for 4 h. The reaction mixture was quenched with sat. aq. $NaHCO_3$, followed by extraction with ethyl acetate. The organic phase was dried (Na_2SO_4), and the solvent was removed under reduced pressure. The crude product was purified by flash chromatography with a gradient of ethyl acetate/acetonitrile:water:methanol (1:1:1) to afford the desired product.

General Procedure B:

To a solution of acid chloride (1 equiv.) in DCM (3 mL) was added a suspension of compound **2.3** (1.1 equiv.) in sat. aq. $NaHCO_3$ (3 mL). The reaction mixture stirred vigorously at room temperature for 10 min. The organic phase was washed with HCl (aq., 10%), sat. aq. $NaHCO_3$ and brine, dried over anhydrous Na_2SO_4 and the solvent removed under reduced

pressure. The crude product was purified by flash chromatography with ethyl acetate/acetonitrile:water:methanol (1:1:1) to afford the desired product.

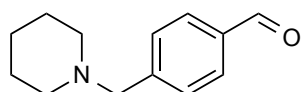
General Procedure C:

To a solution of acid chloride (1 equiv.) in DCM (2 mL) was added a solution of compound **2.3** (1.1 equiv.) and DIPEA (3 equiv.) in DCM (2 mL). The reaction mixture stirred at room temperature for 1 h and the solvent was removed under reduced pressure. The crude product was purified by flash chromatography with ethyl acetate/acetonitrile:water:methanol (1:1:1) to afford the desired product.

General Procedure D:

To a solution of carboxylic acid (1 equiv.) in DCM (2 mL) was added a solution of compound **2.3** (1 equiv.) and DIPEA (3 equiv.) in DCM (2 mL) followed by PyBOP (1.1 equiv.). The reaction mixture stirred at room temperature for 1 h and the solvent was removed under reduced pressure. The crude product was purified by flash chromatography ethyl acetate/acetonitrile:water:methanol (1:1:1) to afford the desired product.

4-(piperidin-1-ylmethyl)benzaldehyde

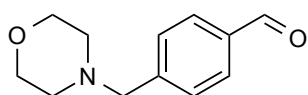


Reaction of terephthalaldehyde (235 mg, 1.75 mmol), piperidine (100 mg, 1.17 mmol) and sodium triacetoxyborohydride (349 mg, 1.64 mmol) according to general procedure A, gave 166 mg (70%) of desired aldehyde as a light yellow oil.

ESI-MS: $C_{13}H_{17}NO$, m/z calculated for $[M+H]^+$: 204.1, Found: 204.3.

1H NMR δ (MeOD) 10.01 (s, 1H), 7.91 (d, $J = 8.2$ Hz, 2H), 7.59 (d, $J = 8.2$ Hz, 2H), 3.64 (s, 2H), 2.52 – 2.46 (m, 4H), 1.70 – 1.60 (m, 4H), 1.53 – 1.49 (m, 2H); **^{13}C NMR** δ (MeOD) 192.4, 144.6, 135.8, 129.9, 129.3, 62.8, 54.1, 25.1, 23.7.

4-(morpholinomethyl)benzaldehyde



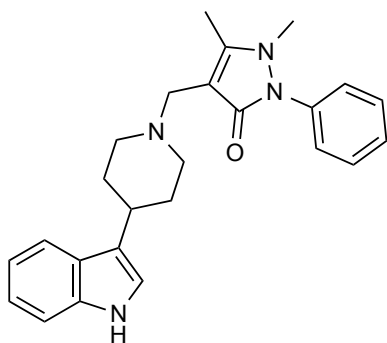
Reaction of terephthalaldehyde (231 mg, 1.73 mmol), morpholine (100 mg, 1.15 mmol) and sodium triacetoxyborohydride (340.6 mg, 1.60 mmol) according to general procedure A, gave 137 mg (58%) of

desired aldehyde as a light yellow oil.

ESI-MS: C₁₂H₁₅NO₂, *m/z* calculated for [M+H]⁺: 206.1, Found: 206.7.

¹H NMR δ (MeOD) 10.01 (s, 1H), 7.92 (d, *J* = 8.2 Hz, 2H), 7.61 (d, *J* = 8.2 Hz, 2H), 3.77 – 3.71 (m, 4H), 3.65 (s, 2H), 2.55 – 2.48 (m, 4H); ¹³C NMR δ (MeOD) 192.4, 144.8, 135.8, 129.6, 125.7, 66.4, 62.4, 53.3.

4-((4-(1*H*-indol-3-yl)piperidin-1-yl)methyl)-1,5-dimethyl-2-phenyl-1,2-dihydro-3*H*-pyrazol-3-one (2.7)

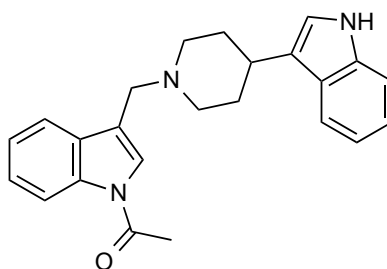


Reaction of compound **2.3** (20 mg, 0.10 mmol), 1,5-dimethyl 3-oxo-2-phenyl-2,3-dihydro-1*H*-pyrazole-4-carbaldehyde (32.4 mg, 0.15 mmol) and sodium triacetoxyborohydride (29.7 mg, 0.14 mmol) according to general procedure A, gave 28.4 mg (79%) of desired compound as a yellow oil.

ESI-MS: C₂₅H₂₈N₄O, *m/z* calculated for [M+H]⁺: 401.2, Found: 401.1.

¹H NMR δ (MeOD) 7.61 (d, *J* = 8.0 Hz, 1H), 7.56 (d, *J* = 8.0 Hz, 2H), 7.47 (ddd, *J* = 7.6, 7.2, 1.2 Hz, 1H), 7.42 (dd, *J* = 8.4, 1.2 Hz, 2H), 7.35 (d, *J* = 8.1 Hz, 1H), 7.10 (ddd, *J* = 8.0, 7.2, 1.2 Hz, 1H), 7.04 (s, 1H), 7.00 (ddd, *J* = 8.0, 7.2, 1.0 Hz, 1H), 3.53 (s, 2H), 3.26 (s, 3H), 3.22 (d, *J* = 10.5 Hz, 2H), 2.90 (m, 1H), 2.49 (t, *J* = 10.5 Hz, 2H), 2.43 (s, 3H), 2.11 (d, *J* = 12.6 Hz, 2H), 1.92 (qd, *J* = 12.1, 3.4 Hz, 2H); ¹³C NMR δ (MeOD) 166.0, 154.4, 136.9, 134.2, 129.2, 127.9, 126.4, 125.9, 120.8, 119.7, 119.4, 118.2, 117.9, 110.9, 101.4, 53.3, 49.3, 33.7, 32.9, 32.0, 10.0.

1-(3-((4-(1*H*-indol-3-yl)piperidin-1-yl)methyl)-1*H*-indol-1-yl)ethan-1-one (2.8)



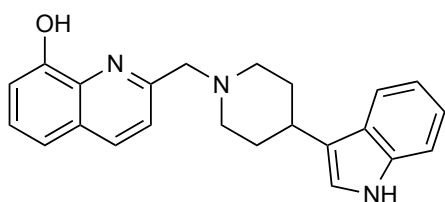
Reaction of compound **2.3** (20.0 mg, 0.10 mmol), 1-acetyl-1*H*-indole-3-carbaldehyde (28.1 mg, 0.15 mmol) and sodium triacetoxyborohydride (29.7 mg, 0.14 mmol) according to general procedure A, gave 25.3 mg (76%) of desired amine as an off-white solid.

ESI-MS: C₂₄H₂₅N₃O, *m/z* calculated for [M+H]⁺: 372.2, Found: 372.4.

¹H NMR δ (CDCl₃) 8.45 (d, *J* = 7.9 Hz, 1H), 8.01 (s, 1H), 7.74 (d, *J* = 8.2 Hz, 1H), 7.64 (d, *J* =

8.0 Hz, 1H), 7.46 – 7.28 (m, 4H), 7.17 (ddd, $J = 8.4, 8.2, 1.2$ Hz 1H), 7.10 (ddd, $J = 8.4, 8.0, 1.0$ Hz, 1H), 6.97 (d, $J = 2.1$ Hz, 1H), 3.75 (s, 2H), 3.15 (d, $J = 11.8$ Hz, 2H), 2.87 (tt, $J = 12.9, 3.6$ Hz, 1H), 2.30 (td, $J = 11.8, 2.1$ Hz, 2H), 2.07 (d, $J = 12.9$ Hz, 2H), 1.88 (qd, $J = 12.3, 3.6$ Hz, 2H); ^{13}C NMR δ (CDCl_3) 169.0, 136.9, 136.4, 131.3, 127.1, 125.7, 124.8, 124.6, 123.9, 123.5, 122.4, 121.8, 120.1, 119.6, 117.0, 111.9, 111.7, 54.9, 54.0, 33.9, 33.4, 24.5.

2-((4-(1H-indol-3-yl)piperidin-1-yl)methyl)quinolin-8-ol (2.9)



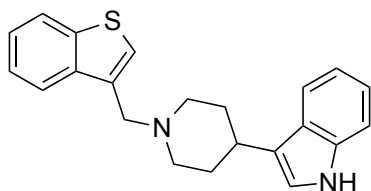
Reaction of compound **2.3** (50 mg, 0.25 mmol), 8-hydroxyquinoline-2-carbaldehyde (64.8 mg, 0.38 mmol) and sodium triacetoxyborohydride (74.1 mg, 0.35 mmol) according to general procedure A, gave 92.6 mg (99%) of

desired amine as a light yellow oil.

ESI-MS: $\text{C}_{23}\text{H}_{23}\text{N}_3\text{O}$, m/z calculated for $[\text{M}+\text{H}]^+$: 358.2, Found: 358.2.

^1H NMR δ (MeOD) 8.17 (d, $J = 8.3$ Hz, 1H), 7.55 (d, $J = 8.5$ Hz, 1H), 7.46 (d, $J = 8.5$ Hz, 1H), 7.39 (d, $J = 8.6$ Hz, 1H), 7.36 – 7.24 (m, 2H), 7.11 (dd, $J = 7.5, 1.3$ Hz, 1H), 7.05 (ddd, $J = 7.5, 6.9, 1.3$ Hz, 1H), 7.01 (s, 1H), 6.96 (ddd, $J = 7.9, 6.9, 1.0$ Hz, 1H), 4.22 (s, 2H), 3.28 – 3.25 (m, 2H), 2.97 (tt, $J = 11.4, 4.1$ Hz, 1H), 2.75 (td, $J = 11.6, 1.6$ Hz, 2H), 2.14 – 1.96 (m, 4H); ^{13}C NMR δ (MeOD) 154.2, 153.7, 139.4, 138.5, 138.3, 129.6, 128.9, 127.7, 122.6, 122.4, 121.3, 119.9, 119.6, 119.0, 118.4, 112.54, 112.4, 63.6, 55.2, 33.5, 32.2.

3-(1-(benzo[b]thiophen-3-ylmethyl)piperidin-4-yl)-1H-indole (2.10)



Reaction of compound **2.3** (50.0 mg, 0.25 mmol), benzo[b]thiophene-3-carbaldehyde (60.7 mg, 0.38 mmol) and sodium triacetoxyborohydride (74.1 mg, 0.35 mmol) according to general procedure A, gave 47.6 mg (55%) of desired amine as a

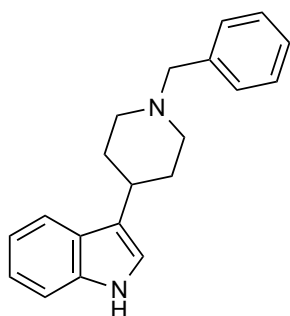
light yellow oil.

ESI-MS: $\text{C}_{22}\text{H}_{22}\text{N}_2\text{S}$, m/z calculated for $[\text{M}+\text{H}]^+$: 347.2, Found: 347.2.

^1H NMR δ (DMSO) 10.77 (s, 1H), 8.03 (d, $J = 7.4$ Hz, 1H), 7.97 (d, $J = 7.5$ Hz, 1H), 7.57 (s, 1H), 7.54 (d, $J = 7.5$ Hz, 1H), 7.45 – 7.31 (m, 3H), 7.10 – 7.01 (m, 2H), 6.95 (t, $J = 7.4$ Hz, 1H), 3.77 (s, 2H), 3.00 (d, $J = 11.2$ Hz, 2H), 2.77 (tt, $J = 12.0, 3.7$ Hz, 1H), 2.18 (t, $J = 10.8$ Hz, 2H), 1.98 – 1.89 (m, 2H), 1.69 (qd, $J = 12.3, 3.7$ Hz, 2H); ^{13}C NMR δ (DMSO) 139.9, 138.8, 136.4,

133.4, 126.3, 124.8, 124.3, 123.9, 122.8, 122.7, 120.8, 120.5, 119.6, 118.5, 118.0, 111.4, 56.2, 53.9, 33.1, 32.8.

3-(1-benzylpiperidin-4-yl)-1H-indole (2.11)

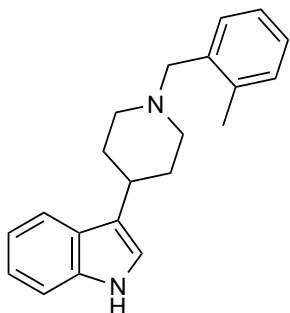


Reaction of compound **2.3** (100 mg, 0.50 mmol), benzaldehyde (79.4 mg, 0.70 mmol) and sodium triacetoxyborohydride (118.6 mg, 0.75 mmol) according to general procedure A, gave 76.2 mg (53%) of desired amine as a dark yellow solid.

ESI-MS: C₂₀H₂₂N₂, *m/z* calculated for [M+H]⁺: 291.2, Found: 291.1.

¹H NMR δ (MeOD) 7.58 (d, *J* = 7.8 Hz, 1H), 7.38 – 7.26 (m, 6H), 7.08 (ddd, *J* = 8.2, 7.0, 1.2 Hz, 1H), 7.03 – 6.96 (m, 2H), 3.56 (s, 2H), 3.00 (m, 2H), 2.80 (tt, *J* = 11.9, 3.8 Hz, 1H), 2.18 (td, *J* = 12.2, 2.6 Hz, 2H), 2.02 – 1.96 (m, 2H), 1.84 (qd, *J* = 12.1, 3.3 Hz, 2H); **¹³C NMR** δ (MeOD) 136.9, 132.8, 129.6, 128.0, 127.9, 127.1, 126.5, 120.8, 119.7, 118.4, 117.9, 110.9, 63.1, 53.8, 33.4, 32.3.

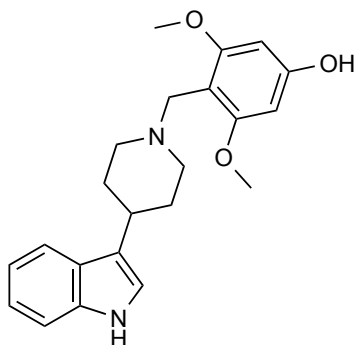
3-(1-(2-methylbenzyl)piperidin-4-yl)-1H-indole (2.12)



Reaction of compound **2.3** (50.0 mg, 0.25 mmol), 2-methylbenzaldehyde (44.9 mg, 0.38 mmol) and sodium triacetoxyborohydride (74.1 mg, 0.35 mmol) according to general procedure A, gave 41.8 mg (55%) of desired amine as a light orange solid.

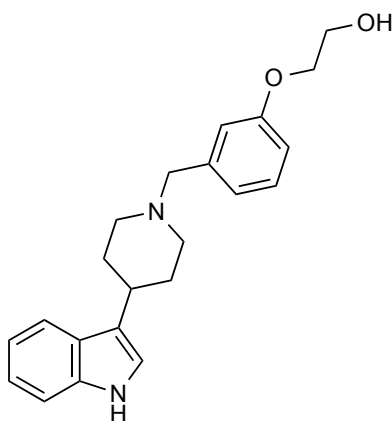
ESI-MS: C₂₁H₂₄N₂, *m/z* calculated for [M+H]⁺: 305.2, Found: 305.2.

¹H NMR δ (CDCl₃) 8.15 (s, 1H), 7.63 (d, *J* = 7.9 Hz, 1H), 7.38 – 7.34 (m, 2H), 7.22 – 7.13 (m, 4H), 7.09 (m, 1H), 6.96 (d, *J* = 2.3 Hz, 1H), 3.62 (s, 2H), 3.09 (d, *J* = 12.1 Hz, 2H), 2.87 (tt, *J* = 12.0, 3.8 Hz, 1H), 2.41 (s, 3H), 2.28 (td, *J* = 12.1, 2.6 Hz, 2H), 2.12 – 1.98 (m, 2H), 1.84 (qd, *J* = 12.2, 3.3 Hz, 2H); **¹³C NMR** δ (CDCl₃) 137.7, 136.5, 130.5, 130.3, 130.3, 127.4, 126.8, 125.8, 121.9, 121.3, 119.9, 119.2, 119.1, 111.3, 60.7, 54.3, 33.5, 32.8, 19.6.

4-((4-(1H-indol-3-yl)piperidin-1-yl)methyl)-3,5-dimethoxyphenol (2.13)

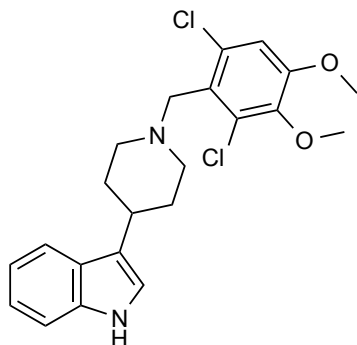
Reaction of compound **2.3** (20.0 mg, 0.10 mmol), 4-hydroxy-2,6-dimethoxybenzaldehyde (27.3 mg, 0.15 mmol) and sodium triacetoxyborohydride (29.7 mg, 0.14 mmol) according to general procedure A, gave 13.6 mg (42%) of desired amine as a yellow solid.

ESI-MS: $C_{22}H_{26}N_2O_3$, m/z calculated for $[M+H]^+$: 367.2, Found: 367.1. **1H NMR** δ (DMSO) 10.91 (s, 1H), 10.12 (s, 1H), 7.65 (d, $J = 7.7$ Hz, 1H), 7.35 (d, $J = 8.2$ Hz, 1H), 7.13 – 7.02 (m, 2H), 6.96 (m, 1H), 6.21 (s, 2H), 4.08 (s, 2H), 3.79 (s, 6H), 3.40 – 3.34 (m, 2H), 3.11 – 2.94 (m, 3H), 2.22 – 1.92 (m, 4H); **^{13}C NMR** δ (DMSO) 161.1, 160.1, 136.4, 125.8, 120.9, 120.8, 118.8, 118.2, 117.7, 111.5, 91.9, 55.8, 55.4, 51.9, 48.8, 43.5, 31.0, 30.7, 29.5, 29.0.

2-(3-((4-(1H-indol-3-yl)piperidin-1-yl)methyl)phenoxy)ethan-1-ol (2.14)

Reaction of compound **2.3** (50 mg, 0.25 mmol), 3-(2-hydroxyethoxy)benzaldehyde (62.3 mg, 0.38 mmol) and sodium triacetoxyborohydride (74.1 mg, 0.35 mmol) according to general procedure A, gave 86.7 mg (99%) of desired amine as an orange oil.

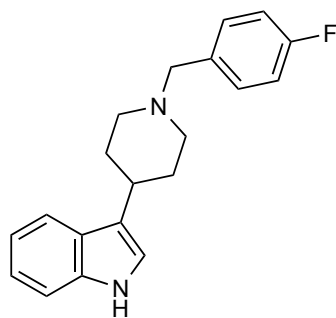
ESI-MS: $C_{22}H_{26}N_2O_2$, m/z calculated for $[M+H]^+$: 351.2, Found: 351.2.
 1H NMR δ ($CDCl_3$) 8.36 (s, 1H), 7.61 (d, $J = 7.9$ Hz, 1H), 7.35 (d, $J = 8.4$ Hz, 1H), 7.27 (m, 1H), 7.19 – 7.12 (m, 2H), 7.08 (ddd, $J = 7.9, 7.1, 1.1$ Hz, 1H), 6.97 (m, 2H), 6.87 (dd, $J = 8.2, 2.5$ Hz, 1H), 4.13 (dd, $J = 5.3, 4.0$ Hz, 2H), 3.96 (dd, $J = 5.3, 4.0$ Hz, 2H), 3.71 (s, 2H), 3.15 (d, $J = 11.5$ Hz, 2H), 2.88 (tt, $J = 11.4, 4.3$ Hz, 1H), 2.36 (t, $J = 10.9$ Hz, 2H), 2.13 – 1.93 (m, 4H); **^{13}C NMR** δ ($CDCl_3$) 159.1, 136.5, 129.5, 126.6, 122.6, 121.9, 120.6, 120.1, 119.2, 119.0, 115.9, 114.4, 111.4, 69.4, 62.8, 61.5, 53.9, 33.1, 32.1.

3-(1-(2,6-dichloro-3,4-dimethoxybenzyl)piperidin-4-yl)-1H-indole (2.15)

Reaction of compound **2.3** (50.0 mg, 0.25 mmol), 2,6-dichloro-3,4-dimethoxybenzaldehyde (87.6 mg, 0.38 mmol) and sodium triacetoxyborohydride (74.1 mg, 0.35 mmol) according to general procedure A, gave 62.9 mg (60%) of desired amine as red solid.

ESI-MS: C₂₂H₂₄Cl₂N₂O₂, *m/z* calculated for [M+H]⁺: 419.1, Found: 419.3.

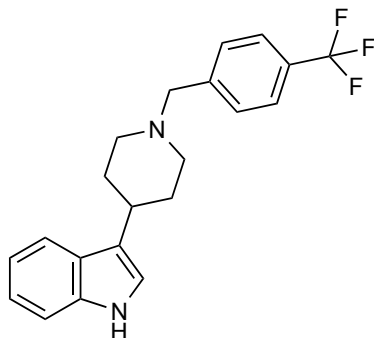
¹H NMR δ (DMSO) 10.74 (s, 1H), 7.52 (dd, *J* = 7.8, 1.2 Hz, 1H), 7.31 (d, *J* = 8.0 Hz, 1H), 7.18 (s, 1H), 7.09 – 7.01 (m, 2H), 6.94 (ddd, *J* = 8.0, 6.9, 1.1 Hz, 1H), 3.86 (s, 3H), 3.75 (s, 3H), 3.68 (s, 2H), 2.92 (d, *J* = 11.1 Hz, 2H), 2.77 (tt, *J* = 12.0, 3.6 Hz, 1H), 2.35 (t, *J* = 11.1 Hz, 2H), 1.92 (d, *J* = 13.7 Hz, 2H), 1.62 (qd, *J* = 12.2, 3.5 Hz, 2H); **¹³C NMR** δ (DMSO) 152.6, 143.9, 136.3, 130.3, 130.2, 126.3, 120.7, 120.4, 119.5, 118.5, 117.9, 112.6, 111.4, 60.1, 56.5, 56.4, 53.7, 32.8.

3-(1-(4-fluorobenzyl)piperidin-4-yl)-1H-indole (2.16)

Reaction of compound **2.3** (50.0 mg, 0.25 mmol), 4-fluorobenzaldehyde (46.4 mg, 0.38 mmol) and sodium triacetoxyborohydride (74.1 mg, 0.35 mmol) according to general procedure A, gave 55 mg (72%) of desired amine as yellow oil.

ESI-MS: C₂₀H₂₁FN₂, *m/z* calculated for [M+H]⁺: 309.2, Found: 309.1.

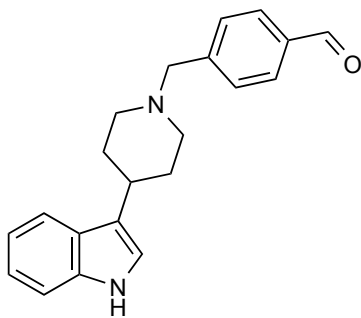
¹H NMR δ (MeOD) 7.60 (d, *J* = 7.9 Hz, 1H), 7.50 – 7.42 (m, 2H), 7.35 (d, *J* = 8.2 Hz, 1H), 7.17 – 7.07 (m, 3H), 7.05 – 6.96 (m, 2H), 3.81 (s, 2H), 3.17 (d, *J* = 12.1 Hz, 2H), 2.94 (tt, *J* = 11.9, 3.8 Hz, 1H), 2.51 (t, *J* = 11.1 Hz, 2H), 2.11 (d, *J* = 12.9 Hz, 2H), 1.93 (qd, *J* = 12.1, 3.3 Hz, 2H); **¹³C NMR** δ (MeOD) 164.1 (d, ¹*J*_{CF} = 245 Hz), 138.3, 133.3, 127.7, 122.3, 121.2, 120.3, 119.6, 119.5, 116.4, 116.2, 112.4, 62.6, 54.7, 34.0, 32.9.

3-(1-(4-(trifluoromethyl)benzyl)piperidin-4-yl)-1H-indole (2.17)

Reaction of compound **2.3** (20 mg, 0.10 mmol), 4-(trifluoromethyl)benzaldehyde (26.1 mg, 0.15 mmol) and sodium triacetoxyborohydride (29.7 mg, 0.14 mmol) according to general procedure A, gave the desired amine as a beige oil 22.2 mg (69%).

ESI-MS: C₂₁H₂₁F₃N₂, *m/z* calculated for [M+H]⁺: 359.2, Found: 359.3.

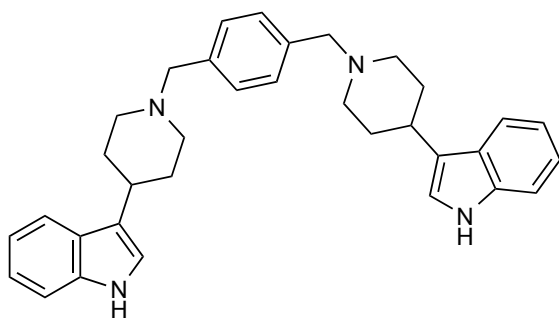
¹H NMR δ (MeOD) 7.72 – 7.55 (m, 5H), 7.34 (d, *J* = 8.1 Hz, 1H), 7.09 (ddd, *J* = 8.1, 7.1, 1.1 Hz, 1H), 7.03 (s, 1H), 7.00 (ddd, *J* = 8.0, 7.1, 1.1 Hz, 1H), 3.72 (s, 2H), 3.06 (d, *J* = 12.3 Hz, 2H), 2.88 (tt, *J* = 12.3, 3.9 Hz, 1H), 2.31 (td, *J* = 12.3, 2.5 Hz, 2H), 2.07 (m, 2H), 1.89 (qd, *J* = 12.3, 3.6 Hz, 2H); **¹³C NMR** δ (MeOD) 143.3, 138.3, 131.3, 127.9, 126.2, 126.2, 126.1, 122.2, 121.1, 121.0, 119.6, 119.3, 112.3, 63.7, 55.3, 34.7, 33.8.

4-((4-(1H-indol-3-yl)piperidin-1-yl)methyl)benzaldehyde (2.18)

Reaction of compound **2.3** (50.0 mg, 0.25 mmol), terephthalaldehyde (50.3 mg, 0.37 mmol) and sodium triacetoxyborohydride (74.1 mg, 0.35 mmol) according to general procedure A, gave 19.9 mg (25%) of desired amine an off-white solid.

ESI-MS: C₂₁H₂₂N₂O, *m/z* calculated for [M+H]⁺: 319.2, Found: 319.2.

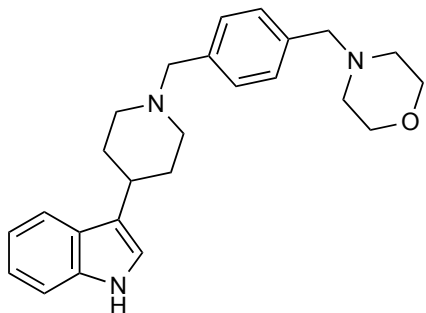
¹H NMR δ (CDCl₃) 10.00 (s, 1H), 8.07 (s, 1H), 7.85 (d, *J* = 8.1 Hz, 2H), 7.64 (d, *J* = 7.9 Hz, 1H), 7.55 (d, *J* = 8.1 Hz, 2H), 7.35 (d, *J* = 8.2 Hz, 1H), 7.18 (ddd, *J* = 8.2, 6.9, 1.2 Hz, 1H), 7.10 (ddd, *J* = 7.9, 7.0, 1.1 Hz, 1H), 6.97 (d, *J* = 1.2 Hz, 1H), 3.66 (s, 2H), 3.01 (d, *J* = 11.8 Hz, 2H), 2.86 (tt, *J* = 11.9, 3.8 Hz, 1H), 2.23 (td, *J* = 11.8, 2.5 Hz, 2H), 2.05 (d, *J* = 13.9 Hz, 2H), 1.86 (qd, *J* = 11.9, 3.3 Hz, 2H); **¹³C NMR** δ (CDCl₃) 191.9, 145.7, 136.2, 135.2, 129.6, 129.5, 126.8, 121.7, 121.1, 119.5, 118.9, 111.0, 62.9, 54.2, 33.2, 32.7.

1,4-bis((4-(1H-indol-3-yl)piperidin-1-yl)methyl)benzene (2.19)

Reaction of compound **2.3** (50.0 mg, 0.25 mmol), terephthalaldehyde (50.3 mg, 0.38 mmol) and sodium triacetoxyborohydride (74.1 mg, 0.35 mmol) according to general procedure A, gave 37.7 mg (30%) of desired amine as an off-white solid.

ESI-MS: C₃₄H₃₈N₄, *m/z* calculated for [M+H]⁺: 503.3, Found: 503.3.

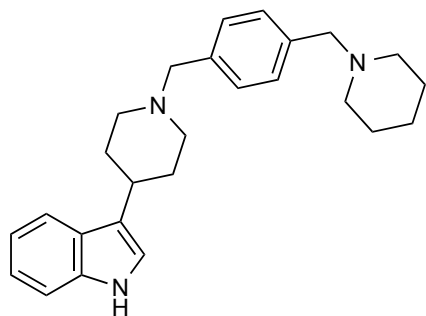
¹H NMR δ (DMSO) 10.74 (s, 2H), 7.53 (d, *J* = 7.6 Hz, 2H), 7.39 – 7.25 (m, 6H), 7.08 (s, 2H), 7.04 (dd, *J* = 7.5, 1.1 Hz, 2H), 6.94 (dd, *J* = 7.6, 1.2 Hz, 2H), 3.49 (s, 4H), 2.91 (d, *J* = 12.1 Hz, 4H), 2.75 (tt, *J* = 12.2, 3.8 Hz, 2H), 2.11 (td, *J* = 11.8, 2.5 Hz, 4H), 1.96 – 1.86 (m, 4H), 1.69 (qd, *J* = 12.0, 3.4 Hz, 4H); **¹³C NMR** δ (DMSO) 137.2, 136.3, 128.6, 126.3, 120.7, 120.5, 119.6, 118.5, 117.9, 111.4, 62.4, 53.8, 33.1, 32.8.

4-(4-((4-(1H-indol-3-yl)piperidin-1-yl)methyl)benzyl)morpholine (2.20)

Reaction of compound **2.3** (20 mg, 0.10 mmol), 4-(morpholinomethyl)benzaldehyde (30.8 mg, 0.15 mmol) and sodium triacetoxyborohydride (29.7 mg, 0.14 mmol) according to general procedure A, gave 14.8 mg (38%) of desired amine as an off-white solid.

ESI-MS: C₂₅H₃₁N₃O, *m/z* calculated for [M+H]⁺: 390.3, Found: 390.2.

¹H NMR δ (CDCl₃) 8.25 (s, 1H), 7.60 (d, *J* = 7.8 Hz, 1H), 7.44 – 7.32 (m, 5H), 7.16 (ddd, *J* = 8.1, 7.1, 1.2 Hz, 1H), 7.08 (ddd, *J* = 7.8, 7.1, 1.1 Hz, 1H), 6.97 (d, *J* = 1.9 Hz, 1H), 3.81 (s, 2H), 3.76 – 3.67 (m, 4H), 3.51 (s, 2H), 3.22 (d, *J* = 11.5 Hz, 2H), 2.90 (m, 1H), 2.52 – 2.37 (m, 6H), 2.10 – 2.06 (m, 4H); **¹³C NMR** δ (CDCl₃) 136.5, 130.4, 130.3, 129.6, 129.6, 126.6, 122.1, 120.1, 119.3, 118.9, 111.5, 67.1, 63.2, 62.2, 53.7, 32.8, 31.7.

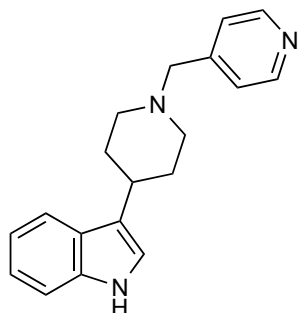
3-(1-(4-(piperidin-1-ylmethyl)benzyl)piperidin-4-yl)-1H-indole (2.21)

Reaction of compound **2.3** (20.0 mg, 0.10 mmol), 4-(piperidin-1-ylmethyl)benzaldehyde (30.5 mg, 0.15 mmol) and sodium triacetoxyborohydride (29.7 mg, 0.14 mmol) according to general procedure A, gave the desired amine as an off-white solid (20.9 mg, 54%).

ESI-MS: C₂₆H₃₃N₃, *m/z* calculated for [M+H]⁺: 388.3,

Found: 388.4.

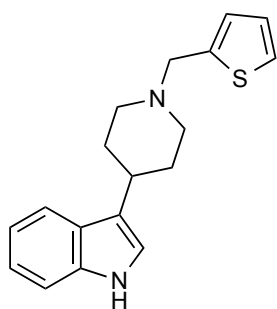
¹H NMR δ (CDCl₃) 8.02 (s, 1H), 7.65 (d, *J* = 7.9 Hz, 1H), 7.35 (d, *J* = 8.1 Hz, 2H), 7.32 – 7.24 (m, 4H), 7.18 (ddd, *J* = 8.1, 6.9, 1.2 Hz, 1H), 7.10 (ddd, *J* = 7.9, 6.9, 1.1 Hz, 1H), 6.96 (d, *J* = 1.8 Hz, 2H), 3.56 (s, 2H), 3.47 (s, 2H), 3.03 (d, *J* = 11.9 Hz, 2H), 2.84 (tt, *J* = 11.9, 3.8 Hz, 1H), 2.45 – 2.31 (m, 4H), 2.17 (td, *J* = 11.9, 2.4 Hz, 2H), 2.08 – 1.98 (m, 2H), 1.83 (qd, *J* = 12.0, 3.5 Hz, 2H), 1.58 (m, 4H), 1.44 (m, 2H); **¹³C NMR** δ (CDCl₃) 137.2, 137.1, 136.4, 129.1, 129.0, 126.7, 121.9, 121.7, 119.6, 119.0, 111.1, 63.7, 63.4, 54.5, 54.4, 33.5, 33.1, 25.9, 24.4.

3-(1-(pyridin-4-ylmethyl)piperidin-4-yl)-1H-indole (2.22)

Reaction of compound **2.3** (50.0 mg, 0.25 mmol), isonicotinaldehyde (40.1 mg, 0.37 mmol) and sodium triacetoxyborohydride (74.1 mg, 0.35 mmol) according to general procedure A, gave 70.6 mg (97%) of desired amine as orange oil.

ESI-MS: C₁₉H₂₁N₃, *m/z* calculated for [M+H]⁺: 292.2, Found: 292.4.

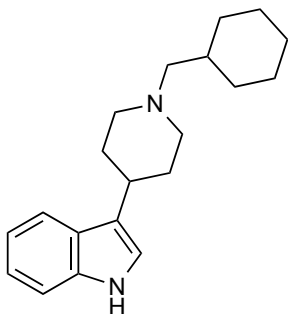
¹H NMR δ (MeOD) 8.49 (d, *J* = 6.0 Hz, 2H), 7.58 (d, *J* = 7.9 Hz, 1H), 7.45 (d, *J* = 6.0 Hz, 2H), 7.33 (d, *J* = 8.1 Hz, 1H), 7.08 (ddd, *J* = 8.1, 6.9, 1.2 Hz, 1H), 7.02 – 6.92 (m, 2H), 3.63 (s, 2H), 3.01 (m, 2H), 2.84 (tt, *J* = 11.9, 3.9 Hz, 1H), 2.27 (t, *J* = 11.9 Hz, 2H), 2.04 (d, *J* = 13.8 Hz, 2H), 1.86 (qd, *J* = 12.0, 3.5 Hz, 2H); **¹³C NMR** δ (MeOD) 150.0, 149.8, 149.7, 138.3, 127.9, 126.0, 122.7, 122.2, 121.1, 120.9, 119.7, 119.4, 112.3, 62.8, 55.4, 34.6, 33.8.

3-(1-(thiophen-2-ylmethyl)piperidin-4-yl)-1H-indole (2.23)

Reaction of compound **2.3** (20.0 mg, 0.10 mmol), thiophene-2-carbaldehyde (16.8 mg, 0.15 mmol) and sodium triacetoxyborohydride (29.7 mg, 0.14 mmol) according to general procedure A, gave 19.2 mg (65%) of desired amine as a light yellow oil.

ESI-MS: C₁₈H₂₀N₂S, *m/z* calculated for [M+H]⁺: 297.1, Found: 297.4.

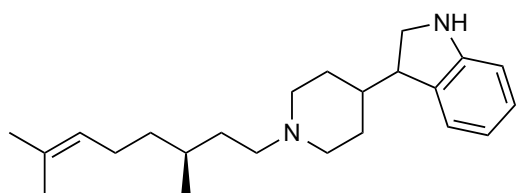
¹H NMR δ (CDCl₃) 8.00 (s, 1H), 7.64 (d, *J* = 7.9 Hz, 1H), 7.35 (d, *J* = 8.1 Hz, 1H), 7.25 (d, *J* = 1.5 Hz, 1H), 7.18 (ddd, *J* = 8.1, 7.1, 1.2 Hz, 1H), 7.10 (ddd, *J* = 7.9, 7.1, 1.1 Hz, 1H), 6.99 – 6.95 (m, 3H), 3.82 (s, 2H), 3.08 (d, *J* = 12.9 Hz, 2H), 2.84 (tt, *J* = 11.9, 3.8 Hz, 1H), 2.24 (t, *J* = 11.8 Hz, 2H), 2.06 (d, *J* = 12.9 Hz, 2H), 1.86 (qd, *J* = 11.8, 3.3 Hz, 2H); ¹³C NMR δ (CDCl₃) 142.0, 136.8, 127.2, 126.9, 126.7, 125.4, 122.4, 121.9, 120.1, 119.6, 119.5, 111.6, 57.9, 54.4, 33.9, 33.4.

3-(1-(cyclohexylmethyl)piperidin-4-yl)-1H-indole (2.24)

Reaction of compound **2.3** (50.0 mg, 0.25 mmol), (*S*)-3,7-dimethyloct-6-enal (42.1 mg, 0.38 mmol) and sodium triacetoxyborohydride (74.1 mg, 0.35 mmol) according to general procedure A, gave 74.1 mg (quantitative yield) of desired amine as orange oil.

ESI-MS: C₂₀H₂₈N₂, *m/z* calculated for [M+H]⁺: 298.2, Found: 298.2.

¹H NMR δ (CDCl₃) 8.19 (s, 1H), 7.64 (d, *J* = 7.9 Hz, 1H), 7.35 (d, *J* = 8.1 Hz, 1H), 7.18 (ddd, *J* = 8.1, 7.0, 1.2 Hz, 1H), 7.10 (ddd, *J* = 7.9, 7.0, 1.1 Hz, 1H), 6.96 (d, *J* = 2.3 Hz, 1H), 3.03 (d, *J* = 11.6 Hz, 2H), 2.83 (tt, *J* = 11.9, 3.8 Hz, 1H), 2.21 (d, *J* = 6.9 Hz, 2H), 2.15 – 1.97 (m, 4H), 1.95 – 1.79 (m, 4H), 1.78 – 1.62 (m, 3H), 1.36 – 1.08 (m, 4H), 1.02 – 0.82 (m, 2H); ¹³C NMR δ (CDCl₃) 136.5, 126.8, 121.9, 121.6, 119.9, 119.2, 119.1, 111.3, 66.3, 55.1, 35.3, 33.7, 32.9, 32.3, 26.9, 26.3.

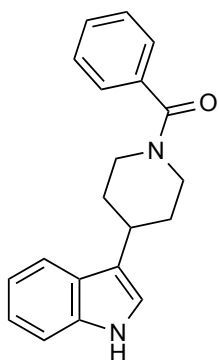
3-(1-((S)-3,7-dimethyloct-6-en-1-yl)piperidin-4-yl)indoline (2.25)

Reaction of compound **2.3** (50.0 mg, 0.25 mmol), (S)-3,7-dimethyloct-6-enal (57.7 mg, 0.38 mmol) and sodium triacetoxyborohydride (74.1 mg, 0.35 mmol) according to general procedure A, gave 83.4 mg

(98%) of desired amine as a dark orange oil.

ESI-MS: C₂₃H₃₆N₂, *m/z* calculated for [M+H]⁺: 341.3, Found: 341.3.

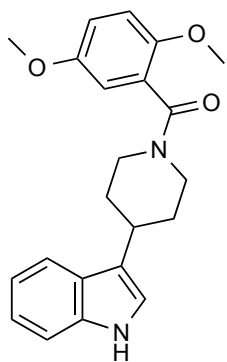
¹H NMR δ (DMSO) 10.75 (s, 1H), 7.52 (d, *J* = 7.9 Hz, 1H), 7.32 (d, *J* = 8.1 Hz, 1H), 7.09 – 7.00 (m, 2H), 6.94 (t, *J* = 7.4 Hz, 1H), 5.01 (m, 1H), 2.94 (d, *J* = 9.3 Hz, 2H), 2.72 (tt, *J* = 11.9, 3.8 Hz, 1H), 2.30 (t, *J* = 7.3 Hz, 2H), 2.11 – 1.80 (m, 6H), 1.67 (m, 1H), 1.65 (s, 3H), 1.58 (s, 3H), 1.46 (m, 2H), 1.39 – 1.07 (m, 4H), 0.87 (d, *J* = 6.3 Hz, 3H); **¹³C NMR** δ (DMSO) 136.4, 130.4, 126.3, 124.7, 120.7, 120.4, 119.7, 118.5, 117.9, 111.4, 58.8, 56.3, 54.3, 53.9, 36.7, 33.6, 33.3, 32.9, 30.2, 25.5, 24.9, 19.6, 17.5.

(4-(1H-indol-3-yl)piperidin-1-yl)(phenyl)methanone (2.26)

Reaction of compound **2.3** (78.6 mg, 0.39 mmol) and benzoyl chloride (50.0 mg, 0.36 mmol) according to general procedure B, gave 59.9 mg (55%) of desired amide as a beige solid.

ESI-MS: C₂₀H₂₀N₂O, *m/z* calculated for [M+H]⁺: 305.2, Found: 305.1.

¹H NMR δ (DMSO) 10.81 (s, 1H), 7.58 (d, *J* = 7.8 Hz, 1H), 7.47 – 7.40 (m, 5H), 7.34 (d, *J* = 7.9 Hz, 1H), 7.14 (d, *J* = 2.3 Hz, 1H), 7.06 (dd, *J* = 7.9, 1.4 Hz, 1H), 6.96 (dd, *J* = 7.8, 1.3 Hz, 1H), 4.61 (br, 1H), 3.68 (br, 1H), 3.23 (br, 1H), 3.08 (tt, *J* = 3.4, 12.2 Hz, 1H), 2.95 (br, 1H), 2.15 – 1.80 (m, 2H), 1.68 – 1.58 (m, 2H); **¹³C NMR** δ (DMSO) 169.4, 137.0, 136.8, 129.7, 128.9, 127.1, 126.6, 121.4, 121.3, 119.4, 118.9, 118.6, 111.9, 48.2, 42.6, 33.6.

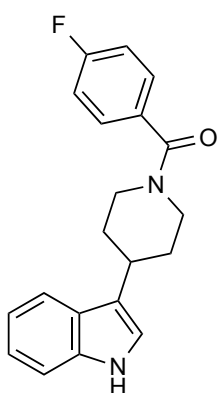
(4-(1H-indol-3-yl)piperidin-1-yl)(2,5-dimethoxyphenyl)methanone (2.27)

Reaction of compound **2.3** (54.9 mg, 0.27 mmol) and 2,5-dimethoxybenzoyl chloride (50.0 mg, 0.25 mmol) according to general procedure B, gave 91.0 mg (quantitative yield) of desired amide as a white solid.

ESI-MS: C₂₂H₂₄N₂O₃, *m/z* calculated for [M+H]⁺: 365.2, Found: 365.2. **¹H**

NMR δ (CDCl₃) 8.37 (s, NH), 7.62 (d, *J* = 7.9 Hz, 1H), 7.35 (d, *J* = 8.1 Hz, 1H), 7.19 (ddd, *J* = 8.1, 7.0, 1.2 Hz, 1H), 7.11 (ddd, *J* = 7.9, 7.0, 1.1 Hz, 1H), 6.93 (d, *J* = 2.2 Hz, 1H), 6.58 (d, *J* = 2.3 Hz, 2H), 6.51 (t, *J* = 2.3 Hz, 1H),

4.85 (br, 1H), 3.91 (br, 1H), 3.80 (s, 6H), 3.20 (br, 1H), 3.13 (tt, *J* = 11.8, 3.6 Hz, 1H), 2.98 (br, 1H), 2.18 (br, 1H), 2.06 (br, 1H), 1.82 (br, 1H), 1.66 (br, 1H); **¹³C NMR** δ (CDCl₃) 170.1, 160.9, 138.3, 136.6, 126.4, 122.1, 120.2, 119.9, 119.3, 118.9, 111.5, 104.8, 101.6, 55.6, 48.4, 42.9, 33.9, 32.6, 29.8.

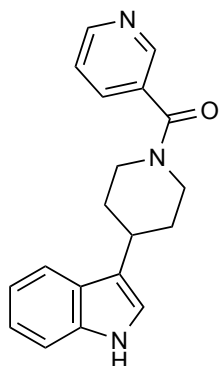
(4-(1H-indol-3-yl)piperidin-1-yl)(4-fluorophenyl)methanone (2.28)

Reaction of compound **2.3** (69.6 mg, 0.35 mmol) and 4-fluorobenzoyl chloride (50.0 mg, 0.32 mmol) according to general procedure B, gave 97.9 mg (95%) of desired amide as a yellow oil.

ESI-MS: C₂₀H₁₉FN₂O, *m/z* calculated for [M+H]⁺: 323.2, Found: 323.3.

¹H NMR δ (DMSO) 10.73 (s, 1H), 7.51 (d, *J* = 7.9 Hz, 1H), 7.47 – 7.40 (m, 2H), 7.30 – 7.16 (m, 3H), 7.06 (d, *J* = 2.4 Hz, 1H), 6.99 (m, 1H), 6.90 (m, 1H), 4.52 (br, 1H), 3.59 (br, 1H), 3.10 (br, 1H), 3.01 (tt, *J* = 11.8, 3.7 Hz, 1H), 2.91 (br, 1H), 1.91 (br, 2H), 1.57 (m, 2H); **¹³C NMR** δ (DMSO) 168.5,

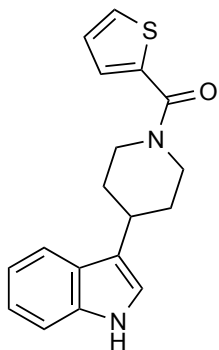
162.9 (d, ¹*J*_{CF} = 246 Hz), 136.8, 133.4, 129.8, 126.6, 121.3, 119.4, 118.9, 118.6, 115.9, 111.9, 48.4, 42.7, 33.6, 33.2, 29.5.

(4-(1H-indol-3-yl)piperidin-1-yl)(pyridin-3-yl)methanone (2.29)

Reaction of compound **2.3** (78.1 mg, 0.39 mmol), nicotinoyl chloride (50.0 mg, 0.35 mmol) and DIPEA (182.9 μ L, 1.05 mmol) according to general procedure C, gave 26.7 mg (25%) of desired amide as an off-white solid.

ESI-MS: $C_{19}H_{19}N_3O$, m/z calculated for $[M+H]^+$: 306.2, Found: 306.4.

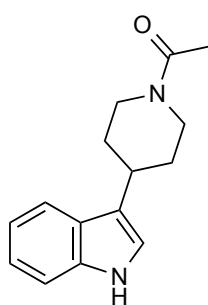
1H NMR δ ($CDCl_3$) 8.73 (d, $J = 2.2$ Hz, 1H), 8.68 (dd, $J = 4.9, 1.7$ Hz, 1H), 8.46 (s, NH), 7.80 (dd, $J = 7.8, 1.9$ Hz, 1H), 7.62 (d, $J = 7.7$ Hz, 1H), 7.42 – 7.32 (m, 2H), 7.19 (dd, $J = 7.7, 1.1$ Hz, 1H), 7.12 (dd, $J = 7.8, 1.2$ Hz, 1H), 6.95 (d, $J = 2.4$ Hz, 1H), 4.88 (br, 1H), 3.85 (br, 1H), 3.28 (br, 1H), 3.15 (tt, $J = 11.9, 3.7$ Hz, 1H), 3.01 (br, 1H), 2.20 (br, 1H), 2.08 (br, 1H), 1.83 (br, 1H), 1.70 (br, 1H); **^{13}C NMR** δ ($CDCl_3$) 167.8, 150.7, 147.9, 136.6, 135.0, 132.3, 126.4, 123.6, 122.2, 120.0, 119.9, 119.3, 118.9, 111.5, 48.6, 43.2, 33.8, 33.7, 32.5.

(4-(1H-indol-3-yl)piperidin-1-yl)(thiophen-2-yl)methanone (2.30)

Reaction of compound **2.3** (76.1 mg, 0.38 mmol) and 2-thiophenecarbonyl chloride (50.0 mg, 0.35 mmol) according to general procedure B, gave 71.1 mg (66%) of desired amide as an off-white solid.

ESI-MS: $C_{18}H_{18}N_2OS$, m/z calculated for $[M+H]^+$: 311.1, Found: 311.3.

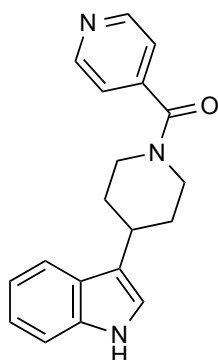
1H NMR δ ($CDCl_3$) 8.12 (s, NH), 7.64 (d, $J = 7.9$ Hz, 1H), 7.44 (dd, $J = 5.0, 1.2$ Hz, 1H), 7.37 (d, $J = 8.1$ Hz, 1H), 7.33 (dd, $J = 3.7, 1.2$ Hz, 1H), 7.20 (ddd, $J = 7.9, 7.1, 1.2$ Hz, 1H), 7.12 (ddd, $J = 8.1, 7.1, 1.1$ Hz, 1H), 7.06 (dd, $J = 5.0, 3.7$ Hz, 1H), 6.98 (d, $J = 2.1$ Hz, 1H), 4.59 (br, 2H), 3.25 – 3.08 (m, 3H), 2.17 (br, 1H), 2.14 (br, 1H), 1.79 (m, 2H); **^{13}C NMR** δ ($CDCl_3$) 163.8, 137.7, 136.6, 128.7, 128.4, 126.8, 126.5, 122.3, 120.5, 119.9, 119.5, 119.0, 111.5, 34.0, 33.3, 29.9, 22.9, 14.3.

1-(4-(1H-indol-3-yl)piperidin-1-yl)ethan-1-one (2.31)

Reaction of compound **2.3** (140 mg, 0.70 mmol) and acetyl chloride (50.0 mg, 0.64 mmol) according to general procedure B, gave 113 mg (73%) of desired amide as a yellow solid.

ESI-MS: C₁₅H₁₈N₂O, *m/z* calculated for [M+H]⁺: 243.1, Found: 243.4.

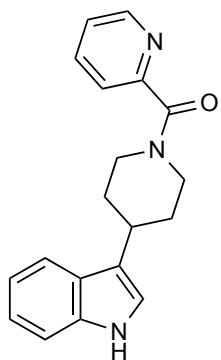
¹H NMR δ (CDCl₃) 8.04 (s, NH), 7.63 (d, *J* = 7.9 Hz, 1H), 7.38 (d, *J* = 8.1 Hz, 1H), 7.20 (ddd, *J* = 8.1, 7.1, 1.2 Hz, 1H), 7.12 (ddd, *J* = 7.9, 7.1, 1.1 Hz, 1H), 6.96 (d, *J* = 2.5 Hz, 1H), 4.77 (m, 1H), 3.92 (m, 1H), 3.26 (ddd, *J* = 13.4, 12.9, 2.7 Hz, 1H), 3.09 (tt, *J* = 11.8, 3.8 Hz, 1H), 2.75 (ddd, *J* = 13.4, 12.9, 2.9 Hz, 1H), 2.15 (s, 3H), 1.76 – 1.60 (m, 4H); **¹³C NMR** δ (CDCl₃) 168.9, 136.4, 126.4, 122.2, 120.5, 119.7, 119.3, 118.9, 111.3, 47.1, 42.3, 33.8, 33.6, 32.3, 21.6.

(4-(1H-indol-3-yl)piperidin-1-yl)(pyridin-4-yl)methanone (2.32)

Reaction of compound **2.3** (20.0 mg, 0.100 mmol), isonicotinic acid (12.3 mg, 0.10 mmol), DIPEA (52.3 μL, 0.30 mmol) and PyBOP (57.2 mg, 0.11 mmol) according to general procedure D, gave 18.30 mg (60%) of desired amide as a yellow oil.

ESI-MS: C₁₉H₁₉N₃O, *m/z* calculated for [M+H]⁺: 306.2, Found: 306.1.

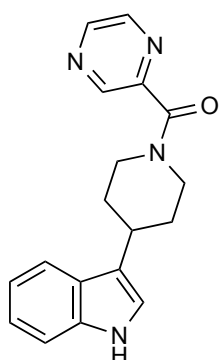
¹H NMR δ (CDCl₃) 8.71 (dd, *J* = 5.9, 1.6 Hz, 2H), 8.06 (s, NH), 7.62 (d, *J* = 7.9 Hz, 1H), 7.38 (d, *J* = 8.1 Hz, 1H), 7.33 (d, *J* = 5.9 Hz, 2H), 7.21 (ddd, *J* = 8.1, 7.1, 1.2 Hz, 1H), 7.13 (ddd, *J* = 7.9, 7.1, 1.0 Hz, 1H), 6.98 (d, *J* = 2.5 Hz, 1H), 4.86 (d, *J* = 13.2 Hz, 1H), 3.74 (d, *J* = 15.9 Hz, 1H), 3.27 (td, *J* = 12.5, 2.3 Hz, 1H), 3.16 (tt, *J* = 3.7, 11.9 Hz, 1H), 3.0 (td, *J* = 12.9, 2.8 Hz, 1H), 2.23 (d, *J* = 13.3 Hz, 1H), 2.08 (d, *J* = 13.0 Hz, 1H), 1.84 (m, 1H), 1.63 (m, 1H); **¹³C NMR** δ (CDCl₃) 167.5, 150.1, 143.9, 136.3, 126.1, 122.1, 120.9, 119.9, 119.5, 119.2, 118.7, 111.2, 48.0, 42.6, 33.6, 32.2, 29.5.

(4-(1H-indol-3-yl)piperidin-1-yl)(pyridin-2-yl)methanone (2.33)

Reaction of compound **2.3** (20.0 mg, 0.10 mmol), picolinic acid (12.3 mg, 0.10 mmol), DIPEA (52.3 μ L, 0.30 mmol) and PyBOP (57.2 mg, 0.11 mmol) according to general procedure D, gave 29.0 mg (95%) of desired amide as a beige solid.

ESI-MS: C₁₉H₁₉N₃O, *m/z* calculated for [M+H]⁺: 306.2, Found: 306.4.

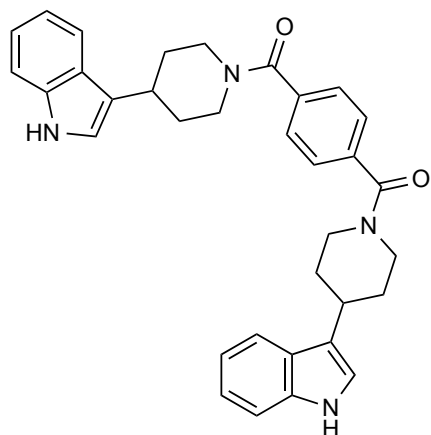
¹H NMR δ (CDCl₃) 8.71 (s, 2H), 8.22 (s, NH), 7.62 (d, *J* = 8.0 Hz, 1H), 7.39 – 7.31 (m, 3H), 7.20 (ddd, *J* = 8.2, 7.1, 1.2 Hz, 1H), 7.12 (ddd, *J* = 8.0, 7.1, 1.1 Hz, 1H), 6.97 (d, *J* = 2.5 Hz, 1H), 4.86 (d, *J* = 12.8 Hz, 1H), 3.73 (d, *J* = 13.0 Hz, 1H), 3.27 (td, *J* = 12.7, 2.9 Hz, 1H), 3.15 (tt, *J* = 11.9, 3.7 Hz, 1H), 3.01 (td, *J* = 12.9, 2.7 Hz, 1H), 2.23 (d, *J* = 13.1 Hz, 1H), 2.08 (d, *J* = 13.0 Hz, 1H), 1.85 (m, 1H), 1.60 (m, 1H); **¹³C NMR** δ (CDCl₃) 167.7, 150.3, 144.0, 136.4, 126.3, 122.2, 121.1, 119.9, 119.8, 119.3, 118.8, 111.4, 48.2, 42.8, 33.7, 33.6, 32.4.

(4-(1H-indol-3-yl)piperidin-1-yl)(pyrazin-2-yl)methanone (2.34)

Reaction of compound **2.3** (20.0 mg, 0.10 mmol), pyrazine-2-carbonyl chloride (14.2 mg, 0.10 mmol), DIPEA (52.3 μ L, 0.30 mmol) and PyBOP (57.2 mg, 0.11 mmol) according to general procedure D, gave 30.6 mg (quantitative yield) of desired amide as a yellow solid.

ESI-MS: C₁₈H₁₈N₄O, *m/z* calculated for [M+H]⁺: 307.2, Found: 307.4.

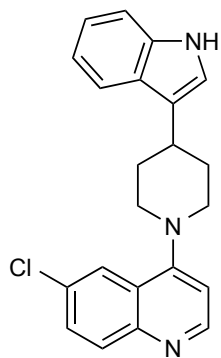
¹H NMR δ (CDCl₃) 8.94 (d, *J* = 1.5 Hz, 1H), 8.63 (d, *J* = 2.5 Hz, 1H), 8.56 (dd, *J* = 2.5, 1.5 Hz, 1H), 8.10 (s, NH), 7.64 (d, *J* = 7.9 Hz, 1H), 7.37 (d, *J* = 8.1 Hz, 1H), 7.20 (ddd, *J* = 8.1, 7.0, 1.2 Hz, 1H), 7.12 (ddd, *J* = 7.9, 7.0, 1.1 Hz, 1H), 6.98 (d, *J* = 2.3 Hz, 1H), 4.89 (d, *J* = 13.3 Hz, 1H), 4.05 (d, *J* = 13.5 Hz, 1H), 3.31 (td, *J* = 12.7, 2.8 Hz, 1H), 3.18 (tt, *J* = 11.8, 3.7 Hz, 1H), 3.04 (td, *J* = 12.9, 2.9 Hz, 1H), 2.23 (d, *J* = 13.2 Hz, 1H), 2.08 (d, *J* = 12.9 Hz, 1H), 1.95 – 1.76 (m, 2H); **¹³C NMR** δ (CDCl₃) 165.7, 150.4, 145.7, 145.6, 143.2, 138.2, 126.8, 122.6, 120.7, 120.3, 119.8, 119.3, 111.8, 48.5, 43.8, 34.2, 33.9, 32.9.

1,4-phenylenebis((4-(1H-indol-3-yl)piperidin-1-yl)methanone) (2.35)

Reaction of compound **2.3** (20.0 mg, 0.10 mmol), terephthalic acid (8.30 mg, 0.05 mmol), DIPEA (52.3 μ L, 0.30 mmol) and PyBOP (57.2 mg, 0.11 mmol) according to general procedure D, gave 53.0 mg (quantitative yield) of desired amide as a white solid.

ESI-MS: $C_{34}H_{34}N_4O_2$, m/z calculated for $[M+H]^+$: 531.3, Found: 531.5.

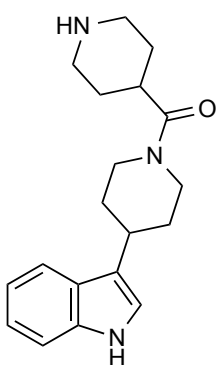
1H NMR δ (DMSO) 10.81 (s, 2H), 7.59 (d, $J = 7.9$ Hz, 2H), 7.50 (s, 4H), 7.33 (d, $J = 8.1$ Hz, 2H), 7.14 (d, $J = 2.3$ Hz, 2H), 7.05 (ddd, $J = 8.1, 7.0, 1.2$ Hz, 2H), 6.96 (ddd, $J = 7.9, 7.0, 1.1$ Hz, 2H), 4.61 (br, 2H), 3.70 (br, 2H), 3.26 (br, 2H), 3.09 (tt, $J = 11.9, 3.6$ Hz, 2H), 2.97 (br, 2H), 2.07 (br, 1H), 1.93 (br, 1H), 1.70 – 1.60 (m, 4H); **^{13}C NMR** δ (DMSO) 168.8, 137.8, 136.8, 127.3, 126.6, 121.4, 121.3, 119.4, 118.9, 118.6, 111.9, 49.1, 48.2, 33.6, 33.1, 14.4.

4-(4-(1H-indol-3-yl)piperidin-1-yl)-6-chloroquinoline (2.36)

To a solution of compound **2.3** (20 mg, 0.10 mmol) and DIPEA (52.3 μ L, 0.30 mmol) in isopropanol (2 mL) was added 4,6-dichloroquinoline (19.8 mg, 0.10 mmol). The reaction mixture stirred under reflux for 56 h. The solvent was removed under reduced pressure and the crude product was purified by flash chromatography using a gradient elution of ethyl acetate/acetonitrile:water:methanol (1:1:1) to afford compound **11** as a yellow oil (9.05 mg, 25%).

ESI-MS: $C_{22}H_{20}ClN_3$, m/z calculated for $[M+H]^+$: 362.1, Found: 361.1.

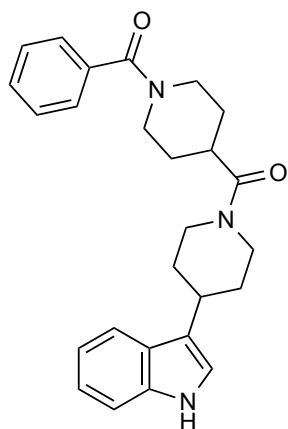
1H NMR (DMSO) 10.89 (s, NH), 8.66 (d, $J = 6.9$ Hz, 1H), 8.22 – 8.09 (m, 2H), 8.02 (dd, $J = 9.1, 1.3$ Hz, 1H), 7.63 (d, $J = 7.8$ Hz, 1H), 7.36 (d, $J = 8.1$ Hz, 1H), 7.28 (d, $J = 7.0$ Hz, 1H), 7.18 (d, $J = 2.3$ Hz, 1H), 7.08 (ddd, $J = 7.8, 7.0, 1.3$ Hz, 1H), 7.00 (m, 1H), 4.28 (d, $J = 13.1$ Hz, 2H), 3.70 (td, $J = 12.8, 2.9$ Hz, 2H), 3.29 (tt, $J = 11.4, 3.8$ Hz, 1H), 2.20 (dd, $J = 11.9, 2.0$ Hz, 2H), 2.02 (qd, $J = 12.9, 2.4$ Hz, 2H); **^{13}C NMR** δ (DMSO) 159.5, 142.0, 138.5, 136.4, 133.5, 131.9, 130.3, 126.1, 125.3, 121.0, 120.9, 120.0, 118.6, 118.4, 118.2, 111.5, 106.2, 52.4, 32.4.

(4-(1H-indol-3-yl)piperidin-1-yl)(piperidin-4-yl)methanone (2.37)

Compound **2.4** (200 mg, 0.49 mmol) was dissolved in a solution of 2 M HCl in MeOH (6 mL) and stirred at room temperature for 40 min. The solvent was removed under reduced pressure and the crude product was purified by reverse phase flash chromatography using a gradient elution of water/acetonitrile to afford the desired product as a yellow solid (151 mg, quantitative yield).

ESI-MS: C₁₉H₂₅N₃O, *m/z* calculated for [M+H]⁺: 312.2, Found: 312.4.

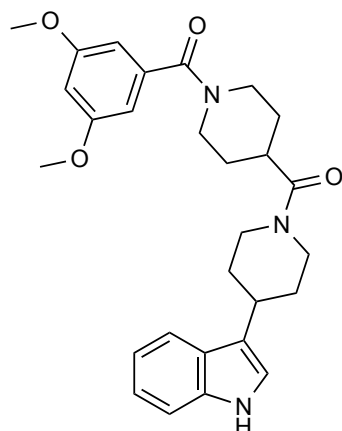
¹H NMR δ (MeOD) 8.49 (s, NH), 7.59 (d, *J* = 7.9 Hz, 1H), 7.36 (d, *J* = 8.1 Hz, 1H), 7.10 (ddd, *J* = 8.1, 6.9, 1.2 Hz, 1H), 7.04 (s, 1H), 7.01 (ddd, *J* = 7.9, 6.9, 1.1 Hz, 1H), 4.66 (d, *J* = 13.3 Hz, 1H), 4.21 (d, *J* = 13.7 Hz, 1H), 3.49 (m, 2H), 3.39 (m, 1H), 3.24 – 3.08 (m, 4H), 2.87 (td, *J* = 12.9, 2.8 Hz, 1H), 2.21 (d, *J* = 13.1 Hz, 2H), 2.12 (d, *J* = 13.9 Hz, 2H), 2.07 – 1.86 (m, 4H), 1.70 (m, 2H); **¹³C NMR** δ (MeOD) 173.7, 138.3, 127.7, 122.3, 121.2, 120.3, 119.5, 119.4, 112.3, 47.5, 44.4, 43.9, 36.7, 35.2, 34.9, 33.9, 26.8, 26.6, 25.9.

(4-(1H-indol-3-yl)piperidin-1-yl)(1-benzoylpiperidin-4-yl)methanone (2.38)

Reaction of compound **2.37** (20 mg, 0.06 mmol) and benzoyl chloride (7.56 mg, 0.05 mmol) according to general procedure B, gave 22.4 mg (80%) of desired product as a beige solid.

ESI-MS: C₂₆H₂₉N₃O₂, *m/z* calculated for [M+H]⁺: 416.2, Found: 416.2.

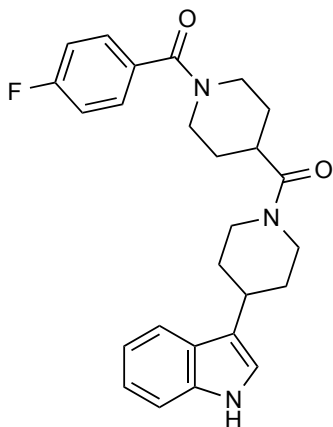
¹H NMR δ (CDCl₃) 8.66 (s, NH), 7.60 (m, 1H), 7.47 – 7.36 (m, 5H), 7.33 (d, *J* = 8.2 Hz, 1H), 7.17 (ddd, *J* = 8.2, 7.0, 1.2 Hz, 1H), 7.10 (ddd, *J* = 8.0, 7.0, 1.1 Hz, 1H), 6.90 (s, 1H), 4.76 (m, 1H), 4.52 (br, 1H), 4.03 (m, 1H), 3.87 (br, 1H), 3.25 (t, *J* = 12.1 Hz, 2H), 3.09 (tt, *J* = 11.9, 3.7 Hz, 1H), 2.96 – 2.70 (m, 5H), 2.23 – 2.05 (m, 2H), 1.92 – 1.80 (m, 2H), 1.74 – 1.59 (m, 2H); **¹³C NMR** δ (CDCl₃) 172.6, 170.7, 136.6, 135.9, 133.1, 129.7, 128.6, 128.4, 126.9, 126.3, 121.9, 120.0, 119.8, 119.1, 118.8, 111.5, 51.9, 47.4, 46.3, 42.9, 42.0, 40.9, 38.4, 33.9, 32.5, 28.9.

(4-(1H-indol-3-yl)piperidin-1-yl)(1-(3,5-dimethoxybenzoyl)piperidin-4-yl)methanone (2.39)

Reaction of compound **2.37** (20.0 mg, 0.06 mmol) and 3,5-dimethoxybenzoyl chloride (10.8 mg, 0.05 mmol) according to general procedure B, gave 19.2 mg (75%) of desired product as a beige oil.

ESI-MS: C₂₈H₃₃N₃O₄, *m/z* calculated for [M+H]⁺: 476.3, Found: 476.4.

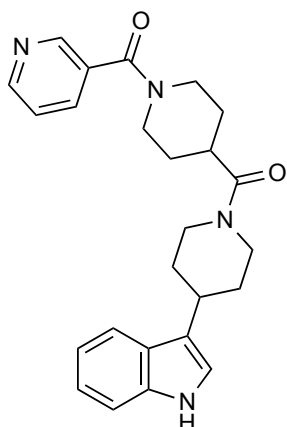
¹H NMR δ (MeOD) 7.61 (d, *J* = 8.2 Hz, 1H), 7.36 (d, *J* = 8.1 Hz, 1H), 7.11 (ddd, *J* = 8.2, 7.0, 1.2 Hz, 1H), 7.07 – 7.00 (m, 2H), 6.61 (dd, *J* = 2.9, 2.3 Hz, 1H), 6.57 (d, *J* = 2.3 Hz, 1H), 4.70 (d, *J* = 13.6 Hz, 2H), 4.24 (d, *J* = 13.1 Hz, 1H), 3.84 (s, 6H), 3.80 (br, 1H), 3.30 – 3.07 (m, 3H), 3.01 (d, *J* = 11.6 Hz, 1H), 2.90 (m, 1H), 2.22 (d, *J* = 12.6 Hz, 1H), 2.14 (d, *J* = 12.6 Hz, 1H), 1.99 – 1.55 (m, 7H); **¹³C NMR** δ (MeOD) 174.8, 172.1, 162.6, 138.9, 138.3, 127.7, 122.3, 121.2, 120.4, 119.5, 119.4, 112.3, 105.5, 102.5, 56.0, 47.4, 43.9, 39.3, 35.3, 35.1, 33.9.

(4-(1H-indol-3-yl)piperidin-1-yl)(1-(4-fluorobenzoyl)piperidin-4-yl)methanone (2.40)

Reaction of compound **2.37** (20.0 mg, 0.06 mmol) and 4-fluorobenzoyl chloride (8.53 mg, 0.05 mmol) according to general procedure B, gave 17.5 mg (75%) of desired product as a beige solid.

ESI-MS: C₂₆H₂₈FN₃O₂, *m/z* calculated for [M+H]⁺: 434.2, Found: 434.2.

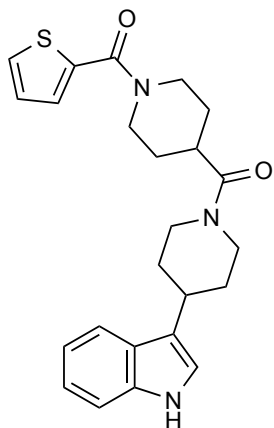
¹H NMR δ (CDCl₃) 8.11 (s, NH), 7.62 (d, *J* = 7.9 Hz, 1H), 7.46 – 7.39 (m, 2H), 7.37 (d, *J* = 8.1 Hz, 1H), 7.20 (dd, *J* = 7.5, 7.1 Hz, 1H), 7.14 – 7.06 (m, 3H), 6.95 (d, *J* = 2.4 Hz, 1H), 4.78 (d, *J* = 12.4 Hz, 1H), 4.67 (br, 1H), 4.03 (d, *J* = 12.4 Hz, 1H), 3.89 (br, 1H), 3.27 (t, *J* = 12.9 Hz, 1H), 3.12 (tt, *J* = 11.9, 3.7 Hz, 1H), 3.01 (br, 1H), 2.93 – 2.69 (m, 2H), 2.19 (d, *J* = 12.3 Hz, 1H), 2.12 (d, *J* = 12.9 Hz, 1H), 1.96 – 1.56 (m, 7H); **¹³C NMR** δ (CDCl₃) 172.3, 169.6, 163.4 (d, ¹*J*_{CF} = 248 Hz), 136.4, 132.0, 129.2, 126.3, 122.2, 120.2, 119.7, 119.3, 118.8, 115.7, 115.5, 111.4, 46.2, 42.7, 40.9, 38.4, 33.9, 32.4.

(4-(1H-indol-3-yl)piperidin-1-yl)(1-nicotinoylpiperidin-4-yl)methanone (2.41)

Reaction of compound **2.6** (20 mg, 0.06 mmol), nicotinoyl chloride (7.61 mg, 0.05 mmol) and DIPEA (52.3 μ L, 0.16 mmol) according to general procedure C, gave 5.6 mg (25%) of desired product as an off-white solid.

ESI-MS: $C_{25}H_{28}N_4O_2$, m/z calculated for $[M+H]^+$: 417.2, Found: 417.4.

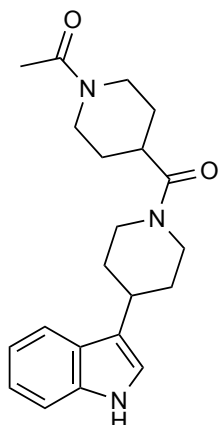
1H NMR δ (CDCl₃) 8.73 – 8.60 (m, 2H), 8.23 (s, NH), 7.76 (dt, $J = 8.0$, 1.9 Hz, 1H), 7.61 (dd, $J = 8.2$, 1.2 Hz, 1H), 7.36 (m, 2H), 7.20 (ddd, $J = 8.2$, 7.0, 1.2 Hz, 1H), 7.11 (ddd, $J = 8.0$, 7.0, 1.1 Hz, 1H), 6.95 (d, $J = 2.9$ Hz, 1H), 4.78 (d, $J = 12.9$ Hz, 1H), 4.69 (br, 1H), 4.02 (d, $J = 12.7$ Hz, 1H), 3.79 (br, $J = 1$ Hz), 3.28 (m, 1H), 3.12 (tt, $J = 11.9$, 3.8 Hz, 1H), 3.01 (br, 1H), 2.86 (td, $J = 9.1$, 4.6 Hz, 1H), 2.77 (t, $J = 11.7$ Hz, 1H), 2.19 (d, $J = 12.4$ Hz, 1H), 2.12 (d, $J = 12.7$ Hz, 1H), 1.95 – 1.79 (m, 3H), 1.77 – 1.58 (m, 4H); **^{13}C NMR δ (CDCl₃)** 172.1, 167.8, 150.7, 147.8, 136.5, 134.9, 131.9, 126.3, 123.5, 122.1, 120.1, 119.8, 119.3, 118.8, 111.4, 50.8, 46.2, 42.7, 38.2, 33.9, 32.4.

(4-(1H-indol-3-yl)piperidin-1-yl)(1-(thiophene-2-carbonyl)piperidin-4-yl)methanone (2.42)

Reaction of compound **2.6** (20 mg, 0.06 mmol) and thiophene-2-carbonyl chloride (7.88 mg, 0.05 mmol) according to general procedure B, gave 16.6 mg (73%) of desired product as a white solid.

ESI-MS: $C_{24}H_{27}N_3O_2S$, m/z calculated for $[M+H]^+$: 422.2, Found: 422.2.

1H NMR δ (CDCl₃) 8.19 (s, NH), 7.62 (d, $J = 7.9$ Hz, 1H), 7.44 (d, $J = 5.0$ Hz, 1H), 7.37 (d, $J = 8.1$ Hz, 1H), 7.30 (d, $J = 3.7$ Hz, 1H), 7.20 (ddd, $J = 8.1$, 7.0, 1.2 Hz, 1H), 7.12 (ddd, $J = 7.9$, 7.0, 1.0 Hz, 1H), 7.04 (dd, $J = 5.0$, 3.7 Hz, 1H), 6.96 (s, 1H), 4.47 (d, $J = 13.9$ Hz, 2H), 3.18–3.01 (m, 4H), 2.91–2.84 (m, 2H), 2.16 (d, $J = 12.2$ Hz, 2H), 2.03–1.52 (m, 8H); **^{13}C NMR δ (CDCl₃)** 172.8, 164.2, 137.6, 136.9, 129.1, 128.9, 127.1, 126.8, 122.6, 120.6, 120.2, 119.7, 119.3, 111.8, 52.4, 41.4, 38.8, 34.3, 29.2, 28.7.

1-(4-(4-(1H-indol-3-yl)piperidine-1-carbonyl)piperidin-1-yl)ethan-1-one (2.43)

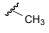
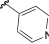
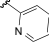
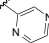
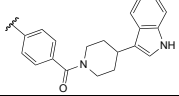
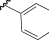
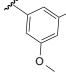
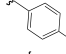
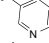
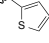
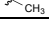
Reaction of compound **2.6** (20 mg, 0.06 mmol) and acetyl chloride (4.21 mg, 0.05 mmol) according to general procedure B, gave 7.62 mg (40%) of desired product as a white solid.

ESI-MS: C₂₁H₂₇N₃O₂, *m/z* calculated for [M+H]⁺: 354.2, Found: 354.2.

¹H NMR δ (CDCl₃) 8.15 (s, NH), 7.62 (d, *J* = 8.0 Hz, 1H), 7.38 (d, *J* = 8.2 Hz, 1H), 7.20 (ddd, *J* = 8.2, 7.0, 1.2 Hz, 1H), 7.12 (ddd, *J* = 8.0, 7.0, 1.1 Hz, 1H), 6.96 (d, *J* = 2.4 Hz, 1H), 4.77 (d, *J* = 13.0 Hz, 1H), 4.60 (d, *J* = 13.2 Hz, 1H), 4.03 (d, *J* = 13.1 Hz, 1H), 3.90 (d, *J* = 13.5 Hz, 1H), 3.26 (t, *J* = 12.9 Hz, 1H), 3.17 – 3.08 (m, 2H), 2.88 – 2.66 (m, 2H), 2.24–2.16 (m, 2H), 2.10 (s, 3H), 1.91 (m, 1H), 1.83–1.56 (m, 6H); **¹³C NMR** δ (CDCl₃) 172.9, 169.4, 136.9, 126.8, 122.6, 120.7, 120.2, 119.7, 119.3, 111.8, 49.6, 46.7, 46.3, 43.1, 41.5, 38.8, 34.4, 32.8, 26.1, 25.4, 21.9.

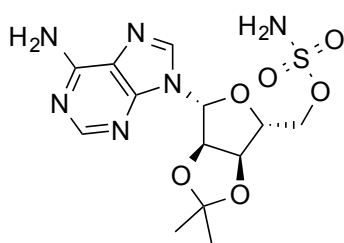
Table 6.1 – Final step and global yield of synthesized compounds.

Series	Compound	R	Yield (%)	Global Yield (%)
Amine	2.7		79	76
	2.8		76	73
	2.9		99	95
	2.10		55	53
	2.11		53	51
	2.12		55	53
	2.13		42	40
	2.14		99	95
	2.15		60	58
	2.16		72	69
	2.17		69	66
	2.18		25	24
	2.19		30	29
	2.20		38	36
	2.21		54	52
2.22		97	93	
2.23		65	62	
2.24		Quant.	96	
2.25		98	94	
Amide	2.26		55	53
	2.27		Quant.	96
	2.28		95	91
	2.29		25	24
	2.30		66	63

Series	Compound	R	Yield (%)	Global Yield (%)
Amide	2.31		73	70
	2.32		60	58
	2.33		95	91
	2.34		Quant.	96
	2.35		Quant.	6.1.2.1 96
	2.36	-	25	24
Bis-amide	2.38		80	77
	2.39		75	72
	2.40		75	72
	2.41		10	10
	2.42		73	70
	2.43		40	38

6.1.3 Synthesis of Sulfamoyl Aminoacyl AMP Analogs

2',3'-*O*-Isopropylidene-5'-*O*-sulfamoyladenosine (**3.17**)



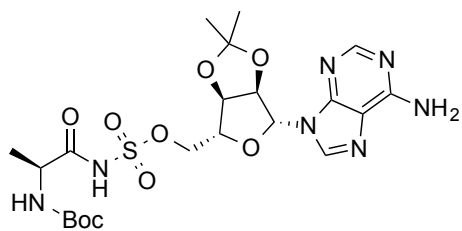
To a magnetically stirred solution of 2',3'-*O*-isopropylideneadenosine (1.00 g, 3.26 mmol) in DME (100 mL) at 0 °C, was added NaH (196 mg of a 60% suspension in mineral oil, 4.89 mmol) under nitrogen atmosphere. After 30 min at 0 °C, a solution of sulfamoyl chloride (565 mg, 4.89 mmol) in DME (30 mL) was added over 5 min. After warming to r.t. and stirring for 4 h, anhydrous methanol (50 mL) was added and the resulting mixture was concentrated *in vacuo* to render a viscous oil. The crude product was purified by flash chromatography with ethyl acetate/acetonitrile:water:methanol (1:1:1) to afford the desired product as a white crystalline solid (0.8 g, 2.1 mmol, 65% yield).

ESI-MS: C₁₃H₁₈N₆O₆S, *m/z* calculated for [M+H]⁺: 387.1, Found: 387.1.

¹H NMR δ (DMSO) 8.31 (s, 1H), 8.17 (s, 1H), 7.61 (brs, 2H), 7.36 (brs, 2H), 6.23 (d, *J* = 2.3 Hz, 1H), 5.44 (dd, *J* = 6.3, 2.3 Hz, 1H), 5.08 (dd, *J* = 6.3, 3.1 Hz, 1H), 4.44 (m, 1H), 4.23 (dd, *J* = 10.8, 5.6 Hz, 1H), 4.15 (dd, *J* = 10.8, 5.6 Hz, 1H), 1.55 (s, 3H), 1.34 (s, 3H). **¹³C NMR** δ (DMSO) 158.8, 150.5, 141.7, 140.7, 121.3, 115.1, 93.6, 87.2, 86.6, 81.8, 59.2, 26.6, 25.2.

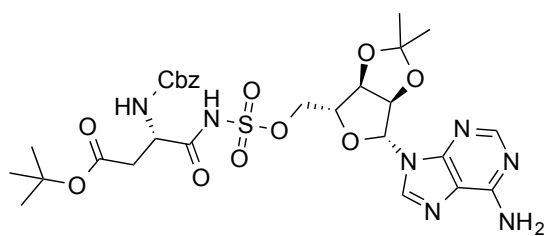
General Procedure E:

To a solution of sulfamoyladenosine **3.17** (250 mg, 1 equiv.) in DMF (10 mL) was added the *N*-protected succinimide activated amino acid (1 equiv.) and DBU (0.23 mL, 2.4 equiv.). The reaction mixture stirred at r.t. for 2 h and the solvent was removed under reduced pressure. The crude product was purified by flash chromatography using ethyl acetate/acetonitrile:water:methanol (1:1:1) to afford the desired product.

2',3'-O-Isopropylidene-5'-O-[N-(Boc-L-alanyl)-sulfamoyl]adenosine (3.18)

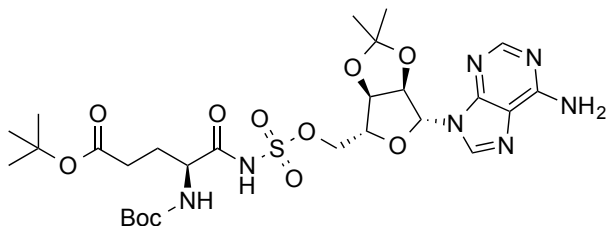
Reaction of compound **3.17** (250 mg, 0.06 mmol) and Boc-L-alanine *N*-hydroxysuccinimide ester (185.4 mg, 0.07 mmol) according to general procedure E, gave 151.6 mg (42%) of desired product as a white solid.

ESI-MS: C₂₁H₃₁N₇O₉S, *m/z* calculated for [M-H]⁻: 556.2, Found: 556.2; *m/z* calculated for [M+H]⁺: 558.2, Found: 558.2.

2',3'-O-Isopropylidene-5'-O-[N-(Z-O-tBu-L-aspartyl)-sulfamoyl]adenosine (3.19)

Reaction of compound **3.17** (250 mg, 0.06 mmol) and Z-O-tButyl-L- aspartate *N*-hydroxysuccinimide ester (272.2 mg, 0.07 mmol) according to general procedure E, gave 179.2 mg (40%) of desired product as a white solid.

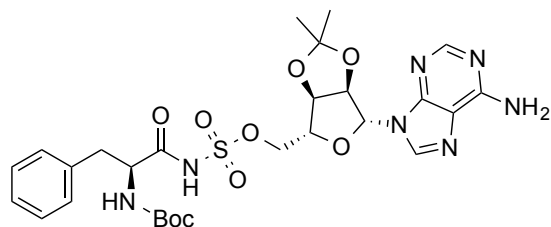
ESI-MS: C₂₉H₃₇N₇O₁₁S, *m/z* calculated for [M-H]⁻: 690.2, Found: 690.2; *m/z* calculated for [M+H]⁺: 692.2, Found: 692.2.

2',3'-O-Isopropylidene-5'-O-[N-(Boc-O-tBu-L-glutamyl)-sulfamoyl]adenosine (3.20)

Reaction of compound **3.17** (250 mg, 0.06 mmol) and Boc-O-tButyl-L- glutamate *N*-hydroxysuccinimide ester (259.3 mg, 0.07 mmol) according to general procedure E, gave 100 mg (23%) of desired product as a white solid.

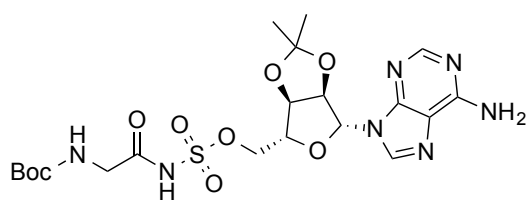
solid.

ESI-MS: C₂₇H₄₁N₇O₁₁S, *m/z* calculated for [M-H]⁻: 670.3, Found: 670.3; *m/z* calculated for [M+H]⁺: 672.3, Found: 672.3.

2',3'-O-Isopropylidene-5'-O-[N-(Boc-L-phenylalanyl)-sulfamoyl]adenosine (3.21)

Reaction of compound **3.17** (250 mg, 0.06 mmol) and Boc-L-phenylalanine *N*-hydroxysuccinimide ester (234.6 mg, 0.07 mmol) according to general procedure E, gave 160 mg (39%) of desired product as a white solid.

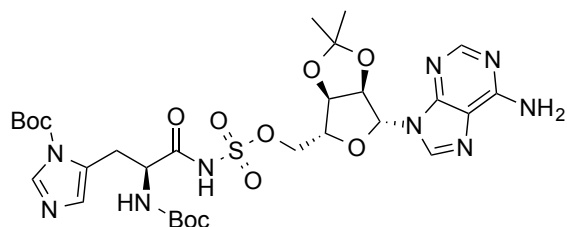
ESI-MS: C₂₇H₃₅N₇O₉S, *m/z* calculated for [M-H]⁻: 632.2, Found: 632.2; *m/z* calculated for [M+H]⁺: 634.2, Found: 634.2.

2',3'-O-Isopropylidene-5'-O-[N-(Boc-L-glyciny)]-sulfamoyl]adenosine (3.22)

Reaction of compound **3.17** (250 mg, 0.06 mmol) and Boc-L-glycine *N*-hydroxysuccinimide ester (176.3 mg, 0.07 mmol) according to general procedure E, gave 147.8 mg (42%) of desired product as a white solid.

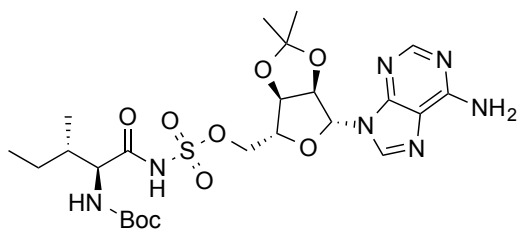
solid.

ESI-MS: C₂₀H₂₉N₇O₉S, *m/z* calculated for [M-H]⁻: 542.2, Found: 542.2; *m/z* calculated for [M+H]⁺: 544.2, Found: 544.2.

2',3'-O-Isopropylidene-5'-O-[N-(Bis-Boc-L-histidinyl)-sulfamoyl]adenosine (3.23)

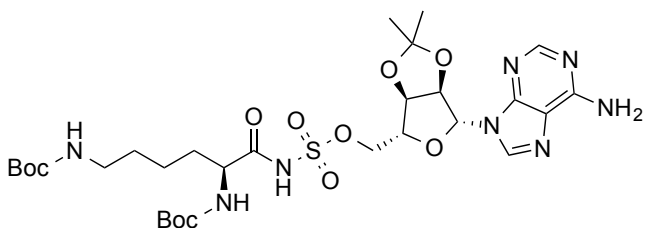
Reaction of compound **3.17** (250 mg, 0.06 mmol) and Bis-Boc-L-histidine *N*-hydroxysuccinimide ester (293 mg, 0.07 mmol) according to general procedure E, gave 135.9 mg (29%) of desired product as a white solid.

ESI-MS: C₂₉H₄₁N₉O₁₁S, *m/z* calculated for [M-H]⁻: 722.3, Found: 722.3; *m/z* calculated for [M+H]⁺: 724.3, Found: 724.3.

2',3'-O-Isopropylidene-5'-O-[N-(Boc-L-isoleucyl)-sulfamoyl]adenosine (3.24)

Reaction of compound **3.17** (250 mg, 0.06 mmol) and Boc-L-isoleucine *N*-hydroxysuccinimide ester (212.6 mg, 0.07 mmol) according to general procedure E, gave 124.2 mg (32%) of desired product as a white solid.

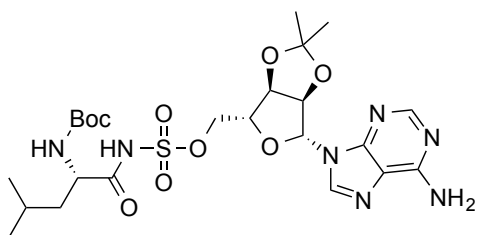
ESI-MS: C₂₄H₃₇N₇O₉S, *m/z* calculated for [M-H]⁻: 598.2, Found: 598.2; *m/z* calculated for [M+H]⁺: 600.2, Found: 600.2.

2',3'-O-Isopropylidene-5'-O-[N-(Bis-Boc-L-lysyl)-sulfamoyl]adenosine (3.25)

Reaction of compound **3.17** (250 mg, 0.06 mmol) and Bis-Boc-L-lysine *N*-hydroxysuccinimide ester (287.1 mg, 0.07 mmol) according to general procedure E, gave 101.8 mg (22%) of desired product as

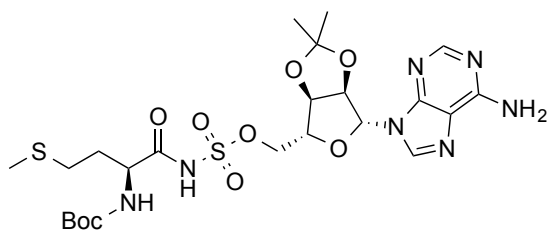
a white solid.

ESI-MS: C₂₉H₄₆N₈O₁₁S, *m/z* calculated for [M-H]⁻: 713.3, Found: 713.3; *m/z* calculated for [M+H]⁺: 715.3, Found: 715.3.

2',3'-O-Isopropylidene-5'-O-[N-(Boc-L-leucyl)-sulfamoyl]adenosine (3.26)

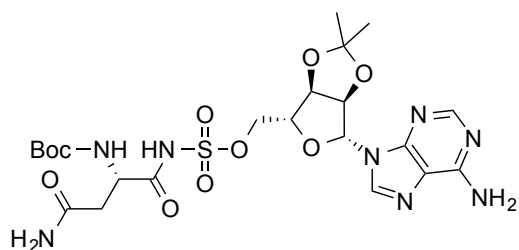
Reaction of compound **3.17** (250 mg, 0.06 mmol) and Boc-L-leucine *N*-hydroxysuccinimide ester (212.6 mg, 0.07 mmol) according to general procedure E, gave 120.4 mg (31%) of desired product as a white solid.

ESI-MS: C₂₄H₃₇N₇O₉S, *m/z* calculated for [M-H]⁻: 598.2, Found: 598.2; *m/z* calculated for [M+H]⁺: 600.2, Found: 600.2.

2',3'-O-Isopropylidene-5'-O-[N-(Boc-L-methionyl)-sulfamoyl]adenosine (3.27)

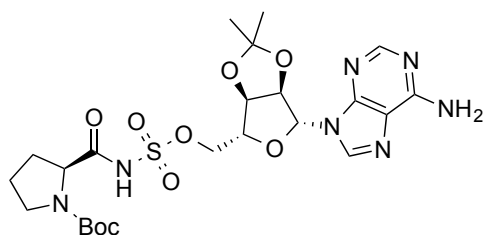
Reaction of compound **3.17** (250 mg, 0.06 mmol) and Boc-L-methionine *N*-hydroxysuccinimide ester (224.3 mg, 0.07 mmol) according to general procedure E, gave 223.9 mg (56%) of desired product as a white solid.

ESI-MS: C₂₃H₃₅N₇O₉S₂, *m/z* calculated for [M-H]⁻: 616.2, Found: 616.2; *m/z* calculated for [M+H]⁺: 618.2, Found: 618.2.

2',3'-O-Isopropylidene-5'-O-[N-(Boc-L-asparginyl)-sulfamoyl]adenosine (3.28)

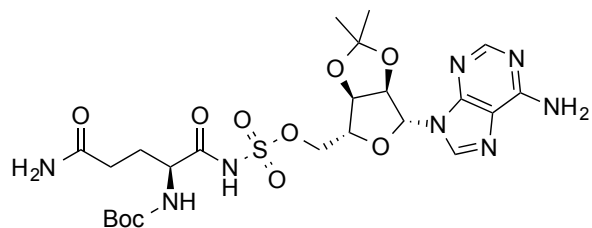
Reaction of compound **3.17** (250 mg, 0.06 mmol) and Z-O-tButyl-L-Asparagine *N*-hydroxysuccinimide ester (213.2 mg, 0.07 mmol) according to general procedure E, gave 58.3 mg (15%) of desired product as a white solid.

ESI-MS: C₂₂H₃₂N₈O₁₀S, *m/z* calculated for [M-H]⁻: 599.2, Found: 599.2; *m/z* calculated for [M+H]⁺: 601.2, Found: 601.2.

2',3'-O-Isopropylidene-5'-O-[N-(Boc-L-prolyl)-sulfamoyl]adenosine (3.29)

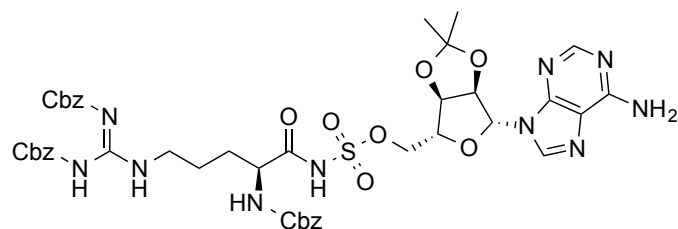
Reaction of compound **3.17** (250 mg, 0.06 mmol) and Boc-L-proline *N*-hydroxysuccinimide ester (202.2 mg, 0.07 mmol) according to general procedure E, gave 151.2 mg (40%) of desired product as a white solid.

ESI-MS: C₂₃H₃₃N₇O₉S, *m/z* calculated for [M-H]⁻: 582.2, Found: 582.2; *m/z* calculated for [M+H]⁺: 584.2, Found: 584.2.

2',3'-O-Isopropylidene-5'-O-[N-(Boc-L-glutamyl)-sulfamoyl]adenosine (3.30)

Reaction of compound **3.17** (250 mg, 0.06 mmol) and Boc-L-glutamine *N*-hydroxysuccinimide ester (222.3 mg, 0.07 mmol) according to general procedure E, gave 119.4 mg (30%) of desired product as a white solid.

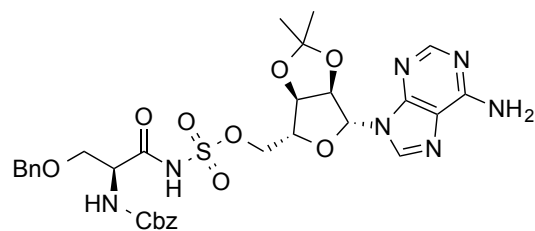
ESI-MS: C₂₃H₃₄N₈O₁₀S, *m/z* calculated for [M-H]⁻: 613.2, Found: 613.2; *m/z* calculated for [M+H]⁺: 615.2, Found: 615.2.

2',3'-O-Isopropylidene-5'-O-[N-(Tris-Z-L-arginyl)-sulfamoyl]adenosine (3.31)

Reaction of compound **3.17** (250 mg, 0.06 mmol) and Tris-Z-L-arginine *N*-hydroxysuccinimide ester (436.2 mg, 0.07 mmol) according to general procedure E, gave 238.6 mg (39%) of desired product

as a white solid.

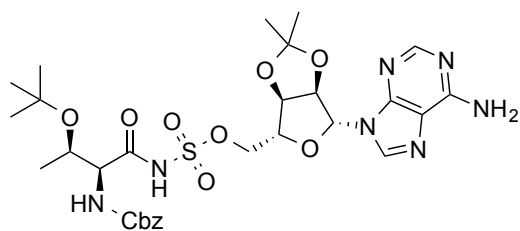
ESI-MS: C₄₃H₄₈N₁₀O₁₃S, *m/z* calculated for [M-H]⁻: 943.3, Found: 943.3; *m/z* calculated for [M+H]⁺: 945.3, Found: 945.3.

2',3'-O-Isopropylidene-5'-O-[N-(Cbz-O-Bn-L-seryl)-sulfamoyl]adenosine (3.32)

Reaction of compound **3.17** (250 mg, 0.06 mmol) and Cbz-O-benzyl-L-serine *N*-hydroxysuccinimide ester (254.1 mg, 0.07 mmol) according to general procedure E, gave 296.5 mg (69%) of desired product as a white solid.

ESI-MS: C₃₁H₃₅N₇O₁₀S, *m/z* calculated for [M-H]⁻: 696.2, Found: 696.2; *m/z* calculated for [M+H]⁺: 698.2, Found: 698.2.

2',3'-O-Isopropylidene-5'-O-[N-(Cbz-O-tBu-L-threonyl)-sulfamoyl]adenosine (3.33)



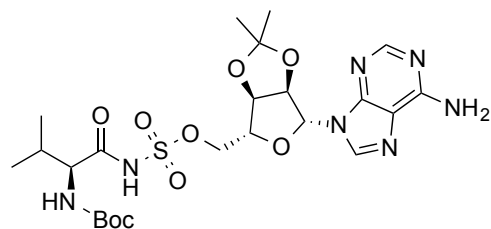
Reaction of compound **3.17** (250 mg, 0.06 mmol) and Cbz-O-tButyl-L-threonine *N*-hydroxysuccinimide ester

(263.2 mg, 0.07 mmol) according to general procedure E, gave 201.86 mg (46%) of desired

product as a white solid.

ESI-MS: C₂₉H₃₉N₇O₁₀S, *m/z* calculated for [M-H]⁻: 676.3, Found: 676.3; *m/z* calculated for [M+H]⁺: 678.3, Found: 678.3.

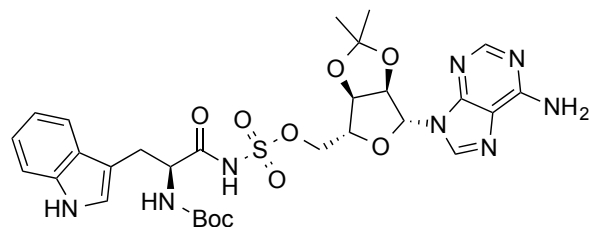
2',3'-O-Isopropylidene-5'-O-[N-(Boc-L-valyl)-sulfamoyl]adenosine (3.34)



Reaction of compound **3.17** (250 mg, 0.06 mmol) and Boc-L-valine *N*-hydroxysuccinimide ester (203.5 mg, 0.07 mmol) according to general procedure E, gave 144.1 mg (38%) of desired product as a white solid.

ESI-MS: C₂₃H₃₅N₇O₉S, *m/z* calculated for [M-H]⁻: 584.2, Found: 584.2; *m/z* calculated for [M+H]⁺: 586.2, Found: 586.2.

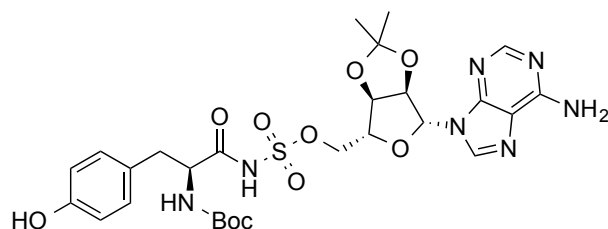
2',3'-O-Isopropylidene-5'-O-[N-(Boc-L-tryptophanyl)-sulfamoyl]adenosine (3.35)



Reaction of compound **3.17** (250 mg, 0.06 mmol) and Boc-L-tryptophan *N*-hydroxysuccinimide ester (259.9 mg, 0.07 mmol) according to general procedure E, gave 52.3 mg (12%) of desired product as a white

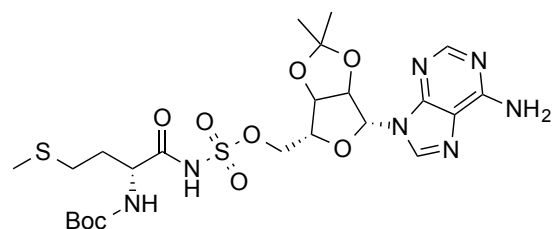
solid.

ESI-MS: C₂₉H₃₆N₈O₉S, *m/z* calculated for [M-H]⁻: 671.2, Found: 671.2; *m/z* calculated for [M+H]⁺: 673.2, Found: 673.2.

2',3'-O-Isopropylidene-5'-O-[N-(Boc-L-tyrosyl)-sulfamoyl]adenosine (3.36)

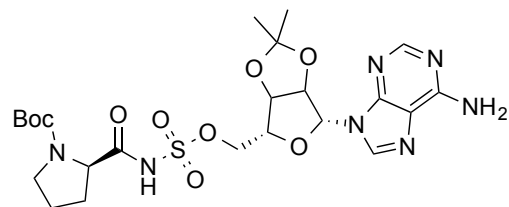
Reaction of compound **3.17** (250 mg, 0.06 mmol) and Boc-L-tyrosine *N*-hydroxysuccinimide ester (245 mg, 0.07 mmol) according to general procedure E, gave 201.9 mg (48%) of desired product as a white solid.

ESI-MS: C₂₇H₃₅N₇O₁₀S, *m/z* calculated for [M-H]⁻: 648.2, Found: 648.2; *m/z* calculated for [M+H]⁺: 650.2, Found: 650.2.

2',3'-O-Isopropylidene-5'-O-[N-(Boc-D-methionyl)-sulfamoyl]adenosine (3.37)

Reaction of compound **3.17** (250 mg, 0.06 mmol) and Boc-D-methionine *N*-hydroxysuccinimide ester (224.3 mg, 0.07 mmol) according to general procedure E, gave 75.99 mg (19%) of desired product as a white solid.

ESI-MS: C₂₃H₃₅N₇O₉S₂, *m/z* calculated for [M-H]⁻: 616.2, Found: 616.2; *m/z* calculated for [M+H]⁺: 618.2, Found: 618.2.

2',3'-O-Isopropylidene-5'-O-[N-(Boc-D-prolyl)-sulfamoyl]adenosine (3.38)

Reaction of compound **3.17** (250 mg, 0.06 mmol) and Boc-D-proline *N*-hydroxysuccinimide ester (202.2 mg, 0.07 mmol) according to general procedure E, gave 132.3 mg (35%) of desired product as a white solid.

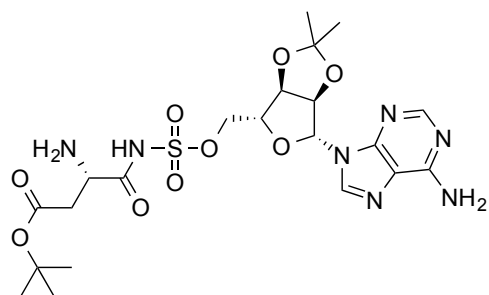
ESI-MS: C₂₃H₃₃N₇O₉S, *m/z* calculated for [M-H]⁻: 582.2, Found: 582.2; *m/z* calculated for [M+H]⁺: 584.2, Found: 584.2.

General Procedure F:

To a solution of the acylsulfamate intermediate (50 mg) in DMF (2 mL) was added 10% Pd/C (50% m/m). The reaction was placed under 1 atm of H₂ (balloon) and stirred at r.t. for 8 h. The reaction mixture was filtered over Celite™ and washed with methanol. The solvent was

removed under reduced pressure and the crude product purified by reverse phase flash chromatography using water/acetonitrile to afford the desired product.

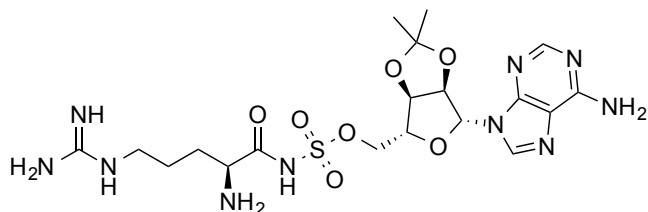
2',3'-O-Isopropylidene-5'-O-[N-(O-*t*Bu-L-aspartyl)-sulfamoyl]adenosine (3.39)



Compound **3.39** was obtained according to general procedure F, as a white solid (2.1 mg, 5%).

ESI-MS: C₂₁H₃₁N₇O₉S, *m/z* calculated for [M-H]⁻: 556.2, Found: 556.2; *m/z* calculated for [M+H]⁺: 558.2, Found: 558.2.

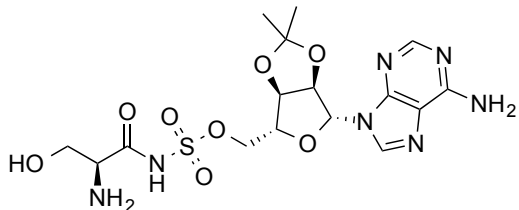
2',3'-O-Isopropylidene-5'-O-[N-(L-arginyl)-sulfamoyl]adenosine (3.40)



Compound **3.40** was obtained according to general procedure F, as a white solid (7.2 mg, 25%).

ESI-MS: C₁₉H₃₀N₁₀O₇S, *m/z* calculated for [M-H]⁻: 541.2, Found: 541.2; *m/z* calculated for [M+H]⁺: 543.2, Found: 543.2.

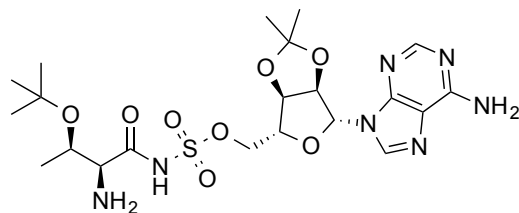
2',3'-O-Isopropylidene-5'-O-[N-(L-seryl)-sulfamoyl]adenosine (3.41)



Compound **3.41** was obtained according to general procedure F, as a white solid (2.14 mg, 60%).

ESI-MS: C₁₆H₂₃N₇O₈S, *m/z* calculated for [M-H]⁻: 472.1, Found: 472.1; *m/z* calculated for [M+H]⁺: 474.1, Found: 474.1.

2',3'-O-Isopropylidene-5'-O-[N-(O-*t*Bu-L-threonyl)-sulfamoyl]adenosine (3.42)

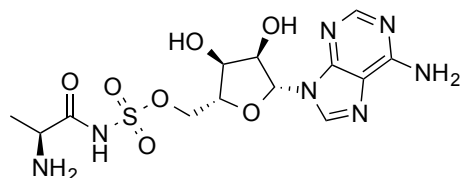


Compound **3.42** was obtained according to general procedure F, as a white solid (2.2 mg, 56%).

ESI-MS: C₂₁H₃₃N₇O₈S, *m/z* calculated for [M-H]⁻: 542.2, Found: 542.2; *m/z* calculated for [M+H]⁺: 544.2, Found: 544.2.

General Procedure G:

A solution of the acylsulfamate intermediate (50 mg) and 2.5 mL of TFA: H₂O (5:1) was stirred at room temperature for 30 min. The solvent was removed under reduced pressure. The crude product was purified by reverse phase flash chromatography using water/acetonitrile to afford the desired product.

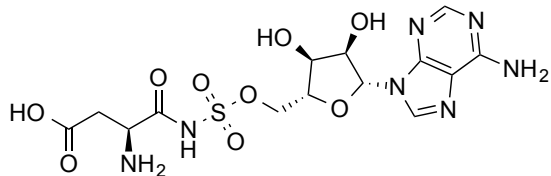
5'-O-[N-(L-alanyl)-sulfamoyl]adenosine (3.43)

The desired AMP analog was obtained according to general procedure G, as a white solid (13.1 mg, 35%).

ESI-MS: C₁₃H₁₉N₇O₇S, *m/z* calculated for [M-H]⁻: 416.1, Found: 416.1; *m/z* calculated for [M+H]⁺: 418.1, Found:

418.1.

¹H NMR δ (D₂O) 8.42 (s, 1H), 8.27 (s, 1H), 6.16 (d, *J* = 5.2 Hz, 1H), 4.77 (1H) 4.54 (dd, *J* = 5.9, 4.7 Hz, 1H), 4.47 (m, 1H), 4.44 – 4.41 (m, 2H), 3.88 (q, *J* = 7.2 Hz, 1H), 1.51 (d, *J* = 7.2 Hz, 3H). **¹³C NMR** δ (D₂O) 176.5 , 152.9 , 139.7 , 114.9 , 100.0 , 87.4 , 82.3 , 79.9 , 74.0 , 70.1 , 68.3 , 51.4 , 16.5 .

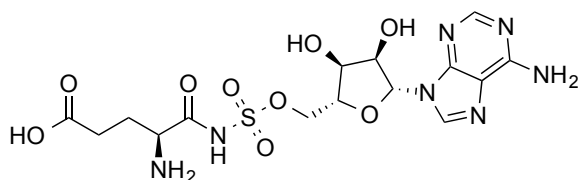
5'-O-[N-(L-aspartyl)-sulfamoyl]adenosine (3.44)

The desired AMP analog was obtained according to general procedure G, as a white solid (3.3 mg, 40%).

ESI-MS: C₁₄H₁₉N₇O₉S, *m/z* calculated for [M-H]⁻:

460.1, Found: 460.1; *m/z* calculated for [M+H]⁺: 462.1, Found: 462.1.

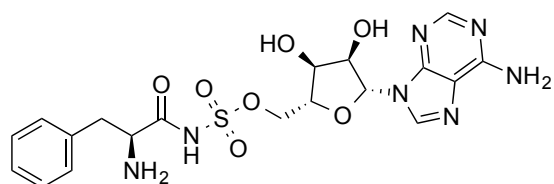
¹H NMR δ (D₂O) 8.47 (s, 1H), 8.25 (s, 1H), 5.94 (d, *J* = 5.7 Hz, 1H), 4.58 (dd, *J* = 7.0, 5.3 Hz, 1H), 4.16 – 4.08 (m, 3H), 3.75 (td, *J* = 7.7, 4.4 Hz, 1H), 3.10 (m, 1H), 2.85 (dd, *J* = 9.6, 5.2 Hz, 1H), 2.62 (dd, *J* = 17.4, 5.2 Hz, 1H). **¹³C NMR** δ (D₂O) 175.6, 171.8, 156.6, 149.3, 139.4, 139.4, 119.5, 93.3, 83.3, 75.4, 70.1, 58.2, 45.6, 35.7.

5'-O-[N-(L-glutamyl)-sulfamoyl]adenosine (3.45)

The desired AMP analog was obtained according to general procedure G, as a white solid (13.8 mg, 39%).

ESI-MS: C₁₅H₂₁N₇O₉S, m/z calculated for [M-H]⁻: 474.1, Found: 474.1; m/z calculated for [M+H]⁺: 476.1, Found: 476.1.

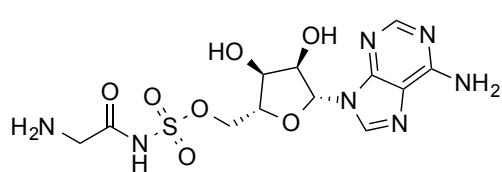
¹H NMR δ (D₂O) 8.43 (s, 1H), 8.26 (s, 1H), 6.15 (d, J = 5.2 Hz, 1H), 4.76 (dd, J = 6.3, 5.2 Hz, 1H), 4.54 (dd, J = 6.3, 4.6 Hz, 1H), 4.47 (dt, J = 4.6, 2.2 Hz, 1H), 4.44 – 4.41 (m, 2H), 3.86 (dd, J = 7.1, 5.0 Hz, 1H), 2.45 (m, 2H), 2.19 (m, 2H). **¹³C NMR** δ (D₂O) 180.3, 175.3, 155.3, 152.4, 148.9, 139.9, 118.6, 114.9, 87.4, 82.3, 74.1, 70.1, 55.3, 32.7, 27.1.

5'-O-[N-(L-phenylalanyl)-sulfamoyl]adenosine (3.46)

The desired AMP analog was obtained according to general procedure G, as a white solid (24.9 mg, 64%).

ESI-MS: C₁₉H₂₃N₇O₇S, m/z calculated for [M-H]⁻: 492.1, Found: 492.1; m/z calculated for [M+H]⁺: 494.1, Found: 494.1.

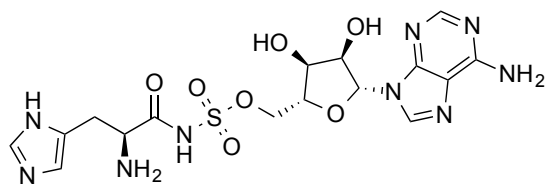
¹H NMR δ (D₂O) 8.33 (s, 1H), 8.19 (s, 1H), 7.34 – 7.02 (m, 5H), 6.10 (d, J = 5.1 Hz, 1H), 4.73 (dd, J = 6.2, 5.1 Hz, 1H), 4.46-4.28 (m, 4H), 4.05 (dd, J = 6.4, 5.8 Hz, 1H), 3.16 (dd, J = 14.4, 7.2 Hz, 1H), 3.06 (dd, J = 14.4, 7.2 Hz, 1H). **¹³C NMR** δ (D₂O) 174.7, 155.4, 152.7, 148.8, 139.7, 134.2, 129.3, 128.8, 127.5, 118.6, 87.4, 82.2, 74.0, 70.0, 68.4, 56.5, 36.6.

5'-O-[N-(L-glycyl)-sulfamoyl]adenosine (3.47)

The desired AMP analog was obtained according to general procedure G, as a white solid (12.6 mg, 34%).

ESI-MS: C₁₂H₁₇N₇O₇S, m/z calculated for [M-H]⁻: 402.1, Found: 402.1; m/z calculated for [M+H]⁺: 404.1, Found: 404.1.

¹H NMR δ (D₂O) 8.34 (s, 1H), 8.15 (s, 1H), 6.13 (d, J = 5.3 Hz, 1H), 4.73 (dd, J = 6.0, 4.6 Hz, 1H), 4.50 - 4.41 (m, 4H), 3.70 (s, 2H). **¹³C NMR** δ (D₂O) 172.7, 156.4, 152.4, 148.8, 139.7, 118.4, 87.4, 82.2, 74.1, 70.1, 68.2, 42.7.

5'-O-[N-(L-histidiny)]-sulfamoyl]adenosine (3.48)

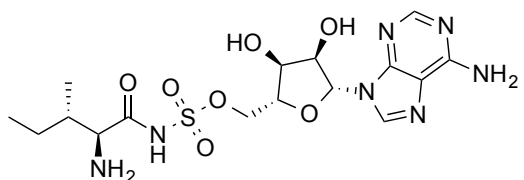
The desired AMP analog was obtained according to general procedure G, as a white solid (9.9 mg, 30%).

ESI-MS: $C_{16}H_{21}N_9O_7S$, m/z calculated for $[M-H]^-$:

482.1, Found: 482.1; m/z calculated for $[M+H]^+$: 484.1, Found: 484.1.

1H NMR δ (D_2O) 8.38 (s, 1H), 8.24 (s, 1H), 7.72 (s, 1H), 7.00 (s, 1H), 6.14 (d, $J = 5.4$, Hz, 1H), 4.75 (1H), 4.52 (dd, $J = 6.3, 4.6$ Hz, 1H), 4.43 (m, 1H), 4.39 – 4.35 (m, 2H), 4.02 (t, $J = 5.1$ Hz, 1H), 3.11 – 3.08 (m, 2H).

^{13}C NMR δ (D_2O) 175.1, 152.9, 148.9, 139.7, 137.8, 136.1, 132.1, 125.4, 120.2, 87.4, 82.2, 74.0, 70.1, 68.4, 55.5, 28.6.

5'-O-[N-(L-isoleuciny)]-sulfamoyl]adenosine (3.49)

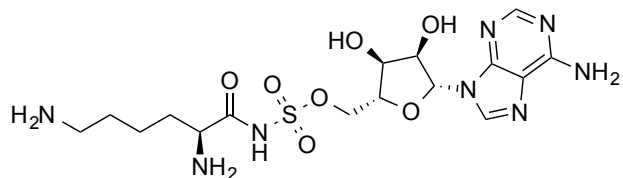
The desired AMP analog was obtained according to general procedure G, as a white solid (15.3 mg, 40%).

ESI-MS: $C_{16}H_{25}N_7O_7S$, m/z calculated for $[M-H]^-$:

458.2, Found: 458.2; m/z calculated for $[M+H]^+$:

460.2, Found: 460.2.

1H NMR δ (D_2O) 8.42 (s, 1H), 8.25 (s, 1H), 6.14 (d, $J = 5.4$ Hz, 1H), 4.76 (dd, $J = 6.2, 5.4$ Hz, 1H), 4.54 (dd, $J = 4.8, 4.4$ Hz, 1H), 4.48 (m, 1H), 4.43 – 4.0 (m, 2H), 3.72 (d, $J = 4.2$ Hz, 1H), 1.97 (m, 1H), 1.95 (m, 1H), 1.42 (m, 1H), 1.18 (d, $J = 6.8$ Hz, 3H), 0.90 (dd, $J = 7.5, 7.3$ Hz, 3H). **^{13}C NMR** δ (D_2O) 175.2, 155.6, 152.9, 149.0, 139.7, 118.6, 87.2, 82.4, 74.0, 70.2, 68.3, 60.1, 36.4, 24.1, 14.4, 10.9.

5'-O-[N-(L-lysyl)]-sulfamoyl]adenosine (3.50)

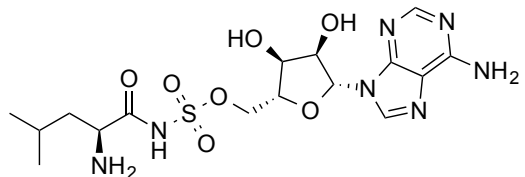
The desired AMP analog was obtained according to general procedure G, as a white solid (11.6 mg, 35%).

ESI-MS: $C_{16}H_{26}N_8O_7S$, m/z calculated for

$[M-H]^-$: 473.2, Found: 473.2; m/z calculated for $[M+H]^+$: 475.2, Found: 475.2.

^1H NMR δ (D_2O) 8.38 (s, 1H), 8.31 (s, 1H), 6.17 (d, $J = 5.4$ Hz, 1H), 4.72 (dd, $J = 5.4, 5.2$ Hz, 1H), 4.54 (dd, $J = 4.6, 4.4$ Hz, 1H), 4.47 – 4.21 (m, 3H), 3.59 (dd, $J = 6.3, 6.2$ Hz, 1H), 2.70 – 2.63 (m, 2H), 1.82 – 1.78 (m, 2H), 1.54 – 1.47 (m, 2H), 1.26 – 1.19 (m, 2H). **^{13}C NMR** δ (D_2O) 175.9, 155.9, 152.1, 149.1, 139.9, 119.4, 97.2, 81.4, 72.9, 70.8, 63.1, 53.2, 42.1, 33.4, 28.7, 22.3.

5'-O-[N-(L-leucinyl)-sulfamoyl]adenosine (3.51)



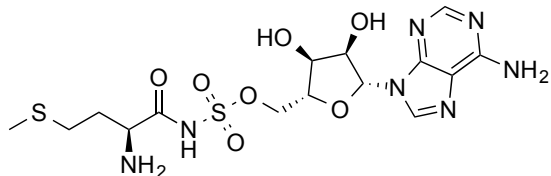
The desired AMP analog was obtained according to general procedure G, as a white solid (7.3 mg, 19%).

ESI-MS: $\text{C}_{16}\text{H}_{25}\text{N}_7\text{O}_7\text{S}$, m/z calculated for $[\text{M}-\text{H}]^-$: 458.2, Found: 458.2; m/z calculated for $[\text{M}+\text{H}]^+$:

460.2, Found: 460.2.

^1H NMR δ (D_2O) 8.41 (s, 1H), 8.25 (s, 1H), 6.14 (d, $J = 5.5$ Hz, 1H), 4.75 (dd, $J = 6.2, 5.5$ Hz, 1H), 4.45 (dd, $J = 4.9, 4.7$ Hz, 1H), 4.47 (m, 1H), 4.42 – 4.38 (m, 2H), 3.80 (m, 1H), 1.96 – 1.94 (m, 2H), 1.01 (m, 1H), 0.89 (d, $J = 6.5, 3\text{H}$), 0.87 (d, $J = 6.5, 3\text{H}$). **^{13}C NMR** δ (D_2O) 176.4, 155.6, 152.9, 149.0, 139.7, 118.6, 87.2, 82.4, 74.0, 70.2, 68.3, 54.2, 40.2, 24.0, 21.8, 20.9.

5'-O-[N-(L-methionyl)-sulfamoyl]adenosine (3.52)

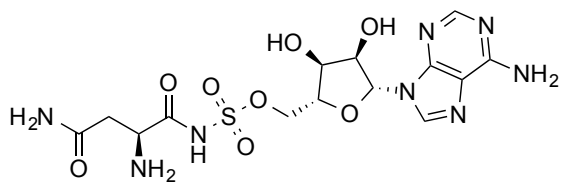


The desired AMP analog was obtained according to general procedure G, as a white solid (13.1 mg, 34%).

ESI-MS: $\text{C}_{15}\text{H}_{23}\text{N}_7\text{O}_7\text{S}_2$, m/z calculated for $[\text{M}-\text{H}]^-$:

476.1, Found: 476.1; m/z calculated for $[\text{M}+\text{H}]^+$: 478.1, Found: 478.1.

^1H NMR δ (D_2O) 8.47 (s, 1H), 8.15 (s, 1H), 6.04 (d, $J = 5.3$ Hz, 1H), 4.75 (1H), 4.59 (dd, $J = 5.4, 5.2$ Hz, 1H), 4.35 (dd, $J = 5.1, 3.6$ Hz, 1H), 4.33 – 4.22 (m, 3H), 3.30 (m, 1H), 2.50 (m, 2H), 2.00 (s, 3H), 1.87 (m, 2H). **^{13}C NMR** δ (D_2O) 172.4, 158.1, 156.5, 149.2, 139.3, 119.4, 93.2, 83.3, 83.2, 75.4, 69.9, 58.1, 30.7, 25.1, 14.3.

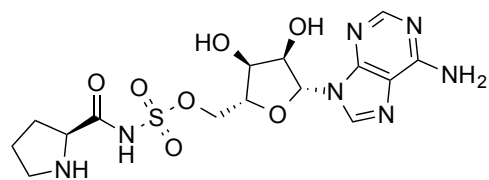
5'-O-[N-(L-asparginy)]-sulfamoyl]adenosine (3.53)

The desired AMP analog was obtained according to general procedure G, as a white solid (37.2 mg, 97%).

ESI-MS: C₁₄H₂₀N₈O₈S, *m/z* calculated for [M-H]⁻:

459.1, Found: 459.1; *m/z* calculated for [M+H]⁺: 461.1, Found: 461.1.

¹H NMR δ (D₂O) 8.60 (s, 1H), 8.36 (s, 1H), 6.48 (d, *J* = 5.3 Hz, 1H), 5.08 (1H), 4.47 (dd, *J* = 4.9, 4.7 Hz, 1H), 4.39 – 4.26 (m, 3H), 4.12 (dd, *J* = 7.9, 3.8 Hz, 1H), 3.03 (m, 2H). **¹³C NMR** δ (D₂O) 163.1, 162.8, 156.5, 149.3, 140.0, 119.6, 114.9, 93.2, 82.9, 75.2, 70.1, 61.2, 58.4, 35.1.

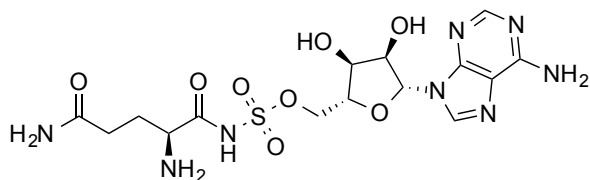
5'-O-[N-(L-prolyl)-sulfamoyl]adenosine (3.54)

Desired AMP analog was obtained according to general procedure G, as a white solid (13.6 mg, 36%).

ESI-MS: C₁₅H₂₁N₇O₇S, *m/z* calculated for [M-H]⁻: 442.1, Found: 442.1; *m/z* calculated for [M+H]⁺: 444.1,

Found: 444.1.

¹H NMR δ (DMSO) 8.36 (s, 1H), 8.15 (s, 1H), 7.27 (s, 2H, -NH₂), 5.91 (d, *J* = 5.2 Hz, 1H), 4.76 (dd, *J* = 5.4, 5.2 Hz, 1H), 4.18 (dd, *J* = 5.4, 4.8 Hz, 1H), 4.16 – 4.06 (m, 3H), 3.90 (dd, *J* = 6.5, 6.3 Hz, 1H), 3.21 (m, 1H), 3.06 (m, 1H), 2.19 (m, 1H), 1.91 (m, 1H), 1.84 – 1.74 (m, 2H). **¹³C NMR** δ (DMSO) 172.2, 156.5, 153.1, 149.9, 139.7, 119.6, 87.4, 82.8, 73.9, 71.1, 68.2, 62.4, 45.2, 29.6, 23.8.

5'-O-[N-(L-glutaminy)]-sulfamoyl]adenosine (3.55)

The desired AMP analog was obtained according to general procedure G, as a white solid (16.9 mg, 44%).

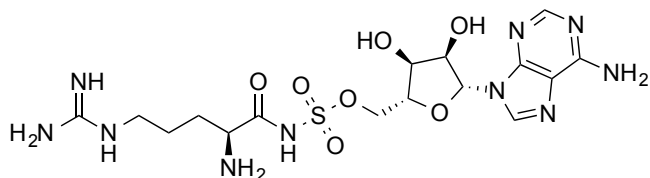
ESI-MS: C₁₅H₂₂N₈O₈S, *m/z* calculated for [M-

H]⁻: 473.1, Found: 473.1; *m/z* calculated for [M+H]⁺: 475.1, Found: 475.1.

¹H NMR δ (D₂O) 8.30 (s, 1H), 8.12 (s, 1H), 6.02 (d, *J* = 5.4 Hz, 1H), 4.75 (1H), 4.60 (dd, *J* = 5.5, 5.4 Hz, 1H), 4.43 (dd, *J* = 4.6, 4.4 Hz, 1H), 4.39 – 4.25 (m, 3H), 3.75 (dd, *J* = 6.3, 6.0 Hz,

1H), 2.40 (m, 1H), 2.14 (m, 1H), 1.50 (m, 1H), 1.33 (m, 1H). ^{13}C NMR δ (D_2O) 177.1, 174.8, 155.5, 152.8, 149.3, 139.9, 113.0, 87.2, 82.2, 73.9, 70.0, 68.3, 54.8, 30.4, 26.4.

5'-O-[N-(L-arginyl)-sulfamoyl]adenosine (3.56)

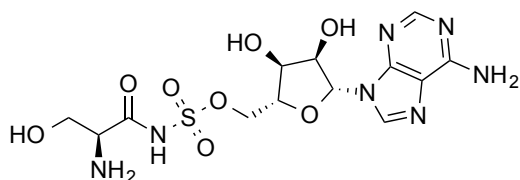


The desired AMP analog was obtained according to general procedure G, as a white solid (3.5 mg, 38%).

ESI-MS: $\text{C}_{16}\text{H}_{26}\text{N}_{10}\text{O}_7\text{S}$, m/z calculated for $[\text{M}-\text{H}]^-$: 501.2, Found: 501.2; m/z calculated for $[\text{M}+\text{H}]^+$: 503.2, Found: 503.2.

^1H NMR δ (D_2O) 8.32 (s, 1H), 8.18 (s, 1H), 6.03 (d, $J = 5.2$ Hz, 1H), 4.85 (1H), 4.48 – 4.14 (m, 4H), 3.81 (m, 1H), 3.08 (m, 2H), 1.84 – 1.81 (m, 2H), 1.57 – 1.53 (m, 2H). ^{13}C NMR δ (D_2O) 175.2, 156.8, 155.5, 152.9, 149.2, 140.0, 87.1, 82.3, 74.2, 68.4, 54.9, 53.3, 40.3, 28.2, 27.9.

5'-O-[N-(L-seryl)-sulfamoyl]adenosine (3.57)

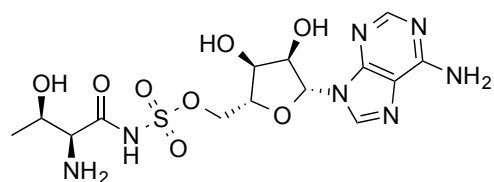


The desired AMP analog was obtained according to general procedure G, as a white solid (6.3 mg, 69%).

ESI-MS: $\text{C}_{13}\text{H}_{19}\text{N}_7\text{O}_8\text{S}$, m/z calculated for $[\text{M}-\text{H}]^-$: 432.1, Found: 432.1; m/z calculated for $[\text{M}+\text{H}]^+$: 434.1, Found: 434.1.

^1H NMR δ (D_2O) 8.50 (s, 1H), 8.21 (s, 1H), 6.09 (d, $J = 5.2$ Hz, 1H), 4.75 (1H), 4.62 (dd, $J = 5.2, 5.0$ Hz, 1H), 4.43 – 4.26 (m, 3H), 3.97 (dd, $J = 11.5, 4.0$ Hz, 1H), 3.93 – 3.78 (m, 2H). ^{13}C NMR δ (D_2O) 170.5, 156.0, 152.9, 149.2, 139.4, 118.9, 87.1, 82.3, 73.5, 70.7, 67.4, 60.9, 57.3.

5'-O-[N-(L-threonyl)-sulfamoyl]adenosine (3.58)



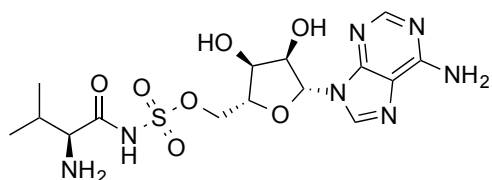
The desired AMP analog was obtained according to general procedure G, as a white solid (3.8 mg, 46%).

ESI-MS: $\text{C}_{14}\text{H}_{21}\text{N}_7\text{O}_8\text{S}$, m/z calculated for $[\text{M}-\text{H}]^-$: 446.1, Found: 446.1; m/z calculated for $[\text{M}+\text{H}]^+$: 448.1, Found: 448.1.

^1H NMR δ (D_2O) 8.51 (s, 1H), 8.19 (s, 1H), 6.08 (d, $J = 5.2$ Hz, 1H), 4.76 (1 H), 4.61 (dd, $J = 4.8, 4.6$ Hz, 1H), 4.45 – 4.27 (m, 3H), 3.99 (dd, $J = 6.1, 5.9$ Hz, 1H), 3.45 (d, $J = 4.5$ Hz, 1H),

1.31 (d, $J = 6.5$ Hz, 3H). ^{13}C NMR δ (D_2O) 174.5, 157.0, 153.9, 149.9, 140.4, 120.1, 89.1, 84.3, 76.5, 71.7, 68.4, 67.6, 62.9, 21.0.

5'-O-[N-(L-valyl)-sulfamoyl]adenosine (3.59)



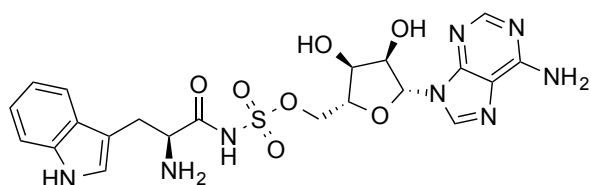
Desired AMP analog was obtained according to general procedure G, as a white solid (16.4 mg, 43%).

ESI-MS: $\text{C}_{15}\text{H}_{23}\text{N}_7\text{O}_7\text{S}$, m/z calculated for $[\text{M}-\text{H}]^-$: 444.1, Found: 444.1; m/z calculated for $[\text{M}+\text{H}]^+$: 446.1,

Found: 446.1.

^1H NMR δ (D_2O) 8.32 (s, 1H), 8.16 (s, 1H), 6.05 (d, $J = 5.2$ Hz, 1H), 4.68 (1H), 4.45 (dd, $J = 4.7, 4.5$ Hz, 1H), 4.38 (m, 1H), 4.36 – 4.33 (m, 2H), 3.55 (d, $J = 4.4$ Hz, 1H), 2.17 (m, 1H), 0.92 (d, $J = 6.9$ Hz, 3H), 0.85 (d, $J = 7.0$ Hz, 3H). ^{13}C NMR δ (D_2O) 175.5, 155.6, 152.9, 149.0, 139.7, 118.6, 87.3, 82.3, 74.0, 70.2, 68.3, 60.9, 29.8, 17.9, 16.3.

5'-O-[N-(L-tryptophanyl)-sulfamoyl]adenosine (3.60)

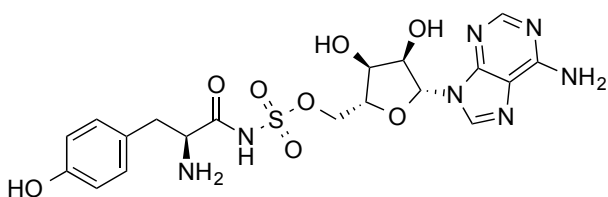


The desired AMP analog was obtained according to general procedure G, as a white solid (13.5 mg, 34%).

ESI-MS: $\text{C}_{21}\text{H}_{24}\text{N}_8\text{O}_7\text{S}$, m/z calculated for $[\text{M}-\text{H}]^-$: 531.2, Found: 531.2; m/z calculated for $[\text{M}+\text{H}]^+$: 533.2, Found: 533.2.

^1H NMR δ (D_2O) 8.40 (s, 1H), 8.14 (s, 1H), 7.57 (d, $J = 7.8$ Hz, 1H), 7.35 (d, $J = 7.9$ Hz, 1H), 7.23 (d, $J = 12.6$ Hz, 1H), 7.05 – 7.01 (m, 2H), 5.92 (d, $J = 5.8$ Hz, 1H), 4.73 (1H), 4.59 (dd, $J = 5.3, 5.1$ Hz, 1H), 4.24 – 4.03 (m, 5H), 3.68 (dd, $J = 8.2, 4.4$ Hz, 1H), 3.05 (dd, $J = 15.1, 8.2$ Hz, 1H). ^{13}C NMR δ (D_2O) 172.5, 156.6, 152.9, 149.7, 139.7, 136.6, 127.3, 124.6, 121.1, 119.0, 118.6, 118.4, 111.5, 108.2, 87.3, 82.3, 74.0, 70.8, 67.3, 55.7, 27.8.

5'-O-[N-(L-tyrosyl)-sulfamoyl]adenosine (3.61)



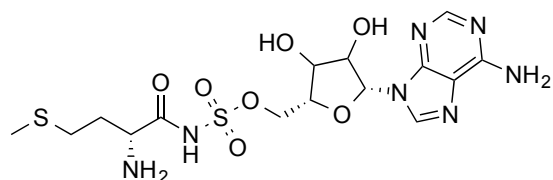
The desired AMP analog was obtained according to general procedure G, as a white solid (11.8 mg, 30%).

ESI-MS: $\text{C}_{19}\text{H}_{23}\text{N}_7\text{O}_8\text{S}$, m/z calculated for $[\text{M}-$

H^- : 508.1, Found: 508.1; m/z calculated for $[\text{M}+\text{H}]^+$: 510.1, Found: 510.1.

$^1\text{H NMR}$ δ (DMSO) 8.40 (s, 1H), 8.15 (s, 1H), 7.23 (br, 2H, $-\text{NH}_2$), 7.05 (d, $J = 8.4$ Hz, 2H), 6.68 (d, $J = 8.4$ Hz, 2H), 5.97 (d, $J = 5.8$ Hz, 1H), 4.62 (dd, $J = 5.1, 4.9$ Hz, 1H), 4.59 (dd, $J = 5.3, 5.1$ Hz, 1H), 4.24 – 4.03 (m, 3H), 3.55 (dd, $J = 8.4, 5.2$ Hz, 1H), 3.04 (dd, $J = 14.3, 4.8$ Hz, 1H), 2.81 (dd, $J = 14.3, 8$ Hz, 1H).

5'-O-[N-(D-methionyl)-sulfamoyl]adenosine (3.62)

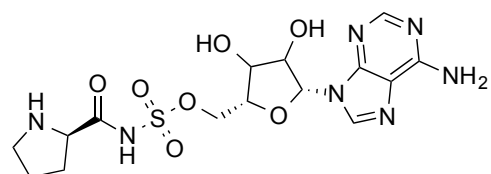


The desired AMP analog was obtained according to general procedure G, as a white solid (11.9 mg, 31%).

ESI-MS: $\text{C}_{15}\text{H}_{23}\text{N}_7\text{O}_7\text{S}_2$, m/z calculated for $[\text{M}-\text{H}]^-$: 476.1, Found: 476.1; m/z calculated for $[\text{M}+\text{H}]^+$: 478.1, Found: 478.1.

$^1\text{H NMR}$ δ (D_2O) 8.47 (s, 1H), 8.13 (s, 1H), 5.99 (d, $J = 5.3$ Hz, 1H), 4.76 (1H), 4.56 (dd, $J = 5.4, 5.2$ Hz, 1H), 4.35 (dd, $J = 5.1, 3.6$ Hz, 1H), 4.33 – 4.22 (m, 3H), 3.27 (m, 1H), 2.50 (m, 2H), 2.00 (s, 3H), 1.87 (m, 2H). $^{13}\text{C NMR}$ δ (D_2O) 172.7, 158.4, 156.6, 149.1, 139.4, 119.1, 93.2, 83.3, 82.9, 75.4, 69.9, 58.1, 30.7, 25.4, 14.5.

5'-O-[N-(D-prolyl)-sulfamoyl]adenosine (3.63)



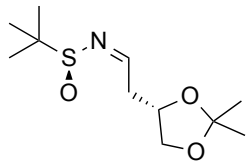
The desired AMP analog was obtained according to general procedure G, as a white solid (14.1 mg, 37%).

ESI-MS: $\text{C}_{15}\text{H}_{21}\text{N}_7\text{O}_7\text{S}$, m/z calculated for $[\text{M}-\text{H}]^-$: 442.1, Found: 442.1; m/z calculated for $[\text{M}+\text{H}]^+$: 444.1, Found: 444.1.

$^1\text{H NMR}$ δ (D_2O) 8.38 (s, 1H), 8.23 (s, 1H), 6.12 (d, $J = 5.2$ Hz, 1H), 4.76 (1H), 4.54 (dd, $J = 5.1, 4.8$ Hz, 1H), 4.49 – 4.36 (m, 3H), 4.19 (dd, $J = 6.5, 6.3$ Hz, 1H), 3.38 – 3.35 (m, 2H), 2.37 (m, 1H), 2.02 (m, 1H), 1.99 – 1.95 (m, 2H). $^{13}\text{C NMR}$ δ (D_2O) 175.3, 155.5, 152.9, 148.9, 139.7, 118.6, 87.4, 82.2, 73.9, 70.1, 68.5, 62.2, 46.2, 29.5, 23.6.

6.1.4 Synthesis of HFG-hybrid Analogs

(S)-tert-Butanesulfinyl aldimine (3.64)



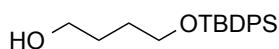
At -60 °C a solution of DMSO (3.95 mL, 56.1 mmol) in DCM (12 mL) was added dropwise to a solution of oxalyl chloride (2.5 mL, 28.1 mmol) in DCM (66 mL). The mixture was stirred for 15 min and then a solution of the primary alcohol (*S*)-2-(2,2-dimethyl-1,3-dioxolan-4-yl)ethan-1-ol (3.6 g, 25.6 mmol) in DCM (12 mL) was added dropwise. The mixture was stirred for 90 min followed by slow addition of Et₃N (17.7 mL, 129 mmol). Stirring was continued for an additional 15 min. The reaction mixture was then warmed up to r.t., stirred for 60 min and H₂O (66 mL) was added. When the mixture became clear, it was extracted with DCM and then washed with citric acid (1 M), saturated NaHCO₃ solution and then brine, and dried over anhydrous Na₂SO₄. The filtered solution was concentrated to give the aldehyde (2.4 g, 67%) without further purification.

To a solution of (*S*)-tert-butanesulfinamide (2.22 g, 18.3 mmol) in DCM (30 mL) was added anhydrous CuSO₄ (6.4 g, 40.3 mmol) followed by the above aldehyde (2.9 g, 20.1 mmol). The mixture was stirred at room temperature for 12 h. The reaction mixture was filtered through a pad of Celite, and the filter cake was washed thoroughly with DCM. The filtrate was concentrated to dryness. The residue was purified by flash chromatography using hexanes/ethyl acetate to afford the desired (*S*)-tert-butanesulfinyl aldimine (2.6 g, 59%) as a yellow oil.

ESI-MS: C₁₁H₂₁NO₃S, *m/z* calculated for [M+H]⁺: 248.1, Found: 248.1; *m/z* calculated for [M+Na]⁺: 270.1, Found: 270.1.

¹H NMR δ (CDCl₃) 7.98 (t, *J* = 4.5 Hz, 1H), 4.46 (p, *J* = 6.3 Hz, 1H), 4.11 (dd, *J* = 8.2, 6.3 Hz, 1H), 3.61 (dd, *J* = 8.2, 6.3 Hz, 1H), 2.82 (dd, *J* = 6.3, 4.6 Hz, 2H), 1.35 (s, 3H), 1.29 (s, 3H), 1.14 (s, 9H). **¹³C NMR** δ (CDCl₃) 165.96, 109.13, 72.37, 69.20, 56.76, 40.50, 26.76, 25.34, 22.28.

4-((tert-butyldiphenylsilyl)oxy)butan-1-ol (3.65a)



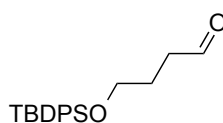
A solution of butanediol (10.32 g, 114.0 mmol), TBDPS-Cl (6.40 g, 23.2 mmol), imidazole (6.48 g, 95.2 mmol), and DMAP (418 mg, 3.4 mmol) in DCM (30 mL) was stirred at room temperature for 12 hours. The reaction mixture was extracted between EtOAc (150 mL) and H₂O (40 mL). The organic layer was washed with brine

(3 x 20 mL), dried over anhydrous Na₂SO₄, filtered and evaporated under reduced pressure. The residue was purified by silica gel column chromatography using hexanes/ethyl acetate to give the title alcohol (3.8 g, 50%).

ESI-MS: C₂₀H₂₈O₂Si, *m/z* calculated for [M+H]⁺: 329.2, Found: 329.2; *m/z* calculated for [M+Na]⁺: 351.2, Found: 351.2.

¹H NMR δ (CDCl₃) 7.75 – 7.60 (m, 4H), 7.50 – 7.35 (m, 6H), 3.75 – 3.55 (m, 4H), 1.97 (brs, 1H), 1.75 – 1.60 (m, 4H), 1.06 (s, 9H). ¹³C NMR δ (CDCl₃) 135.7, 133.8, 129.8, 127.8, 64.2, 62.6, 30.2, 29.4, 27.0, 19.3.

4-((*tert*-butyldiphenylsilyl)oxy)butanal (3.65)

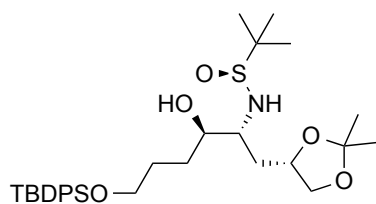


At -60 °C, a solution of DMSO (4.2 mL, 59.2 mmol) in DCM (12 mL) was added dropwise to a solution of oxalyl chloride (2.6 mL, 28.7 mmol) in DCM (70 mL). The mixture was stirred for 15 min and then a solution of the primary alcohol **3.65a** (8.6 g, 26.2 mmol) in DCM (12 mL) was added dropwise. The mixture was stirred for 90 min followed by slow addition of Et₃N (17 mL, 124 mmol). Stirring was continued for an additional 15 min. Then the reaction mixture was warmed up to room temperature, stirred for 60 min and H₂O (90 mL) was added. When the mixture became clear, it was extracted with DCM and then washed with HCl (aqueous, 10%), saturated NaHCO₃ solution and then brine, and dried over anhydrous Na₂SO₄. The filtrate was concentrated. The residue was purified by flash chromatography to afford compound **6** (7.9 g, 93%) as a viscous yellow oil.

ESI-MS: C₂₀H₂₆O₂Si, *m/z* calculated for [M+H]⁺: 327.2, Found: 327.2; *m/z* calculated for [M+Na]⁺: 349.2, Found: 349.2.

¹H NMR δ (CDCl₃) 9.80 (s, 1H), 7.72-7.70 (m, 4H), 7.45-7.34 (m, 6H), 3.68-3.72 (m, 2H), 2.61-2.54 (m, 2H), 1.98-1.89 (m, 2H), 1.05 (s, 9H). ¹³C NMR δ (CDCl₃) 202.9, 136.0, 134.1, 130.1, 128.1, 63.4, 41.2, 27.3, 25.7, 19.7.

β-amido alcohol (3.66)



To a solution of SmI₂ (9 mmol in 100 mL of THF) under argon at -78 °C, was added dropwise the solution of imine **3.64** (1 g, 3.9 mmol), aldehyde **3.65** (1.9 g, 5.9 mmol) and *t*-Butanol (778 μL, 8.2 mmol) in 20 mL of THF. The mixture was stirred vigorously

for 3 h at the same temperature and then quenched by a saturated $\text{Na}_2\text{S}_2\text{O}_3$ solution (10 mL). The organic layer was separated, and the aqueous layer was extracted with ethyl acetate. The combined organic extracts were washed by saturated brine and then dried over anhydrous Na_2SO_4 , filtered, and concentrated under vacuum. The residue was purified by flash chromatography using hexanes/ethyl acetate to afford the desired product (1.3 g, 58%) as yellow oil.

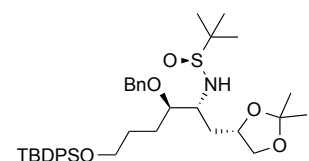
ESI-MS: $\text{C}_{31}\text{H}_{49}\text{NO}_5\text{SSi}$, m/z calculated for $[\text{M}+\text{H}]^+$: 576.3, Found: 576.3; m/z calculated for $[\text{M}+\text{Na}]^+$: 598.3, Found: 598.3; m/z calculated for $[\text{M}-\text{H}]^-$: 574.3, Found: 574.3.

^1H NMR δ (CDCl_3) 7.68–7.63 (m, 4H), 7.46–7.33 (m, 6H), 4.44 (d, $J = 4.8$ Hz, 1H), 4.29 (m, 1H), 4.12 (dd, $J = 8.0, 6.0$ Hz, 1H), 3.77–3.63 (m, 3H), 3.52 (t, $J = 7.9$ Hz, 1H), 3.42 (m, 1H), 2.99 (d, $J = 4.8$ Hz, 1H), 1.94–1.70 (m, 3H), 1.67–1.46 (m, 3H), 1.40 (s, 3H), 1.36 (s, 3H), 1.24 (s, 9H), 1.05 (s, 9H). **^{13}C NMR** δ (CDCl_3) 135.7, 133.9, 129.7, 127.8, 109.8, 73.9, 72.8, 69.9, 64.0, 58.2, 55.8, 32.4, 30.0, 29.4, 27.1, 27.0, 25.9, 22.8, 19.3.

General Procedure H

Sulfonamide **3.66** (250 mg, 0.4 mmol) was dissolved in dry THF (5 mL), and the solution was cooled to -20 °C and stirred under argon. NaHMDS (1 mL, 1 mmol) was added. After 30 min, bromide reagent (1.3 equiv., 0.5 mmol) was added dropwise with a syringe. After the addition, the cooling bath was removed, and the reaction mixture was stirred at r.t. overnight. The reaction was quenched with a saturated solution of NH_4Cl (5 mL), and the mixture was extracted with DCM (3 x 10 mL). The combined organic extracts were washed with brine (10 mL), dried over anhydrous Na_2SO_4 , filtered, and concentrated under vacuum. The residue was purified by flash chromatography using hexanes/ethyl acetate to afford the desired product.

Benzyl ether sulfonamide (3.67)

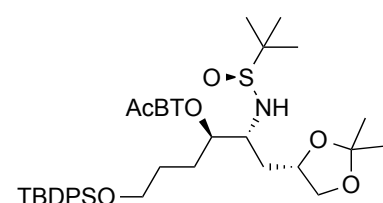


The desired compound **3.67** was obtained according to general procedure H, as yellow oil (138.3 mg, 52%).

ESI-MS: $\text{C}_{38}\text{H}_{55}\text{NO}_5\text{SSi}$, m/z calculated for $[\text{M}+\text{H}]^+$: 666.4, Found: 666.4; m/z calculated for $[\text{M}+\text{Na}]^+$: 688.4, Found: 688.4; m/z calculated for $[\text{M}-\text{H}]^-$: 664.4, Found: 664.4.

¹H NMR δ (CDCl₃) 7.72–7.51 (m, 4H), 7.50–7.36 (m, 6H), 7.36–7.25 (m, 5H), 4.65 (d, J = 11.5 Hz, 1H), 4.50 (d, J = 11.5 Hz, 1H), 4.34 (d, J = 3.7 Hz, 1H), 4.29 (m, 1H), 4.11 (dd, J = 8.0, 6.0 Hz, 1H), 3.71–3.64 (m, 2H), 3.62–3.55 (m, 2H), 3.50 (dd, J = 8.0, 7.7 Hz, 1H), 1.85 (m, 1H), 1.74 (m, 1H), 1.67–1.52 (m, 4H), 1.42 (s, 3H), 1.36 (s, 3H), 1.21 (s, 9H), 1.05 (s, 9H). **¹³C NMR** δ (CDCl₃) 139.1, 136.0, 134.4, 130.0, 128.8, 128.1, 128.1, 128.0, 109.9, 81.6, 75.3, 73.0, 70.1, 64.2, 56.4, 56.1, 34.5, 29.2, 27.7, 27.5, 27.4, 26.2, 23.3, 19.7.

tert-butyl acetate ether sulfonamide (**3.68**)



The desired compound **3.68** was obtained according to general procedure H, as yellow oil (121.3 mg, 44%).

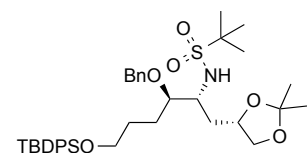
ESI-MS: C₃₇H₅₉NO₇SSi, m/z calculated for [M+H]⁺: 690.4, Found: 690.4; m/z calculated for [M+Na]⁺: 712.4, Found: 712.4; m/z calculated for [M-H]⁻: 688.4, Found: 688.4.

¹H NMR δ (CDCl₃) 7.67–7.63 (m, 4H), 7.46–7.33 (m, 6H), 4.58 (d, J = 4.2 Hz, 1H), 4.31 (m, 1H), 4.12–3.98 (m, 2H), 3.67–3.60 (m, 2H), 3.57–3.43 (m, 3H), 1.89 (m, 1H), 1.75 (m, 1H), 1.68–1.52 (m, 4H), 1.46 (s, 9H), 1.41 (s, 3H), 1.35 (s, 3H), 1.22 (s, 9H), 1.04 (s, 9H). **¹³C NMR** δ (CDCl₃) 169.7, 135.6, 133.9, 129.6, 127.7, 109.3, 83.0, 81.4, 74.8, 69.6, 68.7, 63.8, 56.1, 55.7, 33.7, 29.2, 28.1, 27.2, 26.9, 25.8, 22.8, 19.2.

General Procedure I

To a solution of sulfinamide (100 mg) in DCM (10 mL), was added *m*-CPBA (55%, 1.4 equiv at ambient temperature. After 3 h, the reaction mixture was diluted with a mixture of saturated aqueous NaHSO₃ (5 mL) and NaHCO₃ (5 mL). The aqueous layer was extracted with DCM (2 x 10 mL). The organic extracts were combined, dried over anhydrous Na₂SO₄, filtered, and concentrated under vacuum. The residue was purified by flash chromatography using hexanes/ethyl acetate to afford the desired product.

Benzyl ether sulfonamide (**3.69**)



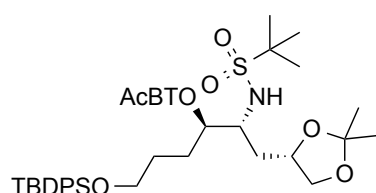
The desired compound **3.69** was obtained according to general procedure I, as colorless oil (101.3 mg, 99%).

ESI-MS: C₃₈H₅₅NO₆SSi, m/z calculated for [M+H]⁺: 682.4, Found:

682.4; m/z calculated for $[M+Na]^+$: 704.4, Found: 704.4; m/z calculated for $[M-H]^-$: 680.4, Found: 680.4.

1H NMR δ ($CDCl_3$) 7.72–7.51 (m, 4H), 7.50–7.36 (m, 6H), 7.36–7.25 (m, 5H), 4.56 (s, 2H), 4.26–4.19 (m, 2H), 4.05 (m, 1H), 3.70–3.42 (m, 5H), 1.96 (m, 1H), 1.74 (m, 1H), 1.67–1.52 (m, 4H), 1.40 (s, 3H), 1.37 (s, 9H), 1.34 (s, 3H), 1.05 (s, 9H); ^{13}C NMR δ ($CDCl_3$) 138.28, 135.47, 133.70, 129.57, 128.35, 127.78, 127.65, 127.60, 109.02, 81.95, 73.86, 72.53, 69.47, 63.35, 59.84, 55.16, 33.44, 28.78, 27.18, 26.92, 26.80, 25.59, 24.08, 19.13.

tert-butyl acetate ether sulfonamide (3.70)



The desired compound **3.70** was obtained according to general procedure I, as colorless oil (100.2 mg, 98%).

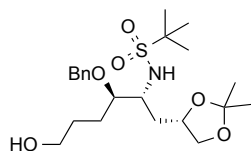
ESI-MS: $C_{37}H_{59}NO_8SSi$, m/z calculated for $[M+H]^+$: 706.4, Found: 706.4; m/z calculated for $[M+Na]^+$: 728.4, Found: 728.4; m/z calculated for $[M-H]^-$: 704.4, Found: 704.4.

1H NMR δ ($CDCl_3$) 7.65–7.55 (m, 4H), 7.45–7.35 (m, 6H), 4.35 (m, 1H), 4.21 (d, $J = 16.8$ Hz, 1H), 4.14 (dd, $J = 8.0, 5.8$ Hz, 1H), 3.94 (d, $J = 16.8$ Hz, 1H), 3.70–3.65 (m, 2H), 3.59–3.49 (m, 2H), 3.42 (m, 1H), 2.04 (m, 1H), 1.73 (m, 1H), 1.67–1.50 (m, 4H), 1.47 (s, 9H), 1.40 (s, 12H), 1.34 (s, 3H), 1.05 (s, 9H). ^{13}C NMR δ ($CDCl_3$) 171.4, 135.5, 133.8, 129.6, 127.7, 108.7, 87.7, 82.2, 74.0, 69.9, 69.6, 63.5, 59.6, 54.9, 33.4, 29.1, 28.1, 27.0, 26.9, 25.7, 24.2, 19.2.

General Procedure J

A solution of the sulfonamide (100 mg) in 3 mL of HF/Pyridine/THF (1/2/7) stirred at r.t. for 16 h, before trimethylmethoxysilane (3 mL) was added. The reaction crude was concentrated under reduced pressure and purified by flash chromatography using DCM/Methanol to afford the desired product.

N-((2*R*,3*R*)-3-(benzyloxy)-1-((*S*)-2,2-dimethyl-1,3-dioxolan-4-yl)-6-hydroxyhexan-2-yl)-2-methylpropane-2-sulfonamide (3.71)



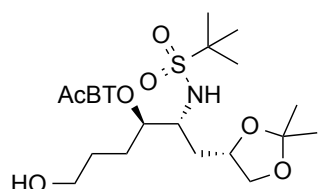
The desired compound **3.71** was obtained according to general procedure J, as colorless oil (50 mg, 77%).

ESI-MS: $C_{22}H_{37}NO_6S$, m/z calculated for $[M+H]^+$: 444.2, Found: 444.2;

m/z calculated for $[M+Na]^+$: 466.2, Found: 466.2; m/z calculated for $[M-H]^-$: 442.2, Found: 442.2.

1H NMR δ ($CDCl_3$) 7.41–7.25 (m, 5H), 4.66 (s, 2H), 4.33 (d, $J = 8.7$ Hz, 1H), 4.28 (m, 1H), 4.11 (dd, $J = 8.1, 5.9$ Hz, 1H), 3.79 (m, 1H), 3.65–3.59 (m, 2H), 3.52 (d, $J = 8.1, 7.6$ Hz, 1H), 1.92 (m, 1H), 1.79 (m, 1H), 1.72–1.47 (m, 4H), 1.40 (s, 3H), 1.38 (s, 9H), 1.34 (s, 3H). ^{13}C NMR δ ($CDCl_3$) 138.3, 128.4, 127.9, 127.8, 109.2, 82.2, 74.0, 73.0, 69.6, 62.5, 60.0, 55.6, 33.5, 28.9, 27.5, 27.0, 25.7, 24.2.

N-((2R,3R)-3-((acetylboranyl-t)oxy)-1-((S)-2,2-dimethyl-1,3-dioxolan-4-yl)-6-hydroxyhexan-2-yl)-2-methylpropane-2-sulfonamide (3.72)



The desired compound **3.72** was obtained according to general procedure J, as colorless oil (51.7 mg, 78%).

ESI-MS: $C_{21}H_{41}NO_8S$, m/z calculated for $[M+H]^+$: 468.3, Found: 468.3; m/z calculated for $[M+Na]^+$: 490.3, Found: 490.3; m/z calculated for $[M-H]^-$: 466.3, Found: 466.3.

1H NMR δ ($CDCl_3$) 4.35 (m, 1H), 4.25 (d, $J = 16.8$ Hz, 1H), 4.14 (dd, $J = 8.1, 5.8$ Hz, 1H), 4.03 (d, $J = 16.8$ Hz, 1H), 3.72–3.59 (m, 3H), 3.59–3.45 (m, 2H), 2.04 (m, 1H), 1.77 (m, 1H), 1.69–1.59 (m, 4H), 1.46 (s, 9H), 1.45 (m, 3H), 1.40 (s, 9H), 1.34 (s, 3H). ^{13}C NMR δ ($CDCl_3$) 171.3, 108.8, 87.5, 82.3, 74.0, 70.0, 69.5, 62.4, 59.7, 55.1, 33.4, 29.1, 28.9, 28.1, 27.0, 25.7, 24.2.

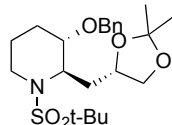
General Procedure K

To an ice-cooled solution of sulfonamide **3.71** or **3.72** (50 mg) in DCM (3 mL), was added methanesulfonyl chloride (1.2 equiv.) and DIPEA (2 equiv.) at -78 °C. The solution was stirred at -78 °C for 3 h followed by addition of a sat. aq. NH_4Cl (5 mL). The aqueous fraction was extracted with DCM (3 x 5 mL). The organic extracts were combined, dried over anhydrous Na_2SO_4 , filtered, and concentrated under vacuum to give the crude product as a yellow solid without further purification.

To a solution of the above crude product in dry THF (5 mL) under argon, was added NaHMDS (1.3 equiv.) at -20 °C. The solution was stirred for 16 h before sat. aq. NH_4Cl (5 mL) was added. The aqueous fraction was extracted with DCM (3 x 5 mL). The organic extracts were combined, dried over anhydrous Na_2SO_4 , filtered, and concentrated under vacuum. The crude residue was

purified by flash column chromatography hexanes/ethyl acetate to afford the desired product.

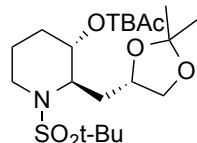
Benzyl ether N-sulfonyl piperidine (3.75)



Desired compound **3.75** was obtained according to general procedure K, as colorless oil (28.8 mg, 60%).

$^1\text{H NMR}$ δ (CDCl_3) 7.82–7.66 (m, 5H), 4.99–4.95 (m, 2H), 4.65 (m, 1H), 4.52–4.49 (m, 2H), 4.09 (dd, $J = 8.2, 6.1$ Hz, 1H), 4.05–3.97 (m, 2H), 3.56 (m, 1H), 2.58–2.32 (m, 3H), 2.26–2.00 (m, 3H), 1.87 (s, 3H), 1.84 (s, 9H), 1.77 (s, 3H). $^{13}\text{C NMR}$ δ (CDCl_3) 138.7, 128.8, 128.1, 128.0, 109.3, 73.5, 70.9, 69.5, 62.2, 42.8, 34.8, 30.1, 27.4, 25.8, 24.9, 23.5, 20.3.

tert-butyl acetate ether N-sulfonyl piperidine (3.76)



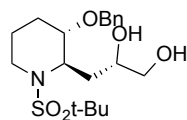
The desired compound **3.76** was obtained according to general procedure K, as colorless oil (24.5 mg, 51%).

$^1\text{H NMR}$ δ (CDCl_3) 4.22 (m, 1H), 4.09 (dd, $J = 8.2, 6.0$ Hz, 1H), 4.03 – 3.92 (m, 3H), 3.66 (dd, $J = 8.2, 7.7$ Hz, 1H), 3.55 – 3.50 (m, 2H), 3.10 (m, 1H), 2.05 – 1.90 (m, 3H), 1.80 – 1.57 (m, 3H), 1.45 (s, 9H), 1.40 (s, 3H), 1.38 (s, 9H), 1.30 (s, 3H). $^{13}\text{C NMR}$ δ (CDCl_3) 170.1, 109.2, 82.0, 73.4, 69.4, 67.0, 62.2, 42.7, 34.4, 30.1, 28.5, 27.4, 25.7, 24.8, 23.8, 20.1.

General Procedure L

To a stirred solution of *N*-sulfonyl piperidine **3.75** or **3.76** (25 mg) in MeOH (3 mL) was added pyridinium *p*-toluenesulfonate (5 mol%) at 60 °C. After 16 h, the reaction crude was concentrated under reduced pressure and purified by flash chromatography using DCM/methanol to afford the desired product.

(S)-3-((2R,3S)-3-(benzyloxy)-1-(tert-butylsulfonyl)piperidin-2-yl)propane-1,2-diol (3.77)

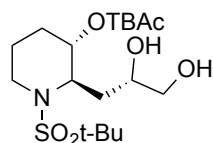


The desired compound **3.77** was obtained according to general procedure L, as colorless oil (13.6 mg, 60%).

ESI-MS: $\text{C}_{19}\text{H}_{31}\text{NO}_5\text{S}$, m/z calculated for $[\text{M}+\text{H}]^+$: 386.2, Found: 386.2; m/z calculated for $[\text{M}+\text{Na}]^+$: 408.2, Found: 408.2; m/z calculated for $[\text{M}-\text{H}]^-$: 385.2, Found: 385.2.

$^1\text{H NMR}$ δ (CDCl_3) 7.38–7.27 (m, 5H), 4.54 (s, 2H), 4.38–3.98 (m, 2H), 3.94–3.26 (m, 5H), 2.06–1.47 (m, 6H), 1.39 (s, 9H). $^{13}\text{C NMR}$ δ (CDCl_3) 138.2, 129.6, 128.3, 127.6, 73.9, 70.5, 66.8, 62.0, 42.8, 37.4, 35.2, 29.7, 24.2, 22.7, 19.7.

tert-butyl ***2-(((2R,3S)-1-(tert-butylsulfonyl)-2-((S)-2,3-dihydroxypropyl)piperidin-3-yl)oxy)acetate (3.78)***



The desired compound **3.78** was obtained according to general procedure L, as colorless oil (17 mg, 75%).

ESI-MS: $\text{C}_{18}\text{H}_{35}\text{NO}_7\text{S}$, m/z calculated for $[\text{M}+\text{H}]^+$: 410.2, Found: 410.2; m/z calculated for $[\text{M}+\text{Na}]^+$: 432.2, Found: 432.2; m/z calculated for $[\text{M}-\text{H}]^-$: 408.2, Found: 408.2.

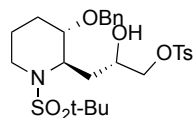
$^1\text{H NMR}$ δ (MeOD) 4.25 (br, 1H), 4.17–4.02 (m, 2H), 3.73–3.66 (m, 2H), 3.62 (br, 1H), 3.54 (d, $J = 5.4$ Hz, 2H), 3.18 (m, 1H), 2.16–1.95 (m, 4H), 1.78–1.72 (m, 2H), 1.54 (s, 9H), 1.45 (s, 9H).

$^{13}\text{C NMR}$ δ (MeOD) 171.7, 82.6, 75.5, 70.4, 67.6, 67.3, 62.6, 55.5, 43.7, 35.3, 28.4, 24.8, 23.9, 20.9.

General Procedure M

To a solution of the diol **3.77** or **3.78** (10 mg) in DCM (3 mL), were added Bu_2SnO (0.2 equiv.), *p*-TsCl (1 equiv.) and Et_3N (1 equiv.). The reaction mixture was stirred for 3 h. The mixture was filtered, and the filtrate was concentrated under reduced pressure, followed by purification with flash chromatography using DCM/Methanol to afford the desired product.

(S)-3-(((2R,3S)-3-(benzyloxy)-1-(tert-butylsulfonyl)piperidin-2-yl)-2-hydroxypropyl ***4-methylbenzenesulfonate (3.79)***



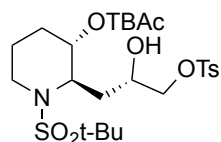
The desired compound **3.79** was obtained according to general procedure M, as colorless oil (13 mg, 93%).

ESI-MS: $\text{C}_{26}\text{H}_{37}\text{NO}_7\text{S}_2$, m/z calculated for $[\text{M}+\text{H}]^+$: 540.2, Found: 540.2; m/z calculated for $[\text{M}+\text{Na}]^+$: 562.2, Found: 562.2; m/z calculated for $[\text{M}-\text{H}]^-$: 538.2, Found: 538.2.

$^1\text{H NMR}$ δ (CDCl_3) 7.78 (d, $J = 8.3$ Hz, 2H), 7.38–7.26 (m, 7H), 4.52 (s, 2H), 4.08 (dd, $J = 6.6$, 6.2 Hz, 1H), 4.03–3.89 (m, 2H), 3.61–3.48 (m, 2H), 3.45 (m, 1H), 3.03 (m, 1H), 2.44 (s, 2H), 2.03–1.83 (m, 3H), 1.66–1.41 (m, 3H), 1.36 (s, 9H).

^{13}C NMR δ (CDCl_3) 145.2, 138.2, 132.7, 130.1, 128.5, 128.1, 127.8, 127.7, 80.4, 73.3, 70.7, 67.6, 62.1, 55.3, 42.9, 35.0, 24.3, 22.9, 21.8, 19.8.

tert-butyl-2-(((2R,3S)-1-(tert-butylsulfonyl)-2-((S)-2-hydroxy-3-(tosyloxy)propyl)piperidin-3-yl)oxy)acetate (3.80)



The desired compound **3.80** was obtained according to general procedure M, as colorless oil (12.8 mg, 93%).

ESI-MS: $\text{C}_{25}\text{H}_{41}\text{NO}_9\text{S}_2$, m/z calculated for $[\text{M}+\text{H}]^+$: 564.2, Found: 564.2; m/z calculated for $[\text{M}+\text{Na}]^+$: 586.2, Found: 586.2; m/z calculated for $[\text{M}-\text{H}]^-$:

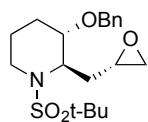
562.2, Found: 562.2.

^1H NMR δ (CDCl_3) 7.78 (d, $J = 8.2$ Hz, 2H), 7.34 (d, $J = 8.2$ Hz, 2H), 4.09–3.97 (m, 2H), 3.96 (s, 2H), 3.92 (m, 1H), 3.60–3.41 (m, 3H), 2.99 (m, 1H), 2.44 (s, 3H), 1.94 (br, 2H), 1.79–1.72 (m, 2H), 1.62–1.55 (m, 2H), 1.46 (s, 9H), 1.38 (s, 9H). ^{13}C NMR δ (CDCl_3) 169.6, 145.0, 132.6, 129.9, 129.0, 128.0, 125.3, 81.8, 75.2, 73.1, 67.3, 66.8, 62.0, 54.9, 42.6, 34.6, 28.1, 24.2, 23.0, 21.6, 19.6.

General Procedure N

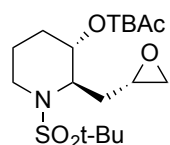
To a solution of the above product (7 mg for **3.79** and 13 mg for **3.80**) in dry THF (2 mL), was added DBU (2 equiv.) at room temperature. The solution was stirred for 16 h and then, concentrated under reduced pressure. The crude residue was purified by flash chromatography using DCM/Methanol to afford the desired product.

(2R,3S)-3-(benzyloxy)-1-(tert-butylsulfonyl)-2-(((S)-oxiran-2-yl)methyl)piperidine (3.81)



The desired compound **3.81** was obtained according to general procedure N, as a colorless oil (4.1 mg, 98%).

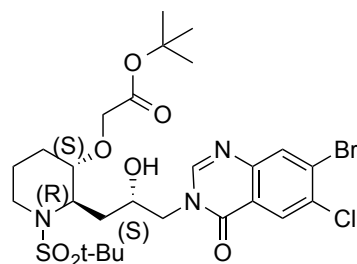
ESI-MS: $\text{C}_{19}\text{H}_{29}\text{NO}_4\text{S}$, m/z calculated for $[\text{M}+\text{H}]^+$: 368.2, Found: 368.2; m/z calculated for $[\text{M}+\text{Na}]^+$: 390.2, Found: 390.2.

***tert-butyl* 2-(((2*R*,3*S*)-1-(*tert*-butylsulfonyl)-2-(((*S*)-oxiran-2-yl)methyl)piperidin-3-yl)oxy)acetate (3.82)**

The desired compound **3.82** was obtained according to general procedure N, as colorless oil (8.2 mg, 91%).

ESI-MS: C₁₈H₃₃NO₆S, *m/z* calculated for [M+H]⁺: 392.2, Found: 392.2; *m/z* calculated for [M+Na]⁺: 414.2, Found: 414.2.

¹H NMR δ (CDCl₃) 4.50 (m, 1H), 4.37 (d, *J* = 8.3 Hz, 2H), 4.00–3.88 (m, 2H), 3.53–3.39 (m, 2H), 3.17 (t, *J* = 4.4 Hz, 1H), 2.91 (dd, *J* = 4.4, 2.6 Hz, 1H), 2.50 (m, 1H), 2.39–2.33 (m, 2H), 2.13 (m, 1H), 2.01 (m, 1H), 1.85 (s, 9H), 1.79 (s, 9H). **¹³C NMR** δ (CDCl₃) 169.6, 81.7, 75.2, 66.8, 61.8, 54.7, 49.6, 47.2, 42.5, 33.2, 28.1, 24.4, 23.2, 19.7.

***tert-butyl* 2-(((2*R*,3*S*)-2-(((*S*)-3-(7-bromo-6-chloro-4-oxoquinazolin-3(4*H*)-yl)-2-hydroxypropyl)-1-(*tert*-butylsulfonyl)piperidin-3-yl)oxy)acetate (3.83)**

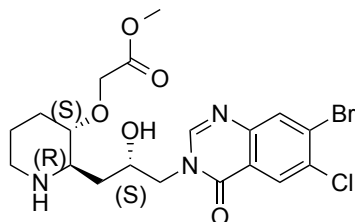
Potassium hydride (4 mg, 0.9 mmol) was suspended in DMF (2 mL). It was cooled in an ice-water bath, and 7-bromo-6-chloro-4-quinazolinone (26 mg, 0.1 mmol) was added in. After 30 min, a solution of oxirane **3.82** (18 mg, 0.05 mmol) in DMF (2 mL) was added in. The reaction mixture was then heated at 80 °C for 72 h under argon atmosphere prior to addition of sat. aq. NH₄Cl (5 mL).

The aqueous fraction was extracted with DCM (3 x 5 mL). The organic extracts were combined, dried over anhydrous Na₂SO₄, filtered, and concentrated under vacuum. The crude residue was purified by flash column chromatography using DCM/Methanol to afford the desired alcohol (27 mg, 84%) as white solid.

ESI-MS: C₂₆H₃₇BrClN₃O₇S, *m/z* calculated for [M+H]⁺: 650.1, Found: 650.1; *m/z* calculated for [M+Na]⁺: 672.1, Found: 672.1; *m/z* calculated for [M-H]⁻: 648.1, Found: 648.1.

¹H NMR δ (MeOD) 8.32 (s, 1H), 8.13 (s, 1H), 8.07 (s, 1H), 4.31–4.20 (m, 2H), 4.11 (s, 2H), 4.07–3.97 (m, 2H), 3.72–3.52 (m, 2H), 3.19 (td, *J* = 13.4, 2.6 Hz, 1H), 2.12–1.61 (m, 6H), 1.50 (s, 9H), 1.44 (s, 9H). **¹³C NMR** δ (MeOD) 170.4, 160.1, 150.0, 146.5, 132.7, 131.8, 128.7, 126.8, 122.0, 81.3, 66.3, 65.9, 61.4, 51.8, 42.1, 34.6, 31.7, 29.4, 27.0, 23.4, 22.3, 19.4.

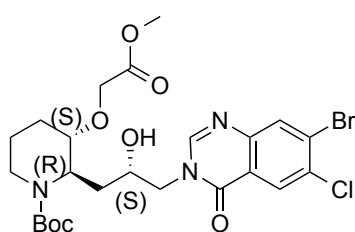
Methyl-2-(((2R,3S)-2-((S)-3-(7-bromo-6-chloro-4-oxoquinazolin-3(4H)-yl)-2-hydroxypropyl)piperidin-3-yl)oxy)acetate (3.84)



A solution of **3.83** (25 mg, 0.04 mmol) in 6 M HCl in MeOH (3 mL) was stirred at r.t. for 3 h, under argon atmosphere. Solvent was removed under pressure and the crude was used without further purification (6.8 mg, 35%).

ESI-MS: C₁₉H₂₃BrClN₃O₅, *m/z* calculated for [M+H]⁺: 488.1, Found: 488.1; *m/z* calculated for [M+Na]⁺: 510.1, Found: 510.1; *m/z* calculated for [M-H]⁻: 486.1, Found: 486.1.

tert-butyl-(2R,3S)-2-(((S)-3-(7-bromo-6-chloro-4-oxoquinazolin-3(4H)-yl)-2-hydroxypropyl)-3-(2-methoxy-2-oxoethoxy)piperidine-1-carboxylate (3.85)



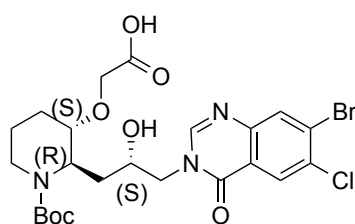
To a solution of **3.84** (5 mg, 0.01 mmol) in DMF (2 mL), was added DIPEA (5 μL, 3 equiv.) followed by Boc₂O (2.5 μL, 1.1 equiv.). The reaction stirred at r.t. for 5 h, under argon atmosphere. The solvent was removed under pressure and the crude was purified by flash column chromatography using DCM/Methanol to

afford the desired compound **3.85** (4 mg, 75%) as a white solid.

ESI-MS: C₂₄H₃₁BrClN₃O₇, *m/z* calculated for [M+H]⁺: 588.1, Found: 588.1; *m/z* calculated for [M+Na]⁺: 610.1, Found: 610.1; *m/z* calculated for [M-H]⁻: 586.1, Found: 586.1.

¹H NMR δ (CDCl₃) 8.33 (s, 1H), 8.20 (s, 1H), 8.04 (s, 1H), 4.52 (m, 1H), 4.33 (m, 1H), 4.15 (s, 2H), 4.10 – 3.95 (m, 2H), 3.74 (s, 3H), 3.60 (m, 1H), 3.55 (t, *J* = 5.1 Hz, 1H), 3.49 (m, 1H), 1.98 – 1.71 (m, 6H), 1.45 (s, 9H).

2-(((2R,3S)-2-(((S)-3-(7-bromo-6-chloro-4-oxoquinazolin-3(4H)-yl)-2-hydroxypropyl)-1-(tert-butoxycarbonyl)piperidin-3-yl)oxy)acetic acid (3.86)



Compound **3.85** (2 mg, 0.003 mmol) was dissolved in 1 M LiOH (20 μL, 0.02 mmol) and stirred at 60 °C for 5 h. The solvent was removed under pressure and the crude was analyzed by LC/MS.

ESI-MS: C₂₃H₂₉BrClN₃O₇, *m/z* calculated for [M+H]⁺: 574.1, Found: 574.1; *m/z* calculated for [M+Na]⁺: 596.1, Found: 596.1;

m/z calculated for $[M-H]^-$: 572.1, Found: 572.1.

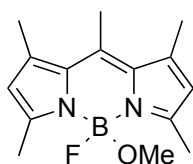
6.1.5 Synthesis of Fluorescent Probes

6.1.5.1 Synthesis of CMA-BODIPYS

General Procedure O

In a round-bottom flask, 1,3,5,7,8-Pentamethyl BODIPY **4.13** (1 equiv.) was dissolved in DCM to give a final concentration of 1.9 mM. The solution was cooled to 0 °C on an ice-water bath and, upon stirring, TMSOTf (5 equiv.) was added from a 10% (v/v) stock-solution in TCM. The reaction was allowed to proceed for 2 minutes and 30 seconds. Then, a premixed solution of alcohol (~100 equiv.) and DIPEA (10 equiv.) was rapidly injected into the reaction. The mixture was then partitioned between DCM: H₂O (1:1). The organics were washed 3 times with H₂O containing 10% NaCl (sat), dried over Na₂SO₄ and gravity filtered. The solvents were removed *in vacuo* at room temperature. All purifications were performed immediately after obtaining the dry crude product, by flash column chromatography using toluene/acetonitrile to afford the desired compound.

1,3,5,7,8-Pentamethyl fluoro methoxy BODIPY (4-fluoro-4-methoxy-1,3,5,7,8-pentamethyl-4-bora-3a,4a-diaza-s-indacene) (4.15)



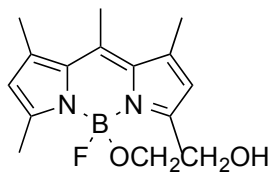
The desired compound **4.15** was obtained according to general procedure O, as an orange powder (14 mg, 0.051 mmol, 46%).

ESI-MS: C₁₅H₂₀BFN₂O, m/z calculated for $[M-H]^-$: 273.2 Found: 273.3; m/z calculated for $[M+Na]^+$: 297.2, Found: 297.2; m/z calculated for $[M-F]^+$

Calculated: 255.2, Found: 255.2.

¹H NMR δ (C₆D₆) 5.76 (s, 2H), 3.11 (s, 3H), 2.66 (s, 6H), 1.99 (s, 6H), 1.87 (s, 3H). **¹³C NMR** δ (C₆D₆) 154.08, 141.42, 139.75, 133.17, 121.25, 49.12 (d, $J = 6.9$ Hz), 17.22, 16.07, 14.75 (d, $J = 2.6$ Hz).

1,3,5,7,8-Pentamethyl fluoro glycol BODIPY (4-fluoro-4-hydroxyethoxy-1,3,5,7,8-pentamethyl-4-bora-3a,4a-diaza-s-indacene) (4.16)

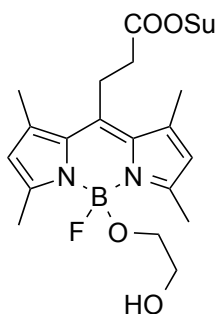


The desired compound **4.16** was obtained according to general procedure O, as an orange powder (20 mg, 0.066 mmol, 43%).

ESI-MS: C₁₆H₂₂BFN₂O₂, *m/z* calculated for [M+Na]⁺: 327.2, Found: 327.2.

¹H NMR δ (C₆D₆) 5.74 (s, 2H), 3.56 (q, *J* = 5.3 Hz, 2H), 3.10 (t, *J* = 4.9 Hz, 2H), 2.60 (s, 6H), 2.21 (t, *J* = 6.2 Hz, 1H), 1.98 (s, 6H), 1.86 (s, 3H). **¹³C NMR** δ (C₆D₆) 154.34, 141.76, 140.26, 133.32, 121.72, 63.93, 63.39 (d, *J* = 5.7 Hz), 17.52, 16.39, 15.12 (d, *J* = 2.8 Hz).

(4-fluoro-4-hydroxyethoxy-1,3,5,7-tetramethyl-8-(N-succinimidyl carboxypropyl)-4-bora-3a,4a-diaza-s-indacene) (4.19)



To BODIPY-NHS **4.17** (20 mg, 0.048 mmol) in CHCl₃ (10 mL) was added TMSOTf from a 10% (v/v) stock solution in CHCl₃ (434 μL, 0.24 mmol) upon stirring at 0 °C. After, 4 min activation, the reaction was rapidly quenched with a premixed solution of ethylene glycol (1.38 mL, 2.4 mmol) and DIPEA (52 μL, 0.30 mmol). After 5 minutes, the reaction was poured into 100 mL of a 1:1 mixture of 2-methyltetrahydrofuran: NaCl (sat). The organic layer was dried over Na₂SO₄, filtered and the solvents removed *in vacuo*. The crude was purified by flash column chromatography using toluene/acetonitrile to afford the desired compound **4.19** (10.4 mg, 0.023 mmol, 47%) as an orange solid.

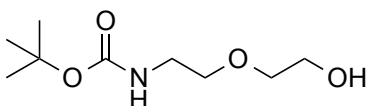
ESI-MS: C₂₂H₂₇BFN₃O₆, *m/z* calculated for [M+Na]⁺: 482.2, Found: 482.2.

¹H NMR δ (CDCl₃) 6.08 (s, 2H), 3.53 (q, *J* = 5.1 Hz, 2H), 3.45–3.40 (m, 2H), 2.96 (t, *J* = 4.8 Hz, 2H), 2.92–2.84 (m, 6H), 2.52 (s, 6H), 2.45 (s, 6H).

6.1.5.2 Synthesis of HaloTag functionalized CMA-BODIPY

HaloTag was synthesized following the procedure published by Neklesa *et al*⁴⁴⁴.

tert-Butyl (2-(2-hydroxyethoxy)ethyl)carbamate (4.20)



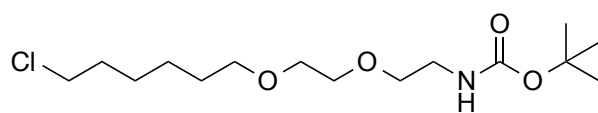
To a solution of 2-(2-aminoethoxy)-ethanol (2.1 g, 20 mmol) in EtOH (5 mL) at 0 °C was added Boc₂O (4.36 g, 20 mmol). The

reaction mixture was stirred at r.t. for 4 h, evaporated, and diluted with DCM (20 mL) and H₂O (20 mL). The mixture was extracted twice with DCM, and the combined extracts were washed with brine, dried over Na₂SO₄, filtered, and concentrated. The residue was purified by flash column chromatography using hexanes/ethyl acetate to afford the desired compound tert-butyl (2-(2-hydroxyethoxy)ethyl)carbamate (4 g, 98%).

ESI-MS: C₉H₁₉NO₄, *m/z* calculated for [M+Na]⁺: 228.4, Found: 228.4.

¹H NMR δ (CDCl₃) 5.01 (br s, 1H), 3.76-3.72 (m, 2H), 3.58-3.54 (m, 4H), 3.35-3.32 (m, 2H), 2.39 (t, *J* = 5.9 Hz, 1H), 1.44 (s, 9H). **¹³C NMR** δ (CDCl₃) 156.1, 79.3, 72.1, 70.3, 61.7, 40.3, 28.7

***tert*-Butyl (2-(2-((6-chlorohexyl)oxy)ethoxy)ethyl)carbamate (4.21)**

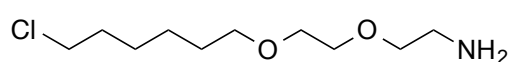


To a solution of tert-butyl (2-(2-hydroxyethoxy)ethyl)carbamate **4.20** (2.2 g, 10.5 mmol) in THF (20 mL) and DMF (10 mL) at 0 °C added portion wise NaH (60% dispersion in mineral oil, 560 mg, 14.0 mmol). After stirring at 0 °C for 0.5 h, 6-chloro-1-iodohexane (2.4 mL, 15.72 mmol) was added to the mixture at 0 °C. The reaction mixture was stirred at 0 °C for 20 min, at r.t. for 3 h, and quenched at 0 °C with saturated NH₄Cl solution in H₂O. The mixture was extracted twice with ethyl acetate and the combined extracts were washed with brine, dried over Na₂SO₄, filtered, and concentrated. The residue was purified by flash chromatography using hexanes/ethyl acetate to afford the tert-butyl (2-(2-((6-chlorohexyl)oxy)ethoxy)ethyl) carbamate **4.21** (1.3 g, 38%).

ESI-MS: C₁₅H₃₀ClNO₄, *m/z* calculated for [M+Na]⁺: 346.2, Found: 346.2.

¹H NMR δ (CDCl₃) 4.98 (br s, 1H), 3.61-3.51 (m, 8H), 3.46 (t, *J* = 6.7 Hz, 2H), 3.31 (t, *J* = 4.7 Hz, 2H), 1.81-1.74 (m, 2H), 1.61-1.57 (m, 2H), 1.49-1.33 (m, 4H), 1.43 (s, 9H). **¹³C NMR** δ (CDCl₃) 155.9, 79.2, 71.2, 70.3, 70.2, 70.0, 45.0, 32.5, 29.4, 28.4, 26.7, 25.4.

***2*-(2-((6-Chlorohexyl)oxy)ethoxy)ethanamine (4.22)**



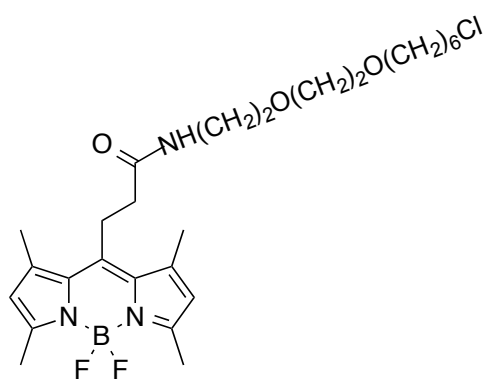
A 2 M HCl solution in MeOH of tert -butyl (2-(2-((6-chlorohexyl)oxy)ethoxy)ethyl)carbamate **4.21** (1.3 g, 4.2 mmol) was stirred at r.t. for 2 h. The solvent was removed under reduced pressure and the crude amine was purified by flash column chromatography using ethyl

acetate/water:methanol:acetonitrile (1:1:1) to give 2-(2-((6-chlorohexyl)oxy)ethoxy)ethanamine **4.22** (727.2 mg, 78%).

ESI-MS: $C_{10}H_{22}ClNO_2$, m/z calculated for $[M+H]^+$: 224.7, Found: 224.7; m/z calculated for $[M+Na]^+$: 246.6, Found: 246.6.

1H NMR δ ($CDCl_3$) 6.47 (br s, 1H), 3.69 (t, $J = 4.9$ Hz, 2H), 3.63-3.60 (m, 2H), 3.56-3.53 (m, 2H), 3.52 (t, $J = 6.6$ Hz, 2H), 3.44 (t, $J = 6.8$ Hz, 2H), 3.12 (t, $J = 4.9$ Hz, 2H), 1.79-1.71 (m, 2H), 1.60-1.53 (m, 2H), 1.46- 1.39 (m, 2H), 1.36-1.28 (m, 2H). **^{13}C NMR** δ ($CDCl_3$) 71.1, 70.1, 69.7, 45.0, 39.4, 32.4, 29.1, 26.5, 25.1.

(4,4-difluoro-1,3,5,7-tetramethyl-8-(3-((2-(2-((6-chlorohexyl)oxy)ethoxy)ethyl)amino)-3-oxopropyl)-4-bora-3a,4a-diaza-s-indacene) (4.23)



BODIPY-NHS **4.17** (12.5 mg, 0.03 mmol) was dissolved in DCM (2 mL).

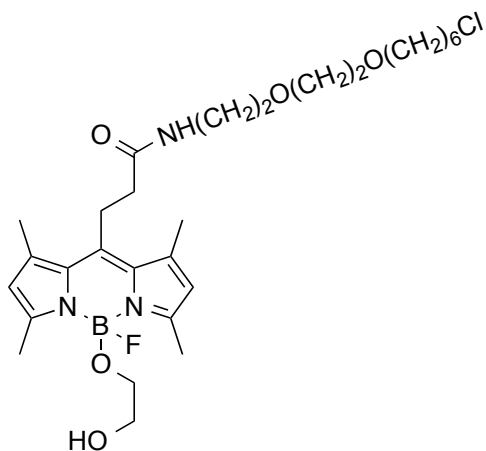
To this solution was added 2-(2-((6-chlorohexyl)oxy)ethoxy)ethanamine hydrochloride (6.7 mg, 0.03 mmol) and DIPEA (16 μ L, 0.09 mmol). The reaction mixture was left to stir at r.t. for 30 min. The solvent was removed *in vacuo* at room temperature. The

crude mixture was purified by flash column chromatography using toluene/acetonitrile to afford an orange solid (5.8 mg, 0.01 mmol, 37%).

ESI-MS: $C_{26}H_{39}BClF_2N_3O_3$, m/z calculated for $[M-H]^-$: 524.2, Found: 524.2; m/z calculated for $[M+Na]^+$: 548.3, Found: 548.3.

1H NMR δ (C_6D_6) 5.67 (s, 2H), 5.41 (br s, 1H, -NH), 3.32-3.30 (m, 6H), 3.21-3.07 (m, 8H), 2.60 (s, 6H), 2.15 (s, 6H), 1.82-1.78 (m, 2H), 1.42-1.36 (m, 4H), 1.16-1.06 (m, 4H). **^{13}C NMR** δ (C_6D_6) 170.40, 154.44, 144.47, 140.49, 131.30, 121.82, 71.29, 70.34, 70.02, 69.60, 44.99, 39.36, 37.39, 32.47, 32.47, 29.45, 26.63, 25.38, 23.84, 16.52, 14.47.

(4-fluoro-4-hydroxyethoxy-1,3,5,7-tetramethyl-8-(3-((2-(2-((6-chlorohexyl)oxy)ethoxy)ethyl)amino)-3-oxopropyl)-4-bora-3a,4a-diaza-s-indacene) (4.24)



To BODIPY **4.23** (3.1 mg, 0.01 mmol) in TCM (3 mL) was added TMSOTf from a 10%(v/v) stock solution in TCM (33 μ L, 0.02 mmol) under stirring at 0 $^{\circ}$ C. After 2 mins and 30 seconds activation, the reaction was quenched with ethylene glycol (~100 equiv.) and the reaction was allowed to stir for an additional two minutes. The mixture was then partitioned between a 1:1 solution of DCM: NaHCO₃ (sat). The organics were washed 3 times with H₂O containing 10% NaCl (sat),

dried over Na₂SO₄ and filtered. The combined organic fractions were removed under reduced pressure at room temperature. The crude was purified by flash column chromatography using toluene/acetonitrile to afford the desired compound **4.24** as an orange solid (2 mg, 0.004 mmol, 60%).

ESI-MS: C₂₈H₄₄BClFN₃O₅, *m/z* calculated for [M-H]⁻: 566.2 Found: 566.2; *m/z* calculated for [M+Na]⁺: 590.3 Found: 590.3.

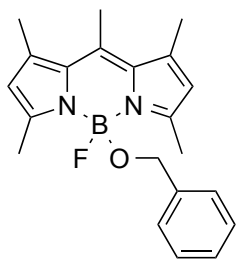
¹H NMR δ (C₆D₆) 5.71 (s, 2H), 5.50 (br s, 1H, -NH), 3.58 (br s, 1H, -OH), 3.32-3.30 (m, 8H), 3.20-3.08 (m, 10H), 2.58 (s, 6H), 2.19 (d, *J* = 5.6 Hz 6H), 1.40-1.30 (m, 6H), 1.15-1.11 (m, 4H).

6.1.5.3 Synthesis of Monoalkoxy BODIPYs

General Procedure P

1,3,5,7,8-Pentamethyl BODIPY (250 mg, 1 equiv.) was dissolved in toluene and heated to 60 $^{\circ}$ C, followed by addition of the appropriate alcohol (1.5 equiv.) and 5 \AA molecular sieves (50 mg of molecular sieves/ mg of fluorophore). The reaction was allowed to proceed for 3 h and gravity filtered. The solvent was removed under reduced pressure and the crude was purified immediately, by flash column chromatography using toluene/acetonitrile to afford the desired compound.

1,3,5,7,8-Pentamethyl fluoro benzyloxy BODIPY (4-fluoro-4-benzyloxy-1,3,5,7,8-pentamethyl-4-bora-3a,4a-diaza-s-indacene) (4.25)



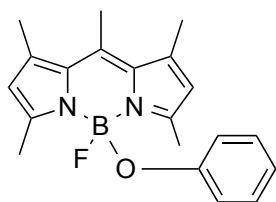
Reaction of 1,3,5,7,8-Pentamethyl BODIPY (250 mg, 0.95 mmol) and benzyl alcohol (149 μ L, 1.43 mmol) according to general procedure P, gave 116.9 mg (35%) of desired fluorophore as an orange solid.

ESI-MS: $C_{20}H_{22}BFN_2O$, m/z calculated for $[M-H]^-$: 349.2 Found: 349.2; m/z calculated for $[M+Na]^+$: 373.2 Found: 373.2; m/z calculated for $[M-F]^+$

Calculated: 331.2, Found: 331.2.

1H NMR δ ($CDCl_3$) 7.24–7.08 (m, 5H), 6.02 (s, 2H), 4.02 (s, 2H), 2.60 (s, 3H), 2.52 (s, 6H), 2.43 (s, 6H). **^{13}C NMR** δ ($CDCl_3$) 153.9, 140.1, 128.4, 127.9, 127.7, 127.3, 127.0, 126.4, 121.3, 64.2, 17.4, 16.4, 14.6.

1,3,5,7,8-Pentamethyl fluoro phenoxy BODIPY (4-fluoro-4-phenoxy-1,3,5,7,8-pentamethyl-4-bora-3a,4a-diaza-s-indacene) (4.26)

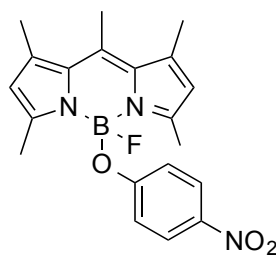


Reaction of 1,3,5,7,8-Pentamethyl BODIPY (250 mg, 0.95 mmol) and phenol (121 μ L, 1.43 mmol) according to general procedure P, gave 144.3 mg (45%) of desired fluorophore as orange solid.

ESI-MS: $C_{20}H_{22}BFN_2O$, m/z calculated for $[M-H]^-$: 335.2 Found: 335.2; m/z calculated for $[M+Na]^+$: 359.3 Found: 359.2; m/z calculated for $[M-F]^+$ Calculated: 317.2, Found: 317.2.

1H NMR δ ($CDCl_3$) 7.03 (dd, $J = 7.2, 7.1$ Hz, 2H), 6.73 (t, $J = 7.1$ Hz, 1H), 6.45 (d, $J = 7.2, 2H$), 6.00 (s, 2H), 2.64 (s, 3H), 2.47 (s, 6H), 2.43 (s, 6H).

1,3,5,7,8-Pentamethyl fluoro 4-nitrophenoxy BODIPY (4-fluoro-4-(4-nitrophenyl)oxy-1,3,5,7,8-pentamethyl-4-bora-3a,4a-diaza-s-indacene) (4.27)

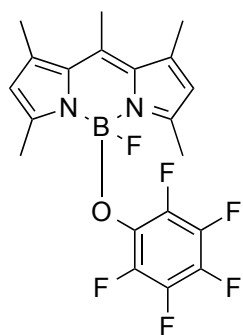


Reaction of 1,3,5,7,8-Pentamethyl BODIPY (250 mg, 0.95 mmol) and *p*-nitrophenol (198.9 mg, 1.43 mmol) according to general procedure P, gave 181.8 mg (50%) of the desired fluorophore as orange solid.

ESI-MS: $C_{20}H_{21}BFN_3O_3$, m/z calculated for $[M-H]^-$: 380.2 Found: 380.2; m/z calculated for $[M+Na]^+$: 404.2 Found: 404.2; m/z calculated for $[M-F]^+$ Calculated: 362.2, Found: 362.2.

¹H NMR δ (CDCl₃) 7.98–7.92 (m, 2H), 6.54 (d, J = 9.2 Hz, 1H), 6.48 (d, J = 9.2 Hz, 1H), 6.03 (s, 2H), 2.49 (s, 3H), 2.46–2.46 (m, 12H). **¹³C NMR** δ (CDCl₃) 162.3, 154.7, 154.1, 142.6, 141.9, 140.7, 140.4, 132.2, 126.1, 125.9, 122.8, 122.0, 118.0, 117.6, 115.7, 17.5, 17.3, 16.5, 15.2, 14.8.

1,3,5,7,8-Pentamethyl fluoro pentafluorophenoxy BODIPY (4-fluoro-4-(pentafluorophenyl)oxy-1,3,5,7,8-pentamethyl-4-bora-3a,4a-diaza-s-indacene) (4.28) Reaction



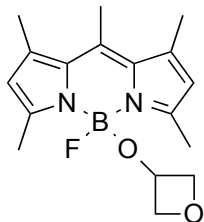
of 1,3,5,7,8-Pentamethyl BODIPY (250 mg, 0.95 mmol) and pentafluorophenol (263.2 mg, 1.43 mmol) according to general procedure P, gave 182.9 mg (45%) of the desired fluorophore as an orange solid.

ESI-MS: C₂₀H₁₇BF₆N₂O, m/z calculated for [M-H]⁻: 425.1 Found: 425.1; m/z calculated for [M+Na]⁺: 449.1 Found: 449.1; m/z calculated for [M-F]⁺ Calculated: 407.1, Found: 407.1.

¹H NMR δ (CDCl₃) 6.04 (s, 2H), 2.53 (s, 3H), 2.49 (s, 6H), 2.40 (s, 6H).

¹³C NMR δ (CDCl₃) 154.3, 141.3, 132.3, 121.6, 17.3, 16.5, 14.6.

1,3,5,7,8-Pentamethyl fluoro oxetan-3-yloxy BODIPY (4-fluoro-4-oxetan-3-yloxy-1,3,5,7,8-pentamethyl-4-bora-3a,4a-diaza-s-indacene) (4.29)



Reaction of 1,3,5,7,8-Pentamethyl BODIPY (50 mg, 0.19 mmol) and 3-oxetanol (14.8 μ L, 0.28 mmol) according to general procedure P, gave 18.5 mg (30%) of the desired fluorophore as an orange solid.

ESI-MS: C₁₇H₂₂BFN₂O₂, m/z calculated for [M-H]⁻: 315.1 Found: 315.1; m/z calculated for [M+Na]⁺: 339.1 Found: 339.1; m/z calculated for [M-F]⁺

Calculated: 297.1, Found: 297.1.

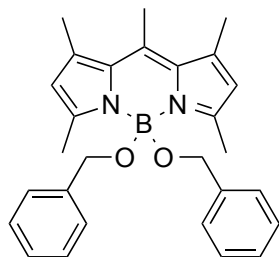
¹H NMR δ (CDCl₃) 6.02 (s, 2H), 4.46–4.28 (m, 2H), 4.26–4.12 (m, 2H), 4.07 (m, 1H), 2.58 (s, 3H), 2.42 (s, 6H), 2.39 (s, 6H).

6.1.5.4 Synthesis of Dialkoxy BODIPYs

General Procedure Q

1,3,5,7,8-Pentamethyl BODIPY (250 mg, 1 equiv.) was dissolved in toluene or THF (5 mL) and heated to 60 °C, followed by addition of the appropriate alcohol (2.5 equiv.) and 5Å molecular sieves (50 mg of molecular sieves/ mg of fluorophore). The reaction was allowed to proceed for 24 h and gravity filtered. The solvent was removed under reduced pressure and the crude was purified immediately by flash column chromatography using toluene/acetonitrile to afford the desired compound.

1,3,5,7,8-Pentamethyl di(benzyloxy) BODIPY (4,4-dibenzyloxy-1,3,5,7,8-pentamethyl-4-bora-3a,4a-diaza-s-indacene) (4.30)

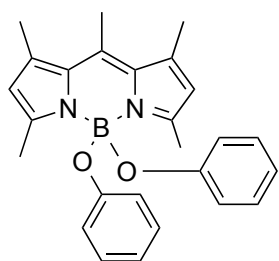


Reaction of 1,3,5,7,8-Pentamethyl BODIPY (250 mg, 0.95 mmol) and benzyl alcohol (247.7 μ L, 2.38 mmol) according to general procedure Q, gave 388.7 mg (93%) of the desired fluorophore as an orange solid.

ESI-MS: $C_{28}H_{31}BN_2O_2$, m/z calculated for $[M-H]^-$: 437.3 Found: 437.3; m/z calculated for $[M+Na]^+$: 461.3 Found: 461.3.

1H NMR δ ($CDCl_3$) 7.33–7.27 (m, 5H), 7.24–7.19 (m, 5H), 5.97 (s, 2H), 4.04 (s, 4H), 2.63 (s, 3H), 2.58 (s, 3H), 2.54 (s, 3H), 2.46 (s, 3H), 2.44 (s, 3H), 2.42 (s, 3H). **^{13}C NMR** δ ($CDCl_3$) 154.1, 141.8, 139.4, 128.3, 127.7, 127.3, 127.0, 126.2, 121.3, 64.2, 17.6, 16.5, 14.8.

1,3,5,7,8-Pentamethyl diphenoxy BODIPY (4,4-diphenoxy-1,3,5,7,8-pentamethyl-4-bora-3a,4a-diaza-s-indacene) (4.31)

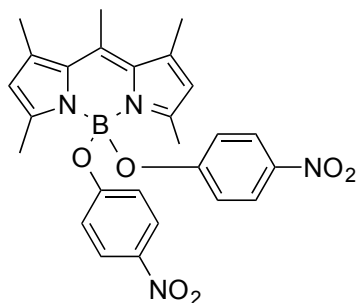


Reaction of 1,3,5,7,8-Pentamethyl BODIPY (250 mg, 0.95 mmol) and phenol (202 μ L, 2.38 mmol) according to general procedure Q, gave 246.5 mg (63%) of the desired fluorophore as an orange solid.

ESI-MS: $C_{26}H_{27}BN_2O_2$, m/z calculated for $[M-H]^-$: 409.2 Found: 409.2; m/z calculated for $[M+Na]^+$: 433.2 Found: 433.2.

1H NMR δ ($CDCl_3$) 7.06 – 6.99 (m, 4H), 6.76 (d, $J = 8.2$ Hz, 1H), 6.70 (d, $J = 8.1$ Hz, 1H), 6.54 – 6.49 (m, 4H), 5.95 (s, 2H), 2.66 (s, 3H), 2.51 (s, 6H), 2.43 (s, 6H). **^{13}C NMR** δ ($CDCl_3$) 156.7, 154.6, 141.0, 132.8, 129.5, 129.1, 122.1, 119.5, 118.6, 17.7, 16.6, 15.2

1,3,5,7,8-Pentamethyl di(4-nitrobenzyloxy) BODIPY (4,4-di(4-nitrobenzyl)oxy-1,3,5,7,8-pentamethyl-4-bora-3a,4a-diaza-s-indacene) (4.32)

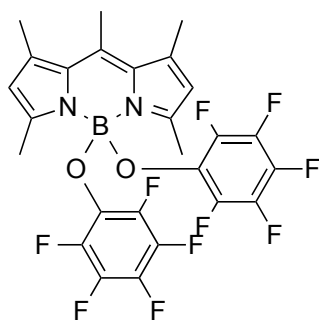


Reaction of 1,3,5,7,8-Pentamethyl BODIPY (250 mg, 0.95 mmol) and *p*-nitrophenol (331.2 mg, 2.38 mmol) according to general procedure Q, gave 365.9 mg (65%) of the desired fluorophore as an orange solid.

ESI-MS: C₂₆H₂₅BN₄O₆, *m/z* calculated for [M-H]⁻: 499.2 Found: 499.2; *m/z* calculated for [M+Na]⁺: 523.2 Found: 523.2.

¹H NMR δ (CDCl₃) 7.90 (d, *J* = 9.2 Hz, 4H), 6.47 (d, *J* = 9.2 Hz, 4H), 5.96 (s, 2H), 2.70 (s, 3H), 2.43 (s, 6H), 2.34 (s, 6H). ¹³C NMR δ (CDCl₃) 162.3, 154.7, 142.6, 141.6, 140.7, 132.5, 125.9, 122.8, 118.0, 17.7, 16.6, 14.9.

1,3,5,7,8-Pentamethyl di(pentafluorobenzyloxy) BODIPY (4,4-di(pentafluorobenzyl)oxy-1,3,5,7,8-pentamethyl-4-bora-3a,4a-diaza-s-indacene) (4.33)

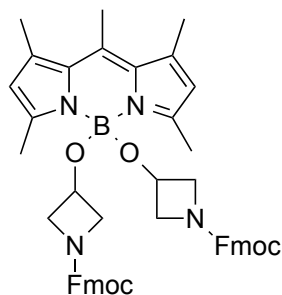


Reaction of 1,3,5,7,8-Pentamethyl BODIPY (250 mg, 0.95 mmol) and pentafluorophenol (438.4 mg, 2.38 mmol) according to general procedure Q, gave 365.9 mg (65%) of the desired fluorophore as an orange solid.

ESI-MS: C₂₆H₁₇BF₁₀N₂O₂, *m/z* calculated for [M-H]⁻: 589.1 Found: 589.1; *m/z* calculated for [M+Na]⁺: 613.1 Found: 613.1.

¹H NMR δ (CDCl₃) 6.02 (s, 2H), 2.58 (s, 3H), 2.42 (s, 6H), 2.39 (s, 6H). ¹³C NMR δ (CDCl₃) 154.5, 142.1, 133.0, 122.5, 18.0, 17.0, 15.1.

1,3,5,7,8-Pentamethyl di(1-Fmoc-3-hydroxyazetidide) BODIPY (4,4-(di(1-Fmoc-3-hydroxyazetidide)-1,3,5,7,8-pentamethyl-4-bora-3a,4a-diaza-s-indacene) (4.34)



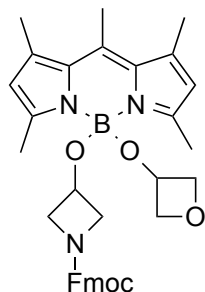
Reaction of 1,3,5,7,8-Pentamethyl BODIPY (250 mg, 0.95 mmol) and 1-Fmoc-3-hydroxyazetidide (703.6 mg, 2.38 mmol) according to general procedure Q, gave 503.6 mg (65%) of desired fluorophore as orange solid.

ESI-MS: $C_{50}H_{49}BN_4O_6$, m/z calculated for $[M-H]^-$: 811.4 Found: 811.4; m/z calculated for $[M+Na]^+$: 835.4 Found: 835.4.

1H NMR δ ($CDCl_3$) 7.66–7.60 (m, 4H), 7.45–7.40 (m, 4H), 7.36–7.11 (m, 8H), 6.04 (s, 2H), 4.23–4.01 (m, 6H), 3.93–3.51 (m, 10H), 2.55 (s, 3H), 2.47 (s, 6H), 2.39 (s, 6H). ^{13}C NMR δ ($CDCl_3$) 156.6, 144.1, 141.5, 141.4, 133.1, 127.7, 127.1, 125.3, 122.1, 120.1, 120.0, 67.1, 60.4, 47.3, 29.8, 22.8, 17.7, 16.7, 15.3.

Reaction of 1,3,5,7,8-Pentamethyl di(1-Fmoc-3-hydroxyazetidide) BODIPY (50 mg, 0.06 mmol) and 3-oxetanol (7.9 μ L, 0.15 mmol) according to general procedure Q for 1 h, yielded a mixture of mono- (4.35) and di-substitution (4.36) by LC/MS.

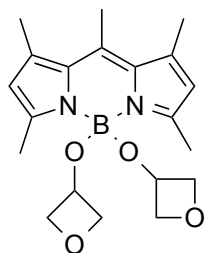
1,3,5,7,8-Pentamethyl 4-(1-Fmoc-3-hydroxyazetidide)-4-(oxetan-3-yloxy) BODIPY (4,4-di(oxetan-3-yloxy)-1,3,5,7,8-pentamethyl-4-bora-3a,4a-diaza-s-indacene) (4.35)



ESI-MS: $C_{35}H_{38}BN_3O_5$, m/z calculated for $[M-H]^-$: 590.3 Found: 590.3; m/z calculated for $[M+Na]^+$: 613.3 Found: 613.3.

1H NMR δ ($CDCl_3$) 7.82 (dd, $J = 9.2, 8.2$ Hz, 2H), 7.66 (dd, $J = 18.5, 8.2$ Hz, 2H), 7.46–7.24 (m, 4H), 6.25–6.07 (m, 2H), 4.46–4.28 (m, 4H), 4.26–4.12 (m, 3H), 4.07 (m, 1H), 3.98 (m, 1H), 3.87–3.71 (m, 2H), 3.59–3.56 (m, 2H), 2.73–2.64 (m, 3H), 2.49 (m, 12H). ^{13}C NMR δ ($CDCl_3$) 158.3, 154.9, 145.2, 145.2, 143.7, 143.3, 143.0, 142.6, 141.8, 134.8, 134.2, 128.8, 128.8, 128.2, 128.1, 126.1, 126.0, 123.0, 122.7, 122.4, 121.0, 120.9, 81.6, 71.7, 69.6, 68.2, 68.0, 65.6, 63.9, 61.7, 17.5, 17.0, 16.9, 15.3, 14.8.

1,3,5,7,8-Pentamethyl di(oxetan-3-yloxy) BODIPY (4,4-di(oxetan-3-yloxy)-1,3,5,7,8-pentamethyl-4-bora-3a,4a-diaza-s-indacene) (4.36)



ESI-MS: C₂₀H₂₇BN₂O₄, *m/z* calculated for [M-H]⁻: 369.2 Found: 369.2; *m/z* calculated for [M+Na]⁺: 393.2 Found: 393.2.

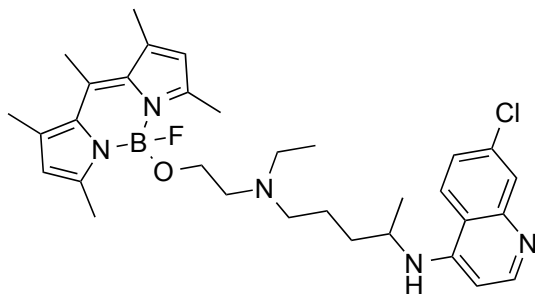
¹H NMR δ (CDCl₃) 6.02 (s, 2H), 4.46–4.28 (m, 4H), 4.26–4.12 (m, 4H), 4.07 (m, 2H), 2.58 (s, 3H), 2.42 (s, 6H), 2.39 (s, 6H).

6.1.5.5 Synthesis of Small Molecule Probes

General Procedure R

1,3,5,7,8-Pentamethyl fluoro methoxy BODIPY **4.15** (10 mg, 1 equiv.) was dissolved in toluene or THF and heated to 60 °C, followed by addition of the appropriate alcohol (1.5 equiv.) and 5Å molecular sieves (50 mg of molecular sieves/ mg of fluorophore). The reaction was allowed to proceed for 8 h and gravity filtered. The solvent was removed under reduced pressure and the crude was purified immediately after obtaining the dry crude product, by reverse flash column chromatography using water/acetonitrile to afford the desired compound.

1,3,5,7,8-Pentamethyl Ethoxychloroquine BODIPY (4.37)



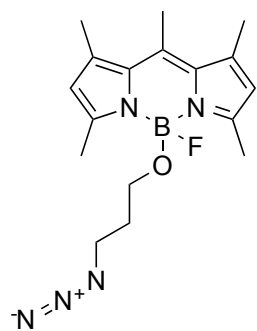
Reaction of 1,3,5,7,8-Pentamethyl fluoro methoxy BODIPY **4.15** (10 mg, 0.04 mmol) and hydroxychloroquine (20.1 mg, 0.06 mmol) in THF, according to general procedure R, gave 8 mg (60%) of the desired fluorophore as an orange solid.

ESI-MS: C₃₂H₄₂BClFN₅O, *m/z* calculated for [M-H]⁻: 576.3, Found: 576.3; *m/z* calculated for [M+Na]⁺: 600.2 Found: 600.2.

¹H NMR δ (DMSO) 8.40–8.32 (m, 2H), 7.78 (dd, *J* = 2.4, 1.9 Hz, 1H), 7.44 (dd, *J* = 9.0, 1.9 Hz, 1H), 6.99 (d, *J* = 9.0 Hz, 1H), 6.53 (s, 1H), 6.10 (s, 1H), 3.55 (t, *J* = 5.9 Hz, 2H), 2.81–2.67 (m, 4H), 2.62–2.53 (m, 3H), 2.45 (s, 3H), 2.35 (s, 3H), 2.11 (s, 3H), 2.01 (s, 3H), 1.70 (s, 3H), 1.63–1.37 (m, 4H), 1.22 (dd, *J* = 12.5, 6.3 Hz, 3H), 1.03 (t, *J* = 7.1 Hz, 3H). **¹³C NMR** δ (DMSO)

152.7, 151.5, 149.7, 148.9, 139.6, 133.5, 127.1, 126.4, 126.2, 124.4, 123.9, 121.0, 120.7, 117.4, 116.2, 108.7, 98.8, 57.3, 54.5, 52.5, 47.5, 47.4, 21.8, 19.8, 16.9, 16.0, 14.5, 12.6, 11.7, 10.1.

1,3,5,7,8-Pentamethyl fluoro 3-azidopropoxy BODIPY (4.38)

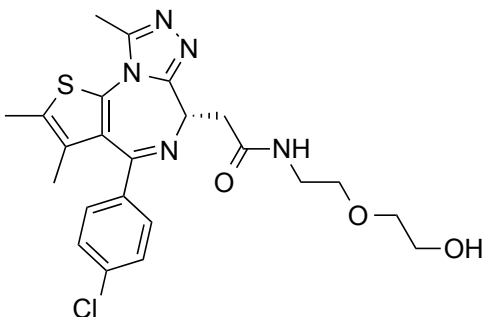


Reaction of 1,3,5,7,8-Pentamethyl fluoro methoxy BODIPY **4.15** (10 mg, 0.04 mmol) and 3-azidopropanol (6.1 mg, 0.06 mmol) in toluene, according to general procedure R, gave 8.9 mg (65%) of the desired fluorophore as an orange solid.

ESI-MS: $C_{17}H_{23}BFN_5O$, m/z calculated for $[M-H]^-$: 342.2 Found: 342.2; m/z calculated for $[M+Na]^+$: 366.2, Found: 366.2.

1H NMR δ (C_6D_6) 6.05 (s, 2H), 3.32 (t, $J = 6.8$ Hz, 2H), 2.95 (t, $J = 6.0$ Hz, 2H), 2.59 (s, 3H), 2.51 (s, 6H), 2.42 (s, 6H), 1.65 (p, $J = 6.5$ Hz, 2H). ^{13}C NMR δ (C_6D_6) 153.8, 141.4, 140.4, 132.9, 121.4, 58.3, 49.0, 31.1, 17.6, 16.6, 14.7.

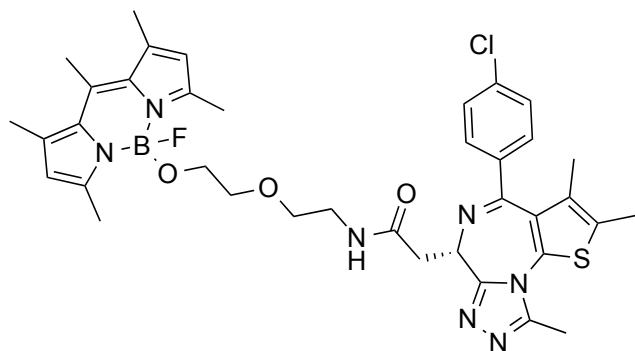
(S)-2-(4-(4-chlorophenyl)-2,3,9-trimethyl-6H-thieno[3,2-f][1,2,4]triazolo[4,3-a][1,4]diazepin-6-yl)-N-(2-(2-hydroxyethoxy)ethyl)acetamide (4.39a)



To a stirring solution of (+)-JQ1-COOH (20 mg, 0.05 mmol) in DMF (2 mL), HCTU (22.8 mg, 1.2 equiv.) was added in one portion. Following 10 minutes of stirring, 2-(2-aminoethoxy)ethan-1-ol (6.1 μ L, 0.06 mmol) and DIPEA (26.1 μ L, 0.15 mmol) were added sequentially. The solution was left to stir at room

temperature for 2 h. The reaction mixture was quenched with sat. aq. $NaHCO_3$, and the product was extracted with DCM. The organic phase was dried (Na_2SO_4), and the solvent was removed under reduced pressure. The crude product was purified by flash chromatography with DCM/methanol to afford the desired product (12.8 mg, 53%).

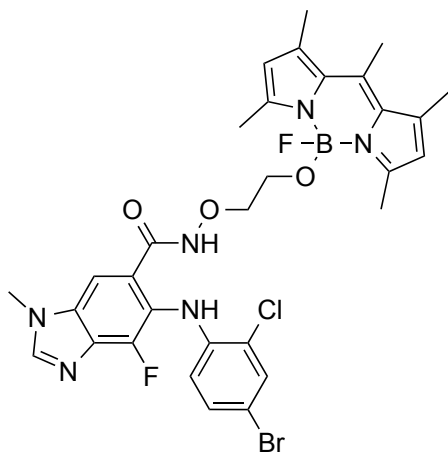
ESI-MS: $C_{23}H_{26}ClN_5O_3S$, m/z calculated for $[M-H]^-$: 486.1 Found: 486.3; m/z calculated for $[M+H]^+$: 488.1, Found: 488.3; m/z calculated for $[M+Na]^+$: 510.1, Found: 510.3.

1,3,5,7,8-Pentamethyl fluoro alkoxy-(+)-JQ1 BODIPY (4.39)

Reaction of 1,3,5,7,8-Pentamethyl fluoro methoxy BODIPY **4.15** (5 mg, 0.02 mmol) and hydroxy-compound **4.39a** (14.6 mg, 0.03 mmol) in toluene, according to general procedure R, gave 5.8 mg (40%) of desired fluorophore as orange solid.

ESI-MS: $C_{37}H_{42}BClFN_7O_3S$, m/z calculated for $[M-H]^-$: 728.3 Found: 728.3; m/z calculated for $[M+Na]^+$: 752.3, Found: 752.3.

1H NMR δ ($CDCl_3$) 7.41 (d, $J = 8.5$ Hz, 2H), 7.31 (d, $J = 8.5$ Hz, 2H), 6.06 (s, 1H), 4.65 (dd, $J = 7.7, 6.3$ Hz, 1H), 3.49 (t, $J = 5.4$ Hz, 2H), 3.47-3.44 (m, 4H), 3.37 (dd, $J = 14.6, 7.7$ Hz, 2H), 3.08 (t, $J = 5.4$ Hz, 2H), 2.66 (s, 3H), 2.59 (s, 3H), 2.55 (s, 6H), 2.42 (s, 6H), 2.39 (s, 3H), 1.67 (s, 3H).

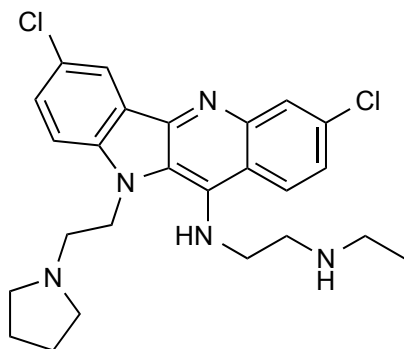
1,3,5,7,8-Pentamethyl fluoro selumetinib BODIPY (4.40)

Reaction of 1,3,5,7,8-Pentamethyl fluoro methoxy BODIPY **4.15** (5 mg, 0.02 mmol) and selumetinib (13.7 mg, 0.03 mmol) in THF, according to general procedure R, gave 6.9 mg (50%) of the desired fluorophore as an orange solid.

ESI-MS: $C_{31}H_{31}BBrClF_2N_6O_3$, m/z calculated for $[M-H]^-$: 697.1 Found: 697.1; m/z calculated for $[M+Na]^+$: 721.1, Found: 721.1.

1H NMR δ ($CDCl_3$) 8.04 (s, 1H), 7.94 (s, 1H), 7.70 (d, $J = 4.1$ Hz, 1H), 7.49 (d, $J = 2.2$ Hz, 1H), 7.45 (dd, $J = 4.1, 2.2$ Hz, 1H), 6.05 (s, 2H), 3.99–3.79 (m, 7H), 2.59 (s, 3H), 2.48 (s, 6H), 2.41 (s, 6H).

*N*¹-(3,7-dichloro-10-(2-(pyrrolidin-1-yl)ethyl)-10*H*-indolo[3,2-*b*]quinolin-11-yl)-*N*²-ethylethane-1,2-diamine (4.41)

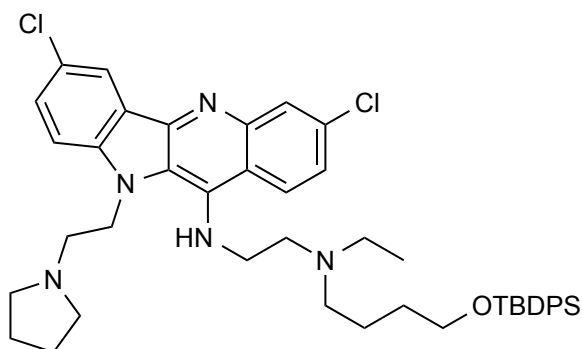


A solution of 3,7,11-trichloro-10-[2-(pyrrolidin-1-yl)ethyl]-10*H*-indolo[3,2-*b*]quinoline (50 mg, 0.1 mmol) in *N*¹-ethylethane-1,2-diamine (1 mL), stirred at 130 °C for 16 h. The solvent was removed under reduced pressure and the crude product was purified by reverse flash column chromatography using water/acetonitrile to afford the desired compound as a dark yellow solid (35 mg, 62%).

ESI-MS: C₂₅H₂₉Cl₂N₅, *m/z* calculated for [M-H]⁻: 468.4, Found: 468.4; *m/z* calculated for [M+H]⁺: 470.4, Found: 470.4.

¹H NMR δ (MeOD) 8.39 (d, *J* = 9.2 Hz, 1H), 8.35 (d, *J* = 2.0 Hz, 1H), 8.10 (d, *J* = 2.2 Hz, 1H), 7.68 (d, *J* = 8.8 Hz, 1H), 7.64 (dd, *J* = 8.8, 2.0 Hz, 1H), 7.56 (dd, *J* = 9.2, 2.2 Hz, 1H), 4.80 (dd, *J* = 7.2, 6.7 Hz, 2H), 3.63 (dd, *J* = 7.9, 6.3 Hz, 2H), 3.57–3.39 (m, 8H), 3.16 (dd, *J* = 7.9, 6.3 Hz, 2H), 2.74 (dd, *J* = 7.2, 6.7 Hz, 2H), 2.66 (q, *J* = 4.3 Hz, 2H), 1.77 (t, *J* = 4.3 Hz, 3H). ¹³C NMR δ (MeOD) 147.0, 145.2, 144.1, 137.0, 133.1, 130.0, 126.5, 126.2, 126.1, 125.4, 123.5, 123.2, 121.5, 120.9, 112.0, 54.0, 53.2, 44.5, 42.8, 41.8, 37.8, 22.9, 11.8, 11.1, 10.2.

*N*¹-(4-((*tert*-butyldiphenylsilyl)oxy)butyl)-*N*²-(3,7-dichloro-10-(2-(pyrrolidin-1-yl)ethyl)-10*H*-indolo[3,2-*b*]quinolin-11-yl)-*N*¹-ethylethane-1,2-diamine (4.42)

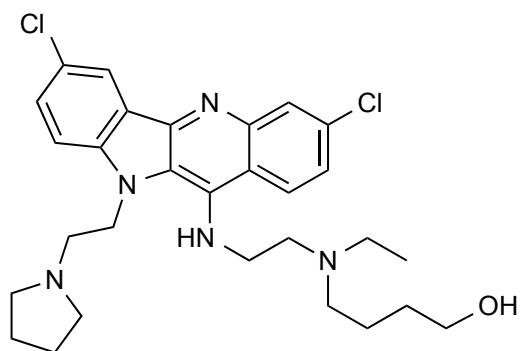


TBDPS-hydroxybutanal (36.4 mg, 0.1 mmol) and amine **4.41** (35mg, 0.07 mmol) were mixed in 1,2-dichloroethane (4 mL), followed by the addition of sodium triacetoxyborohydride (33.1 mg, 0.15 mmol). The reaction was stirred at r.t. under inert atmosphere for 4 h. The reaction mixture was quenched with sat. aq. NaHCO₃, and the product was extracted with ethyl acetate. The organic phase was dried (Na₂SO₄), and the solvent was removed under reduced pressure. The crude product was purified by flash chromatography with ethyl acetate/acetonitrile:water:methanol (1:1:1) to afford the desired product as a dark yellow solid (28 mg, 51%).

ESI-MS: C₄₅H₅₅Cl₂N₅OSi, *m/z* calculated for [M-H]⁻: 778.4, Found: 778.5; *m/z* calculated for [M+H]⁺: 780.4, Found: 780.4.

¹H NMR δ (MeOD) 8.37 (d, *J* = 2.0 Hz, 1H), 8.37 (d, *J* = 9.2 Hz, 1H), 8.10 (d, *J* = 2.1 Hz, 1H), 7.69 – 7.56 (m, 6H), 7.49 (dd, *J* = 9.2, 2.2 Hz, 1H), 7.45 – 7.28 (m, 6H), 4.80 (dd, *J* = 7.2, 6.7 Hz, 2H), 3.61 (dd, *J* = 7.9, 6.3 Hz, 2H), 3.54 (dd, *J* = 7.1, 6.5 Hz, 2H), 2.77 (d, *J* = 7.2, 6.4 Hz, 1H), 2.68 – 2.45 (m, 4H), 2.55 – 2.49 (m, 2H), 1.97 – 1.94 (m, 2H), 1.79 – 1.71 (m, 4H), 1.50 – 1.45 (m, 4H), 1.02 (t, *J* = 7.2 Hz, 3H), 0.98 (s, 9H). **¹³C ¹³C NMR** δ (MeOD) 146.8, 145.4, 144.2, 138.6, 135.2, 133.5, 133.1, 129.8, 129.4, 127.3, 126.3, 126.1, 125.5, 124.9, 123.7, 123.4, 121.0, 120.8, 112.1, 63.3, 54.0, 53.2, 53.1, 53.0, 52.7, 46.6, 42.6, 30.0, 26.0, 22.9, 22.5, 18.6, 9.8.

4-((2-((3,7-dichloro-10-(2-(pyrrolidin-1-yl)ethyl)-10H-indolo[3,2-b]quinolin-11-yl)amino)ethyl)(ethyl)amino)butan-1-ol (4.43)



A solution of compound **4.42** (10 mg, 0.01 mmol) in 2 mL of HF/Pyridine/THF (1/2/7) stirred at r.t., for 16 h, before trimethylmethoxysilane (2 mL) was added. The reaction crude was concentrated under reduced pressure and purified by reverse flash column chromatography using water/acetonitrile to afford the desired compound as a yellow solid (4.1 mg, 58%).

ESI-MS: C₂₉H₃₇Cl₂N₅O, *m/z* calculated for [M-H]⁻: 540.4, Found: 540.4; *m/z* calculated for [M+H]⁺: 542.4, Found: 542.5.

¹H NMR δ (CDCl₃) 8.48 (d, *J* = 9.2 Hz, 1H), 8.25 (d, *J* = 2.1 Hz, 1H), 8.14 (d, *J* = 2.1 Hz, 1H), 7.91 (d, *J* = 8.8 Hz, 1H), 7.69 (dd, *J* = 8.8, 2.1 Hz, 1H), 7.59 (dd, *J* = 9.2, 2.1 Hz, 1H), 4.92 (br, 2H), 3.54 (br, 2H), 3.35 (t, *J* = 6.2 Hz, 2H), 3.12 (br, 2H), 2.99–2.91 (m, 6H), 2.89 (br, 2H), 2.80 (br, 2H), 1.78–1.73 (m, 4H), 1.51 (m, 2H), 1.35 (q, *J* = 7.0 Hz, 2H), 1.05 (t, *J* = 7.0 Hz, 3H). **¹³C NMR** δ (DMSO) 147.1, 146.0, 144.0, 137.3, 132.1, 130.1, 127.8, 126.0, 125.4, 125.2, 125.0, 124.3, 122.0, 120.9, 113.4, 60.6, 54.3, 52.8, 52.4, 52.3, 47.5, 46.0, 41.7, 30.1, 23.3, 21.5, 9.9.

6.2 Physico-chemical Characterization of BODIPYs

6.2.1 Solubility Test

Solubility tests were performed on a monochromator based TECAN Safire 2 multiwell plate reader. Stock solutions for solubility tests were prepared by dissolving each compound (in quantities at least 2 mg and greater) in 1X PBS until fully saturated. Upon reaching saturation, solutions were centrifuged at 15,000 rpm for 10 min to ensure that no free particles were suspended in the supernatant. Aliquots from the saturated solution were removed and dissolved into DMSO (10-fold dilution). 30 μ L aliquots of replicates were transferred into black, flat-bottom 384-well plates and fluorescence intensity readings were acquired. The multiwavelength fluorescence detector settings were optimized for monitoring BODIPY fluorescence (λ_{ex} = 490 nm, λ_{em} = 512 nm). These values were referenced to concentration calibration curves (nM to mM) of each compound dissolved in DMSO acquired under identical instrument settings.

6.2.2 LogD Determination

Determination of LogDs were performed on a monochromator based TECAN Safire 2 multiwell plate reader. Prior to performing the experiment, a 1:1 mixture of 1-octanol (spectrophotometric grade) and 1X PBS were equilibrated for 24 h at room temperature. This equilibrated 1-octanol was used as the nonpolar cosolvent for logD measurements. To perform LogD, aliquots of the saturated 1X PBS stocks, described in the solubility test, were added to an equivalent volume of 1-octanol.

The biphasic solutions were continuously and vigorously shaken for 1 h. Solutions were centrifuged for 2 min at 15,000 rpm to assist in layer separation and then aliquots (in triplicate) were removed from each layer and subsequently dissolved in DMSO (10-fold dilution). 30 μ L aliquots of replicates were transferred into black, flat-bottom 384-well plates and fixed fluorescence intensity readings were acquired. The multiwavelength fluorescence detector settings were optimized for monitoring BODIPY fluorescence (λ_{ex} = 490 nm, λ_{em} = 512 nm). Each set of measurements (sat. 1X PBS layer in DMSO and octanol layer in DMSO) per compound was obtained under identical instrument settings.

6.3 Biological Methods

6.3.1 *Plasmodium falciparum* Blood Stage *in vitro* Drug Sensitivity Assay

Drug assays were performed following reported literature procedures⁴⁴⁵, adapting them for a 384-well format. Briefly, synchronized ring-stage parasites were cultured in the presence of triplicate 12 point 2-fold serial dilutions of test compounds in 40 μ L of RPMI-1640 (Sigma, USA) supplemented with 0.5% AlbuMAX® II (Gibco®, 11021-045) at 1.0% hematocrit and an initial parasitemia of 1.0% in black clear-bottom plates (Greiner Bio-one, 781090). Following a 72 h incubation under standard culture conditions, SYBR Green I dye (Invitrogen, S7563) was added to a dilution of 1:5000, and plates were stored at room temperature until fluorescence signal was read on a Spectramax M5 plate reader (Molecular Devices, ex 494 nm, em 530 nm). After background subtraction and normalization, EC₅₀ values were calculated using a non-linear regression curve fit as implemented in the Mac OS X Prism 6.0c software package (GraphPad Software, Inc.).

6.3.2 *Plasmodium berghei* Liver Stage *in vitro* Drug Sensitivity Assay

As previously published, human liver cells (HepG2) were seeded at 10,000 cells/well and incubated 22 hours at 37 °C, followed by addition of compounds and controls at 1 μ M and 10 μ M. After 2 h, luciferase-expressing *P. berghei* parasites obtained from freshly dissected mosquitoes were added to the plates at 8,500 spz/well and incubated for 48 h. The parasite load and HepG2 viability were quantified using Luciferase and Alamar Blue readout, respectively.³¹⁶ (Work done at the Instituto de Medicina Molecular (Portugal), in Maria Mota's Lab.)

6.3.3 *Plasmodium falciparum* Whole Cell Lysate Western Blot

Dd2 parasites were allowed to grow to asynchrony for 7 replicative cycles. 10 mL aliquots of asynchronous asexual Dd2 parasites were exposed to the experimental treatments for 90 minutes. Drug treated cells were incubated in the presence of small molecule inhibitors in standard RPMI media (GIBCO). Control samples were incubated with either complete RPMI media or PBS (US Biological). The PBS culture served as a positive control for AAR. (29) Protein lysates from each of the 10 mL cultures were prepared by first lysing infected erythrocytes with 0.15% saponin (Sigma) and the resultant parasite pellets were lysed in 1x

Laemmli Sample Buffer (Bio-Rad) supplemented with 5% beta-mercaptoethanol and 2% NP40 (GBiosciences). All lysis buffers contained 1x Complete protease inhibitor cocktail (Roche) and 1x phosphatase inhibitor cocktail PhosStop (Roche). 10 μ L aliquots of lysate were subsequently separated by SDS-PAGE. Proteins were resolved and transferred using standard techniques, and membranes were blotted for a phospho-specific eIF2 α pAb raised to a *Plasmodium falciparum* peptide antigen MSELpSKRRFRS, an eIF2 α pAb raised to *T. gondii* peptide KGYIDLSKRRVS which recognizes total eIF2 α protein (48), and a histone-H3 rabbit pAb (Abcam ab1791).

6.3.4 Yeast Growth Assays

Yeast strains were grown overnight in assay media (0.17% yeast nitrogen base without amino acids, without ammonium sulfate (Bio101), 0.1% glutamic acid, 2% glucose supplemented with complete amino acid mix minus histidine (Sunrise Bioproducts) at 23 °C to maintain log growth phase. The OD600 of cultures was measured and yeast strains were diluted to 0.01 OD600 in assay media with indicated concentrations of drugs or a corresponding volume of DMSO (Sigma). In indicated experiments, media was supplemented with 1 mg/mL proline (Sigma). Cells were grown in 100 μ L of media in covered 96-well Nunc Edge assay plates at 30 °C with interval shaking every 15 minutes in a ThermoScientific Multiskan GO instrument that read OD600 every 15 minutes.

6.3.5 Yeast Western Blots

Pump-deleted yeast strains were grown overnight in assay media at 23 °C, after which either drug or a corresponding volume of DMSO was added to cultures, which were then grown at 30 °C for six hours. Yeast pellets were washed with water and resuspended in lysis buffer (100 mM Tris, pH 8.0, 20 mM NaCl, 2 mM MgCl₂, 50 mM β -mercaptoethanol, 0.025 U/mL benzonase, 1% Triton X-100, 2 x Halt protease inhibitor (Sigma-Aldrich), 1x Halt Phosphatase Inhibitor (Thermo-Fisher) and acid-washed beads and bead beaten for five minutes at 4°C. Supernatants were collected and normalized for total protein content using a BCA assay (Pierce). Proteins were resolved and transferred using standard techniques, and membranes were blotted for His-Tag (27E8) Mouse mAb #2366 (Cell Signaling Technology).

6.3.6 MCF-7 Cell Culture

MCF-7 cells were propagated in RPMI media (+10%FBS +1% L-glutamine +1% Pen/Strep) at 37 °C and 5% CO₂. Cell culture media and supplements were sterile filtered prior to use and were obtained from Gibco (FBS, 1X Attachment Factor), Life Technologies (CO₂ Independent Medium, RPMI 1640, 1X PBS), and Invitrogen (RPMI 1640). Prior to assays, cells were transferred to phenol red free RPMI medium and seeded into black/clear bottom 96-well plates (BD Biosciences #BD356692) at 10,000 cells/well for experiments. One day post plating, compounds were added to cells using an HP D300 Digital Dispenser (Hewlett-Packard).

6.3.7 Cytotoxicity Assay

6.3.7.1 MCF-7

20,000 MCF-7 cells/well were seeded in 96-well cell culture plates. The next day, cells were incubated with varying concentrations of AMP analogues, HFG and oligomycin as positive controls, for 96 h at 37 °C. Assay compounds were dispensed from 10 mM DMSO stock solutions using an HP D300 digital dispenser. Following incubation, cells were washed with 1X PBS and the cytotoxicity was evaluated using CellTiter-Glo Luminescent Cell Viability Assay Kit according to the manufacturer's protocol. Briefly, plates were equilibrated to room temperature for 30 min and CellTiter-Glo reagent was added to each well in a 1:1 volumetric ratio with the culture medium present in the assay wells. After 10 min incubation at room temperature to stabilize luminescent signal, the plates were read in a Luminescent Plate Reader (Envision, PerkinElmer 2103 Multi Reader). Control wells containing medium without cells were prepared to establish background luminescence. All assays were performed with technical triplicates and two biological replicates. The EC₅₀ was estimated for each compound by non-linear interpolation of the dose-dependence curve (GraphPad Software).

6.3.7.2 HepG2

HepG2 A16 human hepatic cell line viability was determined based on the MTT assay. An *in vitro* culture of HepG2 cells was maintained in standard culture conditions. Briefly, cells were seeded in a flat-bottomed 96-well tissue culture plate at a density of 1×10^4 cells/well and allowed to adhere overnight. After removing the medium, 200 µL of fresh medium containing 7 ten-fold dilutions (100 µM – 1 nM) of each compound was added; 200 µL of drug free medium

was added to negative control wells. The plate was incubated for 24 h under standard culture conditions, medium was then substituted by fresh medium containing identical concentrations of the compounds and the plates incubated an additional 24 h. At the end of the incubation period (48 h), 20 μL of 3-(4,5-dimethylthiazol-2-yl)-2,5-diphenyl-2H-tetrazolium (Sigma-Aldrich) (MTT; 5 mg/mL in PBS) was added to each well, wells were incubated for 3 h at standard culture conditions, supernatant was removed and 200 μL of acidified isopropanol was added to each well. Absorbance was read at 570 nm on a multi-mode microplate reader (Triad, Dynex Technologies), to produce a log dose-dependence curve. The EC_{50} was estimated for each compound by non-linear interpolation of the dose-dependence curve (GraphPad Software). (Work done at the Instituto de Medicina Molecular (Portugal), in Maria Mota's Lab.)

6.3.8 MCF-7 Western Blots

MCF-7 cells were propagated to confluency in a 75 cm^2 or 125 cm^2 flask. Cells were incubated with vehicle control or experimental compounds (HFG, HFol or ProSA) at the desired final concentration for 90 min at 37 $^{\circ}\text{C}$. Cells were lysed with RIPA or Native lysis buffer and debris was removed by centrifugation at 14,000 rpm for 15 min, at 4 $^{\circ}\text{C}$. All lysis buffers contained 1x Complete protease inhibitor cocktail (Roche) and 1x phosphatase inhibitor cocktail PhosStop (Roche). Supernatants were collected and normalized for total protein content using a BCA assay (Pierce). 10 μL aliquots of lysate were subsequently separated by SDS-PAGE. Proteins were resolved and transferred using standard techniques, and membranes were blotted for phospho-eIF2 α monoclonal antibody (Ser51) #9721, eIF2 α polyclonal antibody #4837 (Cell Signaling Technology), Anti-Glutamyl Prolyl tRNA synthetase antibody (abcam # 31531).

6.3.9 BRD4 *in vitro* EC_{50} Determination

Following the BRD4 (BD2) TR-FRET Assay Kit (BPSBioscience, Catalog# 32617) protocol, the components were added to a 384-well white plate in a total volume of 30 μL . Assay compounds were dispensed from 10 mM DMSO stock solutions using a HP D300 digital dispenser. The EC_{50} was estimated for each compound by non-linear interpolation of the dose-dependence curve (GraphPad Software). All assays were performed in duplicates in two biological replicas.

6.3.10 Pull-down Assays

6.3.10.1 Dynabeads® His-Tag

Plasmodium falciparum expressed His-tagged PRS protein was affinity-purified with His-Tagged Dynabeads® (Thermo Fisher Scientific #10103D). 50 µL of Dynabeads® slurry were transferred to a microcentrifuge tube and placed on a magnet for 2 min, followed by aspiration of the supernatant. The sample was added to the beads and incubated under continuous end over end rotation at 4 °C for 5-10 minutes. The beads were washed 4 x 2 minutes with 300 µL of wash buffer (which buffer?). Dynabeads® were mixed with an equal volume of SDS loading buffer and bound proteins were eluted by incubation for 2 min at 90°C. 20 µL aliquots of eluted proteins were subsequently separated on SDS-PAGE gels. Proteins were resolved and transferred using standard techniques, and membranes were blotted for His-Tag (27E8) Mouse mAb #2366 (Cell Signaling Technology).

6.3.10.2 His-Tag (27E8) Mouse mAb Magnetic Bead Conjugate

Plasmodium falciparum expressed His-tagged PRS protein was affinity-purified with His-Tag (27E8) Mouse mAb Magnetic Bead Conjugate (Cell Signaling Technology #8811). 10 µL of well-vortexed beads were incubated with 200 µL of sample under continuous end over end rotation at 4 °C for 5-10 minutes. The beads were washed 4 x 2 minutes with 300 µL of lysis buffer. Beads were mixed with an equal volume of SDS loading buffer or elution buffers and bound proteins were eluted by incubation for 2 min. at 90 °C. 20 µL aliquots of eluted proteins were subsequently separated on SDS-PAGE gels. Proteins were resolved and transferred using standard techniques, and membranes were blotted for His-Tag (27E8) Mouse mAb #2366 (Cell Signaling Technology).

6.3.10.3 Dynabeads® Protein A

Mammalian EPRS protein was affinity-purified with Anti-Glutamyl Prolyl tRNA synthetase antibody (abcam # 31531) coupled to Dynabeads® Protein A (Cell Signaling Technology #10002D). To 450 µL of cell lysate, 2.5 µL of the primary antibody was added and incubated with gentle rocking overnight at 4°C. 50 µL of pre-washed protein A magnetic bead (one?) was added to the mix and incubated with gentle rocking for 4 h, at 4 °C. The beads were washed 4 x 2 minutes with 300 µL of lysis buffer. Beads were mixed with an equal volume of

SDS loading buffer or elution buffers and bound proteins were eluted by incubation for 2 min at 90°C. 20 µL aliquots of eluted proteins were subsequently separated on SDS-PAGE gels. Proteins were resolved and transferred using standard techniques, and membranes were blotted for Anti-Glutamyl Prolyl tRNA synthetase antibody (abcam # 31531)

6.3.11 Cell Imaging

Live-cell imaging was performed on a Zeiss Axiovert 100M inverted epifluorescence microscope with a 40X objective. For each region of interest, a bright field view was acquired as well as GFP and DAPI fluorescence channels.

Imaging of mammalian cells: two days prior to imaging, MCF-7 cells were seeded at 10,000 cells/well on a 96-well transparent bottom microwell plate. Imaging media was used for experiments, RPMI 1640 1X [(-) phenol red, (+) 10% FBS]. On the imaging day, each well was incubated for 30 minutes with 10 µM of the title compound suspended in cell imaging media (final DMSO content = 0.1%). Subsequently two washes (5 mins each with medium ...) were performed.

Imaging of *Plasmodium falciparum* cell lines: Chloroquine resistant and sensitive strains, Dd2 and 3D7, respectively, were cultured under standard conditions (cite Trager and Jensen) prior to assay. The day of imaging, asynchronized parasites were incubated for 30 minutes with desired concentration of the title compound suspended in cell imaging media (final DMSO content = 0.1%). Two washes were performed and the live parasites were imaged.

No imaging enhancing processing was performed for acquired data. Imaging data was analyzed with ImageJ software (<http://rsbweb.nih.gov/ij>).

References

References

- World Malaria Report 2014.
http://www.who.int/malaria/publications/world_malaria_report_2014/en/
(accessed August 27 2015).
- Eisenstein, M., Drug development: Holding out for reinforcements. *Nature* **2012**, *484* (7395), S16-18.
- Burrows, J. N.; Chibale, K.; Wells, T. N., The state of the art in anti-malarial drug discovery and development. *Curr Top Med Chem* **2011**, *11* (10), 1226-1254.
- Courtis, A. M.; Santos, S. A.; Guan, Y.; Hendricks, J. A.; Ghosh, B.; Szantai-Kis, D. M.; Reis, S. A.; Shah, J. V.; Mazitschek, R., Monoalkoxy BODIPYs--a fluorophore class for bioimaging. *Bioconjug Chem* **2014**, *25* (6), 1043-1051.
- Figueiras, M.; Coelho, L.; Wicht, K. J.; Santos, S. A.; Lavrado, J.; Gut, J.; Rosenthal, P. J.; Nogueira, F.; Egan, T. J.; Moreira, R.; Paulo, A., N10,N11-di-alkylamine indolo[3,2-b]quinolines as hemozoin inhibitors: design, synthesis and antiplasmodial activity. *Bioorg Med Chem* **2015**, *23* (7), 1530-1539.
- Gamo, F. J.; Sanz, L. M.; Vidal, J.; de Cozar, C.; Alvarez, E.; Lavandera, J. L.; Vanderwall, D. E.; Green, D. V.; Kumar, V.; Hasan, S.; Brown, J. R.; Peishoff, C. E.; Cardon, L. R.; Garcia-Bustos, J. F., Thousands of chemical starting points for antimalarial lead identification. *Nature* **2010**, *465* (7296), 305-310.
- Herman, J. D.; Pepper, L. R.; Cortese, J. F.; Estiu, G.; Galinsky, K.; Zuzarte-Luis, V.; Derbyshire, E. R.; Ribacke, U.; Lukens, A. K.; Santos, S. A.; Patel, V.; Clish, C. B.; Sullivan, W. J., Jr.; Zhou, H.; Bopp, S. E.; Schimmel, P.; Lindquist, S.; Clardy, J.; Mota, M. M.; Keller, T. L.; Whitman, M.; Wiest, O.; Wirth, D. F.; Mazitschek, R., The cytoplasmic prolyl-tRNA synthetase of the malaria parasite is a dual-stage target of febrifugine and its analogs. *Sci Transl Med* **2015**, *7* (288), 288ra277.
- Keller, T. L.; Zocco, D.; Sundrud, M. S.; Hendrick, M.; Edenius, M.; Yum, J.; Kim, Y. J.; Lee, H. K.; Cortese, J. F.; Wirth, D. F.; Dignam, J. D.; Rao, A.; Yeo, C. Y.; Mazitschek, R.; Whitman, M., Halofuginone and other febrifugine derivatives inhibit prolyl-tRNA synthetase. *Nat Chem Biol* **2012**, *8* (3), 311-317.
- White, N. J.; Pukrittayakamee, S.; Hien, T. T.; Faiz, M. A.; Mokuolu, O. A.; Dondorp, A. M., Malaria. *Lancet* **2014**, *383* (9918), 723-735.
- Autino, B.; Noris, A.; Russo, R.; Castelli, F., Epidemiology of malaria in endemic areas. *Mediterr J Hematol Infect Dis* **2012**, *4* (1), e2012060.
- Monge-Maillo, B.; Lopez-Velez, R., Migration and malaria in europe. *Mediterr J Hematol Infect Dis* **2012**, *4* (1), e2012014.
- Odolini, S.; Gautret, P.; Parola, P., Epidemiology of imported malaria in the mediterranean region. *Mediterr J Hematol Infect Dis* **2012**, *4* (1), e2012031.
- Kokwaro, G., Ongoing challenges in the management of malaria. *Malar J* **2009**, *8 Suppl 1*, S2.
- Wellems, T. E.; Hayton, K.; Fairhurst, R. M., The impact of malaria parasitism: from corpuscles to communities. *J Clin Invest* **2009**, *119* (9), 2496-2505.
- Breman, J. G.; Brandling-Bennett, A. D., The challenge of malaria eradication in the twenty-first century: research linked to operations is the key. *Vaccine* **2011**, *29 Suppl 4*, D97-103.

References

16. Popovici, J.; Menard, D., Challenges in Antimalarial Drug Treatment for Vivax Malaria Control. *Trends Mol Med* **2015**, *21* (12), 776-788.
17. Tilley, L.; Dixon, M. W.; Kirk, K., The Plasmodium falciparum-infected red blood cell. *Int J Biochem Cell Biol* **2011**, *43* (6), 839-842.
18. Rowe, J. A.; Claessens, A.; Corrigan, R. A.; Arman, M., Adhesion of Plasmodium falciparum-infected erythrocytes to human cells: molecular mechanisms and therapeutic implications. *Expert Rev Mol Med* **2009**, *11*, e16.
19. Farrow, R. E.; Green, J.; Katsimitsoulia, Z.; Taylor, W. R.; Holder, A. A.; Molloy, J. E., The mechanism of erythrocyte invasion by the malarial parasite, Plasmodium falciparum. *Semin Cell Dev Biol* **2011**, *22* (9), 953-960.
20. Hobbs, C.; Duffy, P., Drugs for malaria: something old, something new, something borrowed. *F1000 Biol Rep* **2011**, *3*, 24.
21. Flannery, E. L.; Chatterjee, A. K.; Winzeler, E. A., Antimalarial drug discovery - approaches and progress towards new medicines. *Nat Rev Microbiol* **2013**, *11* (12), 849-862.
22. Tham, W. H.; Healer, J.; Cowman, A. F., Erythrocyte and reticulocyte binding-like proteins of Plasmodium falciparum. *Trends Parasitol* **2012**, *28* (1), 23-30.
23. Miller, L. H.; Baruch, D. I.; Marsh, K.; Doumbo, O. K., The pathogenic basis of malaria. *Nature* **2002**, *415* (6872), 673-679.
24. Francischetti, I. M.; Seydel, K. B.; Monteiro, R. Q., Blood coagulation, inflammation, and malaria. *Microcirculation* **2008**, *15* (2), 81-107.
25. Moxon, C. A.; Heyderman, R. S.; Wassmer, S. C., Dysregulation of coagulation in cerebral malaria. *Mol Biochem Parasitol* **2009**, *166* (2), 99-108.
26. Miller, L. H.; Ackerman, H. C.; Su, X. Z.; Wellems, T. E., Malaria biology and disease pathogenesis: insights for new treatments. *Nat Med* **2013**, *19* (2), 156-167.
27. Smith, J. D.; Rowe, J. A.; Higgins, M. K.; Lavstsen, T., Malaria's deadly grip: cytoadhesion of Plasmodium falciparum-infected erythrocytes. *Cell Microbiol* **2013**, *15* (12), 1976-1983.
28. Idro, R.; Marsh, K.; John, C. C.; Newton, C. R., Cerebral malaria: mechanisms of brain injury and strategies for improved neurocognitive outcome. *Pediatr Res* **2010**, *68* (4), 267-274.
29. Walker, P. G.; ter Kuile, F. O.; Garske, T.; Menendez, C.; Ghani, A. C., Estimated risk of placental infection and low birthweight attributable to Plasmodium falciparum malaria in Africa in 2010: a modelling study. *Lancet Glob Health* **2014**, *2* (8), e460-467.
30. Steketee, R. W.; Nahlen, B. L.; Parise, M. E.; Menendez, C., The burden of malaria in pregnancy in malaria-endemic areas. *Am J Trop Med Hyg* **2001**, *64* (1-2 Suppl), 28-35.
31. Autino, B.; Corbett, Y.; Castelli, F.; Taramelli, D., Pathogenesis of malaria in tissues and blood. *Mediterr J Hematol Infect Dis* **2012**, *4* (1), e2012061.
32. Kappe, S. H.; Vaughan, A. M.; Boddey, J. A.; Cowman, A. F., That was then but this is now: malaria research in the time of an eradication agenda. *Science* **2010**, *328* (5980), 862-866.
33. Jana, S.; Paliwal, J., Novel molecular targets for antimalarial chemotherapy. *Int J Antimicrob Agents* **2007**, *30* (1), 4-10.
34. Siciliano, G.; Alano, P., Enlightening the malaria parasite life cycle: bioluminescent Plasmodium in fundamental and applied research. *Front Microbiol* **2015**, *6*, 391.

35. Muller, I. B.; Hyde, J. E., Antimalarial drugs: modes of action and mechanisms of parasite resistance. *Future Microbiol* **2010**, *5* (12), 1857-1873.
36. Castelli, F.; Tomasoni, L. R.; Matteelli, A., Advances in the treatment of malaria. *Mediterr J Hematol Infect Dis* **2012**, *4* (1), e2012064.
37. Hyde, J. E., Drug-resistant malaria - an insight. *FEBS J* **2007**, *274* (18), 4688-4698.
38. Martinelli, A.; Moreira, R.; Ravo, P. V., Malaria combination therapies: advantages and shortcomings. *Mini Rev Med Chem* **2008**, *8* (3), 201-212.
39. A research agenda for malaria eradication: drugs. *PLoS Med* **2011**, *8* (1), e1000402.
40. Gelb, M. H., Drug discovery for malaria: a very challenging and timely endeavor. *Curr Opin Chem Biol* **2007**, *11* (4), 440-445.
41. Nwaka, S.; Hudson, A., Innovative lead discovery strategies for tropical diseases. *Nat Rev Drug Discov* **2006**, *5* (11), 941-955.
42. Brown, C., Malaria vaccine not perfect, but still useful. *Cmaj* **2015**.
43. Aguiar, J. C.; Bolton, J.; Wanga, J.; Sacci, J. B.; Iriko, H.; Mazeika, J. K.; Han, E. T.; Limbach, K.; Patterson, N. B.; Sedegah, M.; Cruz, A. M.; Tsuboi, T.; Hoffman, S. L.; Carucci, D.; Hollingdale, M. R.; Villasante, E. D.; Richie, T. L., Discovery of Novel Plasmodium falciparum Pre-Erythrocytic Antigens for Vaccine Development. *PLoS One* **2015**, *10* (8), e0136109.
44. Moreno, A.; Joyner, C., Malaria vaccine clinical trials: what's on the horizon. *Curr Opin Immunol* **2015**, *35*, 98-106.
45. de Koning-Ward, T. F.; Gilson, P. R.; Crabb, B. S., Advances in molecular genetic systems in malaria. *Nat Rev Microbiol* **2015**, *13* (6), 373-387.
46. Renslo, A. R., Antimalarial Drug Discovery: From Quinine to the Dream of Eradication. *ACS Med Chem Lett* **2013**, *4* (12), 1126-1128.
47. Schlitzer, M., Malaria chemotherapeutics part I: History of antimalarial drug development, currently used therapeutics, and drugs in clinical development. *ChemMedChem* **2007**, *2* (7), 944-986.
48. Kumar, A.; Katiyar, S. B.; Agarwal, A.; Chauhan, P. M., Perspective in antimalarial chemotherapy. *Curr Med Chem* **2003**, *10* (13), 1137-1150.
49. Schlitzer, M., Antimalarial drugs - what is in use and what is in the pipeline. *Arch Pharm (Weinheim)* **2008**, *341* (3), 149-163.
50. Olliaro, P., Mode of action and mechanisms of resistance for antimalarial drugs. *Pharmacol Ther* **2001**, *89* (2), 207-219.
51. Sigala, P. A.; Crowley, J. R.; Henderson, J. P.; Goldberg, D. E., Deconvoluting heme biosynthesis to target blood-stage malaria parasites. *Elife* **2015**, *4*.
52. Eshar, S.; Dahan-Pasternak, N.; Weiner, A.; Dzikowski, R., High resolution 3D perspective of Plasmodium biology: advancing into a new era. *Trends Parasitol* **2011**, *27* (12), 548-554.
53. Egan, T. J., Recent advances in understanding the mechanism of hemozoin (malaria pigment) formation. *J Inorg Biochem* **2008**, *102* (5-6), 1288-1299.
54. O'Neill, P. M.; Ward, S. A.; Berry, N. G.; Jeyadevan, J. P.; Biagini, G. A.; Asadollaly, E.; Park, B. K.; Bray, P. G., A medicinal chemistry perspective on 4-aminoquinoline antimalarial drugs. *Curr Top Med Chem* **2006**, *6* (5), 479-507.
55. Goldberg, D. E., Hemoglobin degradation. *Curr Top Microbiol Immunol* **2005**, *295*, 275-291.

References

56. Orjih, A. U., Hemozoin accumulation in Garnham bodies of Plasmodium falciparum gametocytes. *Parasitol Res* **2012**, *111* (6), 2353-2359.
57. O'Neill, P. M.; Park, B. K.; Shone, A. E.; Maggs, J. L.; Roberts, P.; Stocks, P. A.; Biagini, G. A.; Bray, P. G.; Gibbons, P.; Berry, N.; Winstanley, P. A.; Mukhtar, A.; Bonar-Law, R.; Hindley, S.; Bambal, R. B.; Davis, C. B.; Bates, M.; Hart, T. K.; Gresham, S. L.; Lawrence, R. M.; Brigandi, R. A.; Gomez-delas-Heras, F. M.; Gargallo, D. V.; Ward, S. A., Candidate selection and preclinical evaluation of N-tert-butyl isoquine (GSK369796), an affordable and effective 4-aminoquinoline antimalarial for the 21st century. *J Med Chem* **2009**, *52* (5), 1408-1415.
58. Sigala, P. A.; Goldberg, D. E., The peculiarities and paradoxes of Plasmodium heme metabolism. *Annu Rev Microbiol* **2014**, *68*, 259-278.
59. Gorka, A. P.; de Dios, A.; Roepe, P. D., Quinoline drug-heme interactions and implications for antimalarial cytostatic versus cytotoxic activities. *J Med Chem* **2013**, *56* (13), 5231-5246.
60. de Villiers, K. A.; Marques, H. M.; Egan, T. J., The crystal structure of halofantrine-ferriprotoporphyrin IX and the mechanism of action of arylmethanol antimalarials. *J Inorg Biochem* **2008**, *102* (8), 1660-1667.
61. Kuter, D.; Chibale, K.; Egan, T. J., Linear free energy relationships predict coordination and pi-stacking interactions of small molecules with ferriprotoporphyrin IX. *J Inorg Biochem* **2011**, *105* (5), 684-692.
62. de Dios, A. C.; Casabianca, L. B.; Kosar, A.; Roepe, P. D., Structure of the amodiaquine-FPIX mu oxo dimer solution complex at atomic resolution. *Inorg Chem* **2004**, *43* (25), 8078-8084.
63. Leed, A.; DuBay, K.; Ursos, L. M.; Sears, D.; De Dios, A. C.; Roepe, P. D., Solution structures of antimalarial drug-heme complexes. *Biochemistry* **2002**, *41* (32), 10245-10255.
64. Bray, P. G.; Ward, S. A.; O'Neill, P. M., Quinolines and artemisinin: chemistry, biology and history. *Curr Top Microbiol Immunol* **2005**, *295*, 3-38.
65. Weissbuch, I.; Leiserowitz, L., Interplay between malaria, crystalline hemozoin formation, and antimalarial drug action and design. *Chem Rev* **2008**, *108* (11), 4899-4914.
66. Buller R., P. M. L., Almarsson O. and Leiserowitz L., "Quinoline Binding Site on Malaria Pigment Crystal: A Rational Pathway for Antimalaria Drug Design.". *Crystal Growth & Design* **2002**, (2), 553-562.
67. Fitch, C. D., Ferriprotoporphyrin IX, phospholipids, and the antimalarial actions of quinoline drugs. *Life Sci* **2004**, *74* (16), 1957-1972.
68. Vale, N.; Moreira, R.; Gomes, P., Primaquine revisited six decades after its discovery. *Eur J Med Chem* **2009**, *44* (3), 937-953.
69. Fernando, D.; Rodrigo, C.; Rajapakse, S., Primaquine in vivax malaria: an update and review on management issues. *Malar J* **2011**, *10*, 351.
70. Hocart, S. J.; Liu, H.; Deng, H.; De, D.; Krogstad, F. M.; Krogstad, D. J., 4-aminoquinolines active against chloroquine-resistant Plasmodium falciparum: basis of antiparasite activity and quantitative structure-activity relationship analyses. *Antimicrob Agents Chemother* **2011**, *55* (5), 2233-2244.
71. Egan, T. J.; Hunter, R.; Kaschula, C. H.; Marques, H. M.; Mispion, A.; Walden, J., Structure-function relationships in aminoquinolines: effect of amino and chloro groups on

- quinoline-hematin complex formation, inhibition of beta-hematin formation, and antiplasmodial activity. *J Med Chem* **2000**, *43* (2), 283-291.
72. Saenz, F. E.; Mutka, T.; Udenze, K.; Oduola, A. M.; Kyle, D. E., Novel 4-aminoquinoline analogs highly active against the blood and sexual stages of Plasmodium in vivo and in vitro. *Antimicrob Agents Chemother* **2012**, *56* (9), 4685-4692.
73. Aguiar, A. C.; Santos Rde, M.; Figueiredo, F. J.; Cortopassi, W. A.; Pimentel, A. S.; Franca, T. C.; Meneghetti, M. R.; Krettli, A. U., Antimalarial activity and mechanisms of action of two novel 4-aminoquinolines against chloroquine-resistant parasites. *PLoS One* **2012**, *7* (5), e37259.
74. Fidock, D. A.; Eastman, R. T.; Ward, S. A.; Meshnick, S. R., Recent highlights in antimalarial drug resistance and chemotherapy research. *Trends Parasitol* **2008**, *24* (12), 537-544.
75. White, N. J., Antimalarial drug resistance. *J Clin Invest* **2004**, *113* (8), 1084-1092.
76. Shujatullah, F.; Khan, H. M.; Khatoon, A.; Khan, P. A.; Ashfaq, M., In Vitro Chloroquine Resistance in Plasmodium falciparum Isolates from Tertiary Care Hospital. *Malar Res Treat* **2012**, *2012*, 538481.
77. Witkowski, B.; Berry, A.; Benoit-Vical, F., Resistance to antimalarial compounds: methods and applications. *Drug Resist Updat* **2009**, *12* (1-2), 42-50.
78. Ecker, A.; Lehane, A. M.; Clain, J.; Fidock, D. A., PfCRT and its role in antimalarial drug resistance. *Trends Parasitol* **2012**, *28* (11), 504-514.
79. Wells, T. N.; Hooft van Huijsduijnen, R.; Van Voorhis, W. C., Malaria medicines: a glass half full? *Nat Rev Drug Discov* **2015**, *14* (6), 424-442.
80. White, N. J., Primaquine to prevent transmission of falciparum malaria. *Lancet Infect Dis* **2012**.
81. Myint, H. Y.; Berman, J.; Walker, L.; Pybus, B.; Melendez, V.; Baird, J. K.; Ohrt, C., Review: Improving the therapeutic index of 8-aminoquinolines by the use of drug combinations: review of the literature and proposal for future investigations. *Am J Trop Med Hyg* **2011**, *85* (6), 1010-1014.
82. Tekwani, B. L.; Walker, L. A., 8-Aminoquinolines: future role as antiprotozoal drugs. *Curr Opin Infect Dis* **2006**, *19* (6), 623-631.
83. Schlagenhauf, P.; Adamcova, M.; Regep, L.; Schaerer, M. T.; Rhein, H. G., The position of mefloquine as a 21st century malaria chemoprophylaxis. *Malar J* **2010**, *9*, 357.
84. Schlagenhauf, P.; Adamcova, M.; Regep, L.; Schaerer, M. T.; Bansod, S.; Rhein, H. G., Use of mefloquine in children - a review of dosage, pharmacokinetics and tolerability data. *Malar J* **2011**, *10*, 292.
85. Bohorquez, E. B.; Juliano, J. J.; Kim, H. S.; Meshnick, S. R., Mefloquine exposure induces cell cycle delay and reveals stage-specific expression of the pfmdr1 gene. *Antimicrob Agents Chemother* **2012**.
86. Yuthavong, Y.; Tarnchompoo, B.; Vilaivan, T.; Chitnumsub, P.; Kamchonwongpaisan, S.; Charman, S. A.; McLennan, D. N.; White, K. L.; Vivas, L.; Bongard, E.; Thongphanchang, C.; Taweechai, S.; Vanichtanankul, J.; Rattanajak, R.; Arwon, U.; Fantauzzi, P.; Yuvaniyama, J.; Charman, W. N.; Matthews, D., Malarial dihydrofolate reductase as a paradigm for drug development against a resistance-compromised target. *Proc Natl Acad Sci U S A* **2012**, *109* (42), 16823-16828.
87. Miller, L. H.; Su, X., Artemisinin: discovery from the Chinese herbal garden. *Cell* **2011**, *146* (6), 855-858.

References

88. de Ridder, S.; van der Kooy, F.; Verpoorte, R., Artemisia annua as a self-reliant treatment for malaria in developing countries. *J Ethnopharmacol* **2008**, *120* (3), 302-314.
89. Yeung, S.; Socheat, D.; Moorthy, V. S.; Mills, A. J., Artemisinin resistance on the Thai-Cambodian border. *Lancet* **2009**, *374* (9699), 1418-1419.
90. Meshnick, S., Perspective: artemisinin-resistant malaria and the wolf. *Am J Trop Med Hyg* **2012**, *87* (5), 783-784.
91. Tulloch, J.; David, B.; Newman, R. D.; Meek, S., Artemisinin-resistant malaria in the Asia-Pacific region. *Lancet* **2012**.
92. Mbengue, A.; Bhattacharjee, S.; Pandharkar, T.; Liu, H.; Estiu, G.; Stahelin, R. V.; Rizk, S. S.; Njimoh, D. L.; Ryan, Y.; Chotivanich, K.; Nguon, C.; Ghorbal, M.; Lopez-Rubio, J. J.; Pfrender, M.; Emrich, S.; Mohandas, N.; Dondorp, A. M.; Wiest, O.; Haldar, K., A molecular mechanism of artemisinin resistance in Plasmodium falciparum malaria. *Nature* **2015**, *520* (7549), 683-687.
93. Pantaleo, A.; Pau, M. C.; Chien, H. D.; Turrini, F., Artemisinin resistance, some facts and opinions. *J Infect Dev Ctries* **2015**, *9* (6), 597-599.
94. Ariey, F.; Witkowski, B.; Amaratunga, C.; Beghain, J.; Langlois, A. C.; Khim, N.; Kim, S.; Duru, V.; Bouchier, C.; Ma, L.; Lim, P.; Leang, R.; Duong, S.; Sreng, S.; Suon, S.; Chuor, C. M.; Bout, D. M.; Menard, S.; Rogers, W. O.; Genton, B.; Fandeur, T.; Miotto, O.; Ringwald, P.; Le Bras, J.; Berry, A.; Barale, J. C.; Fairhurst, R. M.; Benoit-Vical, F.; Mercereau-Puijalon, O.; Menard, D., A molecular marker of artemisinin-resistant Plasmodium falciparum malaria. *Nature* **2014**, *505* (7481), 50-55.
95. Dondorp, A. M.; Nosten, F.; Yi, P.; Das, D.; Phyto, A. P.; Tarning, J.; Lwin, K. M.; Ariey, F.; Hanpithakpong, W.; Lee, S. J.; Ringwald, P.; Silamut, K.; Imwong, M.; Chotivanich, K.; Lim, P.; Herdman, T.; An, S. S.; Yeung, S.; Singhasivanon, P.; Day, N. P.; Lindergardh, N.; Socheat, D.; White, N. J., Artemisinin resistance in Plasmodium falciparum malaria. *N Engl J Med* **2009**, *361* (5), 455-467.
96. Kano, S., Artemisinin-based combination therapies and their introduction in Japan. *J Infect Chemother* **2010**, *16* (6), 375-382.
97. O'Neill, P. M.; Barton, V. E.; Ward, S. A., The molecular mechanism of action of artemisinin--the debate continues. *Molecules* **2010**, *15* (3), 1705-1721.
98. Wang, J.; Zhang, C. J.; Chia, W. N.; Loh, C. C.; Li, Z.; Lee, Y. M.; He, Y.; Yuan, L. X.; Lim, T. K.; Liu, M.; Liew, C. X.; Lee, Y. Q.; Zhang, J.; Lu, N.; Lim, C. T.; Hua, Z. C.; Liu, B.; Shen, H. M.; Tan, K. S.; Lin, Q., Haem-activated promiscuous targeting of artemisinin in Plasmodium falciparum. *Nat Commun* **2015**, *6*, 10111.
99. Meshnick, S. R., Artemisinin: mechanisms of action, resistance and toxicity. *Int J Parasitol* **2002**, *32* (13), 1655-1660.
100. Eckstein-Ludwig, U.; Webb, R. J.; Van Goethem, I. D.; East, J. M.; Lee, A. G.; Kimura, M.; O'Neill, P. M.; Bray, P. G.; Ward, S. A.; Krishna, S., Artemisinins target the SERCA of Plasmodium falciparum. *Nature* **2003**, *424* (6951), 957-961.
101. Krungkrai, J.; Burat, D.; Kudan, S.; Krungkrai, S.; Prapunwattana, P., Mitochondrial oxygen consumption in asexual and sexual blood stages of the human malarial parasite, Plasmodium falciparum. *Southeast Asian J Trop Med Public Health* **1999**, *30* (4), 636-642.
102. Cui, L.; Su, X. Z., Discovery, mechanisms of action and combination therapy of artemisinin. *Expert Rev Anti Infect Ther* **2009**, *7* (8), 999-1013.

103. O'Neill, P. M.; Posner, G. H., A medicinal chemistry perspective on artemisinin and related endoperoxides. *J Med Chem* **2004**, *47* (12), 2945-2964.
104. Gautam, A.; Ahmed, T.; Batra, V.; Paliwal, J., Pharmacokinetics and pharmacodynamics of endoperoxide antimalarials. *Curr Drug Metab* **2009**, *10* (3), 289-306.
105. Golenser, J.; Waknine, J. H.; Krugliak, M.; Hunt, N. H.; Grau, G. E., Current perspectives on the mechanism of action of artemisinins. *Int J Parasitol* **2006**, *36* (14), 1427-1441.
106. Nosten, F.; White, N. J., Artemisinin-based combination treatment of falciparum malaria. *Am J Trop Med Hyg* **2007**, *77* (6 Suppl), 181-192.
107. Delves, M.; Plouffe, D.; Scheurer, C.; Meister, S.; Wittlin, S.; Winzeler, E. A.; Sinden, R. E.; Leroy, D., The activities of current antimalarial drugs on the life cycle stages of Plasmodium: a comparative study with human and rodent parasites. *PLoS Med* **2012**, *9* (2), e1001169.
108. Rodrigues, T.; Lopes, F.; Moreira, R., Inhibitors of the mitochondrial electron transport chain and de novo pyrimidine biosynthesis as antimalarials: The present status. *Curr Med Chem* **2010**, *17* (10), 929-956.
109. Crofts, A. R.; Lhee, S.; Crofts, S. B.; Cheng, J.; Rose, S., Proton pumping in the bc1 complex: a new gating mechanism that prevents short circuits. *Biochim Biophys Acta* **2006**, *1757* (8), 1019-1034.
110. Moser, C. C.; Farid, T. A.; Chobot, S. E.; Dutton, P. L., Electron tunneling chains of mitochondria. *Biochim Biophys Acta* **2006**, *1757* (9-10), 1096-1109.
111. Barton, V.; Fisher, N.; Biagini, G. A.; Ward, S. A.; O'Neill, P. M., Inhibiting Plasmodium cytochrome bc1: a complex issue. *Curr Opin Chem Biol* **2010**, *14* (4), 440-446.
112. Fisher, N.; Meunier, B., Molecular basis of resistance to cytochrome bc1 inhibitors. *FEMS Yeast Res* **2008**, *8* (2), 183-192.
113. Nixon, G. L.; Moss, D. M.; Shone, A. E.; Laloo, D. G.; Fisher, N.; O'Neill, P. M.; Ward, S. A.; Biagini, G. A., Antimalarial pharmacology and therapeutics of atovaquone. *J Antimicrob Chemother* **2013**, *68* (5), 977-985.
114. Biagini, G. A.; Fisher, N.; Shone, A. E.; Mubaraki, M. A.; Srivastava, A.; Hill, A.; Antoine, T.; Warman, A. J.; Davies, J.; Pidathala, C.; Amewu, R. K.; Leung, S. C.; Sharma, R.; Gibbons, P.; Hong, D. W.; Pacorel, B.; Lawrenson, A. S.; Charoensutthivarakul, S.; Taylor, L.; Berger, O.; Mbekeani, A.; Stocks, P. A.; Nixon, G. L.; Chadwick, J.; Hemingway, J.; Delves, M. J.; Sinden, R. E.; Zeeman, A. M.; Kocken, C. H.; Berry, N. G.; O'Neill, P. M.; Ward, S. A., Generation of quinolone antimalarials targeting the Plasmodium falciparum mitochondrial respiratory chain for the treatment and prophylaxis of malaria. *Proc Natl Acad Sci U S A* **2012**, *109* (21), 8298-8303.
115. Dong, C. K.; Uргаonkar, S.; Cortese, J. F.; Gamo, F. J.; Garcia-Bustos, J. F.; Lafuente, M. J.; Patel, V.; Ross, L.; Coleman, B. I.; Derbyshire, E. R.; Clish, C. B.; Serrano, A. E.; Cromwell, M.; Barker, R. H., Jr.; Dvorin, J. D.; Duraisingh, M. T.; Wirth, D. F.; Clardy, J.; Mazitschek, R., Identification and validation of tetracyclic benzothiazepines as Plasmodium falciparum cytochrome bc1 inhibitors. *Chem Biol* **2011**, *18* (12), 1602-1610.
116. Murteira, S.; Ghezaiel, Z.; Karray, S.; Lamure, M., Drug reformulations and repositioning in pharmaceutical industry and its impact on market access: reassessment of nomenclature. *2013* **2013**.
117. Abdulla, S.; Sagara, I., Dispersible formulation of artemether/lumefantrine: specifically developed for infants and young children. *Malar J* **2009**, *8* Suppl 1, S7.

References

118. Eastman, R. T.; Fidock, D. A., Artemisinin-based combination therapies: a vital tool in efforts to eliminate malaria. *Nat Rev Microbiol* **2009**, *7* (12), 864-874.
119. Nwaka, S.; Hudson, A., Innovative lead discovery strategies for tropical diseases. *Nat Rev Drug Discov* **2006**, *5* (11), 941-955.
120. Tshefu, A. K.; Gaye, O.; Kayentao, K.; Thompson, R.; Bhatt, K. M.; Sesay, S. S.; Bustos, D. G.; Tjitra, E.; Bedu-Addo, G.; Borghini-Fuhrer, I.; Duparc, S.; Shin, C. S.; Fleckenstein, L., Efficacy and safety of a fixed-dose oral combination of pyronaridine-artesunate compared with artemether-lumefantrine in children and adults with uncomplicated *Plasmodium falciparum* malaria: a randomised non-inferiority trial. *Lancet* **2010**, *375* (9724), 1457-1467.
121. Chandra, R. S.; Orazem, J.; Ubben, D.; Duparc, S.; Robbins, J.; Vandebroucke, P., Creative solutions to extraordinary challenges in clinical trials: methodology of a phase III trial of azithromycin and chloroquine fixed-dose combination in pregnant women in Africa. *Malar J* **2013**, *12*, 122.
122. Aguiar, A. C.; Rocha, E. M.; Souza, N. B.; Franca, T. C.; Krettli, A. U., New approaches in antimalarial drug discovery and development: a review. *Mem Inst Oswaldo Cruz* **2012**, *107* (7), 831-845.
123. Wu, T.; Nagle, A. S.; Chatterjee, A. K., Road towards new antimalarials - overview of the strategies and their chemical progress. *Curr Med Chem* **2011**, *18* (6), 853-871.
124. Leroy, D.; Campo, B.; Ding, X. C.; Burrows, J. N.; Cherbuin, S., Defining the biology component of the drug discovery strategy for malaria eradication. *Trends Parasitol* **2014**, *30* (10), 478-490.
125. Burrows, J. N.; van Huijsduijnen, R. H.; Mohrle, J. J.; Oeuvray, C.; Wells, T. N., Designing the next generation of medicines for malaria control and eradication. *Malar J* **2013**, *12*, 187.
126. Sharma, R.; Lawrenson, A. S.; Fisher, N. E.; Warman, A. J.; Shone, A. E.; Hill, A.; Mbekeani, A.; Pidathala, C.; Amewu, R. K.; Leung, S.; Gibbons, P.; Hong, D. W.; Stocks, P.; Nixon, G. L.; Chadwick, J.; Shearer, J.; Gowers, I.; Cronk, D.; Parel, S. P.; O'Neill, P. M.; Ward, S. A.; Biagini, G. A.; Berry, N. G., Identification of novel antimalarial chemotypes via chemoinformatic compound selection methods for a high-throughput screening program against the novel malarial target, PfNDH2: increasing hit rate via virtual screening methods. *J Med Chem* **2012**, *55* (7), 3144-3154.
127. de Beer, T. A.; Wells, G. A.; Burger, P. B.; Joubert, F.; Marechal, E.; Birkholtz, L.; Louw, A. I., Antimalarial drug discovery: in silico structural biology and rational drug design. *Infect Disord Drug Targets* **2009**, *9* (3), 304-318.
128. Brown, L. E.; Chih-Chien Cheng, K.; Wei, W. G.; Yuan, P.; Dai, P.; Trilles, R.; Ni, F.; Yuan, J.; MacArthur, R.; Guha, R.; Johnson, R. L.; Su, X. Z.; Dominguez, M. M.; Snyder, J. K.; Beeler, A. B.; Schaus, S. E.; Inglese, J.; Porco, J. A., Jr., Discovery of new antimalarial chemotypes through chemical methodology and library development. *Proc Natl Acad Sci U S A* **2011**, *108* (17), 6775-6780.
129. Crowther, G. J.; Napuli, A. J.; Gilligan, J. H.; Gagaring, K.; Borboa, R.; Francek, C.; Chen, Z.; Dagostino, E. F.; Stockmyer, J. B.; Wang, Y.; Rodenbough, P. P.; Castaneda, L. J.; Leibly, D. J.; Bhandari, J.; Gelb, M. H.; Brinker, A.; Engels, I. H.; Taylor, J.; Chatterjee, A. K.; Fantauzzi, P.; Glynn, R. J.; Van Voorhis, W. C.; Kuhnen, K. L., Identification of inhibitors for putative malaria drug targets among novel antimalarial compounds. *Mol Biochem Parasitol* **2011**, *175* (1), 21-29.

130. Andrews, K. T.; Fisher, G.; Skinner-Adams, T. S., Drug repurposing and human parasitic protozoan diseases. *Int J Parasitol Drugs Drug Resist* **2014**, *4* (2), 95-111.
131. Gardiner, D. L.; Skinner-Adams, T. S.; Brown, C. L.; Andrews, K. T.; Stack, C. M.; McCarthy, J. S.; Dalton, J. P.; Trenholme, K. R., Plasmodium falciparum: new molecular targets with potential for antimalarial drug development. *Expert Rev Anti Infect Ther* **2009**, *7* (9), 1087-1098.
132. Pink, D.; Bertz-Lepel, J.; Busemann, C.; Bitz, U.; Reichardt, P., Efficacy of trabectedin in patients with advanced or metastatic alveolar soft-part sarcoma. *Onkologie* **2012**, *35* (5), 249-252.
133. Chong, C. R.; Chen, X.; Shi, L.; Liu, J. O.; Sullivan, D. J., Jr., A clinical drug library screen identifies astemizole as an antimalarial agent. *Nat Chem Biol* **2006**, *2* (8), 415-416.
134. Weisman, J. L.; Liou, A. P.; Shelat, A. A.; Cohen, F. E.; Guy, R. K.; DeRisi, J. L., Searching for new antimalarial therapeutics amongst known drugs. *Chem Biol Drug Des* **2006**, *67* (6), 409-416.
135. Yuan, J.; Cheng, K. C.; Johnson, R. L.; Huang, R.; Pattaradilokrat, S.; Liu, A.; Guha, R.; Fidock, D. A.; Inglesse, J.; Wellems, T. E.; Austin, C. P.; Su, X. Z., Chemical genomic profiling for antimalarial therapies, response signatures, and molecular targets. *Science* **2011**, *333* (6043), 724-729.
136. da Cruz, F. P.; Martin, C.; Buchholz, K.; Lafuente-Monasterio, M. J.; Rodrigues, T.; Sonnichsen, B.; Moreira, R.; Gamo, F. J.; Marti, M.; Mota, M. M.; Hannus, M.; Prudencio, M., Drug screen targeted at Plasmodium liver stages identifies a potent multistage antimalarial drug. *J Infect Dis* **2012**, *205* (8), 1278-1286.
137. Lucantoni, L.; Avery, V., Whole-cell in vitro screening for gametocytocidal compounds. *Future Med Chem* **2012**, *4* (18), 2337-2360.
138. Bathula, C.; Singh, S.; Sen, S., Diversity oriented synthesis for novel anti-malarials. *Syst Synth Biol* **2015**, *9* (Suppl 1), 49-53.
139. Weiwer, M.; Mulrooney, C.; Massi, D.; Heidebrecht, R.; Wiegand, R.; Lukens, A. K.; Dick, J.; Wirth, D.; Ekland, E.; Cheng, C. C.; Zhao, J.; Yuan, J.; Su, X. Z.; Johnson, R. L.; Guha, R.; Dandapani, S.; Munoz, B.; Palmer, M.; Thomas, C.; Austin, C. P.; Fidock, D.; Schreiber, S. L., ML238: An Antimalarial Small Molecule of a Unique Structural Class. In *Probe Reports from the NIH Molecular Libraries Program*, National Center for Biotechnology Information (US): Bethesda (MD), 2010.
140. Heidebrecht, R. W., Jr.; Mulrooney, C.; Austin, C. P.; Barker, R. H., Jr.; Beaudoin, J. A.; Cheng, K. C.; Comer, E.; Dandapani, S.; Dick, J.; Duvall, J. R.; Ekland, E. H.; Fidock, D. A.; Fitzgerald, M. E.; Foley, M.; Guha, R.; Hinkson, P.; Kramer, M.; Lukens, A. K.; Masi, D.; Marcaurelle, L. A.; Su, X. Z.; Thomas, C. J.; Weiwer, M.; Wiegand, R. C.; Wirth, D.; Xia, M.; Yuan, J.; Zhao, J.; Palmer, M.; Munoz, B.; Schreiber, S., Diversity-Oriented Synthesis Yields a Novel Lead for the Treatment of Malaria. *ACS Med Chem Lett* **2012**, *3* (2), 112-117.
141. Passemar, C.; Sallery, M.; Soh, P. N.; Linas, M. D.; Ahond, A.; Poupat, C.; Benoit-Vical, F., Indole and aminoimidazole moieties appear as key structural units in antiplasmodial molecules. *Phytomedicine* **2011**, *18* (13), 1118-1125.
142. Wolfender, J. L.; Queiroz, E. F., New approaches for studying the chemical diversity of natural resources and the bioactivity of their constituents. *Chimia (Aarau)* **2012**, *66* (5), 324-329.

References

143. Perez-Moreno, G.; Cantizani, J.; Sanchez-Carrasco, P.; Ruiz-Perez, L. M.; Martin, J.; El Aouad, N.; Perez-Victoria, I.; Tormo, J. R.; Gonzalez-Menendez, V.; Gonzalez, I.; de Pedro, N.; Reyes, F.; Genilloud, O.; Vicente, F.; Gonzalez-Pacanowska, D., Discovery of New Compounds Active against *Plasmodium falciparum* by High Throughput Screening of Microbial Natural Products. *PLoS One* **2016**, *11* (1), e0145812.
144. Wells, T. N., Discovering and developing new medicines for malaria control and elimination. *Infect Disord Drug Targets* **2013**, *13* (4), 292-302.
145. Guantai, E.; Chibale, K., How can natural products serve as a viable source of lead compounds for the development of new/novel anti-malarials? *Malar J* **2011**, *10 Suppl 1*, S2.
146. Bero, J.; Quetin-Leclercq, J., Natural products published in 2009 from plants traditionally used to treat malaria. *Planta Med* **2011**, *77* (6), 631-640.
147. Cordier, C.; Morton, D.; Murrison, S.; Nelson, A.; O'Leary-Steele, C., Natural products as an inspiration in the diversity-oriented synthesis of bioactive compound libraries. *Nat Prod Rep* **2008**, *25* (4), 719-737.
148. Rishton, G. M., Natural products as a robust source of new drugs and drug leads: past successes and present day issues. *Am J Cardiol* **2008**, *101* (10a), 43d-49d.
149. Burns, W. R., East meets West: how China almost cured malaria. *Endeavour* **2008**, *32* (3), 101-106.
150. Lavrado, J.; Moreira, R.; Paulo, A., Indoloquinolines as scaffolds for drug discovery. *Curr Med Chem* **2010**, *17* (22), 2348-2370.
151. Derbyshire, E. R.; Mota, M. M.; Clardy, J., The next opportunity in anti-malaria drug discovery: the liver stage. *PLoS Pathog* **2011**, *7* (9), e1002178.
152. Chatterjee, A. K.; Yeung, B. K., Back to the future: lessons learned in modern target-based and whole-cell lead optimization of antimalarials. *Curr Top Med Chem* **2012**, *12* (5), 473-483.
153. Payne, D. J.; Gwynn, M. N.; Holmes, D. J.; Pompliano, D. L., Drugs for bad bugs: confronting the challenges of antibacterial discovery. *Nat Rev Drug Discov* **2007**, *6* (1), 29-40.
154. Coteron, J. M.; Marco, M.; Esquivias, J.; Deng, X.; White, K. L.; White, J.; Koltun, M.; El Mazouni, F.; Kokkonda, S.; Katneni, K.; Bhamidipati, R.; Shackelford, D. M.; Angulo-Barturen, I.; Ferrer, S. B.; Jimenez-Diaz, M. B.; Gamo, F. J.; Goldsmith, E. J.; Charman, W. N.; Bathurst, I.; Floyd, D.; Matthews, D.; Burrows, J. N.; Rathod, P. K.; Charman, S. A.; Phillips, M. A., Structure-guided lead optimization of triazolopyrimidine-ring substituents identifies potent *Plasmodium falciparum* dihydroorotate dehydrogenase inhibitors with clinical candidate potential. *J Med Chem* **2011**, *54* (15), 5540-5561.
155. Guiguemde, W. A.; Shelat, A. A.; Garcia-Bustos, J. F.; Diagona, T. T.; Gamo, F. J.; Guy, R. K., Global phenotypic screening for antimalarials. *Chem Biol* **2012**, *19* (1), 116-129.
156. Swinney, D. C.; Anthony, J., How were new medicines discovered? *Nat Rev Drug Discov* **2011**, *10* (7), 507-519.
157. Dembele, L.; Gego, A.; Zeeman, A. M.; Franetich, J. F.; Silvie, O.; Rametti, A.; Le Grand, R.; Dereuddre-Bosquet, N.; Sauerwein, R.; van Gemert, G. J.; Vaillant, J. C.; Thomas, A. W.; Snounou, G.; Kocken, C. H.; Mazier, D., Towards an in vitro model of *Plasmodium* hypnozoites suitable for drug discovery. *PLoS One* **2011**, *6* (3), e18162.

158. Sanders, N. G.; Sullivan, D. J.; Mlambo, G.; Dimopoulos, G.; Tripathi, A. K., Gametocytocidal screen identifies novel chemical classes with *Plasmodium falciparum* transmission blocking activity. *PLoS One* **2014**, *9* (8), e105817.
159. Tanaka, T. Q.; Dehdashti, S. J.; Nguyen, D. T.; McKew, J. C.; Zheng, W.; Williamson, K. C., A quantitative high throughput assay for identifying gametocytocidal compounds. *Mol Biochem Parasitol* **2013**, *188* (1), 20-25.
160. Brancucci, N. M.; Goldowitz, I.; Buchholz, K.; Werling, K.; Marti, M., An assay to probe *Plasmodium falciparum* growth, transmission stage formation and early gametocyte development. *Nat Protoc* **2015**, *10* (8), 1131-1142.
161. Zuzarte-Luis, V.; Sales-Dias, J.; Mota, M. M., Simple, sensitive and quantitative bioluminescence assay for determination of malaria pre-patent period. *Malar J* **2014**, *13*, 15.
162. Derbyshire, E. R.; Prudencio, M.; Mota, M. M.; Clardy, J., Liver-stage malaria parasites vulnerable to diverse chemical scaffolds. *Proc Natl Acad Sci U S A* **2012**, *109* (22), 8511-8516.
163. Calderon, F.; Barros, D.; Bueno, J. M.; Coteron, J. M.; Fernandez, E.; Gamo, F. J.; Lavandera, J. L.; Leon, M. L.; Macdonald, S. J. F.; Mallo, A.; Manzano, P.; Porras, E.; Fiandor, J. M.; Castro, J., An Invitation to Open Innovation in Malaria Drug Discovery: 47 Quality Starting Points from the TCAMS. *Acs Medicinal Chemistry Letters* **2011**, *2* (10), 741-746.
164. Medicines for Malaria Venture. <http://www.mmv.org/> (accessed August 28 2015).
165. Burrows, J. N.; Burlot, E.; Campo, B.; Cherbuin, S.; Jeanneret, S.; Leroy, D.; Spangenberg, T.; Waterson, D.; Wells, T. N.; Willis, P., Antimalarial drug discovery - the path towards eradication. *Parasitology* **2014**, *141* (1), 128-139.
166. Drinkwater, N.; McGowan, S., From crystal to compound: structure-based antimalarial drug discovery. *Biochem J* **2014**, *461* (3), 349-369.
167. Mandal, S.; Moudgil, M.; Mandal, S. K., Rational drug design. *Eur J Pharmacol* **2009**, *625* (1-3), 90-100.
168. Katsuno, K.; Burrows, J. N.; Duncan, K.; Hooft van Huijsduijnen, R.; Kaneko, T.; Kita, K.; Mowbray, C. E.; Schmatz, D.; Warner, P.; Slingsby, B. T., Hit and lead criteria in drug discovery for infectious diseases of the developing world. *Nat Rev Drug Discov* **2015**, *14* (11), 751-758.
169. Manly, C. J.; Chandrasekhar, J.; Ochterski, J. W.; Hammer, J. D.; Warfield, B. B., Strategies and tactics for optimizing the Hit-to-Lead process and beyond--a computational chemistry perspective. *Drug Discov Today* **2008**, *13* (3-4), 99-109.
170. Rottmann, M.; McNamara, C.; Yeung, B. K.; Lee, M. C.; Zou, B.; Russell, B.; Seitz, P.; Plouffe, D. M.; Dharia, N. V.; Tan, J.; Cohen, S. B.; Spencer, K. R.; Gonzalez-Paez, G. E.; Lakshminarayana, S. B.; Goh, A.; Suwanarusk, R.; Jegla, T.; Schmitt, E. K.; Beck, H. P.; Brun, R.; Nosten, F.; Renia, L.; Dartois, V.; Keller, T. H.; Fidock, D. A.; Winzeler, E. A.; Diagana, T. T., Spiroindolones, a potent compound class for the treatment of malaria. *Science* **2010**, *329* (5996), 1175-1180.
171. Kuhen, K. L.; Chatterjee, A. K.; Rottmann, M.; Gagaring, K.; Borboa, R.; Buenviaje, J.; Chen, Z.; Francek, C.; Wu, T.; Nagle, A.; Barnes, S. W.; Plouffe, D.; Lee, M. C.; Fidock, D. A.; Graumans, W.; van de Vegte-Bolmer, M.; van Gemert, G. J.; Wirjanata, G.; Sebayang, B.; Marfurt, J.; Russell, B.; Suwanarusk, R.; Price, R. N.; Nosten, F.; Tungtaeng, A.; Gettayacamin, M.; Sattabongkot, J.; Taylor, J.; Walker, J. R.; Tully, D.;

References

- Patra, K. P.; Flannery, E. L.; Vinetz, J. M.; Renia, L.; Sauerwein, R. W.; Winzeler, E. A.; Glynn, R. J.; Diagana, T. T., KAF156 is an antimalarial clinical candidate with potential for use in prophylaxis, treatment, and prevention of disease transmission. *Antimicrob Agents Chemother* **2014**, *58* (9), 5060-5067.
172. Oliveira, R.; Miranda, D.; Magalhaes, J.; Capela, R.; Perry, M. J.; O'Neill, P. M.; Moreira, R.; Lopes, F., From hybrid compounds to targeted drug delivery in antimalarial therapy. *Bioorg Med Chem* **2015**, *23* (16), 5120-5130.
173. Oliveira, R.; Guedes, R. C.; Meireles, P.; Albuquerque, I. S.; Goncalves, L. M.; Pires, E.; Bronze, M. R.; Gut, J.; Rosenthal, P. J.; Prudencio, M.; Moreira, R.; O'Neill, P. M.; Lopes, F., Tetraoxane-pyrimidine nitrile hybrids as dual stage antimalarials. *J Med Chem* **2014**, *57* (11), 4916-4923.
174. Miranda, D.; Capela, R.; Albuquerque, I. S.; Meireles, P.; Paiva, I.; Nogueira, F.; Amewu, R.; Gut, J.; Rosenthal, P. J.; Oliveira, R.; Mota, M. M.; Moreira, R.; Marti, F.; Prudencio, M.; O'Neill, P. M.; Lopes, F., Novel endoperoxide-based transmission-blocking antimalarials with liver- and blood-schizontocidal activities. *ACS Med Chem Lett* **2014**, *5* (2), 108-112.
175. Muregi, F. W.; Ishih, A., Next-Generation Antimalarial Drugs: Hybrid Molecules as a New Strategy in Drug Design. *Drug Dev Res* **2010**, *71* (1), 20-32.
176. Rodrigues, C. A.; Frade, R. F.; Albuquerque, I. S.; Perry, M. J.; Gut, J.; Machado, M.; Rosenthal, P. J.; Prudencio, M.; Afonso, C. A.; Moreira, R., Targeting the erythrocytic and liver stages of malaria parasites with s-triazine-based hybrids. *Chem Med Chem* **2015**, *10* (5), 883-890.
177. Dambuza, N. S.; Smith, P.; Evans, A.; Norman, J.; Taylor, D.; Andayi, A.; Egan, T.; Chibale, K.; Wiesner, L., Antiplasmodial activity, in vivo pharmacokinetics and antimalarial efficacy evaluation of hydroxypyridinone hybrids in a mouse model. *Malar J* **2015**, *14* (1), 505.
178. Vandekerckhove, S.; D'Hooghe, M., Quinoline-based antimalarial hybrid compounds. *Bioorg Med Chem* **2015**, *23* (16), 5098-5119.
179. Coslédan, F.; Fraisse, L.; Pellet, A.; Guillou, F.; Mordmüller, B.; Kremsner, P. G.; Moreno, A.; Mazier, D.; Maffrand, J.-P.; Meunier, B., Selection of a trioxaquine as an antimalarial drug candidate. *Proc Natl Acad Sci* **2008**, *105* (45), 17579-17584.
180. Jones, R. A.; Panda, S. S.; Hall, C. D., Quinine conjugates and quinine analogues as potential antimalarial agents. *Eur J Med Chem* **2015**, *97*, 335-355.
181. de Souza, N. B.; Carmo, A. M.; Lagatta, D. C.; Alves, M. J.; Fontes, A. P.; Coimbra, E. S.; da Silva, A. D.; Abramo, C., 4-aminoquinoline analogues and its platinum (II) complexes as antimalarial agents. *Biomed Pharmacother* **2011**, *65* (4), 313-316.
182. Biot, C.; Nosten, F.; Fraisse, L.; Ter-Minassian, D.; Khalife, J.; Dive, D., The antimalarial ferroquine: from bench to clinic. *Parasite* **2011**, *18* (3), 207-214.
183. Nilsen, A.; LaCrue, A. N.; White, K. L.; Forquer, I. P.; Cross, R. M.; Marfurt, J.; Mather, M. W.; Delves, M. J.; Shackelford, D. M.; Saenz, F. E.; Morrissey, J. M.; Steuten, J.; Mutka, T.; Li, Y.; Wirjanata, G.; Ryan, E.; Duffy, S.; Kelly, J. X.; Sebayang, B. F.; Zeeman, A. M.; Noviyanti, R.; Sinden, R. E.; Kocken, C. H.; Price, R. N.; Avery, V. M.; Angulo-Barturen, I.; Jimenez-Diaz, M. B.; Ferrer, S.; Herreros, E.; Sanz, L. M.; Gamo, F. J.; Bathurst, I.; Burrows, J. N.; Siegl, P.; Guy, R. K.; Winter, R. W.; Vaidya, A. B.; Charman, S. A.; Kyle, D. E.; Manetsch, R.; Riscoe, M. K., Quinolone-3-diarylethers: a new class of antimalarial drug. *Sci Transl Med* **2013**, *5* (177), 177ra137.

184. Charman, S. A.; Arbe-Barnes, S.; Bathurst, I. C.; Brun, R.; Campbell, M.; Charman, W. N.; Chiu, F. C.; Chollet, J.; Craft, J. C.; Creek, D. J.; Dong, Y.; Matile, H.; Maurer, M.; Morizzi, J.; Nguyen, T.; Papastogiannidis, P.; Scheurer, C.; Shackleford, D. M.; Sriraghavan, K.; Stingelin, L.; Tang, Y.; Urwyler, H.; Wang, X.; White, K. L.; Wittlin, S.; Zhou, L.; Vennerstrom, J. L., Synthetic ozonide drug candidate OZ439 offers new hope for a single-dose cure of uncomplicated malaria. *Proc Natl Acad Sci U S A* **2011**, *108* (11), 4400-4405.
185. Stocks, P. A.; Barton, V.; Antoine, T.; Biagini, G. A.; Ward, S. A.; O'Neill, P. M., Novel inhibitors of the Plasmodium falciparum electron transport chain. *Parasitology* **2014**, *141* (1), 50-65.
186. Cross, R. M.; Monastyrskyi, A.; Mutka, T. S.; Burrows, J. N.; Kyle, D. E.; Manetsch, R., Endochin optimization: structure-activity and structure-property relationship studies of 3-substituted 2-methyl-4(1H)-quinolones with antimalarial activity. *J Med Chem* **2010**, *53* (19), 7076-7094.
187. Winter, R.; Kelly, J. X.; Smilkstein, M. J.; Hinrichs, D.; Koop, D. R.; Riscoe, M. K., Optimization of endochin-like quinolones for antimalarial activity. *Exp Parasitol* **2011**, *127* (2), 545-551.
188. Miley, G. P.; Pou, S.; Winter, R.; Nilsen, A.; Li, Y.; Kelly, J. X.; Stickles, A. M.; Mather, M. W.; Forquer, I. P.; Pershing, A. M.; White, K.; Shackleford, D.; Saunders, J.; Chen, G.; Ting, L. M.; Kim, K.; Zakharov, L. N.; Donini, C.; Burrows, J. N.; Vaidya, A. B.; Charman, S. A.; Riscoe, M. K., ELQ-300 prodrugs for enhanced delivery and single-dose cure of malaria. *Antimicrob Agents Chemother* **2015**, *59* (9), 5555-5560.
189. Abbat, S.; Jain, V.; Bharatam, P. V., Origins of the specificity of inhibitor P218 toward wild-type and mutant PfDHFR: a molecular dynamics analysis. *J Biomol Struct Dyn* **2015**, *33* (9), 1913-1928.
190. Mokmak, W.; Chunsriviro, S.; Hannongbua, S.; Yuthavong, Y.; Tongsim, S.; Kamchonwongpaisan, S., Molecular dynamics of interactions between rigid and flexible antifolates and dihydrofolate reductase from pyrimethamine-sensitive and pyrimethamine-resistant Plasmodium falciparum. *Chem Biol Drug Des* **2014**, *84* (4), 450-461.
191. Vennerstrom, J. L.; Arbe-Barnes, S.; Brun, R.; Charman, S. A.; Chiu, F. C.; Chollet, J.; Dong, Y.; Dorn, A.; Hunziker, D.; Matile, H.; McIntosh, K.; Padmanilayam, M.; Santo Tomas, J.; Scheurer, C.; Scorneaux, B.; Tang, Y.; Urwyler, H.; Wittlin, S.; Charman, W. N., Identification of an antimalarial synthetic trioxolane drug development candidate. *Nature* **2004**, *430* (7002), 900-904.
192. Dong, Y.; Wittlin, S.; Sriraghavan, K.; Chollet, J.; Charman, S. A.; Charman, W. N.; Scheurer, C.; Urwyler, H.; Santo Tomas, J.; Snyder, C.; Creek, D. J.; Morizzi, J.; Koltun, M.; Matile, H.; Wang, X.; Padmanilayam, M.; Tang, Y.; Dorn, A.; Brun, R.; Vennerstrom, J. L., The structure-activity relationship of the antimalarial ozonide arterolane (OZ277). *J Med Chem* **2010**, *53* (1), 481-491.
193. Moehrle, J. J.; Duparc, S.; Siethoff, C.; van Giersbergen, P. L.; Craft, J. C.; Arbe-Barnes, S.; Charman, S. A.; Gutierrez, M.; Wittlin, S.; Vennerstrom, J. L., First-in-man safety and pharmacokinetics of synthetic ozonide OZ439 demonstrates an improved exposure profile relative to other peroxide antimalarials. *Br J Clin Pharmacol* **2013**, *75* (2), 524-537.

References

194. Smith, P. W.; Diagana, T. T.; Yeung, B. K., Progressing the global antimalarial portfolio: finding drugs which target multiple Plasmodium life stages. *Parasitology* **2014**, *141* (1), 66-76.
195. Diagana, T. T., Supporting malaria elimination with 21st century antimalarial agent drug discovery. *Drug Discov Today* **2015**.
196. Leong, F. J.; Zhao, R.; Zeng, S.; Magnusson, B.; Diagana, T. T.; Pertel, P., A first-in-human randomized, double-blind, placebo-controlled, single- and multiple-ascending oral dose study of novel Imidazolopiperazine KAF156 to assess its safety, tolerability, and pharmacokinetics in healthy adult volunteers. *Antimicrob Agents Chemother* **2014**, *58* (11), 6437-6443.
197. Younis, Y.; Douelle, F.; Feng, T. S.; Gonzalez Cabrera, D.; Le Manach, C.; Nchinda, A. T.; Duffy, S.; White, K. L.; Shackleford, D. M.; Morizzi, J.; Mannila, J.; Katneni, K.; Bhamidipati, R.; Zabiulla, K. M.; Joseph, J. T.; Bashyam, S.; Waterson, D.; Witty, M. J.; Hardick, D.; Wittlin, S.; Avery, V.; Charman, S. A.; Chibale, K., 3,5-Diaryl-2-aminopyridines as a novel class of orally active antimalarials demonstrating single dose cure in mice and clinical candidate potential. *J Med Chem* **2012**, *55* (7), 3479-3487.
198. Baldwin, J.; Michnoff, C. H.; Malmquist, N. A.; White, J.; Roth, M. G.; Rathod, P. K.; Phillips, M. A., High-throughput screening for potent and selective inhibitors of Plasmodium falciparum dihydroorotate dehydrogenase. *J Biol Chem* **2005**, *280* (23), 21847-21853.
199. McNamara, C.; Winzeler, E. A., Target identification and validation of novel antimalarials. *Future Microbiol* **2011**, *6* (6), 693-704.
200. Ursu, A.; Waldmann, H., Hide and seek: Identification and confirmation of small molecule protein targets. *Bioorg Med Chem Lett* **2015**, *25* (16), 3079-3086.
201. Tashiro, E.; Imoto, M., Target identification of bioactive compounds. *Bioorg Med Chem* **2012**, *20* (6), 1910-1921.
202. Wilson, D. W.; Langer, C.; Goodman, C. D.; McFadden, G. I.; Beeson, J. G., Defining the timing of action of antimalarial drugs against Plasmodium falciparum. *Antimicrob Agents Chemother* **2013**, *57* (3), 1455-1467.
203. Horn, D.; Duraisingh, M. T., Antiparasitic chemotherapy: from genomes to mechanisms. *Annu Rev Pharmacol Toxicol* **2014**, *54*, 71-94.
204. Dharia, N. V.; Sidhu, A. B.; Cassera, M. B.; Westenberger, S. J.; Bopp, S. E.; Eastman, R. T.; Plouffe, D.; Batalov, S.; Park, D. J.; Volkman, S. K.; Wirth, D. F.; Zhou, Y.; Fidock, D. A.; Winzeler, E. A., Use of high-density tiling microarrays to identify mutations globally and elucidate mechanisms of drug resistance in Plasmodium falciparum. *Genome Biol* **2009**, *10* (2), R21.
205. Hoepfner, D.; McNamara, C. W.; Lim, C. S.; Studer, C.; Riedl, R.; Aust, T.; McCormack, S. L.; Plouffe, D. M.; Meister, S.; Schuierer, S.; Plikat, U.; Hartmann, N.; Staedtler, F.; Cotesta, S.; Schmitt, E. K.; Petersen, F.; Supek, F.; Glynn, R. J.; Tallarico, J. A.; Porter, J. A.; Fishman, M. C.; Bodenreider, C.; Diagana, T. T.; Movva, N. R.; Winzeler, E. A., Selective and specific inhibition of the plasmodium falciparum lysyl-tRNA synthetase by the fungal secondary metabolite cladosporin. *Cell Host Microbe* **2012**, *11* (6), 654-663.
206. Herman, J. D.; Rice, D. P.; Ribacke, U.; Silterra, J.; Deik, A. A.; Moss, E. L.; Broadbent, K. M.; Neafsey, D. E.; Desai, M. M.; Clish, C. B.; Mazitschek, R.; Wirth, D. F., A

- genomic and evolutionary approach reveals non-genetic drug resistance in malaria. *Genome Biol* **2014**, *15* (11), 511.
207. Dyer, M.; Jackson, M.; McWhinney, C.; Zhao, G.; Mikkelsen, R., Analysis of a cation-transporting ATPase of *Plasmodium falciparum*. *Mol Biochem Parasitol* **1996**, *78* (1-2), 1-12.
208. Krishna, S.; Woodrow, C.; Webb, R.; Penny, J.; Takeyasu, K.; Kimura, M.; East, J. M., Expression and functional characterization of a *Plasmodium falciparum* Ca²⁺-ATPase (PfATP4) belonging to a subclass unique to apicomplexan organisms. *J Biol Chem* **2001**, *276* (14), 10782-10787.
209. Trottein, F.; Thompson, J.; Cowman, A. F., Cloning of a new cation ATPase from *Plasmodium falciparum*: conservation of critical amino acids involved in calcium binding in mammalian organellar Ca(2+)-ATPases. *Gene* **1995**, *158* (1), 133-137.
210. Spillman, N. J.; Allen, R. J.; McNamara, C. W.; Yeung, B. K.; Winzeler, E. A.; Diagana, T. T.; Kirk, K., Na(+) regulation in the malaria parasite *Plasmodium falciparum* involves the cation ATPase PfATP4 and is a target of the spiroindolone antimalarials. *Cell Host Microbe* **2013**, *13* (2), 227-237.
211. Kruger, T.; Sanchez, C. P.; Lanzer, M., Complementation of *Saccharomyces cerevisiae* pik1ts by a phosphatidylinositol 4-kinase from *Plasmodium falciparum*. *Mol Biochem Parasitol* **2010**, *172* (2), 149-151.
212. Cho, Y. S.; Kwon, H. J., Identification and validation of bioactive small molecule target through phenotypic screening. *Bioorg Med Chem* **2012**, *20* (6), 1922-1928.
213. Bantscheff, M., Mass spectrometry-based chemoproteomic approaches. *Methods Mol Biol* **2012**, *803*, 3-13.
214. Bantscheff, M.; Drewes, G., Chemoproteomic approaches to drug target identification and drug profiling. *Bioorg Med Chem* **2012**, *20* (6), 1973-1978.
215. Vincent, I. M.; Barrett, M. P., Metabolomic-based strategies for anti-parasite drug discovery. *J Biomol Screen* **2015**, *20* (1), 44-55.
216. Creek, D. J.; Barrett, M. P., Determination of antiprotozoal drug mechanisms by metabolomics approaches. *Parasitology* **2014**, *141* (1), 83-92.
217. Lakshmanan, V.; Rhee, K. Y.; Daily, J. P., Metabolomics and malaria biology. *Mol Biochem Parasitol* **2011**, *175* (2), 104-111.
218. Park, Y. H.; Shi, Y. P.; Liang, B.; Medriano, C. A.; Jeon, Y. H.; Torres, E.; Uppal, K.; Slutsker, L.; Jones, D. P., High-resolution metabolomics to discover potential parasite-specific biomarkers in a *Plasmodium falciparum* erythrocytic stage culture system. *Malar J* **2015**, *14*, 122.
219. Bulusu, V.; Jayaraman, V.; Balaram, H., Metabolic fate of fumarate, a side product of the purine salvage pathway in the intraerythrocytic stages of *Plasmodium falciparum*. *J Biol Chem* **2011**, *286* (11), 9236-9245.
220. Storm, J.; Perner, J.; Aparicio, I.; Patzewitz, E. M.; Olszewski, K.; Llinas, M.; Engel, P. C.; Muller, S., *Plasmodium falciparum* glutamate dehydrogenase a is dispensable and not a drug target during erythrocytic development. *Malar J* **2011**, *10*, 193.
221. Schenone, M.; Dancik, V.; Wagner, B. K.; Clemons, P. A., Target identification and mechanism of action in chemical biology and drug discovery. *Nat Chem Biol* **2013**, *9* (4), 232-240.

References

222. Prieto, J. H.; Fischer, E.; Koncarevic, S.; Yates, J.; Becker, K., Large-scale differential proteome analysis in *Plasmodium falciparum* under drug treatment. *Methods Mol Biol* **2015**, *1201*, 269-279.
223. Prieto, J. H.; Koncarevic, S.; Park, S. K.; Yates, J., III; Becker, K., Large-Scale Differential Proteome Analysis in *Plasmodium falciparum* under Drug Treatment. *PLoS One* **2008**, *3* (12).
224. Radfar, A.; Diez, A.; Bautista, J. M., Chloroquine mediates specific proteome oxidative damage across the erythrocytic cycle of resistant *Plasmodium falciparum*. *Free Radic Biol Med* **2008**, *44* (12), 2034-2042.
225. Bunnage, M. E.; Chekler, E. L.; Jones, L. H., Target validation using chemical probes. *Nat Chem Biol* **2013**, *9* (4), 195-199.
226. Vinegoni, C.; Dubach, J. M.; Thurber, G. M.; Miller, M. A.; Mazitschek, R.; Weissleder, R., Advances in measuring single-cell pharmacology in vivo. *Drug Discov Today* **2015**, *20* (9), 1087-1092.
227. Dubach, J. M.; Vinegoni, C.; Mazitschek, R.; Fumene Feruglio, P.; Cameron, L. A.; Weissleder, R., In vivo imaging of specific drug-target binding at subcellular resolution. *Nat Commun* **2014**, *5*, 3946.
228. Hartwig, C. L.; Lauterwasser, E. M.; Mahajan, S. S.; Hoke, J. M.; Cooper, R. A.; Renslo, A. R., Investigating the antimalarial action of 1,2,4-trioxolanes with fluorescent chemical probes. *J Med Chem* **2011**, *54* (23), 8207-8213.
229. Liu, Y.; Lok, C. N.; Ko, B. C.; Shum, T. Y.; Wong, M. K.; Che, C. M., Subcellular localization of a fluorescent artemisinin derivative to endoplasmic reticulum. *Org Lett* **2010**, *12* (7), 1420-1423.
230. Stocks, P. A.; Bray, P. G.; Barton, V. E.; Al-Helal, M.; Jones, M.; Araujo, N. C.; Gibbons, P.; Ward, S. A.; Hughes, R. H.; Biagini, G. A.; Davies, J.; Amewu, R.; Mercer, A. E.; Ellis, G.; O'Neill, P. M., Evidence for a common non-heme chelatable-iron-dependent activation mechanism for semisynthetic and synthetic endoperoxide antimalarial drugs. *Angew Chem Int Ed Engl* **2007**, *46* (33), 6278-6283.
231. Loh, C. C.; Suwanarusk, R.; Lee, Y. Q.; Chan, K. W.; Choy, K. Y.; Renia, L.; Russell, B.; Lear, M. J.; Nosten, F. H.; Tan, K. S.; Chow, L. M., Characterization of the commercially-available fluorescent chloroquine-BODIPY conjugate, LynxTag-CQGREEN, as a marker for chloroquine resistance and uptake in a 96-well plate assay. *PLoS One* **2014**, *9* (10), e110800.
232. Leeson, P. D.; Springthorpe, B., The influence of drug-like concepts on decision-making in medicinal chemistry. *Nat Rev Drug Discov* **2007**, *6* (11), 881-890.
233. Jensen, K.; Plichta, D.; Panagiotou, G.; Kouskoumvekaki, I., Mapping the genome of *Plasmodium falciparum* on the drug-like chemical space reveals novel anti-malarial targets and potential drug leads. *Mol Biosyst* **2012**, *8* (6), 1678-1685.
234. White, N. J.; Pukrittayakamee, S.; Phyo, A. P.; Rueangweerayut, R.; Nosten, F.; Jittamala, P.; Jeeyapant, A.; Jain, J. P.; Lefevre, G.; Li, R.; Magnusson, B.; Diagana, T. T.; Leong, F. J., Spiroindolone KAE609 for falciparum and vivax malaria. *N Engl J Med* **2014**, *371* (5), 403-410.
235. Yeung, B. K.; Zou, B.; Rottmann, M.; Lakshminarayana, S. B.; Ang, S. H.; Leong, S. Y.; Tan, J.; Wong, J.; Keller-Maerki, S.; Fischli, C.; Goh, A.; Schmitt, E. K.; Krastel, P.; Francotte, E.; Kuhlen, K.; Plouffe, D.; Henson, K.; Wagner, T.; Winzeler, E. A.; Petersen, F.; Brun, R.; Dartois, V.; Diagana, T. T.; Keller, T. H., Spirotetrahydro beta-carbolines

- (spiroindolones): a new class of potent and orally efficacious compounds for the treatment of malaria. *J Med Chem* **2010**, *53* (14), 5155-5164.
236. Urgaonkar, S.; Cortese, J. F.; Barker, R. H.; Cromwell, M.; Serrano, A. E.; Wirth, D. F.; Clardy, J.; Mazitschek, R., A concise silylamine approach to 2-amino-3-hydroxy-indoles with potent in vivo antimalaria activity. *Org Lett* **2010**, *12* (18), 3998-4001.
237. Cully, M., Trial watch: Next-generation antimalarial from phenotypic screen shows clinical promise. *Nat Rev Drug Discov* **2014**, *13* (10), 717.
238. Barker, R. H., Jr.; Urgaonkar, S.; Mazitschek, R.; Celatka, C.; Skerlj, R.; Cortese, J. F.; Tyndall, E.; Liu, H.; Cromwell, M.; Sidhu, A. B.; Guerrero-Bravo, J. E.; Crespo-Llado, K. N.; Serrano, A. E.; Lin, J. W.; Janse, C. J.; Khan, S. M.; Duraisingh, M.; Coleman, B. I.; Angulo-Barturen, I.; Jimenez-Diaz, M. B.; Magan, N.; Gomez, V.; Ferrer, S.; Martinez, M. S.; Wittlin, S.; Papastogiannidis, P.; O'Shea, T.; Klinger, J. D.; Bree, M.; Lee, E.; Levine, M.; Wiegand, R. C.; Munoz, B.; Wirth, D. F.; Clardy, J.; Bathurst, I.; Sybertz, E., Aminoindoles, a novel scaffold with potent activity against Plasmodium falciparum. *Antimicrob Agents Chemother* **2011**, *55* (6), 2612-2622.
239. Abdel-Magid, A. F.; Carson, K. G.; Harris, B. D.; Maryanoff, C. A.; Shah, R. D., Reductive Amination of Aldehydes and Ketones with Sodium Triacetoxyborohydride. Studies on Direct and Indirect Reductive Amination Procedures(1). *J Org Chem* **1996**, *61* (11), 3849-3862.
240. Crick, F. H., On protein synthesis. *Symp Soc Exp Biol* **1958**, *12*, 138-163.
241. Crick, F., Central dogma of molecular biology. *Nature* **1970**, *227* (5258), 561-563.
242. Havrylenko, S.; Mirande, M., Aminoacyl-tRNA synthetase complexes in evolution. *Int J Mol Sci* **2015**, *16* (3), 6571-6594.
243. Gadakh, B.; Van Aerschot, A., Aminoacyl-tRNA synthetase inhibitors as antimicrobial agents: a patent review from 2006 till present. *Expert Opin Ther Pat* **2012**, *22* (12), 1453-1465.
244. Datt, M.; Sharma, A., Novel and unique domains in aminoacyl-tRNA synthetases from human fungal pathogens *Aspergillus niger*, *Candida albicans* and *Cryptococcus neoformans*. *BMC Genomics* **2014**, *15*, 1069.
245. Dewan, V.; Reader, J.; Forsyth, K. M., Role of aminoacyl-tRNA synthetases in infectious diseases and targets for therapeutic development. *Top Curr Chem* **2014**, *344*, 293-329.
246. Pham, J. S.; Dawson, K. L.; Jackson, K. E.; Lim, E. E.; Pasaje, C. F.; Turner, K. E.; Ralph, S. A., Aminoacyl-tRNA synthetases as drug targets in eukaryotic parasites. *Int J Parasitol Drugs Drug Resist* **2014**, *4* (1), 1-13.
247. Li, R.; Macnamara, L. M.; Leuchter, J. D.; Alexander, R. W.; Cho, S. S., MD Simulations of tRNA and Aminoacyl-tRNA Synthetases: Dynamics, Folding, Binding, and Allostery. *Int J Mol Sci* **2015**, *16* (7), 15872-15902.
248. Pang, Y. L.; Poruri, K.; Martinis, S. A., tRNA synthetase: tRNA aminoacylation and beyond. *Wiley Interdiscip Rev RNA* **2014**, *5* (4), 461-480.
249. Ibba, M.; Soll, D., The renaissance of aminoacyl-tRNA synthesis. *EMBO Rep* **2001**, *2* (5), 382-387.
250. Krab, I. M.; Parmeggiani, A., Mechanisms of EF-Tu, a pioneer GTPase. *Prog Nucleic Acid Res Mol Biol* **2002**, *71*, 513-551.
251. Hotokezaka, Y.; Tobben, U.; Hotokezaka, H.; Van Leyen, K.; Beatrix, B.; Smith, D. H.; Nakamura, T.; Wiedmann, M., Interaction of the eukaryotic elongation factor 1A with newly synthesized polypeptides. *J Biol Chem* **2002**, *277* (21), 18545-18551.

References

252. Jackson, K. E.; Habib, S.; Frugier, M.; Hoen, R.; Khan, S.; Pham, J. S.; Ribas de Pouplana, L.; Royo, M.; Santos, M. A.; Sharma, A.; Ralph, S. A., Protein translation in Plasmodium parasites. *Trends Parasitol* **2011**, *27* (10), 467-476.
253. Ribas de Pouplana, L.; Schimmel, P., Aminoacyl-tRNA synthetases: potential markers of genetic code development. *Trends Biochem Sci* **2001**, *26* (10), 591-596.
254. Schimmel, P., Development of tRNA synthetases and connection to genetic code and disease. *Protein Sci* **2008**, *17* (10), 1643-1652.
255. Ribas de Pouplana, L.; Schimmel, P., Two classes of tRNA synthetases suggested by sterically compatible dockings on tRNA acceptor stem. *Cell* **2001**, *104* (2), 191-193.
256. Jakubowski, H., Quality control in tRNA charging. *Wiley Interdiscip Rev RNA* **2012**, *3* (3), 295-310.
257. Guo, M.; Schimmel, P., Structural analyses clarify the complex control of mistranslation by tRNA synthetases. *Curr Opin Struct Biol* **2012**, *22* (1), 119-126.
258. Yadavalli, S. S.; Ibba, M., Quality control in aminoacyl-tRNA synthesis its role in translational fidelity. *Adv Protein Chem Struct Biol* **2012**, *86*, 1-43.
259. Ling, J.; Reynolds, N.; Ibba, M., Aminoacyl-tRNA synthesis and translational quality control. *Annu Rev Microbiol* **2009**, *63*, 61-78.
260. Yadavalli, S. S.; Musier-Forsyth, K.; Ibba, M., The return of pretransfer editing in protein synthesis. *Proc Natl Acad Sci U S A* **2008**, *105* (49), 19031-19032.
261. Brown, M. V.; Reader, J. S.; Tzima, E., Mammalian aminoacyl-tRNA synthetases: cell signaling functions of the protein translation machinery. *Vascul Pharmacol* **2010**, *52* (1-2), 21-26.
262. Guo, M.; Yang, X. L.; Schimmel, P., New functions of aminoacyl-tRNA synthetases beyond translation. *Nat Rev Mol Cell Biol* **2010**, *11* (9), 668-674.
263. Smirnova, E. V.; Lakunina, V. A.; Tarassov, I.; Krasheninnikov, I. A.; Kamenski, P. A., Noncanonical functions of aminoacyl-tRNA synthetases. *Biochemistry (Mosc)* **2012**, *77* (1), 15-25.
264. Yao, P.; Poruri, K.; Martinis, S. A.; Fox, P. L., Non-catalytic regulation of gene expression by aminoacyl-tRNA synthetases. *Top Curr Chem* **2014**, *344*, 167-187.
265. Yao, P.; Fox, P. L., Aminoacyl-tRNA synthetases in medicine and disease. *EMBO Mol Med* **2013**, *5* (3), 332-343.
266. Park, S. G.; Schimmel, P.; Kim, S., Aminoacyl tRNA synthetases and their connections to disease. *Proc Natl Acad Sci U S A* **2008**, *105* (32), 11043-11049.
267. Kim, S.; You, S.; Hwang, D., Aminoacyl-tRNA synthetases and tumorigenesis: more than housekeeping. *Nat Rev Cancer* **2011**, *11* (10), 708-718.
268. Kim, D.; Kwon, N. H.; Kim, S., Association of aminoacyl-tRNA synthetases with cancer. *Top Curr Chem* **2014**, *344*, 207-245.
269. Nangle, L. A.; Zhang, W.; Xie, W.; Yang, X. L.; Schimmel, P., Charcot-Marie-Tooth disease-associated mutant tRNA synthetases linked to altered dimer interface and neurite distribution defect. *Proc Natl Acad Sci U S A* **2007**, *104* (27), 11239-11244.
270. Park, S. G.; Park, H. S.; Jeong, I. K.; Cho, Y. M.; Lee, H. K.; Kang, Y. S.; Kim, S.; Park, K. S., Autoantibodies against aminoacyl-tRNA synthetase: novel diagnostic marker for type 1 diabetes mellitus. *Biomarkers* **2010**, *15* (4), 358-366.
271. Ida, H.; Huang, M.; Hida, A.; Origuchi, T.; Kawakami, A.; Migita, K.; Tsujihata, M.; Mimori, T.; Eguchi, K., Characterization of anticytoplasmic antibodies in patients with systemic autoimmune diseases. *Mod Rheumatol* **2003**, *13* (4), 333-338.

272. Deval, C.; Chaveroux, C.; Maurin, A. C.; Cherasse, Y.; Parry, L.; Carraro, V.; Milenkovic, D.; Ferrara, M.; Bruhat, A.; Jousse, C.; Fafournoux, P., Amino acid limitation regulates the expression of genes involved in several specific biological processes through GCN2-dependent and GCN2-independent pathways. *FEBS J* **2009**, *276* (3), 707-718.
273. Palii, S. S.; Kays, C. E.; Deval, C.; Bruhat, A.; Fafournoux, P.; Kilberg, M. S., Specificity of amino acid regulated gene expression: analysis of genes subjected to either complete or single amino acid deprivation. *Amino Acids* **2009**, *37* (1), 79-88.
274. Peng, T.; Golub, T. R.; Sabatini, D. M., The immunosuppressant rapamycin mimics a starvation-like signal distinct from amino acid and glucose deprivation. *Mol Cell Biol* **2002**, *22* (15), 5575-5584.
275. Duan, Y.; Li, F.; Tan, K.; Liu, H.; Li, Y.; Liu, Y.; Kong, X.; Tang, Y.; Wu, G.; Yin, Y., Key mediators of intracellular amino acids signaling to mTORC1 activation. *Amino Acids* **2015**, *47* (5), 857-867.
276. Sancak, Y.; Peterson, T. R.; Shaul, Y. D.; Lindquist, R. A.; Thoreen, C. C.; Bar-Peled, L.; Sabatini, D. M., The Rag GTPases bind raptor and mediate amino acid signaling to mTORC1. *Science* **2008**, *320* (5882), 1496-1501.
277. Harding, H. P.; Zhang, Y.; Zeng, H.; Novoa, I.; Lu, P. D.; Calton, M.; Sadri, N.; Yun, C.; Popko, B.; Paules, R.; Stojdl, D. F.; Bell, J. C.; Hettmann, T.; Leiden, J. M.; Ron, D., An integrated stress response regulates amino acid metabolism and resistance to oxidative stress. *Mol Cell* **2003**, *11* (3), 619-633.
278. Liwak, U.; Faye, M. D.; Holcik, M., Translation control in apoptosis. *Exp Oncol* **2012**, *34* (3), 218-230.
279. Holcik, M.; Sonenberg, N., Translational control in stress and apoptosis. *Nat Rev Mol Cell Biol* **2005**, *6* (4), 318-327.
280. Fennell, C.; Babbitt, S.; Russo, I.; Wilkes, J.; Ranford-Cartwright, L.; Goldberg, D. E.; Doerig, C., Pfk1K1, a eukaryotic initiation factor 2 α kinase of the human malaria parasite *Plasmodium falciparum*, regulates stress-response to amino-acid starvation. *Malar J* **2009**, *8*, 99.
281. Istvan, E. S.; Dharia, N. V.; Bopp, S. E.; Gluzman, I.; Winzeler, E. A.; Goldberg, D. E., Validation of isoleucine utilization targets in *Plasmodium falciparum*. *Proc Natl Acad Sci USA* **2011**, *108* (4), 1627-1632.
282. Hoen, R.; Novoa, E. M.; Lopez, A.; Camacho, N.; Cubells, L.; Vieira, P.; Santos, M.; Marin-Garcia, P.; Bautista, J. M.; Cortes, A.; Ribas de Pouplana, L.; Royo, M., Selective inhibition of an apicoplastic aminoacyl-tRNA synthetase from *Plasmodium falciparum*. *Chembiochem* **2013**, *14* (4), 499-509.
283. Castilho, B. A.; Shanmugam, R.; Silva, R. C.; Ramesh, R.; Himme, B. M.; Sattlegger, E., Keeping the eIF2 α kinase Gcn2 in check. *Biochim Biophys Acta* **2014**, *1843* (9), 1948-1968.
284. Bullwinkle, T. J.; Ibba, M., Emergence and evolution. *Top Curr Chem* **2014**, *344*, 43-87.
285. Khan, S.; Sharma, A.; Jamwal, A.; Sharma, V.; Pole, A. K.; Thakur, K. K.; Sharma, A., Uneven spread of cis- and trans-editing aminoacyl-tRNA synthetase domains within translational compartments of *P. falciparum*. *Sci Rep* **2011**, *1*, 188.
286. Bhatt, T. K.; Kapil, C.; Khan, S.; Jairajpuri, M. A.; Sharma, V.; Santoni, D.; Silvestrini, F.; Pizzi, E.; Sharma, A., A genomic glimpse of aminoacyl-tRNA synthetases in malaria parasite *Plasmodium falciparum*. *BMC Genomics* **2009**, *10*, 644.

References

287. Jackson, K. E.; Pham, J. S.; Kwek, M.; De Silva, N. S.; Allen, S. M.; Goodman, C. D.; McFadden, G. I.; Ribas de Pouplana, L.; Ralph, S. A., Dual targeting of aminoacyl-tRNA synthetases to the apicoplast and cytosol in *Plasmodium falciparum*. *Int J Parasitol* **2012**, *42* (2), 177-186.
288. Pino, P.; Aeby, E.; Foth, B. J.; Sheiner, L.; Soldati, T.; Schneider, A.; Soldati-Favre, D., Mitochondrial translation in absence of local tRNA aminoacylation and methionyl tRNA Met formylation in Apicomplexa. *Mol Microbiol* **2010**, *76* (3), 706-718.
289. Sharma, A.; Sharma, A., *Plasmodium falciparum* mitochondria import tRNAs along with an active phenylalanyl-tRNA synthetase. *Biochem J* **2015**, *465* (3), 459-469.
290. Tao, J.; Schimmel, P., Inhibitors of aminoacyl-tRNA synthetases as novel anti-infectives. *Expert Opin Investig Drugs* **2000**, *9* (8), 1767-1775.
291. Schimmel, P.; Tao, J.; Hill, J., Aminoacyl tRNA synthetases as targets for new anti-infectives. *Faseb j* **1998**, *12* (15), 1599-1609.
292. Poovelikunnel, T.; Gethin, G.; Humphreys, H., Mupirocin resistance: clinical implications and potential alternatives for the eradication of MRSA. *J Antimicrob Chemother* **2015**, *70* (10), 2681-2692.
293. Boyce, J. M., MRSA patients: proven methods to treat colonization and infection. *J Hosp Infect* **2001**, *48 Suppl A*, S9-14.
294. Gupta, A. K.; Daigle, D., Tavaborole (AN-2690) for the treatment of onychomycosis of the toenail in adults. *Expert Rev Anti Infect Ther* **2014**, *12* (7), 735-742.
295. Nass, G.; Poralla, K.; Zahner, H., Effect of the antibiotic Borrelidin on the regulation of threonine biosynthetic enzymes in *E. coli*. *Biochem Biophys Res Commun* **1969**, *34* (1), 84-91.
296. Ogilvie, A.; Wiebauer, K.; Kersten, W., Inhibition of leucyl-transfer ribonucleic acid synthetase. *Biochem J* **1975**, *152* (3), 511-515.
297. Werner, R. G.; Thorpe, L. F.; Reuter, W.; Nierhaus, K. H., Indolmycin inhibits prokaryotic tryptophanyl-tRNA ligase. *Eur J Biochem* **1976**, *68* (1), 1-3.
298. Tanaka, K.; Tamaki, M.; Watanabe, S., Effect of furanomycin on the synthesis of isoleucyl-tRNA. *Biochim Biophys Acta* **1969**, *195* (1), 244-245.
299. Konrad, I.; Roschenthaler, R., Inhibition of phenylalanine tRNA synthetase from *Bacillus subtilis* by ochratoxin A. *FEBS Lett* **1977**, *83* (2), 341-347.
300. Konishi, M.; Nishio, M.; Saitoh, K.; Miyaki, T.; Oki, T.; Kawaguchi, H., Cispentacin, a new antifungal antibiotic. I. Production, isolation, physico-chemical properties and structure. *J Antibiot (Tokyo)* **1989**, *42* (12), 1749-1755.
301. Hurdle, J. G.; O'Neill, A. J.; Chopra, I., Prospects for aminoacyl-tRNA synthetase inhibitors as new antimicrobial agents. *Antimicrob Agents Chemother* **2005**, *49* (12), 4821-4833.
302. Farrera-Sinfreu, J.; Espanol, Y.; Geslain, R.; Guitart, T.; Albericio, F.; Ribas de Pouplana, L.; Royo, M., Solid-phase combinatorial synthesis of a lysyl-tRNA synthetase (LysRS) inhibitory library. *J Comb Chem* **2008**, *10* (3), 391-400.
303. Van de Vijver, P.; Ostrowski, T.; Sproat, B.; Goebels, J.; Rutgeerts, O.; Van Aerschot, A.; Waer, M.; Herdewijn, P., Aminoacyl-tRNA synthetase inhibitors as potent and synergistic immunosuppressants. *J Med Chem* **2008**, *51* (10), 3020-3029.
304. Ding, D.; Meng, Q.; Gao, G.; Zhao, Y.; Wang, Q.; Nare, B.; Jacobs, R.; Rock, F.; Alley, M. R.; Plattner, J. J.; Chen, G.; Li, D.; Zhou, H., Design, synthesis, and structure-activity

- relationship of *Trypanosoma brucei* leucyl-tRNA synthetase inhibitors as antitrypanosomal agents. *J Med Chem* **2011**, *54* (5), 1276-1287.
305. Nakama, T.; Nureki, O.; Yokoyama, S., Structural basis for the recognition of isoleucyl-adenylate and an antibiotic, mupirocin, by isoleucyl-tRNA synthetase. *J Biol Chem* **2001**, *276* (50), 47387-47393.
306. Cestari, I.; Stuart, K., Inhibition of isoleucyl-tRNA synthetase as a potential treatment for human African Trypanosomiasis. *J Biol Chem* **2013**, *288* (20), 14256-14263.
307. Jiang, S.; Zeng, Q.; Gettayacamin, M.; Tungtaeng, A.; Wannaying, S.; Lim, A.; Hansukjariya, P.; Okunji, C. O.; Zhu, S.; Fang, D., Antimalarial activities and therapeutic properties of febrifugine analogs. *Antimicrob Agents Chemother* **2005**, *49* (3), 1169-1176.
308. Edgar, S. A.; Flanagan, C., Efficacy of Stenrol (halofuginone). I. Against recent field isolates of six species of chicken coccidia. *Poult Sci* **1979**, *58* (6), 1469-1475.
309. Pines, M.; Spector, I., Halofuginone - the multifaceted molecule. *Molecules* **2015**, *20* (1), 573-594.
310. Pines, M., Halofuginone for fibrosis, regeneration and cancer in the gastrointestinal tract. *World J Gastroenterol* **2014**, *20* (40), 14778-14786.
311. Sundrud, M. S.; Koralov, S. B.; Feuerer, M.; Calado, D. P.; Kozhaya, A. E.; Rhule-Smith, A.; Lefebvre, R. E.; Unutmaz, D.; Mazitschek, R.; Waldner, H.; Whitman, M.; Keller, T.; Rao, A., Halofuginone inhibits TH17 cell differentiation by activating the amino acid starvation response. *Science* **2009**, *324* (5932), 1334-1338.
312. Zhou, H.; Sun, L.; Yang, X. L.; Schimmel, P., ATP-directed capture of bioactive herbal-based medicine on human tRNA synthetase. *Nature* **2013**, *494* (7435), 121-124.
313. Jain, V.; Yogavel, M.; Oshima, Y.; Kikuchi, H.; Touquet, B.; Hakimi, M. A.; Sharma, A., Structure of Prolyl-tRNA Synthetase-Halofuginone Complex Provides Basis for Development of Drugs against Malaria and Toxoplasmosis. *Structure* **2015**, *23* (5), 819-829.
314. Son, J.; Lee, E. H.; Park, M.; Kim, J. H.; Kim, J.; Kim, S.; Jeon, Y. H.; Hwang, K. Y., Conformational changes in human prolyl-tRNA synthetase upon binding of the substrates proline and ATP and the inhibitor halofuginone. *Acta Crystallogr D Biol Crystallogr* **2013**, *69* (Pt 10), 2136-2145.
315. Jain, V.; Kikuchi, H.; Oshima, Y.; Sharma, A.; Yogavel, M., Structural and functional analysis of the anti-malarial drug target prolyl-tRNA synthetase. *J Struct Funct Genomics* **2014**.
316. Derbyshire, E. R.; Mazitschek, R.; Clardy, J., Characterization of Plasmodium liver stage inhibition by halofuginone. *ChemMedChem* **2012**, *7* (5), 844-849.
317. Takeuchi, Y.; Oshige, M.; Azuma, K.; Abe, H.; Harayama, T., Concise synthesis of dl-febrifugine. *Chem Pharm Bull (Tokyo)* **2005**, *53* (7), 868-869.
318. Pang, Y. L.; Martinis, S. A., A paradigm shift for the amino acid editing mechanism of human cytoplasmic leucyl-tRNA synthetase. *Biochemistry* **2009**, *48* (38), 8958-8964.
319. Rock, F. L.; Mao, W.; Yaremchuk, A.; Tukalo, M.; Crepin, T.; Zhou, H.; Zhang, Y. K.; Hernandez, V.; Akama, T.; Baker, S. J.; Plattner, J. J.; Shapiro, L.; Martinis, S. A.; Benkovic, S. J.; Cusack, S.; Alley, M. R., An antifungal agent inhibits an aminoacyl-tRNA synthetase by trapping tRNA in the editing site. *Science* **2007**, *316* (5832), 1759-1761.
320. Baker, S. J.; Zhang, Y. K.; Akama, T.; Lau, A.; Zhou, H.; Hernandez, V.; Mao, W.; Alley, M. R.; Sanders, V.; Plattner, J. J., Discovery of a new boron-containing antifungal

References

- agent, 5-fluoro-1,3-dihydro-1-hydroxy-2,1- benzoxaborole (AN2690), for the potential treatment of onychomycosis. *J Med Chem* **2006**, *49* (15), 4447-4450.
321. Liu, C. T.; Tomsho, J. W.; Benkovic, S. J., The unique chemistry of benzoxaboroles: current and emerging applications in biotechnology and therapeutic treatments. *Bioorg Med Chem* **2014**, *22* (16), 4462-4473.
322. Zhang, Y. H.; Xue, M. Q.; Bai, Y. C.; Yuan, H. H.; Zhao, H. L.; Lan, M. B., 3,5-Dicaffeoylquinic acid isolated from *Artemisia argyi* and its ester derivatives exert anti-leucyl-tRNA synthetase of *Giardia lamblia* (GILeuRS) and potential anti-giardial effects. *Fitoterapia* **2012**, *83* (7), 1281-1285.
323. Bowers, G. D.; Tenero, D.; Patel, P.; Huynh, P.; Sigafos, J.; O'Mara, K.; Young, G. C.; Dumont, E.; Cunningham, E.; Kurtinecz, M.; Stump, P.; Conde, J. J.; Chism, J. P.; Reese, M. J.; Yueh, Y. L.; Tomayko, J. F., Disposition and metabolism of GSK2251052 in humans: a novel boron-containing antibiotic. *Drug Metab Dispos* **2013**, *41* (5), 1070-1081.
324. Hu, Q. H.; Liu, R. J.; Fang, Z. P.; Zhang, J.; Ding, Y. Y.; Tan, M.; Wang, M.; Pan, W.; Zhou, H. C.; Wang, E. D., Discovery of a potent benzoxaborole-based anti-pneumococcal agent targeting leucyl-tRNA synthetase. *Sci Rep* **2013**, *3*, 2475.
325. Zhao, Y.; Wang, Q.; Meng, Q.; Ding, D.; Yang, H.; Gao, G.; Li, D.; Zhu, W.; Zhou, H., Identification of *Trypanosoma brucei* leucyl-tRNA synthetase inhibitors by pharmacophore- and docking-based virtual screening and synthesis. *Bioorg Med Chem* **2012**, *20* (3), 1240-1250.
326. Zhang, F.; Du, J.; Wang, Q.; Hu, Q.; Zhang, J.; Ding, D.; Zhao, Y.; Yang, F.; Wang, E.; Zhou, H., Discovery of N-(4-sulfamoylphenyl)thioureas as *Trypanosoma brucei* leucyl-tRNA synthetase inhibitors. *Org Biomol Chem* **2013**, *11* (32), 5310-5324.
327. Zhang, Y. K.; Plattner, J. J.; Freund, Y. R.; Easom, E. E.; Zhou, Y.; Ye, L.; Zhou, H.; Waterson, D.; Gamo, F. J.; Sanz, L. M.; Ge, M.; Li, Z.; Li, L.; Wang, H.; Cui, H., Benzoxaborole antimalarial agents. Part 2: Discovery of fluoro-substituted 7-(2-carboxyethyl)-1,3-dihydro-1-hydroxy-2,1-benzoxaboroles. *Bioorg Med Chem Lett* **2012**, *22* (3), 1299-1307.
328. Zhang, Y. K.; Plattner, J. J.; Easom, E. E.; Jacobs, R. T.; Guo, D.; Sanders, V.; Freund, Y. R.; Campo, B.; Rosenthal, P. J.; Bu, W.; Gamo, F. J.; Sanz, L. M.; Ge, M.; Li, L.; Ding, J.; Yang, Y., Benzoxaborole antimalarial agents. Part 4. Discovery of potent 6-(2-(alkoxycarbonyl)pyrazinyl-5-oxy)-1,3-dihydro-1-hydroxy-2,1-benzoxaboroles. *J Med Chem* **2015**, *58* (13), 5344-5354.
329. Guo, M.; Chong, Y. E.; Beebe, K.; Shapiro, R.; Yang, X. L.; Schimmel, P., The C-Ala domain brings together editing and aminoacylation functions on one tRNA. *Science* **2009**, *325* (5941), 744-747.
330. Novoa, E. M.; Vargas-Rodriguez, O.; Lange, S.; Goto, Y.; Suga, H.; Musier-Forsyth, K.; Ribas de Pouplana, L., Ancestral AlaX editing enzymes for control of genetic code fidelity are not tRNA-specific. *J Biol Chem* **2015**, *290* (16), 10495-10503.
331. Lee, J. W.; Beebe, K.; Nangle, L. A.; Jang, J.; Longo-Guess, C. M.; Cook, S. A.; Davisson, M. T.; Sundberg, J. P.; Schimmel, P.; Ackerman, S. L., Editing-defective tRNA synthetase causes protein misfolding and neurodegeneration. *Nature* **2006**, *443* (7107), 50-55.

332. Liu, Y.; Satz, J. S.; Vo, M. N.; Nangle, L. A.; Schimmel, P.; Ackerman, S. L., Deficiencies in tRNA synthetase editing activity cause cardioproteinopathy. *Proc Natl Acad Sci U S A* **2014**, *111* (49), 17570-17575.
333. Kron, M. A.; Metwali, A.; Vodanovic-Jankovic, S.; Elliott, D., Nematode asparaginyl-tRNA synthetase resolves intestinal inflammation in mice with T-cell transfer colitis. *Clin Vaccine Immunol* **2013**, *20* (2), 276-281.
334. Kron, M.; Marquard, K.; Hartlein, M.; Price, S.; Leberman, R., An immunodominant antigen of *Brugia malayi* is an asparaginyl-tRNA synthetase. *FEBS Lett* **1995**, *374* (1), 122-124.
335. Crepin, T.; Peterson, F.; Haertlein, M.; Jensen, D.; Wang, C.; Cusack, S.; Kron, M., A hybrid structural model of the complete *Brugia malayi* cytoplasmic asparaginyl-tRNA synthetase. *J Mol Biol* **2011**, *405* (4), 1056-1069.
336. Sukuru, S. C.; Crepin, T.; Milev, Y.; Marsh, L. C.; Hill, J. B.; Anderson, R. J.; Morris, J. C.; Rohatgi, A.; O'Mahony, G.; Grotli, M.; Danel, F.; Page, M. G.; Hartlein, M.; Cusack, S.; Kron, M. A.; Kuhn, L. A., Discovering new classes of *Brugia malayi* asparaginyl-tRNA synthetase inhibitors and relating specificity to conformational change. *J Comput Aided Mol Des* **2006**, *20* (3), 159-178.
337. Danel, F.; Caspers, P.; Nuoffer, C.; Hartlein, M.; Kron, M. A.; Page, M. G., Asparaginyl-tRNA synthetase pre-transfer editing assay. *Curr Drug Discov Technol* **2011**, *8* (1), 66-75.
338. Yu, Z.; Vodanovic-Jankovic, S.; Ledebor, N.; Huang, S. X.; Rajski, S. R.; Kron, M.; Shen, B., Tirandamycins from *Streptomyces* sp. 17944 inhibiting the parasite *Brugia malayi* asparagine tRNA synthetase. *Org Lett* **2011**, *13* (8), 2034-2037.
339. Yu, Z.; Vodanovic-Jankovic, S.; Kron, M.; Shen, B., New WS9326A congeners from *Streptomyces* sp. 9078 inhibiting *Brugia malayi* asparaginyl-tRNA synthetase. *Org Lett* **2012**, *14* (18), 4946-4949.
340. Novoa, E. M.; Camacho, N.; Tor, A.; Wilkinson, B.; Moss, S.; Marin-Garcia, P.; Azcarate, I. G.; Bautista, J. M.; Mirando, A. C.; Francklyn, C. S.; Varon, S.; Royo, M.; Cortes, A.; Ribas de Pouplana, L., Analogs of natural aminoacyl-tRNA synthetase inhibitors clear malaria in vivo. *Proc Natl Acad Sci U S A* **2014**, *111* (51), E5508-5517.
341. Guiguemde, W. A.; Guy, R. K., An all-purpose antimalarial drug target. *Cell Host Microbe* **2012**, *11* (6), 555-557.
342. Khan, S.; Sharma, A.; Belrhali, H.; Yogavel, M.; Sharma, A., Structural basis of malaria parasite lysyl-tRNA synthetase inhibition by cladosporin. *J Struct Funct Genomics* **2014**, *15* (2), 63-71.
343. Fang, P.; Han, H.; Wang, J.; Chen, K.; Chen, X.; Guo, M., Structural Basis for Specific Inhibition of tRNA Synthetase by an ATP Competitive Inhibitor. *Chem Biol* **2015**, *22* (6), 734-744.
344. Novoa, E. M.; Ribas de Pouplana, L., Cooperation for Better Inhibiting. *Chem Biol* **2015**, *22* (6), 685-686.
345. Critchley, I. A.; Green, L. S.; Young, C. L.; Bullard, J. M.; Evans, R. J.; Price, M.; Jarvis, T. C.; Guiles, J. W.; Janjic, N.; Ochsner, U. A., Spectrum of activity and mode of action of REP3123, a new antibiotic to treat *Clostridium difficile* infections. *J Antimicrob Chemother* **2009**, *63* (5), 954-963.
346. Green, L. S.; Bullard, J. M.; Ribble, W.; Dean, F.; Ayers, D. F.; Ochsner, U. A.; Janjic, N.; Jarvis, T. C., Inhibition of methionyl-tRNA synthetase by REP8839 and effects of

References

- resistance mutations on enzyme activity. *Antimicrob Agents Chemother* **2009**, *53* (1), 86-94.
347. Shibata, S.; Gillespie, J. R.; Kelley, A. M.; Napuli, A. J.; Zhang, Z.; Kovzun, K. V.; Pefley, R. M.; Lam, J.; Zucker, F. H.; Van Voorhis, W. C.; Merritt, E. A.; Hol, W. G.; Verlinde, C. L.; Fan, E.; Buckner, F. S., Selective inhibitors of methionyl-tRNA synthetase have potent activity against *Trypanosoma brucei* Infection in Mice. *Antimicrob Agents Chemother* **2011**, *55* (5), 1982-1989.
348. Larson, E. T.; Kim, J. E.; Zucker, F. H.; Kelley, A.; Mueller, N.; Napuli, A. J.; Verlinde, C. L.; Fan, E.; Buckner, F. S.; Van Voorhis, W. C.; Merritt, E. A.; Hol, W. G., Structure of *Leishmania major* methionyl-tRNA synthetase in complex with intermediate products methionyladenylate and pyrophosphate. *Biochimie* **2011**, *93* (3), 570-582.
349. Koh, C. Y.; Kim, J. E.; Wetzel, A. B.; de van der Schueren, W. J.; Shibata, S.; Ranade, R. M.; Liu, J.; Zhang, Z.; Gillespie, J. R.; Buckner, F. S.; Verlinde, C. L.; Fan, E.; Hol, W. G., Structures of *Trypanosoma brucei* methionyl-tRNA synthetase with urea-based inhibitors provide guidance for drug design against sleeping sickness. *PLoS Negl Trop Dis* **2014**, *8* (4), e2775.
350. Koh, C. Y.; Kim, J. E.; Shibata, S.; Ranade, R. M.; Yu, M.; Liu, J.; Gillespie, J. R.; Buckner, F. S.; Verlinde, C. L.; Fan, E.; Hol, W. G., Distinct states of methionyl-tRNA synthetase indicate inhibitor binding by conformational selection. *Structure* **2012**, *20* (10), 1681-1691.
351. Ranade, R. M.; Gillespie, J. R.; Shibata, S.; Verlinde, C. L.; Fan, E.; Hol, W. G.; Buckner, F. S., Induced resistance to methionyl-tRNA synthetase inhibitors in *Trypanosoma brucei* is due to overexpression of the target. *Antimicrob Agents Chemother* **2013**, *57* (7), 3021-3028.
352. Pedro-Rosa, L.; Buckner, F. S.; Ranade, R. M.; Eberhart, C.; Madoux, F.; Gillespie, J. R.; Koh, C. Y.; Brown, S.; Lohse, J.; Verlinde, C. L.; Fan, E.; Bannister, T.; Scampavia, L.; Hol, W. G.; Spicer, T.; Hodder, P., Identification of potent inhibitors of the *Trypanosoma brucei* methionyl-tRNA synthetase via high-throughput orthogonal screening. *J Biomol Screen* **2015**, *20* (1), 122-130.
353. Hussain, T.; Yogavel, M.; Sharma, A., Inhibition of protein synthesis and malaria parasite development by drug targeting of methionyl-tRNA synthetases. *Antimicrob Agents Chemother* **2015**, *59* (4), 1856-1867.
354. Ruan, B.; Bovee, M. L.; Sacher, M.; Stathopoulos, C.; Poralla, K.; Francklyn, C. S.; Soll, D., A unique hydrophobic cluster near the active site contributes to differences in borrelidin inhibition among threonyl-tRNA synthetases. *J Biol Chem* **2005**, *280* (1), 571-577.
355. Fang, P.; Yu, X.; Jeong, S. J.; Mirando, A.; Chen, K.; Chen, X.; Kim, S.; Francklyn, C. S.; Guo, M., Structural basis for full-spectrum inhibition of translational functions on a tRNA synthetase. *Nat Commun* **2015**, *6*, 6402.
356. Ishiyama, A.; Iwatsuki, M.; Namatame, M.; Nishihara-Tsukashima, A.; Sunazuka, T.; Takahashi, Y.; Omura, S.; Otoguro, K., Borrelidin, a potent antimalarial: stage-specific inhibition profile of synchronized cultures of *Plasmodium falciparum*. *J Antibiot (Tokyo)* **2011**, *64* (5), 381-384.
357. Sugawara, A.; Tanaka, T.; Hirose, T.; Ishiyama, A.; Iwatsuki, M.; Takahashi, Y.; Otoguro, K.; Omura, S.; Sunazuka, T., Borrelidin analogues with antimalarial activity:

- design, synthesis and biological evaluation against Plasmodium falciparum parasites. *Bioorg Med Chem Lett* **2013**, *23* (8), 2302-2305.
358. Koh, C. Y.; Kim, J. E.; Napoli, A. J.; Verlinde, C. L.; Fan, E.; Buckner, F. S.; Van Voorhis, W. C.; Hol, W. G., Crystal structures of Plasmodium falciparum cytosolic tryptophanyl-tRNA synthetase and its potential as a target for structure-guided drug design. *Mol Biochem Parasitol* **2013**, *189* (1-2), 26-32.
359. Khan, S.; Garg, A.; Sharma, A.; Camacho, N.; Picchioni, D.; Saint-Leger, A.; Ribas de Pouplana, L.; Yogavel, M.; Sharma, A., An appended domain results in an unusual architecture for malaria parasite tryptophanyl-tRNA synthetase. *PLoS One* **2013**, *8* (6), e66224.
360. Pham, J. S.; Sakaguchi, R.; Yeoh, L. M.; De Silva, N. S.; McFadden, G. I.; Hou, Y. M.; Ralph, S. A., A dual-targeted aminoacyl-tRNA synthetase in Plasmodium falciparum charges cytosolic and apicoplast tRNACys. *Biochem J* **2014**, *458* (3), 513-523.
361. Bour, T.; Akaddar, A.; Lorber, B.; Blais, S.; Balg, C.; Candolfi, E.; Frugier, M., Plasmodial aspartyl-tRNA synthetases and peculiarities in Plasmodium falciparum. *J Biol Chem* **2009**, *284* (28), 18893-18903.
362. Kim, S.; Lee, S. W.; Choi, E. C.; Choi, S. Y., Aminoacyl-tRNA synthetases and their inhibitors as a novel family of antibiotics. *Appl Microbiol Biotechnol* **2003**, *61* (4), 278-288.
363. Bernier, S.; Akochy, P. M.; Lapointe, J.; Chenevert, R., Synthesis and aminoacyl-tRNA synthetase inhibitory activity of aspartyl adenylate analogs. *Bioorg Med Chem* **2005**, *13* (1), 69-75.
364. Vondenhoff, G. H.; Van Aerschot, A., Aminoacyl-tRNA synthetase inhibitors as potential antibiotics. *Eur J Med Chem* **2011**, *46* (11), 5227-5236.
365. Heacock, D.; Forsyth, C. J.; Shiba, K.; Musier-Forsyth, K., Synthesis and Aminoacyl-tRNA Synthetase Inhibitory Activity of Prolyl Adenylate Analogs. *Bioorg Chem* **1996**, *24* (3), 273-289.
366. Brown, P.; Richardson, C. M.; Mensah, L. M.; O'Hanlon, P. J.; Osborne, N. F.; Pope, A. J.; Walker, G., Molecular recognition of tyrosinyl adenylate analogues by prokaryotic tyrosyl tRNA synthetases. *Bioorg Med Chem* **1999**, *7* (11), 2473-2485.
367. Schwarz, S.; Thieme, I.; Richter, M.; Undeutsch, B.; Henkel, H.; Elger, W., Synthesis of estrogen sulfamates: compounds with a novel endocrinological profile. *Steroids* **1996**, *61* (12), 710-717.
368. Farrera-Sinfreu, J.; Albericio, F.; Royo, M., Solid-phase synthesis of sulfamate peptidomimetics. *J Comb Chem* **2007**, *9* (3), 501-506.
369. Forrest, A. K.; Jarvest, R. L.; Mensah, L. M.; O'Hanlon, P. J.; Pope, A. J.; Sheppard, R. J., Aminoalkyl adenylate and aminoacyl sulfamate intermediate analogues differing greatly in affinity for their cognate Staphylococcus aureus aminoacyl tRNA synthetases. *Bioorg Med Chem Lett* **2000**, *10* (16), 1871-1874.
370. Rui Wang, K. F., Bing-Feng Sun, Ming-Hua Xu, Guo-Qiang Lin, Concise Asymmetric Synthesis of Antimalarial Alkaloid (+)-Febrifugine. *Synlett* **2009**, *2009* (14), 2301-2304.
371. Szostak, M.; Spain, M.; Procter, D. J., Preparation of samarium(II) iodide: quantitative evaluation of the effect of water, oxygen, and peroxide content, preparative methods, and the activation of samarium metal. *J Org Chem* **2012**, *77* (7), 3049-3059.
372. Hinnebusch, A. G., Translational regulation of GCN4 and the general amino acid control of yeast. *Annu Rev Microbiol* **2005**, *59*, 407-450.

References

373. Meyer, K.; Selbach, M., Quantitative affinity purification mass spectrometry: a versatile technology to study protein-protein interactions. *Front Genet* **2015**, *6*, 237.
374. Gomez, Y. R.; Gallien, S.; Huerta, V.; van Oostrum, J.; Domon, B.; Gonzalez, L. J., Characterization of protein complexes using targeted proteomics. *Curr Top Med Chem* **2014**, *14* (3), 344-350.
375. Carneiro, D. G.; Clarke, T.; Davies, C. C.; Bailey, D., Identifying novel protein interactions: Proteomic methods, optimisation approaches and data analysis pipelines. *Methods* **2015**.
376. McNamara, C. W.; Lee, M. C.; Lim, C. S.; Lim, S. H.; Roland, J.; Nagle, A.; Simon, O.; Yeung, B. K.; Chatterjee, A. K.; McCormack, S. L.; Manary, M. J.; Zeeman, A. M.; Dechering, K. J.; Kumar, T. R.; Henrich, P. P.; Gagaring, K.; Ibanez, M.; Kato, N.; Kuhlen, K. L.; Fischli, C.; Rottmann, M.; Plouffe, D. M.; Bursulaya, B.; Meister, S.; Rameh, L.; Trappe, J.; Haasen, D.; Timmerman, M.; Sauerwein, R. W.; Suwanarusk, R.; Russell, B.; Renia, L.; Nosten, F.; Tully, D. C.; Kocken, C. H.; Glynn, R. J.; Bodenreider, C.; Fidock, D. A.; Diagana, T. T.; Winzeler, E. A., Targeting Plasmodium PI(4)K to eliminate malaria. *Nature* **2013**, *504* (7479), 248-253.
377. Fidock, D. A.; Rosenthal, P. J.; Croft, S. L.; Brun, R.; Nwaka, S., Antimalarial drug discovery: efficacy models for compound screening. *Nat Rev Drug Discov* **2004**, *3* (6), 509-520.
378. Wongsrichanalai, C.; Meshnick, S. R., Declining artesunate-mefloquine efficacy against falciparum malaria on the Cambodia-Thailand border. *Emerg Infect Dis* **2008**, *14* (5), 716-719.
379. Li, N.; Overkleeft, H. S.; Florea, B. I., Activity-based protein profiling: an enabling technology in chemical biology research. *Curr Opin Chem Biol* **2012**, *16* (1-2), 227-233.
380. Cravatt, B. F.; Wright, A. T.; Kozarich, J. W., Activity-based protein profiling: from enzyme chemistry to proteomic chemistry. *Annu Rev Biochem* **2008**, *77*, 383-414.
381. Speers, A. E.; Adam, G. C.; Cravatt, B. F., Activity-based protein profiling in vivo using a copper(i)-catalyzed azide-alkyne [3 + 2] cycloaddition. *J Am Chem Soc* **2003**, *125* (16), 4686-4687.
382. Yang, K. S.; Budin, G.; Reiner, T.; Vinegoni, C.; Weissleder, R., Bioorthogonal imaging of aurora kinase A in live cells. *Angew Chem Int Ed Engl* **2012**, *51* (27), 6598-6603.
383. Cabrera, M.; Natarajan, J.; Paguio, M. F.; Wolf, C.; Urbach, J. S.; Roepe, P. D., Chloroquine transport in Plasmodium falciparum. 1. Influx and efflux kinetics for live trophozoite parasites using a novel fluorescent chloroquine probe. *Biochemistry* **2009**, *48* (40), 9471-9481.
384. Kanaoka, Y., Organic fluorescence reagents in the study of enzymes and proteins. *Angew Chem Int Ed Engl* **1977**, *16* (3), 137-147.
385. Lavis, L. D.; Raines, R. T., Bright ideas for chemical biology. *ACS Chem Biol* **2008**, *3* (3), 142-155.
386. Lakowicz, J. R., *Principles of Fluorescence Spectroscopy*. 3rd edition ed.; Springer: New York, 2006.
387. Lavis, L. D.; Raines, R. T., Bright building blocks for chemical biology. *ACS Chem Biol* **2014**, *9* (4), 855-866.
388. Pepperkok, R.; Ellenberg, J., High-throughput fluorescence microscopy for systems biology. *Nat Rev Mol Cell Biol* **2006**, *7* (9), 690-696.

389. Weissleder, R.; Pittet, M. J., Imaging in the era of molecular oncology. *Nature* **2008**, *452* (7187), 580-589.
390. Wennmalm, S.; Simon, S. M., Studying individual events in biology. *Annu Rev Biochem* **2007**, *76*, 419-446.
391. Chan, J.; Dodani, S. C.; Chang, C. J., Reaction-based small-molecule fluorescent probes for chemoselective bioimaging. *Nat Chem* **2012**, *4* (12), 973-984.
392. Yang, J.; Karver, M. R.; Li, W.; Sahu, S.; Devaraj, N. K., Metal-catalyzed one-pot synthesis of tetrazines directly from aliphatic nitriles and hydrazine. *Angew Chem Int Ed Engl* **2012**, *51* (21), 5222-5225.
393. Kneuer R, G. H., Beckmann N,; Jetzfellner T, N. V., In vivo fluorescence optical and multi-modal imaging in pharmacological research: from chemistry to therapy monitoring. *RSC Drug Discovery Series* **2012**, 343-370.
394. Ntziachristos, V., Fluorescence molecular imaging. *Annu Rev Biomed Eng* **2006**, *8*, 1-33.
395. Terai, T.; Nagano, T., Small-molecule fluorophores and fluorescent probes for bioimaging. *Pflugers Arch* **2013**, *465* (3), 347-359.
396. Goncalves, M. S., Fluorescent labeling of biomolecules with organic probes. *Chem Rev* **2009**, *109* (1), 190-212.
397. Johnson, T. W.; Dress, K. R.; Edwards, M., Using the Golden Triangle to optimize clearance and oral absorption. *Bioorg Med Chem Lett* **2009**, *19* (19), 5560-5564.
398. Shank, N. I.; Pham, H. H.; Waggoner, A. S.; Armitage, B. A., Twisted cyanines: a non-planar fluorogenic dye with superior photostability and its use in a protein-based fluoromodule. *J Am Chem Soc* **2013**, *135* (1), 242-251.
399. Egawa, T.; Koide, Y.; Hanaoka, K.; Komatsu, T.; Terai, T.; Nagano, T., Development of a fluorescein analogue, TokyoMagenta, as a novel scaffold for fluorescence probes in red region. *Chem Commun (Camb)* **2011**, *47* (14), 4162-4164.
400. Lukinavicius, G.; Umezawa, K.; Olivier, N.; Honigmann, A.; Yang, G.; Plass, T.; Mueller, V.; Reymond, L.; Correa, I. R., Jr.; Luo, Z. G.; Schultz, C.; Lemke, E. A.; Heppenstall, P.; Eggeling, C.; Manley, S.; Johnsson, K., A near-infrared fluorophore for live-cell super-resolution microscopy of cellular proteins. *Nat Chem* **2013**, *5* (2), 132-139.
401. Wang, S.; Guo, J.; Ono, T.; Kool, E. T., DNA polyfluorophores for real-time multicolor tracking of dynamic biological systems. *Angew Chem Int Ed Engl* **2012**, *51* (29), 7176-7180.
402. Ulrich, G.; Ziessel, R.; Harriman, A., The chemistry of fluorescent bodipy dyes: versatility unsurpassed. *Angew Chem Int Ed Engl* **2008**, *47* (7), 1184-1201.
403. Didier, P.; Ulrich, G.; Mely, Y.; Ziessel, R., Improved push-pull-push E-Bodipy fluorophores for two-photon cell-imaging. *Org Biomol Chem* **2009**, *7* (18), 3639-3642.
404. Zheng, Q.; Xu, G.; Prasad, P. N., Conformationally restricted dipyrromethene boron difluoride (BODIPY) dyes: highly fluorescent, multicolored probes for cellular imaging. *Chemistry* **2008**, *14* (19), 5812-5819.
405. Hapuarachchige, S.; Montano, G.; Ramesh, C.; Rodriguez, D.; Henson, L. H.; Williams, C. C.; Kadavakkollu, S.; Johnson, D. L.; Shuster, C. B.; Arterburn, J. B., Design and synthesis of a new class of membrane-permeable triazaborolopyridinium fluorescent probes. *J Am Chem Soc* **2011**, *133* (17), 6780-6790.
406. Beatty, K. E.; Szychowski, J.; Fisk, J. D.; Tirrell, D. A., A BODIPY-cyclooctyne for protein imaging in live cells. *Chembiochem* **2011**, *12* (14), 2137-2139.

References

407. Li, L.; Han, J.; Nguyen, B.; Burgess, K., Syntheses and spectral properties of functionalized, water-soluble BODIPY derivatives. *J Org Chem* **2008**, *73* (5), 1963-1970.
408. Loudet, A.; Burgess, K., BODIPY dyes and their derivatives: syntheses and spectroscopic properties. *Chem Rev* **2007**, *107* (11), 4891-4932.
409. Bura, T.; Ziessel, R., Water-soluble phosphonate-substituted BODIPY derivatives with tunable emission channels. *Org Lett* **2011**, *13* (12), 3072-3075.
410. Niu, S. L.; Ulrich, G.; Ziessel, R.; Kiss, A.; Renard, P. Y.; Romieu, A., Water-soluble BODIPY derivatives. *Org Lett* **2009**, *11* (10), 2049-2052.
411. Zhu, S.; Zhang, J.; Vegesna, G.; Luo, F. T.; Green, S. A.; Liu, H., Highly water-soluble neutral BODIPY dyes with controllable fluorescence quantum yields. *Org Lett* **2011**, *13* (3), 438-441.
412. Gabe, Y.; Ueno, T.; Urano, Y.; Kojima, H.; Nagano, T., Tunable design strategy for fluorescence probes based on 4-substituted BODIPY chromophore: improvement of highly sensitive fluorescence probe for nitric oxide. *Anal Bioanal Chem* **2006**, *386* (3), 621-626.
413. Tahtaoui, C.; Thomas, C.; Rohmer, F.; Klotz, P.; Duportail, G.; Mely, Y.; Bonnet, D.; Hibert, M., Convenient method to access new 4,4-dialkoxy- and 4,4-diaryloxy-diaza-s-indacene dyes: Synthesis and spectroscopic evaluation. *J Org Chem* **2007**, *72* (1), 269-272.
414. Jiang, X. D.; Zhang, J.; Furuyama, T.; Zhao, W., Development of mono- and di-AcO substituted BODIPYs on the boron center. *Org Lett* **2012**, *14* (1), 248-251.
415. Frath, D.; Azizi, S.; Ulrich, G.; Ziessel, R., Chemistry on Boranils: an entry to functionalized fluorescent dyes. *Org Lett* **2012**, *14* (18), 4774-4777.
416. Hendricks, J. A.; Keliher, E. J.; Wan, D.; Hilderbrand, S. A.; Weissleder, R.; Mazitschek, R., Synthesis of [¹⁸F]BODIPY: bifunctional reporter for hybrid optical/positron emission tomography imaging. *Angew Chem Int Ed Engl* **2012**, *51* (19), 4603-4606.
417. Njaria, P. M.; Okombo, J.; Njuguna, N. M.; Chibale, K., Chloroquine-containing compounds: a patent review (2010 - 2014). *Expert Opin Ther Pat* **2015**, *25* (9), 1003-1024.
418. Pagola, S.; Stephens, P. W.; Bohle, D. S.; Kosar, A. D.; Madsen, S. K., The structure of malaria pigment beta-haematin. *Nature* **2000**, *404* (6775), 307-310.
419. Lavrado, J.; Cabal, G. G.; Prudencio, M.; Mota, M. M.; Gut, J.; Rosenthal, P. J.; Diaz, C.; Guedes, R. C.; dos Santos, D. J.; Bichenkova, E.; Douglas, K. T.; Moreira, R.; Paulo, A., Incorporation of basic side chains into cryptolepine scaffold: structure-antimalarial activity relationships and mechanistic studies. *J Med Chem* **2011**, *54* (3), 734-750.
420. Lavrado, J.; Gani, K.; Nobre, P. A.; Santos, S. A.; Figueiredo, P.; Lopes, D.; Rosario, V.; Gut, J.; Rosenthal, P. J.; Moreira, R.; Paulo, A., Bis-alkylamine quindolone derivatives as new antimalarial leads. *Bioorg Med Chem Lett* **2010**, *20* (19), 5634-5637.
421. Lavrado, J.; Paulo, A.; Gut, J.; Rosenthal, P. J.; Moreira, R., Cryptolepine analogues containing basic aminoalkyl side-chains at C-11: synthesis, antiplasmodial activity, and cytotoxicity. *Bioorg Med Chem Lett* **2008**, *18* (4), 1378-1381.
422. Paulo, A.; Figueiras, M.; Machado, M.; Charneira, C.; Lavrado, J.; Santos, S. A.; Lopes, D.; Gut, J.; Rosenthal, P. J.; Nogueira, F.; Moreira, R., Bis-alkylamine Indolo[3,2-b]quinolines as hemozoin ligands: implications for antimalarial cytostatic and cytotoxic activities. *J Med Chem* **2014**, *57* (8), 3295-3313.

423. Krettli, A. U.; Adebayo, J. O.; Krettli, L. G., Testing of natural products and synthetic molecules aiming at new antimalarials. *Curr Drug Targets* **2009**, *10* (3), 261-270.
424. Kaur, K.; Jain, M.; Kaur, T.; Jain, R., Antimalarials from nature. *Bioorg Med Chem* **2009**, *17* (9), 3229-3256.
425. Onyeibor, O.; Croft, S. L.; Dodson, H. I.; Feiz-Haddad, M.; Kendrick, H.; Millington, N. J.; Parapini, S.; Phillips, R. M.; Seville, S.; Shnyder, S. D.; Taramelli, D.; Wright, C. W., Synthesis of some cryptolepine analogues, assessment of their antimalarial and cytotoxic activities, and consideration of their antimalarial mode of action. *J Med Chem* **2005**, *48* (7), 2701-2709.
426. Lavrado, J.; Paulo, A.; Bichenkova, E.; Douglas, K. T.; Moreira, R., ¹H NMR spectroscopic identification of protonable sites in cryptolepines with C-11 substituents containing two amino functionalities. *Magn Reson Chem* **2012**, *50* (3), 216-220.
427. Solomon, V. R.; Lee, H., Quinoline as a privileged scaffold in cancer drug discovery. *Curr Med Chem* **2011**, *18* (10), 1488-1508.
428. Kumar, E. V.; Etukala, J. R.; Ablordeppey, S. Y., Indolo[3,2-b]quinolines: synthesis, biological evaluation and structure activity-relationships. *Mini Rev Med Chem* **2008**, *8* (6), 538-554.
429. Brito, H.; Martins, A. C.; Lavrado, J.; Mendes, E.; Francisco, A. P.; Santos, S. A.; Ohnmacht, S. A.; Kim, N. S.; Rodrigues, C. M.; Moreira, R.; Neidle, S.; Borralho, P. M.; Paulo, A., Targeting KRAS Oncogene in Colon Cancer Cells with 7-Carboxylate Indolo[3,2-b]quinoline Tri-Alkylamine Derivatives. *PLoS One* **2015**, *10* (5), e0126891.
430. Lavrado, J.; Borralho, P. M.; Ohnmacht, S. A.; Castro, R. E.; Rodrigues, C. M.; Moreira, R.; dos Santos, D. J.; Neidle, S.; Paulo, A., Synthesis, G-quadruplex stabilisation, docking studies, and effect on cancer cells of indolo[3,2-b]quinolines with one, two, or three basic side chains. *ChemMedChem* **2013**, *8* (10), 1648-1661.
431. Lavrado, J.; Brito, H.; Borralho, P. M.; Ohnmacht, S. A.; Kim, N. S.; Leitao, C.; Pisco, S.; Gunaratnam, M.; Rodrigues, C. M.; Moreira, R.; Neidle, S.; Paulo, A., KRAS oncogene repression in colon cancer cell lines by G-quadruplex binding indolo[3,2-c]quinolines. *Sci Rep* **2015**, *5*, 9696.
432. Rocha e Silva, L. F.; Montoia, A.; Amorim, R. C.; Melo, M. R.; Henrique, M. C.; Nunomura, S. M.; Costa, M. R.; Andrade Neto, V. F.; Costa, D. S.; Dantas, G.; Lavrado, J.; Moreira, R.; Paulo, A.; Pinto, A. C.; Tadei, W. P.; Zacardi, R. S.; Eberlin, M. N.; Pohlit, A. M., Comparative in vitro and in vivo antimalarial activity of the indole alkaloids ellipticine, olivacine, cryptolepine and a synthetic cryptolepine analog. *Phytomedicine* **2012**, *20* (1), 71-76.
433. Gao, B. G. X. P. A. C. Y. W. M. T. L. Z. X. C. Y., Synthesis and spectral properties of new boron dipyrromethene dyes. *Dyes and Pigments* **2007**, *73* (2), 206-210.
434. Bonnier, C.; Piers, W. E.; Parvez, M.; Sorensen, T. S., Borenium cations derived from BODIPY dyes. *Chem Commun (Camb)* **2008**, (38), 4593-4595.
435. Hudnall, T. W.; Gabbai, F. P., A BODIPY boronium cation for the sensing of fluoride ions. *Chem Commun (Camb)* **2008**, (38), 4596-4597.
436. Los, G. V.; Encell, L. P.; McDougall, M. G.; Hartzell, D. D.; Karassina, N.; Zimprich, C.; Wood, M. G.; Learish, R.; Ohana, R. F.; Urh, M.; Simpson, D.; Mendez, J.; Zimmerman, K.; Otto, P.; Vidugiris, G.; Zhu, J.; Darzins, A.; Klaubert, D. H.; Bulleit, R. F.; Wood, K. V., HaloTag: a novel protein labeling technology for cell imaging and protein analysis. *ACS Chem Biol* **2008**, *3* (6), 373-382.

References

437. S, N. P.; Kwon, K., The HaloTag: Improving Soluble Expression and Applications in Protein Functional Analysis. *Curr Chem Genomics* **2012**, *6*, 8-17.
438. Correa, I. R., Jr., Considerations and protocols for the synthesis of custom protein labeling probes. *Methods Mol Biol* **2015**, *1266*, 55-79.
439. Burkhard, J. A.; Wuitschik, G.; Rogers-Evans, M.; Muller, K.; Carreira, E. M., Oxetanes as versatile elements in drug discovery and synthesis. *Angew Chem Int Ed Engl* **2010**, *49* (48), 9052-9067.
440. Horisawa, K., Specific and quantitative labeling of biomolecules using click chemistry. *Front Physiol* **2014**, *5*, 457.
441. Al-Bari, M. A., Chloroquine analogues in drug discovery: new directions of uses, mechanisms of actions and toxic manifestations from malaria to multifarious diseases. *J Antimicrob Chemother* **2015**, *70* (6), 1608-1621.
442. Filippakopoulos, P.; Qi, J.; Picaud, S.; Shen, Y.; Smith, W. B.; Fedorov, O.; Morse, E. M.; Keates, T.; Hickman, T. T.; Felletar, I.; Philpott, M.; Munro, S.; McKeown, M. R.; Wang, Y.; Christie, A. L.; West, N.; Cameron, M. J.; Schwartz, B.; Heightman, T. D.; La Thangue, N.; French, C. A.; Wiest, O.; Kung, A. L.; Knapp, S.; Bradner, J. E., Selective inhibition of BET bromodomains. *Nature* **2010**, *468* (7327), 1067-1073.
443. Bergstrom, F.; Mikhalyov, I.; Hagglof, P.; Wortmann, R.; Ny, T.; Johansson, L. B., Dimers of dipyrrometheneboron difluoride (BODIPY) with light spectroscopic applications in chemistry and biology. *J Am Chem Soc* **2002**, *124* (2), 196-204.
444. Neklesa, T. K.; Tae, H. S.; Schneekloth, A. R.; Stulberg, M. J.; Corson, T. W.; Sundberg, T. B.; Raina, K.; Holley, S. A.; Crews, C. M., Small-molecule hydrophobic tagging-induced degradation of HaloTag fusion proteins. *Nat Chem Biol* **2011**, *7* (8), 538-543.
445. Johnson, J. D.; Denu, R. A.; Gerena, L.; Lopez-Sanchez, M.; Roncal, N. E.; Waters, N. C., Assessment and continued validation of the malaria SYBR green I-based fluorescence assay for use in malaria drug screening. *Antimicrob Agents Chemother* **2007**, *51* (6), 1926-1933.

Appendices

Chemical Structures

- Chapter 1: Compounds **1.1-1.37**
- Chapter 2: Compounds **2.1-2.43**
- Chapter 3: Compounds **3.1-3.86**
- Chapter 4: Compounds **4.1-4.43**

